

AIAA Education Series



EUGENE L. FLITMAN

TACTICAL MISSILE DESIGN

AIAA

Education Series

AIAA Books
www.aaa.org

Tactical Missile Design

Tactical Missile Design

Eugene L. Fleeman



EDUCATION SERIES

J. S. Przemieniecki
Series Editor-in-Chief

Published by
American Institute of Aeronautics and Astronautics, Inc.
1801 Alexander Bell Drive, Reston, VA 20191-4344

American Institute of Aeronautics and Astronautics, Inc., Reston, Virginia

1 2 3 4 5

Library of Congress Cataloging-in-Publication Data

Fleeman, Eugene L.

Tactical missile design / Eugene L. Fleeman.

p. cm.—(AIAA education series)

Includes bibliographical references and index.

1. Guided missiles—Design and construction. I. Title. II. Series.

UG1310.F58 2001 623.4'519—dc21 2001033398

ISBN 1-56347-494-8 (hardcover: alk. paper)

Copyright © 2001 by the American Institute of Aeronautics and Astronautics, Inc. All rights reserved.
Printed in the United States of America. No part of this publication may be reproduced, distributed, or transmitted, in any form or by any means, or stored in a database or retrieval system, without the prior written permission of the publisher.

Data and information appearing in this book are for informational purposes only. AIAA is not responsible for any injury or damage resulting from use or reliance, nor does AIAA warrant that use or reliance will be free from privately owned rights.

To my family, especially my grandchildren Nicholas and Christopher

Foreword

Tactical Missile Design, by Eugene L. Fleeman, is truly a vademecum for every aeronautical engineer involved in the design and development of tactical missiles. This text is based on materials used in short courses presented by the author for many years, and it reflects his extensive experience and knowledge of the current state-of-the art for tactical missile technology. It describes the design process starting with the mission requirements and missile characteristics followed by the conceptual design and development process. It includes consideration of the important missile technologies such as aerodynamics, propulsion, structure, weight, flight performance, warhead lethality, and launch platform integration. The text is particularly suitable for graduate level courses in aeronautical engineering.

A novel feature for the AIAA Education Series, included with this text for the first time, is a CD that provides electronic versions of the figures and illustrative videos of the various aspects of tactical missile design and operation. Missile carriage, store separation, flyout trajectory, target intercept, warhead detonation, and other design and operation elements, are depicted in this way. Also included on the CD is a tactical missile design spreadsheet for conceptual design and analysis.

The AIAA Education Series of textbooks and monographs, inaugurated in 1984, embraces a broad spectrum of theory and application of different disciplines in aeronautics and astronautics, including aerospace design practice. The series also includes texts on defense science, engineering, and management. The books serve as both teaching texts for students and reference materials for practicing engineers, scientists, and managers. The complete list of textbooks published in the series (over 70 titles) can be found on the end pages of this volume.

J. S. Przemieniecki
Editor-in-Chief
AIAA Education Series

Table of Contents

Preface	xv
Chapter 1. Introduction/Key Drivers in the Design Process	1
1.1 Tactical Missile Characteristics	1
1.2 Conceptual Design Process	3
1.3 Examples of State-of-the-Art Missiles	6
1.4 Aerodynamic Configuration Sizing Parameters	7
1.5 Example of Alternatives in Establishing Mission Requirements	8
1.6 Baseline Missile	13
1.7 Summary	16
Chapter 2. Aerodynamic Considerations in Tactical Missile Design	17
2.1 Missile Diameter Tradeoff	17
2.2 Nose Fineness Tradeoff	21
2.3 Boattail	25
2.4 Lifting Body Versus Axisymmetric Body	26
2.5 Wings Versus No Wings	29
2.6 Normal Force Prediction for Surfaces	30
2.7 Wing Aerodynamic Center Prediction	32
2.8 Wing Drag Prediction	33
2.9 Surface Planform Geometry Tradeoffs	35
2.10 Flight Control Alternatives	36
2.11 Maneuver Alternatives	48
2.12 Roll Orientation	50
2.13 Static Stability	51
2.14 Tail Area Sizing	52
2.15 Stability and Control Conceptual Design Criteria	55
2.16 Body Buildup	56
2.17 Summary	57
Chapter 3. Propulsion Considerations in Tactical Missile Design	59
3.1 Propulsion Alternatives Assessment	59
3.2 Ideal Ramjet Mach Number and Temperature Technology Limit	64
3.3 Ramjet Specific Impulse Prediction	65
3.4 Ramjet Thrust Prediction	66
3.5 Ramjet Engine/Booster Integration	67
3.6 Ramjet Inlet Options	69
3.7 Ramjet Inlet Spillage	72

3.8 Inlet Shock Loss	75
3.9 Ramjet Missile Drag Due to Booster Integration	76
3.10 Fuel Alternatives	77
3.11 Rocket Motor Performance	77
3.12 Solid Motor Grain Alternatives	81
3.13 Solid Rocket Thrust Control	82
3.14 Solid Propellant Material Alternatives	84
3.15 Motor Case Alternatives	86
3.16 Rocket Nozzle Material Alternatives	87
3.17 Summary	88
Chapter 4. Weight Considerations in Tactical Missile Design	89
4.1 Benefits of Lighter Weight Missile	89
4.2 Subsystem Weight Sensitivity to Flight Performance	89
4.3 Missile Weight Prediction	90
4.4 Center-of-Gravity and Moment-of-Inertia Prediction	92
4.5 Factor of Safety	93
4.6 Micro-Machined Electro-Mechanical Systems (MEMS)	94
4.7 Manufacturing Processes	95
4.8 Airframe Material Alternatives	97
4.9 Aerodynamic Heating Prediction	101
4.10 Insulation Trades	103
4.11 Insulation Material Alternatives	104
4.12 Structure Design	106
4.13 Seeker Dome Materials	111
4.14 Thermal Stress	112
4.15 Localized Aerodynamic Heating	113
4.16 Summary	114
Chapter 5. Flight Performance Considerations in Tactical Missile Design	115
5.1 Flight Performance Envelope	115
5.2 Equations of Motion Modeling	116
5.3 Driving Parameters for Flight Performance	117
5.4 Cruise Flight Performance	119
5.5 Steady-State Flight	120
5.6 Flight Trajectory Shaping	120
5.7 Turn Radius	122
5.8 Turn Rate Performance	123
5.9 Coast Flight Performance	124
5.10 Boost Flight Performance	125
5.11 Intercept Lead Angle and Velocity	126
5.12 Comparison with Performance Requirements	126
5.13 Summary	127
Chapter 6. Measures of Merit and Launch Platform Integration	129
6.1 Robustness	129
6.2 Warhead Lethality	142

6.3	Miss Distance	153
6.4	Carriage and Launch Observables	164
6.5	Other Survivability Considerations	167
6.6	Reliability	168
6.7	Cost	168
6.8	Launch Platform Integration	175
6.9	Summary	183
Chapter 7. Sizing Examples		185
7.1	Air-to-Air Range Requirement	185
7.2	Wing Sizing for Maneuverability	198
7.3	Weight and Miss Distance Harmonization	199
7.4	Ramjet Missile Range Robustness	202
7.5	Ramjet Propulsion/Fuel Alternatives	211
7.6	Ramjet Missile Surface Impact Velocity	212
7.7	Computer-Aided Sizing for Conceptual Design	213
7.8	Verification Process	217
7.9	Summary	218
Chapter 8. Development Process		219
8.1	Technology Assessment/Roadmap	219
8.2	Phases of Development/Design Maturity	219
8.3	Tactical Missile Follow-On Programs	223
8.4	Subsystem Integration	224
8.5	Example of Technology Development	227
8.6	Examples of State-of-the-Art Advancement	229
8.7	New Technologies for Tactical Missiles	230
8.8	Summary	232
Chapter 9. Summary and Lessons Learned		233
9.1	Iterate-the System-of-Systems Analysis	233
9.2	Exploit Diverse Skills	233
9.3	Apply Creative Skills	233
9.4	Identify High-Payoff Measures of Merit	234
9.5	Start with a Good Baseline Design	235
9.6	Conduct Balanced Tradeoffs	235
9.7	Evaluate a Broad Range of Alternatives	235
9.8	Refine the Design	236
9.9	Evaluate Technology Risk	237
9.10	Maintain Real-Time Documentation	238
9.11	Develop Good Documentation	238
9.12	Utilize Group Skills	240
9.13	Balance the Tradeoff of Importance Versus Priority	241
9.14	Iterate the Configuration Design	241
9.15	Configuration Sizing Conceptual Design Criteria	241
9.16	Wrap-Up	243
Appendix A: Nomenclature		245

Appendix B: Acronyms	251
Appendix C: Conversion Factors	254
References	257
Index	261

Preface

The material in this book is oriented toward the needs of aerospace engineering students, missile engineers, and missile program managers. An objective is to provide a reference text for the aerospace engineering curriculum of universities. Although the tactical missile community is large, receives a significant amount of funding, and has many technical and system problems to address, few universities offer courses in missile design. It is hoped that this introduction to tactical missiles will spark the interest of young engineers to make a career in the tactical missile community. Also, the text is a reference for missile engineers and missile program managers.

The text is a summary of information that I have collected during my 36 years of experience in the development of tactical missiles and their technologies. It distills the technical knowledge that I have gathered into an integrated handbook method for missile design. The handbook method generally uses simple closed-form analytical expressions that are physics-based, to provide insight into the primary driving parameters. Closed-form analytical expressions are used in lieu of computers—a throwback to the way missile design was conducted over 30 years ago. The text also provides example calculations of rocket-powered and ramjet-powered baseline missiles, typical values of missile parameters, examples of the characteristics of current operational missiles, discussion of the enabling subsystems and technologies of tactical missiles, and the current/projected state of the art of tactical missiles.

In recent years we have seen increased use of tactical missile systems for military operations. Moreover, tactical missiles are expected to have an even larger share of military operations in the future. A key contributor to the increased effectiveness is the advancement in technology. Examples of advancement in missile system effectiveness include improved range, firepower, maneuverability, accuracy, lethality, and adverse weather capability.

A historical example of the value of guided weapons is the Thanh Hoa Bridge in Vietnam. For over six years, a total of 871 aircraft sorties dropped unguided bombs but failed to close the bridge. However, the first operational application of laser-guided bombs on 13 May 1972 resulted in direct hits on the supporting piers, dropping the center span and closing the bridge. It is noted that 11 aircraft were lost using unguided munitions in the 871 previous sorties. No aircraft were lost in the four sorties using precision guided munitions.

The organization of the material in this text is as follows. Chapter 1 gives an overview of the missile design process. Chapter 2 discusses conceptual design methods and the technologies emphasizing low aspect ratio wing and wingless configurations. Conceptual design methods and technologies for rocket and ramjet propulsion are included in Chapter 3, and conceptual design methods and

technologies emphasizing lower cost and high temperature structure are included in Chapter 4. Conceptual design methods for predicting flight range, time to target, and maneuverability are given in Chapter 5. Chapter 6 includes conceptual analysis methods and technologies in the areas of robustness, lethality, miss distance, carriage and launch observables, other survivability considerations, reliability, cost, and launch platform integration/firepower. Sizing examples for a rocket-powered missile, sizing examples for a ramjet-powered missile, and examples of conceptual design computer programs are presented in Chapter 7. The sizing examples for a rocket-powered missile are flight range and time-to-target evaluation, wing sizing for maneuverability, and weight/miss distance harmonization. The sizing examples for a ramjet-powered missile are range robustness assessment, propulsion and fuel alternatives evaluation, and impact velocity analysis. The examples for conceptual design computer programs are a computer program that combines missile aerodynamics prediction with a flight trajectory and an electronic spreadsheet for conceptual design and missile design criteria. Chapter 8 discusses the relationship of the missile design process to the missile development process. A summary of this text and the lessons learned in missile development are given in Chapter 9. References of the data and methods used in this text and a bibliography of other reports and web sites that are related to tactical missiles are provided at the end of all of the chapters. The appendices include a list of the symbols and acronyms used in this text, as well as a table for conversion of English to metric units.

A compact disk is included with this book. Included in the CD is an electronic version of the figures in this text. It is a Microsoft PowerPoint presentation. The viewgraphs are in color and have embedded tabular data. Also embedded in the viewgraphs are 16 videos in Microsoft Windows Media Player format. The 16 videos include examples of loading missiles on rail and ejection launchers and missile carriage on launch platforms; pilot actions prior to launching missiles; store separation trajectories (safe as well as unsafe); flight trajectories, intercepts, and warhead detonations for air and surface targets; plume observables of high-smoke, reduced-smoke, and minimum-smoke motors; missile countermeasures and counter-countermeasures; and development facilities, development testing, and manufacturing processes. The CD also includes a tactical missile design spreadsheet in Microsoft Excel format. The spreadsheet models the configuration sizing methods of this text.

I would like to thank the faculty and students at the Georgia Institute of Technology for their input and comments. Special appreciation is expressed to Dimitri Mavris, Director of the Aerospace Systems Design Laboratory, and to the following students: Bryce Roth, Andrew Frits, Jack Zentner, Brian German, Peter Hollingsworth, Javier Rosario, Caleb Branscome, and Nick Yiakas. In addition to providing comments on the text, Andrew Frits and Jack Zentner also developed the tactical missile design spreadsheet on the CD.

I also would like to express my appreciation to the following persons who have supported my work in the areas of missile design, advanced weapon concepts, and advanced weapons technologies: Bill Lamar and Charles Westbrook of the U.S. Air Force Research Laboratory and Thad Sandford of the Boeing Company Phantom Works.

Finally, I would appreciate receiving comments and corrections on this text, as well as any data, examples, or references that you may offer. E-mail to: GeneFleeman@msn.com or Eugene.Fleeman@asdl.gatech.edu; Web site <http://www.asdl.gatech.edu>. Write to: 4472 Anne Arundel Court, Lilburn, GA 30047, or call: +1-770-925-4635.

Eugene L. Fleeman

March 2001

Introduction/Key Drivers in the Design Process

The primary area of emphasis in the text is the methods and technology for aerodynamic configuration sizing (Fig. 1.1). Aerodynamic configuration sizing is conducted to develop the configuration geometry and the dimensions of the missile. The output of aerodynamic configuration sizing includes the missile diameter, length, nose geometry, stabilizer size and geometry, and the control surface size and geometry. The configuration sizing methods of this text are physics-based methods to allow analytical sizing of the missile configuration. Other areas that are addressed with secondary emphasis include aerodynamic stability and control, aerodynamic flight performance, propulsion, structure, weight, warhead, and miss distance. These are addressed to a level that is consistent with their impact on the aerodynamic configuration sizing. Tertiary emphasis is given to the areas of seeker, cost, additional measures of merit, and launch platform integration. Although the areas of secondary and tertiary emphasis are important at the system level, they generally have lesser impact on the aerodynamic design.

1.1 Tactical Missile Characteristics

Tactical missiles are different from other flight vehicles, such as combat aircraft, and are a technical specialty in their own right. Figure 1.2 is a state-of-the-art comparison of tactical missile characteristics with the current state of the art (SOTA) of fighter aircraft. Examples are shown where missiles are driving technology. Also shown are other areas where the missile is not driving technology.

As an example, the lateral and longitudinal acceleration SOTA of missiles exceeds that of combat aircraft. Missile lateral maneuverability of $30g^+$ and longitudinal acceleration of $30g^+$ have been demonstrated. Notable examples of missiles with high acceleration and maneuverability include the AGM-88 HARM and the AA-11 Archer missiles. Missile speed is also usually greater than that of combat aircraft; an example is the PAC-3 hypersonic missile. Another difference is the dynamic pressure loading on a missile, which is usually greater than that of combat aircraft. For example, the PAC-3 missile operates at much higher dynamic pressure than that of aircraft. Another difference is the relatively small size and lighter weight of missiles in comparison to combat aircraft, such as in the Stinger and Javelin man-portable missiles. Related to cost, missiles are a throwaway. As a result, they are more cost driven than combat aircraft. Development cost is lower for missiles, and the difference in production cost is even more dramatic. An example is the GBU-31 JDAM, with a cost of approximately \$10–20,000, compared to a cost of tens of millions of dollars for typical combat aircraft. Finally, cruise missiles such as AGM-129 achieve low radar cross section without the other design limitations associated with piloted aircraft.

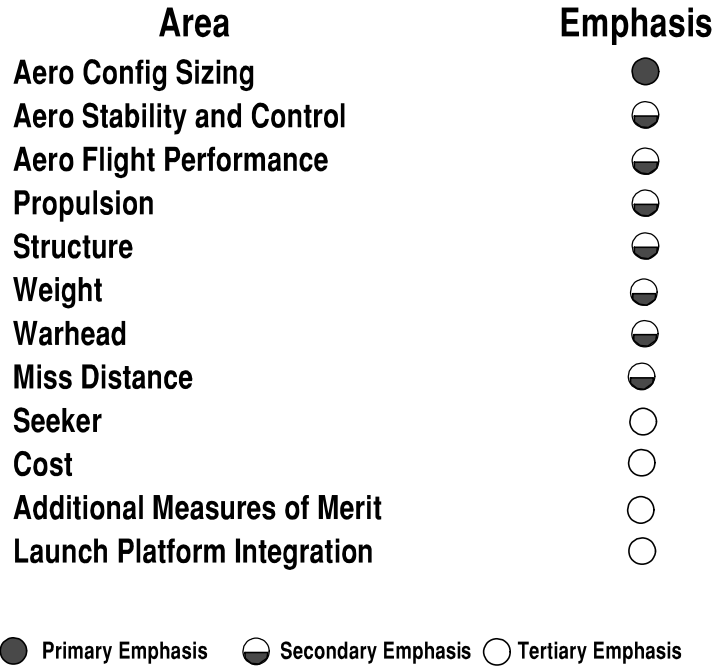


Fig. 1.1 Emphasis of this text is on physics-based, analytical sizing of aerodynamic configuration.

Areas where the combat aircraft generally have superior capability include range, targets killed per use, and target acquisition. Although the conventional version of the AGM-86 cruise missile (CALCM) has a flight range that can exceed 700 n miles, combat aircraft can have a much longer range. In the area of target kill capability, precision strike missiles have become more efficient in recent years, with a single target kill probability approaching one and a capability for multiple target kills. The Apache missile is an example of an efficient precision

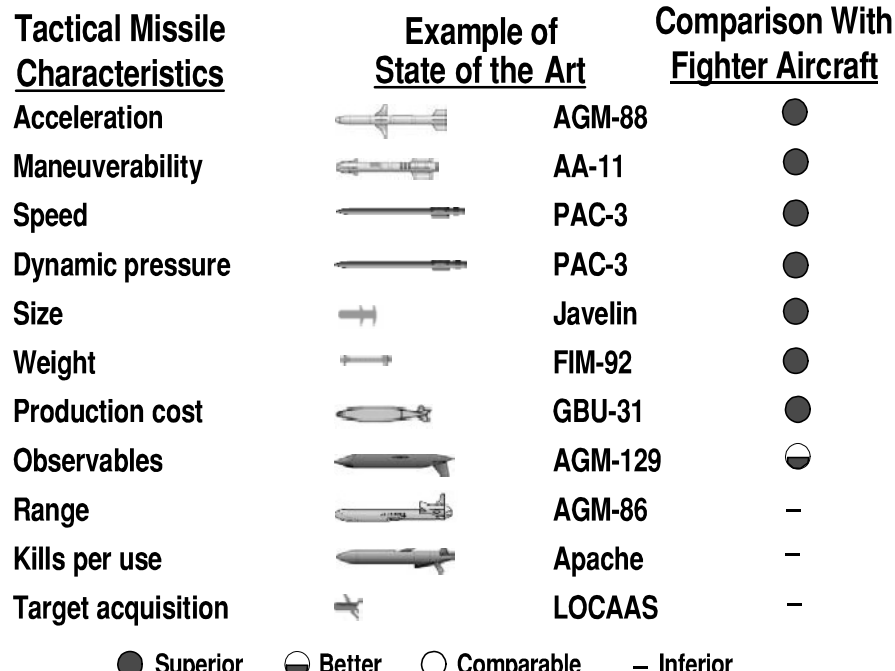


Fig. 1.2 Tactical missiles are different from fighter aircraft.

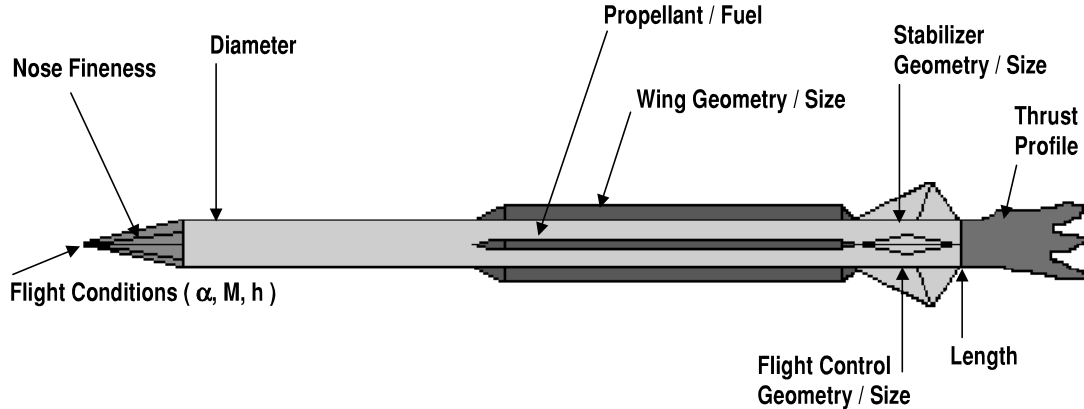


Fig. 1.3 Aerodynamic configuration sizing parameters emphasized in this text.

strike missile. It has high accuracy and is capable of dispensing submunitions, exhibiting high firepower. However, the same missiles are load-outs on combat aircraft, and so the enhancement in missiles also enhances the combat aircraft effectiveness and firepower. Finally, although smart powered submunitions such as LOCAAS have demonstrated a capability for automatic target recognition (ATR), a combat aircraft with a human pilot continues to have superior capability for target recognition, discrimination, and acquisition. Autonomous target acquisition by missiles is a relatively immature technology that will improve in the future with new technologies such as multimode and multispectral seekers.

Figure 1.3 is a summary of the aerodynamic configuration sizing parameters emphasized in this text. These are flight conditions (α , M , h), nose fineness, diameter, propellant/fuel type and weight, wing geometry/size, stabilizer geometry/size, flight control geometry/size, length, and thrust profile. Flight condition parameters that are most important in the design of tactical missiles are angle of attack α , Mach number M , and altitude h . For the aerodynamic configuration, the missile diameter and length have a first-order effect on characteristics such as missile drag, subsystem packaging available volume, launch platform integration, seeker and warhead effectiveness, and body bending. Another configuration driver is nose fineness, an important contributor to missile drag for supersonic missiles. Also, nose fineness affects seeker performance, available propellant length, and missile observables. Another example is missile propellant/fuel type and weight, which drive flight performance range and velocity. The aerodynamic configuration wing geometry and size are often set by maneuverability requirements and aerodynamic efficiency. Stabilizer geometry and size are often established by static margin requirements. In the flight control area, the geometry and size of the flight control surfaces determine the maximum achievable angle of attack and the resulting maneuverability. Finally, the thrust profile determines the missile velocity time history.

1.2 Conceptual Design Process

Figure 1.4 shows a typical missile conceptual design process. Conceptual design is an iterative process, requiring a number of design iterations to achieve a balance of emphasis from the diverse inputs and outputs. The major tasks of conceptual design are 1) mission/scenario definition; 2) weapon requirements,

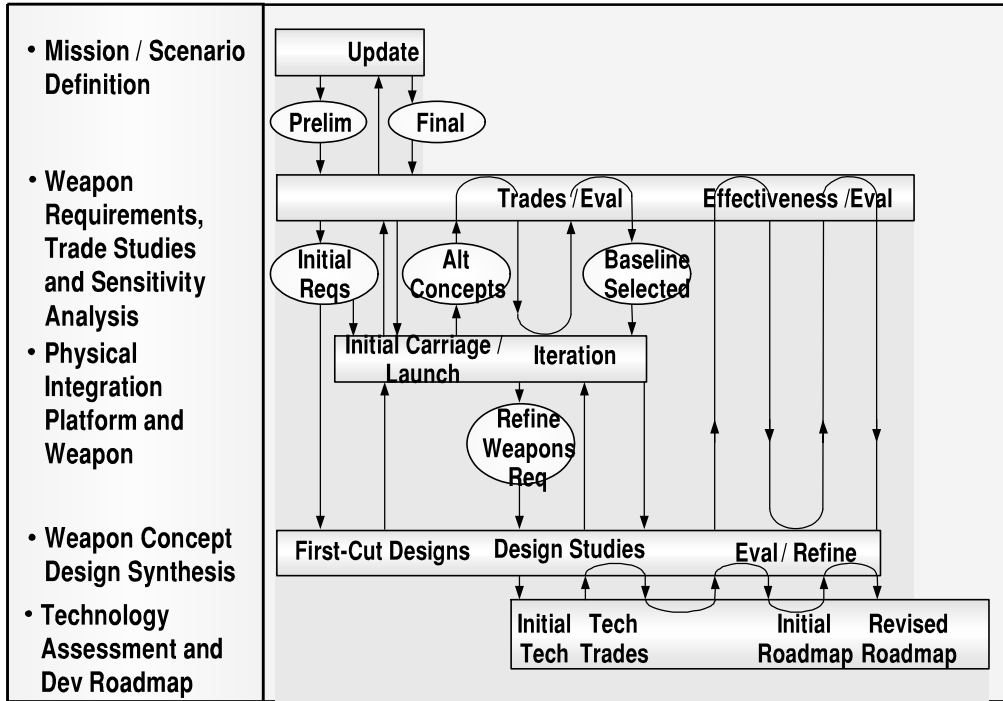


Fig. 1.4 Conceptual design process requires iteration; typical design cycle is 3–9 months.

trade studies, and sensitivity analysis; 3) physical integration of the missile with the launch platform; 4) weapon concept design synthesis; and 5) technology assessment and technology development roadmap. The initial design process begins with a general definition of the mission/scenario. Mission/scenario definition can have one or more updates during the design process. The initial input is a “requirements pull” desired capability from the military customer. It is evaluated against the “technology push” potential technology availability provided by the technical community. The weapon requirements, trade studies, and sensitivity analysis task provide the high level requirements on the missile such as range, time to target, and other measures of merit. This task is oriented toward an operations analysis of a system-of-systems, including targeting. The high level requirements are initially provided by the military customer and may be refined through computer modeling. The system-level computer models may be characterized as campaign, raid, or engagement models. In a campaign model many different types of systems are interacting over a simulated time interval from days to weeks. A raid model has multiple platforms engaging multiple targets during a single raid. An engagement model may be that of a single launch platform and missile engaging a single target or threat. The third task, physical integration of the missile with the launch platform, provides constraints such as length, span, and weight. This task is oriented towards systems integration. The fourth task, weapon concept design synthesis, is the most iterative and arguably the most creative. Characteristics such as the aerodynamic shape, propellant or fuel type and weight, flight trajectory range, time to intercept, maneuverability, seeker detection range, accuracy, lethality, and cost are evaluated; and the missile is resized and reconfigured in an iterative process. For example, the tail stabilizers and flight control surfaces may be resized for improved stability or maneuverability. Another example is adding propellant

or fuel to match the flight range requirement. As the design matures and becomes better defined through iteration, the number of alternative solutions is reduced from a broad range of possibilities to a smaller set of preferred candidates that are more reasonable and cost effective. More in-depth information is provided for the design subsystems as the design matures. Finally, a technology assessment task further defines the subsystems and selects the best technology from the candidate approaches. The technology trades lead to a set of preferred, enabling technologies. A technology roadmap documents the development plan for maturing the enabling technologies.

A typical duration for a conceptual design activity is three to nine months. The products of the missile design activity include refined mission/scenario definitions, system-of-systems definition of the missile requirements, launch platform compatibility compliance, advanced missile concepts, identification of the enabling technologies, and a technology roadmap.

Figure 1.5 shows the iterative process used for conceptual design synthesis. Based on mission requirements, an initial baseline from an existing missile with similar propulsion is established. It is used as a starting point to expedite the design convergence. Advantages of a baseline missile include the prior consideration of balanced system engineering for the subsystems and the use of an accurate benchmark based on existing test data (e.g., wind-tunnel data). Changes are made in the baseline missile aerodynamics, propulsion, weight, and flight trajectory to reflect the new requirements of the new missile concept. The new conceptual design is evaluated against its flight performance requirements (e.g., range, time to target, maneuver footprint). The aerodynamics portion of the conceptual design process is an investigation of alternatives in configuration geometry. The output of the aerodynamics calculation is then inputted to the propulsion system design to size the propulsion system. Propulsion sizing includes providing sufficient propellant or

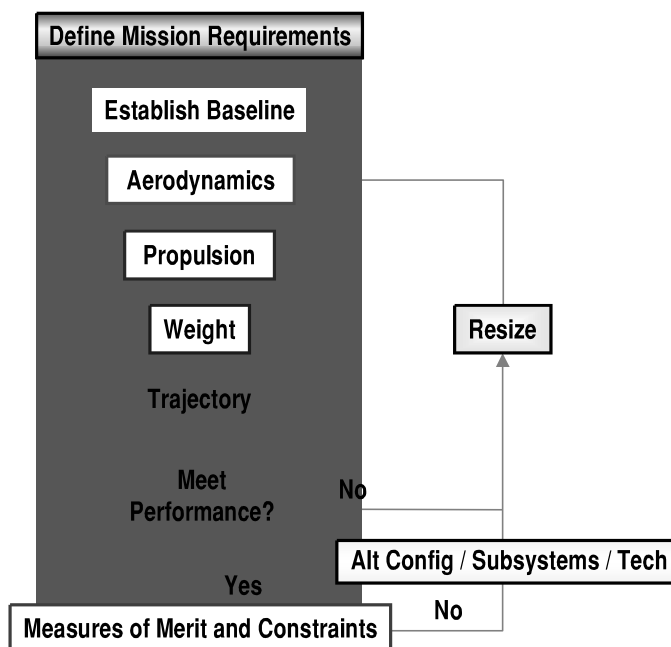


Fig. 1.5 Missile concept synthesis requires iteration.

fuel to meet the range and time-to-target requirements. The next step is to estimate the weight of the new missile with its modified aerodynamics and propulsion. Much of this activity is focused on structural design, which is sensitive to changes in flight performance. Following the weight sizing, flight trajectories are computed for the new missile. The range, terminal velocity, maneuverability, and other flight performance parameters are then compared with the mission flight performance requirements. If the missile does not meet the flight performance requirements, it is resized and reiterated. After completing a sufficient number of iterations to meet the flight performance requirements, the next step is evaluating the new missile against the other measures of merit and constraint requirements. If the missile does not meet the requirements, the design is changed (alternative configuration, subsystems, technologies) and resized for the next iteration and evaluation.

A synthesized missile will differ from the starting point baseline in several respects. For example, the wing area may have been resized to meet the maneuverability requirement. The tail area may have been resized to meet static margin and maximum trim angle-of-attack requirements. The rocket motor or the ramjet engine may have been modified to improve its efficiency at the selected design altitude or Mach number. Additionally, the length of the propulsion system may have been changed to accommodate additional propellant/fuel necessary to satisfy flight range requirements. The design changes are reflected in revisions to the mass properties, configuration geometry, thrust profile, and flight trajectory for the missile. Typically, three to six design iterations are required before a synthesized missile converges to meet the flight performance requirements.

1.3 Examples of State-of-the-Art Missiles

Shown in Figs. 1.6 and 1.7 are examples of state-of-the-art missiles for the mission areas of air to air, air to surface, surface to surface, and surface to air (see Missile.index online at <http://www.index.ne.jp/missile-e/>).

◆ Air to air		Example SOTA	← 10 feet →
• Short-range ATA. AA-11.	Maneuverability		
• Medium-range ATA. AIM-120.	Performance / weight		
• Long-range ATA. AIM-54.	Range		
◆ Air to surface			
• Short-range ATS. AGM-65.	Accuracy		
• Antiradar ATS. AGM-88.	Speed		
• Medium-range ATS. Apache.	Modularity		
• Antitank ATS. AGM-114.	Versatility		
• Long-range ATS. AGM-86.	Range		

Fig. 1.6 Examples of air-launched missile missions/types (used with permission of Missile Index, 1997, online at <http://www.index.ne.jp/missile-e/>).

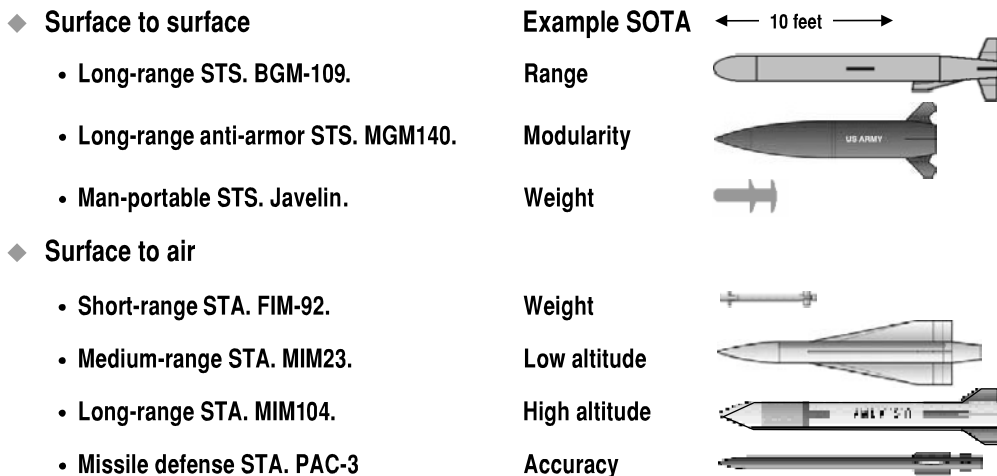


Fig. 1.7 Examples of surface-launched missile missions/types (used with permission of Missile Index, 1997, online at <http://www.index.ne.jp/missile-e/>).

Three examples are shown in the top of Fig. 1.6 of the state-of-the-art drivers of air-to-air missiles. The selected drivers are air-to-air maneuverability, performance with light weight, and range. The examples are a short-range air-to-air missile represented by the highly maneuverable AA-11 Archer, a medium-range air-to-air missile represented by the high-performance/lightweight AIM-120 AMRAAM, and a long-range air-to-air missile represented by the AIM-54 Phoenix.

Five examples are shown in the bottom of Fig. 1.6 of the state-of-the-art drivers of air-to-surface missile types. The selected drivers are air-to-surface accuracy, speed, modularity, versatility, and range. The example missiles are the short-range precision strike AGM-65 Maverick, the antiradar defense suppression high-speed AGM-88 HARM, the medium-range precision strike modular Apache, the antitank versatile AGM-114 Hellfire, and the long-range precision strike AGM-86 cruise missile.

Examples are shown in the top of Fig. 1.7 of tactical surface-to-surface missiles that illustrate the state-of-the-art drivers. The selected drivers are surface-to-surface range, modularity, and light weight. The example missiles are the long-range BGM-109 Tomahawk, the long-range modular anti-armor MGM 140 ATACMS, and the man-portable Javelin antitank missile.

Surface-to-air missile state-of-the art drivers are shown in the bottom of Fig. 1.7. The selected drivers are surface-to-air weight, altitude, and accuracy. The missiles shown are the short-range lightweight FIM-92 Stinger, medium-range low-altitude MIM23 Hawk, long-range high-altitude MIM104 PAC-2 Patriot, and the medium-range missile defense PAC-3 hit-to-kill missile.

1.4 Aerodynamic Configuration Sizing Parameters

Aerodynamic configuration sizing parameters have an impact on missile requirements. Figure 1.8 is an assessment of the relative impact of aerodynamic configuration sizing parameters on flight performance measures of merit (e.g., weight, range, maneuver footprint, and time to target). Also shown is the impact of aerodynamic configuration sizing parameters on other measures of merit

Aero Configuration Sizing Parameter	Impact on Weapon Requirement									
	Aero Measures of Merit			Other Measures of Merit					Constraint	
	Weight	Range / Maneuver	Time to Target	Robustness	Lethality	Miss Distance	Observables	Survivability	Cost	Launch Platform
Nose Fineness	●	●	●	○	●	●	●	●	●	○
Diameter	●	●	●	○	●	●	○	○	●	●
Length	●	●	●	●	●	●	○	○	●	●
Wing Geometry / Size	●	●	●	●	●	●	●	●	●	●
Stabilizer Geometry / Size	●	●	●	○	○	●	●	●	●	●
Flight Control Geometry / Size	●	●	●	○	○	●	●	●	●	●
Propellant / Fuel	●	●	●	○	●	●	●	●	●	●
Thrust Profile	●	●	●	●	●	●	●	●	●	-
Flight Conditions (α, M, h)	●	●	●	●	●	●	●	●	●	○

● Very Strong ○ Strong ○ Moderate — Relatively Low

Fig. 1.8 Aerodynamic configuration sizing has high impact on mission requirements.

(e.g., robustness, lethality, miss distance, observables, survivability, and cost), as well as their impact on constraints (e.g., launch platform integration weight, length, and span constraints).

The aerodynamic configuration sizing parameters that are addressed in this text are listed on the left side of the figure. These are nose fineness, diameter, length, wing geometry/size, stabilizer geometry/size, flight control geometry/size, propellant/fuel, thrust profile, and flight conditions (angle of attack, Mach number, altitude). Note from the figure that the aforementioned parameters have very strong impact on missile requirements in the areas of weight, range, and maneuverability. The aerodynamic configuration sizing parameters also have a strong impact in the areas of lethality, miss distance, and cost.

1.5 Example of Alternatives in Establishing Mission Requirements

Figure 1.9 is an example of alternative approaches that should be considered in establishing mission requirements. It illustrates an assessment of alternative approaches for precision strike. The assessment includes the approaches that are used today by current systems, as well as a projection of capabilities that may be used in the future for new missile systems. Three measures of merit are assumed in comparing future precision strike missiles with the current systems. These are cost per shot, number of launch platforms required, and the effectiveness against time-critical targets. For the current systems, two approaches are used: 1) penetrating aircraft with relatively short-range subsonic precision guided munitions or missiles and 2) standoff platforms (ships, submarines, or aircraft) using subsonic cruise missiles. The penetrating aircraft systems include the F-117 with subsonic precision guided munitions such as JDAM. As shown, penetrating aircraft/subsonic precision guided munitions have an advantage of low cost per shot, about \$20,000. However, the experience in Desert Storm showed that

Alternatives for Precision Strike	Cost per Shot	Number of Launch Platforms Required	TCT Effectiveness
Future Systems			
◆ Standoff platforms / hypersonic missiles	○	●	●
◆ Overhead loitering UCAVs / hypersonic missiles	●	●	●
◆ Overhead loitering UCAVs / lightweight PGMs	●	○	●
Current Systems			
◆ Penetrating aircraft / subsonic PGMs	●	—	—
◆ Standoff platforms / subsonic missiles	○	●	—
Note: ● Superior ○ Good ○ Average — Poor			

Fig. 1.9 Example of assessment of alternatives to establish mission requirements.

subsonic penetrating aircraft do not have the capability to counter time-critical targets (TCTs) such as theater ballistic missiles (TBMs). Another current approach using standoff platforms such as ships, submarines, and large aircraft outside the threat borders requires fewer launch platforms, resulting in lower logistics costs. However, standoff platforms with subsonic cruise missiles (e.g., Tomahawk, CALCM) are also ineffective against time-critical targets such as theater ballistic missiles.

Also shown in the figure are future missile system alternatives for precision strike. Technology development work is under way in all three of the areas; the best approach has yet to be demonstrated. One approach is based on a standoff platform, with an aircraft, ship, or submarine standing off outside the threat country border. Hypersonic long-range precision strike missiles would provide broad coverage, holding a large portion of the threat country at risk. This approach is attractive because of the small number of launch platforms required and the effectiveness against time-critical targets. Based on current technology programs such as the Affordable Rapid Response Missile Demonstrator (ARRMD) Program, the cost of future hypersonic missiles is projected to be comparable to that of current cruise missiles.

Another alternative approach is to use overhead loitering unmanned combat air vehicles (UCAVs) with hypersonic missiles. The number of UCAVs required is dependent upon the speed and range of their onboard missiles and the loiter altitude. A high loiter altitude tends to reduce the available payload weight/firepower. This approach would probably provide the fastest response time against time-critical targets because of the shorter required flight range of the missile.

A third approach is overhead loitering UCAVs with advanced lightweight precision guided munitions. Again, a design consideration is the loiter altitude required for survivability vs the weapon payload. This approach would have the lowest cost per shot but would also require a larger number of UCAVs.

An enabling synergistic capability for precision strike is the application of near-real-time, accurate targeting from either overhead tactical satellite or overhead

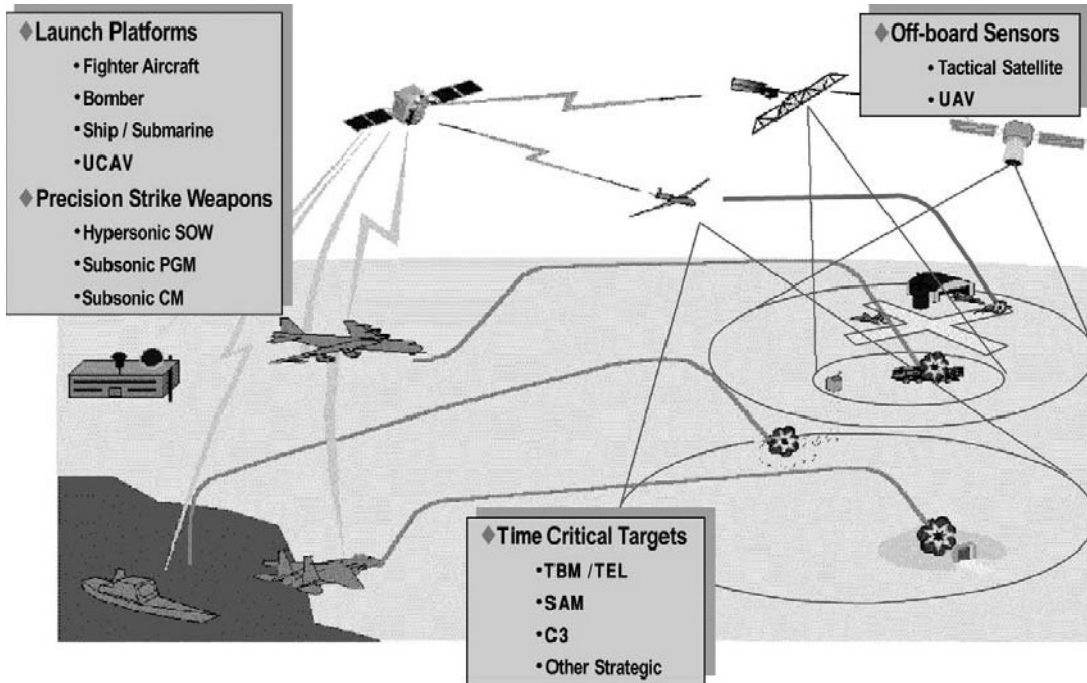


Fig. 1.10 Future C4ISR tactical satellites and UAVs will have high impact on mission requirements.

unmanned air vehicle (UAV) sensors. It is projected that an advanced command, control, communication, computers, intelligence, surveillance, reconnaissance (C4ISR) network will be available around the year 2010 to support near-real-time and high accuracy targeting of time-critical targets. The C4ISR network could be used by all types of launch platforms (e.g., fighter aircraft, bombers, helicopters, UCAVs, ships, submarines, and ground vehicles). Illustrated in Fig. 1.10 are examples of a ground station, overhead satellite sensors and satellite relays, and the overhead UAV sensor platform elements of the assumed C4ISR architecture. The assumed C4ISR of the year 2010 is projected to have a capability for a target location error (TLE) of less than 1 m (1σ) and sensor-to-shooter connectivity time of less than 2 min (1σ). A data link from the launch platform to the missile will allow in-flight target updates and battle damage indication/battle damage assessment (BDI/BDA). An enabling technology for a lightweight/low-volume missile data link is phased array antenna. A phased array antenna can be conformally mounted on the missile airframe.

Figure 1.11 is an illustration of system-of-systems analysis. The example is a system analysis to develop mission requirements for precision strike around the year 2010. A comparison is made of a subsonic cruise missile vs a hypersonic missile. In the initial activity, requirements are defined for the targeting time of the two missiles. In the example both missiles rely on receiving the target location in near real time, with a fast response time for launch. The second activity (shown in the lower left section of the figure) develops a solution matrix of time to target vs average speed and range. Shown in the figure are three assumptions of the flight range. Based on the knee of the curve, an average speed is selected and a third activity is initiated, involving tradeoffs of flight attitude vs the level of reduced observables required for survivability. In the fourth activity (lower right section of the figure)

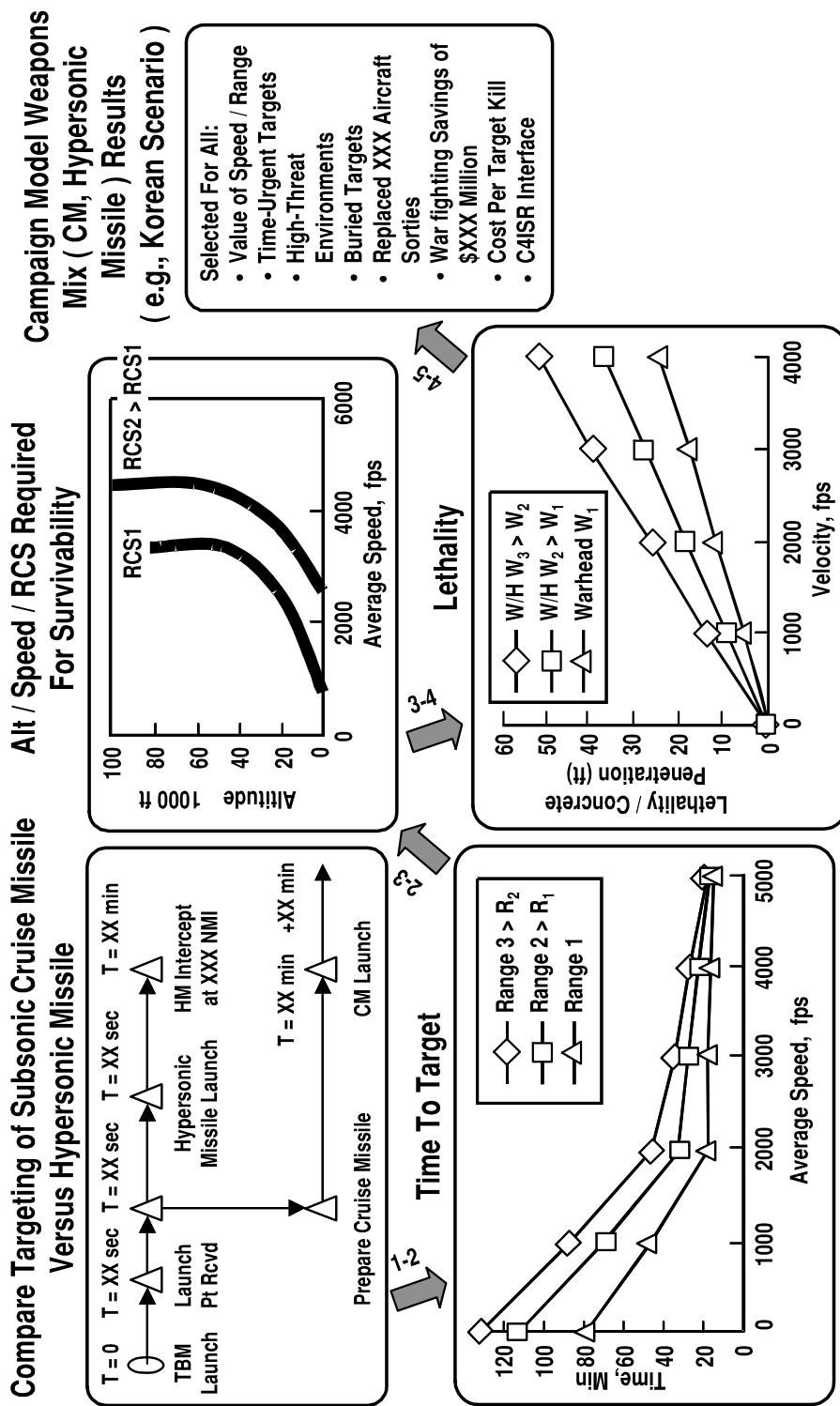


Fig. 1.11 Example of system-of-systems analysis to develop mission requirements.

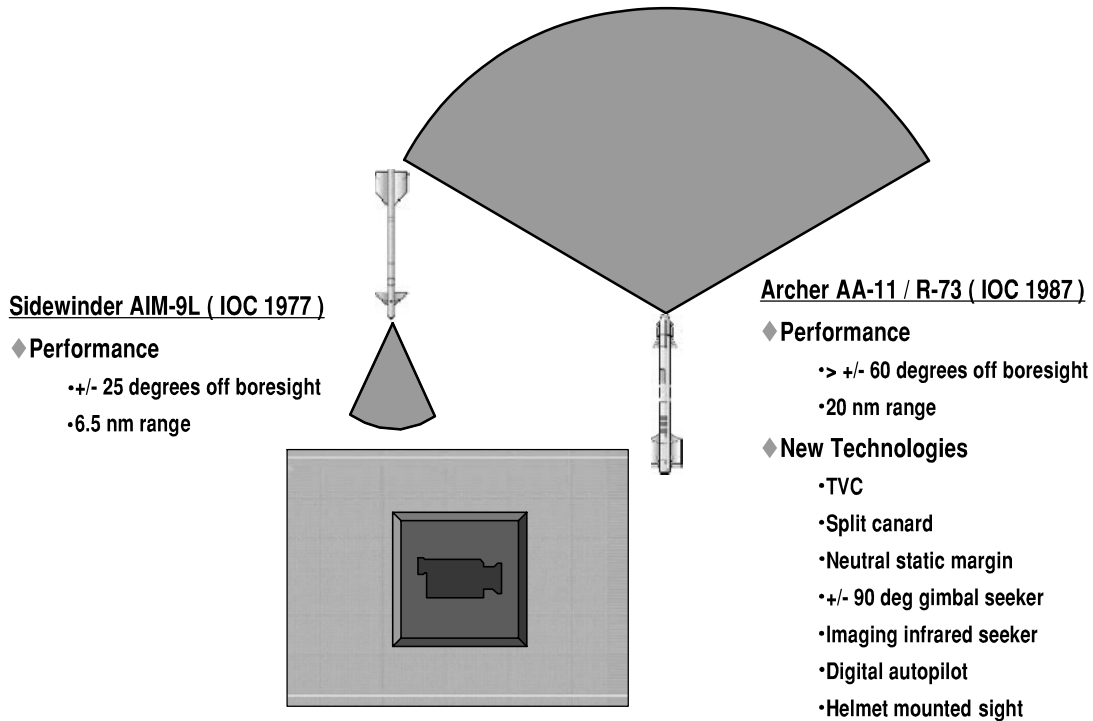


Fig. 1.12 Example of evolution of short-range air-to-air missile range and off-boresight requirements.

a tradeoff is made of the missile impact velocity required for penetration of a buried target as a function of warhead weight. Finally, a system-of-systems analysis campaign modeling activity is initiated (upper right section of the figure) to derive the weapon system-of-system requirements such as the best mix of cruise missiles and hypersonic missiles for a representative scenario. Measures of merit include the value of speed and range, capability against time-urgent targets, survivability in a high-threat environment, effectiveness against buried targets, replacement for aircraft sorties, war fighting savings, cost per target kill, and the requirements for the C4ISR interface.

Figure 1.12 is another illustration of the impact of mission requirements on missile design. It shows the impact of mission requirements for short-range air-to-air missiles. A comparison is made of the older technology AIM-9L Sidewinder with the newer technology, highly maneuverable Archer AA-11/R-73 missile.

Shown on the left side of the figure are the flight range and off-boresight capability of the AIM-9L Sidewinder. The initial operational capability (IOC) for AIM-9L was the year 1977. The performance of the AIM-9L is $+/- 25$ deg off boresight and approximately 6.5 n miles range. Contrasting with AIM-9L is a more recent missile, the Archer AA-11/R-73. The Archer is described in the right section of the figure. The Archer has a more recent IOC, 1987. Its performance is $+/- 60$ deg off boresight and 20 miles range. New technologies developed for the Archer missile include thrust vector control, split canard, neutral static margin, $+/- 90$ deg gimbaled seeker, imaging infrared seeker, digital autopilot, and integration with a helmet mounted sight. These provide higher maneuverability and longer range.

Also shown at the bottom of the figure is a video comparing the flight performance of the Sidewinder vs the Archer and an example of the large off-boresight

conditions and pilot activities that are required for short-range air-to-air combat. The Archer can be launched at a much larger off boresight than Sidewinder, allowing an earlier launch of an Archer in a short-range air-to-air engagement. Because Archer has a superior short-range air-to-air capability, an older, relatively low maneuverability aircraft that uses the highly maneuverable Archer missile may be able to defeat a more modern, highly maneuverable aircraft that uses an older, lower technology missile.

1.6 Baseline Missile

Mission concept synthesis is an iterative process that requires evaluation of alternative configurations, alternative subsystems, alternative technologies, and resizing the missile. As shown in Fig. 1.13, following the definition of mission requirements, a baseline missile is selected. For the purpose of this text, two alternative baselines are available for conceptual design, a rocket-powered medium-range missile based on the AIM-7 Sparrow and a ramjet-powered long-range missile based on the Advanced Strategic Air Launched Missile (ASALM). Detailed information on the baseline missiles is provided in Chapter 7.

Using a baseline missile to initiate the design process has benefits that include a faster design process and a more accurate design. Because a baseline missile is a real missile that is anchored with test data, it allows simple conceptual design methods to be used with reasonable accuracy. The existing documentation and the configuration control of a baseline missile provide traceability between cause and effect as the conceptual design process is conducted. System engineering has already been applied to the baseline missile, providing a benchmark for balanced subsystems. The startup time for conceptual design is greatly reduced by using a baseline—the default values for the conceptual design missile are the baseline

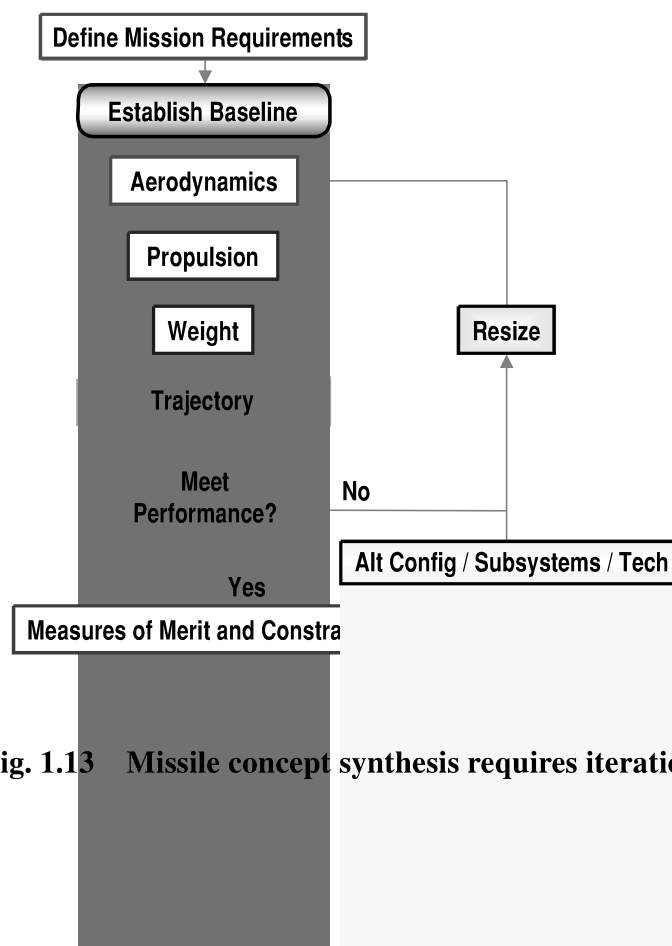


Fig. 1.13 Missile concept synthesis requires iteration.

missile. It is noted that no one baseline can cover all the range of possible solutions. Typically the propulsion system of the new conceptual missile should be the same type as that of the baseline missile. The baseline missile characteristics can be extrapolated about $+/-50\%$ with reasonable accuracy.

Note that, when using a baseline missile, it is important not to get locked in by the baseline but to be creative in exploring design alternatives. Also, because the baseline is based on an existing missile, whereas the conceptual design usually involves a missile projected for the future, the state of the art must often be projected into the future, particularly for the electronic and sensor subsystems.

Shown in Fig. 1.14 is an example of the baseline missile data that is used in conceptual design sizing. The example is based on the chin inlet, integral rocket ramjet baseline described in Chapter 7. In the upper left of the figure is an illustration of a configuration drawing of the baseline missile. The configuration drawing is a dimensioned layout with an inboard profile showing the major subsystems (guidance, warhead, fuel, booster/engine, and flight control surfaces). In the upper center of the figure are examples of tables for a missile weight statement and geometry data. Missile weight and center-of-gravity location are provided for launch, booster burnout, and engine burnout flight conditions. Weight and geometry data are also provided for the major subsystems. The upper right corner of the figure is an illustration of a description of the ramjet internal flowpath geometry. The internal flowpath geometry data include the inlet design capture area and the internal areas of the inlet throat, diffuser exit, flame holder plane, combustor exit, nozzle throat, and nozzle exit. Examples of aerodynamic data plots are illustrated in the left center section of the figure. The aerodynamic data of the ramjet baseline cover angles of attack up to 16 deg and Mach numbers up to 4.0. Aerodynamic coefficients and derivatives include zero-lift drag coefficient C_{D_0} , normal force coefficient C_N , pitching moment coefficient C_m , pitching moment control effectiveness derivative C_{m_δ} , and normal force control effectiveness derivative C_{N_δ} . Examples of ramjet propulsion thrust T and the ramjet specific impulse I_{SP} are shown in the center of the figure. Thrust of the ramjet baseline is a function of Mach number, altitude, and fuel-to-air ratio. Specific impulse of the ramjet baseline is a function of Mach number. Rocket booster propulsion thrust, boost range, and burnout Mach number are illustrated in the right center of the figure as a function of launch Mach number and altitude. The left bottom section of the figure shows the maximum flight range of the ramjet baseline. Maximum flight range is a function of the launch Mach number, launch altitude, cruise Mach number, and the cruise altitude. Finally, the right bottom section of the figure is an example of the sensitivity of design parameters on maximum flight range. Sensitivity parameters include inert weight, fuel weight, zero-lift drag coefficient, lift-curve-slope derivative C_{L_α} , ramjet thrust, and ramjet specific impulse. The sensitivity study in the example was conducted for cruise flight conditions ranging from Mach 2.4, sea level, to Mach 3.0, 60,000 ft in altitude.

Shown in Fig. 1.15 is the process of using baseline missile data to provide enhanced accuracy to prediction methods. The predicted values of the design parameters from the conceptual design prediction methods are corrected by the baseline missile data. First, an uncorrected prediction is made of the conceptual design parameter $P_{CD,U}$. Second, a prediction is made of the baseline missile parameter $P_{B,U}$. The correction in the prediction for the baseline missile $P_{B,C}/P_{B,U}$

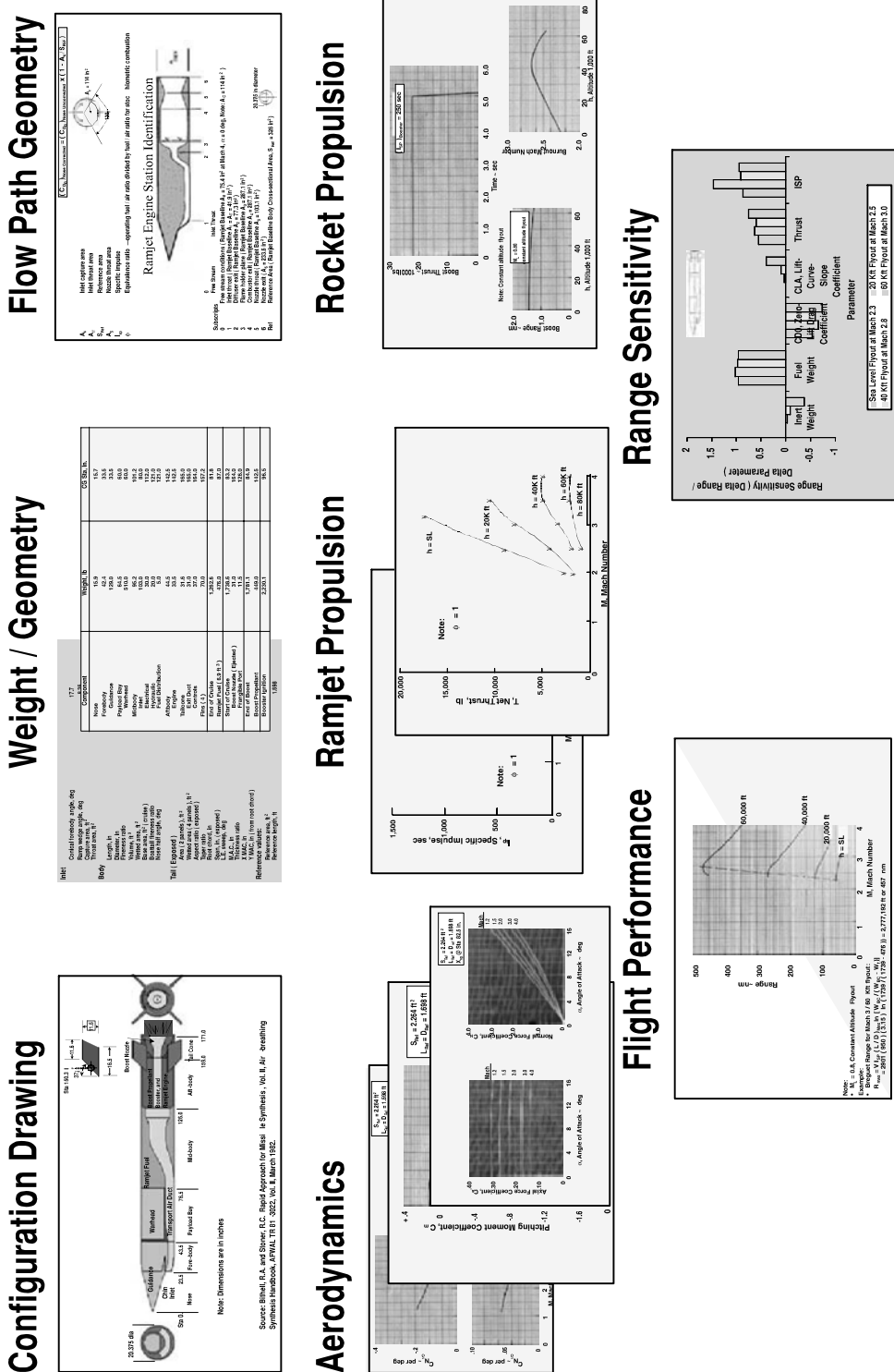


Fig. 1.14 Example of missile baseline data.

$$P_{CD,C} = (P_{B,C} / P_{B,U}) P_{CD,U}$$

- ◆ $P_{CD,C}$ Parameter of conceptual design, corrected
- ◆ $P_{B,C}$ Parameter of baseline, corrected (actual data)
- ◆ $P_{B,U}$ Parameter of baseline, uncorrected (computed)
- ◆ $P_{CD,U}$ Parameter of conceptual design, uncorrected (computed)
- ◆ Example

- Ramjet Baseline with RJ-5 fuel (heating value = 11,300,000 ft-lbf / lbm)
- Advanced Concept with slurry fuel (40% JP-10 / 60% boron carbide = 18,500,000 ft-lbf / lbm)
- Flight conditions: Mach 3.5 cruise, 60K ft altitude, combustion temperature 4,000 Rankine
- Calculate specific impulse (I_{SP})_{CD,C} for conceptual design, based on corrected baseline data
- (I_{SP})_{B,C} = 1,120 sec
- (I_{SP})_{B,U} = 1,209 sec
- (I_{SP})_{CD,U} = 1,979 sec
- (I_{SP})_{CD,C} = [$(I_{SP})_{B,C} / (I_{SP})_{B,U}$] (I_{SP})_{CD,U}
= [(1120) / (1209)] (1979) = (0.93) (1979) = 1,830 sec



Fig. 1.15 Baseline design data allow the correction of computed parameters in conceptual design.

provides a correction to the prediction method. Finally, the corrected conceptual design parameter $P_{CD,C}$ is computed by $P_{CD,C} = (P_{B,C}/P_{B,U}) P_{CD,U}$.

In the example the ramjet baseline fuel is RJ-5, with a heating value of 11,300,000 ft · lb force per lbm (14,525 per lbm). The assumed fuel of the conceptual design missile is a high-density slurry fuel consisting of 40% JP-10 and 60% boron carbide. It has a higher heating value of 18,500,000 ft · lb force per lbm. The assumed cruise condition of this example is Mach 3.5, 60,000 ft in altitude. The ramjet combustion temperature is assumed to be 4000°R. Finally, the uncorrected specific impulse predicted for the high-density fuel [$(I_{SP})_{CD,U} = 1979$ s] is corrected by the ratio of the actual specific impulse of the baseline [$(I_{SP})_{B,C} = 1120$ s] to the predicted specific impulse of the baseline [$(I_{SP})_{B,U} = 1209$ s], giving a corrected specific impulse for the high-density fuel of $(I_{SP})_{CD,C} = 1830$ s.

1.7 Summary

This chapter provided an overview of the missile design process. Also included were examples of tactical missile characteristics. A comparison was made of tactical missile capabilities with those of combat aircraft. In many cases tactical missiles drive the state of the art more than combat aircraft. The aerodynamic configuration sizing parameters of tactical missiles were identified. It was shown that the aerodynamic configuration sizing parameters have a strong impact on the missile system measures of merit and constraints. The chapter also gave examples of the process and considerations for establishing mission requirements. Included was an example of an analysis of a mix of hypersonic strike missiles with subsonic cruise missiles. Another example was a comparison of the short-range air-to-air capability of a relatively new highly maneuverable missile with the lesser capability of a relatively old less maneuverable missile. Finally, Chapter 1 presented a process for correcting design predictions using baseline missile data. The following chapters of this text will address the specific methods and technologies for tactical missile design.

2

Aerodynamic Considerations in Tactical Missile Design

This chapter addresses aerodynamic considerations for tactical missile design. The conceptual design methods, design tradeoffs, design criteria, and technologies emphasize low aspect ratio wing and wingless configurations. Consideration is given to missile diameter tradeoffs; nose fineness tradeoffs; boattail considerations; lifting body vs axisymmetric body; calculation of body and surfaces normal force, lift-to-drag ratio, zero-lift drag coefficient, and center-of-pressure location; wings vs no wings; surface planform geometry alternatives; flight control alternatives; maneuver alternatives; roll orientation; static stability; tail area sizing; stability and control conceptual design criteria; and body buildup aerodynamics.

As shown in the Fig. 2.1, aerodynamic configuration synthesis follows the initial activities of defining mission requirements and establishing a baseline missile. Aerodynamic configuration synthesis requires consideration of alternative configurations, aerodynamic technology, and the process for resizing the missile. The output of aerodynamic configuration synthesis includes the missile diameter, length, nose geometry, wing size and geometry, stabilizer and control surfaces size and geometry, and the aerodynamic coefficients and derivatives. The output of the aerodynamic configuration synthesis is an input to the propulsion system design.

2.1 Missile Diameter Tradeoff

Missile diameter tradeoff has drivers toward a small diameter as well as drivers toward a large diameter. These must be harmonized. The drivers toward a small diameter missile include lower drag and smaller lateral dimensions for improved launch platform compatibility. However, these must be harmonized with the other drivers toward a large diameter missile. These include 1) increased range, higher resolution, better tracking, and lower noise for the seeker, 2) increased warhead effectiveness due to higher fragment velocity and higher blast overpressure for a blast fragmentation warhead or a longer and faster jet for a shaped charge warhead, 3) increased body bending frequency, which improves the flight control characteristics, 4) improved subsystem packaging for diameter limited subsystems, and 5) shorter length for launch platform compatibility.

The typical range in missile body fineness ratio (length-to-diameter ratio) is from 5 to about 25. An example of a low fineness missile is the Javelin man-portable anti-armor missile, which has an l/d equal to 8.5. An example of a high fineness missile is the AIM-120 AMRAAM air-to-air missile, with l/d equal to 20.5.

Drag is a major design parameter in satisfying the flight range requirement of tactical missiles, especially supersonic missiles. It is a function of drag coefficient, dynamic pressure, and reference area, given by the equation $D = C_D q S_{Ref}$. For a missile configuration, the reference area is the body cross-sectional area.

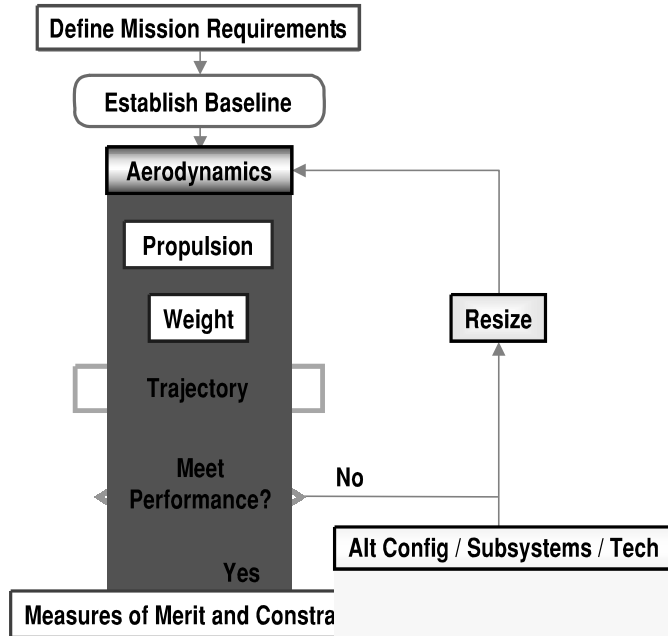


Fig. 2.1 Missile concept synthesis requires iteration.

Substituting missile diameter gives $D = C_D q (\pi/4) d^2 = 0.785 C_D q d^2$. Shown in Fig. 2.2 is D/C_D as a function of diameter and dynamic pressure for a typical range in the values of the parameters for tactical missiles.

As an example of missile drag, consider the rocket baseline missile. The rocket baseline missile has a reference area of 0.349 ft^2 and a reference length (diameter) of 8 in. At a typical flight condition of Mach 2 and flight altitude of 20,000 ft, the dynamic pressure $q = 2725 \text{ psf}$. Also, at Mach 2, the rocket baseline

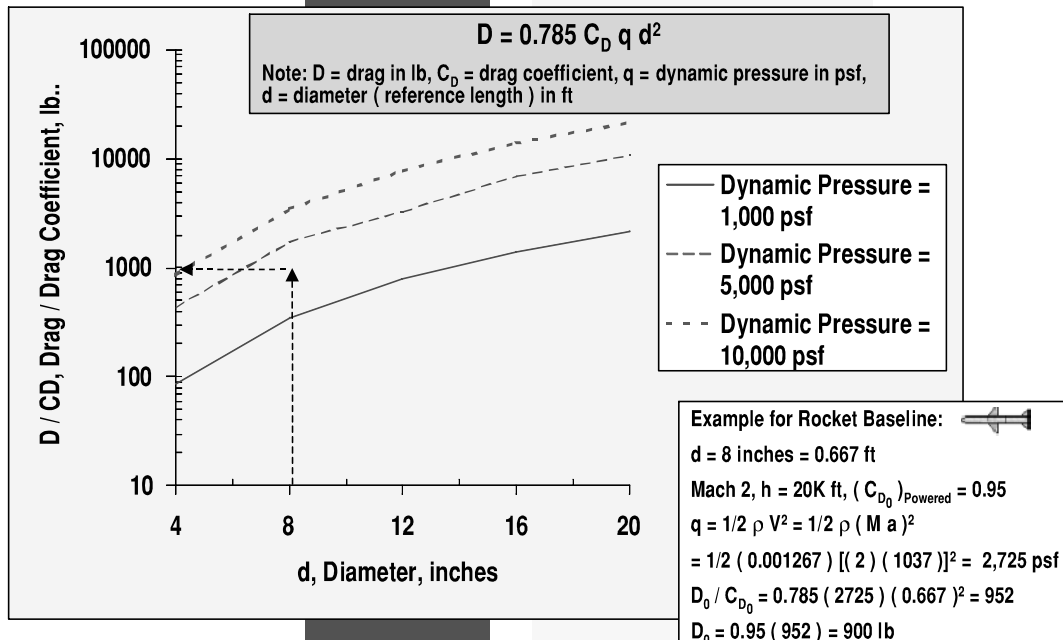


Fig. 2.2 Small diameter missiles have low drag.

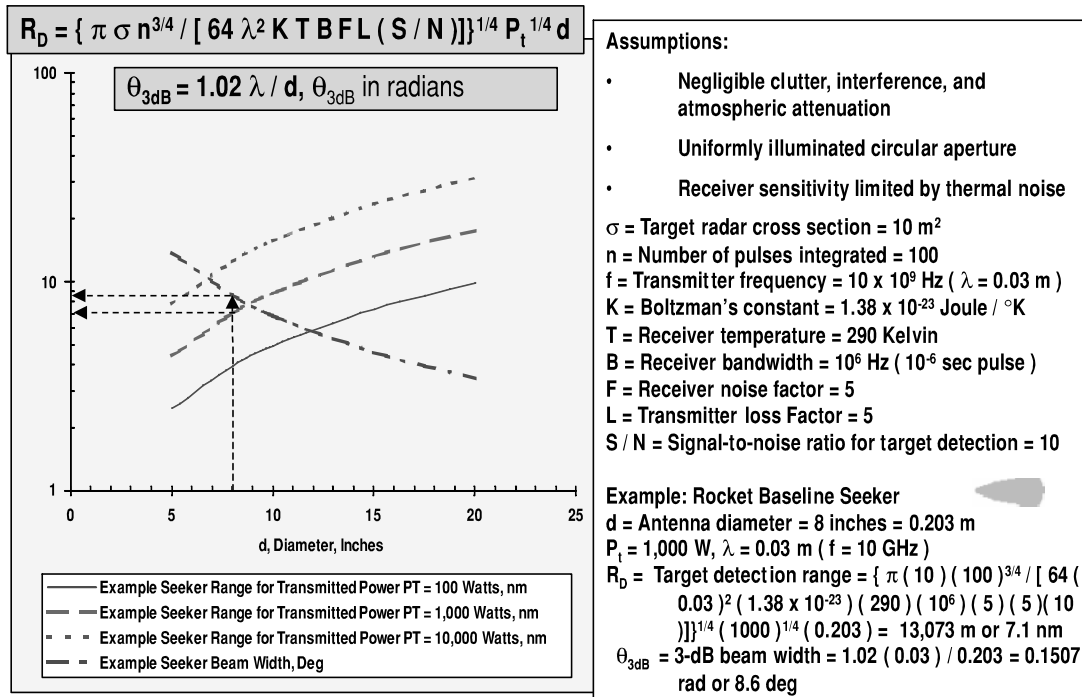


Fig. 2.3 Large diameter seeker provides longer detection range and higher resolution.

zero-lift drag coefficient for power-on flight $C_{D_0} = 0.95$. Substituting into the drag equation, the zero-lift powered flight drag of the rocket 8-in.-diam baseline is $D_0 = 900 \text{ lb}$. A missile with configuration geometry similar to the rocket baseline, but with one-half the diameter (4 in.) would have one-fourth the drag (225 lb). A similar configuration with twice the diameter (16 in.) would have four times the drag (3600 lb).

Figure 2.3 shows the benefit of a large diameter in enhancing seeker detection range and resolution. It is based on the two-way radar range equation, given by

$$R_D = \{ \pi \sigma n^{3/4} [64 \lambda^2 k T B F L (S/N)] \}^{1/4} P_T^{1/4} d$$

Assumptions are a uniformly illuminated circular aperture, negligible clutter, negligible interference, negligible atmospheric attenuation, and thermal noise-limited receiver sensitivity. The receiver threshold sensitivity P_r (in Watts) is given by the equation $P_r = k T B F$. Assumptions are a nominal receiver temperature $T = 290 \text{ K}$, bandwidth $B = 10^6 \text{ Hz}$ (pulse width of about 10^{-6} s), and noise factor $F = 5$. Boltzman's constant is the term $k = 1.38 \times 10^{-23} \text{ J/K}$. Substituting,

$$P_r = 1.38 \times 10^{-23} (290) (10^6) (5) = 2.0 \times 10^{-14} \text{ W}$$

Other assumptions for the example plotted in the figure are a target radar cross section $\sigma = 10 \text{ m}^2$, number of pulses integrated $n = 100$, transmitter frequency $f = 10 \text{ GHz}$, transmitter loss factor $L = 5$, and target detection signal-to-noise ratio $S/N = 10$. The assumed value of $S/N = 10$ provides a false alarm of about 1% for a probability of detection of 90%. It is noted that for a typical transmitter duty cycle of 20% and a loss factor of 5, the average output power is about 20% of the peak power and the input power is comparable to the peak power. The maximum

allowable transmitted power by the seeker is limited by the transmitter technology, power available from the battery, and the maximum allowable temperature due to heating.

As an example, the rocket baseline missile has an antenna diameter of about $d = 8$ in. and a transmitted power $P_T = 1000$ W. Detection range is computed to be $R_D = 13,073$ m or 7.1 n miles. Beam width is given by the equation $-3\text{dB} = 1.02/d$. The 3-dB beam width for a frequency of 10 GHZ and a diameter of 8 in. is $-3\text{dB} = 0.151$ rad or 8.6 deg.

A larger diameter or higher frequency provides longer range, more precise tracking, and finer resolution. For example, an increase of 100% in diameter (to 16 in.) provides an increase in the seeker range of 100% (to 14.1 n miles) and a decrease in the seeker beam width of 50% (to 4.3 deg). Also, a longer pulse width would provide longer detection range, with disadvantages of degraded range measurement accuracy, higher false alarm rate, and potentially receiving overlapping pulses. Pulse modulation (e.g., chirp) can be used to avoid range ambiguity for a long-duration pulse. Pulse compression is another approach to improve range. Processing provides the equivalence of an increase in the pulse width. Pulse compression has advantages of not degrading the range measurement accuracy, pulse nonambiguity, and false alarm rate.

Figure 2.4 illustrates that high fineness missiles may be limited by aeroelasticity problems from the body bending frequency. Shown is the nondimensional first mode body bending frequency as a function of body fineness ratio. The equation is $\omega_{BB} = 18.75 \{ Et / [W(l/d)] \}^{1/2}$. The equation is derived from Ref. 1. The assumptions are a thin wall cylinder structure with no stiffening from surfaces or bulkheads. Note that the body bending frequency is highest for a missile that has low fineness ratio, light weight, high modulus of elasticity, and high airframe skin thickness.

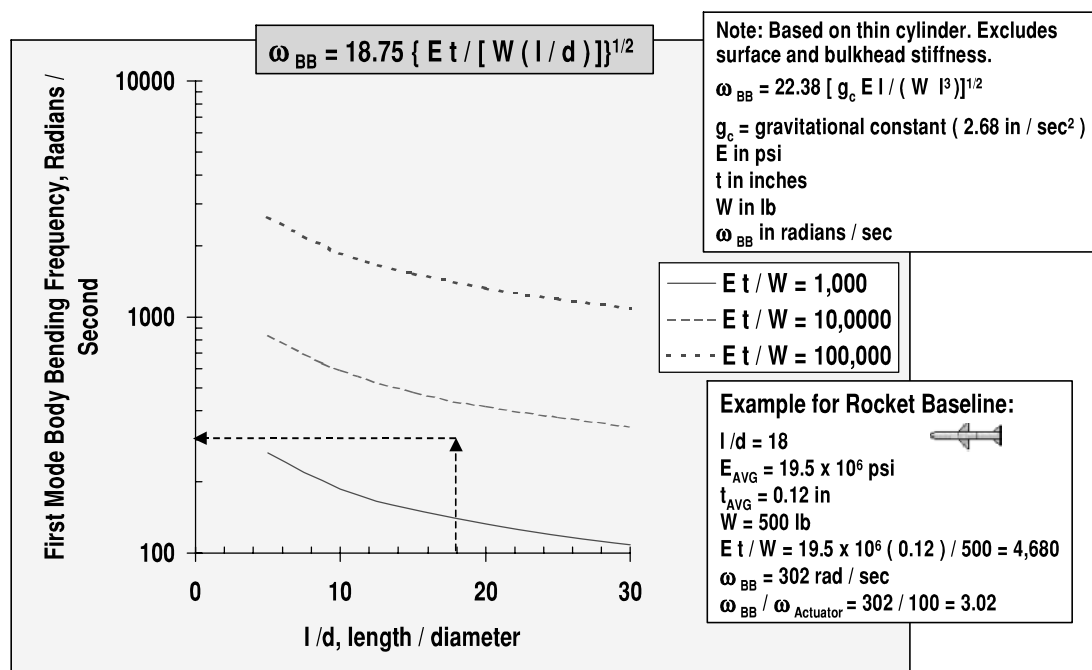


Fig. 2.4 Maximum fineness ratio may be limited through the impact of body bending modes on the flight control system (from Ref. 1).

An example is given for the rocket baseline missile. The contribution due to the wing is neglected. The rocket missile body is a combination of the pyroceram dome, aluminum airframe structure (including the aft body structure that shrouds the rocket nozzle), and the steel motor case. The modulus of elasticity of the steel motor case is 29.5×10^6 psi, the thickness of the case is 0.074 in., and the length of the case is 59.4 in. The modulus of elasticity of the aluminum body structure is 10.5×10^6 psi, thickness is 0.16 in., and the total length is 65.3 in. The contribution due to the radome is neglected for this conceptual analysis due to the relatively short length and the geometric stiffness of the tangent ogive radome. Using a weighted average based on length, the average modulus of elasticity is $E_{AVG} = 19.5 \times 10^6$ psi and the average thickness $t_{AVG} = 0.12$ in. The rocket baseline missile launch weight is 500 lb, and the fineness ratio is 18. Substituting into the equation, the first mode body bending frequency is computed to be 302 rad/s or 48 Hz. As a rule of thumb, the first mode body bending frequency should be at least twice the actuator bandwidth of the flight control system. For the rocket baseline missile, the actuator frequency is 100 rad/s, providing a design margin in body bending frequency for the fineness ratio $l/d = 18$.

2.2 Nose Fineness Tradeoff

As shown in Fig. 2.5, nose fineness tradeoff has some drivers toward high fineness ratio. It also has other drivers toward low fineness ratio. These must be harmonized. A high fineness nose, such as $l_N/d = 5$, is ideal aerodynamically and has low observables. A low fineness nose, such as $l_N/d = 0.5$, is ideal electromagnetically and also allows more propellant length and volume for a length limited missile. For supersonic missiles, a moderate nose fineness compromise dome is a nose length-to-diameter ratio of about 2.

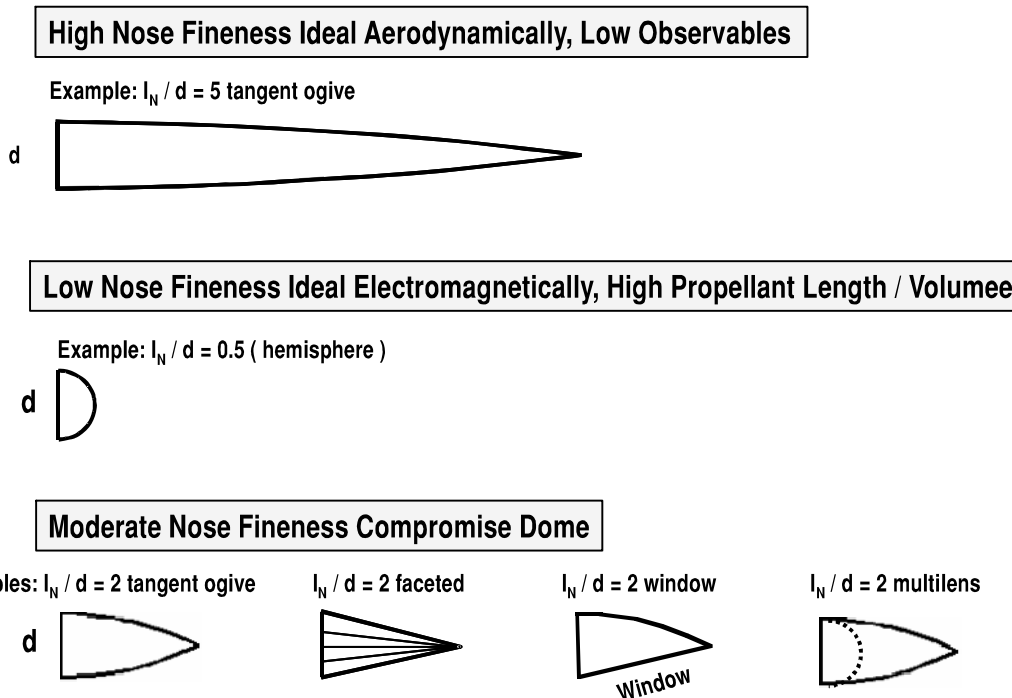
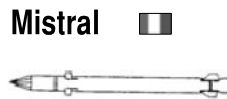


Fig. 2.5 Nose fineness alternatives.

◆ Faceted Dome



◆ Flat Window

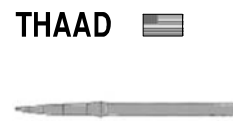
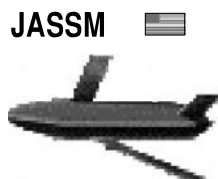
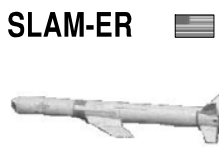


Fig. 2.6 Examples of high fineness domes that also have low dome error slope.

Alternative dome geometry includes tangent ogive, faceted or pyramidal, flat window, and multilens domes. A tangent ogive dome has a circular arc surface. Although a tangent ogive dome has low drag, the curved surface results in high error slope for a seeker tracking the target. An alternative dome is a faceted dome. A faceted dome is composed of six to eight triangular surfaces that form a pyramid. A faceted dome has the advantage of low error slope due to the flat surfaces. The bond line between the facets must be small to minimize optical distortion. A disadvantage of a faceted dome for an infrared seeker is the solar energy reflection off the facets into the seeker. A third type of dome is a window dome composed of a single flat surface. The window dome also has an advantage of low dome error slope. A disadvantage of a window dome is that it limits the field of regard of the seeker, which may limit the ability of the seeker to acquire an off-boresight target. Finally, a multilens dome is composed of two or more concentric domes. A multilens dome has both low drag and low dome error slope. The interior dome(s) provide optical correction to the dome error slope induced by the low drag exterior dome.

Shown in Fig. 2.6 are current missiles with infrared (IR) domes that have high fineness but also have low dome error slope. Faceted dome technology has been applied to supersonic surface-to-air and air-to-air missiles to provide low drag combined with low dome error slope. Supersonic missiles that have a high fineness faceted dome for low drag combined with low dome error slope are the Russian SA-16 missile and the French Mistral missile. Window dome technology has been applied to cruise missiles to provide low radar cross section combined with low dome error slope. Cruise missiles that have a high fineness window for low radar cross section combined with low dome error slope are the U.S. SLAM-ER missile and the U.S. JASSM missile. The SLAM-ER and JASSM seekers have limited field of regard and are biased downward to look through the window. Finally, the U.S. THAAD antimissile missile has a high fineness window that provides both low drag and low dome error slope. The THAAD seeker also has a limited field of regard, and is biased to look through the side window.

Figure 2.7 shows the benefit of a high fineness nose to reduce supersonic drag. For supersonic missiles, skin friction drag and base drag are relatively small.

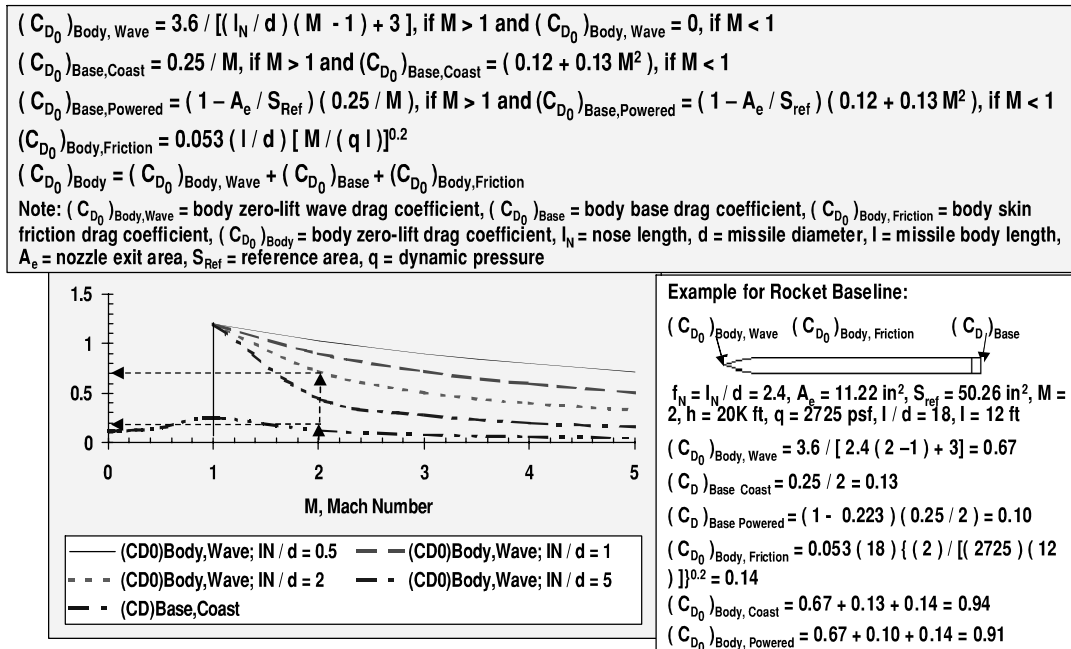
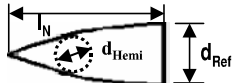


Fig. 2.7 High nose fineness reduces supersonic drag.

Supersonic drag is dominated by the drag due to the shock wave on the nose. $(C_{D_0})_{\text{Body, Wave}}$ is a function of nose fineness and Mach number. The equation for body wave drag coefficient is $(C_{D_0})_{\text{Body, Wave}} = 3.6 / [(l_N/d)(M - 1) + 3]$. Note from the figure that $(C_{D_0})_{\text{Body, Wave}}$ decreases with increasing fineness ratio and Mach number. The figure also shows body base drag coefficient during coasting flight $(C_D)_{\text{Body, Coast}}$ as a function of Mach number. Body base drag can be a major contributor to the total drag during coasting flight, because of the low pressure in the base. For coasting flight at supersonic Mach number, $(C_D)_{\text{Base, Coast}} = 0.25/M$. For coasting flight at subsonic Mach number, $(C_D)_{\text{Base, Coast}} = 0.12 + 0.13M^2$. During powered flight the base drag is reduced by the factor $(1 - A_e/S_{\text{Ref}})$. For a nozzle exit area that is nearly as large as the missile base area, the base drag is negligible during powered flight. Finally, note from the figure that skin friction drag is a major contributor to subsonic drag. $(C_{D_0})_{\text{Body, Friction}}$ is primarily driven by body fineness ratio. It is also a weak function of Mach number, dynamic pressure, and body length. The equation for the body skin friction drag coefficient is $(C_{D_0})_{\text{Body, Friction}} = 0.053(l/d)[M/(ql)]^{0.2}$. Assumptions are that the body wetted area can be approximated by the wetted area of a cylinder, the variation in the free stream speed of sound and viscosity with altitude is relatively small, and a turbulent boundary layer.

An example is shown for the rocket baseline missile, which has a nose fineness ratio of $f_N = 2.4$, body fineness ratio $l/d = 18$, and body length $l = 12 \text{ ft}$. At a nominal Mach number of 2, the predicted zero-lift wave drag coefficient is $(C_{D_0})_{\text{Body, Wave}} = 0.67$. The base drag coefficient during coasting flight at Mach 2 is $(C_D)_{\text{Body, Coast}} = 0.13$, which is only 19% of $(C_{D_0})_{\text{Body, Wave}}$. During powered flight at Mach 2, the base drag coefficient is smaller, $(C_D)_{\text{Body, powered}} = 0.10$. The skin friction drag coefficient at Mach 2 and a nominal altitude of 20,000 ft (corresponding to a dynamic pressure of $q = 2725 \text{ psf}$) is $(C_{D_0})_{\text{Body, Friction}} = 0.14$.

- ◆ Relate blunted nose tip geometry to pointed nose tip geometry



- ◆ Compute $(C_{D_0})_{\text{Wave}}$ for sharp nose based on the body reference area is

$$\cdot (C_{D_0})_{\text{Wave, SharpNose}} = 3.6 / [(l_N / d)(M - 1) + 3]$$

- ◆ C_{D_0} of the hemispherical nose tip based on the nose tip area is

$$\cdot (C_{D_0})_{\text{Wave,Hemi}} = 3.6 / [(l_N / d)(M - 1) + 3] = 3.6 / [0.5 / (M - 1) + 3]$$

- ◆ Finally, compute (C_{D_0}) of the blunt nose based on the body reference area

$$\cdot (C_{D_0})_{\text{Wave,BluntNose}} = (C_{D_0})_{\text{Wave,SharpNose}} (S_{\text{Ref}} - S_{\text{Hemi}}) / S_{\text{Ref}} + (C_{D_0})_{\text{Wave,Hemi}} S_{\text{Hemi}} / S_{\text{Ref}}$$

- ◆ Example rocket baseline ($d_{\text{Ref}} = 8$ in) with 10% nose tip bluntness at Mach 2

$$\cdot (C_{D_0})_{\text{Wave,SharpNose}} = 3.6 / [(2.4)(2 - 1) + 3] = 0.67$$

$$\cdot d_{\text{Hemi}} = 0.10(8) = 0.8 \text{ in}$$

$$\cdot S_{\text{Hemi}} = \pi d_{\text{Hemi}}^2 / 4 = 3.1416 (0.8)^2 / 4 = 0.503 \text{ in}^2 = 0.00349 \text{ ft}^2$$

$$\cdot (C_{D_0})_{\text{Wave,Hemi}} = 3.6 / [0.5 / (2 - 1) + 3] = 1.03$$

$$\cdot (C_{D_0})_{\text{Wave,BluntNose}} = 0.67 (0.349 - 0.003) / 0.349 + (1.03)(0.003) / (0.349) = 0.66 + 0.01 = 0.67$$

Fig. 2.8 Moderate nose tip bluntness causes only a small increase in drag.

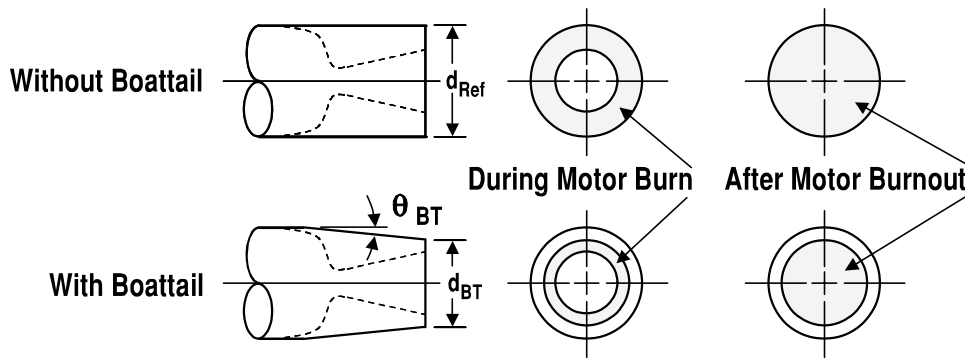
This is only 21% of the value of $(C_{D_0})_{\text{Body, Wave}}$. Finally, the body power-off drag is computed as the sum of the contributions from the wave drag plus the base drag plus the skin friction drag. At Mach 2 and 20,000-ft altitude, the predicted body drag coefficient during coasting flight of the rocket baseline missile is $(C_{D_0})_{\text{Body, Coast}} = 0.94$. The body drag coefficient in powered flight is slightly lower, $(C_{D_0})_{\text{Body, Powered}} = 0.91$.

A small amount of nose tip bluntness is usually desirable for a tactical missile. Nose tip bluntness alleviates problems of localized stress concentration and nose tip heating, usually with a negligible change in drag. Figure 2.8 illustrates the effect of nose tip bluntness on zero-lift wave drag. First, the zero-lift wave drag coefficient is calculated for a sharp nose. The equation is $(C_{D_0})_{\text{Wave, SharpNose}} = 3.6 / [(l_N / d)(M - 1) + 3]$. Next, the zero-lift drag wave coefficient of the hemispherical nose tip is calculated. The equation is $(C_{D_0})_{\text{Wave, Hemi}} = 3.6 / [0.5 / (M - 1) + 3]$, where $(C_{D_0})_{\text{Wave, Hemi}}$ is based on the nose tip cross sectional area. Finally, the zero-lift wave drag coefficient of a missile with a blunt nose tip is the summation of the wave drag coefficient of the sharp nose plus the wave drag coefficient of the hemispherical nose tip, scaled by their areas. The equation is

$$(C_{D_0})_{\text{Wave, BluntNose}} = (C_{D_0})_{\text{Wave, SharpNose}} (S_{\text{Ref}} - S_{\text{Hemi}}) / S_{\text{Ref}}$$

$$+ (C_{D_0})_{\text{Wave, Hemi}} S_{\text{Hemi}} / S_{\text{Ref}}$$

As an example, the wave drag coefficient of the rocket baseline with a sharp nose of fineness ratio $l_N / d = 2.4$ and flying at Mach 2 has a nose zero-lift wave drag coefficient $(C_{D_0})_{\text{Wave, SharpNose}} = 0.67$. The wave drag coefficient of a hemispherical nose tip is given by $(C_{D_0})_{\text{Wave, Hemi}} = 1.03$, where $(C_{D_0})_{\text{Wave, Hemi}}$ is based on the nose tip cross sectional area. Finally, the rocket baseline missile ($d_{\text{Ref}} = 8$ in.) with 10% nose tip bluntness at Mach 2 has a predicted zero-lift wave drag coefficient of $(C_{D_0})_{\text{Wave, BluntNose}} = 0.67$, which is the same value as that of a sharp nose.



Note: Boattail limited by propulsion nozzle packaging, tail flight control packaging, and flow separation

Fig. 2.9 Boattail decreases base pressure drag area (from Ref. 3).

2.3 Boattail

Boattailing has its best payoff for subsonic missiles; supersonic missiles are susceptible to aft flow separation due to boattailing. Figure 2.9 from Ref. 2 illustrates the benefit of a moderate amount of boattailing. Without a boattail, during motor burn the entire base area outside the nozzle has base pressure drag. After motor burnout, the base pressure coefficient occupies the entire base area. However, with boattailing the area occupied by the boattail has a larger base pressure, reducing the base drag in the area of the boattail. A design consideration if the missile has a boattail is that there is less volume available for subsystems such as tail control actuators.

Figure 2.10 from Ref. 3 shows that the payoff for boattailing is greatest for subsonic missiles. The example body has an overall fineness ratio of 10.5, a nose fineness ratio of 3.00, a center body fineness ratio of 6.00, and a boattail fineness

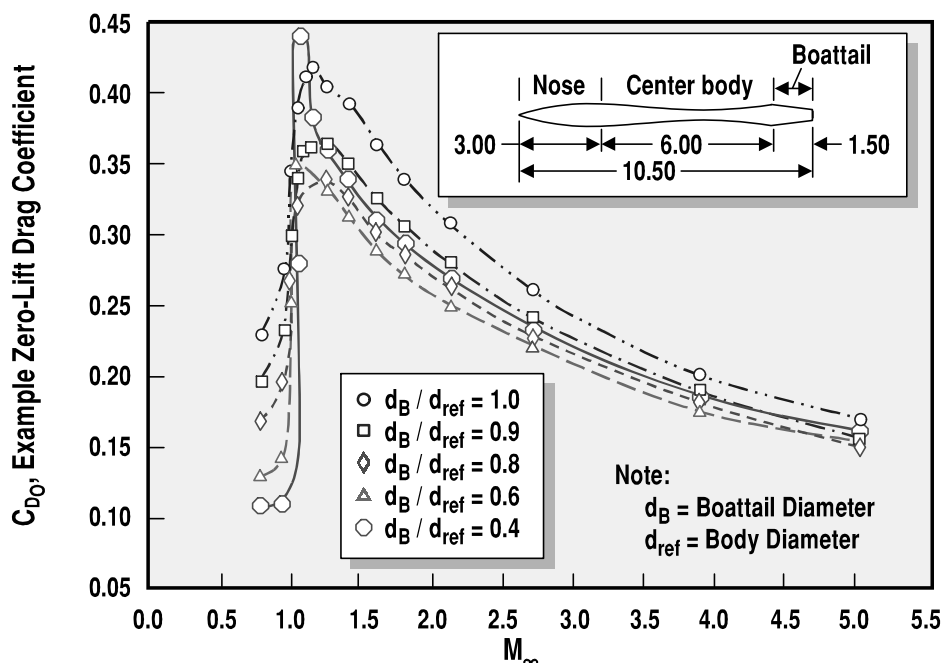


Fig. 2.10 Boattailing has greatest payoff for subsonic missiles (from Ref. 2).

ratio 1.50. Note that for subsonic Mach number, boattailing reduces the drag by over 50%. However, at supersonic to hypersonic Mach number there is only a slight reduction in drag with moderate boattailing, and large boattailing actually causes an increase in drag. At high Mach number, a large boattail angle can cause flow separation over the boattail, resulting in increased drag.

2.4 Lifting Body Versus Axisymmetric Body

As shown in Fig. 2.11, the maximum normal force of a lifting body is higher than that of an axisymmetric body. The normal force prediction is based on combining slender body theory⁴ and body cross flow theory.⁵ The equation for normal force coefficient is

$$|C_N| = [| (a/b) \cos \phi + (b/a) \sin \phi |] [|\sin(2\alpha) \cos(\alpha/2)| + 2(l/d) \sin^2 \alpha]$$

Normal force coefficient of a slender body is independent of Mach number. For an elliptical cross section, an equivalent diameter is based on a circular cross section of the same area. The figure shows normal force coefficient as a function of angle of attack α and the body cross section major-to-minor axis ratio (a/b). The normal force coefficient increases with α (up to $\alpha = 90\text{-deg}$) and a/b . As an example, at a 90-deg angle of attack, the normal force coefficient for an elliptical cross section with a major-to-minor axis ratio of $a/b = 2$ is twice that of a circular cross section.

The body normal force curve slope due to angle of attack is used in sizing the tail to meet the static stability requirement. $(C_{N_\alpha})_{\text{Body}}$ is the derivative of the equation for body normal force coefficient. At low angle of attack, $(C_{N_\alpha})_{\text{Body}} = 2[(a/b) \cos \varphi + (b/a) \sin \varphi]$, measuring per rad.

The equation for aerodynamic efficiency is

$$L/D = (C_N \cos \alpha - C_{D_0} \sin \alpha) / (C_N \sin \alpha + C_{D_0} \cos \alpha)$$

$$|C_N| = [| (a/b) \cos (\phi) + (b/a) \sin (\phi) |] [|\sin (2\alpha) \cos (\alpha/2)| + 2(l/d) \sin^2 \alpha]$$

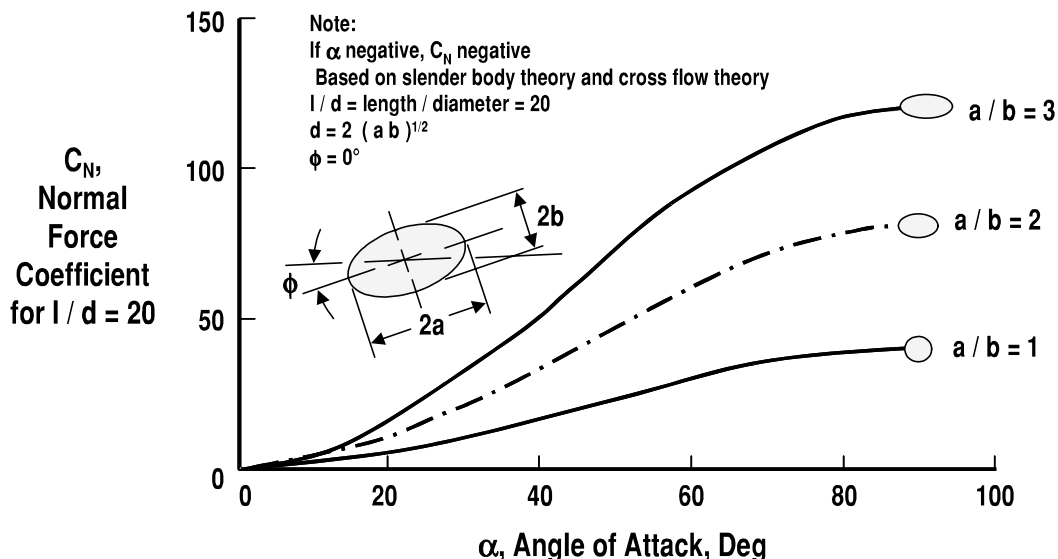


Fig. 2.11 Lifting body has higher normal force coefficient.

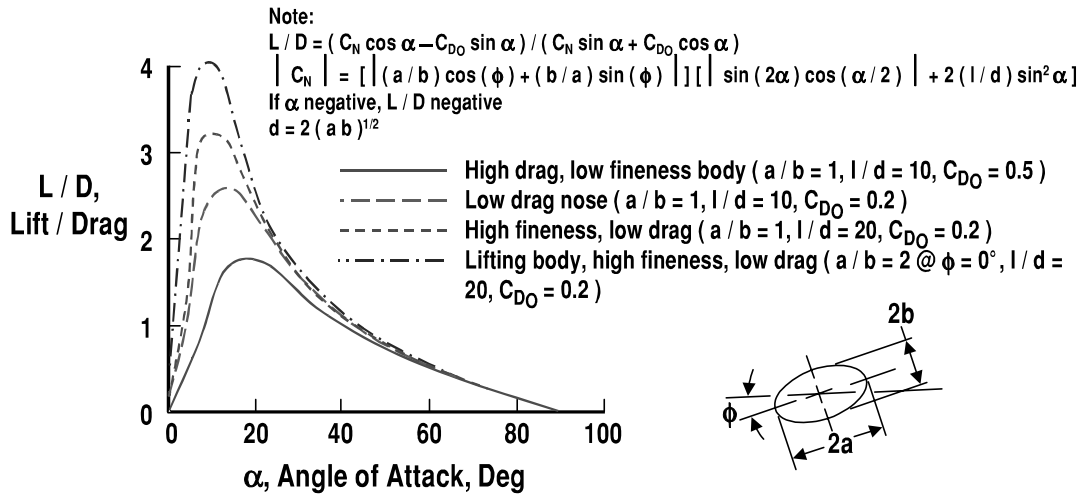


Fig. 2.12 C_{D_0} , body fineness, and lifting body impact L/D .

L/D is a function of primarily angle of attack for a body-lift missile. As shown in Fig. 2.12, an increase in L/D can be achieved by reducing the zero-lift drag coefficient, increasing the body fineness, and providing a lifting body configuration ($a/b > 1$). Note that as a higher L/D is achieved, the angle of attack in which $(L/D)_{Max}$ is achieved is decreased. Again, the prediction is based on combining slender body theory⁴ with cross flow theory.⁵ Note that other considerations, such as launch platform lateral and length constraints, may limit the aerodynamic shaping that is practical. Also note that for 1-g constant altitude flight the angle of attack is usually much lower than the angle of attack for $(L/D)_{Max}$. The L/D during the flyout of most rocket powered missiles is usually much lower than $(L/D)_{Max}$.

Although a lifting body configuration has a higher $(L/D)_{Max}$ than an axisymmetric cross-sectional configuration, for 1-g flight at low angles of attack the axisymmetric configuration usually provides higher L/D . Figure 2.13 compares the

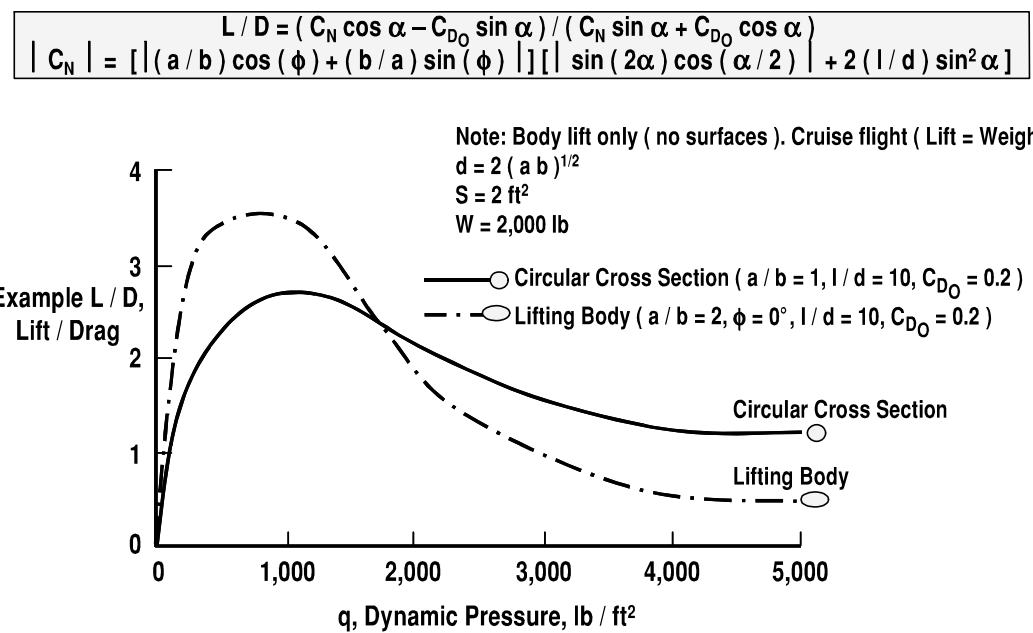


Fig. 2.13 A lifting body has high efficiency at low dynamic pressure.

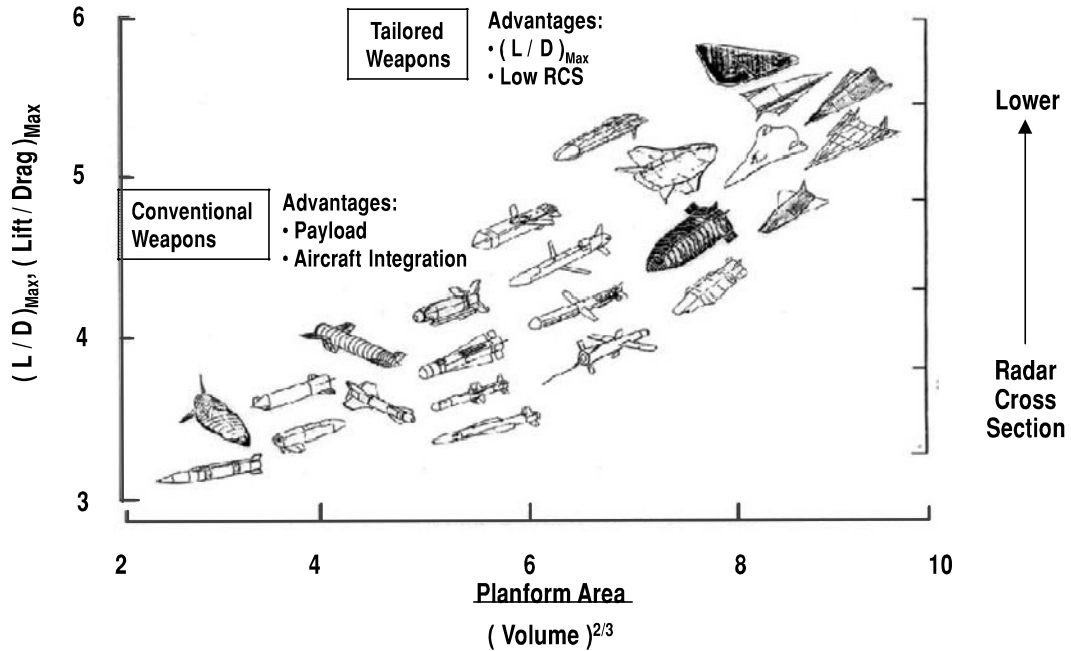


Fig. 2.14 Tradeoff of low observables and $(L/D)_{\text{Max}}$ vs volumetric efficiency.

L/D of a lifting body configuration ($a/b = 2$) with that of a circular cross-sectional configuration. Typical values are given for a precision strike missile configuration of 2 ft^2 cross-sectional area and 2000 lb weight. As before, the L/D is based on combining slender body theory with cross flow theory. Maximum L/D for the lifting body configuration occurs at a dynamic pressure $q = 700 \text{ psf}$. The maximum L/D for the circular cross-sectional configuration occurs at a higher dynamic pressure, $q = 1000 \text{ psf}$. Note that the circular body cross-sectional configuration provides a higher L/D if the dynamic pressure is greater than 1700 psf. For a dynamic pressure less than 1700 psf, the lifting body has a higher L/D . A more highly tailored lifting body ($a/b > 2$) or adding a wing further increases $(L/D)_{\text{Max}}$, reduces $\alpha_{(L/D)_{\text{Max}}}$, and reduces $q_{(L/D)_{\text{Max}}}$. For example, the rocket baseline missile has a relatively high L/D , because of its wing. At Mach 0.8, $(L/D)_{\text{Max}} = 6.2$, $\alpha_{(L/D)_{\text{Max}}} = 4.5 \text{ deg}$, and $q_{(L/D)_{\text{Max}}} = 350 \text{ psf}$. Supersonic missiles usually fly at a dynamic pressure greater than 1000 psf. The L/D for a supersonic missile in 1-g flight is usually much less than $(L/D)_{\text{Max}}$. As an example, the rocket baseline during 1-g powered flight at Mach 2, 20,000-ft altitude has an $L/D = 0.41$.

Figure 2.14 compares weapon configurations that have a conventional cylindrical cross section to other weapons that are highly tailored, using aerodynamic shaping of their lifting body configurations. An advantage of a tailored lifting body missile is higher aerodynamic efficiency (lift-to-drag ratio) for extended range cruise performance and enhanced maneuverability. Also shown is the synergy of tailored missiles with reduced radar cross section. Tailored missiles are also synergistic with ramjets in areas such as inlet integration and liquid hydrocarbon fuel packaging. Disadvantages of tailored missiles include their relative inefficiency for solid subsystems packaging and an adverse impact on launch platform integration due to a larger span. Improved methods and tests are required for the prediction of the aerodynamics and the structural loads of nonaxisymmetric weapons. This includes more extensive wind tunnel tests, computational fluid dynamics (CFD) predictions, and finite element modeling (FEM) of structural integrity.

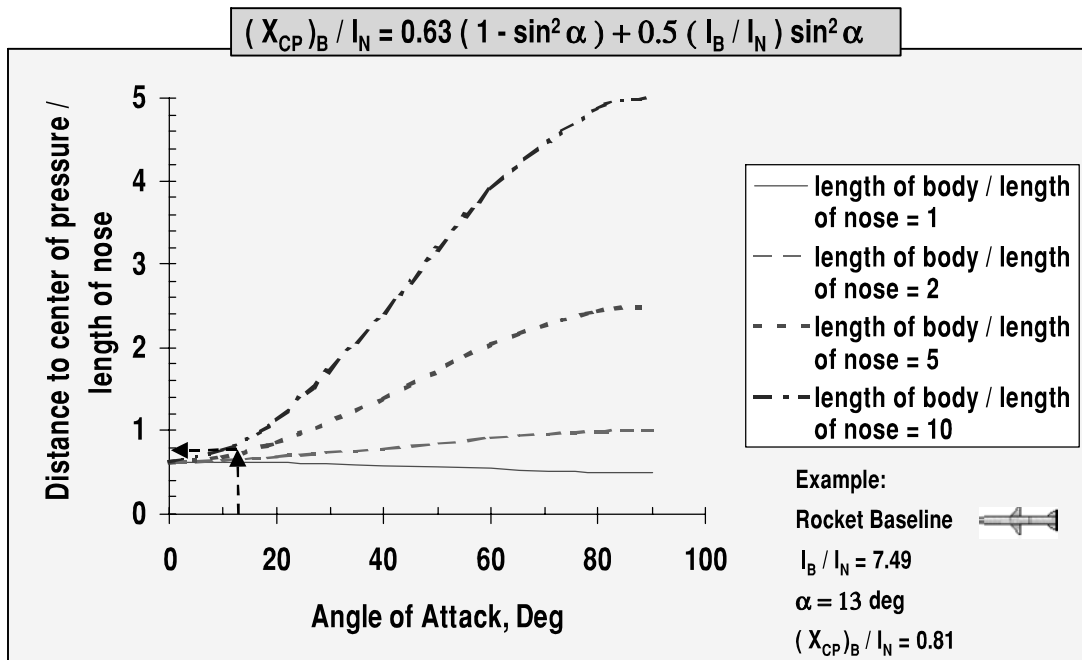


Fig. 2.15 Body center-of-pressure location is a function of angle of attack and fineness.

Body center-of-pressure location x_{CP} depends mostly on two parameters, angle of attack and aftbody fineness. For conceptual design, the dependence on Mach number may be neglected. As shown in Fig. 2.15, at low angle of attack, x_{CP} is located about 0.63 diameters from the nose tip. At angles of attack approaching 90 deg, x_{CP} approaches the center of the body. Results in the figure are shown as a function of the body-length-to-nose-length ratio l_B/l_N and angle of attack α . As before, results are based on combining slender body theory⁴ with cross flow theory,⁵ giving the equation $(x_{CP})_B/l_N = 0.63(1 - \sin^2 \alpha) + 0.5(l_B/l_N) \sin^2 \alpha$. As an example, the rocket baseline missile has a ratio of body length to nose length of $l_B/l_N = 7.49$. For an angle of attack of $\alpha = 13$ deg, the center of pressure of the body $(x_{CP})_B$ is located at 81% of the length of the nose.

2.5 Wings Versus No Wings

There are many considerations in the tradeoff of small wing/no wing vs a larger wing. A small wing or no wing has the advantages of range in high supersonic flight/high dynamic pressure, stability and control at high angles of attack (less induced roll), launch platform compatibility, lower radar cross section, and volume and weight available for propellant/fuel in a volume or weight limited missile. A larger wing has the advantages of range in subsonic flight/low dynamic pressure, lower guidance time constant, normal acceleration, high altitude intercept, less aeroelasticity (stiffens body), less seeker tracking error due to dome error slope (lower angle of attack), less wipe velocity for the warhead (lower angle of attack), and lower gimbal angle requirement for the seeker. Note that the advantages of lower guidance time constant, normal acceleration, and high altitude intercept are based on the assumption of aerodynamic flight control. Unconventional flight control (e.g., thrust vector control, reaction jet/jet interaction control) for a wingless missile can provide a small guidance time constant, high normal acceleration or maneuverability, and a high altitude intercept capability at low dynamic pressure.

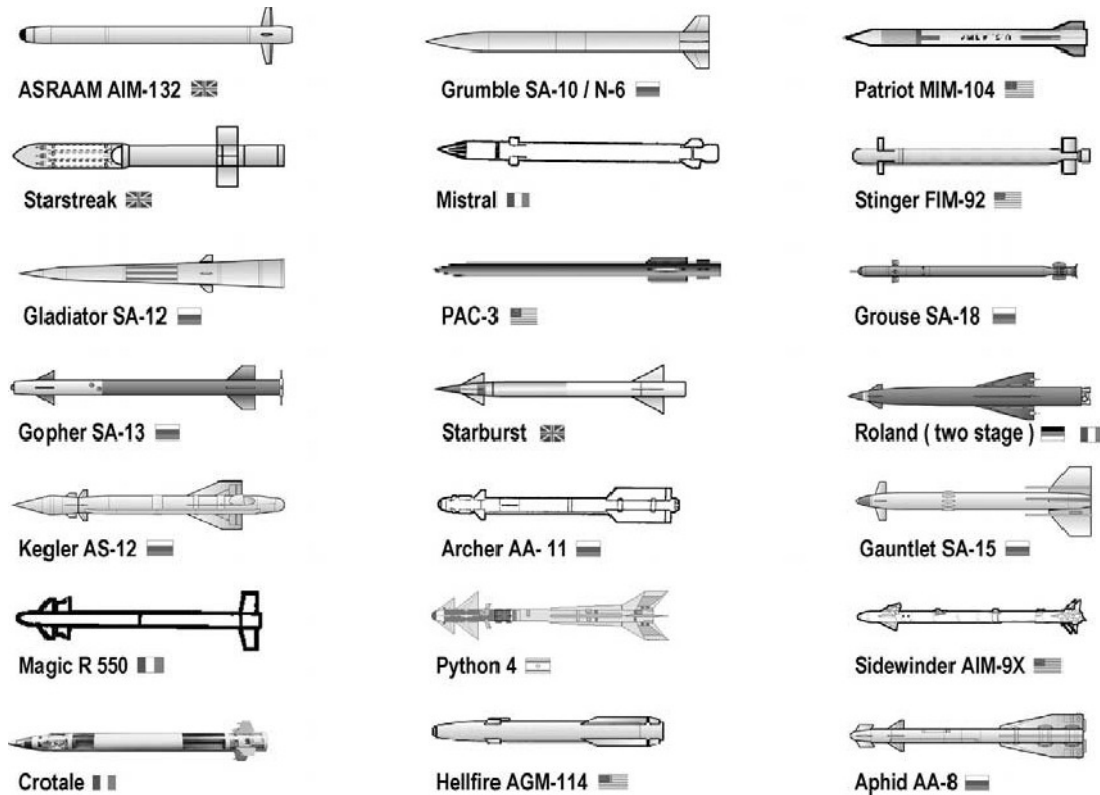


Fig. 2.16 Examples of supersonic missiles that are wingless (used with permission of Missile Index, 1997, online at <http://www.index.ne.jp/missile-e/>).

Because supersonic missiles generally operate at relatively high dynamic pressure, body lift may be sufficient for the required aerodynamic efficiency L/D and maneuverability. Shown in Fig. 2.16 are examples of supersonic missiles that do not have wings. Many of these missiles also have high maneuverability and are capable of operating at high angle of attack. Wingless missiles that use canard control have enhanced maneuverability from the additional lift of the canard surface. Thirteen of the 21 wingless missiles shown in the figure use canard control, and eight of the missiles have tail control. Unconventional flight control may also be used if additional maneuverability is required to supplement the body lift. An example of a supersonic wingless missile that uses thrust vector control combined with canard control is the Archer AA-11.

2.6 Normal Force Prediction for Surfaces

Tactical missile surface planforms include wing, tail, and canard surfaces. These may be fixed or movable (i.e., control surfaces). As shown in the equations of Fig. 2.17, the wing surface normal force coefficient (C_N)_{Wing} is a function of Mach number, local angle of attack, aspect ratio, and the wing surface planform area. (C_N)_{Wing}, based on the missile reference area, decreases with increasing supersonic Mach number and increases with angle of attack and the wing surface area. The prediction is based on the method of Ref. 4. In the figure, linear wing theory plus Newtonian impact theory are applied at high supersonic Mach number, with $M^2 > 1 + [8/(\pi A)]^2$. The equation is

$$|(C_N)_{\text{Wing}}| = [4|\sin \alpha' \cos \alpha'|/(M^2 - 1)^{1/2} + 2 \sin^2 \alpha'] (S_W/S_{\text{Ref}})$$

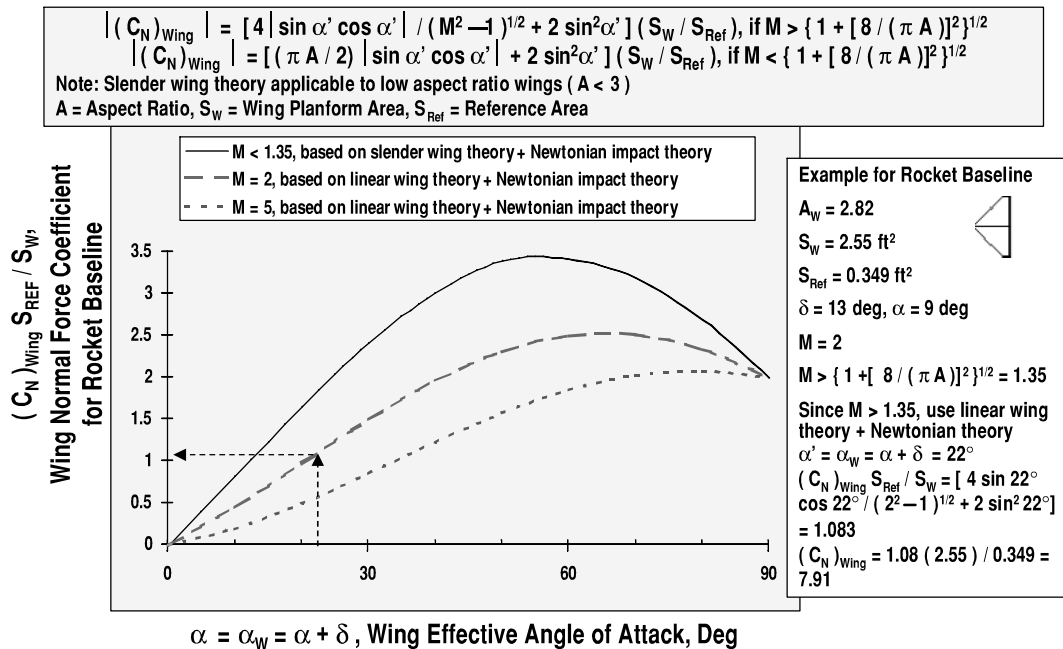


Fig. 2.17 C_N of a surface is a function of Mach number, angle of attack, aspect ratio, and surface area.

Note that $(C_N)_{Wing}$, based on linear wing theory, is independent of aspect ratio. For the rocket baseline missile wing with an aspect ratio of $A_W = 2.82$, linear wing theory is applicable for Mach numbers greater than 1.35. Slender wing theory plus Newtonian impact theory is more applicable at subsonic and low supersonic Mach number, with $M^2 < 1 + [8/(\pi A)]^2$. The equation is

$$|(C_N)_{Wing}| = [(\pi A/2) |\sin \alpha' \cos \alpha'| + 2 \sin^2 \alpha'] (S_W / S_{Ref})$$

Note that $(C_N)_{Wing}$ based on slender wing theory is independent of Mach number. Slender wing theory is accurate for low aspect ratio wings ($A < \approx 3$). For the rocket baseline missile wing ($A_W = 2.82$), slender wing theory is applicable for Mach numbers less than 1.35.

As an example, the rocket baseline missile is evaluated at Mach 2. The rocket baseline missile wing is limited to a maximum local angle of attack of 22 deg due to stall of the wing. This results in a maximum angle of attack of 9.4 deg for a maximum wing control deflection of 12.6 deg. For this condition, the normal force coefficient of the wing, based on wing area, is equal to 1.08. The normal force coefficient of the wing, based on the body reference cross-sectional area, is equal to 7.91. Because the rocket baseline missile has a large wing, most of the normal force for the missile comes from the wing.

The rocket baseline has fixed tail surfaces with an exposed aspect ratio $A_T = 2.59$ and planform area $S_T = 1.54 \text{ ft}^2$. At Mach 2 and an angle of attack $\alpha = 9.4$ deg, the normal force coefficient of the tail is computed to be $(C_N)_{Tail} = 0.425$, based on the tail surface planform area. Based on the missile reference area, $(C_N)_{Tail} = 1.88$. Note that for the trimmed flight condition of Mach 2 and $\alpha = 9.4$ deg, the tail provides only 24% of the normal force of the deflected wing.

The total normal force coefficient of the wing–tail–body configuration is assumed to be the sum of the contributions from the wing plus the tail plus the body. As shown previously, the body normal force coefficient is a function of angle of attack, fineness ratio, and cross section geometry. The rocket baseline has a circular cross section ($a/b = 1$) and a fineness ratio $l/d = 17.99$. At an angle of attack of $\alpha = 9.4$ deg, the body normal force coefficient is computed to be

$$(C_N)_{\text{Body}} = \sin(2\alpha) \cos(\alpha/2) + 2(l/d) \sin^2 \alpha = 1.28$$

Note that the body normal force coefficient is only 16% of that provided by the deflected wing. Substituting, the total trimmed normal force coefficient at Mach 2, $\alpha = 9.4$ deg, and $\delta = 12.6$ deg is

$$C_N = (C_N)_{\text{Wing}} + (C_N)_{\text{Tail}} + (C_N)_{\text{Body}} = 7.91 + 1.88 + 1.28 = 11.1$$

A similar approach can be used to determine the wing normal force curve slope due to angle of attack. $(C_{N_\alpha})_{\text{Wing}}$ is used in sizing the tail to meet the static stability requirement. It is the derivative of the equation for wing normal force coefficient. At low angle of attack, $(C_{N_\alpha})_{\text{Wing}} = 4/(M^2 - 1)^{1/2}$, if the parameter $M^2 > 1 + [8/(\pi A)]^2$. If the parameter $M^2 < 1 + [8/(\pi A)]^2$, then the appropriate equation is $(C_{N_\alpha})_{\text{Wing}} = \pi A/2$. Note that $(C_{N_\alpha})_{\text{Wing}}$ in these equations is based on the wing planform area and is measured per rad.

The total normal force curve slope due to angle of attack is assumed to be the sum of the contributions from the wing plus the tail plus the body. As shown previously, the body normal force curve slope is $(C_{N_\alpha})_{\text{Body}} = 2[(a/b) \cos \varphi + (b/a) \sin \varphi]$. For the rocket baseline with a circular cross section, $(C_{N_\alpha})_{\text{Body}} = 2$ per rad. At Mach 2, the total normal force curve based on body cross-sectional reference area is

$$\begin{aligned} (C_{N_\alpha}) &= (C_{N_\alpha})_{\text{Wing}}(S_W/S_{\text{Ref}}) + (C_{N_\alpha})_{\text{Tail}}(S_T/S_{\text{Ref}}) + (C_{N_\alpha})_{\text{Body}} \\ &= 4/(2^2 - 1)^{1/2}(2.55/0.349) + 4/(2^2 - 1)^{1/2}(1.54/0.349) + 2 \\ &= 16.9 + 10.2 + 2 = 29.1 \text{ per rad} \end{aligned}$$

The total normal force curve slope due to angle of attack from Chapter 7, which is based on wind tunnel data, is $C_{N_\alpha} = 34.4$ per rad. The predicted value of C_{N_α} has an error of 14%.

2.7 Wing Aerodynamic Center Prediction

Shown in Fig. 2.18 is the variation of aerodynamic center $(x_{AC})_{\text{Wing}}$ of a surface with Mach number, and aspect ratio. Results are applicable to low angles of attack ($\alpha < 10$ deg). At low Mach number, $(x_{AC})_{\text{Wing}}$ is located near 25% of the mean aerodynamic chord C_{MAC} . At hypersonic Mach number, $(x_{AC})_{\text{Wing}}$ shifts to 50% of C_{MAC} . Note that low aspect ratio wings have less variation in the aerodynamic center. The prediction at supersonic Mach number is based on linear wing theory,⁴ giving

$$(x_{AC}/C_{\text{MAC}})_{\text{Wing}} = [A(M^2 - 1)^{1/2} - 0.67]/[2A(M^2 - 1)^{1/2} - 1]$$

The rocket baseline missile wing has an exposed aspect ratio of 2.82, a mean aerodynamic chord length of 13.3 in., and a location of the leading edge of the

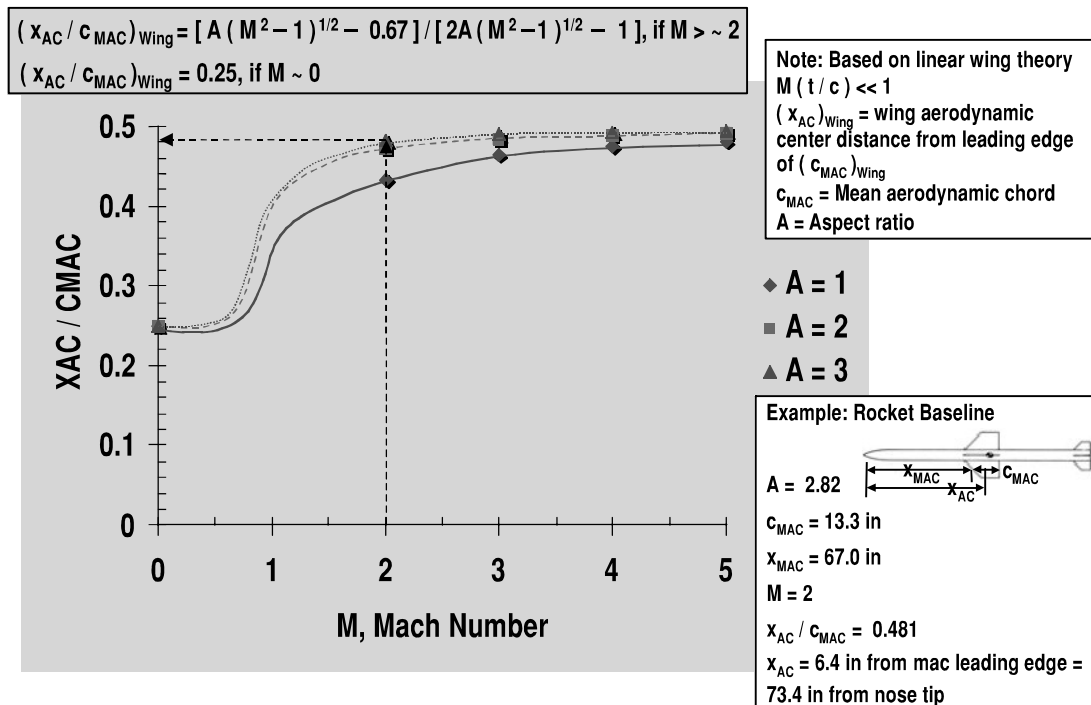


Fig. 2.18 Wing aerodynamic center has a large variation with Mach number.

mean aerodynamic chord at 67.0 in. from the nose tip. As shown in the figure, at Mach 2 the aerodynamic center of the exposed wing is located at 48% of the length of the mean aerodynamic chord, providing a location of 73.4 in. from the nose tip. At subsonic Mach number the wing aerodynamic center is located at approximately 25% of the mean aerodynamic chord, providing a location of 70.3 in. from the nose tip. The center-of-gravity location of the rocket baseline missile is 84.6 in. from the nose tip at launch and 76.2 in. at burnout. Because the distance between the wing aerodynamic center and the missile center of gravity is always relatively small (less than 14.3 in.) for all flight conditions, the deflection of the wing control causes a relatively small change in missile angle of attack. If either tail control or canard control were used for the rocket baseline missile instead of wing control, the change in angle of attack with control surface deflection would be larger because of the larger moment arm of a tail or canard control.

2.8 Wing Drag Prediction

Equations for predicting the wing surface drag coefficient are shown in Fig. 2.19. The wave drag prediction is based on modified Newtonian theory from Ref. 6, with the equation

$$(C_{D_0})_{\text{Wing, Wave}} = n_W [2/(\gamma M_{\Lambda_{LE}}^2)] \{[(\gamma + 1)M_{\Lambda_{LE}}^2]/2\}^{\gamma/(\gamma-1)} \{(\gamma + 1)/[2\gamma M_{\Lambda_{LE}}^2 - (\gamma - 1)]\}^{1/(\gamma-1)} - 1 \sin^2 \delta_{LE} \cos \Lambda_{LE} t_{MAC} b / S_{\text{Ref}}$$

Newtonian theory is modified by calculating the pressure across the normal shock as a function of Mach number. Note that a thin wing with a small leading edge section angle has very small wave drag compared with that of a wing with a blunt

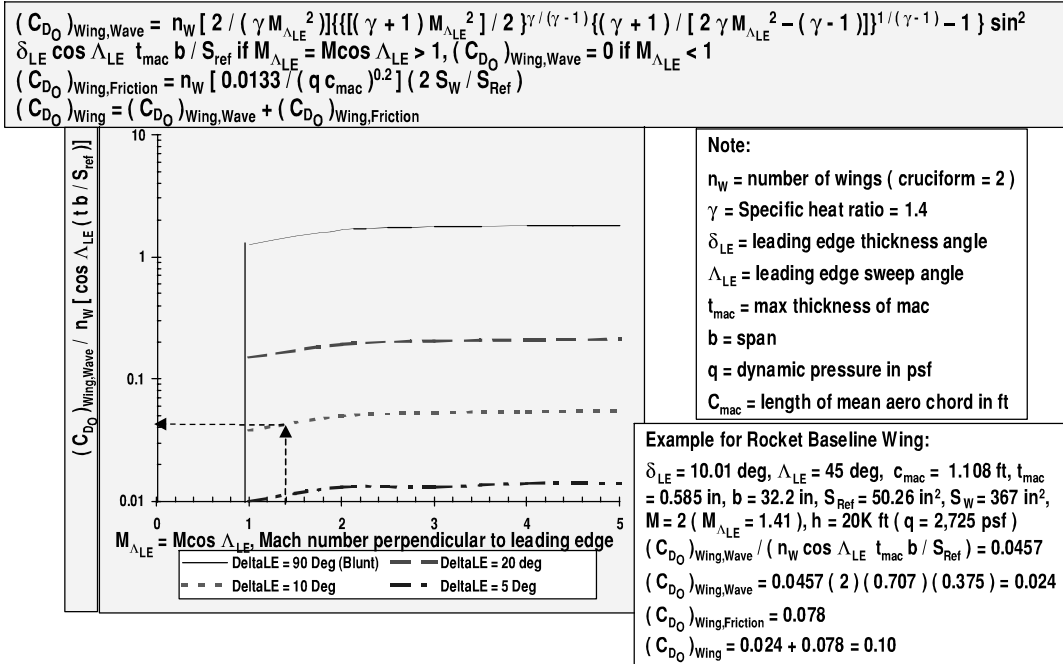


Fig. 2.19 Thin wing reduces supersonic wave drag.

leading edge. Also, leading edge sweep reduces the effect of Mach number by the factor of $\cos \Lambda_{LE}$, maintaining a subsonic leading edge until $M \cos \Lambda_{LE} = 1$. A second contributor to wing zero-lift drag is skin friction. The equation is

$$(C_{D_0})_{Wing,Friction} = n_w [0.0133 / (q c_{MAC})^{0.2}] (2 S_w / S_{Ref})$$

Major contributors to the skin friction drag coefficient are the number of wings n_w and the wing planform area S_w . Wing skin friction drag coefficient is also a weak function of dynamic pressure and the length of the mean aerodynamic chord. The expansion region on the aft portion of the wing and the lower pressure on the base of the wing normally have negligible contributions to wing drag, especially for thin wings.

As an example, the rocket baseline missile has cruciform wings ($n_w = 2$), wing leading edge sweep angle of $\Lambda_{LE} = 45 \text{ deg}$, exposed planform area of each wing $S_w = 2.55 \text{ ft}^2$, leading edge section angle $\delta_{LE} = 10.01 \text{ deg}$, length of the mean aerodynamic chord $C_{MAC} = 1.108 \text{ ft}$, maximum thickness of the mean aerodynamic chord $t_{MAC} = 0.585 \text{ in.}$, and exposed span $b = 32.2 \text{ in.}$ At Mach 2, the zero-lift wave drag coefficient of the cruciform wing (four panels) based on the reference area (body cross-sectional reference) is $(C_{D_0})_{Wing,Wave} = 0.024$. The contribution of skin friction to the drag coefficient for an assumed altitude of 20,000 ft is larger, with $(C_{D_0})_{Wing,Friction} = 0.078$. The total zero-lift drag coefficient is $(C_{D_0})_{Wing} = 0.10$. It is noted that the rocket baseline missile wing has a zero-lift drag coefficient that is only 13% of the body coast zero-lift drag coefficient (0.10 vs 0.81). At supersonic Mach number the nose wave drag is the major contributor to the missile zero-lift drag.

The rocket baseline has cruciform tail surfaces ($n_w = 2$), tail leading edge sweep angle of $\Lambda_{LE} = 57 \text{ deg}$, exposed planform area of $S_T = 1.54 \text{ ft}^2$, leading edge thickness angle $\delta_{LE} = 6.17 \text{ deg}$, mean aerodynamic chord $C_{MAC} = 1.025 \text{ ft}$,

maximum thickness of the mean aerodynamic chord $c_{MAC} = 0.33$ in., and exposed span $b = 24.0$ in. At Mach 2 and an altitude of 20,000 ft, the zero-lift drag coefficient of the tail surfaces is computed to be

$$(C_{D_0})_{\text{Tail}} = (C_{D_0})_{\text{Tail, Wave}} + (C_{D_0})_{\text{Tail, Friction}} = 0.003 + 0.048 = 0.051$$

based on the missile reference area. The zero-lift drag of the tail is much smaller than that of the wing, primarily due to the smaller leading edge section angle (6.17 deg vs 10.01 deg). Note that for the flight condition of Mach 2 and 20,000-ft altitude, the tail provides only 6% of the zero-lift drag compared with that of the body.

Finally, the total zero-lift drag coefficient is assumed to be the sum of the contributions from the body plus the wing plus the tail. Substituting, the total zero-lift drag coefficient of the rocket baseline during coasting flight at Mach 2 and 20,000-ft altitude is computed to be

$$C_{D_0} = (C_{D_0})_{\text{Body}} + (C_{D_0})_{\text{Wing}} + (C_{D_0})_{\text{Tail}} = 0.81 + 0.10 + 0.05 = 0.96$$

2.9 Surface Planform Geometry Tradeoffs

Shown in Fig. 2.20 are alternative surface planform geometries for missile tails, canards, and wings. The figure is a comparison of a triangular (delta) planform, a trapezoidal planform with an aft swept leading edge, a trapezoidal planform with a forward swept leading edge, and a rectangular surface planform. An example of new aeromechanics technology is forward swept surfaces. Forward swept surfaces are beneficial for missiles that require low radar cross section (RCS) or have small span requirements for aircraft compatibility. A forward swept wing has low frontal RCS because of the wing sweep and the attenuation of backscatter bouncing off the

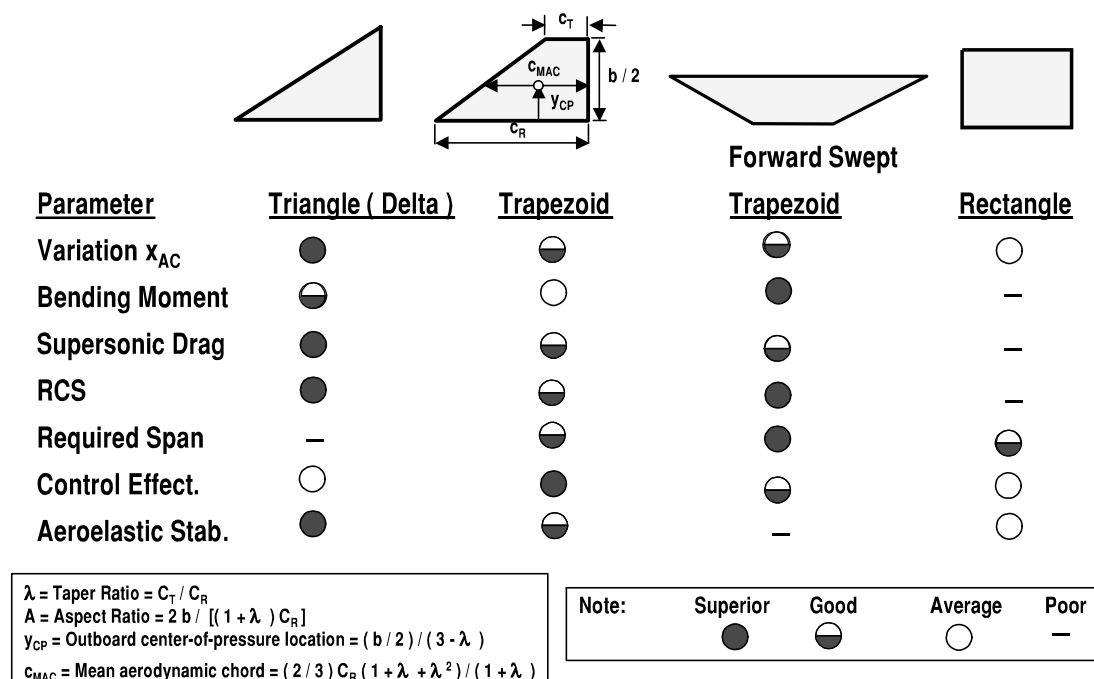


Fig. 2.20 Surface planform alternatives.

adjacent body. In addition to a low RCS and smaller span, forward swept surfaces have good-to-superior characteristics of low variation in aerodynamic center, low bending moment, low supersonic drag, and high control effectiveness. An inherent disadvantage of a forward swept surface is increased potential for aeroelastic instability. Composite structure is synergistic with forward swept surfaces because the higher stiffness of composites mitigates aeroelastic instability and facilitates aeroelastic tailoring of the wing. Composite material may also be used in radar absorbing structure. The U.S. AGM-129 Advanced Cruise Missile and the Russian AA-10 are examples of missiles with a forward swept wing. An alternative surface planform geometry based on triangular (delta) surfaces is attractive if the span can be accommodated within the launch platform span constraints. A delta surface has strengths of a small variation in aerodynamic center, low supersonic drag, low radar cross section, and high structural stiffness. AGM-65 and AIM-54 are examples of missiles with triangular wings. Another alternative, a trapezoidal surface with an aft swept leading edge is often selected for missile wing, canard, and tail surfaces because it has high control effectiveness and does not have any serious weaknesses in the other attributes. Patriot and AIM-9X are examples of missiles with aft-swept trapezoidal tails. Finally, rectangular surfaces have many disadvantages and are used less often, but rectangular surfaces do allow a large surface area within launch platform chord and span constraints. The AGM-130, AGM-65, and AIM-54 are examples of missiles with rectangular tails.

The surface planform geometry parameters shown in the figure include taper ratio, aspect ratio, outboard location of the center of pressure, and the mean aerodynamic chord. Taper ratio λ is the tip chord to root chord ratio, C_T/C_R . Aspect ratio A is defined as the square of the surface span divided by the surface area, b^2/S . In terms of span, taper ratio, and root chord, $A = 2b/[(1 + \lambda)C_R]$. The outboard location of the mean aerodynamic chord, or center-of-pressure location, is given by $y_{CP} = (b/2)/(3 - \lambda)$. Finally, the length of the mean aerodynamic chord is $C_{MAC} = (2/3)C_R(1 + \lambda + \lambda^2)/(1 + \lambda)$. The aerodynamic center, which is the same as the center of pressure for a surface with a symmetrical noncambered cross section, is located on the mean aerodynamic chord.

2.10 Flight Control Alternatives

The types of flight control (tail, canard, wing, unconventional) and the alternative approaches for design and integration with fixed surfaces are shown in Fig. 2.21. For tail control, the control surface design alternatives include the number of tails (three or four) and the launch platform integration (no compressed carriage, folded, wraparound, switchblade). A tail control missile may also have forward surfaces (fixed wings, strakes, canards). The forward fixed surfaces may be either inline or interdigitated with the tail controls. The forward surfaces of a tail control missile may have two surfaces (usually used with bank-to-turn maneuvering), three surfaces (usually used with a tri-tail), or four forward (cruciform) fixed surfaces.

For canard control there are similar control alternatives. Canard control has an additional design alternative of only two control surfaces, which reduces cost and subsystem volume. Examples of missiles with two control surfaces are the 5-in.-diam Rolling Airframe Missile (RAM) and the 2.75-in.-diam Stinger missile.

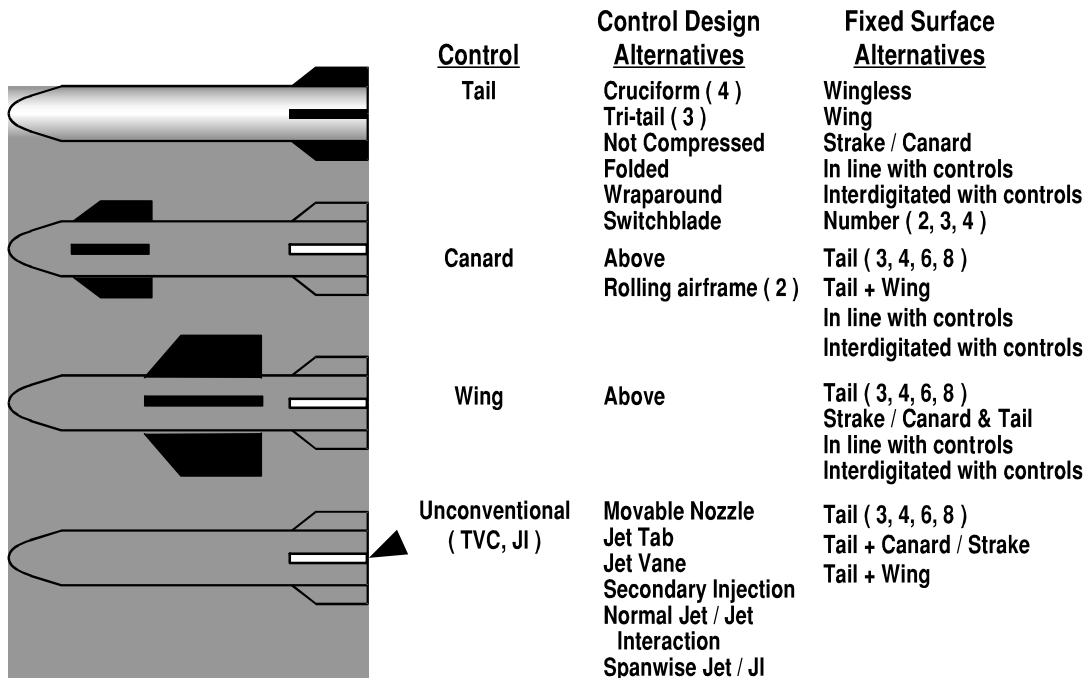


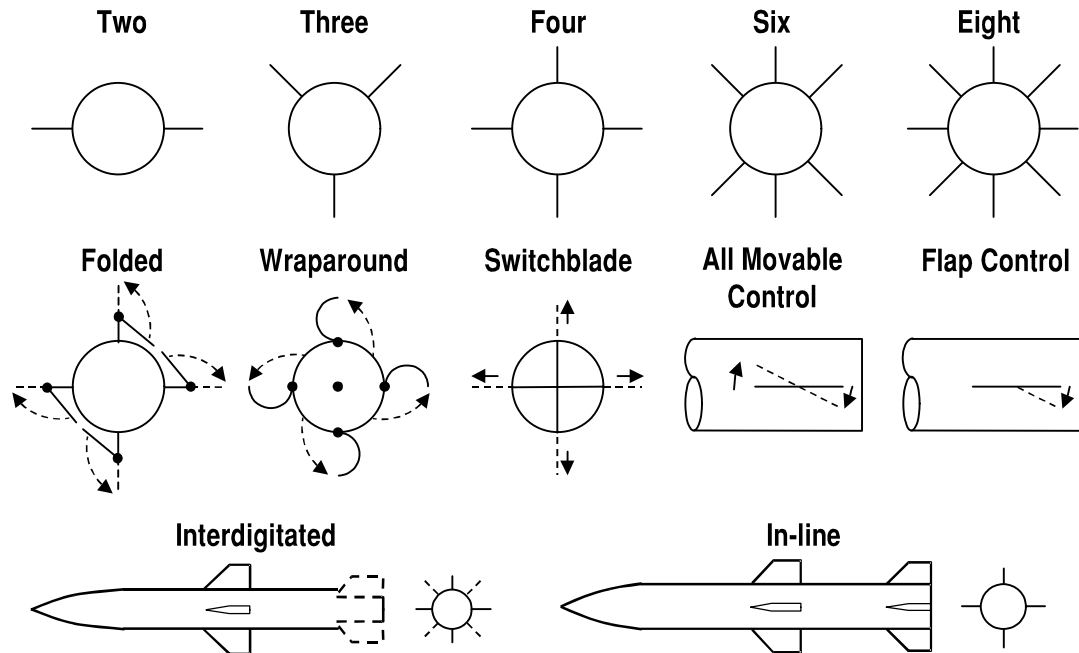
Fig. 2.21 Flight control alternatives.

The number of tail surfaces for a canard control missile may be tri-tail (three), cruciform (four), or more (six, eight) surfaces. The missile may have free-to-roll tails to minimize the rolling moment at high angle of attack. An example of a highly maneuverable canard control missile with free-to-roll tails is the Python 4.

Wing control requires three or more tail surfaces for static stability, similar to canard control. Wing control may also have fixed forward surfaces (canards/strakes), although this is rare because of problems at high angle of attack due to vortex shedding.

Finally, unconventional flight control includes thrust vector control (TVC) and jet interaction/reaction jet control. There are a number of approaches to unconventional flight control, with considerations including performance, cost, weight, packaging, and the capability for roll control. Unconventional flight control is used when aerodynamic control has either insufficient control effectiveness or an excessive response time. Unconventional flight control is usually augmented by aerodynamic control for flight at higher dynamic pressure. Fixed surfaces used with unconventional flight control include tails (three or more), tails plus canards/strakes, and tails plus wings.

Wing, stabilizer, and control surface integration alternatives are shown in Fig. 2.22 for a number of surfaces (two to eight), folding arrangements (folded, wraparound, switchblade), control surface deflection (all movable, flap control), and tandem surface orientation (interdigitated, inline). Note that at least three tail surfaces are required for static stability. For wing and control surfaces, four surfaces are typical, consistent with skid-to-turn maneuvering. For bank-to-turn maneuvering missiles, two wing surfaces are usually used with at least three tail surfaces. If more than six tail surfaces are used, the reasons are often due to either a span limit imposed by launch platform integration or to an attempt to reduce the rolling moment due to vortices.



Note: Eight tails are usually free-to-roll pitch / yaw stabilizers, with low induced roll.

Fig. 2.22 Surface arrangement alternatives.

Surfaces may be folded to reduce the span requirement for compressed carriage integration with the launch platform. A folded surface usually has a ballistic actuator that deploys the surface after separation from the launch platform. The AGM-86 cruise missile has folded tail surfaces for flight control. Another approach to compressed carriage is wraparound surfaces. These are particularly suited for tube launch. A third approach is switchblade surfaces. The switchblade surfaces are stored inside the missile prior to launch. After separation of the missile from the launch platform, the surfaces are deployed. The BGM-109 Tomahawk cruise missile has switchblade wings. Finally, reduced span surfaces that are not folded provide compressed carriage. An example is the compressed carriage AMRAAM.

Alternatives for the location of the flight control actuators are near the aerodynamic center of the surface (all movable control) or near the trailing edge of the surface (flap control). All movable control has advantages of lower hinge moment and lower drag. Flap control has advantages of a stable hinge moment and generally has a lower radar cross section.

Tandem surfaces include canard-tail and wing-tail planforms. Alternative orientations of the surfaces are inline or interdigitated. Inline surfaces are usually preferred because of lower drag and radar cross section (RCS).

Advantages and disadvantages of tail control are illustrated in Fig. 2.23. Advantages of tail control include an efficient packaging of the subsystems around a blast tube, a low hinge moment and a low actuator torque because of the small local angle of attack, and a low induced rolling moment because the vortices shed by tail deflection trail behind the missile. Note from the figure that, for a statically stable tail control missile, the control surface deflection to trim the missile reduces the local angle of attack at the control surface. A disadvantage of tail control is

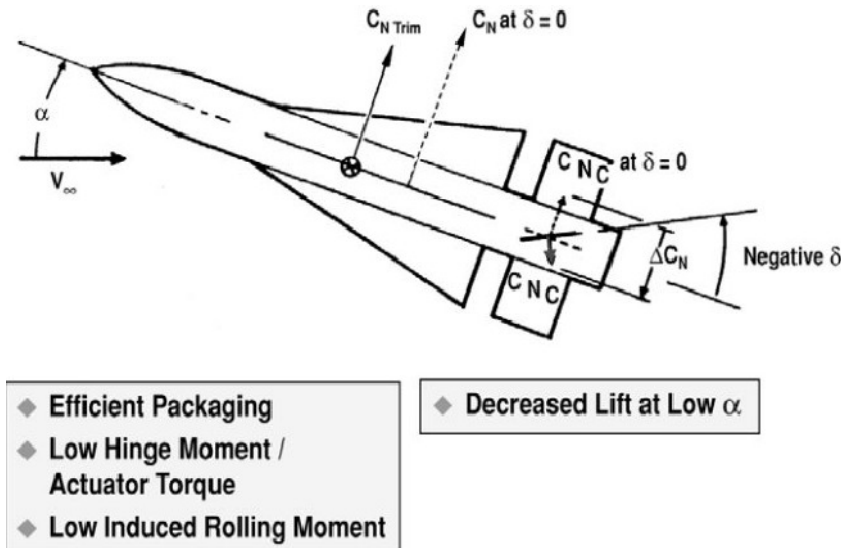


Fig. 2.23 Tail control missile is efficient at high angle of attack.

decreased lift for a statically stable missile, because of the negative incremental lift from the control surface deflection. As shown in the figure, for a statically stable tail control missile, the control deflection force is opposite that of the force on the body. Conversely, for a statically unstable missile, the control deflection force adds to the force on the body.

For a statically stable missile, tail control is usually more effective than a single canard control at high angle of attack. As shown in Fig. 2.24, the deflection of the tail to trim the missile reduces the local angle of attack at the tail. As a result the tail can be deflected to a high deflection angle without stall. In the case of single

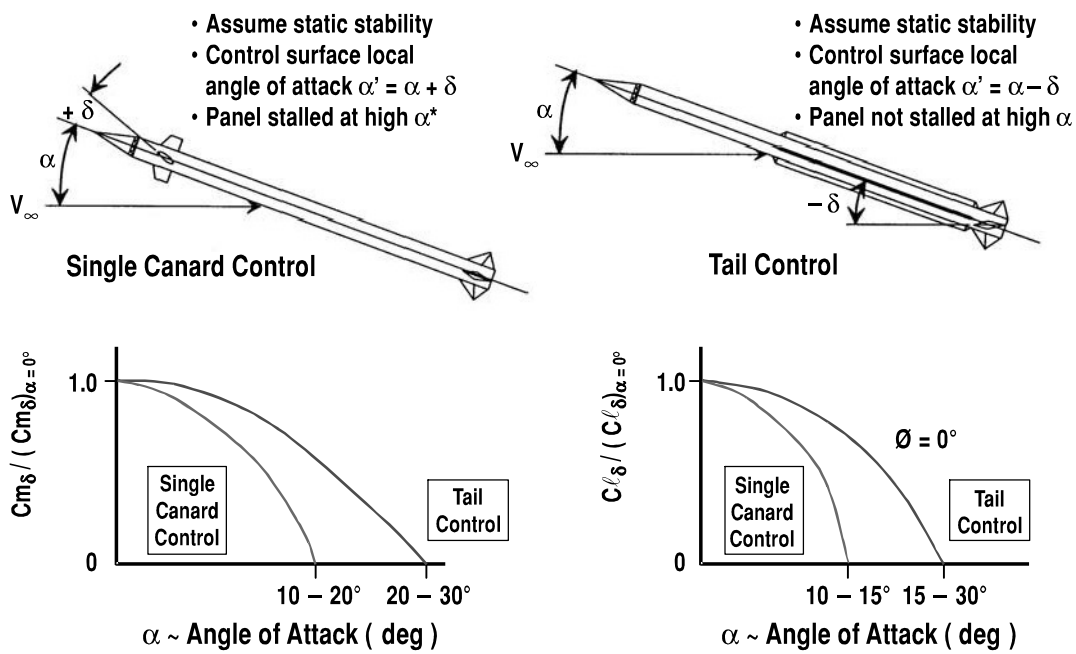


Fig. 2.24 Tail control is more effective than single canard control at high angle of attack.

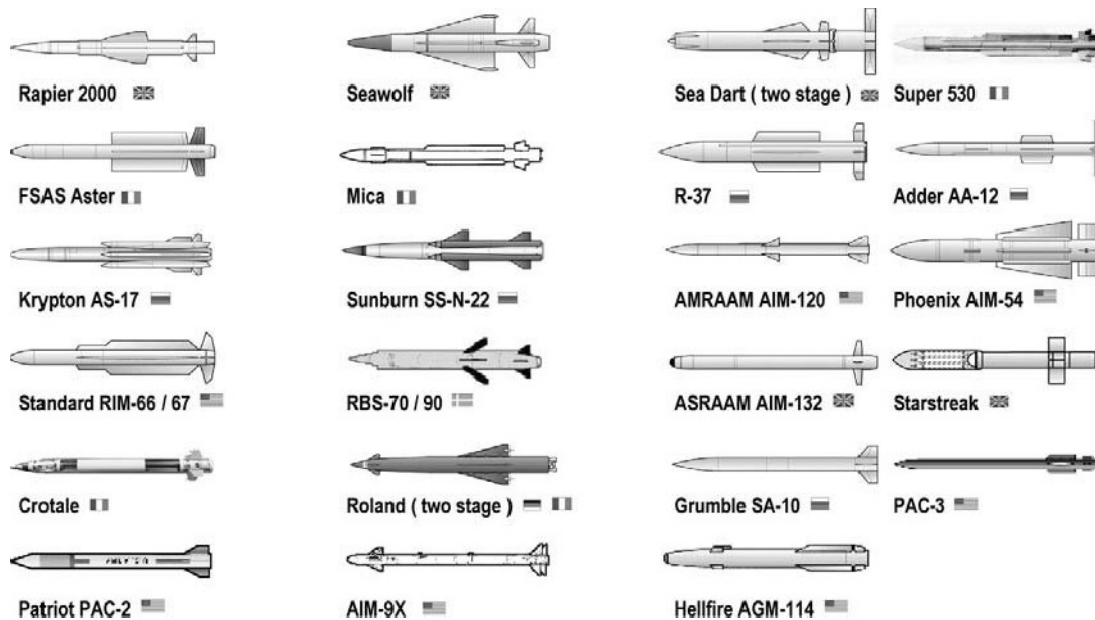


Fig. 2.25 Most tail control missiles have wings (used with permission of Missile Index, 1997, online at <http://www.index.ne.jp/missile-e/>).

canard control, the deflection of the canard to trim the missile increases the local angle of attack at the canard. The canard can be deflected only to relatively small angles before stalling. Also, the vortices shed by the canard can interact with the tail, resulting in a loss of roll control and large induced roll.

Note that a fixed forward surface in front of the movable canard (such as the split canards of Python 4) alleviates the problems of stall, loss of roll control, and induced roll at high angle of attack. Also, free-to-roll tails (such as the free-to-roll tails of Python 4) alleviate the problems of loss of roll control and induced roll at high angle of attack. The Python 4 free-to-roll tails are mounted on bearings that are decoupled from the airframe. Finally, a statically unstable missile alleviates the problem of stall. The required deflection of the canard for trim is opposite the angle of attack, reducing the local angle of attack at the canard.

Most tail control missiles also have wings for greater aerodynamic efficiency L/D and higher maneuverability. Shown in Fig. 2.25 are examples of operational missiles that have tail control. Of the 23 examples, 18 have wings and four are wingless. The wingless tail control missiles shown in the figure generally have less maneuverability at subsonic Mach number than the tail control missiles with wings. An exception is the wingless tail control AIM-9X, which also uses unconventional control to augment tail control.

An example of a new aeromechanics technology is lattice tail control. Lattice fins have advantages of lower hinge moment and higher control effectiveness at supersonic Mach number. Figure 2.26 shows a comparison of lattice tail control with two conventional approaches to tail control, all movable surface control and flap control. Except for radar cross section, lattice tail control has good-to-superior performance for supersonic missiles. RCS is particularly high when there is a resonance of a lattice dimension with the radar wavelength. For example, a lattice with individual compartments of $1 \times 1 \times 1$ in. will have high RCS if it is illuminated by an X-band (10 GHz frequency or 1-in. wavelength) radar. Also shown in the

Type of Tail Control	Control Effectiveness	Drag	Hinge Moment	RCS
◆ All Movable Surface (Example: ASRAAM AIM-132)	●	●	●	●
◆ Movable Flap (Example: Hellfire AGM-114)	○	●	—	●
◆ Lattice (Example: Adder AA-12)	●	●	●	—

Note: ● Superior ○ Good ○ Average — Poor

Fig. 2.26 Tail control alternatives: all movable surface, movable flap, and lattice.

figure are examples of supersonic missiles with the tail control alternatives of lattice tail control (Adder AA-12), all movable surface tail control (ASRAAM AIM-132), and flap tail control (Hellfire AGM-114). The smaller chord length of lattice control results in less variation in the location of the center of pressure of the tail and a lower hinge moment.

Lattice fins, such as the fin shown in the top right section of Fig. 2.27, are most appropriate for either subsonic or high supersonic missiles. The bottom right section of the figure shows the flow through the lattice at a transonic, a low supersonic, and a high supersonic Mach number. At subsonic Mach number the drag of lattice fins is comparable to that of traditional flight control. At transonic Mach number lattice fins have higher drag and lower control effectiveness than traditional flight control. At a low transonic freestream Mach number less than 1, the local

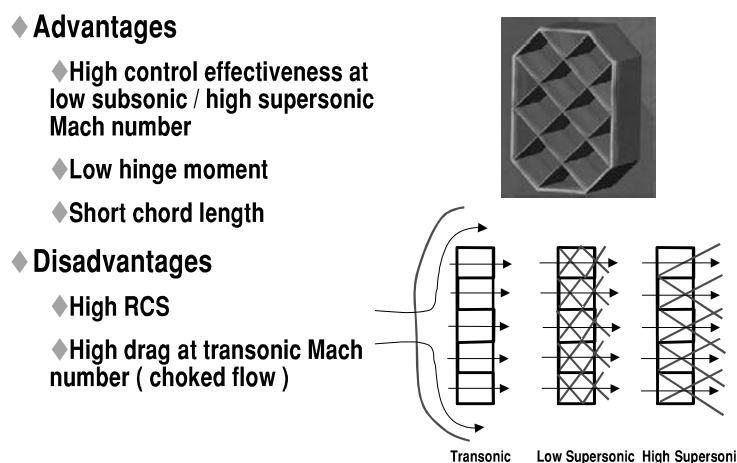


Fig. 2.27 Lattice fins have advantages for low subsonic and high supersonic missiles.

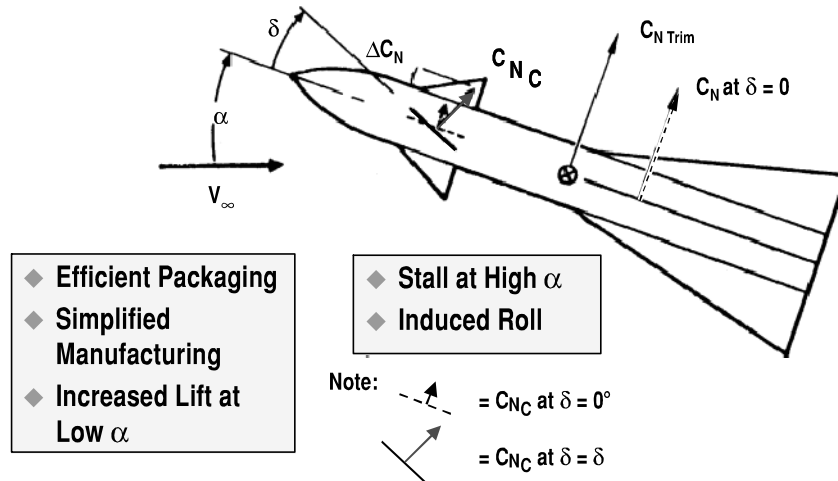


Fig. 2.28 Single canard control missile is most efficient at low angle of attack.

flow through the lattice can accelerate to Mach 1, choking the flow. For a transonic freestream Mach number slightly greater than 1, the flow through the lattice remains choked. A detached, normal shock wave in front of the lattice spills excess air around the lattice. The lattice remains choked until the supersonic Mach number is sufficiently high to allow the lattice to swallow the shock. An oblique shock is then formed on each leading edge of the surfaces of the lattice. At low supersonic Mach number, the oblique shock of each leading edge is large, and the oblique shocks are reflected downstream, off the lattice surfaces. The large number of reflected shocks results in a relatively high drag. At higher Mach number the oblique shock angle of each leading edge is smaller, passing through the lattice without intersecting a lattice surface. In summary, lattice fins have their best application at low subsonic and high supersonic Mach number, where they have low drag and high control effectiveness.

The leading edges of the lattice can be thin because of the efficiency of the box structure. The small thickness provides low drag.

Figure 2.28 shows the advantages and disadvantages of single canard control. Advantages of canard control include 1) efficient packaging of the guidance, navigation, and control subsystems in the same location, 2) simplified manufacturing and ease of integration of the guidance, navigation, and control subsystems, and 3) for a statically stable missile, increased lift at low angle of attack. The figure illustrates the incremental normal force to trim the missile, providing additional lift. Disadvantages of single canard control include 1) a tendency to stall at high angles of attack for a statically stable missile and 2) a large induced roll at high angles of attack. As noted previously, these problems are alleviated by the use of split canards and free-to-roll tails.

Shown in Fig. 2.29 are examples of operational missiles that have canard control and are also wingless. Most canard control missiles do not have wings because 1) the additional surface area of the canard and the larger tail required for stability usually provide sufficient aerodynamic efficiency L/D and maneuverability and the 2) vortex shedding from the canard makes it difficult to integrate a wing. Because of the location of the canard forward of the center of gravity, the canard is destabilizing, requiring a larger tail for stability. Shown in the figure are 12

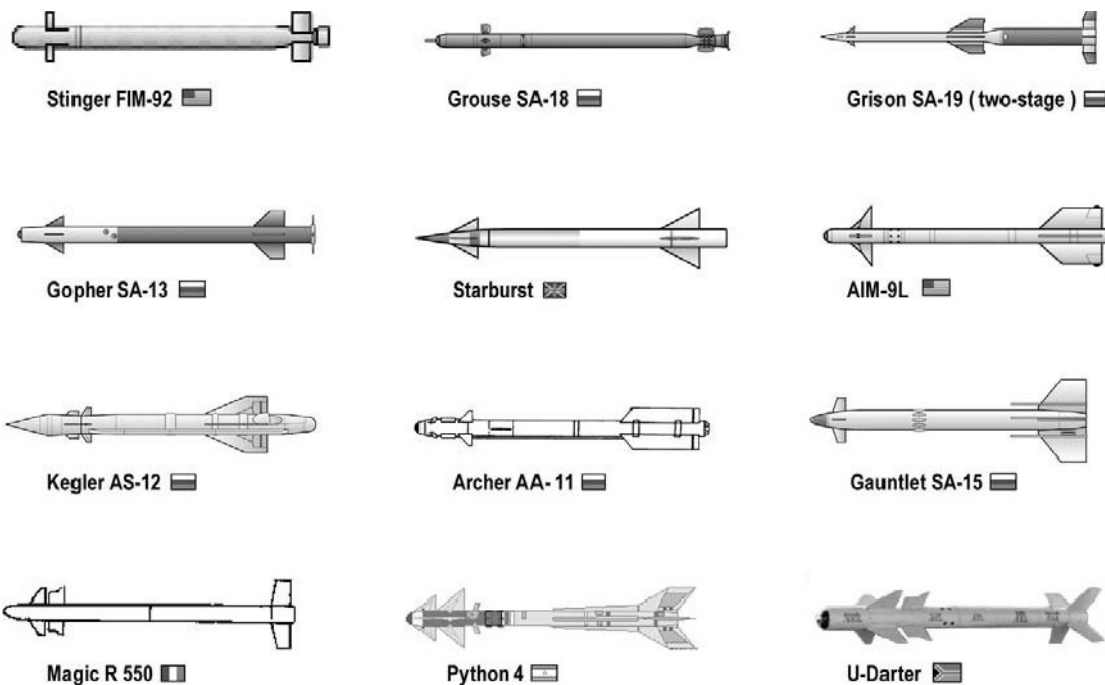


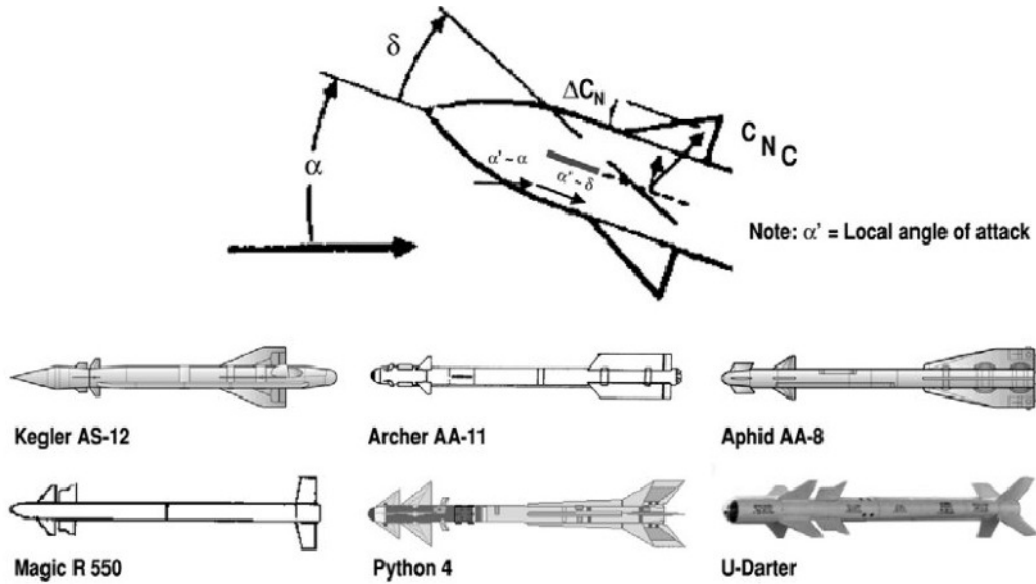
Fig. 2.29 Most canard control missiles are wingless (used with permission of Missile Index, 1997, online at <http://www.index.ne.jp/missile-e/>).

operational wingless missiles that use canard control. Except for the Kegler AS-12, 11 of the 12 wingless canard control missiles in the figure are air intercept missiles (SAM or AAM).

A split canard has a smaller local angle of attack, enhancing the maneuverability at high angle of attack. Modern highly maneuverable missiles use split canards for flight control. Split canard control has a fixed surface in front of the movable canard. Shown in Fig. 2.30 is a schematic of the local flow that illustrates the advantage of split canards. The incremental normal force coefficient ΔC_N in the figure is the difference between the normal force coefficient of the deflected control surface and the normal force coefficient of an undeflected control surface. Note that the forward surface reduces the local effective angle of attack α' . Because the trailing canard control surface has a smaller local angle of attack, it is more effective at higher control surface deflection δ and higher angle of attack α , operating without stall. All modern canard control missiles use split canard control, including Kegler AS-12, Archer AA-11, Aphid AA-8, Magic R-550, Python 4, and U-Darter.

Figure 2.31 shows advantages and disadvantages of wing control. The advantages of wing control are few and the disadvantages are many. An advantage of wing control is that only a small body rotation is required to maneuver. This results in smaller seeker tracking error due to dome error slope. A second advantage is fast response for maneuverability, particularly for skid-to-turn maneuvers. As shown in the figure, most of the missile lift is derived from deflecting the wing. Because the wing can usually be deflected faster than body rotation, the time required to achieve maneuver g is shorter.

One disadvantage of wing control is the limited space available for packaging of the large actuators. For a high performance missile, the wing may be located over the motor case. Another disadvantage is the larger hinge moment required



Note: Forward fixed surface reduces local angle-of-attack for movable canard, providing higher stall angle of attack.
 Python 4 has free-to-roll tails to alleviate induced roll at high α .

Fig. 2.30 Missiles with split canards have enhanced maneuverability at high angle of attack.

to deflect the wing. A third disadvantage is that the wing must be larger. It must be sized for maneuverability in addition to aerodynamic efficiency L/D . A fourth disadvantage is the large induced roll produced by the wing.

The strong vortex shedding for a wing control missile often has adverse effects on missile stability and control. Figure 2.32 illustrates wing and body vortex shedding for a body-wing-tail configuration at high angle of attack [see Nielsen Engineering & Research (NEAR) Aerodynamic Software Products online at <http://www.NEAR.com>].

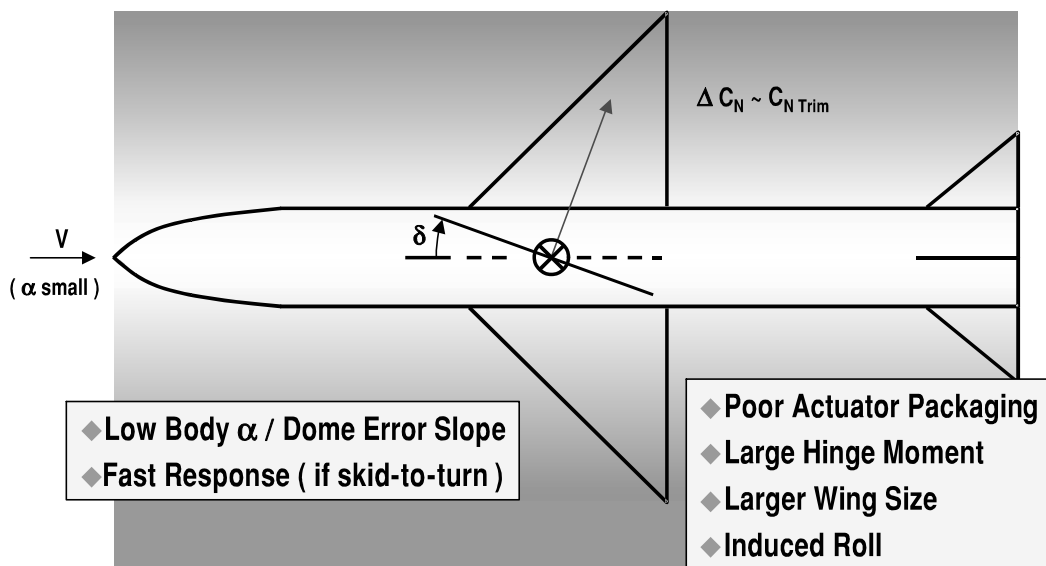


Fig. 2.31 Wing control missile requires less body rotation but also has higher induced roll.

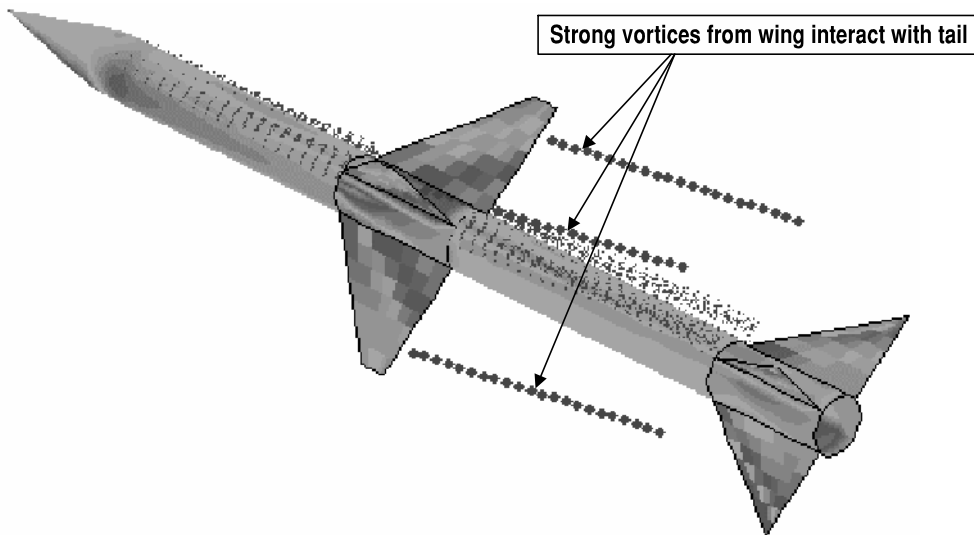


Fig. 2.32 Wing control missile has high vortex shedding [used with permission of Nielsen Engineering & Research (NEAR) Aerodynamic Software Products online at <http://www.nearinc.com/near/software.htm>].

[nearinc.com/near/software.htm](http://www.nearinc.com/near/software.htm)]. As shown in the figure, wing vortices are shed near the wing tips, trailing back with the free stream. Body vortices are shed near the nose center of pressure, approximately two-thirds of the length of the nose. At high angles of attack, additional body vortices may be shed from the cylindrical body downstream of the nose. Surfaces aft of the wing, particularly aft surfaces with a span comparable to that of the wing, are susceptible to the strong vortices shed from the wing, and the missile may have large adverse induced roll, a loss in stability, and a loss in control effectiveness.

Examples of operational missiles that use wing control are shown in Fig. 2.33. Note that the wings are generally large and located near the center of gravity. The configurations of Skyflash, HARM, and Aspide are similar to that of the Sparrow missile developed in 1956. The AA-10/R-27 Alamo configuration is different from

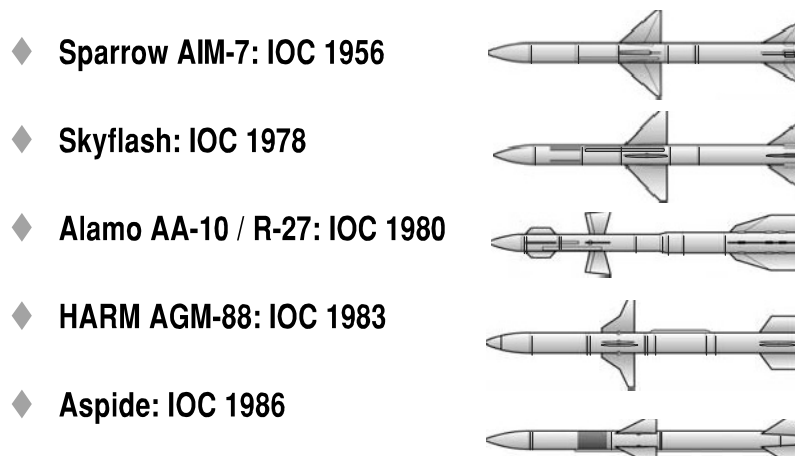


Fig. 2.33 Most wing control missiles are older technology (used with permission of Missile Index, 1997, online at <http://www.index.ne.jp/missile-e/>).

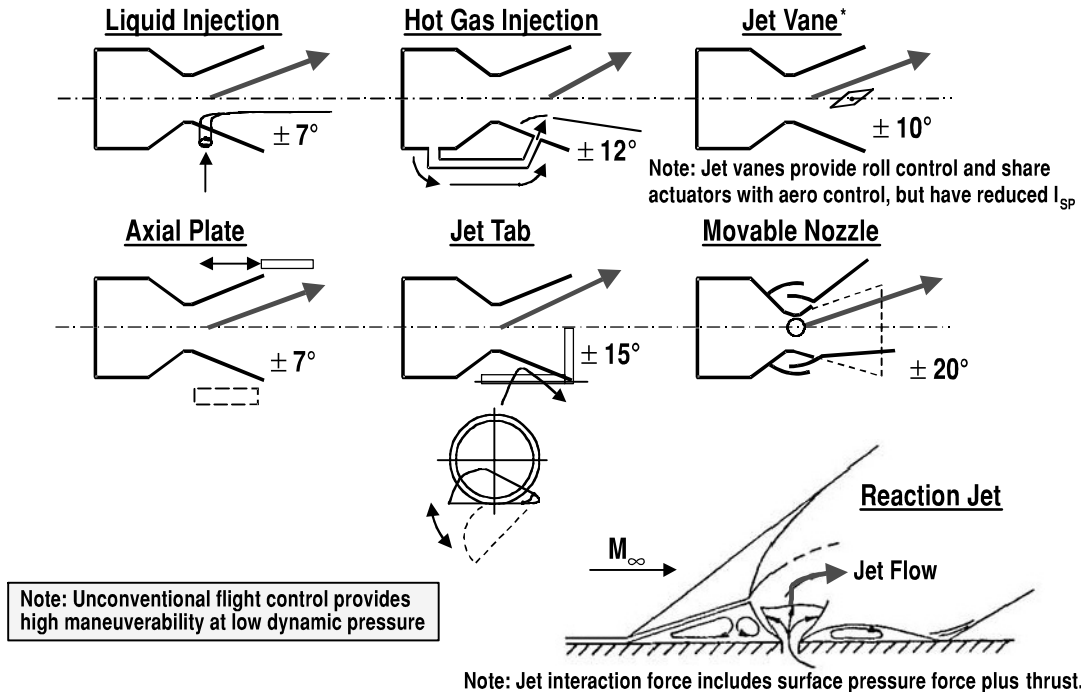


Fig. 2.34 Alternatives for unconventional flight control.

the Sparrow, with a fixed forward strake surface and a forward swept movable wing. The Alamo geometry of body-strake-movable wing-tail has complex vortex shedding at high angle of attack from the body and the multiple surfaces.

A wing control missile has not been developed in recent years because of deficiencies such as actuator packaging, hinge moment, wing size, and induced roll. Modern missiles use tail, canard, or unconventional flight control. Although the wing control Sparrow has been largely replaced by the tail control AMRAAM as a preferred medium-range air-to-air missile, the Sparrow was selected as a rocket baseline for this text because of the availability of unclassified data for the Sparrow missile.

Alternative approaches to unconventional flight control are shown in Fig. 2.34. The figure is a schematic of seven different types of unconventional flight control. It also shows a relative deflection of the thrust for each of the flight control types. Liquid injection TVC uses a fluid such as freon, injected normal to the local stream, which causes a bow shock wave inside the nozzle. Deflection is on the order of $+/-7$ deg. Another type is hot gas injection TVC, which ducts hot gas products from the motor chamber into the nozzle. Hot gas injection has high deflection, although there may be problems for the high-temperature valves, which must operate with gas products up to 5500°F . A third type is jet vanes, which are control surfaces inside the nozzle. Jet vanes have an advantage in that differential deflection also provides roll control. However, jet vanes are continually exposed to the rocket exhaust plume, providing a loss in specific impulse even if they are not deflected. Axial plate thrust vector control is a fourth type, consisting of a plate that extends back and forth. When the plate is fully extended, the plume attaches to the plate because of the Coanda effect. A fifth type is jet tabs, which are simple devices that switch in and out of the plume. The jet tab sets up a bow shock inside the nozzle, similar to that of liquid injection thrust vector control. A sixth type of thrust

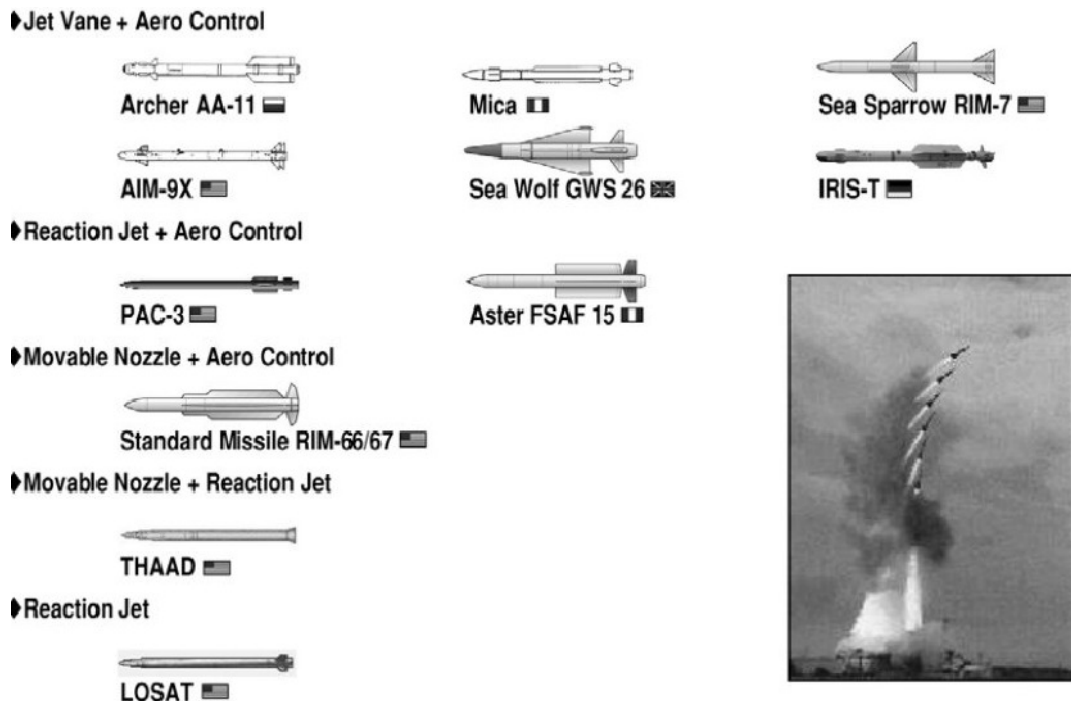


Fig. 2.35 Most missiles with unconventional flight control also use aerodynamic control.

vector control is movable nozzle. Although movable nozzle TVC is often used with strategic ballistic missiles, its application in tactical missiles, because of its high cost, is primarily limited to expensive, high-performance missiles such as Standard Missile and THAAD. A seventh type of unconventional flight control is reaction jet control. Reaction jet control operates on the free stream air. The total force is a combination of the thrust force and the jet interaction force. The jet interaction force results from the pressure distribution on the airframe surface. As illustrated in the figure, the free stream flow separates from the airframe surface because of the obstruction of the jet. This causes a higher local pressure in the separated flow region in front of the nozzle and a lower local pressure in the separated flow region behind the nozzle. Although the jet interaction force usually augments the thrust force, there is relatively high uncertainty and risk in the magnitude of the jet interaction force.

Most unconventional flight control provides higher maneuverability and faster response. It is especially suited for short duration operation to enhance the maneuverability and response of aerodynamic control. Cost, weight, subsystem packaging, risk, and the capability for roll control are design considerations.

Shown in Fig. 2.35 are examples of operational missiles that use unconventional flight control. Jet vane plus aerodynamic control is the most popular type of thrust vector control. Examples of missiles that use jet vane plus aerodynamic control include the Russian Archer AA-11, the French Mica, the U.S. Sea Sparrow RIM-7 and Sidewinder AIM-9X, the U.K. Seawolf GWS 26, and the German IRIS-T. Jet vanes provide large off-boresight maneuvering after launch, whereas aerodynamic control provides terminal maneuvering after motor burnout. Jet vanes must be constructed from materials with a very high temperature capability, such as tungsten or carbon-carbon.

Two examples of missiles that use reaction jet plus aerodynamic control are the U.S. PAC-3 and the French Aster FSAF 15 surface-to-air missile defense missiles. Reaction jets are usually used for hit-to-kill antimissile missiles because reaction jets have a smaller time constant (\sim milliseconds) than thrust vector control, providing smaller miss distance.

The Standard Missile RIM-66/67 uses movable nozzle TVC for launch stabilization and off-boresight maneuverability. Aerodynamic control provides terminal maneuvering. Examples of missiles that do not use aerodynamic control are THAAD and LOSAT. THAAD uses movable nozzle TVC for launch stabilization and off-boresight maneuverability. LOSAT uses only reaction jet control. Reaction jet control provides hit-to-kill accuracy and terminal maneuvering.

Shown in the bottom right of Fig. 2.35 is a launch flight trajectory of the Aster FSAF 15. Note the high maneuverability and rapid heading change following launch.

2.11 Maneuver Alternatives

Figure 2.36 compares missile maneuver alternatives of skid-to-turn maneuvering, bank-to-turn maneuvering, and rolling airframe maneuvering. Bank-to-turn maneuvering is a relatively new technology for tactical missiles. Missiles using bank-to-turn maneuvering will first roll until the wings or the major axis of a lifting body are oriented perpendicular to the target line of sight. Following the roll maneuver, the missile then maneuvers in pitch, maintaining the preferred roll orientation. A benefit of bank-to-turn maneuvering is higher maneuverability for a lifting body with noncircular cross section or for a missile with wings. Another benefit is a smaller sideslip angle for missiles with inlets. Bank-to-turn maneuvering is particularly suited for midcourse guidance maneuvers prior to

- ◆ **Skid-To-Turn (STT)**
 - Advantage: Fast response
 - Features
 - No roll commands from autopilot
 - Works best for axisymmetric cruciform missiles
- ◆ **Bank-To-Turn (BTT)**
 - Advantage: Provides higher maneuverability for wings, noncircular / lifting bodies, and airbreathers
 - Disadvantages
 - Time to roll
 - Requires fast roll rate
 - May have higher dome error slope
 - Features
 - Roll attitude commands from autopilot
 - Small sideslip
- ◆ **Rolling airframe (RA)**
 - Advantage: Requires only two sets of gyros / accelerometers / actuators
 - Disadvantages
 - Reduced maneuverability
 - Potential for roll resonance
 - Features
 - Aileron bias / constant roll rate command from auto pilot
 - Can use impulse steering
 - Compensates for thrust offset

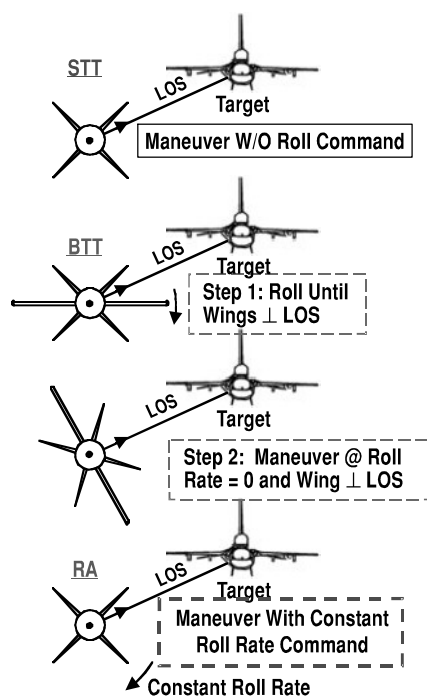


Fig. 2.36 Maneuver law alternatives.

seeker lock-on to the target. A disadvantage of bank-to-turn maneuvering is slower response in terminal maneuvers that could degrade guidance accuracy, increasing the missile miss distance. Alternative approaches to alleviate this problem include faster actuators for roll control, faceted or multilens dome, and switching from bank-to-turn maneuvering to skid-to-turn maneuvering for terminal flight. Bank-to-turn missiles may also have higher dome error slope, because the seeker looks through a dome with large variation in radial angle in addition to the variation in off-boresight angle.

Most missiles use skid-to-turn maneuvering. Skid-to-turn maneuvering is particularly applicable to axisymmetric, cruciform missiles with low aspect ratio surfaces. As shown in the figure, a skid-to-turn maneuver is a commanded maneuver along the line of sight of the seeker without rolling. An advantage of skid-to-turn maneuvering is fast response because the maneuver is immediately made along the line of sight without delay.

A third type of maneuver is the rolling airframe maneuver. Rolling airframe maneuvering is similar to skid-to-turn maneuvering except the missile also has a roll control bias input to provide continuous roll rate. Advantages of rolling airframe missiles include lower cost because of the requirement for fewer flight control gyros, accelerometers, and actuators; lower volume requirement to package less flight control hardware; compensation for thrust misalignment; and compatibility with reaction jet impulse control. The 5-in.-diam rolling airframe missile (RAM) and the 2.75-in.-diam Stinger missile are examples of rolling airframe missiles. RAM and Stinger missiles use two-axis flight control, requiring less flight control hardware packaging within the small diameter. Disadvantages of rolling airframe missiles include reduced maneuverability from using fewer controls and susceptibility to roll-pitch-yaw cross coupling instability. Roll-pitch-yaw cross coupling tends to occur from roll resonance when the roll rate is comparable to the missile natural frequency in pitch or yaw. Note that the miss distance due to the seeker dome error slope may be reduced due to the averaging effect of roll rate. However, the miss distance may also be increased due to susceptibility to roll resonance.

Twin inlet and chin inlet ramjets usually require bank-to-turn maneuvering to avoid loss of inlet efficiency due to sideslip. Figure 2.37 shows examples of ramjet missiles that use bank-to-turn maneuvering. The French ASMP is an example of an operational ramjet missile with twin axisymmetric inlets that are separated by a radial angle of 180 deg. Also shown are two configurations of the Future Medium-Range Air-to-Air Missile (FMRAAM) as examples of developmental missiles with twin two-dimensional inlets. The inlets are in tandem with the two bottom cruciform tails and are separated by a radial angle of 90 deg. A major difference between the U.S. FMRAAM and the U.K. FMRAAM (Meteor) is the propulsion system. The U.S. FMRAAM engine is a liquid hydrocarbon fuel ramjet. An advantage of a liquid fuel ramjet is a low observable plume. The Meteor engine is a variable flow boron fuel ducted rocket. An advantage of a ducted rocket is simpler logistics and higher acceleration capability. Finally, shown in the bottom of the figure is an example of a developmental ramjet missile with a chin inlet, the U.S. Advanced Strategic Air Launched Missile (ASALM). The ASALM uses angle of attack α and angle of sideslip β feedback in the flight control system to provide a coordinated turn in bank-to-turn maneuvering. The ASALM was selected

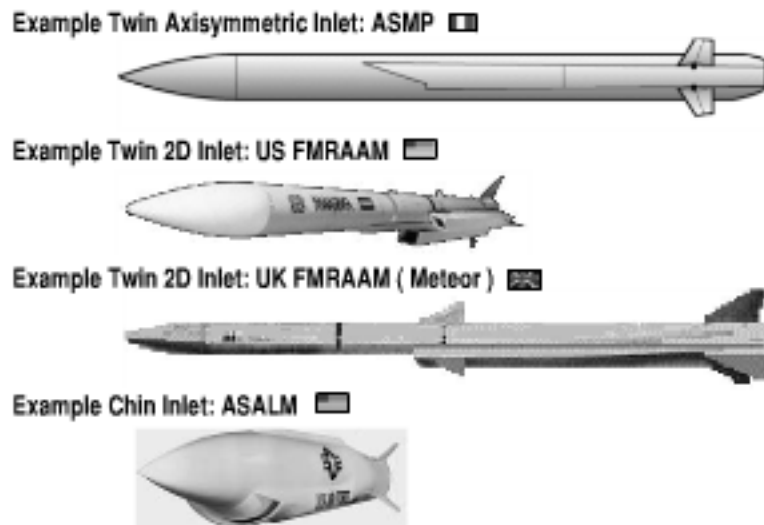


Fig. 2.37 Twin inlet and chin inlet ramjets usually require bank-to-turn maneuvering.

as a ramjet baseline for this text because of the availability of unclassified data and its high performance.

2.12 Roll Orientation

Figure 2.38 compares roll attitude and maneuver control deflection alternatives. Approaches to symmetric roll orientation during missile flight, with no induced roll, are + and \times orientations. Each has advantages and disadvantages. The + configuration has the simplest control mechanization. For pitch command, two surfaces provide normal force into the pitch direction. Similarly for yaw command, two surfaces provide side force into the yaw direction. For roll command, all four surfaces are deflected clockwise to provide clockwise roll and counterclockwise to provide counterclockwise roll. The + configuration usually has an advantage of lower trim drag. A disadvantage is that it usually has a statically unstable rolling moment derivative ($C_{l\phi} > 0$).

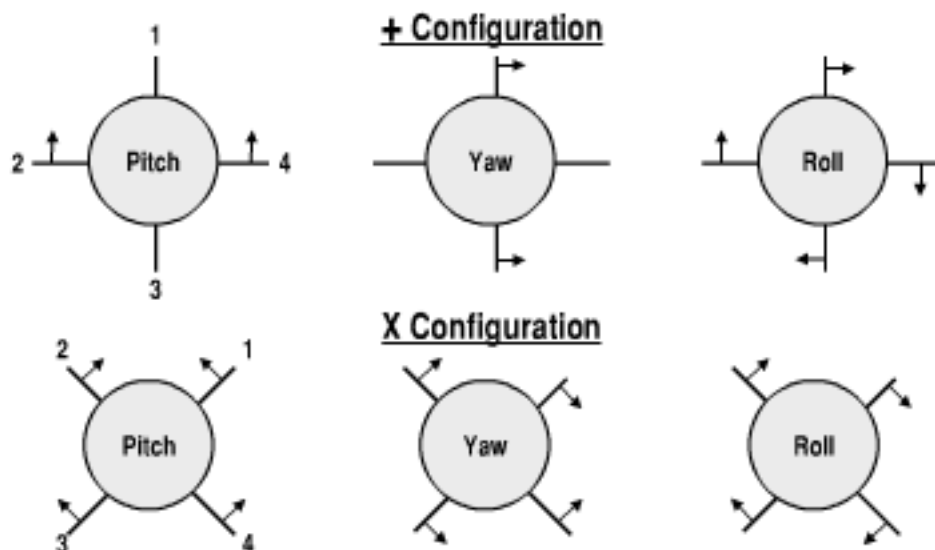


Fig. 2.38 Roll attitude and maneuver control deflection alternatives.

An alternative approach of the x configuration during missile flight is somewhat more complex in its control mechanization. For pitch command all four surfaces are deflected to provide normal force without side force. For yaw command all four surfaces are deflected to provide side force without normal force. The roll command is similar to that of the + configuration. For roll control all four surfaces are deflected clockwise to provide clockwise roll and counterclockwise to provide counterclockwise roll. The x configuration often has advantages of better fit for launch platform compatibility, higher aerodynamic efficiency L/D , and a statically stable rolling moment derivative ($C_{l\delta} < 0$).

2.13 Static Stability

Static stability in pitch is defined by the slope of the pitching moment vs angle of attack. Shown in the top left portion of Fig. 2.39 is an example of the pitching moment coefficient vs angle of attack curve for a statically stable missile. For a statically stable missile, the slope of the pitching moment coefficient vs angle of attack is negative. An increase in angle of attack (nose up) causes a negative incremental pitching moment (nose down), which then tends to decrease the angle of attack. Control surface deflections allow the missile to trim ($C_m = 0$) at the desired angle of attack. The bottom left portion of the figure shows the decay of an incremental disturbance in the angle of attack as a function of time. It assumes a statically stable missile without an autopilot correction. For a highly stable, highly damped missile, the convergence is usually nonoscillatory. Most missiles have small tail surfaces and small static margin, and they are lightly damped in free flight without autopilot feedback (e.g., unguided flight trajectory during store separation). The lightly damped missiles have an oscillatory convergence from a disturbance in angle of attack. The ideal damping for autopilot feedback is $\zeta \approx 0.7$.

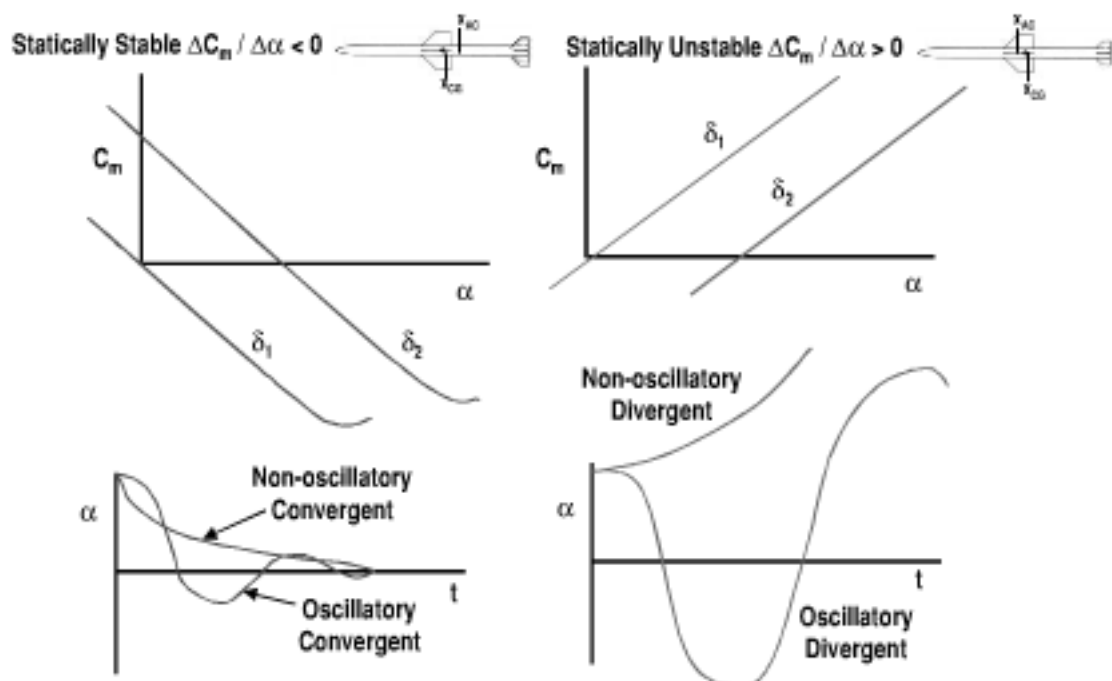


Fig. 2.39 $\Delta C_m / \Delta \alpha$ defines static stability.

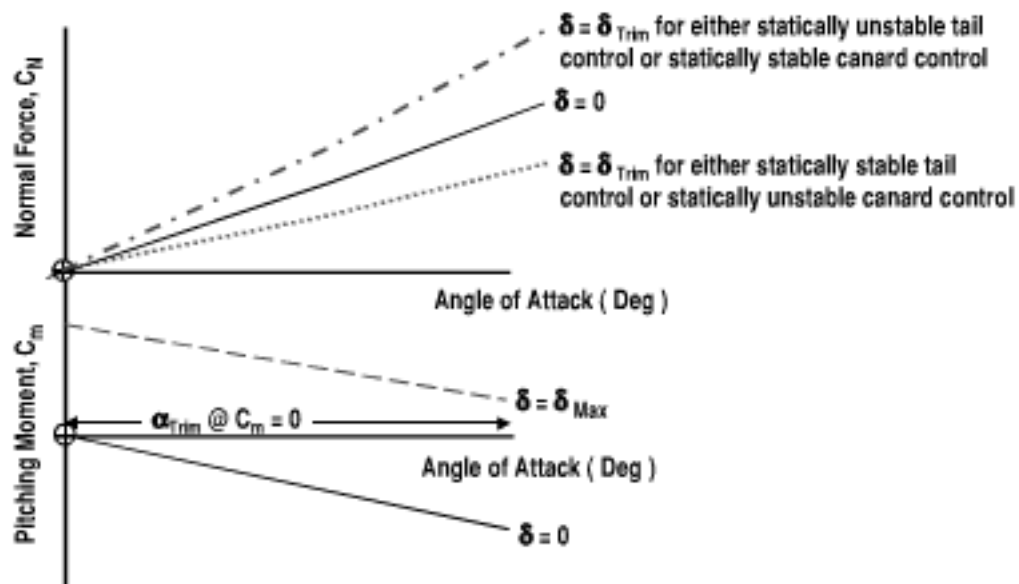


Fig. 2.40 Trimmed normal force is defined at zero pitching moment.

As shown in the upper right of the figure, a statically unstable missile has the opposite trend. The slope of the pitching moment coefficient vs angle of attack is positive. An increase in angle of attack causes an increase in pitching moment, which tends to cause a further increase in angle of attack. If the autopilot is sufficiently fast, it is possible to trim and control a statically unstable missile. A statically unstable missile might be desirable to improve responsiveness and maneuverability. The bottom right portion of the figure shows the divergence of a statically unstable missile without an autopilot correction. A highly unstable missile will diverge monotonically. A statically unstable missile that is slightly unstable will tend to oscillate with increasing divergence.

Trim is defined at zero pitching moment. As shown in Fig. 2.40, the normal force at a trimmed flight condition is lower for either a statically stable missile using tail control or a statically unstable missile using canard control. Conversely, the trimmed normal force is higher for a statically unstable missile using tail control or a statically stable missile using canard control. A rule of thumb for conceptual design of a tail or canard control missile is that the change in angle of attack due to control deflection should be greater than one ($|\alpha/\delta| > 1$). Most control surfaces have deflection limits less than $+/-30$ deg; $|\alpha/\delta| > 1$ usually allows a trim angle of attack up to about 30 deg.

Relaxed static margin allows the missile to trim at a higher angle of attack, providing higher maneuverability. Shown in Fig. 2.41 is the benefit of relaxed static stability for the rocket baseline missile. The rocket baseline missile has excessive static margin (e.g., 0.88 diameter at Mach 2), resulting in a relatively low maximum angle of attack and a relatively low maximum trimmed normal force ($C_N = 9$). Reducing the static margin increases the maximum angle of attack and the maximum trimmed normal force. In the example a neutrally stable missile ($\alpha/\delta = \infty$ or static margin = 0) has a 130% increase in maximum angle of attack ($\alpha = 9.4$ to 21.8 deg) and an 80% increase in maximum available normal force ($C_N = 9\text{--}16$).

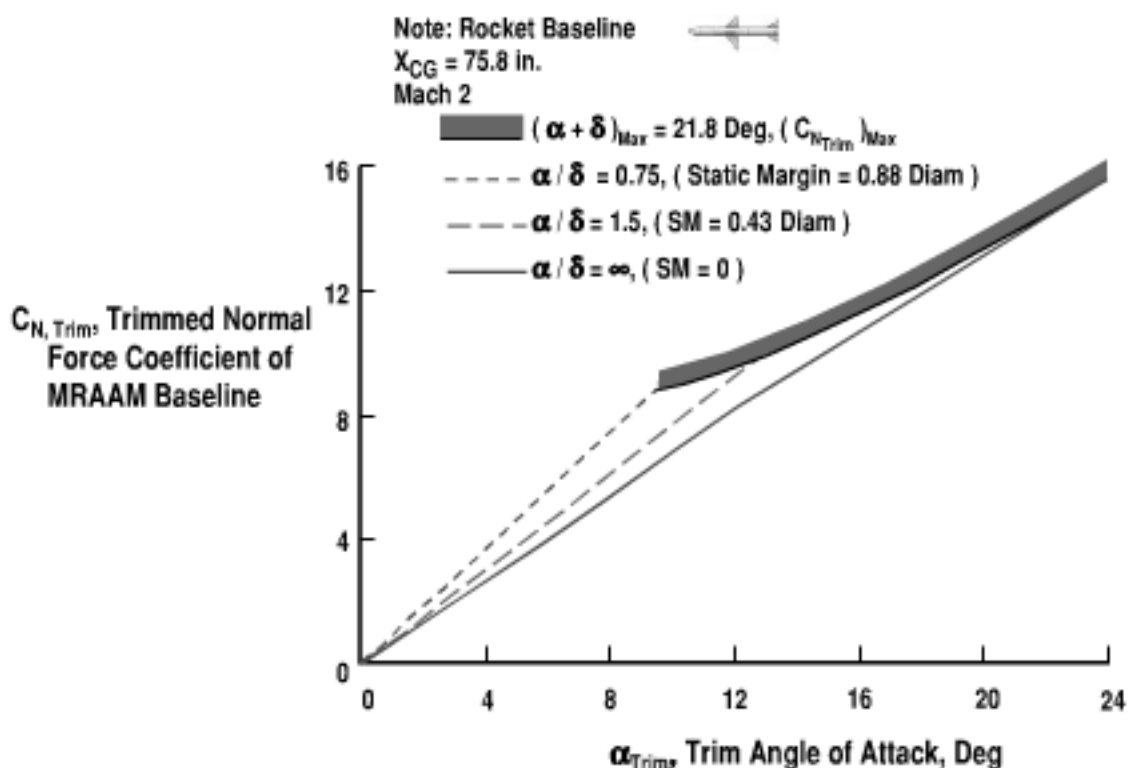


Fig. 2.41 Relaxed static margin allows higher trim angle of attack and higher normal force.

2.14 Tail Area Sizing

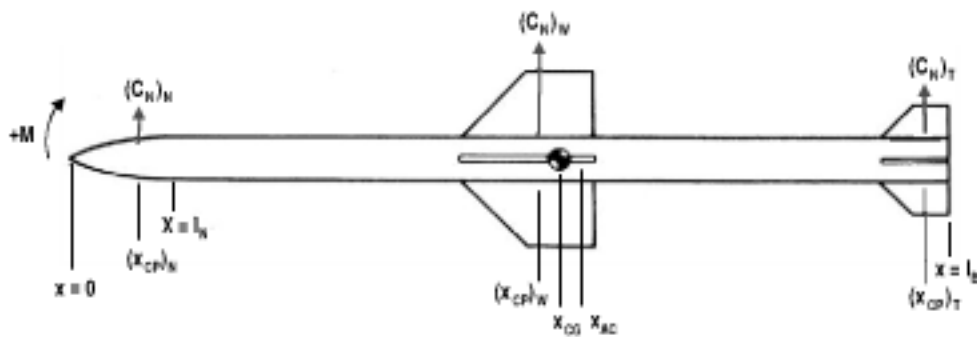
Much of the conceptual design configuration sizing process is oriented toward tail sizing. Because missiles are usually volume limited and the subsystems are of comparable density, the center-of-gravity location is usually near 50% of the length of the missile. Because the nose and any forward surfaces (strakes/canards) are destabilizing, the tails must be sized to provide static stability. Shown in Fig. 2.42 is an example of tail area sizing to meet static margin requirements for a body-wing-tail configuration. The tail contribution to pitching moment stability, provided by the tail normal force effectiveness ($C_{N,\alpha}$)_T (S_T/S_{Ref}) times its moment arm to the center of gravity [$x_{CG} - (x_{CP})_T$], must balance the contributions to pitching moment from the nose and wing. Shown in the figure are equations for the required tail area.

Of particular interest is the required tail area for neutral stability. The equation is

$$S_T = \left\{ (C_{N,\alpha})_N [x_{CG} - (x_{CP})_N]/d + (C_{N,\alpha})_W [(x_{CG} - (x_{CP})_W)/d] (S_W/S_{Ref}) \right\} \\ \times [d/[(x_{CP})_T - x_{CG}]] S_{Ref}/(C_{N,\alpha})_T$$

Note that for a small tail area the wing center of pressure should be located near the center of gravity [$(x_{CP})_W - x_{CG} \approx 0$].

Figure 2.43 shows the required tail area for neutral static margin as a function of Mach number and wing location. Note that the required tail area for neutral static stability must be larger as the Mach number increases toward hypersonic.



$$(C_{N_x})_N \{ [x_{CG} - (x_{CP})_N] / d \} + (C_{N_x})_W \{ [x_{CG} - (x_{CP})_W] / d \} S_W / S_{Ref} + (C_{N_x})_T \{ [x_{CG} - (x_{CP})_T] / d \} S_T / S_{Ref}$$

$$= - [(C_{N_x})_N + (C_{N_x})_W S_W / S_{Ref} + (C_{N_x})_T S_T / S_{Ref}] \{ (x_{AC} - x_{CG}) / d \}$$

Solving for tail area

$$S_T = \{ [(C_{N_x})_N + (C_{N_x})_W S_W / S_{Ref} + (C_{N_x})_T S_T / S_{Ref}] \{ (x_{AC} - x_{CG}) / d \} + (C_{N_x})_N \{ [x_{CG} - (x_{CP})_N] / d \} + (C_{N_x})_W \{ [x_{CG} - (x_{CP})_W] / d \} \}$$

$$\{ (S_W / S_{Ref}) / \{ d / [(x_{CP})_T - x_{CG}] \} \} S_{Ref} / (C_{N_x})_T$$

For neutral stability, $x_{AC} - x_{CG} = 0$

$$S_T = \{ (C_{N_x})_N \{ x_{CG} - (x_{CP})_N \} / d + (C_{N_x})_W \{ x_{CG} - (x_{CP})_W \} / d \} \{ S_W / S_{Ref} \} / \{ d / [(x_{CP})_T - x_{CG}] \} S_{Ref} / (C_{N_x})_T$$

Fig. 2.42 Tail area sizing for desired static margin.

The tail loses its aerodynamic efficiency as Mach number increases. Also note that placing the wing such that its aerodynamic center is forward of the center-of-gravity location is destabilizing, requiring a larger tail area for compensation. The rocket baseline wing aerodynamic center is forward of the center of gravity, and therefore the rocket baseline has a large tail. Placing the wing aft of the center of gravity is stabilizing, allowing a smaller tail area to meet the static margin requirement. It is noted that for a typical missile wing without camber, the location of the wing aerodynamic center is the same as the wing center-of-pressure location.

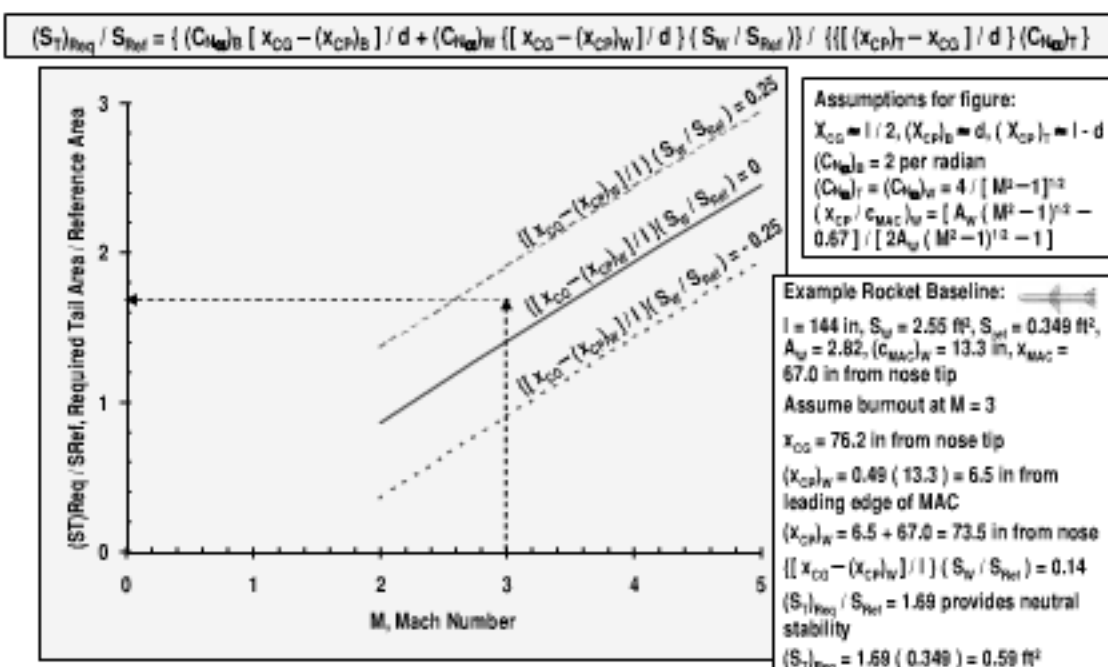


Fig. 2.43 Example of tail area sizing for neutral static stability.

The figure is based on analytical prediction of aerodynamics from slender body theory ($C_{N_a}B = 2/\text{rad}$ and $(x_{CP})_B \approx d$) and linear wing theory [$(C_{N_a})_W$ or $(C_{N_a})_T = 4/(M^2 - 1)^{1/2}$] and $(x_{CP}/c_{MAC})_W = [A_W(M^2 - 1)^{1/2} - 0.67]/[2A_W(M^2 - 1)^{1/2} - 1]$). The moment arm from the tail center-of-pressure location to the missile center of gravity is assumed to be equal to the moment arm from the body (nose) center of pressure location to the center of gravity.

In the example of the rocket baseline at Mach 3, the required tail area must be 0.59 square foot for neutral static stability. The required tail area is 1.69 times the body reference cross sectional area. The actual rocket baseline missile has a tail area that is over four times the reference body cross-sectional area. This is an indication that the rocket baseline missile has excessive static margin from a tail surface area that is too large. Also, the wing center-of-pressure location of the rocket baseline is in front of the missile center of gravity, requiring a larger tail area.

2.15 Stability and Control Conceptual Design Criteria

Stability and control has an impact on the aerodynamic configuration design, particularly tail sizing, and should be considered early in conceptual design. Because tactical missiles tend to have near-neutral static stability, it may be difficult to accurately predict static margin and control effectiveness. Although the actual stability and control derivatives prediction may have large error, it is often possible to size the canard, wing, or tail surfaces with less than 10% error in the surface area. Predicting stability and control derivatives usually requires much iteration as the surfaces are resized and the center-of-gravity location changes during the design convergence. It is helpful to start with baseline missiles, such as the rocket and ramjet baselines in this text, that have a balance of system engineering in their stability and control derivatives. It is also useful to compare stability and control derivatives with conceptual design criteria to facilitate design convergence. Figure 2.44 shows conceptual design criteria for roll cross coupling (rolling

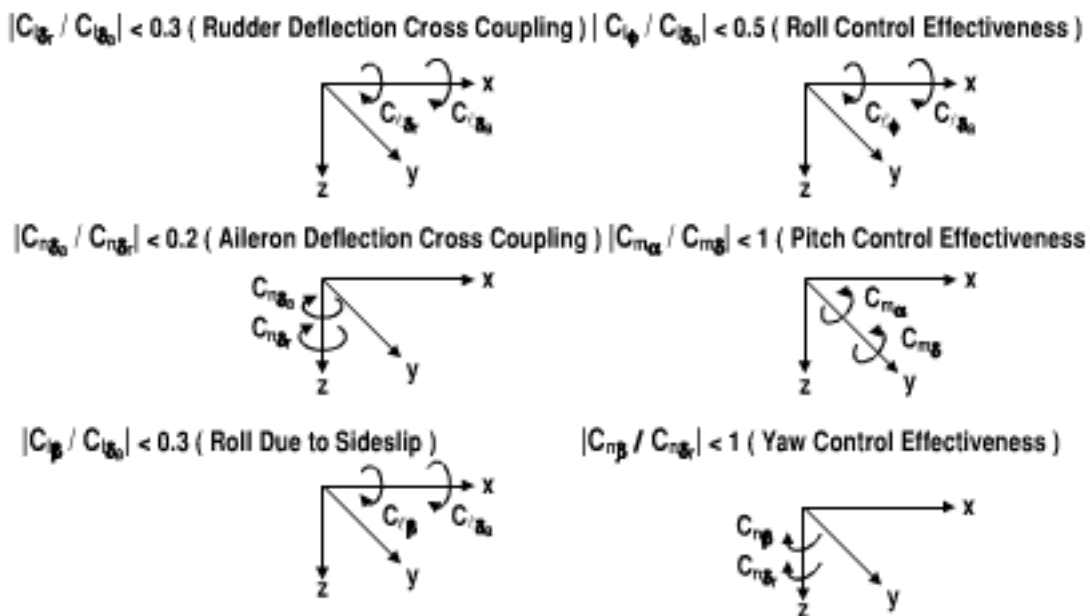


Fig. 2.44 Stability and control derivatives conceptual design criteria.

moment due to rudder deflection C_{l_r}), yaw cross coupling (yawing moment due to aileron deflection $C_{n_{sa}}$), rolling moment due to sideslip C_{l_β} , roll control effectiveness $C_{l_{\alpha_e}}$, pitch control effectiveness C_{m_s} , and yaw control effectiveness $C_{n_{\alpha_e}}$. Stability and control cross coupling or out-of-plane moments should generally be less than 30% of the “pure” in-plane moments to maximize the control power and minimize the time constant for maneuvers. Stability and control conceptual design criteria are as follows:

- 1) $|C_{l_r}| < 0.3 |C_{l_{\alpha_e}}|$, rolling moment due to rudder deflection should be less than 30% of the aileron control effectiveness to have adequate control margin.
- 2) $|C_{n_{sa}}| < 0.2 |C_{n_{\alpha_e}}|$, yawing moment due to aileron deflection should be less than 20% of the rudder control effectiveness to have adequate control margin.
- 3) $|C_{l_\beta}| < 0.3 |C_{l_{\alpha_e}}|$, rolling moment due to sideslip should be less than 30% of the aileron control effectiveness to have adequate control margin.
- 4) $|C_{l_\phi}| < 0.5 |C_{l_{\alpha_e}}|$, rolling moment due to roll attitude should be less than 50% of the aileron control effectiveness to have adequate control margin.
- 5) $|C_{m_s}| < C_{m_s}$, pitching moment due to angle of attack should be less than the elevator control effectiveness to have adequate control margin.
- 6) $|C_{n_\beta}| < |C_{n_{\alpha_e}}|$, yawing moment due to sideslip should be less than the rudder control effectiveness to have adequate control margin.

2.16 Body Buildup

A first-order estimate of total normal force, suitable for conceptual design, is to assume a body buildup of the contribution due to the body plus the contribution due to each surface. For a wing–body–tail configuration the equation is $(C_N)_{\text{Total}} = (C_N)_{\text{Wing-Body-Tail}} \approx (C_N)_{\text{Body}} + (C_N)_{\text{Wing}} + (C_N)_{\text{Tail}}$. Figure 2.45 shows a body buildup of the normal force coefficient of the rocket baseline

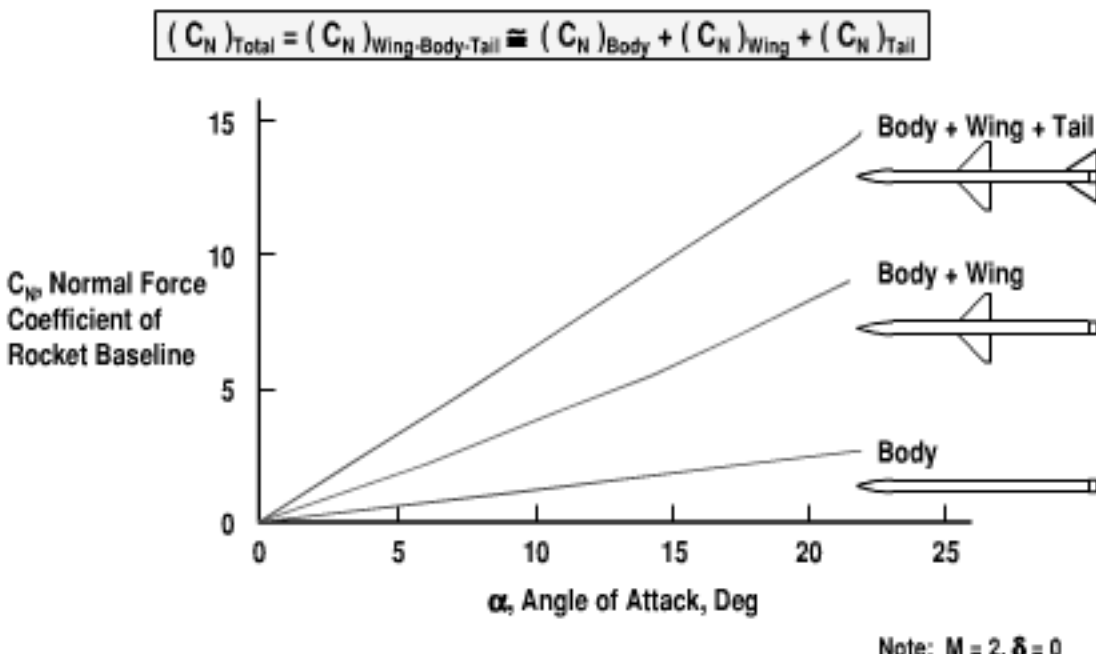


Fig. 2.45 Most of the normal force of the rocket baseline missile is provided by the wing.

missile. The body buildup in the figure is based on undeflected control surfaces. Note that for the rocket baseline missile most of the normal force is provided by the wing contribution. Deflecting the wing control provides an additional contribution to normal force. The second largest contributor to normal force is from the tail. As mentioned previously, the rocket baseline has a large tail and a large static margin. Finally, the body provides a relatively small contribution to normal force. This has an implication in the design for maneuverability. The maneuverability requirements of the rocket baseline missile are satisfied through sizing the wing.

For conceptual design it is assumed that the total normal force is the summation of that of an isolated body + wing (exposed) + tail (exposed). The effects of wing-body, body-wing, tail-body, body-tail, and wing-tail interference are assumed to be small when compared to the contributions from the isolated configuration geometries.

The body buildup approach based on summing the isolated contributions from the body plus each surface is used in the conceptual design prediction of normal force, drag, and pitching moment. For preliminary design more accurate methods based on including the effects due to wing-body, body-wing, tail-body, body-tail, and wing-tail interference are used. For the conceptual design prediction methods of this text, the conceptual design predictions without interference effects are corrected by the baseline missile aerodynamics, which include interference effects.

2.17 Summary

Chapter 2 provided conceptual design methods, design tradeoffs, design criteria, and technologies for the aerodynamics of tactical missiles. The emphasis was on the aerodynamics of low aspect ratio wing and wingless missiles. The conceptual design prediction methods of this text addressed the normal force coefficient, drag force coefficient, and the pitching moment coefficient of bodies and surfaces. Design tradeoffs addressed missile diameter, nose fineness, boattail, lifting body vs axisymmetric body, wings vs no wings, surface planform geometry, flight control alternatives, maneuver alternatives, and roll orientation. A process was given for tail area sizing. Stability and control design criteria were provided for static stability, control effectiveness, and cross coupling. New aerodynamic technologies were identified that have high payoff for tactical missiles. These include faceted/window/multilens dome geometry, bank-to-turn maneuvering, lifting body airframe, forward swept surfaces, neutral static margin, lattice tails, split canard control, and free-to-roll tails.

Propulsion Considerations in Tactical Missile Design

Tactical missile propulsion considerations that are addressed in this text emphasize conceptual design methods, design trades, and technologies for rocket and ramjet propulsion. Consideration is given to propulsion system alternatives of turbojet, ramjet, ducted rocket, scramjet, and rocket propulsion. Ramjet propulsion topics are ideal Mach number and temperature technology limit, specific impulse prediction, thrust prediction, engine/booster integration options, inlet options, inlet spillage prediction, shock loss, drag due to booster integration, and fuel alternatives. Rocket propulsion topics are maximum incremental flight velocity, burn area requirement, throat area requirement, specific impulse prediction, thrust prediction, grain alternatives, thrust magnitude control, propellant alternatives, motor case material alternatives, and nozzle material alternatives. Consideration is also given to inlet shock loss, ramjet missile drag due to booster integration, fuel alternatives, maximum incremental flight velocity for rocket propulsion, solid rocket grain alternatives, solid rocket thrust magnitude control, solid propellant alternatives, motor case alternatives, and rocket nozzle design considerations.

Figure 3.1 shows that, after aerodynamic configuration design, the next step in the missile configuration synthesis process is propulsion system design. Propulsion system design is an iterative process requiring consideration of alternative propulsion systems, alternative propulsion subsystems, alternative technologies, and propulsion system resizing. The propulsion sizing output includes the thrust, specific impulse, and the propellant/fuel weight of the propulsion system.

3.1 Propulsion Alternatives Assessment

Figure 3.2 compares the efficiency of tactical missile propulsion alternatives across the Mach number ranges of subsonic through hypersonic. Shown is a typical specific impulse envelope for the alternatives of turbofan/turbojet, ramjet, ducted rocket, scramjet, and solid rocket propulsion.

Turbojet/turbofan propulsion is a relatively mature technology. It is most suited for subsonic cruise missiles, providing high efficiency against non-time-critical targets. Beyond Mach 2 increasingly complex inlet systems are required to match the delivered inlet airflow to compressor capacity, and expensive cooling is required to avoid exceeding the material temperature limit at the turbine inlet.

A ramjet is efficient from Mach 2.5 to 5. Above Mach 5 the combustor material maximum temperature limits the achievable exit velocity and thrust. Also, the deceleration of the inlet airflow to a subsonic velocity results in chemical dissociation of the air, which absorbs heat and negates a portion of the energy input of the combustor. For a subsonic launch platform, a rocket boosts the missile to the ramjet thrust takeover at about Mach 2.5.

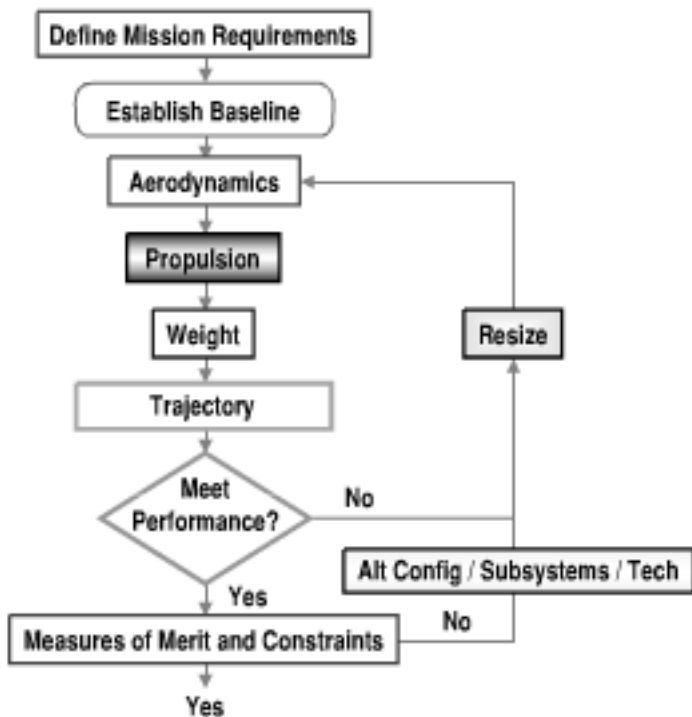


Fig. 3.1 Missile concept synthesis requires iteration.

The maximum specific impulse of ducted rocket propulsion is about 800 s, which is intermediate to that of a solid rocket and a ramjet. Ducted rockets are most efficient for a Mach number range of about 2.5 to 4.0. Ducted rockets have higher acceleration capability (higher thrust) than ramjets and generally have longer range capability (higher specific impulse) than solid propellant rockets.

Scramjet propulsion has supersonic flow through the entire flowpath, including supersonic combustion. Scramjet propulsion challenges include fuel mixing,

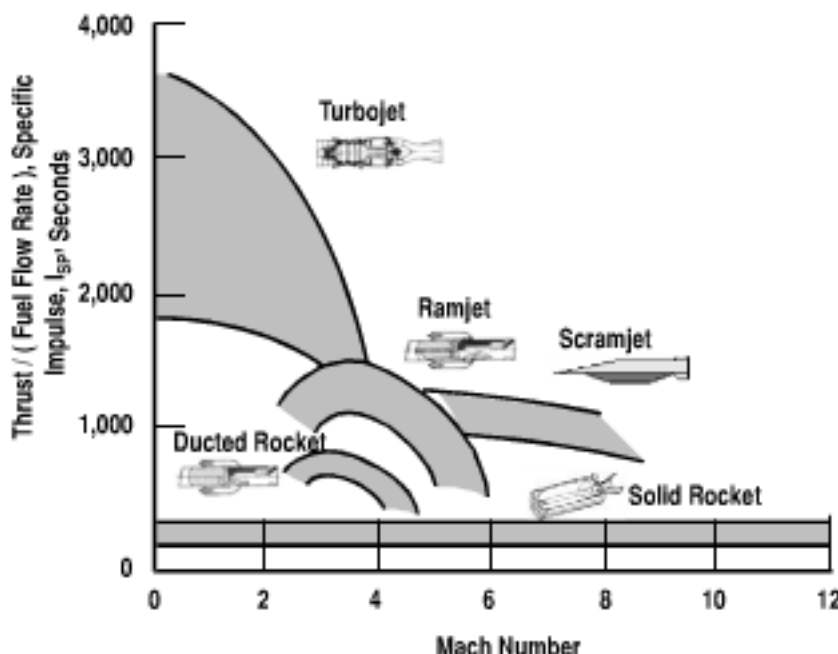


Fig. 3.2 Specific impulse of tactical missile propulsion alternatives.

efficient combustion, and airframe integration. A longer combustion chamber is required for a scramjet compared to a ramjet, because of the longer mixing time for supersonic combustion. The airframe integration alternatives are using an internal nozzle vs using the aft airframe bottom surface as an equivalent nozzle. The scramjet is boosted to a thrust takeover speed of about Mach 4, requiring a large booster for a subsonic launch. Efficient cruise is about Mach 6, 100,000 ft in altitude.

Dual-combustion ramjet-scramjet (DCR) propulsion separates the inlet airflow into two streams. The main airflow remains supersonic. The smaller airflow is decelerated to subsonic speed for combustion, after which it accelerates through a nozzle. After the smaller airflow is accelerated to supersonic speed, it mixes with the main airflow in the supersonic combustion chamber. The mixing enhances the supersonic combustion. Efficient flight is Mach 3–7.

Solid rockets are capable of providing thrust across the entire Mach number range. Although the specific impulse of tactical rockets is relatively low, on the order of 250 s, rockets have an advantage of much higher acceleration capability than airbreathing propulsion. Also, their ability to operate at high altitude enables a boost-climb-glide trajectory to extend range by minimizing drag.

Figure 3.3 compares four propulsion alternatives for a long-range precision strike missile. The alternatives are subsonic cruise turbojet propulsion, supersonic cruise liquid hydrocarbon fuel ramjet propulsion, hypersonic cruise liquid hydrocarbon fuel scramjet propulsion, and supersonic cruise solid propellant rocket propulsion. All four propulsion types are held to a missile launch weight of 2000 lb, a representative weight limit for carriage on a small fighter aircraft such as the F-18C.

Note from the figure that subsonic cruise turbojet propulsion is the preferred approach for long-range strike against targets that are not time critical. Subsonic cruise turbojet propulsion has 120% greater range than the next best alternative, a supersonic cruise liquid-fuel ramjet (1800 n miles vs 830 n miles). An examination

$$R = (L/D) I_{sp} V \ln [W_L / (W_L - W_P)], \text{ Breguet Range Equation}$$

Parameter	Typical Value for 2,000 lb Precision Strike Missile			
	Subsonic Turbojet Missile	Liquid Fuel Ramjet Missile	Hydrocarbon Fuel Scramjet Missile	Solid Rocket
L/D , Lift / Drag	10	5	3	5
I_{sp} , Specific Impulse	3,000 sec	1,300 sec	1,000 sec	250 sec
V_{AVG} , Average Velocity	1,000 ft / sec	3,500 ft / sec	6,000 ft / sec	3,000 ft / sec
W_P / W_L , Cruise Propellant or Fuel Weight / Launch Weight	0.3	0.2	0.1	0.4
R, Cruise Range	1,800 nm	830 nm	310 nm	250 nm

Note: Ramjet and Scramjet missiles propellant for Mach 2.5 to 4 take-over speed not included in W_P .
Rockets require thrust magnitude control (e.g., pinfire, pulse motor) for effective cruise. Max range for a rocket is usually a semi-ballistic flight profile, instead of cruise flight.

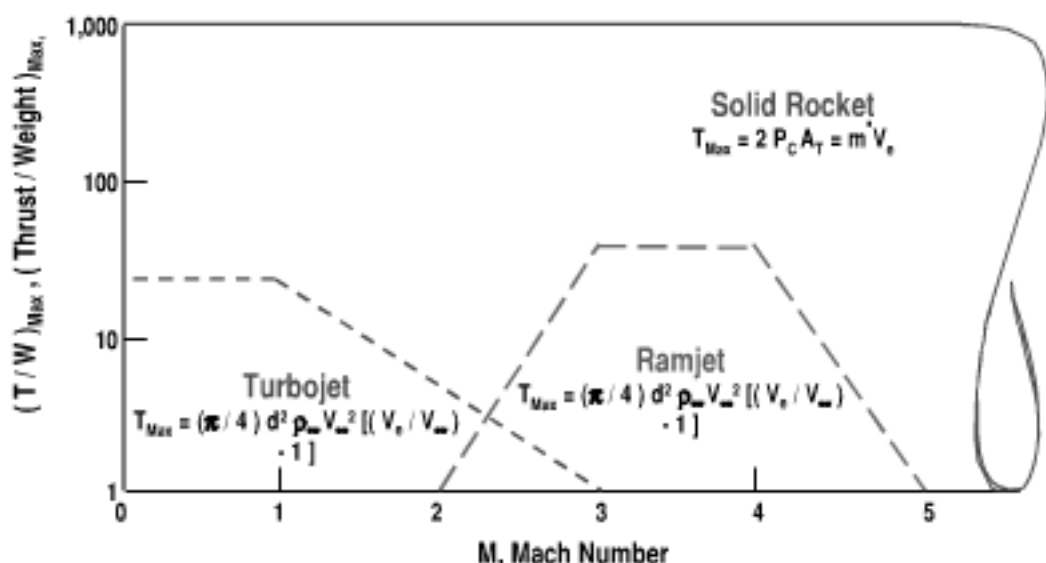
Fig. 3.3 Cruise range is driven by the parameters L/D , I_{sp} , velocity, and propellant or fuel weight fraction.

of the Breguet range equation explains the difference in performance. The subsonic cruise turbojet missile is superior to the supersonic cruise ramjet missile in its aerodynamics, with a maximum lift-to-drag ratio $L/D = 10$ vs 5 for the ramjet. The subsonic cruise missile also has superior propulsion efficiency, with a specific impulse $I_{SP} = 3000$ s vs 1300 s for a ramjet. Finally, the subsonic cruise missile has more weight available for fuel, for a missile launch weight limited to 2000 lb, with 600 lb of fuel vs 400 lb of fuel for a ramjet. The ramjet missile has less available weight for fuel because it requires a rocket to boost the missile up to about Mach 2.5 for transition to ramjet propulsion. However, a ramjet missile has an advantage of a shorter response time against time-critical targets. It may also have an advantage in survivability because of the higher flight altitude and higher speed. If time-critical targets are of utmost importance, scramjet propulsion may be preferred. As shown in the figure, the scramjet missile example is 70% faster than the ramjet (6000 ft/s vs 3500 ft/s). However, the maximum range of a scramjet missile that is limited to 2000 lb launch weight is only 37% that of a liquid-fuel ramjet (310 n miles vs 830 n miles). Again, examining the Breguet range equation is instructive. The liquid-fuel ramjet missile is superior to the scramjet in the aerodynamic efficiency ($L/D = 5$ vs 3), specific impulse ($I_{SP} = 1300$ s vs 1000 s), and available fuel for a missile limited to 2000-lb launch weight (400 lb of fuel vs 200 lb of fuel). The scramjet missile has less available weight for fuel because it requires a larger rocket booster for a higher takeover Mach number (Mach 4 vs 2.5), requires a longer combustor for efficient combustion, and requires more insulation. Finally, the supersonic cruise rocket has a maximum flight range of 250 n miles. The most efficient cruise condition for the long-range rocket was found to be Mach 3 cruise at high altitude. The solid propellant rocket example uses thrust magnitude control from a pintle motor for more efficient acceleration and cruise. Although it is not shown, a semiballistic flight trajectory (e.g., launch, pitch-up, ballistic climb, glide) would have provided a more efficient flight trajectory for the rocket because of the lower drag and higher L/D in high altitude flight.

Based on an examination of the Breguet range equation, new technology development has payoff in the areas of higher cruise velocity, aerodynamic efficiency (lift/drag), specific impulse, lightweight structure, lightweight/low volume subsystems, and higher density fuel/propellant.

Shown in Fig. 3.4 is a comparison of tactical missile propulsion alternatives based on acceleration capability. It is a typical envelope of the maximum thrust-to-weight ratio. The comparison is shown as a function of Mach number. Note that the solid rocket has the highest thrust-to-weight ratio. This is due to higher exit velocity, the independence of the exit velocity from that of the freestream velocity, and the capability for higher mass flow rate. The exit velocity of a solid rocket is about 6000 ft/s, much higher than that of a typical ramjet (exit velocity about 4000 ft/s) or a typical turbojet (exit velocity about 2000 ft/s). Note from the maximum thrust equation for airbreathing propulsion $T_{Max} = (\pi/4)d^2\rho_\infty V_\infty^2[(V_e/V_\infty) - 1]$, turbojets and ramjets produce thrust only if the exit velocity is greater than the freestream velocity ($V_e > V_\infty$). The maximum velocity of an airbreathing missile is less than the exit velocity.

Figure 3.5 illustrates tactical missile ramjet propulsion alternatives of liquid-fuel ramjet, solid-fuel ramjet, and ducted rocket. The examples are based on an integral rocket-ramjet, with the rocket booster occupying the same volume as the



Note:

P_C = Chamber pressure, A_T = Nozzle throat area, \dot{m} = Mass flow rate

d = Diameter, ρ_∞ = Freestream density, V_∞ = Freestream velocity,

V_e = Nozzle exit velocity (Turbojet: $V_e \sim 2,000$ ft/sec, Ramjet: $V_e \sim 4,000$ ft/sec, Rocket: $V_e \sim 6,000$ ft/sec)

Fig. 3.4 Solid rockets have high acceleration capability.

ramjet engine combustor. Shown in the upper portion of example is the rocket booster configuration during boost. Shown in the bottom portion of each example is the ramjet engine configuration during sustain. Ramjet propulsion is relatively simple compared with turbojet propulsion; it has no moving parts. Air enters the inlet at supersonic velocity and is decelerated to low subsonic speed (e.g., Mach 0.2) at the combustor entrance. Downstream of the combustor is a convergent-divergent nozzle, which accelerates the airflow back to supersonic velocity. The

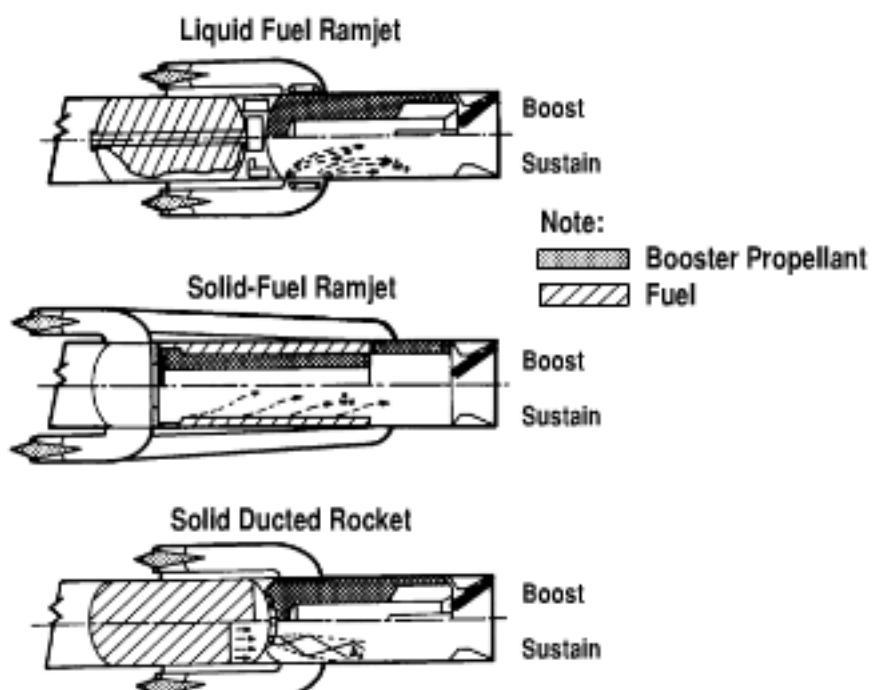


Fig. 3.5 Ramjet propulsion alternatives for tactical missiles.

maximum specific impulse of a hydrocarbon liquid-fuel ramjet is about 1500 s, much higher than the specific impulse of a solid rocket. An efficient cruise condition for a liquid-fuel ramjet is about Mach 4, 80,000 ft in altitude. As mentioned previously, the maximum Mach number is about 5. Because a ramjet is inefficient at low supersonic Mach number, a rocket is required for subsonic launch to boost the missile to the ramjet thrust takeover at about Mach 2.5. Liquid-fuel ramjets are synergistic with noncircular, lifting body airframes because fuel can be stored in noncircular tanks. Liquid-fuel ramjets can be throttled for efficient matching of the fuel with the inlet airflow over a broad flight envelope of Mach number and altitude.

A variation of the traditional liquid-fuel ramjet is the solid-fuel ramjet. The solid-fuel ramjet has a fuel grain with a hollow center core for the inlet airflow. An advantage of the higher density solid fuel is its volumetric performance. Disadvantages are limited throttle capability and the reduced volumetric loading of the fuel because of the hollow center grain. Some passive fuel flow compensation is achieved from changing flight conditions. If a larger variation in fuel flow rate is required, shaping of the fuel grain is needed, at a loss in volumetric loading. Other means of thrust management, such as variable geometry inlets or nozzles, are usually not cost effective for tactical missiles.

As mentioned previously, a ducted rocket has a maximum specific impulse of about 800 s, intermediate to that of a solid rocket and a ramjet. Ducted rockets are most efficient for Mach 2.5–4.0. Ducted rockets have higher acceleration (higher thrust) than ramjets and longer range (higher specific impulse) than solid rockets. A gas generator provides fuel-rich products to the combustor. The gas generator flow rate can be controlled, providing a throttle capability for thrust magnitude control.

The integration of the ramjet booster affects the missile compatibility for launch platform length and diameter constraints. Integral boosters that occupy the combustor case improve volumetric efficiency and reduce weight, enhancing integration with the launch platform. Another integration challenge for the booster is to minimize fratricide by having no ejecta. A nozzleless booster with a common booster case/ramjet combustor avoids nozzle and booster ejecta. A nozzleless booster has a cast propellant grain that maintains the throat and divergence geometry during motor burn.

3.2 Ideal Ramjet Mach Number and Temperature Technology Limit

Higher combustion temperature has a payoff in improving the specific impulse and thrust of ramjet missiles, enabling flight at higher Mach number. Figure 3.6, based on Ref. 7, shows the ideal combustion temperature for maximum specific impulse and thrust of an ideal ramjet as a function of Mach number and ratio of specific heat. The equation for the combustion temperature that provides maximum specific impulse is

$$(T_4/T_0)_{(ISP)_{Max}} = \left\{ [(\gamma - 1)/2]M_0^2 - 1 \right\}^2 \left\{ 1 + [(\gamma - 1)/2]M_0^2 \right\}$$

The equation for the combustion temperature that provides maximum thrust per unit frontal area is

$$(T_4/T_0)_{(T/A_3)_{Max}} = \left\{ 1 + [(\gamma - 1)/2]M_0^2 \right\}^3 / \left\{ 1 + [(\gamma - 1)/4]M_0^2 \right\}^2$$

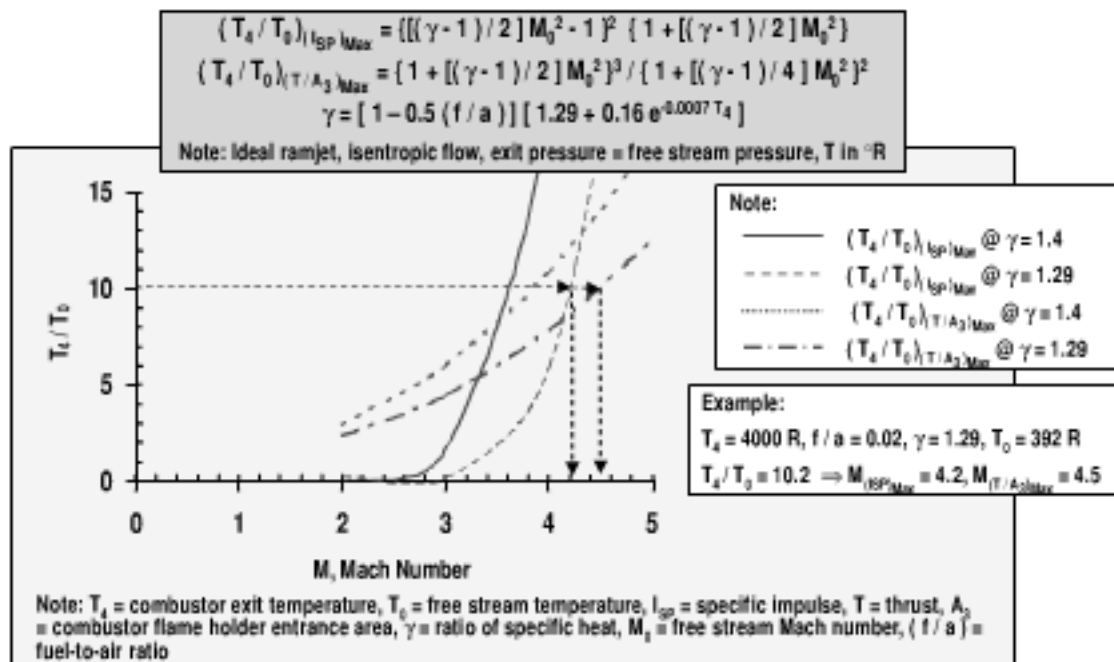


Fig. 3.6 High combustion temperature is required for ramjet-efficient operation at high Mach number (from Ref. 7).

Finally, the ratio of specific heat of air is given by the equation

$$\gamma = (1 - f/a)(1.29 + 0.16e^{-0.0007 T_4})$$

Results are based on the assumptions of an ideal ramjet, isentropic flow and expansion of the nozzle exit pressure to atmospheric pressure. Temperature is in Rankine.

As an example, assume that the ramjet baseline missile is operating at 80,000-ft altitude with a combustion temperature of 4000°R and a fuel-to-air ratio of 0.02. The ratio of the combustion temperature to the freestream temperature is 10.2, and the ratio of specific heat is 1.29. As shown in the figure, for a combustion temperature of 4000°R, maximum specific impulse for a ramjet is produced at a Mach number of about 4.2. Also shown is the Mach number for maximum thrust per unit frontal area. The maximum thrust per unit frontal area for a combustion temperature $T_4 = 4000 \text{ }^{\circ}\text{R}$ is produced at a Mach number of about 4.5. Improvement in the technology for maximum allowable temperature of insulated combustor materials allows ramjets to operate at higher Mach number. Also shown in the figure are examples of the ideal Mach number at a specific heat ratio of $\gamma = 1.4$, corresponding to a low value of the combustion temperature. The ideal Mach numbers are lower for a low combustion temperature.

3.3 Ramjet Specific Impulse Prediction

Shown in Fig. 3.7 is an example of the specific impulse of an ideal ramjet.⁷ The equation is

$$(I_{SP})(a_0)/H_f = (\gamma - 1)M_0 / \left\{ \left\{ 1 + [(\gamma - 1)/2]M_0^2 \right\} \times \left[\left\{ (T_4/T_0) / \left\{ 1 + [(\gamma - 1)/2]M_0^2 \right\} \right\}^{1/2} + 1 \right] \right\}$$

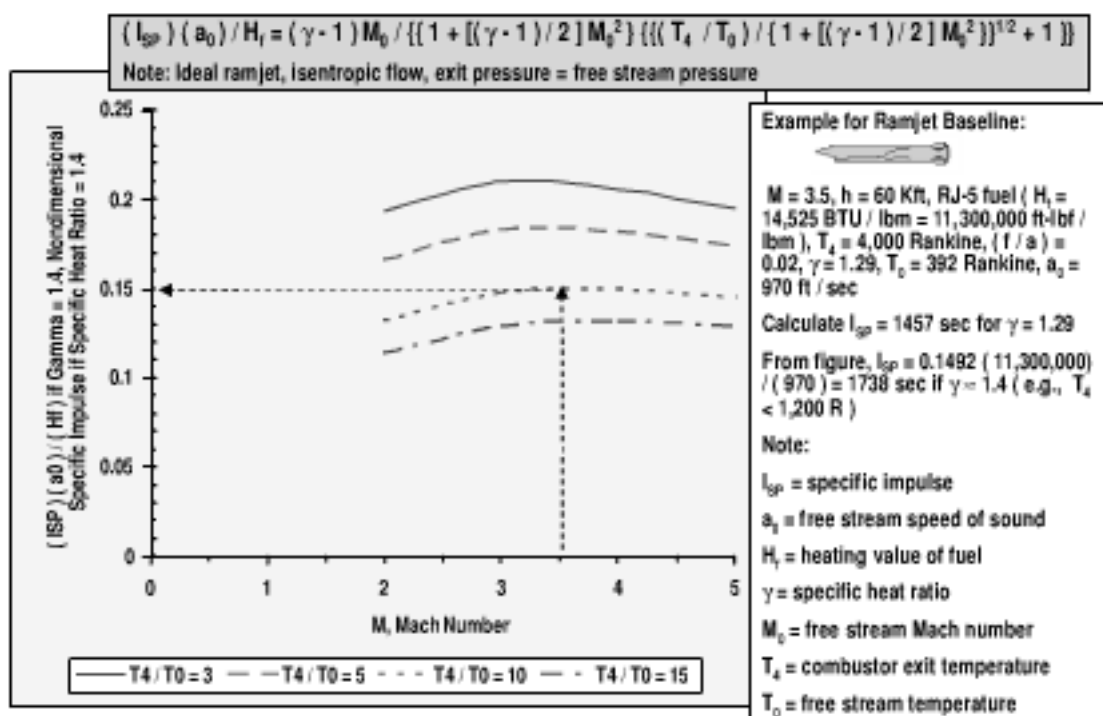


Fig. 3.7 High specific impulse for a ramjet occurs using high heating value fuel at Mach 3–4.

Note that specific impulse is a function of Mach number, heating value of fuel, combustion temperature, freestream temperature, speed of sound, and combustion specific heat ratio. Results for the ideal ramjet are based on assumptions of isentropic flow, perfect gas, and ideal expansion. It is also assumed that the ramjet combustor is sufficiently long to provide complete combustion. This may be a problem for flight at a dynamic pressure less than 500 psf and an altitude above 60,000 ft. A design guideline for a typical length-limited combustor is that the pressure inside the combustor should be greater than 5 psi, to ensure complete combustion.

An example is given for the ramjet baseline at Mach 3.5, 60,000 ft in altitude. The fuel is RJ-5 fuel (heating value of 14,525 Btu per lb of fuel). The assumed combustion temperature is 4000°R and the fuel-to-air ratio is 0.02, giving a ratio of specific heat of 1.29. Specific impulse is calculated to be 1457 s. The actual specific impulse is lower, because of inlet shock loss. Also note from the figure that ambient temperature gas ($\gamma = 1.4$) would provide a 19% higher value of specific impulse (1738 s vs 1457 s).

3.4 Ramjet Thrust Prediction

Shown in Fig. 3.8 is the thrust of an ideal ramjet.⁷ The equation is

$$T = p_0 A_3 \gamma M_0^2 \left\{ \left[\frac{T_4}{T_0} \right] / \left\{ 1 + [(\gamma - 1)/2] M_0^2 \right\} \right\}^{1/2} - 1$$

Note that thrust is a function of the combustion temperature, combustor area, Mach number, freestream pressure and temperature, and the ratio of specific heat. For typical values of the parameters, maximum thrust occurs at a Mach number between Mach 3 and 5. Results are based on an ideal ramjet with isentropic flow, perfect gas, stoichiometric ($\phi = 1$) combustion, and ideal expansion of the nozzle exit pressure

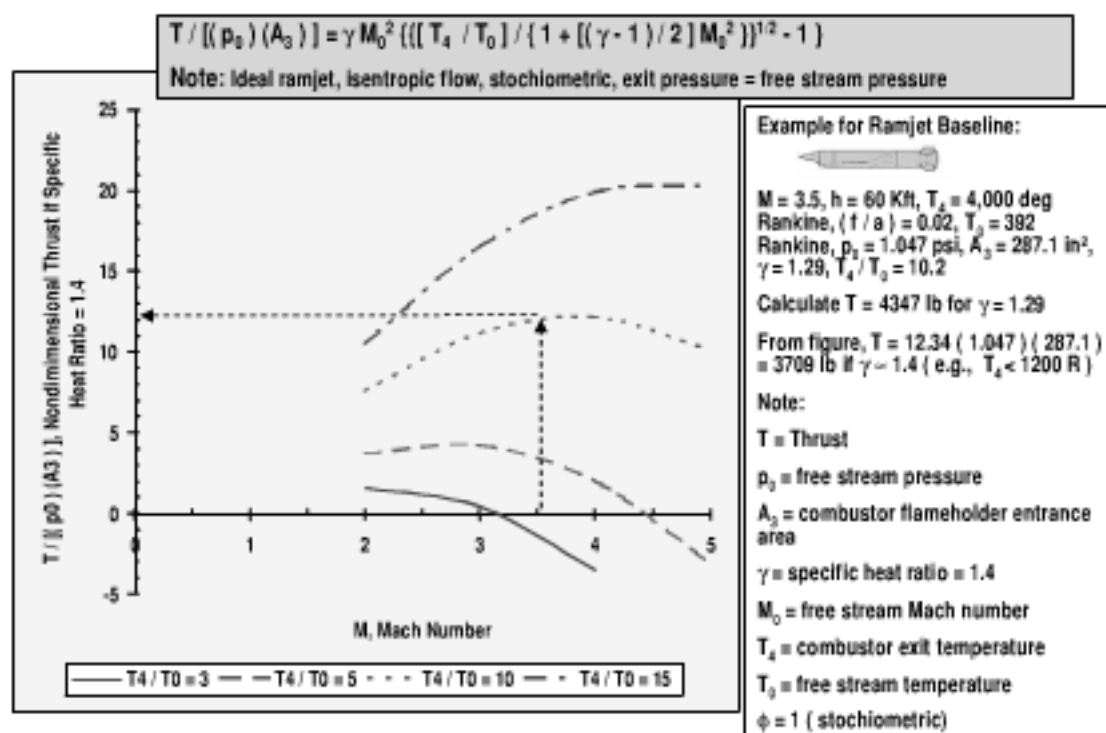


Fig. 3.8 High thrust for a ramjet occurs from Mach 3 to 5 with high combustion temperature.

to the freestream static pressure. For fuel-to-air ratios less than stoichiometric, it is assumed that thrust is proportional to ϕ .

An example is shown for the ramjet baseline at Mach 3.5 and an altitude of 60,000 ft. It assumes a combustion temperature of 4000°R and a fuel-to-air ratio of 0.02, which gives a specific heat ratio of 1.29. The thrust is calculated to be $T = 4347$ lb. The actual thrust is lower, because of inlet shock loss. Also note from the figure that ambient temperature gas ($\gamma = 1.4$) would provide a value of thrust that is 15% lower (3709 lb vs 4307 lb) than the value for $\gamma = 1.29$.

3.5 Ramjet Engine/Booster Integration

Figure 3.9 from Ref. 8 characterizes ramjet engine/booster integration options according to their cruise drag. Low cruise drag ramjets are tandem integral rocket ramjet (IRR), aft drop-off booster, forward-located booster, and podded drop-off booster. The high cruise drag ramjets that are shown in the figure are the podded ramjet, podded integral rocket ramjet, and the podded ramjet with a drop-off booster. Most modern ramjets have low cruise drag. The integral rocket ramjet is particularly attractive. After booster burnout, an IRR uses the booster case as the combustion chamber for the ramjet. The IRR is often preferred because of advantages of low cruise drag, low volume, lighter weight, and small diameter.

A further comparison of ramjet engine/booster integration options is given in Fig. 3.10 based on Ref. 8. The integral rocket ramjet engine has above-average-to-superior characteristics for the selection factors of length, diameter, weight, no ejecta, cruise drag, launch platform carriage drag, cost, compatibility of the ramjet engine with the booster, and compatibility of the ramjet engine with the inlet. The other candidate engines are below average in one or more of the selection

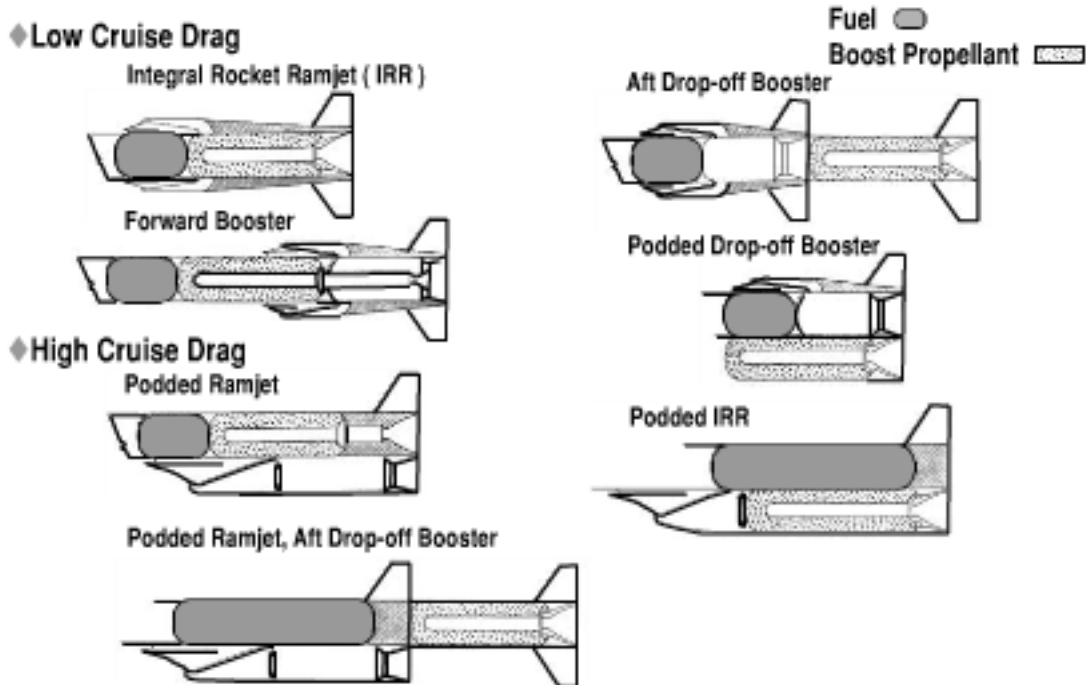


Fig. 3.9 Ramjet engine/booster intergration options (from Ref. 8).

factors. However, depending upon the weighting of the selection factors and the mission, one or more of the other candidate engines may also be acceptable, or even preferable. The strengths and potential weaknesses of the other candidate ramjet engine alternatives to an integral rocket ramjet include the following:

1) Aft drop-off booster attractive features include small diameter, low cruise drag, low cost, and compatibility of the engine with the inlet. Disadvantages of an aft drop-off booster include long length and ejecta.

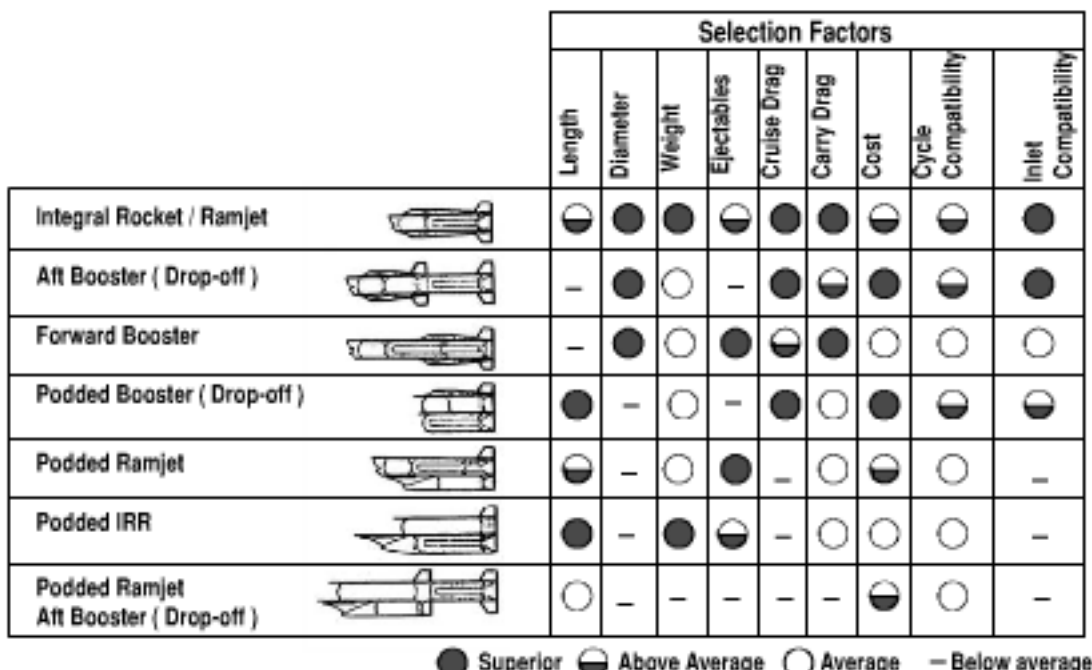


Fig. 3.10 Ramjet engine/booster integration selection factors (from Ref. 8).

- 2) Forward booster has attractive features of small diameter, no ejecta, and low launch platform carriage drag. A disadvantage is long length.
- 3) Podded drop-off booster has attractive features of short length, low cruise drag, and low cost. Disadvantages include a large diameter and ejecta.
- 4) Podded ramjet has an attractive feature of no ejecta. Disadvantages of a podded ramjet include a large diameter, high cruise drag, and a potential problem of inlet compatibility. The disadvantages make it unsuitable for most modern applications.
- 5) Podded integral rocket ramjet has attractive features of short length and lighter weight. Disadvantages include large diameter, high cruise drag, and a potential problem of inlet compatibility. The disadvantages make it unsuitable for most modern applications.
- 6) Podded ramjet with a drop-off booster has disadvantages of large diameter, heavy weight, ejecta, high cruise drag, high carriage drag, and a potential problem of inlet compatibility. The disadvantages make it unsuitable for most modern applications.

3.6 Ramjet Inlet Options

Ramjet inlet design considerations include the type of opening, location of the inlet on the body, and the number of inlets. Figure 3.11 from Ref. 8 shows the inlet placement and geometry of the following nine ramjet inlet options:

- 1) Annular nose inlet. The inlet surrounds the body. It may rely only on the cowl lip oblique shock for the initial compression, or it may also have a center spike for compression.
- 2) Chin inlet located forward underneath the nose. The nose compression angle provides an oblique shock in front of the inlet.
- 3) Forward cruciform axisymmetric inlet. The nose compression angle provides an oblique shock in front of the inlet. The inlets are usually in tandem with cruciform tails.

Type Inlet	Sketch	Placement
Nose		Nose-full axisymmetric
Chin		Forward underside in nose compression field-partial axisymmetric
Forward Cruciform Axisymmetric		Forward in nose compression field-cruciform (four) axisymmetric
Aft Cruciform Axisymmetric		Aft-cruciform (four) axisymmetric
Underwing Axisymmetric		In planar wing compression field-twin axisymmetric
Twin Two-dimensional		Aft-twin cheek-mounted two-dimensional
Underslung Axisymmetric		Aft underside-full axisymmetric
Underslung Two-dimensional		Aft underside-belly mounted two-dimensional
Cruciform Two-dimensional		Aft-cruciform (four) two-dimensional

Fig. 3.11 Ramjet inlet options (from Ref. 8).

Type Inlet	Selection Factors									
	Pressure Recovery	Carriage Envelope	Alpha Capability	Weight	Drag	Warhead Shrouding	Inlet Cost	Preferred Steering	Preferred Control	Prime Mission Suitability
○ -	●	●	○	●	●	-	●	STT	W, C	ATS, STA
○ -	●	●	●	○	●	○	○	BTT	T	ATS, ATA, STA
□ -	●	○	●	-	○	-	-	STT	T	ATS, ATA, STA
□ -	○	●	○	●	○	●	○	STT	T	ATS
○ -	●	-	●	●	○	●	●	BTT	T	ATA, STA
○ -	●	○	●	●	●	○	○	BTT	T	ATS, ATA, STA
○ -	○	-	○	●	○	●	●	BTT	T	ATS
○ -	-	●	●	●	●	●	●	BTT	T	ATS, ATA, STA
□ -	-	○	○	●	●	●	○	STT	T	ATS

Note:
 BTT = Bank to Turn
 STT = Skid to Turn
 W = Wing C = Canard T = Tall
 ● Superior ○ Above Average ○ Average - Below average

Fig. 3.12 Ramjet inlet concept selection factors (from Ref. 8).

4) Aft cruciform axisymmetric inlet. There are four inlets located near the center of the missile. The inlets are usually in tandem with cruciform tails.

5) Underwing axisymmetric inlet. There are two inlets located near the center of the missile, under a planar wing. The wing provides an initial compression.

6) Twin two-dimensional inlet. This concept has two inlets on the lower portion of the body, separated by a radial angle of about 90 deg. The inlets are usually in tandem with the bottom cruciform tails.

7) Underslung axisymmetric inlet. The underslung inlet is located near the center of the missile.

8) Underslung two-dimensional inlet. This is similar to the above.

9) Cruciform two-dimensional inlet. This is similar to the aft cruciform axisymmetric inlet.

Trades of inlet alternatives are shown in Fig. 3.12 from Ref. 8. The selection factors are:

1) Higher pressure recovery. The chin inlet and the forward cruciform axisymmetric inlet benefit from the relatively high recovery pressure provided by an oblique shock from the forebody in front of the inlet. The nose inlet, underwing axisymmetric inlet, and twin two-dimensional inlet also have relatively good pressure recovery. The underwing axisymmetric inlet benefits from the wing compression, whereas the twin two-dimensional inlet benefits from the underbody compression.

2) Small carriage envelope on the launch platform. The annular inlet and the chin inlet require only a small inlet height to capture airflow, because of the large wraparound angle.

3) High angle of attack capability. The chin inlet allows high positive angles of attack, providing a relatively high recovery pressure for bank-to-turn maneuvering.

- 4) Light weight. The underwing axisymmetric inlet and the underslung axisymmetric inlet, located aft on the missile body, require less material for structure.
- 5) Low drag. The annular nose inlet and the chin inlet have reduced drag on the nose.
- 6) No shrouding of the warhead. The aft cruciform axisymmetric inlet, aft twin axisymmetric inlet, and the aft cruciform two-dimensional inlet shown in the figure are located aft of the warhead section of the missile.
- 7) Low cost. The lowest cost, simplest fabrication inlet is probably an underslung axisymmetric inlet.
- 8) Preferred steering approach (skid to turn, bank to turn). Cruciform inlets are consistent with skid-to-turn maneuvering, whereas chin, twin, or underslung inlets are consistent with bank-to-turn maneuvering.
- 9) Preferred type of flight control (tail, canard, wing). An annular inlet has volume available for the forward packaging of flight control actuators for canard or wing control. The other inlets are more compatible with tail control.
- 10) Preferred mission application (air to surface, air to air, or surface to air). The air intercept mission requires high maneuverability and high angle of attack, which is especially consistent with the capability of the chin inlet. The relatively low angle of attack capability of the aft cruciform and cruciform two-dimensional inlets makes them more suitable for surface target missions.

There is no single inlet that is best for all missions. The selection factors must be weighted for the mission as part of the inlet selection.

The current operational ramjet missiles are shown in Fig. 3.13. The current operational ramjets have either a nose inlet (U.K. Sea Dart) or aft axisymmetric inlets (France ASMP, Russia AS 17/Kh-31, Kh-41, SS-N-22/3M80, and

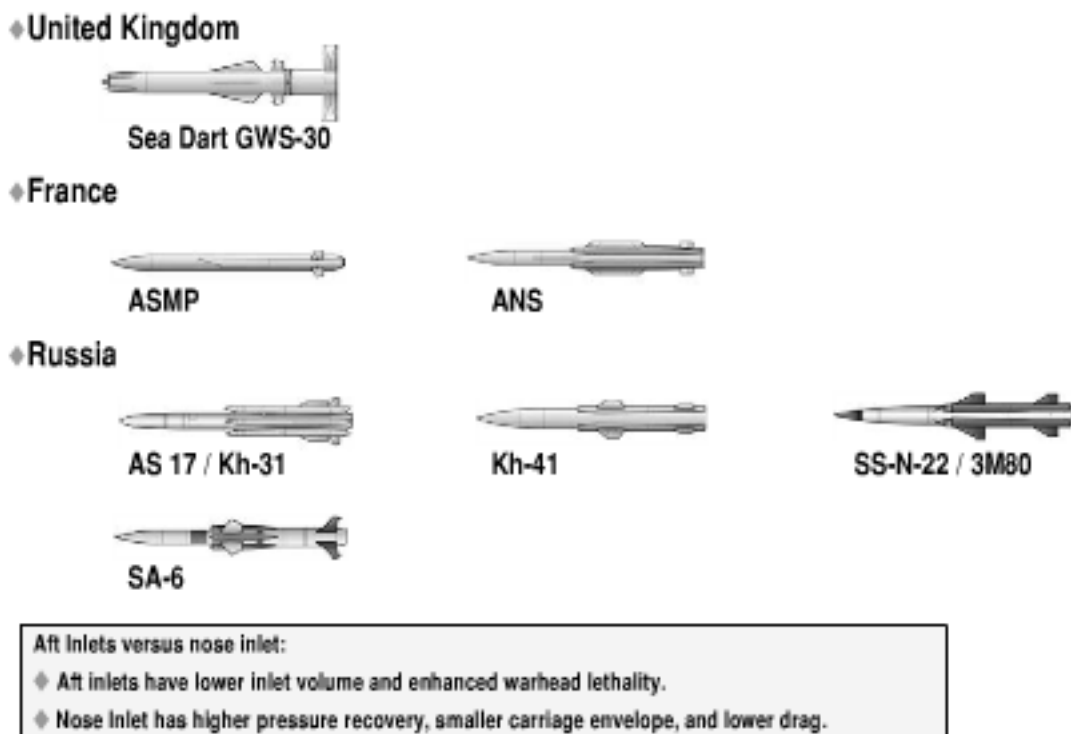


Fig. 3.13 Current operational ramjet missiles have either a nose inlet or have axisymmetric aft inlets.

SA-6). A nose inlet has an advantage of lower drag. Aft axisymmetric inlets have advantages of lighter weight and lower volume, and they do not shroud/degrade warhead effectiveness. Also note that the flight control for all of the current operational ramjets is based on tail control surfaces. The tail flight control actuators are packaged around the ramjet nozzle.

Inlet design for a supersonic or hypersonic tactical missile involves a host of considerations, including matching the flow delivered to the ramjet nozzle, swallowing capacity, and inlet start. It is not possible to consider all of these in conceptual design. The inlet design considerations that are addressed in this text are those that have a large effect on the aerodynamic configuration.

3.7 Ramjet Inlet Spillage

Figure 3.14 shows a comparison of the shock wave location for an annular inlet with the shock wave location for an oblique shock external compression inlet. The oblique shock external compression inlet has a body deflection angle in front of the inlet. The annular inlet shown at the top of the figure has an advantage in that it swallows 100% of the oncoming air, with no spillage. A disadvantage is that it may have lower pressure recovery because of a strong normal shock inside the inlet. A center spike reduces the problem of a strong normal shock, but it adds an additional concern of matching the airflow of the inlet with the requirement of the engine. The oblique shock external compression inlet is shown at the middle and bottom of the figure, operating in two conditions. The first condition, shown in the middle of the figure, is a lower Mach number where the oblique shocks have high shock wave angles, passing over the inlet. This results in spillage air, which tends to increase drag. The second condition for the oblique shock external compression inlet is shown at the bottom of the figure. It is a higher Mach number condition

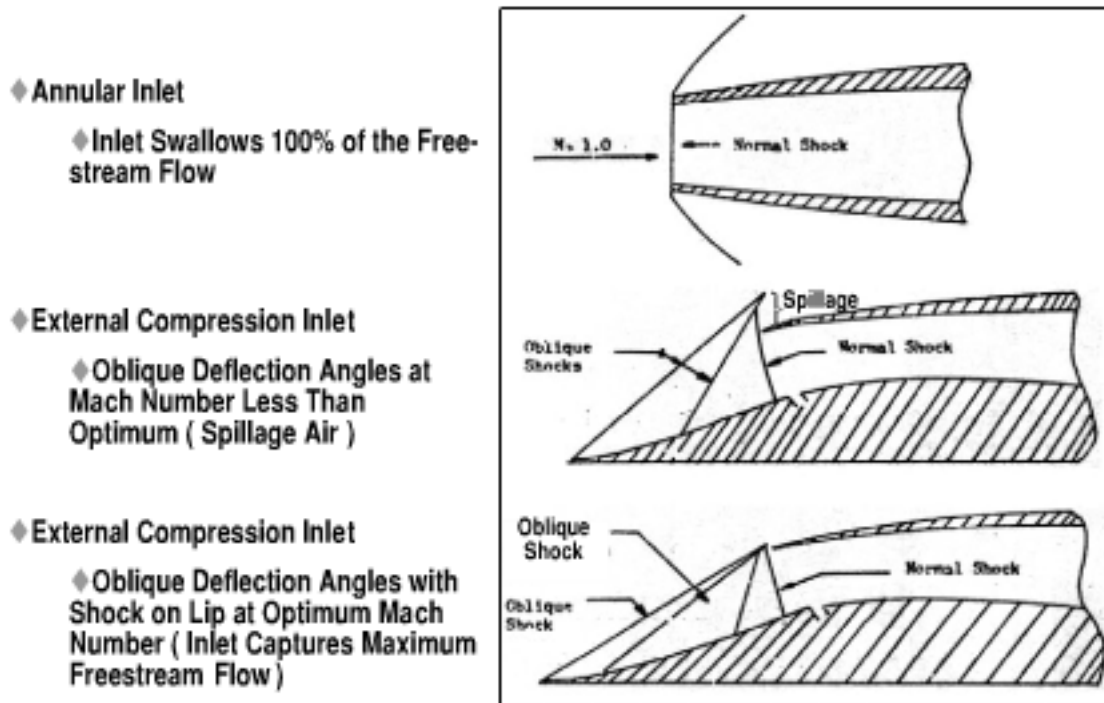


Fig. 3.14 Shock on inlet cowl lip prevents spillage.

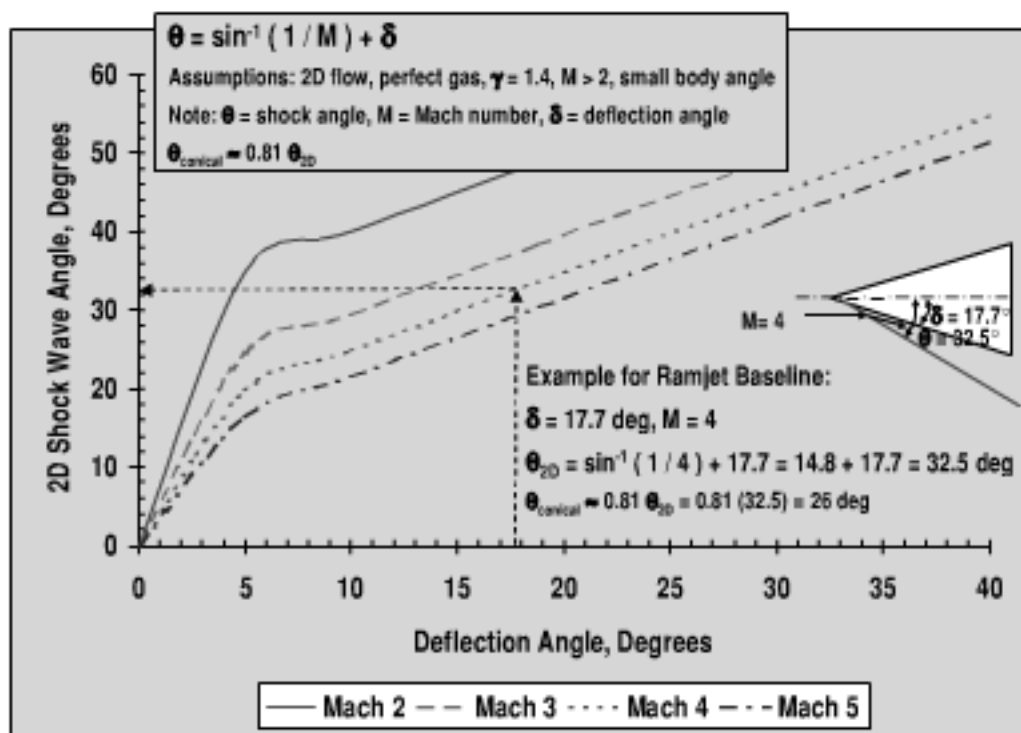


Fig. 3.15 Shock wave angle increases with body deflection angle.

with the oblique shocks converging on the inlet lip. In this condition the oblique shock inlet swallows 100% of the oncoming air.

A first-order estimate of the two-dimensional shock wave angle, suitable for conceptual design, is to assume that the shock wave angle is the sum of the Mach angle plus the body deflection angle. The equation is $\theta = \sin^{-1}(1/M) + \delta$ shown in Fig. 3.15 is a prediction of the two-dimensional oblique shock wave angle. The prediction is based on assumptions of two-dimensional flow, perfect gas, specific heat ratio of 1.4, Mach number greater than 2, and a small body deflection angle. The assumption of small body deflection angle becomes less accurate as the body deflection angle increases beyond 20 deg. Note from the figure that the oblique shock wave angle is larger for a large body deflection angle and a low Mach number. As a result, the inlet height to avoid air spillage must be greater for a missile with a low fineness nose at low supersonic Mach number. Note that the shock wave angle for conical flow around a conical nose is about 81% of the two-dimensional shock wave angle.

An example is shown of the shock wave angle for the ramjet baseline, which has a 17.7-deg half-angle conical nose. At Mach 4 the Mach angle is 14.8 deg, resulting in a two-dimensional oblique shock wave angle of approximately 32.5 deg. The conical shock wave angle for the ramjet baseline is 26 deg (81% of a two-dimensional shock wave angle). The estimate of the oblique shock wave angle provides a guideline for the inlet height that is required to achieve a shock-on-lip condition.

Figure 3.16 shows the capture efficiency of an annular inlet compared with that of an oblique shock external compression inlet. The figure is based on the equation $(A_0/A_C) = (h/l)(1 + \delta M)/[(\delta + (h/l))]$. The annular inlet captures 100% of the freestream flow at all Mach numbers. The oblique shock external compression inlet

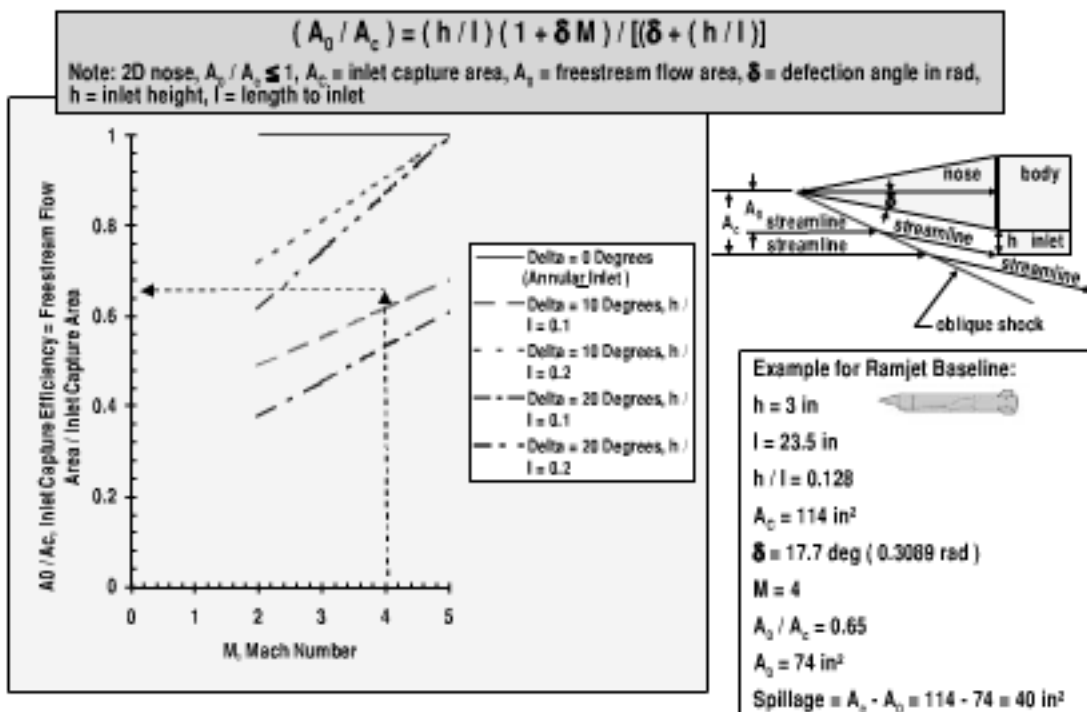


Fig. 3.16 Inlet capture efficiency increases with Mach number.

capture efficiency for a two-dimensional (wedge) forebody is shown as a function of Mach number ($2 < M < 5$), body deflection angle ($\delta = 10, 20$ deg), and the inlet height compared with the length from the nose tip ($h = 0.1$ length, 0.2 length). Most inlets are designed for shock-on-lip operation at the highest Mach number cruise condition. Greater spillage tends to occur at lower Mach number because of greater shock wave angle.

An example of the inlet spillage for the ramjet baseline is shown in the figure. Note that there is an error in the prediction because of the conical forebody of the ramjet baseline vs the two-dimensional wedge forebody assumption of the prediction method. The chin inlet ramjet baseline has an inlet height $h = 3$ in., length to the inlet from the nose tip $l = 23.5$ in., capture area $A_C = 114 \text{ in}^2$, and a nose half-angle $\delta = 17.7$ deg. From the equation in the figure, the ramjet baseline at Mach 4 cruise has a freestream capture efficiency of 65%. The freestream flow area at Mach 4 is computed to be $A_0 = 74 \text{ in}^2$ and the air spillage is given by $A_C - A_0 = 40 \text{ in}^2$. A higher value of inlet height would be required for shock-on-lip at Mach 4. However, this was not possible for the ramjet baseline because of the constraint of ASALM fitment compatibility with the B-1 rotary launcher and its weapons bay.

Figure 3.17 from Ref. 9 presents the optimum deflection angle of a single cone forebody compared with the optimum body deflection angles for a double cone forebody. The figure shows that the required deflection angle(s) for optimum pressure recovery increases with Mach number. It also shows that two oblique shocks have smaller optimum deflection angles than the optimum deflection angle of a single oblique shock. Note that there is higher pressure recovery for two oblique shocks than for one oblique shock.

As an example, at Mach 4 the optimum deflection angles for two oblique shocks are a 22-deg half-angle for the first oblique shock and a 23-deg half-angle for the second oblique shock. As a comparison, the ramjet baseline has two oblique shock

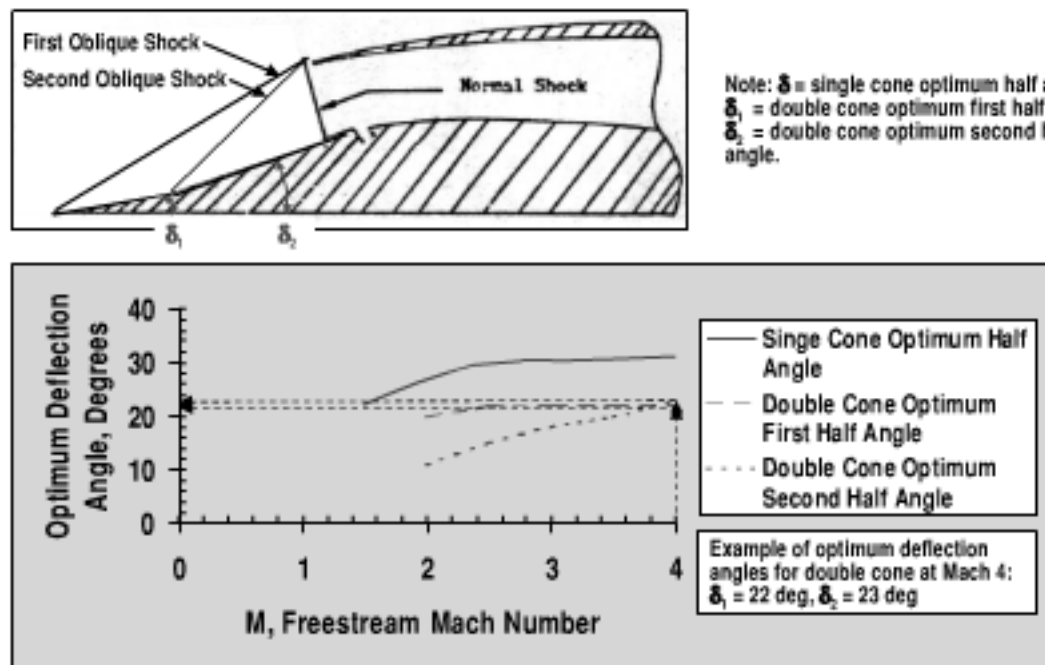


Fig. 3.17 Optimum oblique deflection angle for high pressure recovery increases with Mach number (from Ref. 9).

deflections consisting of a nose half-angle of 17.7 deg, followed by an inlet cowl ramp angle of 8.36 deg. The oblique shock deflection angles of the ramjet baseline are more compatible with the lower Mach number cruise condition of Mach 2.5, sea level.

3.8 Inlet Shock Loss

Because ramjet combustion is subsonic, there must be a normal shock in the inlet to provide subsonic flow into the combustor. Small oblique shocks prior to the normal shock alleviate the problem of total (stagnation) pressure loss across the normal shock. Figure 3.18 is based on Ref. 10, and compares a single, normal shock total pressure recovery with that of one, two, and three oblique shocks prior to the normal shock. Note that three oblique shocks prior to the normal shock provide a relatively high stagnation pressure recovery. Ramjet inlet/airframe integration through external forebody compression (such as a chin inlet), an optimized inlet cowl lip angle, and internal turning provide higher specific impulse and higher thrust. At hypersonic Mach number a mixed compression inlet [external compression from oblique shock(s) on the forebody, followed by internal oblique shock(s) inside the inlet] is often required. A mixed compression inlet may be desirable to avoid excessive flow turning away from the axial direction.

An example is shown of the chin inlet ramjet baseline, which has mixed compression consisting of three oblique shocks. There are two external oblique shocks (from a conical forebody half angle of 17.7 deg and an inlet ramp angle of 8.36 deg) plus an internal oblique shock of 8.24 deg. As shown in the example, the stagnation pressure recovery ratio at Mach 3.5 is 83% if there are three oblique shocks. The specific impulse and thrust are 83% of the values of a perfect inlet. The specific impulse is $0.83(1457) = 1209$ s. The thrust is $0.83(4347) = 3608$ lb.

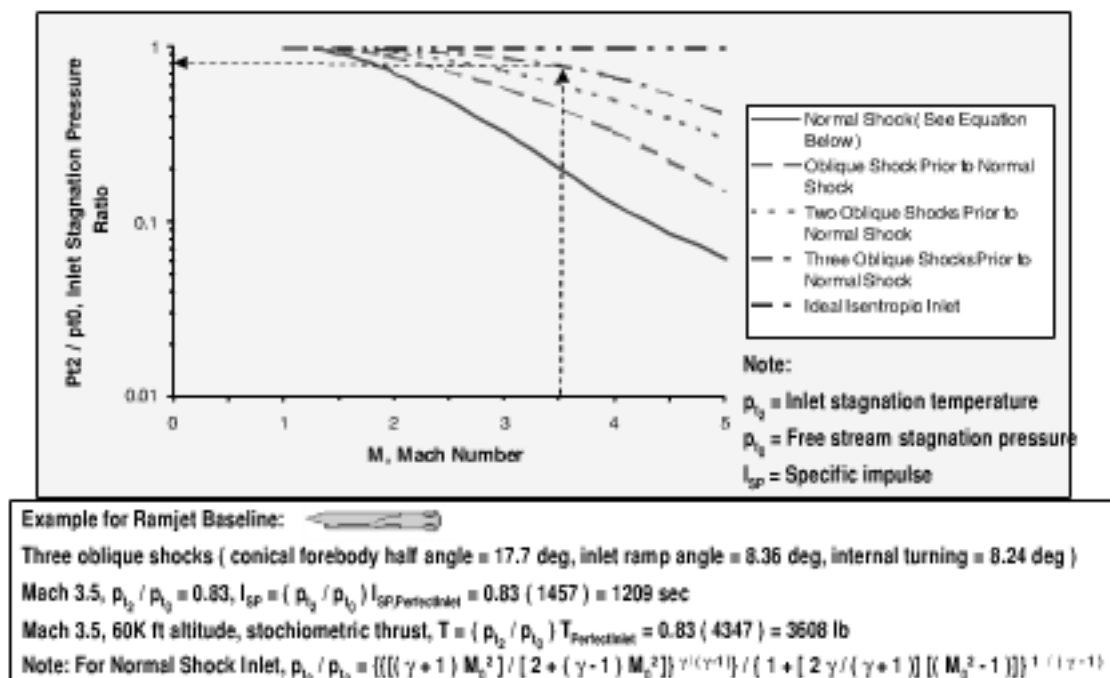


Fig. 3.18 Oblique shocks prior to the inlet normal shock provide higher pressure recovery (from Ref. 10).

3.9 Ramjet Missile Drag Due to Booster Integration

A first-order estimate of ramjet zero-lift drag, based on Ref. 8, is given in Fig. 3.19. The examples of ramjets that have low cruise drag are wingless ramjets based on one of the following: an integral rocket ramjet (IRR), an aft dropoff booster, a forward-located booster, or a podded dropoff booster. As an example, the wingless missiles have a zero-lift drag coefficient at Mach 2 of $C_{D_0} \approx 0.3$ –0.6. Adding wings to the low drag ramjets increases the drag. At Mach 2 the value of the

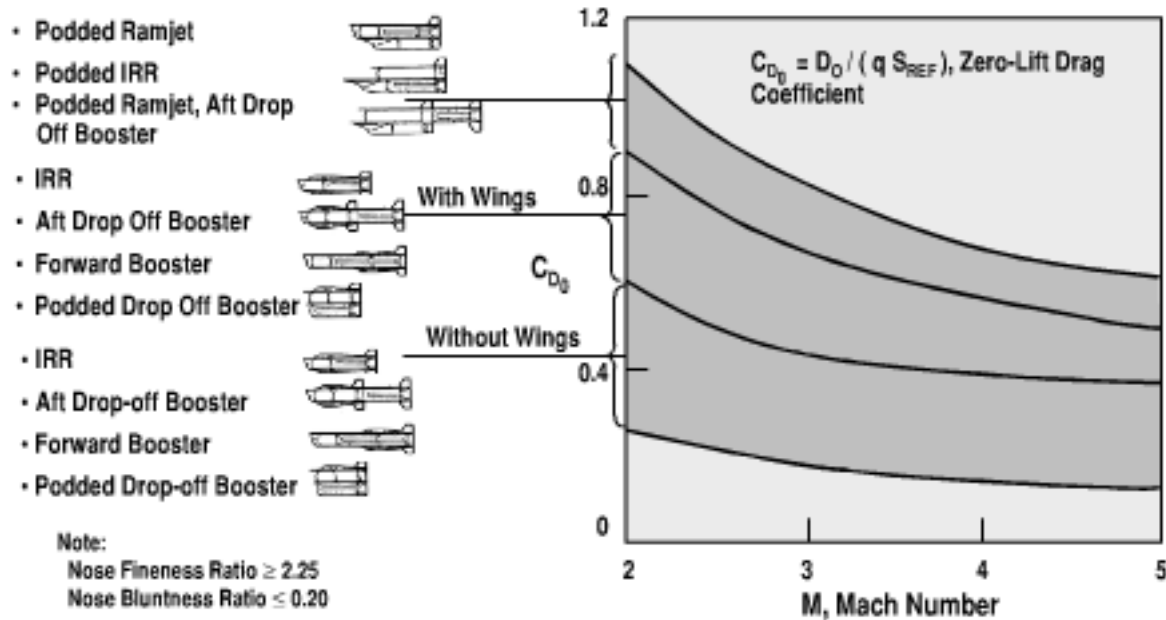


Fig. 3.19 Ramjets with internal boosters have low drag (from Ref. 8).

Type	Volumetric Performance, BTU / in ³	Low Observables
Turbine (JP-4, JP-5, JP-7, JP-10), $\rho \sim 0.028 \text{ lb/in}^3$	○ 559	●
Liquid Ramjet (RJ-4, RJ-5, RJ-6, RJ-7), $\rho \sim 0.040 \text{ lb/in}^3$	○ 581	●
Slurry (40% JP-10 / 60% carbon), $\rho \sim 0.049 \text{ lb/in}^3$	● 801	○
Solid Hydrocarbon, $\rho \sim 0.075 \text{ lb/in}^3$	● 1132	○
Slurry (40% JP-10 / 60% aluminum), $\rho \sim 0.072 \text{ lb/in}^3$	● 866	-
Slurry (40% JP-10 / 60% boron carbide), $\rho \sim 0.050 \text{ lb/in}^3$	● 1191	-
Solid Mg, $\rho \sim 0.068 \text{ lb/in}^3$	● 1300	-
Solid Al, $\rho \sim 0.10 \text{ lb/in}^3$	● 1300	-
Solid Boron, $\rho \sim 0.082 \text{ lb/in}^3$	● 2040	-
● Superior ● Above average ○ Average — Below average		

Fig. 3.20 High density fuels provide higher volumetric performance but have higher observables.

zero-lift drag coefficient is $C_{D_0} \approx 0.6\text{--}0.9$. Examples of high drag configurations are the podded ramjets. As shown in the figure, at Mach 2 the zero-lift drag coefficient for podded ramjets is the highest, $C_{D_0} \approx 0.9\text{--}1.1$. As stated previously, the high drag podded ramjets are unsuitable for most modern applications.

3.10 Fuel Alternatives

An area of high payoff propulsion technology is that of higher density fuels. As shown in Fig. 3.20, the higher density fuels provide high volumetric performance for volume limited missiles. Current fuels for turbines such as JP-4, JP-5, JP-7, and JP-10 have relatively low density, on the order of 0.028 lb/in^3 , and low volumetric performance, on the order of 559 Btu/in^3 . Liquid fuel ramjet hydrocarbon fuels such as RJ-4, RJ-5, RJ-6, and RJ-7 have somewhat higher density (0.040 lb/in^3) and higher volumetric performance (581 Btu/in^3). Slurry fuels, such as JP-10 with carbon slurry, and solid hydrocarbon fuels have much higher volumetric performance at the expense of somewhat higher visual observables. Even better volumetric performance can be achieved with high density solid metal fuels such as magnesium, aluminum, and boron. For example, solid boron fuel, with a theoretical solids loading of 100%, would provide over three times the volumetric performance of a liquid hydrocarbon fuel. Disadvantages of solid metal fuels are high visual observables from their plumes and the reduced volumetric efficiency from the hollow center grain core that is required for the inlet airflow.

3.11 Rocket Motor Performance

Figure 3.21 shows the relationship of the maximum incremental velocity of a rocket as a function of the propellant weight fraction and the specific impulse. The

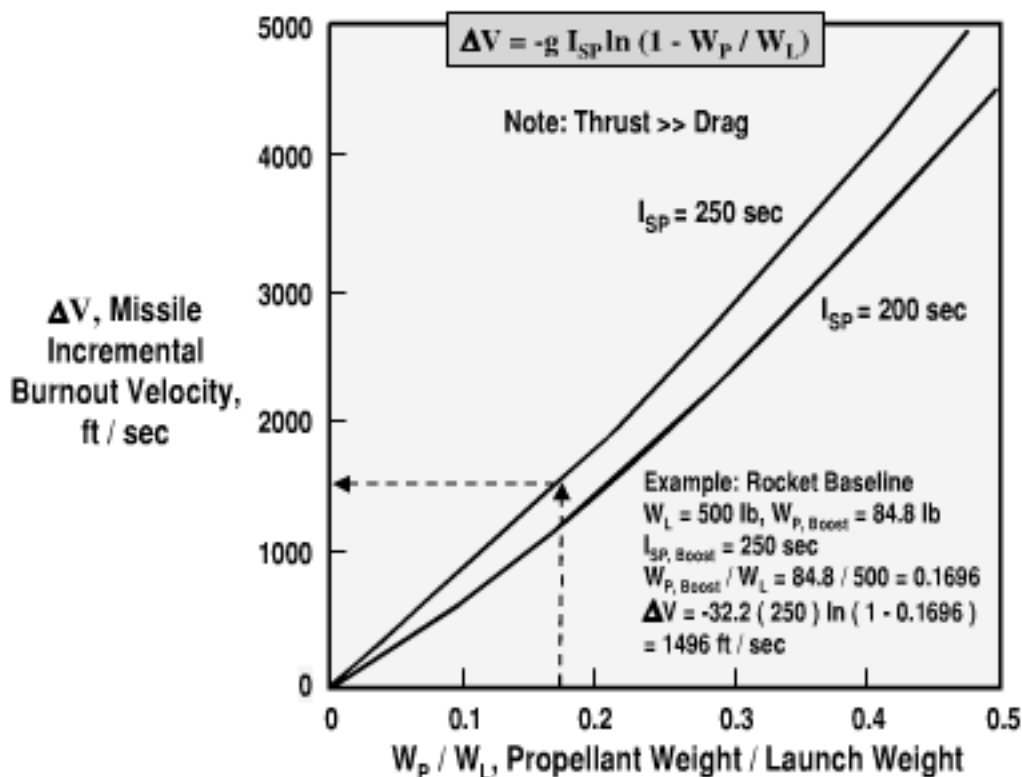


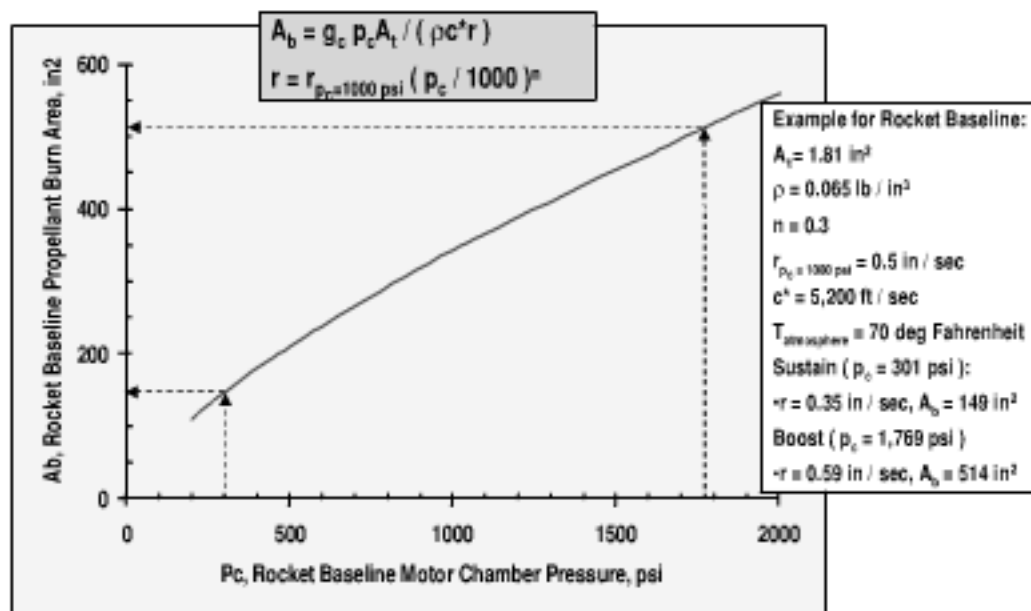
Fig. 3.21 High propellant fraction increases the missile burnout velocity.

equation is $\Delta V = -g_c I_{SP} \ln(1 - W_p / W_L)$. The figure is based on the assumption of a high thrust motor with thrust much larger than drag. Note that hypersonic Mach number can be achieved at a low speed launch only if the propellant weight is more than one-half of the missile launch weight. Higher specific impulse also gives higher burnout velocity.

For the rocket baseline missile, the launch weight is $W_L = 500$ lb, boost propellant weight is $W_p = 84.9$ lb, and the specific impulse during boost is $I_{SP} = 250$ s. The maximum incremental velocity due to boost is computed to be $\Delta V = 1496$ ft/s. For a typical launch condition of Mach 0.8, 20,000 ft in altitude, the launch velocity is 820 ft/s, resulting in a theoretical end-of-boost velocity of 2316 ft/s. The actual end-of-boost velocity is lower, because of drag.

Figure 3.22 shows a relationship of the propellant burn area to the burn pressure of the rocket baseline. The equations are $A_b = g_c p_c A_t / (\rho c^* r)$ and $r = r_{p_c=1000\text{psi}} (p_c / 1000)^n$. The required burn area is a function of the chamber pressure, throat area, propellant density, characteristic velocity, and the propellant burn rate. Unlike airbreathing or liquid propellant propulsion, the combustion chamber of a solid propellant rocket does not need additional volume to complete combustion. Because the oxidizer and fuel are already mixed in the propellant, combustion occurs nearly instantaneously at the burning surface.

The rocket baseline has a throat area $A_T = 1.81$ in.² and a propellant density $\rho = 0.065$ lb/in.³ The burn rate exponent is $n = 0.3$, referenced to a nominal chamber pressure of 1000 psi and a nominal atmospheric temperature of 70°F. The nominal burn rate at standard conditions (chamber pressure of 1000 psi, atmospheric temperature of 70°F) is $r_B = 0.5$ in./s. Note from the figure that during sustain, with a chamber pressure of $p_c = 301$ psi, the required burn area $A_B = 149$ in.²



Note: A_b = propellant burn area, g_c = gravitation constant, A_t = Nozzle throat area, ρ = density of propellant, c^* = characteristic velocity, r = propellant burn rate, $r_{p_c=1000\text{ psi}}$ = propellant burn rate at $p_c = 1,000 \text{ psi}$, p_c = chamber pressure, n = burn rate exponent

Fig. 3.22 Large propellant burn area is required for high chamber pressure.

For the 8-in.-diam rocket baseline, the body cross-sectional area is 50 in.². An end-burning grain for the rocket baseline nozzle geometry and propellant would not provide the required chamber pressure. A center cavity grain is used by the rocket baseline to obtain the required burn surface area for boost and sustain thrust. For the rocket baseline boost chamber pressure $p_c = 1769 \text{ psi}$, the required burn area is larger, $A_b = 514 \text{ in}^2$.

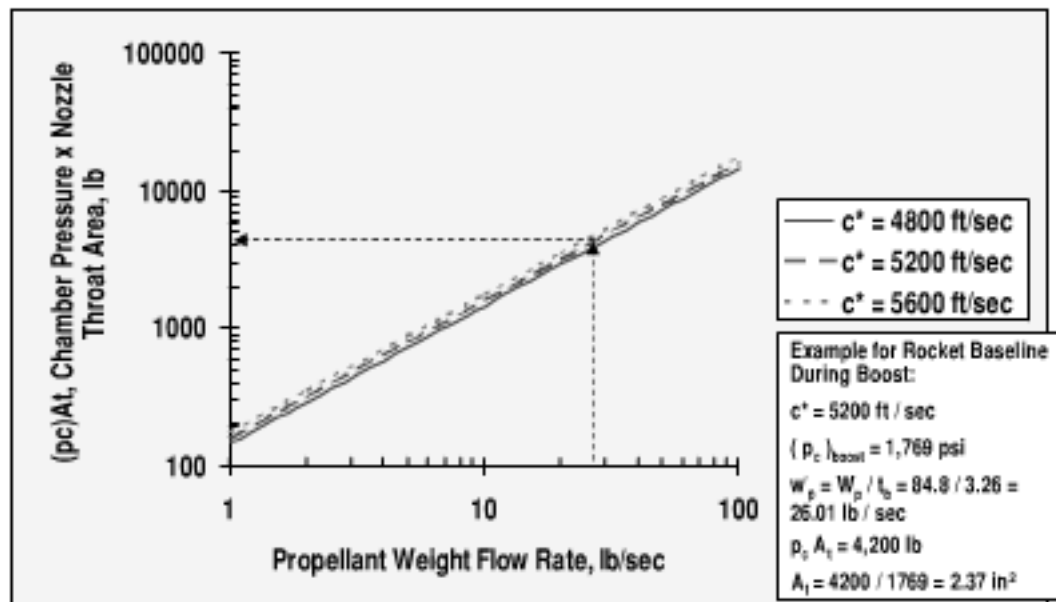
Shown in Fig. 3.23 is the area of the nozzle throat that is necessary to provide a required propellant weight flow rate. The equation is $A_t = c^* w_p^* / (g_c p_c)$. Note that the necessary throat area A_t increases with increased values of the design propellant burn rate w_p^* and characteristic velocity c^* . Also note that the necessary throat area decreases with an increased value of the design chamber pressure p_c . The range of values shown in the figure are typical values of A_t , w_p^* , c^* , and p_c for tactical missiles.

As an example, the rocket baseline has a propellant characteristic velocity of $c^* = 5200 \text{ ft/s}$. At the boost condition the motor chamber pressure is $p_c = 1769 \text{ psi}$ and the propellant weight flow rate is $w_p^* = 26.01 \text{ lb/s}$. The necessary nozzle throat area is computed to be $A_t = 5200(26.01) / [32.2(1769)] = 2.37 \text{ in}^2$. The computed nozzle throat area is 27% higher than the actual nozzle throat area of the rocket baseline (2.37 vs 1.81).

Nozzle exit area and nozzle throat area define the nozzle expansion ratio ($\epsilon = A_e / A_t$). It may not be possible to use the value of expansion ratio that gives the maximum value of specific impulse and thrust. The expansion ratio that provides $(I_{SP})_{max}$ and T_{max} may not allow sufficient volume for packaging subsystems around the nozzle, or it may exceed the diameter of the missile. A lower value of the design ϵ may be required, reducing the value of the achievable specific impulse and thrust.

Specific impulse, thrust, and nozzle expansion are initial considerations in the motor sizing process. Another primary design parameter is the chamber pressure.

$$A_t = c^* w_p / (g_c p_c)$$



Note: A_t = nozzle throat area, c^* = characteristic velocity, w_p = propellant weight flow rate, g_c = gravitational constant, p_c = chamber pressure

Fig. 3.23 High propellant weight flow rate requires a large nozzle.

The equations are

$$I_{\text{SP}} = c_d \left\{ \left[2\gamma^2 / (\gamma - 1) \right] \left[2 / (\gamma + 1) \right]^{(\gamma-1)/(\gamma+1)} \left[1 - (p_e/p_c)^{(\gamma-1)/\gamma} \right] \right\}^{1/2} + (p_e/p_c)\varepsilon - (p_0/p_c)\varepsilon \cdot c^* / g_c$$

$$T = (g_c/c^*) p_c A_t I_{\text{SP}}$$

$$\varepsilon = \left\{ \left[2 / (\gamma + 1)^{1/(\gamma-1)} \right] \left[(\gamma - 1) / (\gamma + 1) \right]^{1/2} \right\} / \left\{ (p_e/p_c)^{1/\gamma} \times \left[1 - (p_e/p_c)^{(\gamma-1)/\gamma} \right]^{1/2} \right\}$$

Specific impulse of a rocket is shown in Fig. 3.24 as a function of nozzle expansion ratio, chamber pressure, and altitude. These results are based on typical values of specific heat ratio ($\gamma = 1.18$), discharge coefficient ($c_d = 0.96$), and characteristic velocity ($c^* = 5200 \text{ ft/s}$). The assumed characteristic velocity of 5200 ft/s is a representative value for a high smoke propellant. The value of c^* may be less than 4800 ft/s for a low performance minimum smoke propellant at low chamber pressure and low ambient temperature. It may be greater than 5600 ft/s for a high performance high smoke propellant at high chamber pressure and high ambient temperature. Referring again to the figure, note that for low-altitude flight conditions and low chamber pressure a relatively small value of nozzle expansion is desired. At high-altitude flight conditions and high chamber pressure, a high value of nozzle expansion is desirable within the limit of the missile diameter.

As an example, the rocket baseline has a nozzle exit-area-to-throat-area ratio of $\varepsilon = 6.2$ and a nozzle throat area $A_t = 1.81 \text{ in}^2$. At an altitude of 20,000 ft, the specific impulse and thrust during boost ($p_c = 1769 \text{ psi}$) are computed to be $I_{\text{SP}} = 257 \text{ s}$ and $T = 5096 \text{ lb}$. During the lower chamber pressure sustain

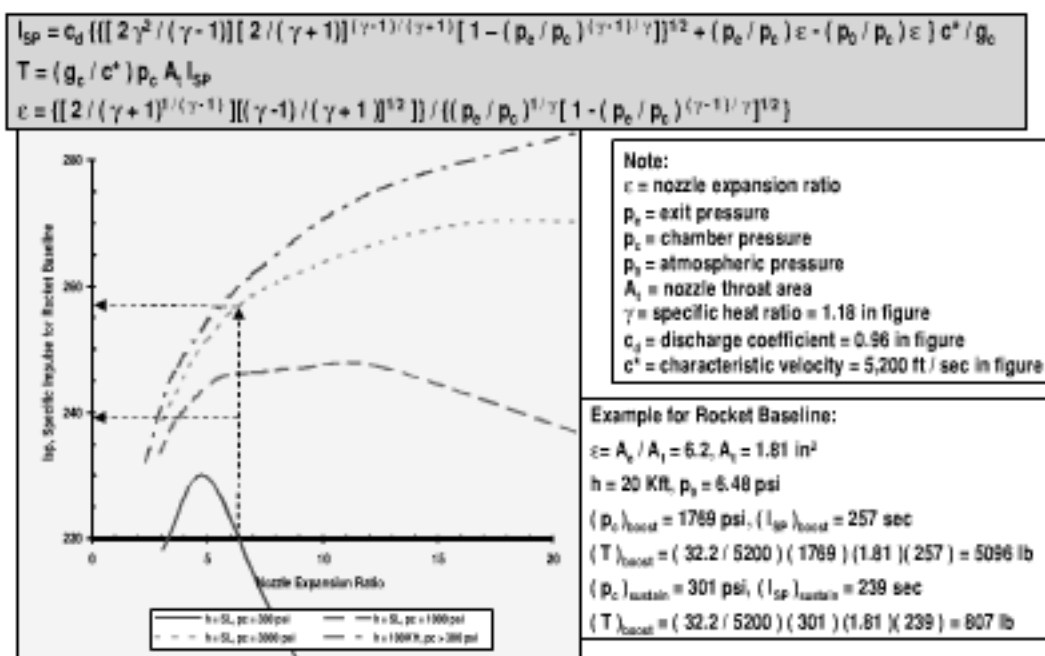


Fig. 3.24 Specific impulse of a rocket is maximized at high chamber pressure and altitude.

($p_c = 301 \text{ psi}$), the computed specific impulse and thrust are $I_{SP} = 239 \text{ s}$ and $T = 807 \text{ lb}$. It is noted that the actual specific impulse of the rocket baseline is about 3% lower than prediction (250 s vs 257 s during boost and 230 s vs 239 s during sustain). The actual thrust of the rocket baseline is about 20% higher than prediction (5750 lb vs 5096 lb during boost and 1018 lb vs 807 lb during sustain). The predicted burn time is about 20% longer than the actual burn time. A possible contributor to the differences between prediction and data is the specific heat ratio (γ) of the nozzle gases. Although the gases experience a large variation in temperature, the prediction is based on an assumption that γ is constant during the expansion of the gases through the nozzle.

3.12 Solid Motor Grain Alternatives

To define a varying thrust-time profile, a cavity through the center of the propellant grain can be used to provide the required burning surface area time profile. As shown in Fig. 3.25, a variety of shapes (e.g., wagon wheel, star) provide larger or smaller burn area and thus more or less hot gas, providing more or less thrust. The change in the burn area as a function of time provides the desired thrust-time profile. If the thrust increases with burn time, it is referred to as progressive burning. If the grain design produces a decrease in thrust with burn time, the rocket motor is said to have regressive burning characteristics. Shown in the figure are typical volumetric loadings for grain design. The volumetric efficiency of the propellant grain cavity loading for operational missiles varies from about 79% to about 87%. A disadvantage of high volumetric loading of the propellant grain cavity is that there may be problems of localized stress and cracks. Note that the length of a radial burn motor also affects the thrust. The greater burn area of a longer motor also provides higher thrust.

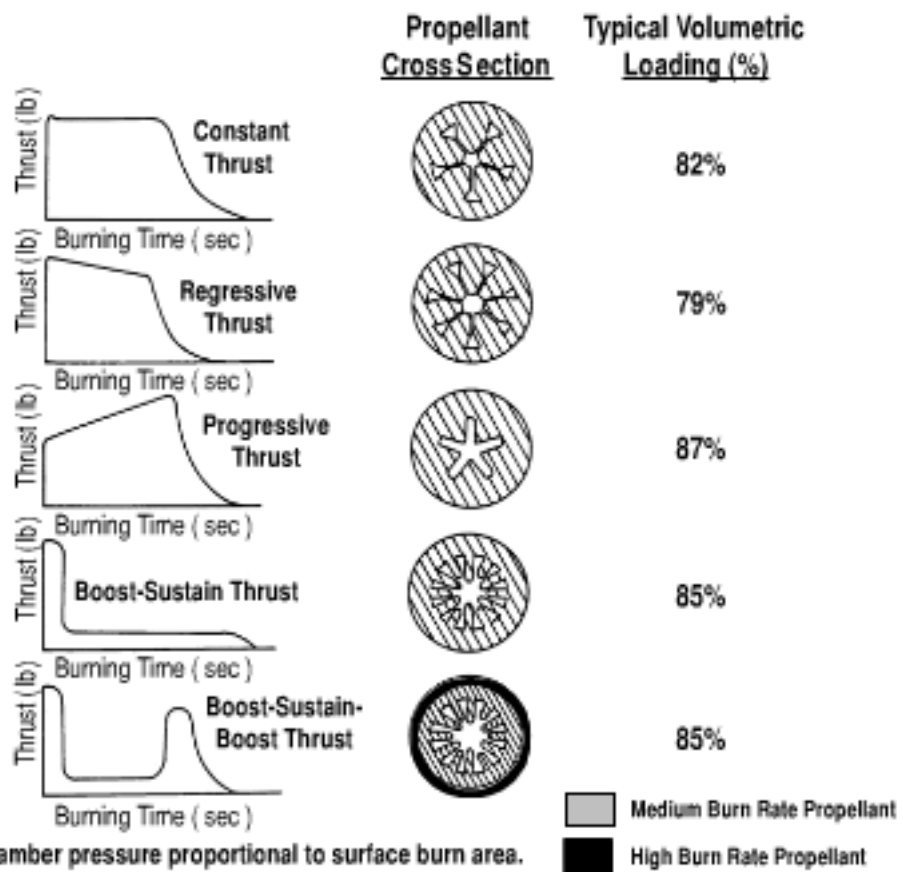


Fig. 3.25 Single burn solid rocket thrust-time design alternatives are a function of propellant cross section.

If there is no cavity, only the end of the grain burns. An end-burning grain has nearly constant burning area and thus nearly constant thrust.

3.13 Solid Rocket Thrust Control

Examples are shown in Fig. 3.26 of solid propellant motor concepts for boost-coast, boost-sustain-coast, and boost-coast-boost-coast thrust profiles. At the top of the figure are examples of single burn boost concepts based on end-burning and radial-burning grain designs. The radial-burning grain has higher burn area, providing higher thrust. In the center of the figure are two examples of single-burn concepts capable of a boost-sustain-coast thrust profile. The left middle concept has a radial-burn boost using a high burn rate propellant, continuing with an end burning sustain using a lower burn rate propellant. The right middle concept has concentric radial burn, with a high burn rate propellant for boost, followed by a low burn rate propellant for sustain. The bottom concepts in the figure are examples of thrust magnitude control, with a controlled time delay between boost and sustain. The left bottom concept is a pulse motor with a radial-burn boost using a high burn rate propellant. A barrier is provided (either mechanical or chemical) for a controlled delay in initiating the second burn. Following coast, the second burn in the example is a sustain thrust using an end-burning grain and a low burn rate propellant. Finally, the right bottom concept is another pulse motor concept based on a radial grain for boost (with high burn rate propellant), followed by second

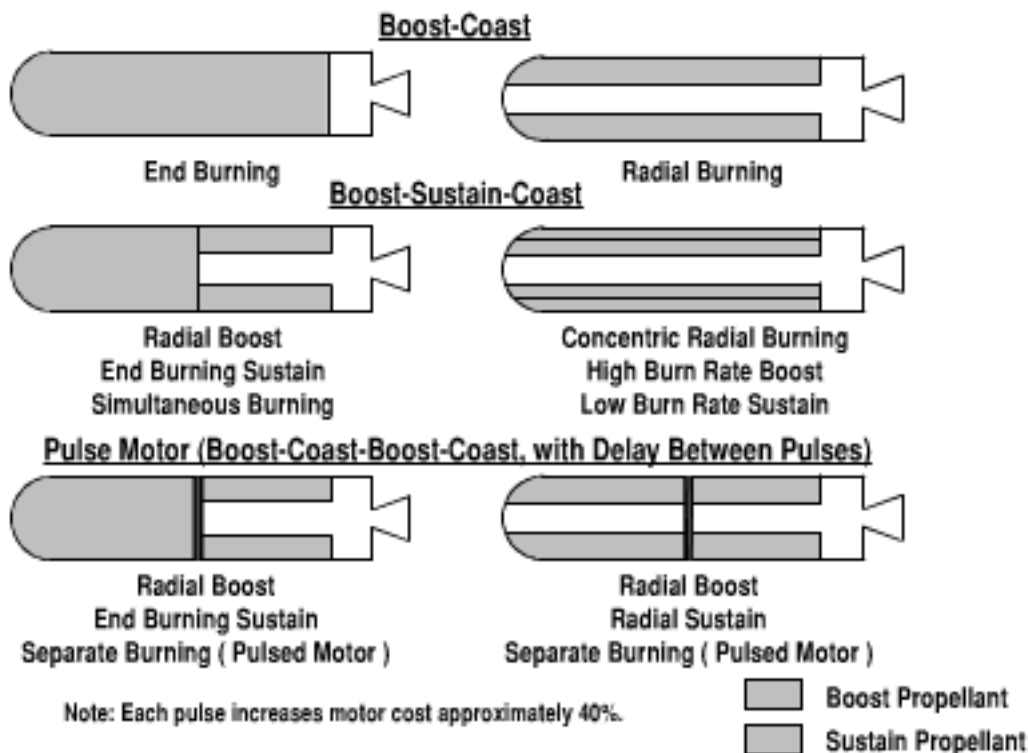


Fig. 3.26 Solid rocket alternatives of boost-coast motor, boost-sustain-coast motor, and pulsed motor.

radial grain for sustain (with lower burn rate propellant). Note that pulse motors are more expensive than continuous burn motors. Each pulse of a pulse motor increases the motor production cost by about 40%.

A design concern of layering a high burn rate propellant on top of a low burn rate propellant is the difference in the thermal expansion of the two different propellants. Localized stress and cracks can develop because of thermal expansion.

Approaches to energy management for a solid rocket using thrust magnitude control include pulsed, pintle, and gel propulsion. Figure 3.27 shows alternatives of pulsed and pintle motors.

The solid pulse motor uses thermal or mechanical barriers to separate two or more pulses. The time delay between pulses can be controlled to optimize the flight trajectory profile. As a result, a boost-coast-boost-coast pulse motor can have longer range and reduced aerodynamic heating compared with conventional single-burn boost-coast or boost-sustain-coast motors.

The second approach to thrust magnitude control, a solid pintle motor, has a pintle plug that is moved in and out of the throat area. A pintle must be constructed from a material with a very high temperature capability, such as tungsten or carbon/carbon. Moving the pintle into the throat area provides increased chamber pressure and higher thrust, whereas moving the pintle out of the throat area decreases the chamber pressure and thrust. Pintle motors have demonstrated maximum-to-minimum thrust ratios of up to 10:1. However, the larger thrust ratio is at the expense of reduced specific impulse.

A third potential alternative for thrust magnitude control is a gel propellant motor using a nonhydrocarbon gelled fuel and a chemical gelled oxidizer. Gelled

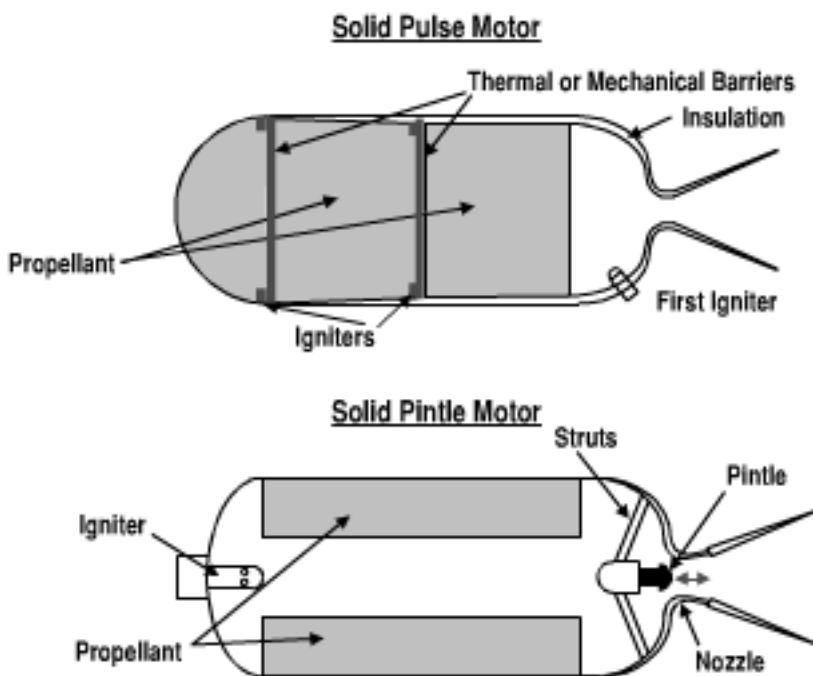


Fig. 3.27 Solid rocket motor thrust magnitude control.

nonhydrocarbon fuels and chemical oxidizers have not yet been accepted for tactical missile applications, particularly for naval platforms, because of concerns of toxicity.

3.14 Solid Propellant Alternatives

Figure 3.28 shows a comparison of solid propellant alternatives based on visual observables. Tradeoffs are rocket motor performance vs safety and observable concerns. In high smoke and reduced smoke motors, the solid propellant is a composite consisting of a fuel and an oxidizer, blended together and mixed into a binder, or polymer. The mixture is cast (poured) into the motor case and cured. The highest performance solid propellants are composite propellants based on binding a metal fuel with an oxidizer such as ammonium perchlorate. Powdered aluminum is the metallic fuel most widely used in solid rocket propellants. Benefits of a metal fuel include 1) increased combustion temperature, resulting in an increase in specific impulse; 2) increased density of the propellant, resulting in an improved volumetric performance; and 3) improved combustion stability. Binders have been based on both natural and man-made materials. The organic prepolymers have rubbery properties following cure and form a strong binding within the inorganic fuels and chemical oxidizers. The most commonly used liquid prepolymers cure much like rubber. The prepolymers used as binders in composite propellants are initially liquid, so that the fuel and oxidizer can be blended in more easily prior to the start of the polymerization cure. The polymers cure to an irreversible solid form. Unfortunately, metal fuels such as aluminum have high observable smoke particles (e.g., Al_2O_3). An initial approach to reduce plume observables is reduced smoke motors. Reduced smoke motors replace the metal fuel with a binder fuel, such as hydroxyl terminated polybutadiene binder (HTPB). The performance and

Type	I_{SP} , Specific Impulse, sec	ρ , Density, lb/in ³	Burn Rate @ 1,000 psi, in/sec	Hazard	Observables
• Min Smoke. No Al fuel or AP oxidizer. Nitramine XLDB (CL-20, ADN, HMX, RDX). Very low contrail (H_2O).	- 220 - 255	- 0.055 - 0.062	O 0.25 - 1.0	-	●
• Reduced Smoke. No Al (binder fuel), AP oxidizer. Low contrail (HCl)	O 250 - 260	O 0.062	● 0.1 - 1.5	O	O
• High Smoke. Al fuel, AP oxidizer. High smoke (Al_2O_3).	● 260 - 265	● 0.065	● 0.1 - 3.0	●	-

● Superior ● Above Average ○ Average - Below Average

Fig. 3.28 Solid rocket propellant alternatives.

insensitive munition capability of reduced smoke motors are slightly lower than that of high smoke motors. Reduced smoke propellants can still have visual observables from a hydrogen chloride contrail. The HCl contrail occurs at low atmospheric temperature.

A third type of propellant is minimum smoke propellant. Minimum smoke propellants eliminate the HCl contrail by eliminating ammonium perchlorate as an oxidizer, resulting in lower visual observables. The performance and safety of current minimum smoke propellants is not as good as that of high smoke propellants. Current minimum smoke propellants are cross-linked double-base (XLDB) propellants. In the older minimum smoke double-base propellants, the propellant consists generally of cotton (cellulose) combined with nitric acid to form nitrocellulose (guncotton), which in turn is combined with nitroglycerin, another fuel oxidizer. In the double-base propellant, the nitrocellulose serves as the binder, and the nitroglycerin causes it to solidify. Examples of current minimum smoke propellants are HMX (Her Majesty's Explosive, cyclotetramethylene tetranitramine) and RDX (Royal Demolition Explosive, cyclotrimethylene trinitramine). An example of a new minimum smoke propellant is the U.S. Navy China Lake CL-20 propellant. CL-20 is a cyclic polynitramine with a unique caged structure that provides higher crystal density, heat of formation, and oxidizer-to-fuel ratio. CL-20 propellant has 10–20% higher performance than HMX and RDX. CL-20 also has reduced shock sensitivity (Class 1.3 vs 1.1) and milder cookoff reaction than either HMX or RDX. A disadvantage of CL-20 propellant is high cost (currently more than \$400 per pound).

Another example of a new minimum smoke propellant developed by Russia is ammonium dinitramine (ADN). ADN performance and cost are similar to that of CL-20.

3.15 Motor Case Material Alternatives

Primary design considerations in selecting the materials for the motor case are shown in Fig. 3.29. These are high maximum temperature, high volumetric efficiency, light weight, ease of attachment to the airframe or launcher, and low cost. Other considerations include manufacturing, handling, storage, and environment (e.g., sea salt corrosion in a naval environment).

The most common types of motor cases are conventional quench and temper steel (hardened by heating then plunging into liquid to cool suddenly) and nickel precipitation-hardening alloy steel, aluminum alloys, strip metal/epoxy laminate (e.g., steel/epoxy laminate), titanium alloys, and composite (e.g., fiberglass reinforced plastics). If a combination of high performance and relatively low cost is required, steel is often the best material. If low cost is a factor and the motor has relatively low heating, aluminum is often the best material. A strip metal/epoxy laminate may be the best choice of moderate performance and cost. Titanium and composite cases have had relatively little application to date because of their higher current cost. The cost of a composite motor case is expected to decrease in the future, resulting in increased application of composite motor cases.

For a volume-limited missile, such as a missile packaged inside a Vertical Launch System (VLS) canister with a diameter limit, the volumetric efficiency of the material may be as important as the weight efficiency. As an example, a composite motor case may have the lightest weight, but also the largest thickness. The larger thickness of the composite case may limit the available volume for propellant, resulting in a reduction in flight range.

Internal insulation protects the motor case from the high flame temperature (e.g., 5200°F) of combustion. The internal insulator also provides the bonding of the propellant to the motor case, and must have sufficient strength to prevent the

Type	Temperature	Volumetric Efficiency	Weight	Airframe and Launcher Attachment	Cost
◆ Steel	●	●	○	●	○
◆ Aluminum	-	-	-	●	●
◆ Strip Metal / Epoxy Laminate	○	●	●	-	●
◆ Titanium	●	●	●	-	-
◆ Composite	○	-	●	-	-

● Superior ● Above Average ○ Average - Below Average

Fig. 3.29 Motor case material alternatives.

propellant from de-bonding. Most of the internal motor case insulators are rubber-based materials such as hydroxyl terminated polybutadiene or ethylene propylene dimethyl monomer.

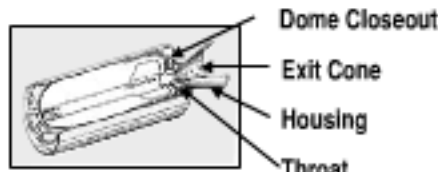
Upon exposure to the combustion flame temperature the insulator chars. A design consideration is the required insulation thickness to compensate for the recession and the change in thermal conductivity as a result of char. Another design consideration is the potential debonding from the motor case due to outgassing.

3.16 Rocket Nozzle Material Alternatives

The rocket nozzle is attached to the end of the motor case. It controls the flow of gases, converting the chemical energy released from combustion into kinetic energy. Figure 3.30 shows material alternatives for the components of the rocket nozzle, i.e., housing, dome closeout, blast tube, throat, and exit cone.

The housing is the overall structure of the nozzle. It may be made of high temperature steel for a high heating motor case, or lower temperature materials such as cellulose/phenolic or aluminum for a low heating motor. The inside of the housing usually must be insulated to maintain structural integrity.

The dome closeout is a convergent section of the nozzle that is downstream of the motor case and upstream of the throat. In the dome closeout the flow area is reduced, and the speed of the subsonic exhaust gas is increased as it is channeled to the throat. For a high heating motor with high chamber pressure and long duration, there must be an insulation insert in the dome closeout housing. The candidate dome closeout insulation materials include silica/phenolic, graphite/phenolic, and silicone elastomer. For a relatively low heating motor, low-cost glass/phenolic is a candidate insulation material for the dome closeout. For a very low heating motor



Rocket Nozzle Element	High Heating (High Chamber Pressure or Long Burn) \Rightarrow High Cost Nozzle	Low Heating (Low Chamber Pressure or Short Burn) \Rightarrow Low Cost Nozzle
<ul style="list-style-type: none"> + Housing Material Alternatives + Throat Material Alternatives + Exit Cone, Dome Closeout, and Blast Tube Material Alternatives 	<ul style="list-style-type: none"> + Steel + Tungsten Insert + Molybdenum Insert + Silica / Phenolic Insert + Graphite / Phenolic Insert + Silicone Elastomer Insert 	<ul style="list-style-type: none"> + Cellulose / Phenolic + Aluminum + Cellulose / Phenolic Insert + Silica / Phenolic Insert + Graphite Insert + Carbon – Carbon Insert + No Insert + Glass / Phenolic Insert

Fig. 3.30 Heating drives rocket nozzle materials and cost.

with low chamber pressure and short burn duration, it may not be necessary to have an insulation insert in the housing of the dome closeout.

A blast tube may be downstream of the dome closeout, if it is necessary to have additional volume to package subsystems, such as flight control actuators, around the nozzle. Ideally, the blast tube should have a small diameter to allow maximum packaging volume for the surrounding subsystems. However, as the blast tube diameter approaches the throat diameter, the local gas Mach number approaches Mach 1. Because of severe erosion from the hot gas at Mach 1, the blast tube diameter is normally larger than the throat, so that the local Mach number is less than Mach 0.8. The material alternatives for the blast tube are the same as those for the dome closeout. The material selection is driven by heating and cost considerations.

The nozzle throat is the smallest internal diameter of the nozzle assembly. At the nozzle throat the exhaust gas passes through the minimum flow area and reaches the speed of sound. Because of the high erosion at the throat, it may be necessary to have a refractory metal insert such as tungsten or molybdenum at the throat of a high performance motor. For a low heating motor, a lighter weight insert such as cellulose/phenolic, silica/phenolic, graphite, or carbon/carbon may be used.

Downstream of the throat the gases expand in the exit cone to supersonic speed. The exit cone may be contoured or conical. A contoured nozzle provides higher I_{SP} whereas a conical nozzle is lower in cost. Finally, the exit plane is at the end of the exit cone, where the static pressure of the gas is ideally nearly equal to the atmospheric pressure. The exit cone material alternatives are the same as those for the dome closeout. The material selection is driven by heating and cost considerations.

3.17 Summary

Chapter 3 provided conceptual design methods, discussed design trades, and identified high payoff technologies for tactical missile propulsion. The emphasis was on rocket and ramjet propulsion. Conceptual design methods were provided for predicting the thrust and specific impulse. Design trades included ramjet engine/booster integration alternatives, ramjet inlet options, ramjet fuel alternatives, rocket motor grain alternatives, solid propellant alternatives, motor case material alternatives, and nozzle material alternatives. New propulsion technologies were identified that have high payoff for tactical missiles. These include ramjets, ducted rockets, scramjets, high temperature combustor, oblique shock airframe compression, mixed compression inlet, low drag inlet, higher density fuel, ramjet throttle fuel control, endothermic fuel, solid rocket thrust magnitude control, and low observable fuel/propellant.

Weight Considerations in Tactical Missile Design

Conceptual design methods and technologies for tactical missile weight that are addressed in this chapter emphasize low cost and high temperature/short duration structure. Weight considerations include benefits of designing a lightweight missile, subsystem weight sensitivity to flight performance, missile system and subsystem weight prediction, methodology for center-of-gravity and moment-of-inertia prediction, guidelines for factors of safety, applications of micro-machined electro-mechanical systems (MEMS), airframe manufacturing processes and technology, airframe material alternatives, aerodynamic heating prediction, airframe structure/insulation trades, insulation material alternatives, structure design, seeker dome material trades, thermal stress concerns, and areas of localized aerodynamic heating.

Figure 4.1 shows that the next step in the missile synthesis process following propulsion sizing is weight estimation and optimization. Weight estimation and optimization is an iterative process that includes subsystem packaging, weight and balance bookkeeping, and structure weight prediction/optimization.

4.1 Benefits of Lighter Weight Missile

The benefits of designing a lighter weight missile are numerous. They include lower production cost, lower logistics cost, smaller size, higher firepower for a weight-limited/volume-limited launch platform, and reduced observables. The benefits also include better mission flexibility from the capability of carriage on multiple launch platforms (e.g., bombers, fighter aircraft, helicopters, UCAVs, ships, submarines, ground vehicles) and synergy with expeditionary warfare. The rapid force deployment requirement of expeditionary warfare requires lightweight missiles.

4.2 Subsystem Weight Sensitivity to Flight Performance

As shown in Fig. 4.2, the weight of most missile subsystems is sensitive to flight performance requirements such as speed, range, and maneuverability. Missile subsystem weights that are highly impacted by flight performance are propulsion, structure, flight control hardware, surfaces (e.g., wings, stabilizers, flight control surfaces), and aerothermal insulation. Other subsystem weights that have a second-order sensitivity to flight performance requirements are warhead/fusing and power supply. Finally, subsystem weights that are relatively insensitive to flight performance are the seeker dome, seeker, and guidance and control.

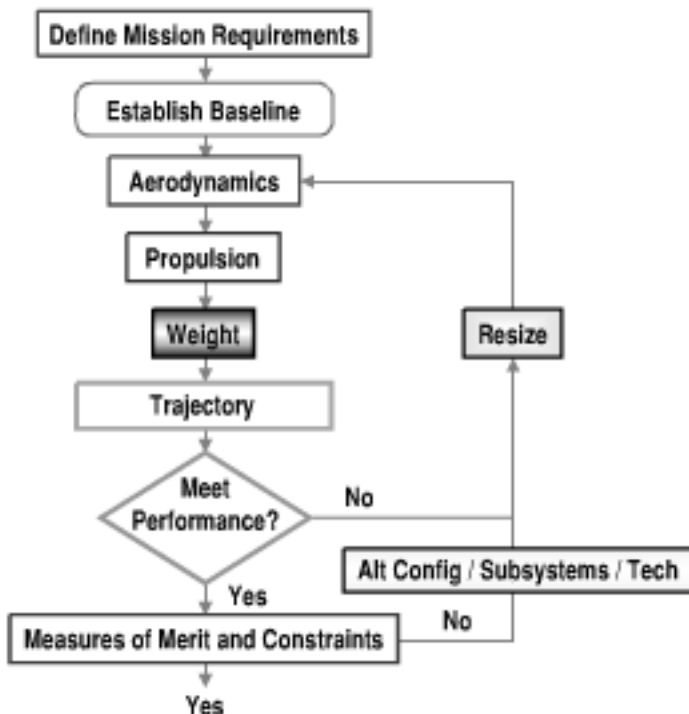


Fig. 4.1 Missile concept synthesis requires iteration.

4.3 Missile Weight Prediction

The average subsystem density of a tactical missile is about 0.05 lb/in.^3 . Except for the nose section, most missile bodies can be represented as a cylinder of diameter d and length l . The volume of a cylinder is $V = (\pi/4)ld^2$. Neglecting the geometry difference of the missile nose from that of a cylinder and neglecting the weight of the surfaces, the missile weight should correlate as the average density times the volume of a cylindrical body [$W_L = \rho_M V = 0.05(\pi/4)ld^2 = 0.04ld^2$].

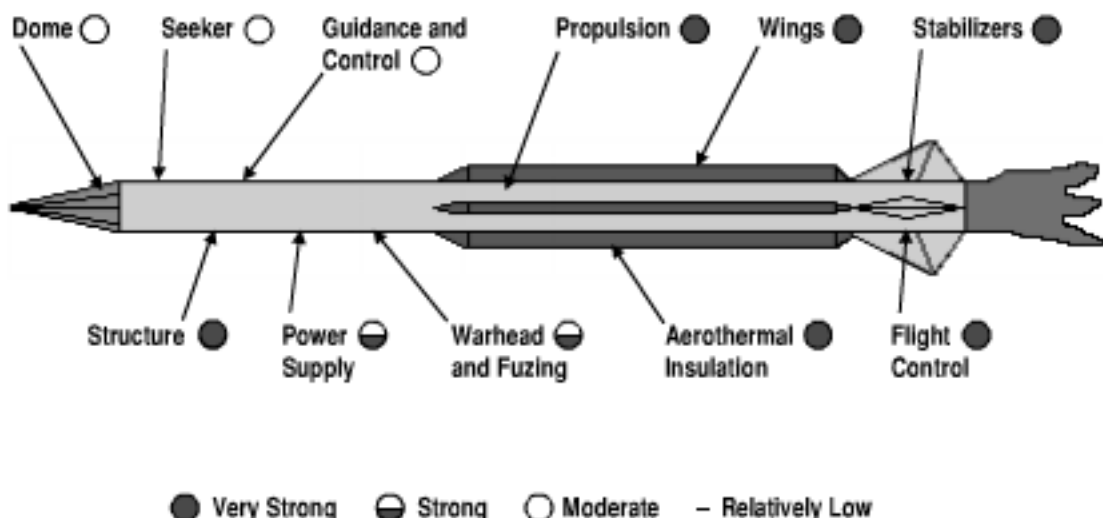


Fig. 4.2 Subsystem weight is sensitive to flight performance (range, speed, maneuverability).

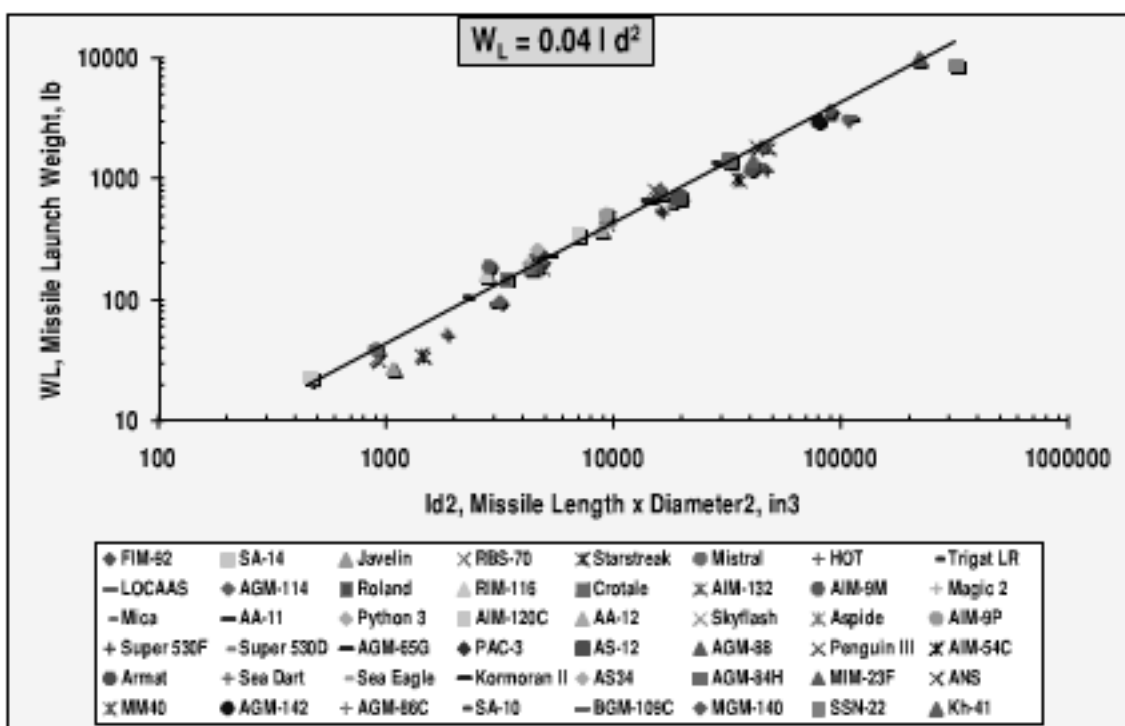


Fig. 4.3 Missile weight is a function of diameter and length.

Figure 4.3, which is based on the weight of 48 tactical missiles, shows the correlation of the predicted weight with the actual weight. The scatter in the data includes the effects of differences in the launch environment, maneuverability, subsystem density, nose fineness, body cross-sectional geometry, boattailing, and the surface planform geometry. Note from the figure that the lightest weight missiles (FIM-92, SA-14, Javelin, RBS-70, Starstreak, Mistral) are man-portable, tube launched missiles with a relatively benign launch environment, relatively small warhead, and small surfaces.

A more detailed description of missile weight at the subsystem level is shown in Fig. 4.4. Shown are typical values of subsystem density for rocket-powered missiles. Except for structure density, the subsystem density varies from 0.04 to 0.07 lb/in.³ A more accurate estimate of missile weight is obtained by estimating the individual subsystem volumes, densities, and weights through a missile weight statement.

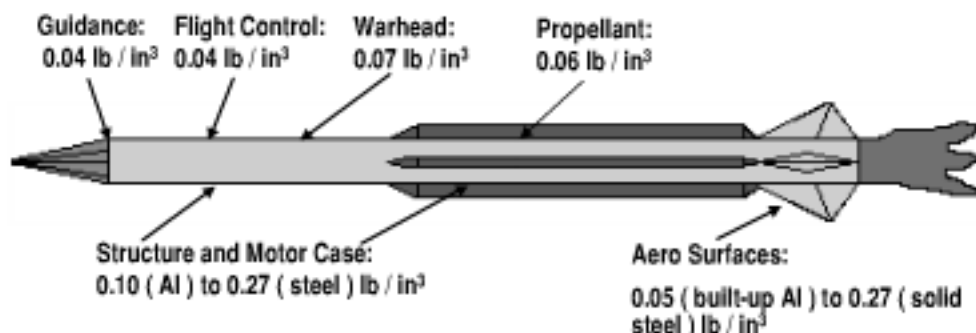


Fig. 4.4 Subsystems densities for rocket-powered missiles.

4.4 Center-of-Gravity and Moment-of-Inertia Prediction

The methodology for missile weight, balance, and moment-of-inertia prediction is shown in Fig. 4.5. Missile weight is the summation of the individual weights of the subsystems, structure, surfaces, and fuel/propellant. Launch weight and burnout weight estimates are required for analysis of the missile flight performance.

The missile center of gravity is estimated by summing each subsystem weight times its distance from the nose tip, divided by the missile weight. As an example, the longitudinal location of the center of gravity is

$$x_{CG} = \sum (x_{\text{subsystem}1} W_{\text{subsystem}1} + x_{\text{subsystem}2} W_{\text{subsystem}2} + \dots) / W_{\text{total}}$$

Again, x_{CG} must be calculated for launch and burnout.

The moment of inertia about the missile center of gravity is calculated by summing the local moment of inertia of each subsystem about its center of gravity, plus the weight of each subsystem times the square of the distance of the subsystem from the missile center of gravity. As an example, the moment of inertia about the y axis is

$$I_y = \sum [(I_{y,\text{subsystem}1})_{\text{local}} + W_{\text{subsystem}1}(x_{\text{subsystem}1} - x_{CG})^2/g_c + (I_{y,\text{subsystem}2})_{\text{local}} + W_{\text{subsystem}2}(x_{\text{subsystem}2} - x_{CG})^2/g_c + \dots]$$

Moment of inertia is calculated for both the launch and burnout conditions.

Figure 4.6 shows the local moment of inertia (I_y)_{local} variation with body fineness ratio l/d for cylindrical and conical bodies. Note the large increase in the moment of inertia with increasing fineness ratio. As an example, the ramjet baseline can be approximated as a cone-cylinder configuration for the moment-of-inertia calculation. The local moment of inertia of the conical nose about its center of gravity is

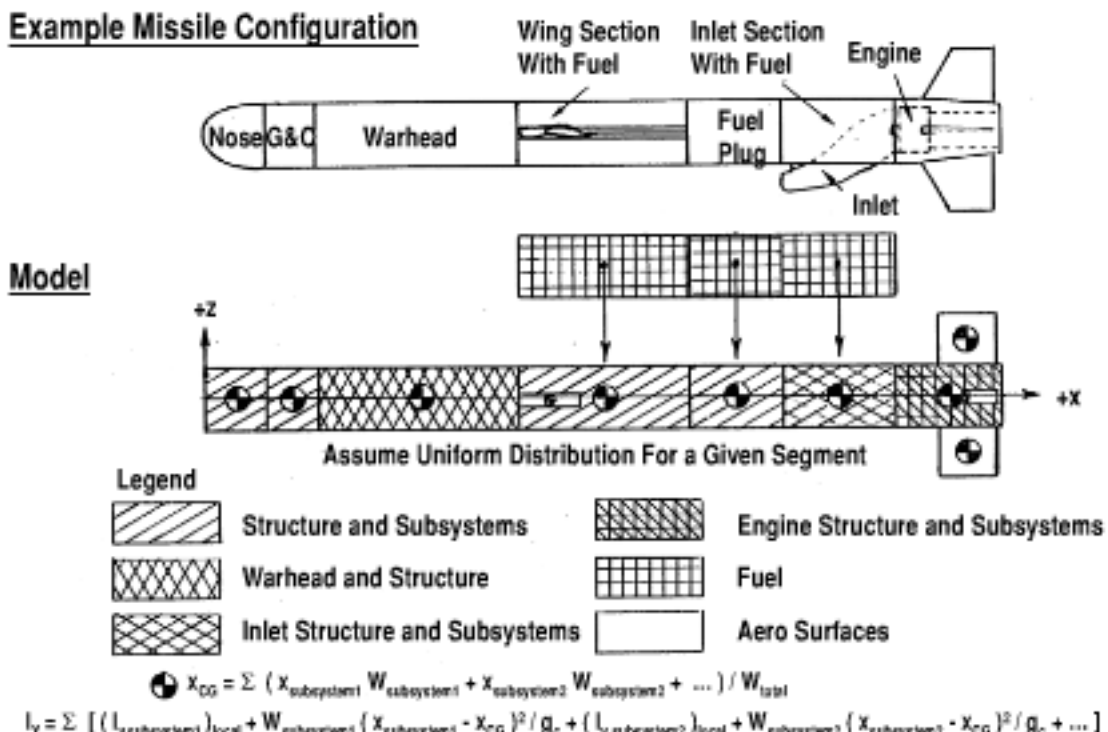


Fig. 4.5 Modeling weight, balance, and moment of inertia.

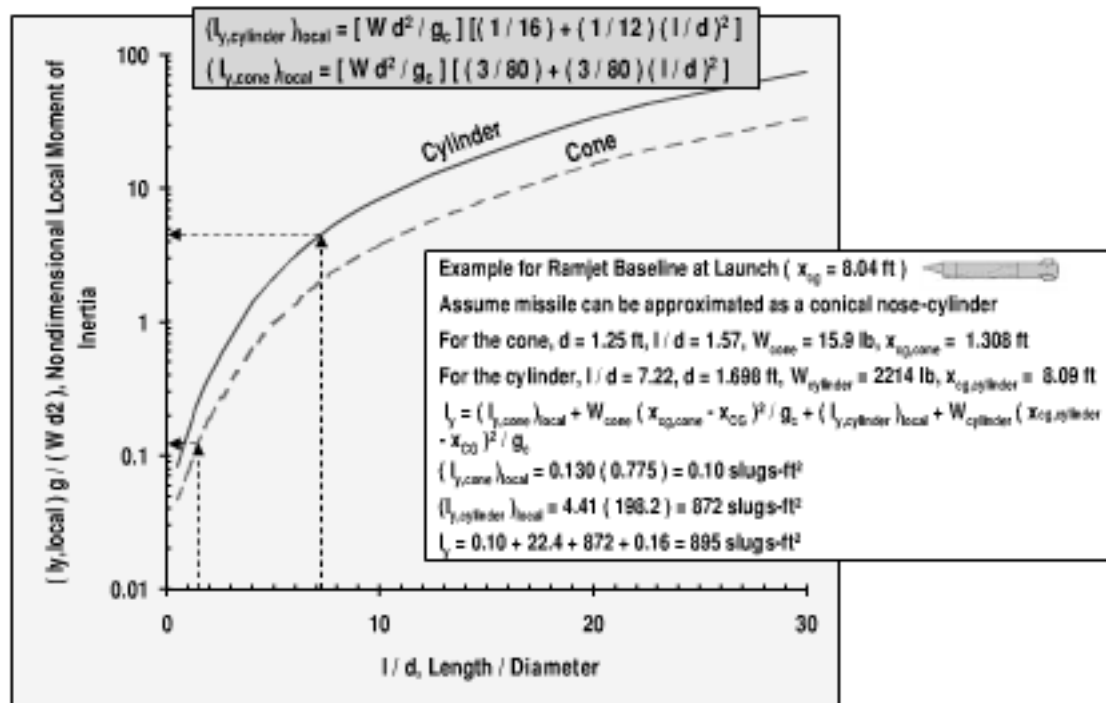


Fig. 4.6 Missile moment of inertia is higher for a high fineness ratio body.

$(I_{y,cone})_{local} = 0.13 \text{ slugs}\cdot\text{ft}^2$. The local moment of the cylindrical approximation of the rest of the missile is $(I_{y,cylinder})_{local} = 872 \text{ slugs}\cdot\text{ft}^2$. The moment of inertia about the missile center of gravity is given by

$$I_y = (I_{y,cone})_{local} + W_{cone}(x_{cg,cone} - x_{CG})^2 / g_c + (I_{y,cylinder})_{local} + W_{cylinder}(x_{cg,cylinder} - x_{CG})^2 / g_c$$

Substitution gives the total moment of inertia of the ramjet baseline at launch as $I_y = 895 \text{ slugs}\cdot\text{ft}^2$.

4.5 Factor of Safety

Typical factors of safety for tactical missiles are shown in Fig. 4.7. The factor of safety of a missile tends to be high where there is a danger of fratricide. As an example, pressure bottle ultimate and yield factors of safety are typically 2.5 and 1.5, respectively. Missile gas bottles may be pressurized up to 10,000 psi. Because gas bottles require periodic logistics maintenance and inspection by ground personnel, the required factor of safety is high. Another area where the factor of safety is high is in the area of ground handling loads, such as cross-country transportation. Factors of safety for ground handling loads are about 1.5 for ultimate loads and 1.15 for yield loads. Other examples of high factor of safety are launch platform carriage and separation. During carriage or during aircraft separation, missile factors of safety are required to be about 1.5 for ultimate and 1.15 for yield. The motor case is designed not only for conditions of environmental extremes, such as a hot day, but also for consideration of safety. The ultimate and yield factors of safety for the motor maximum effective operating pressure are about 1.5 and 1.1, respectively. The required factors of safety are lower for flight conditions where the missile is safely away from the launch platform. For example, missile-free flight

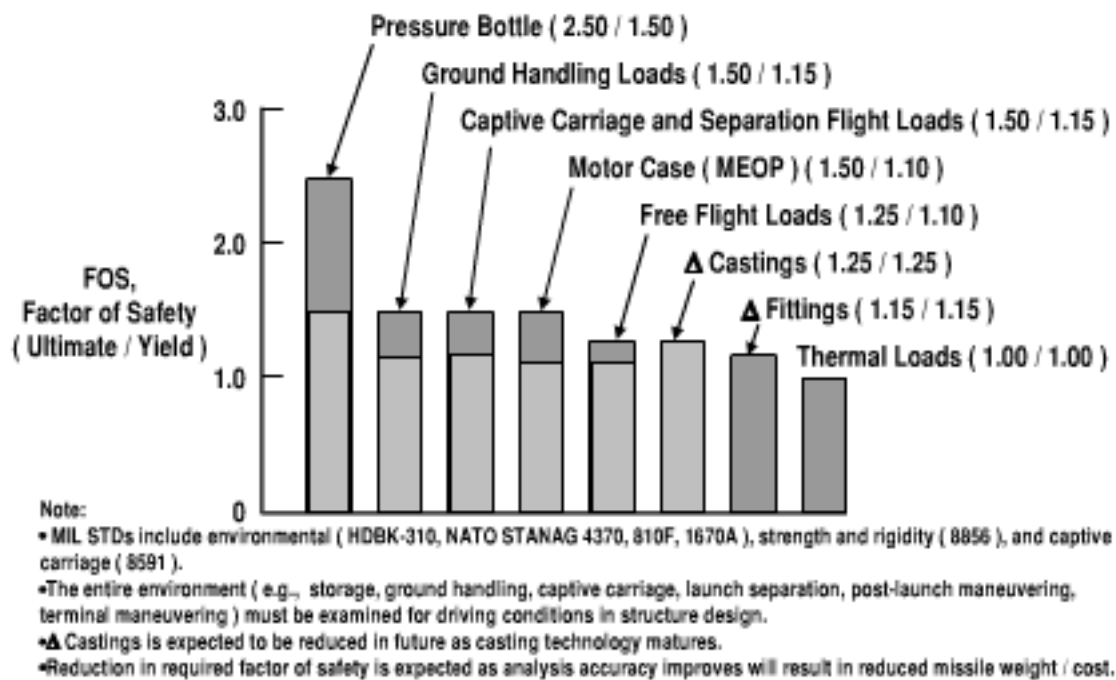


Fig. 4.7 Structure design criteria factor of safety for missiles.

load factors of safety are about 1.25 and 1.1, respectively, and the thermal loads, which occur near the end of flight, are just design considerations with a factor of safety of 1.0. A distinguishing characteristic of tactical missiles is a lower factor of safety compared with manned aircraft or even unmanned air vehicles (UAVs). Because missiles are a throwaway, the factor of safety can be reduced if there is no danger involved to friendly forces. This would result in lighter weight compared with an aircraft or a UAV. Note that an additional factor of safety is required for structural areas where there is a relatively large design uncertainty. An example is castings, which can have hidden voids. Castings currently require an incremental factor of safety of about 1.25 in addition to the normal design factors of safety. Fittings also require an additional factor of safety of about 1.15 because of the uncertainty in the analysis for attachment integrity. The applicable military standards in the United States that are considered in factors of safety include environmental (HDBK-310, NATO STANAG 4370, MIL-STD-810F, MIL-1670A), strength and rigidity (MIL-STD-8856), and captive carriage (MIL-STD-8591) military standards.

A technology opportunity to reduce missile weight is to develop more accurate predictions of the missile environment, loads, and strength. This would allow a reduction in the factor of safety (i.e., factor of ignorance).

4.6 Micro-Machined Electro-Mechanical Systems (MEMS)

Because high performance missiles such as ramjets are weight and volume limited, there is leverage in reducing weight. Reduced weight is consistent with reduced cost, improved performance, and improved launch platform compatibility. One approach to reduce missile weight is to reduce the required factors of safety. Technology in improved analysis and development tools will provide reductions in missile weight and cost by reducing the design uncertainty and the required factors of safety. An example is the MEMS technology illustrated in Fig. 4.8.

- ◆ Micro-machined Electro-Mechanical Systems (MEMS)
 - ◆ Small size / low cost
 - ◆ Semiconductor manufacturing process
 - ◆ 2,000 to 5,000 sensors on a 5 inch silicon wafer
- ◆ Missile Development Application
 - ◆ Wireless (RF) Data Collection and Health Monitoring
- ◆ Distributed Sensors Over Missile
 - ◆ Stress / strain
 - ◆ Vibration
 - ◆ Acoustics
 - ◆ Temperature
 - ◆ Pressure
- ◆ Allows Reduced Design Uncertainty / Factor of Safety
 - ◆ Provides reduced weight and cost



Fig. 4.8 Small-size MEMS sensors can reduce required factor of safety, saving missile weight.

MEMS devices are fabricated from a single piece of silicon by semiconductor manufacturing processes, resulting in a small size, low-cost package. For example, between 2000 and 5000 MEMS sensor devices can be produced from a single 5-in. silicon wafer. Future tactical missiles will have low-cost/small size MEMS sensors for data collection during missile development and for health monitoring after production. Localized stress/strain, vibration, acoustics, temperature, pressure, and other measurements can be monitored through many sensors distributed around the airframe. The higher confidence because of MEMS data will allow weight reduction in the overdesigned structure.

4.7 Manufacturing Processes

Figure 4.9 shows examples of manufacturing processes that are used for tactical missile airframes and surfaces. A driving consideration for cost reduction is to minimize the parts count. Examples of manufacturing processes that reduce the parts count include vacuum assisted resin transfer molding (RTM), filament winding, pultrusion, casting, vacuum bag/autoclave forming, metal forming, strip laminate, and compression molding.

Examples of low-cost manufacturing processes that are particularly applicable to complex shapes are precision casting, vacuum assisted RTM, filament winding, and pultrusion. Precision casting is particularly suitable. It has high payoff for reducing the cost of high temperature metal airframes with complex shape. A historical limitation in applying castings to complex configurations is the tight manufacturing tolerances required for the complex configurations. However, new technology such as ceramic tooling allows low-cost precision castings suitable for complex airframe configurations such as ramjets. Castings reduce the parts count with a resulting cost savings. Large precision cast structures are in development for complex missile shapes, such as ramjets. A one-piece cast airframe design integrates

Geometry Alternatives	Structure Concept Alternatives	Structure Manufacturing Process Alternatives								
		Composites					Metals			
		Vacuum Assist RTM	Compression Mold	Filament Wind	Pultrusion	Thermal Form	Vacuum Bag / Autoclave	Cast	High Speed Machine	Forming
Lifting Body Airframe 	Monocoque Integrally Hoop Stiffened Integrally Longitudinal Stiffened	● ● ●	● ● ○	● ● ●	● ● ●	● ● ●	● ● ●	● ● ●	-	● ●
Axisymmetric Airframe 	Monocoque Integrally Hoop Stiffened Integrally Longitudinal Stiffened	● ● ●		● ● ●		● ● ●	● ● ●	● ● ●	● ●	● ●
Fin or Wing 	Monocoque Sandwich	● ●	● ●		● ●	● ●	● ●	● ●	● ●	● ○

Note: Manufacturing process cost is a function of recurring cost (unit material, unit labor) and non-recurring cost (tooling).

Note: ● Very Low Parts Count ○ Low Parts Count □ Moderate Parts Count - High Parts Count

Fig. 4.9 Structure concepts and manufacturing processes for low parts count.

all of the secondary structure to minimize parts count. Precision casting minimizes subsequent machine and hand finishing of mating surfaces by achieving a precision surface finish “as-cast.” Fuel cells can be an integral part of the structure and not require bladders. Structural attachment points (e.g., ejector attachments, payload supports, booster attachments) and self-indexing/aligning features can be integral to the structure. This minimizes or eliminates mating/alignment/assembly tooling and test/inspection requirements. Precision castings have been demonstrated for missile aluminum, titanium, and steel airframes, motor cases, and combustors.

Shown in Fig. 4.10 are schematics of the manufacturing processes for vacuum assisted RTM, composite filament winding, composite pultrusion, and metal casting. As stated previously, these processes are particularly suited to lifting body airframes with complex shapes, providing cost benefits from the reduced parts count.

The vacuum assisted resin transfer molding process consists of inserting fibers into a mold, pulling a vacuum, injecting resin into the fibers, and curing the part. The vacuum assisted RTM process has advantages of high production rate and good tolerances (e.g., $+/- 0.005$ in.).

Filament winding is an automated process that is suited to circular and elliptical cross-sectional shapes such as airframes and motor cases. The filament fibers are pulled through a resin bath and wound around a mandrel. The resin is usually worked into the fibers by roll coaters or by breaker bars in dip tanks. Cycle time is about 1 h for winding and about 3 h for oven curing. Because the winding action itself compacts the laminate, vacuum bagging or other compaction methods are not necessary.

Pultrusion is a continuous, automated closed-molding process that is cost effective for high volume production of circular and elliptical cross-sectional shapes. The process pulls the fiber and resin continuously through a heated steel die, where the part cures.

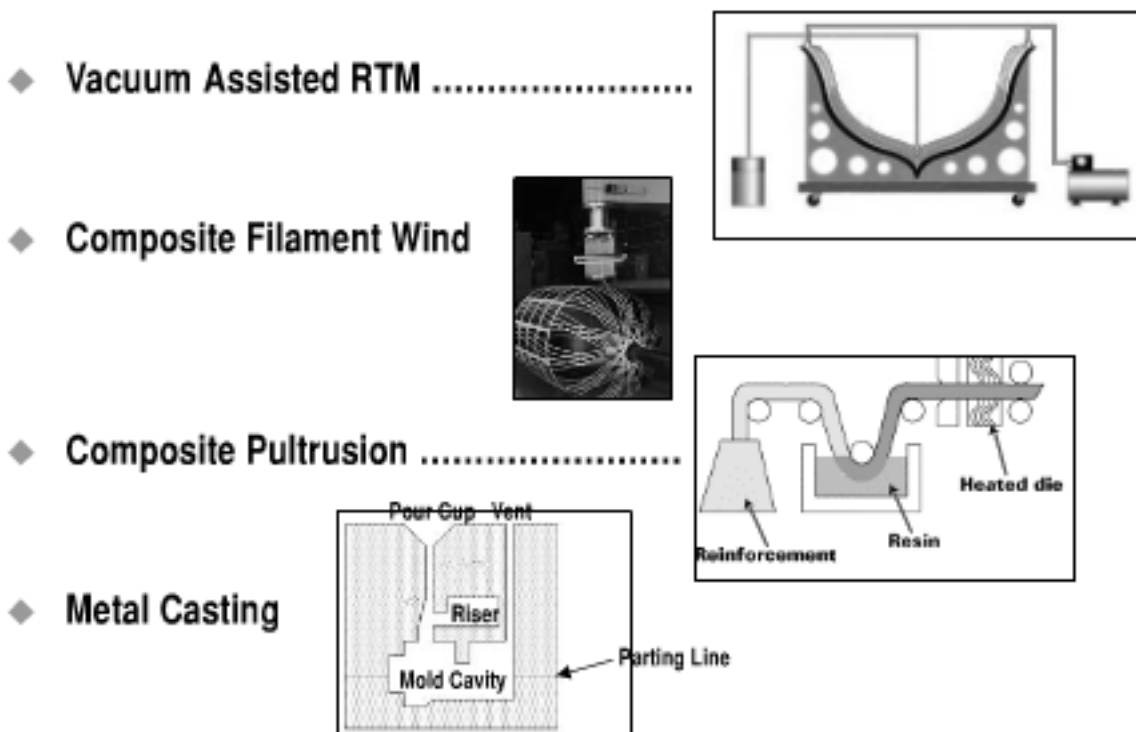


Fig. 4.10 Low parts count manufacturing processes for lifting body airframe.

Metal casting is particularly suited to reducing the parts count and cost of complex, nonaxisymmetric airframes, such as ramjets. It is also applicable to surfaces. Precision casting is based on a permanent precision die, such as a ceramic die. The mold cavity is filled with molten metal by gravity pouring. As the metal cools, the mold cavity, riser, and pour cup become one solid casting. When the metal has cooled and solidified, the ceramic die is opened at the parting line and the part is removed by techniques such as vibration and water blasting.

4.8 Airframe Material Alternatives

Examples of tactical missile alternative airframe materials and their tradeoffs are shown in Fig. 4.11. Metallic airframe material alternatives of Aluminum 2219, Steel PH 15-7Mo, and Titanium 6Al-4V are shown in the order of increasing cost. Similarly, composite airframe material alternatives of 1) S994 glass/epoxy and S994 glass/polyimide, 2) glass or graphite reinforced molding, and 3) graphite/epoxy and graphite/polyimide are shown in the order of increasing cost. Design considerations for airframe materials are maximum allowable stress, compression stability, maximum temperature for the short-duration flight of tactical missiles, sensitivity to thermal stress, ease of joining to adjacent structure/subsystems, low cost, and light weight.

For a lightweight tactical missile airframe at moderate temperatures, graphite/epoxy and graphite/polyimide materials may be preferred. For a high temperature airframe, titanium or steel materials are often preferred. For a low-cost airframe the preferred materials are usually aluminum, steel, S994 glass/epoxy, or S994 glass/polyimide.

Figure 4.12 shows the strength of typical airframe materials. Shown are the tensile strength and the stress-strain curves of small diameter graphite, Kevlar,

Type	Material	Tension (FTU/p)	Compression Stability (FCR/p)	Max Short-Life Temp	Thermal Stress	Joining	Cost	Weight
Metallic Increasing Cost ↓	Aluminum 2219	○	●	-	-	●	●	○
	Steel PH 15-7Mo	●	-	●	○	●	●	-
	Titanium 6Al-4V	●	○	●	●	○	-	○
Composite Increasing Cost ↓	S994 Glass / Epoxy and S994 Glass / Polyimide	●	○	○	●	○	●	●
	Glass or Graphite Reinforce Molding	-	○	○	●	○	○	●
	Graphite / Epoxy and Graphite Polyimide	●	○	●	●	-	-	●

Note: ● Superior ○ Above Average ○ Average - Below Average

Fig. 4.11 Tactical missile airframe material alternatives.

and glass fibers (without a composite matrix); high strength steel (such as precipitation hardening stainless steel); titanium alloy; and aluminum alloy material alternatives. Note that the strength capability of advanced small diameter fibers is very high. For example, as shown in the figure, the unidirectional tensile strength of graphite (carbon) fiber is more than 400,000 psi. Small diameter Kevlar and glass fibers may have comparable strength to graphite or carbon fiber, but also exhibit relatively high strain under load. In addition to small diameter fibers, advanced

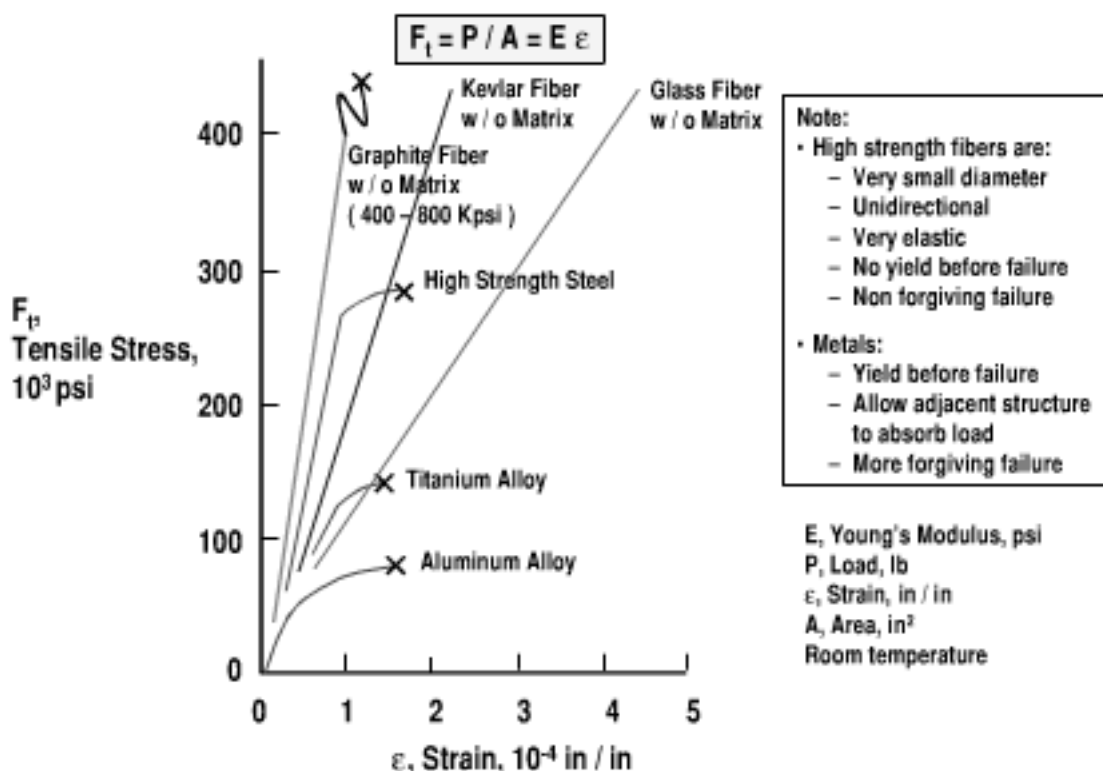


Fig. 4.12 Strength, elasticity of airframe material alternatives.

composite structures have long, continuous fibers and a fiber/matrix ratio that is greater than 50% fibers by volume. Fibers can be graphite (carbon), Kevlar, glass, boron, ceramic, silicon carbide, quartz, polyethylene, and others. As an example of strength at the structure level, a 50% volume graphite composite structure can have strength in a tailored laminate that is above 200,000 psi, much greater than that of aluminum, or even most steels. Also, the low density of composites further reduces the weight compared with metals. Graphite fiber composite materials have extremely high moduli of elasticity, resulting in low strain and deflection compared to metals. However, note with caution that composites are not fault-tolerant. The fiber has a nearly linear stress-strain curve out to the ultimate load, at which it suddenly fails. Unlike metals that generally yield gracefully before ultimate failure, composite fibers generally fail suddenly without yield. Another disadvantage of composite structure is that failure of the structure may be hidden inside the laminate. Microcracks can spread through the matrix, decreasing the ability of the fiber to transfer load.

Figure 4.13 shows the structural efficiency advantage of composites compared to conventional materials. The example is based on a 0- \pm 45-90-deg orientation tailoring of the laminate. For short duration temperatures up to about 300°F, graphite/epoxy is a good candidate material based on its characteristics of high strength and low density. Graphite/polyimide can be used at higher temperatures, up to about 1100°F short duration temperature. Epoxy and polyimide matrices are thermoset polymer matrices. Thermosets have relatively high temperature

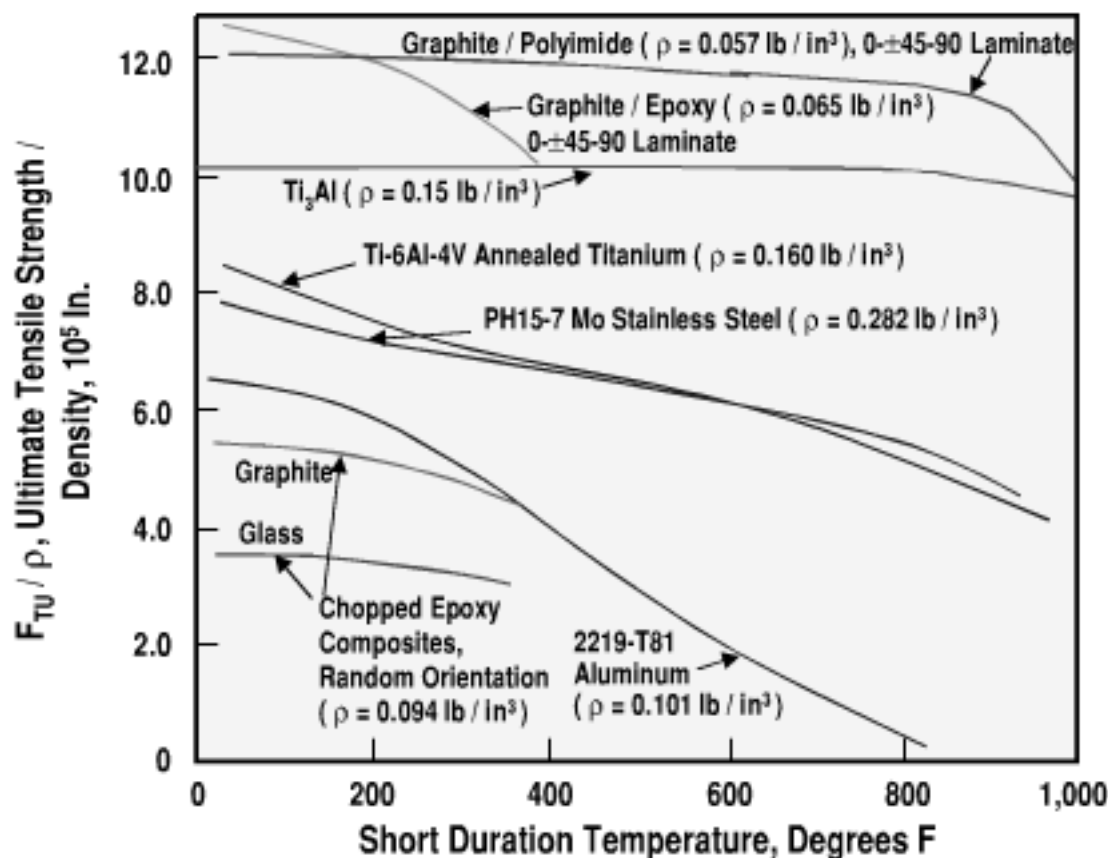


Fig. 4.13 Structural efficiency at high temperature of short-duration airframe material alternatives.

capability, good dimensional stability and solvent resistance, but they require a relatively long cure time. A common high temperature thermoset resin is phenolic. Phenolics are based on phenol (carbolic acid) and formaldehydes. An alternative low-cost polymer matrix with a shorter processing time is thermoplastic. Thermoplastics are most suitable to subsonic missiles because of a relatively low temperature capability. Examples of thermoplastic polymer matrices include polyetheretherketone (PEEK), polyphenylene (PPE), and polyetherketone (PEK). Above 1100°F, titanium and steel alloys are the best materials based on strength-to-weight ratio.

A consideration in developing a design based on composites is complexity. In addition to the material itself having greater complexity, the structures are not as straightforward as metal structures. The designer of a metal structure has two primary design considerations, material choice and the geometric configuration. Composites require another design consideration, the composite matrix orientation. Two structures of identical geometric configuration, weight and composite material, but with different layup, will have different stress-strain and failure modes as a function of orientation. The failure modes of composites, which include exploding laminate, fibers pulling free from a matrix, first-ply failure, matrix cracking, and delamination, are difficult to predict.

Metal matrix composites and ceramic matrix composites are in development for strategic missile, space, UAV, and aircraft applications. An example is titanium matrix/silicon carbide. Although the performance is very high, cost is a factor. Metal matrix and ceramic matrix composites may not be cost effective for tactical missiles.

Examples of uninsulated structure materials that are cost effective for the short-duration flight of tactical missiles are shown in Fig. 4.14. An assumption is that

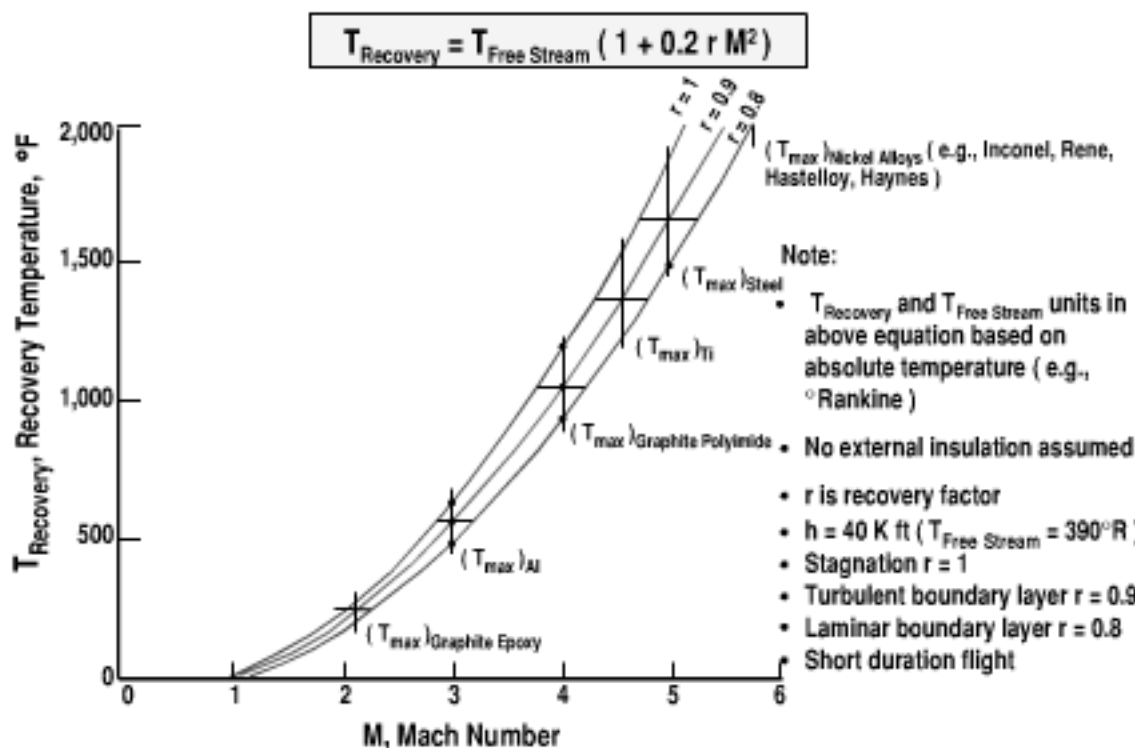


Fig. 4.14 Hypersonic missiles require high temperature structure.

the heat conducted to the airframe is large compared to the heat radiated by the airframe. This assumption is most applicable at low altitude/high atmospheric density. The airframe temperature would be lower at high altitude, due to the relative importance of radiation from the airframe. The example airframe materials selected for the figure are based on the consideration of weight, cost, and maximum temperature capability. Composite materials are a new technology that will find increased use in new missile airframe structure. High temperature composites have particular benefits for hypersonic missiles, providing weight reduction. Titanium alloy technology also enables lighter weight missiles in a hypersonic, high temperature flight environment.

As shown in the figure, at subsonic and low supersonic Mach number, graphite/epoxy and aluminum or aluminum alloys are attractive choices for a lighter weight structure without external insulation. Graphite/epoxy and aluminum alloys have high strength-to-weight ratio, are easily fabricated, have good corrosion resistance, and are low cost. For higher Mach number, graphite/polyimide composite structure has an advantage of high structure efficiency at higher temperature for Mach numbers to about Mach 4. For flight to about Mach 4.5 without external insulation, titanium structure and its alloys are preferred. A disadvantage of a titanium structure is higher material and machining cost. For example, a titanium part has a material cost that is up to 18 times that of aluminum and a machining cost that is up to 13 times that of aluminum. However, the cost to cast a part made of titanium is comparable to the cost to cast an aluminum part. Small tolerance (e.g., ± 0.001 in.) is required to avoid expensive touchup machining. Up to Mach 5.7 without external insulation (about 2000°F), super nickel alloys such as Inconel, Rene, Hastelloy, and Haynes must be used. Precision casting should be used to minimize the expensive machining and material cost associated with super alloys. Above Mach 5.7 the super alloys require either external insulation or active cooling. Active cooling is usually not cost effective for tactical missiles.

The Mach number and temperature application relationships shown in the figure are somewhat dependent upon the temperature recovery factor. At a stagnation region, such as the nose or leading edges, the recovery factor is about 1, resulting in the highest (stagnation) temperature. A turbulent or laminar boundary layer downstream of the nose or leading edge will have temperature recovery factors of about 0.9 and 0.8, respectively, with local temperatures less than stagnation.

4.9 Aerodynamic Heating Prediction

The heat flux input due to aerodynamic heating shown in Fig. 4.15 is a function of Mach number, altitude, and location from the leading edge. It is based on Ref. 11. The equation is $Q = 345\rho^{0.8}M^{2.8}/x^{0.2}$. Note that the heat transfer rate increases with higher Mach number, lower altitude, and shorter distance from the leading edge. The results are based on the assumptions of a turbulent boundary layer, a local angle of attack of 0 deg, and insulation behind the airframe (i.e., adiabatic wall).

An example is shown in the figure of the heat transfer rate of the rocket baseline missile. For an assumed distance of 1 ft from the leading edge, the heat transfer rate of the rocket baseline at Mach 2, 20,000 ft in altitude is 12 Btu/ft²/s.

An example of the skin temperature rate of increase for the rocket baseline airframe is shown in Fig. 4.16. The figure is based on Ref. 11. Note from the

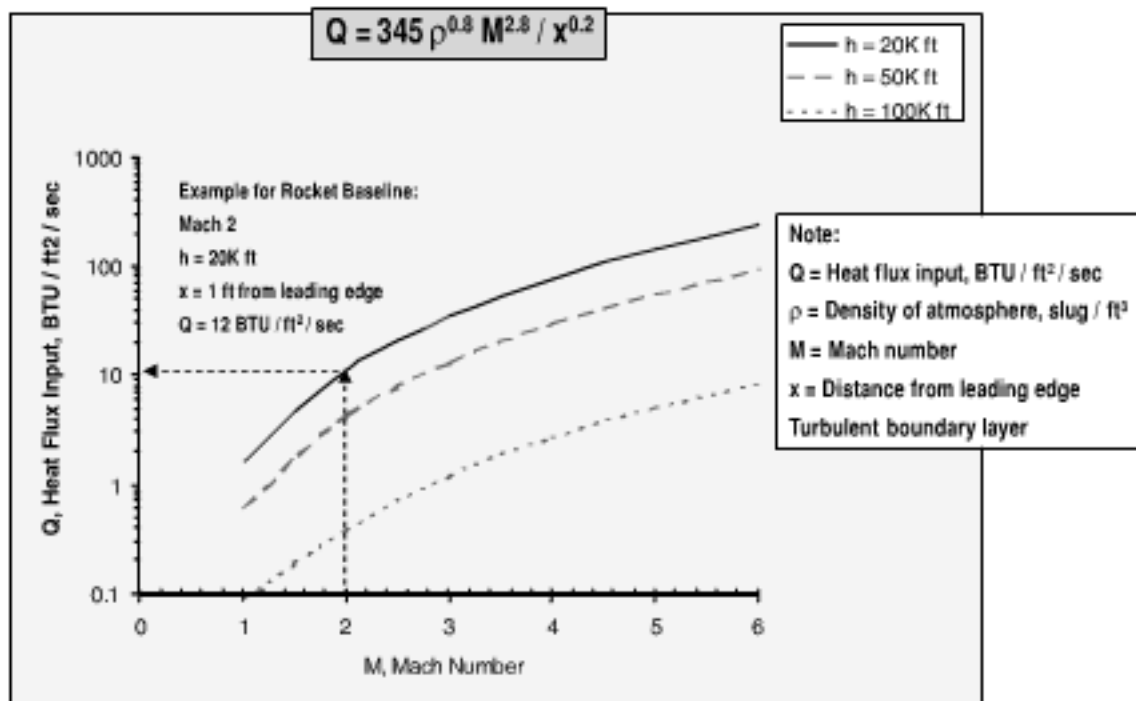
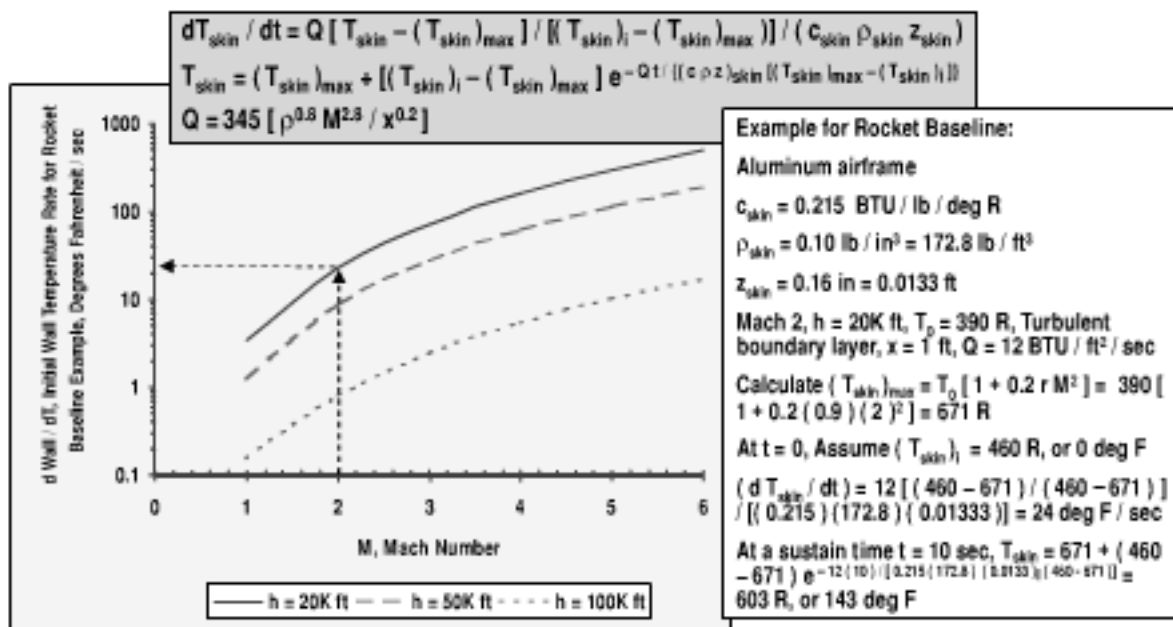


Fig. 4.15 Hypersonic missiles at low altitude have high aerodynamic heating (from Ref. 11).



Note: Insulation behind skin (adiabatic); 1-D heat transfer; Radiation neglected; Turbulent boundary layer; $x = 1 \text{ ft from leading edge}$; dT_{skin} / dt = Skin temperature rate, deg F/sec; Q = Heat flux input, BTU / ft² / sec; c_{skin} = Specific heat of skin (airframe) material, BTU / lb / deg R; ρ_{skin} = Density of skin material, lb / ft³; z_{skin} = Skin thickness, ft

Fig. 4.16 High temperature rate occurs at high Mach number and low altitude (from Ref. 11).

equation

$$\frac{dT_{\text{skin}}}{dt} = Q \{ [T_{\text{skin}} - (T_{\text{skin}})_{\text{max}}] / [(T_{\text{skin}})_i - (T_{\text{skin}})_{\text{max}}] \} / ((c_{\text{skin}} \rho_{\text{skin}} z_{\text{skin}}))$$

that the airframe skin temperature rate is a function of heat flux input, skin temperature, skin conductivity, skin density, and skin thickness. Also note from the figure that the skin temperature rate is highest at high Mach number and low altitude. The assumptions for the rocket baseline missile are an aluminum airframe, airframe skin thickness of 0.16 in., and insulation behind the airframe skin (i.e., adiabatic wall). As shown previously, at Mach 2 and 20,000 ft in altitude, the heat flux input at 1 ft behind the leading edge is 12 Btu/ft²/s. For this flight condition, the initial skin temperature rate is computed to be 24°F/s.

The equation for airframe skin temperature as a function of time is

$$T_{\text{skin}} = (T_{\text{skin}})_{\text{max}} + [(T_{\text{skin}})_i - (T_{\text{skin}})_{\text{max}}] e^{-Qt/((c\rho z)_{\text{skin}}(T_{\text{skin}})_{\text{max}} - (T_{\text{skin}})_i)}$$

For a short duration time of flight, the rocket baseline airframe will not reach thermal equilibrium. As an example, the maximum temperature at Mach 2, 20,000 ft in altitude for a turbulent boundary layer ($r = 0.9$) is

$$(T_{\text{skin}})_{\text{max}} = T_0 [1 + 0.2rM^2] = 390[1 + 0.9(2)^2] = 671^{\circ}\text{R}$$

Assuming an airframe skin initial temperature of $(T_{\text{skin}})_i = 460^{\circ}\text{R}$, the skin temperature after 10-s exposure is $T_{\text{skin}} = 603^{\circ}\text{R}$, or 143°F .

4.10 Insulation Trades

Thermal insulators are used to provide short-duration protection of structural materials from aerodynamic and propulsion heating. Airframe structure/insulation trades for tactical missiles include hot structure/internal insulation, external insulation/“cold” structure, and a one-piece self-insulating composite structure. These are shown in Fig. 4.17. A consideration for a volume-limited missile is the total thickness of the structure/insulation. Large thickness means less volume for fuel or propellant, resulting in less range. An uninsulated metal structure has the smallest thickness at low Mach number/stagnation temperature. For a relatively short duration flight at very high Mach number/stagnation temperature, an external insulator/ablator over a metal airframe with internal insulation is the lightest weight approach, at the expense of large thickness. The external insulation maintains the airframe below its maximum allowable temperature, and the internal insulation maintains subsystems (e.g., warhead, propellant/fuel, electronics) below their maximum allowable temperature. At intermediate (supersonic) Mach number, the lightest weight approach for a relatively short duration flight is either an uninsulated metal airframe with internal insulation (to protect the subsystems) or a self-insulating composite structure.

The figure also shows typical values of the insulation parameters for the alternative insulation approaches. Values of maximum temperature T_{max} , thermal conductivity k , heat capacity c , density ρ , and diffusivity α for a typical metal structure (aluminum), composite structure (graphite/polyimide), internal insulation (Min-K), and external insulation (microquartz paint) are shown. As an external insulator, microquartz paint provides a high temperature capability ($T_{\text{max}} = 2000^{\circ}\text{F}$). It protects a low temperature airframe such as aluminum ($T_{\text{max}} = 600^{\circ}\text{F}$)

Example Structure / Insulation Concepts	T_{max}	k	c	ρ	α
Metal Structure Without Insulation (e.g., Aluminum)	600	0.027	0.22	0.101	0.000722
Metal Structure	600	0.027	0.22	0.101	0.000722
Internal Insulation (e.g., Min-K)	2000	0.0000051	0.24	0.012	0.00000106
Composite Structure (e.g., Graphite Polyimide)	1100	0.000109	0.27	0.057	0.00000410
Ext Insulation (e.g., Micro-Quartz Paint)	1200	0.0000131	0.28	0.012	0.00000226
Metal Structure	600	0.027	0.22	0.101	0.000722
Internal Insulation	2000	0.0000051	0.24	0.012	0.00000106

Note:

- Small thickness allows more propellant / fuel for diameter constrained missiles (e.g., VLS launcher)
- Weight and cost are application specific
- T_{max} = max temp, deg F; k = thermal conductivity, BTU / sec / ft / deg F; c = thermal capacity, BTU / lbm / deg F; ρ = density, lbm / in³; α = thermal diffusivity = $k / (\rho c)$, ft² / sec

Fig. 4.17 Structure/insulation trades.

in a short-term, high temperature environment. Similarly the low conductivity of Min-K ($k = 0.0000051$ Btu/s/ft/ $^{\circ}$ F) as an internal insulator protects warhead, electronics, and other subsystems. As a combined structure and insulator material, graphite/polyimide has good characteristics of maximum temperature ($T_{max} = 1100^{\circ}$ F) and thermal conductivity ($k = 0.000109$ Btu/s/ft/ $^{\circ}$ F). The thickness that is required for insulation is a design consideration. Thermal diffusivity is a measure of the insulation thickness efficiency of a material. It is a function of the thermal conductivity, heat capacity, and density of the material, given by the equation $\alpha = k / (\rho c)$. As a comparison, the thermal diffusivity of Min-K is 0.1% that of aluminum. Microquartz paint and graphite/polyimide also have low thermal diffusivity compared with aluminum (0.3% and 0.6% respectively).

For environmental control of a tactical missile, an actively cooled (refrigerator) approach is usually not cost effective. Passive insulation using thermal inertia is usually a superior approach for the short-duration flight of a tactical missile. In the case of a ramjet, the fuel can provide a thermal sink.

4.11 Insulation Material Alternatives

Because missiles have volume and weight constraints, higher density insulation materials are in development. Higher density insulation materials permit more fuel/propellant for a volume-limited missile, resulting in longer range. Figure 4.18 shows the maximum temperature and short-duration insulation efficiency of candidate insulation materials.

Note that composite materials are good candidates for lightweight insulation. For insulating high-speed airframes, engines, and motor cases, the medium density plastic composites are often used. An example is a fiberglass-reinforced phenolic resin containing nylon, silica, graphite, or carbon. Phenolics have good resistance to erosion, allow high surface temperatures over 5000 $^{\circ}$ R, and exhibit good

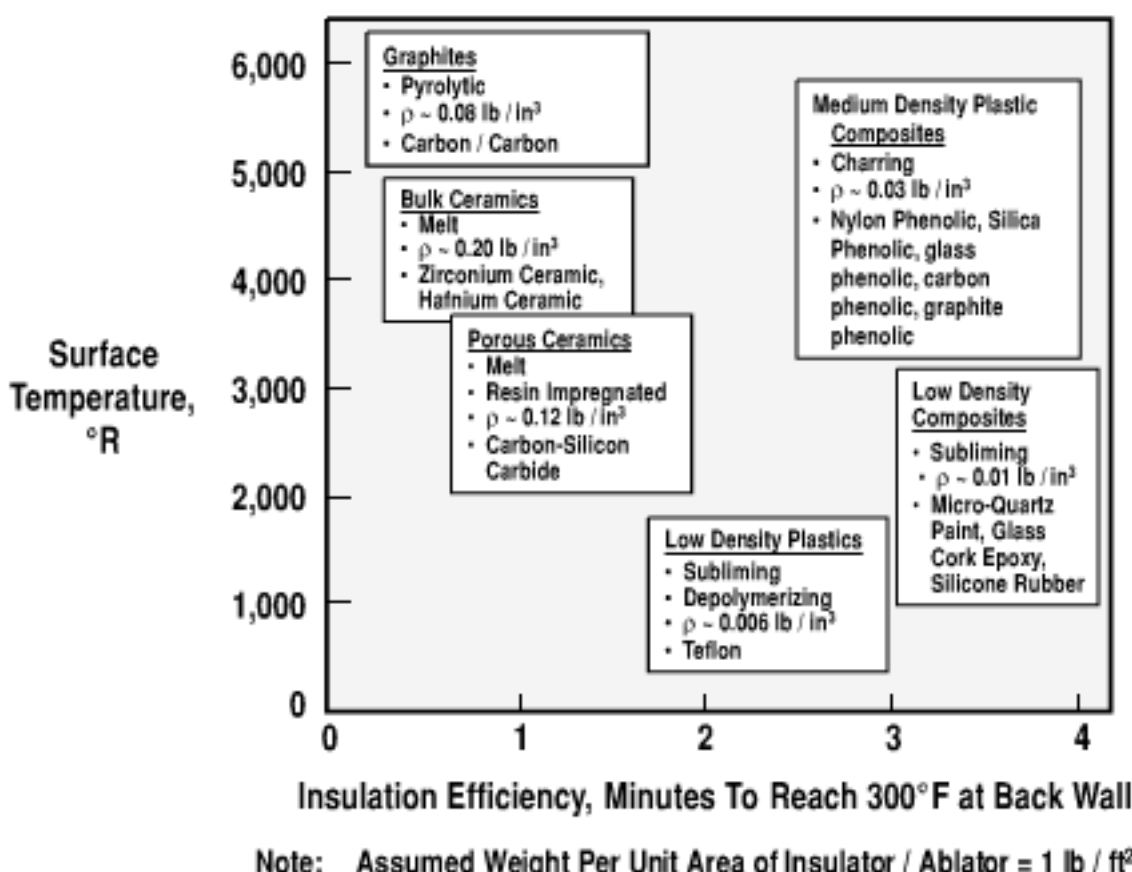


Fig. 4.18 Composites are good insulators/ablatives at high temperature.

insulation performance. These materials char at high temperature, but they generally maintain their thickness and aerodynamic shape. They are usually fabricated by wrapping fiberglass tape over a metal form mandrel, so that the grain of the finished unit is oriented for minimum erosion. Another example of a good insulator at somewhat lower temperatures is low density composites. Low density composites such as microquartz paint, glass cork epoxy, or silicone rubber may be used for temperatures up to about 3000°R. These require periodic maintenance touch-up. A third approach based on lower density plastics is rarely used for hypersonic missiles. Low density plastics have a disadvantage of decomposing at high temperature into gas, resulting in decreased thickness and changes in the aerodynamic shape.

Ceramic refractory materials and graphite materials are also candidate insulators for high speed airframes, engines, and motor cases. Although ceramic refractory materials and graphites have high temperature capability, the insulation efficiency for a given weight of material is not as good as that of plastic composite materials. An example of a porous ceramic, with a maximum temperature up to about 3500°R, is resin impregnated carbon/silicon carbide. At high temperatures the resin melts, providing cooling for the structure. Examples of bulk ceramics are zirconium ceramic and hafnium ceramic. Bulk ceramics are capable of withstanding temperatures up to 5000°R, but like porous ceramics, they have relatively poor insulation efficiency. Finally, graphite insulators provide the highest temperature capability. Graphites are capable of withstanding temperatures greater than 5000°R. However, graphites have relatively poor insulation efficiency.

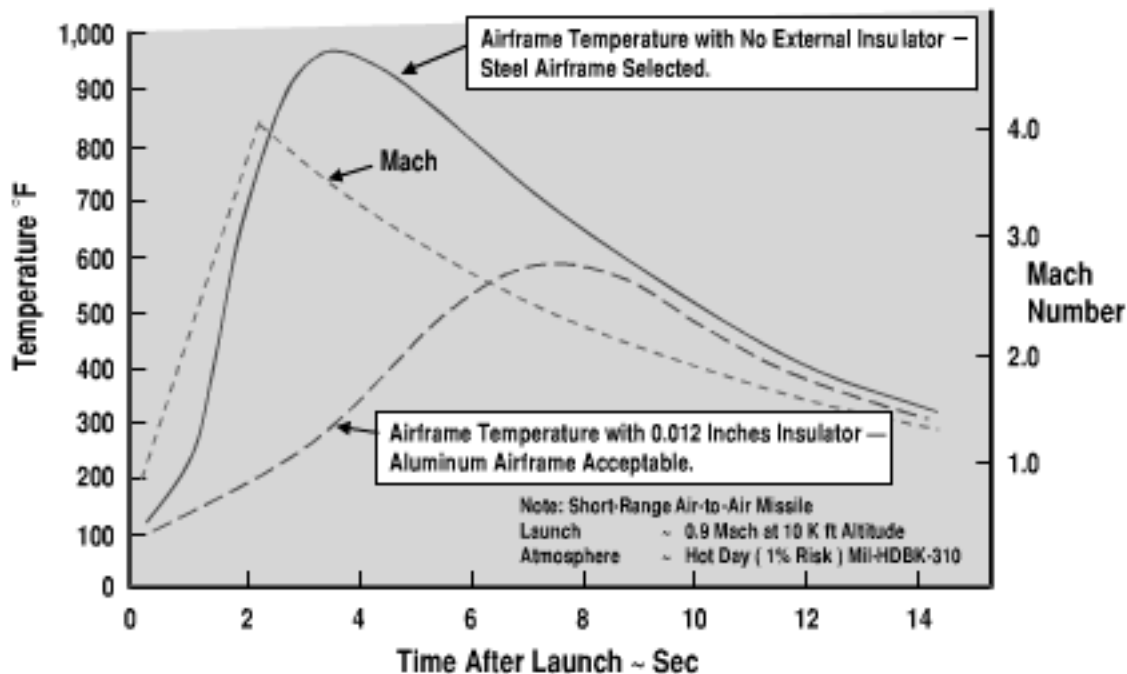


Fig. 4.19 External insulation has high payoff for short-duration flight.

Figure 4.19 compares the temperature for an insulated airframe vs an uninsulated airframe for short-duration flight. The example is based on a short-range air-to-air missile launched on a hot day at Mach 0.9 and 10,000 ft in altitude. The missile motor burnout is at 2.5 s, providing a burnout Mach number of 4.0. Note from the figure that for an uninsulated airframe a steel structure was selected because of the high maximum temperature (950°F). An alternative is to use a lighter weight, lower cost aluminum airframe that is protected by a thin layer of spray-on insulation. The peak temperature on the insulated structure is only 600°F , allowing the use of aluminum in the short-duration flight at high Mach number.

4.12 Structure Design

Localized buckling, bending moment loads, and motor case pressure loads are structure design considerations for tactical missiles. The equation for localized buckling stress due to bending is $\sigma_{\text{buckling,bending}}/E \cong 0.35(t/r)$. The equation for localized buckling stress due to compression is $\sigma_{\text{buckling,axial compression}}/E \cong 0.25(t/r)$. Localized buckling stress in bending and compression is shown in Fig. 4.20 as a function of thickness ratio and modulus of elasticity. Note that for small thickness the allowable stress for localized buckling is very low. Localized buckling may occur in a thin-wall structure prior to exceeding the yield stress.

An example is shown of the required motor case wall thickness to avoid localized buckling. It is based on the bending moment of the rocket baseline missile. The rocket baseline motor case is 4130 steel, with a modulus of elasticity $E = 29.5 \times 10^6$ psi. The case thickness $t = 0.074$ in. and the case radius $r = 4$ in. For a value of $t/r = 0.0185$, the maximum allowable localized buckling stress due to bending moment is $\sigma_{\text{buckling,bending}} = 191,000$ psi, which is comparable to the yield stress $\sigma_{\text{yield}} = 170,000$ psi.

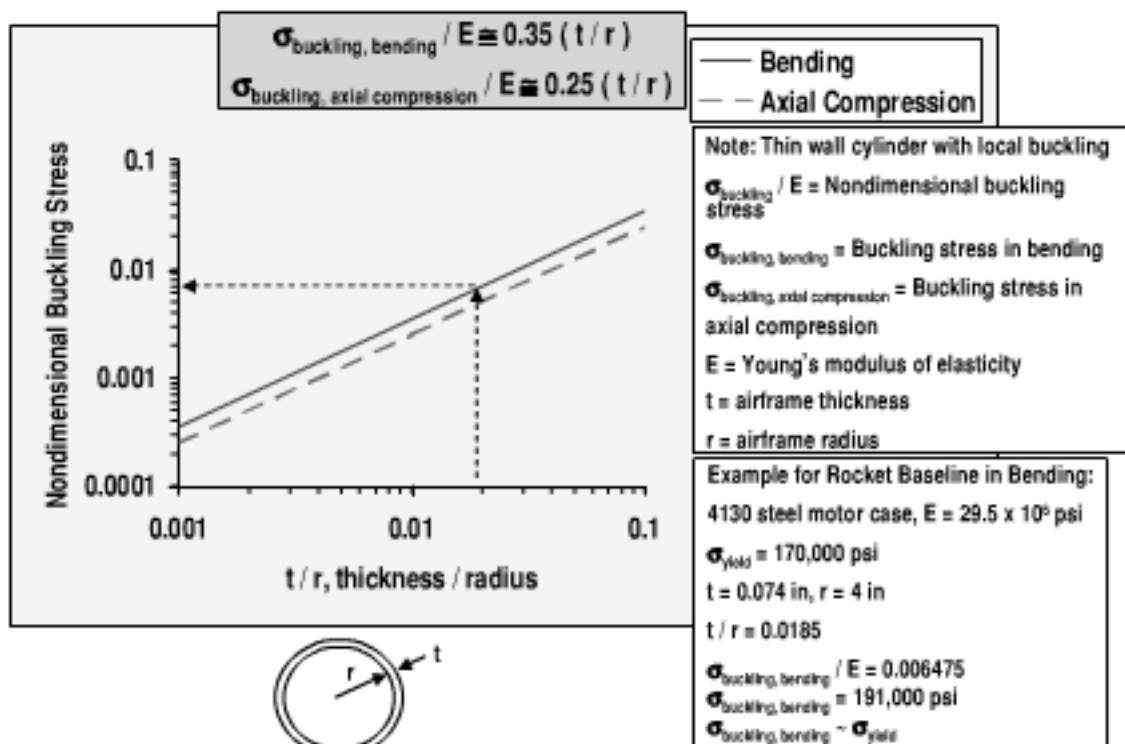


Fig. 4.20 Localized buckling for thin-wall missile structure.

Flight carriage impact on missile design is illustrated in Fig. 4.21. A comparison is shown of a representative distribution of missile free-flight maneuver loads vs launch platform carriage loads. The left section of the figure shows a typical free-flight maneuvering air-load distribution and the weight-load distribution on each bulkhead. The right section of the figure shows a typical maneuvering aircraft carriage air-load distribution, carriage weight-load distribution, and carriage suspension loads. The missile free-flight loads are usually higher than the carriage loads because missile maximum maneuverability is usually greater than that of aircraft (e.g., 30 g vs 9 g). The missile skin thickness is usually not sized by aircraft maneuver loads. As shown in the right section of the figure, carriage loads are taken out through a suspension system. It is usually possible to get a fairly accurate prediction of the missile free-flight loads. Also, wind-tunnel tests are usually conducted to determine free-flight air loads. Unfortunately, this is usually not the case for carriage flight loads, as it is difficult to accurately predict the two-body problem of a store in the flow field of the launch aircraft. In addition, it is difficult to get accurate wind-tunnel data because of the small size of the missile model for aircraft carriage wind-tunnel tests. As a result, the current approach to estimating carriage loads is usually based on the conservative process of Military Standard (MIL STD) MIL-A-8591. As missile loads estimation becomes more accurate in the future, there is a potential for structure weight savings based on improving the estimation accuracy for carriage loads.

Shown in Fig. 4.22 is a nomogram that calculates the bending moment M_B as a function of force N , length l , and the type of loading c . The scales of the nomogram cover the typical maximum/minimum ranges of the values of the parameters for tactical missiles. An advantage of using a nomogram is insight into the design drivers.

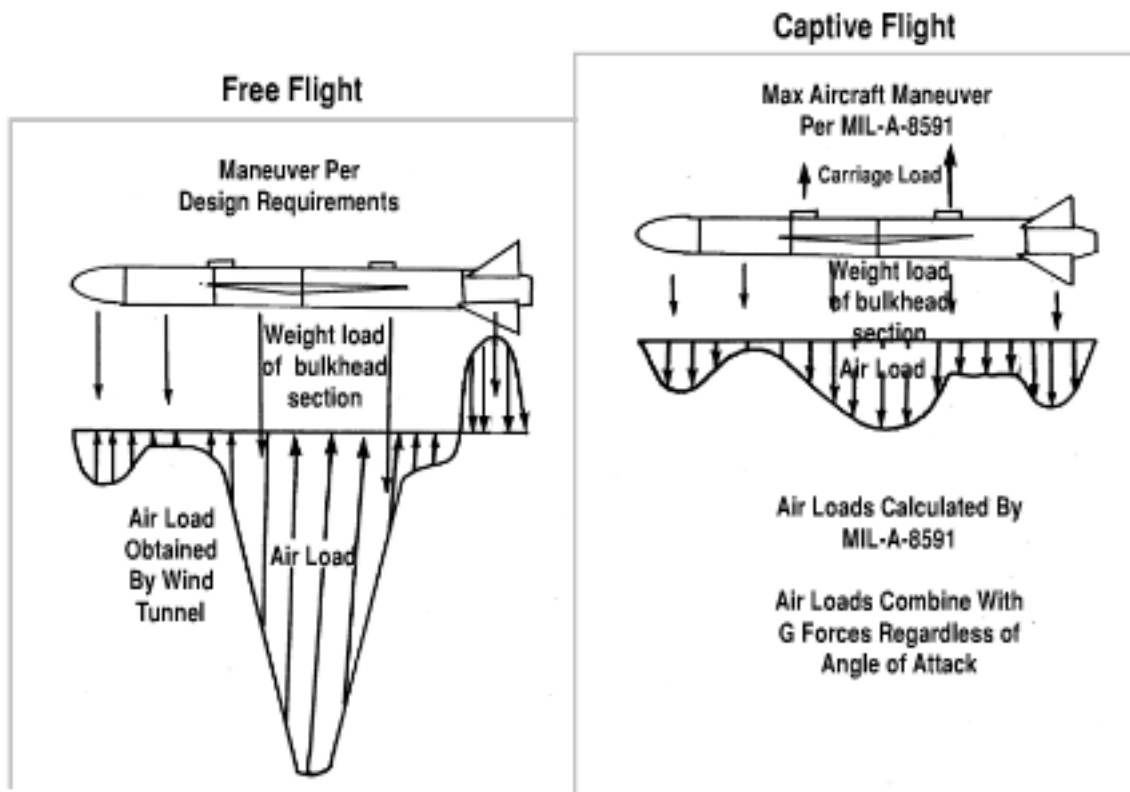


Fig. 4.21 Process for captive and free-flight loads calculation.

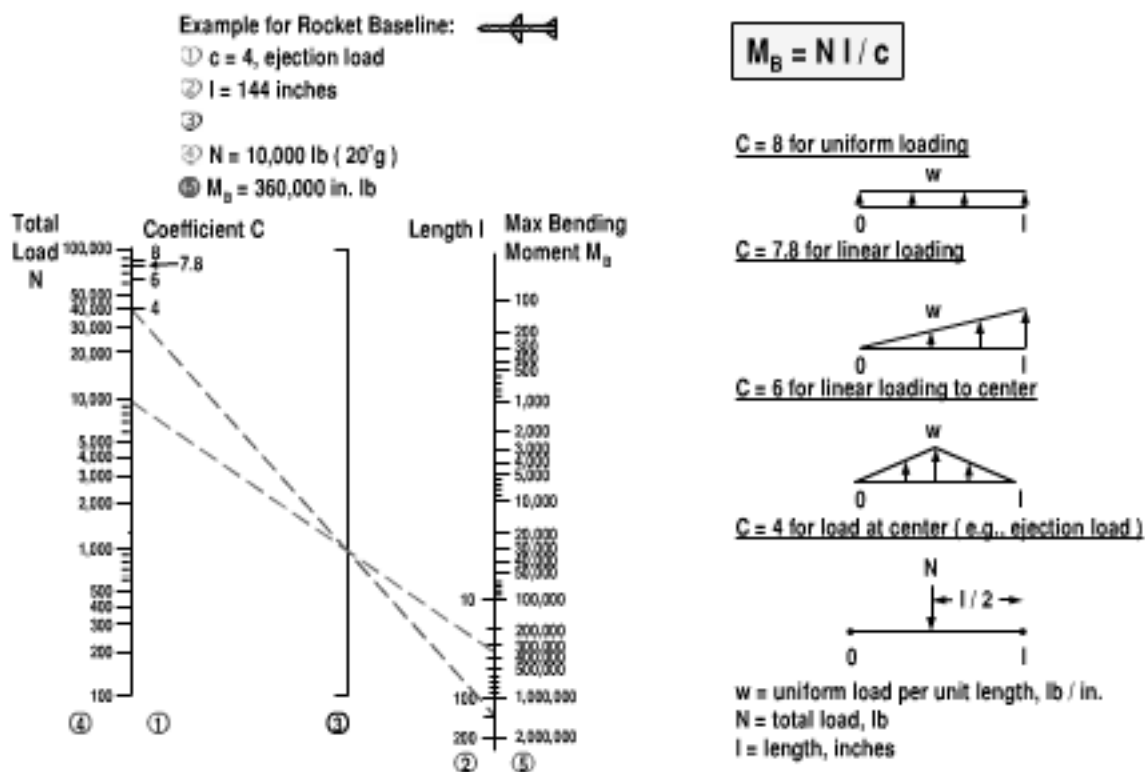


Fig. 4.22 Maximum bending moment depends upon load distribution.

Referring again to the figure, note the shape of the typical load distributions. The load distributions are uniform loading ($c = 8$), linear loading increasing from the nose tip to the base ($c = 7.8$), linear loading increasing from the nose tip to the center of the missile and returning to zero at the base ($c = 6$), and point loading (e.g., ejection load) at the center ($c = 4$).

As an example for the rocket baseline missile subjected to an ejection load of 20 g (10,000 lb), the bending moment is calculated as $M_B = NI/c = 10,000(144)/4 = 360,000 \text{ in.} \cdot \text{lb}$. The bending moment is estimated in the nomogram by drawing a straight line from line 1 ($c = 4$) to line 2 ($l = 144$) to determine a turning point on line 3. A second straight line is drawn from line 4 ($N = 10,000$) through the turning point on line 3 to intersect the value of the bending moment on line 5 ($M_B = 360,000 \text{ in.} \cdot \text{lb}$).

The simple nomogram shown in the figure is a throwback to the way engineering estimates were made more than 30 years ago, before the advent of high-speed computers. Although nomograms are still in use in areas such as medicine, they have fallen out of use in aerospace engineering. Until about the year 1970 nomograms, including complex special slide rules with three or more sliders, were used in aerospace design and as an aerospace engineering teaching tool in universities.

An example is shown in Fig. 4.23 of the required thickness of the rocket baseline missile airframe to maintain bending moment stress below the yield stress. The required thickness is calculated as a function of bending moment, airframe radius, maximum allowable stress, and factor of safety. The equation is $t = M_B(\text{FOS}) / [\pi r^2 \sigma_{\text{Max}}]$. Assumptions for the equation are a thin cylinder of circular cross section, solid skin, longitudinal bending moment, negligible axial (thrust and drag) stress, and negligible thermal stress. As noted in the previous discussion, the rocket baseline subjected to an ejection load of 20 g will have a bending moment $M_B = 360,000 \text{ in.} \cdot \text{lb}$. Based on a factor of safety for an ultimate load

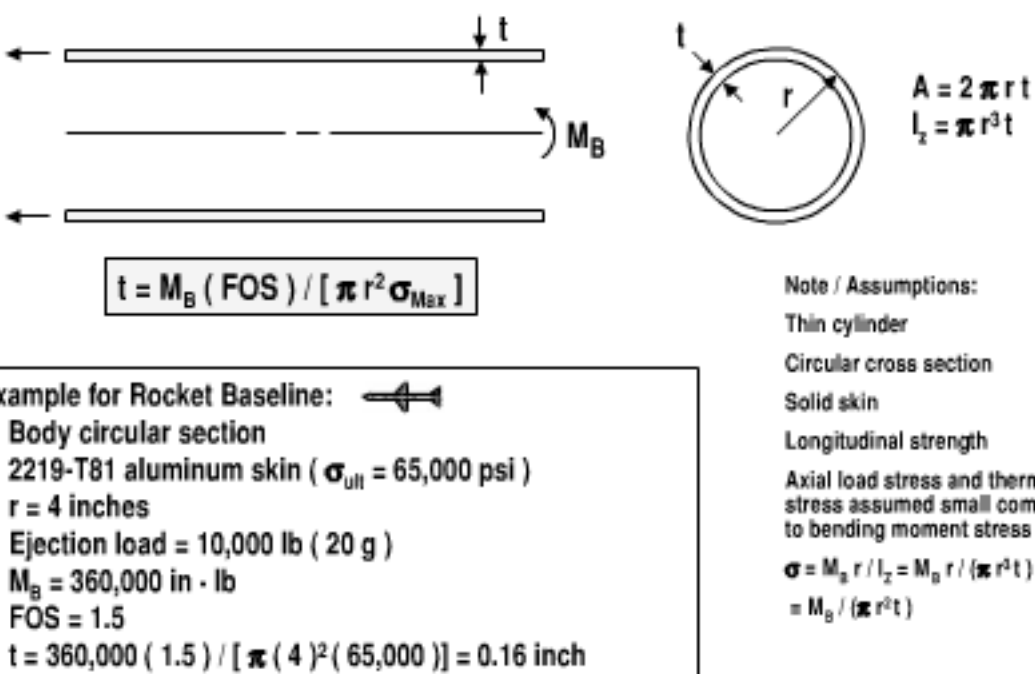
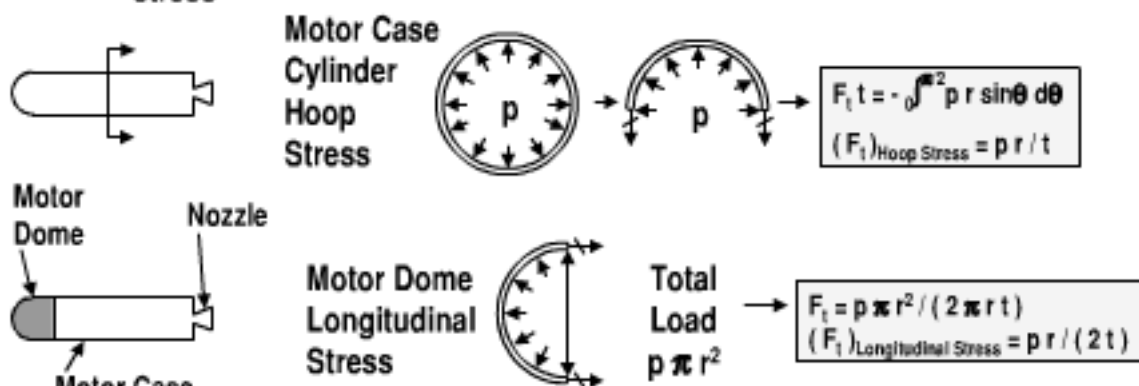


Fig. 4.23 Bending moment load may drive body structure design.

- ◆ For an axisymmetric motor case with a hemispherical dome, motor case cylinder hoop stress is twice the motor dome longitudinal stress



- ◆ With metals – the extra longitudinal material reacts body bending
- ◆ In filament wound motor designs, extra fibers must usually be added to accommodate body bending

Fig. 4.24 Motor case stresses may be determined from the pressure vessel.

of FOS = 1.5, an aluminum airframe structure ultimate stress $\sigma_{\text{ult}} = 65,000$ psi, and an airframe radius $r = 4$ in., the required airframe thickness is computed to be $t = 0.16$ in.

The rocket motor case is subjected to a variety of loads. Determining the type of load and its value that sizes the motor case requires an evaluation of a variety of loads. The loads on the motor case include internal pressure from the gas produced during propellant combustion; thrust produced by the motor during operation; localized buckling, aerodynamic bending, and the ground handling loads developed during a variety of flight conditions (e.g., handling, storage, launch platform carriage, ejection, and flight); and thermal expansion stress.

The dominant load on the motor case is often due to internal pressure. Figure 4.24 illustrates the motor case stress from the internal pressure. The motor case hoop stress is a function of the internal pressure p , case thickness t , and case radius r . Hoop stress is the radial stress in the cylindrical section of the motor case. It is given by the equation $(F_t)_{\text{Hoop Stress}} = pr/t$. The motor case longitudinal stress is the stress in the forward dome. For a hemispherical dome it is one-half of the hoop stress and is given by $(F_t)_{\text{Longitudinal Stress}} = pr/(2t)$.

Because the motor case cylindrical section and the forward dome section are often the same thickness, a dome thickness set by internal pressure often has additional material, providing additional design margin to react to other loads such as body bending loads. In the case of a composite motor case, the case thickness may not be set by internal pressure but by body bending loads, requiring a greater thickness to accommodate body bending.

The following example calculates the required thickness of the steel motor case of the rocket baseline as a function of pressure, factor of safety, radius, and the maximum allowable stress. The calculation shows the weight savings of a composite motor case over a steel motor case.

Step 1. Calculate maximum effective operating pressure (MEOP):

- 1) $MEOP = (OP)_{RT} e^{\pi k \Delta T} x$ (margin for ignition spike and other design uncertainty).
- 2) Rocket baseline: motor diameter = 8 in., motor length = 55 in.
- 3) $(OP)_{RT}$ = operating pressure at room temperature = 1769 psi average boost pressure at room temperature (RT).
- 4) $\pi_k = (\Delta p / \Delta T) / p_c = 0.14\% / {}^\circ F$, where π_k = sensitivity of motor pressure to temperature.
- 5) Assume hot day = 140° F, calculate $e^{\pi k \Delta T} = e^{0.0014(140-70)} = 1.10$.
- 6) For a 3σ design margin, $MEOP = 1769 \times (1.10)^3 = 2355$ psi.

Step 2. Assume an ultimate factor of safety FOS = 1.5.

Step 3a. First try the rocket baseline steel material for the motor case. The maximum allowable tensile stress is $F_t = 200,000$ psi ultimate. Calculate:

- 1) $t_{Hoop} = (MEOP) \times r \times (FOS) / F_t = 2355 \times 4.0 \times 1.5 / 200,000 = 0.071$ in.
- 2) $t_{Dome} = 0.035$ in.
- 3) Weight = $W_{Cylinder} + W_{Dome} = \rho \pi d t_{Hoop} \ell + \rho (\pi/2) d^2 t_{Dome} = 29.9$ lb for a steel motor case (without attachments and insulation).

Step 3b. Next, try an alternative composite glass/epoxy material for the motor case. The maximum allowable stress in the glass is $F_t = 450,000$ psi ultimate. Assume 60% glass/40% epoxy. Calculate:

- 1) $t_{Hoop} = 2355 \times 4.0 \times 1.5 / [(450,000)(0.60)] = 0.052$ in.
- 2) $t_{Dome} = 0.026$ in. May need to add additional thickness to react body bending load.
- 3) Weight = 10.1 lb for composite case (one-third of the weight of the rocket baseline steel motor case).

4.13 Seeker Dome Materials

Shown in Fig. 4.25 is a comparison of alternative dome materials for missile seekers. The dome materials are grouped based on their best applicability to multimode (RF/IR), RF-only, and mid-wave IR-only seekers. Measures of merit are dielectric constant, combined mid-wave/long wave infrared bandpass, transverse strength, thermal expansion, erosion resistance, and maximum short-duration temperature. Dome materials that are especially suited for combined radar and infrared seekers are zinc sulfide and zinc selenide. Zinc sulfide has advantages in dielectric constant, transverse strength, and rain erosion. Zinc sulfide is generally the multimode dome material of choice for Mach numbers up to 3. For Mach number greater than 3, new materials are required for multimode seekers. Candidate materials include spinel/sapphire, quartz/fused silicon, and silicon nitride. These materials are more expensive than zinc sulfide and zinc selenide. A new candidate dome material that is under development for missile defense applications is diamond. Obviously cost is very high for a diamond dome. In addition to high material cost, diamond dome assembly cost is high. Diamond domes must be assembled as a built-up mosaic because the present manufacturing processes produce relatively small size diamonds.

For RF-only seekers, two popular radome materials are pyroceram and polyimide. Pyroceram is commonly used in supersonic missiles, such as Sparrow and the Patriot PAC-2. Polyimide radomes are used on relatively low speed, low cost

Seeker Dome Material	Density (gm / cm ³)	Dielectric Constant	MWIR / LWIR Bandpass	Transverse Strength (psi)	Thermal Expansion (10 ⁻⁶ / °F)	Erosion, Knoop (kg / mm ²)	Max Short-Duration Temp (°F)
RF-IR Seeker							
Zinc Sulfide (ZnS)	4.05	○ 8.4	●	○ 18	○ 4	○ 350	○ 700
Zinc Selenide (ZnSe)	5.16	◐ 9.0	●	◐ 8	○ 4	○ 150	○ 600
Spinel (MgAl ₂ O ₄)	3.68	○ 8.5	◐	○ 28	○ 3	● 1650	● 1800
Quartz / Fused Silicon (SiO ₂)	2.20	● 3.7	○	◐ 8	● 0.3	● 600	● 2000
Silicon Nitride (Si ₃ N ₄)	3.18	● 6.1	◐	● 90	● 2	● 2200	● 2700
Diamond (C)	3.52	● 5.6	◐	● 400	● 1	● 8800	● 3500
RF Seeker							
Pyroceram	2.55	● 5.8	◐	○ 25	○ 3	● 700	● 2200
Polyimide	1.54	● 3.2	◐	○ 17	◐ 40	◐ 70	◐ 200
MWIR Seeker							
Magnesium Fluoride (MgF ₂)	3.18	● 5.5	●	◐ 7	◐ 6	● 420	● 1000
Alon (Al ₂ O ₃ N ₅)	3.67	◐ 9.3	○	● 44	○ 3	● 1900	● 1800

● Superior ○ Above Average ○ Average ◐ Below Average

Fig. 4.25 Dome material selection is driven by the type of seeker.

missiles such as the millimeter wave (mmW) Brimstone. Polyimide radomes have excellent dielectric characteristics. For MWIR-only seekers, additional dome materials include magnesium fluoride and Alon. Although both are suitable for supersonic missiles, Alon is less susceptible to rain and dust erosion and is capable of operating at higher Mach number. Multispectral dome materials may also be used for MWIR-only and RF-only seekers. Zinc sulfide is suitable for MWIR seekers at supersonic Mach number. Spinel or sapphire domes may be used with MWIR seekers at high supersonic/low hypersonic Mach numbers. Silicon nitride is suitable for RF and mmW seekers at low hypersonic Mach number.

4.14 Thermal Stress

The thermal stress trouble spots shown in Fig. 4.26 are the dome, joints, and leading edges. Radomes and IR domes often have thermal stress problems at the attachment of the dome to the metal airframe because of a difference in thermal expansion. Domes have their thickness set by electromagnetic or electro-optical (EO) considerations in addition to structural considerations. Because many dome materials have low strength, domes are susceptible to failure.

Body joints are also susceptible to local stress concentration. For a supersonic or hypersonic missile, the difference in temperature of the hot outer airframe (due to aerodynamic heating) and the relatively cold inner bulkhead (due to the thermal heat sink of the interior bulkhead material) may lead to high local thermal stress at the body joint. This may cause premature buckling.

Finally, leading edges contribute to high aerodynamic heating for hypersonic missiles. The leading edges are subjected to stagnation heating and could erode. Downstream of the hot leading edge, the additional thickness of the wing, canard, or tail surface is relatively cold. The difference in temperature may cause the

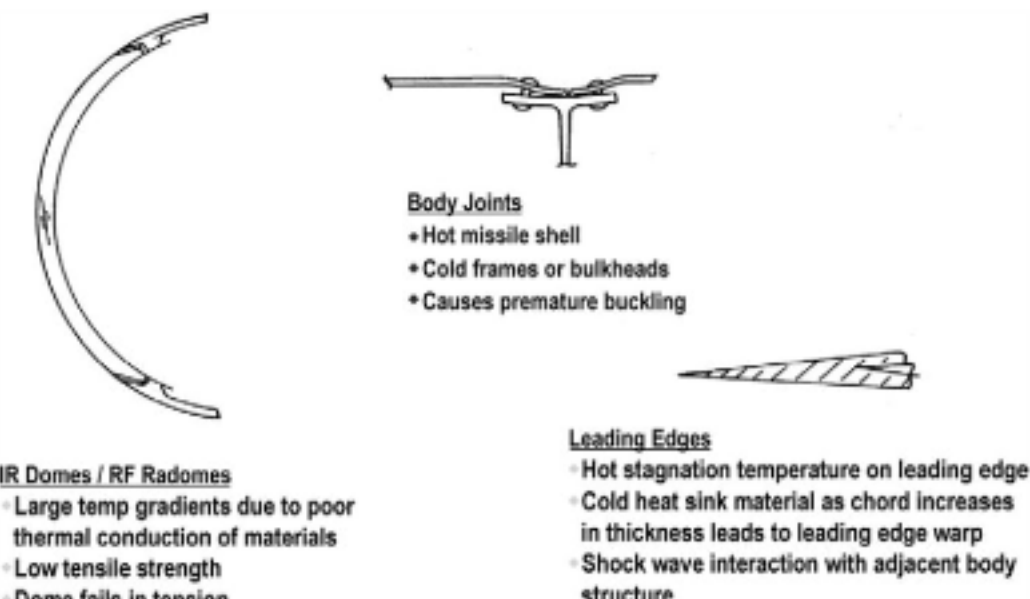


Fig. 4.26 Thermal stress trouble spots.

leading edge to warp. Another concern is the impingement of the shock wave from the leading edge on an adjacent surface. Shock-wave/boundary-layer interaction causes localized high heating.

4.15 Localized Aerodynamic Heating

Shown in Fig. 4.27 are examples of aerodynamic hot spots for a supersonic or hypersonic tactical missile. Note the high aerodynamic heating at the nose tip, leading edge of surfaces, corner flow at the cylinder-flare junction, and the reattachment of the separated boundary layer downstream of the cylinder-flare junction. The aerodynamic heating is higher on the windward side of the missile. Note

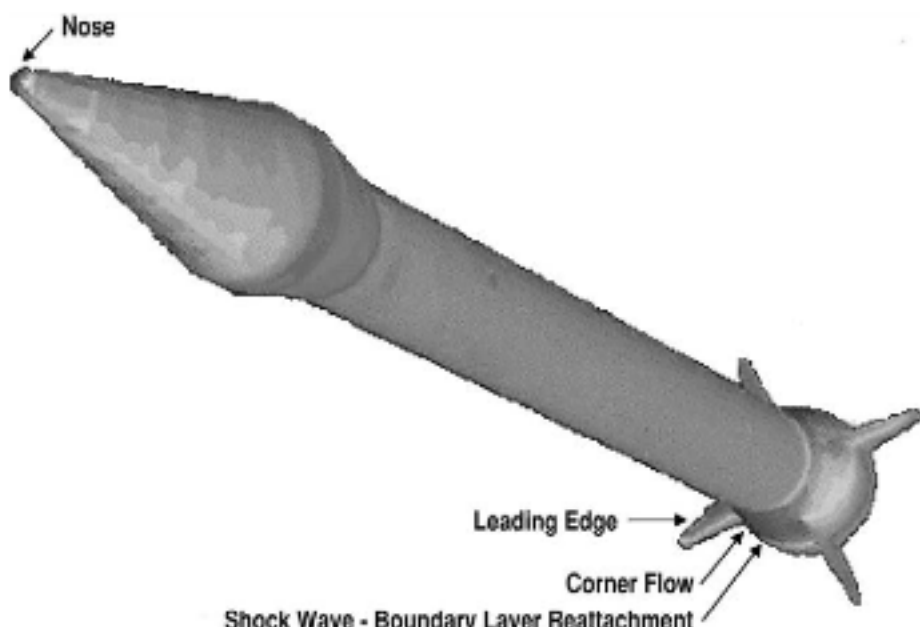


Fig. 4.27 Examples of aerodynamic hot spots.

that the expansion region aft of the bulge is a relatively cool region of low aerodynamic heating. The aerodynamic hot spots may require either additional local insulation or the use of a high temperature airframe material to withstand the high local heating.

4.16 Summary

This chapter addressed design methods, manufacturing processes, design considerations, and the technologies for lightweight, low-cost tactical missiles. Design methods included weight prediction, center-of-gravity and moment-of-inertia prediction, factors of safety, aerodynamic heating prediction, and structure design methodology. Manufacturing processes include low parts count/low-cost processes such as precision castings, vacuum assisted resin transfer molding, pultrusion, extrusion, and filament winding. Design considerations included airframe material alternatives, insulation material alternatives, seeker dome material alternatives, thermal stress, and aerodynamic heating. Finally, new technologies were identified for lighter weight missiles. These included MEMS diagnostic technology, composites, titanium alloys, and higher density insulation.

Flight Performance Considerations in Tactical Missile Design

This chapter addresses the conceptual design modeling and computer prediction of missile flight performance. It is oriented toward predicting the missile flight range, time to target, and off-boresight maneuverability. Flight performance considerations that are addressed include flight performance envelope, equations of motion modeling, driving parameters in flight performance, Breguet range equation prediction of cruise range, steady-state flight relationships, benefit of flight trajectory shaping, turn radius prediction, coast flight performance prediction, boost flight performance prediction, intercept lead angle and velocity requirement, and flight performance comparison with mission requirements.

Figure 5.1 illustrates the next step in the missile configuration synthesis process, flight trajectory evaluation. Simulations of the forward, beam, and rear flight trajectories are conducted to determine maximum/minimum range envelopes, time to target, off-boresight envelope, and maneuverability limits.

5.1 Flight Performance Envelope

The missile flight envelope may be characterized by the maximum and the minimum flight ranges in forward and off-boresight flight. In the example shown in Fig. 5.2, the missile has a large off-boresight capability, up to $+/-180$ deg off boresight. Illustrated in the figure are the maximum and minimum ranges for straight-ahead flight, beam flight, and flight to the rear of the launch aircraft. Note that a supersonic missile at 1-g flight and at low altitude flies near zero angle of attack. The maximum range for a supersonic missile in straight-ahead flight is driven by the zero-lift drag coefficient. The maximum range may be established by the speed and maneuverability required for an intercept. The minimum range may be established by the maneuverability required to correct an initial heading error. For a beam flight (to the side of the launch platform), the missile must operate at high angle of attack to rapidly turn the velocity vector to 90 deg off boresight. The maximum/minimum range for a beam intercept may be a combination of the seeker gimbal limit, maneuverability, stability, and drag due to lift. For flight to the rear of the launch platform, the missile must make a heading change of 180 deg. The drivers for a rear intercept may be a combination of zero-lift drag and the drag due to lift.

If practical, the missile should have a long maximum range, a small minimum range, and a large off-boresight capability. This provides robustness for long-range, short-range, and off-boresight targets.

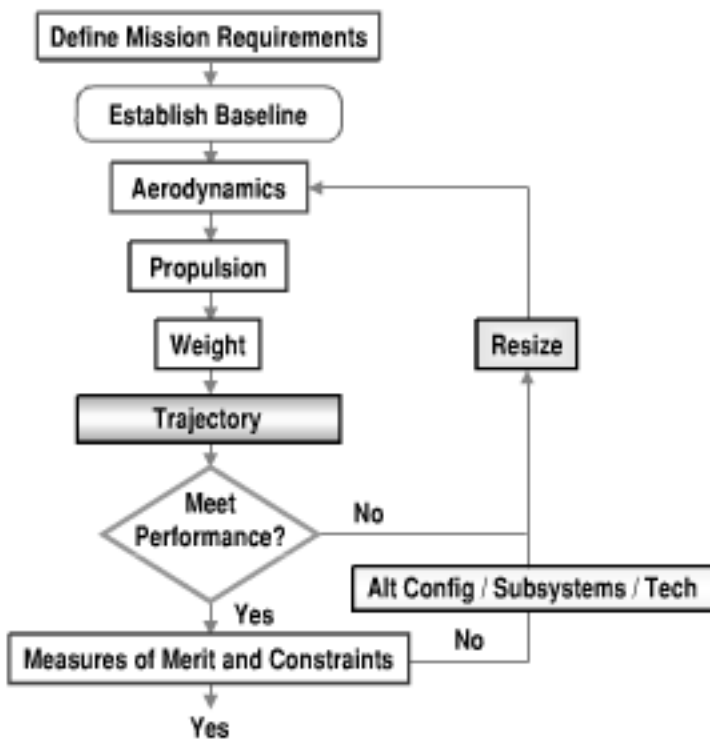


Fig. 5.1 Missile concept synthesis requires iteration.

5.2 Equations of Motion Modeling

The flight trajectory evaluation activity under missile concept synthesis requires consideration of the degrees of freedom (DOF) to be simulated. Figure 5.3 compares the simulation modeling degrees of freedom that are usually used in conceptual design with the degrees of freedom that are appropriate for preliminary design. As discussed previously, conceptual design is the rapid evaluation of a large range of alternatives. It requires that the design methods be fast, be easy to

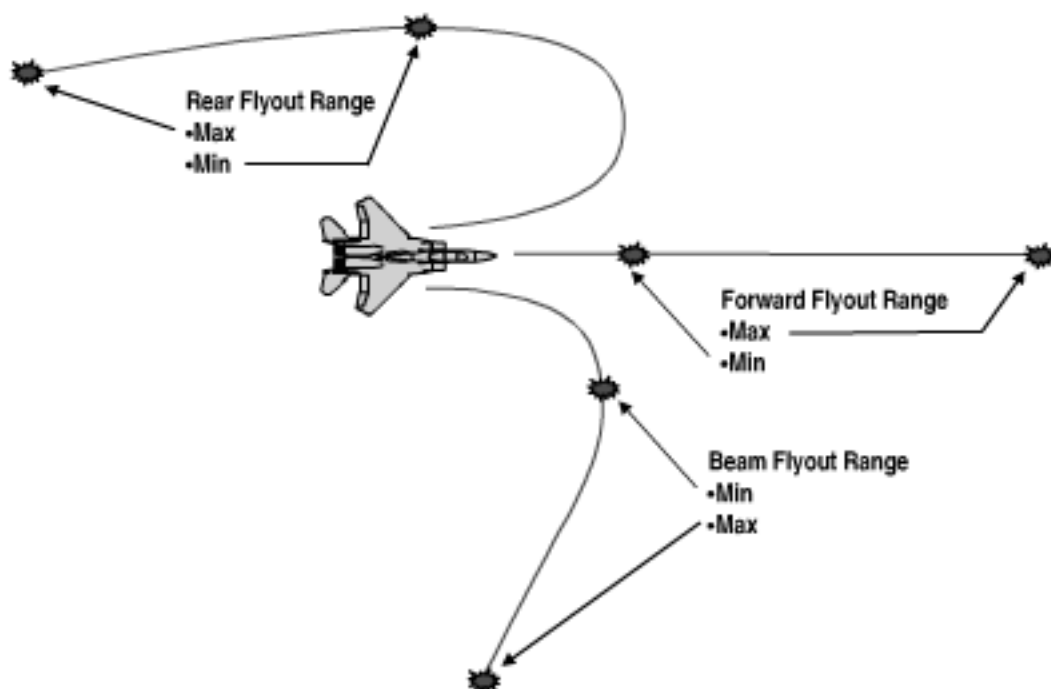
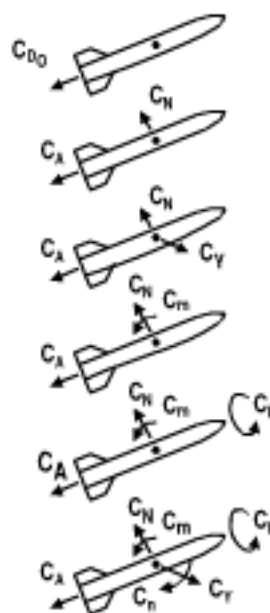


Fig. 5.2 Definition of missile flight performance envelope.

◆ Conceptual Design Modeling

- ◆ 1 DOF (Axial force (C_{D_0}), thrust, weight)
- ◆ 2 DOF (Normal force (C_N), axial force, thrust, weight)
- ◆ 3 DOF point mass (3 forces (normal, axial, side), thrust, weight)
- ◆ 3 DOF pitch (2 forces (normal, axial), 1 moment (pitch), thrust, weight)
- ◆ 4 DOF (2 forces (normal, axial), 2 moments (pitch, roll), thrust, weight)



◆ Preliminary Design Modeling

- ◆ 6 DOF (3 forces (normal, axial, side), 3 moments (pitch, roll, yaw), thrust, weight)

Fig. 5.3 Conceptual design modeling vs preliminary design modeling.

use, and have a broad range of applicability. The simplest model, often acceptable for the conceptual design of high-speed missiles, is one degree of freedom. One-degree-of-freedom modeling requires only the zero-lift drag coefficient, thrust, and weight. Analytical equations can be used to model a one-degree-of-freedom simulation. Other models used for conceptual design are two-degrees-of-freedom point-mass modeling, three-degrees-of-freedom point-mass modeling, three-degrees-of-freedom pitch modeling, and four-degrees-of-freedom roll modeling. In the 4-DOF roll modeling, the normal force, axial force, pitching moment, rolling moment, thrust, and weight are modeled for a rolling airframe missile. Finally, missile simulation during preliminary design is usually modeled in six degrees of freedom (6 DOF). The 6-DOF simulation includes three forces (normal force, axial force, side force), three moments (pitching moment, rolling moment, yawing moment), thrust, and weight. Missile degrees of freedom greater than 6 DOF describe the structure bending modes. Because most tactical missiles are relatively stiff, modeling at greater than 6 DOF is usually not required for aerodynamic control missiles but may be required for impulse reaction jet control missiles.

The one-degree-of-freedom coast equation is compared in Fig. 5.4 with the more accurate 2-DOF coast equation. Results are for the rocket baseline missile coasting in horizontal flight at Mach 2 and 20,000 ft in altitude, following motor burnout. Note that the one-degree-of-freedom (1-DOF) coast equation has less than 10% error in the deceleration \dot{V} for angles of attack up to about 3 deg. For the rocket baseline coasting in horizontal flight at Mach 2 with an altitude of 20,000 ft, the angle of attack for 1-g flight is only 0.3 deg. The 1-DOF coast equation provides sufficient accuracy for conceptual design assessment of the flight trajectory of the rocket baseline missile. Note that the rocket baseline aerodynamic efficiency L/D during constant altitude 1-g flight is much lower than $(L/D)_{Max}$.

5.3 Driving Parameters for Flight Performance

It is instructive to examine the equations of motion for missile design drivers. Figure 5.5 shows the simplified equations of motion for three degrees of freedom

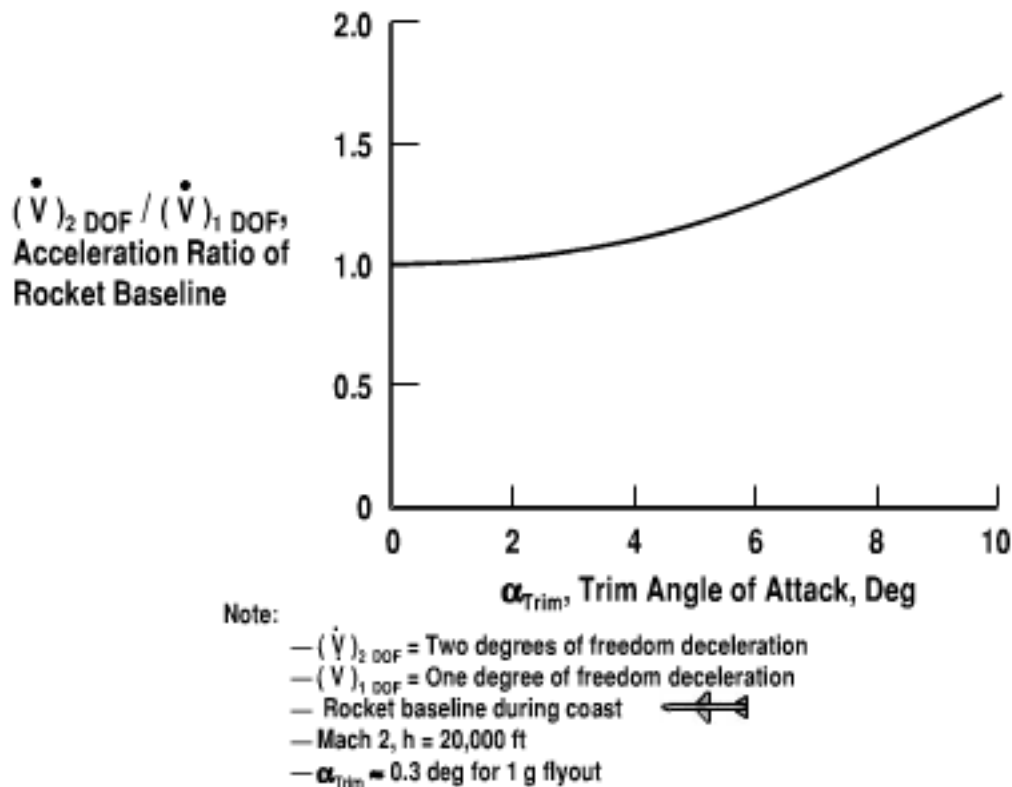


Fig. 5.4 One-degree-of-freedom coast equation has good accuracy near zero angle of attack.

with pitch modeling. Aerodynamic control is assumed. The equations describe missile angular acceleration $\ddot{\theta}$, rate of change in the flight path angle $\dot{\gamma}$, and the rate of change in the velocity \dot{V} . The configuration sizing implication from examining the angular acceleration equation shows the importance of control effectiveness. High control effectiveness is provided by high pitching moment control effectiveness C_{m_δ} , low static stability C_{m_α} , and small moment of inertia I_y . A small moment of inertia is a characteristic of a lightweight missile. The second equation shows

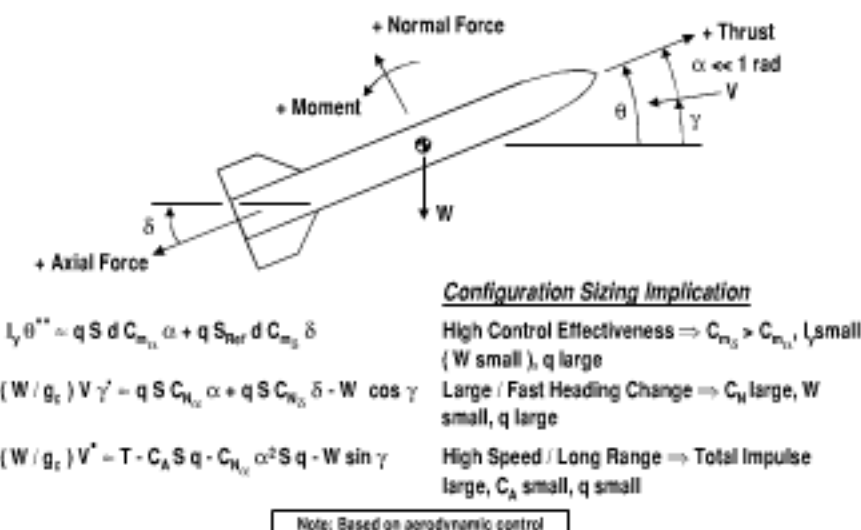


Fig. 5.5 Three-degrees-of-freedom simplified equations of motion show the drivers for configuration sizing.

the design drivers for missile maneuverability. High maneuverability is the capability to make large and rapid changes in the flight-path angle. This occurs for large normal force coefficient C_N , light weight W , and low velocity V . Large C_N is achievable through large values of $C_{N\alpha}$, α , $C_{N\delta}$, and δ . Implications of the third equation are missile speed and range. High speed and long range are provided by large total impulse, or the integral of thrust for the burn time duration ($\int T dt$). There is also payoff for flight range in using higher density propellant/fuel. Higher density propellant/fuel increases the total impulse of a volume-limited propulsion system. The third equation also shows that low axial force coefficient C_A provides longer range. Axial force coefficient is approximately equal to the zero-lift drag coefficient C_{D_0} .

5.4 Cruise Flight Performance

The Breguet range equation provides an estimate of the missile flight range during cruise flight. Assumptions in the derivation of the Breguet range equation are constant velocity, constant lift-to-drag ratio, and constant specific impulse. The derivation is as follows: The missile flight range is the time integral of velocity

$$R = \int V dt$$

Incremental time dt is related to fuel flow rate, thrust, and specific impulse by

$$dW/dt = T/I_{SP}$$

For nonaccelerating flight, lift equals weight and thrust equals drag. Therefore

$$L/D = W/T$$

Substitution and integration gives the Breguet cruise range equation

$$R = (VI_{SP})(L/D) \ln [W_{BC}/(W_{BC} - W_P)]$$

Note that the Breguet cruise range equation is a function of the missile weight at the beginning of cruise W_{BC} , propellant weight W_P , aerodynamic efficiency L/D , specific impulse I_{SP} , and velocity V . Figure 5.6 shows the maximum cruise range for a typical rocket, an axisymmetric ramjet, and a lifting body ramjet. The typical maximum value of the rocket propulsion parameter is $VI_{SP}(L/D) = 2 \times 10^6$ ft. The typical maximum value of the ramjet propulsion parameter for an axisymmetric, low L/D airframe is $VI_{SP}(L/D) = 10 \times 10^6$ ft. Finally, the maximum value for a high aerodynamic efficiency ramjet is $VI_{SP}(L/D) = 25 \times 10^6$ ft. The curves are a function of the fuel or propellant fraction of the missile weight at the beginning of cruise (W_P/W_{BC}). Note from the figure that the high L/D ramjet has the longest cruise range whereas the rocket has the shortest cruise range. As mentioned previously, the rocket usually has a longer range in semiballistic flight than in constant altitude cruise flight.

Note that in most cases for supersonic missiles in low altitude flight the cruise flight range is much less than that of the maximum value. One-g flight (lift equals weight) at high dynamic pressure results in a cruise L/D that is usually much lower than $(L/D)_{Max}$.

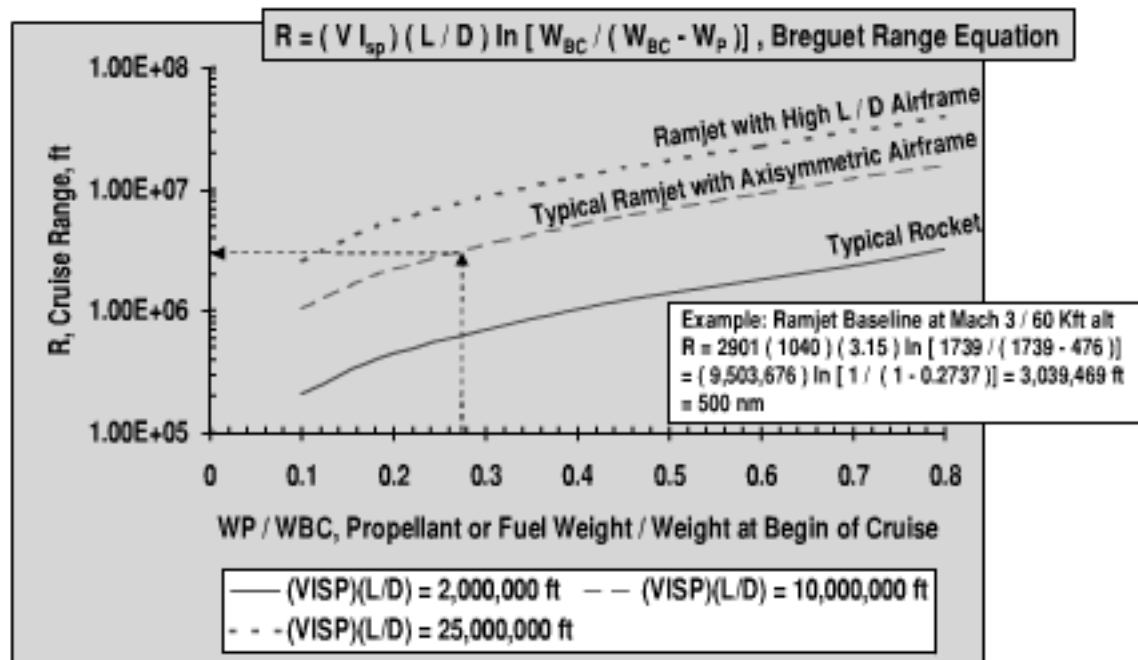


Fig. 5.6 For long-range cruise, maximize $V I_{sp}$, L/D , and fuel or propellant weight fraction.

As an example of the Breguet range equation, the ramjet baseline is evaluated at Mach 3, 60,000 ft in altitude. At Mach 3 the ramjet baseline has a specific impulse $I_{sp} = 1040$ s. At the beginning of cruise the missile weight $W_{BC} = 1739$ lb and the fuel weight $W_p = 476$ lb. Computing the range for Mach 3 cruise at 60,000 ft in altitude gives $R = 3.0 \times 10^6$ ft or 500 n miles.

5.5 Steady-State Flight

The steady-state level flight, steady climb, and steady dive relationships from Ref. 3 are shown in Fig. 5.7. In steady-state level flight at low angle of attack, the lift L is approximately equal to the weight W , and the thrust T is approximately equal to the drag D . Note that the thrust required for steady-state level flight is the missile weight divided by the aerodynamic efficiency [$T = W/(L/D)$]. High L/D has the benefit of reducing the required thrust, resulting in a lower fuel flow rate. Note from the steady climb equation in the figure, the flight path angle γ_C and climb velocity V_C are proportional to the excess thrust ($T - D$). High thrust and low drag provide higher climb angle and higher climb velocity. Similarly in a steady dive, the flight path angle γ_D and dive velocity V_D are proportional to the excess drag ($D - T$). Low drag allows a shallow glide angle after burnout ($T = 0$), providing an extended glide range.

5.6 Flight Trajectory Shaping

Figure 5.8 illustrates the extended range advantage of missiles that use flight trajectory shaping. Flight trajectory shaping is particularly beneficial for high performance supersonic missiles, which have large propellant or fuel weight fraction. To take advantage of flight trajectory shaping, the missile must rapidly pitch up

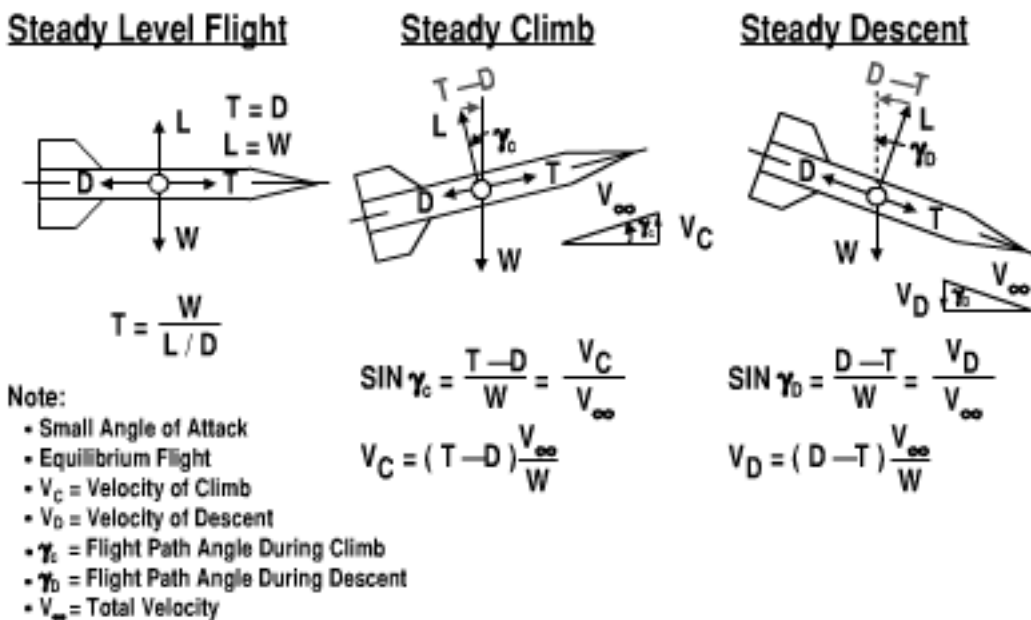
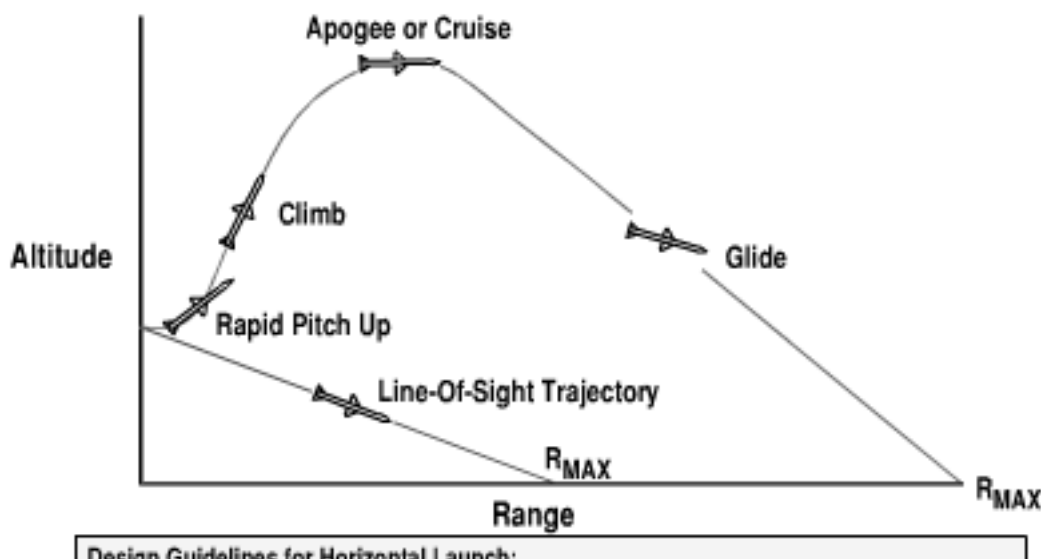


Fig. 5.7 For high rate of climb, maximize thrust and velocity while minimizing drag and weight (from Ref. 3).

and climb to an efficient cruise altitude. During the climb, the missile angle of attack should be small to minimize drag. Missile thrust-to-weight ratio for safe separation should be high (≈ 10), followed by a relatively low (≈ 2) thrust-to-weight during climb. A thrust-to-weight ratio greater than about 2 will result in a high dynamic pressure, increasing drag. After reaching higher altitude, the missile benefits from cruising at an improved lift-to-drag ratio, such as $(L/D)_{MAX}$. Dynamic pressure for efficient cruise of a high performance supersonic missile is



Design Guidelines for Horizontal Launch:

- Rapid pitch up minimizes time / propellant to reach efficient altitude
- Climb at $\alpha = 0$ deg with thrust-to-weight = 2 and $q = 700$ psf minimizes drag / propellant to reach efficient cruise altitude for $(L/D)_{MAX}$
- High altitude cruise at $(L/D)_{MAX}$ and $q = 700$ psf to maximizes range
- Glide from high altitude at $(L/D)_{MAX}$ and $q = 700$ psf provides extended range

Fig. 5.8 Flight trajectory shaping provides extended range.

on the order of 500–1000 psf. Following burnout, the missile can have extended range through glide at a dynamic pressure of about 700 psf, providing an aerodynamic efficiency approximately equal to $(L/D)_{Max}$.

5.7 Turn Radius

Figure 5.9 shows an example of missile horizontal turn radius using aerodynamic control of the flight path. The example is based on a wingless missile with a circular body cross section. The horizontal turn radius is a function of missile weight, normal force coefficient, reference area, and atmospheric density. It is given by the equation $R_T = 2 W / (g_c C_N S_{Ref} \rho)$. The term g_c in the equation is the gravitational constant ($g_c = 32.2 \text{ ft/s}^2$). Results are based on slender body theory⁴ plus cross flow theory.⁵ The example supersonic missile has a weight $W = 2000 \text{ lb}$, length that is 10 times the diameter ($l/d = 10$), cross-sectional area $S = 2 \text{ ft}^2$, and zero-lift drag coefficient $C_{D_0} = 0.2$. Note from the figure that the horizontal turn radius increases rapidly as the altitude increases. As an example, at an altitude of 40,000 ft, the horizontal turn radius of the supersonic wingless missile for an incremental angle of attack of $\Delta\alpha = 10 \text{ deg}$ is very large, $R_T = 161,000 \text{ ft}$. Adding a wing or shaping the missile into an elliptical body cross section would provide higher normal force capability and a smaller turn radius.

Also noted in the figure are the efficient cruise conditions for the wingless missile. At an altitude of 40,000 ft, the Mach number for $(L/D)_{Max}$ is $M = 1.9$. As the altitude increases, the wingless missile is more efficient cruising at a higher Mach number. For example, at an altitude of 100,000 ft, a hypersonic Mach number is required for high aerodynamic efficiency [$(L/D)_{Max}$ occurs at $M = 7.9$].

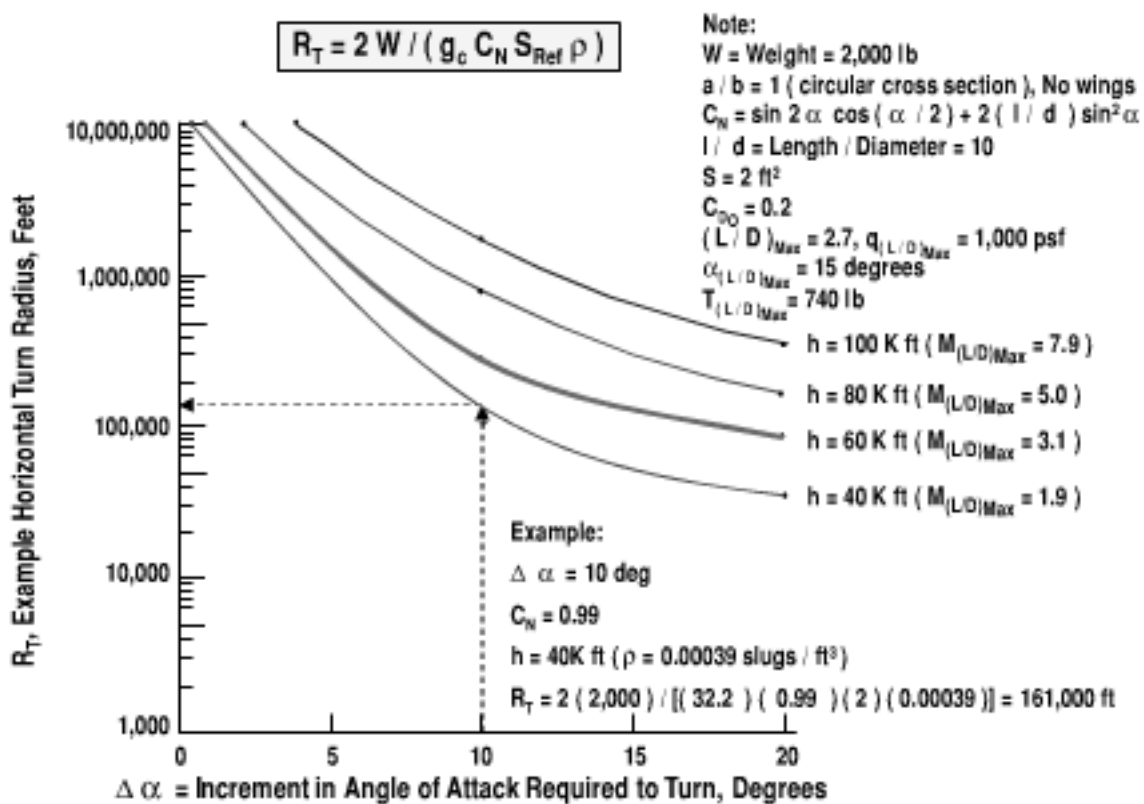


Fig. 5.9 Small turn radius requires high angle of attack and low-altitude flight.

The angle of attack for maximum aerodynamic efficiency of the wingless axisymmetric missile is $\alpha_{(L/D)\text{Max}} = 15$ deg. The dynamic pressure required to fly in 1-g horizontal steady flight at $(L/D)_{\text{Max}}$ for the wingless missile is $q_{(L/D)\text{Max}} = 1000$ psf. The thrust required for 1-g steady-state horizontal flight of the wingless missile at $(L/D)_{\text{Max}}$ is $T_{(L/D)\text{Max}} = 740$ lb. The required thrust is 37% of the missile weight.

5.8 Turn Rate Performance

Turn rate performance is the capability to make a rapid rate of change in the flight path angle γ . As shown previously, the equation is

$$\dot{\gamma} = g_c n / V = [q S C_{N_a} \alpha + q S C_{N_b} \delta - W \cos \gamma] / [(W/g_c)V]$$

An example of a requirement for turn rate performance is the capability of an antiaircraft missile to match the turn rate of the target for a successful intercept. For manned combat aircraft, the maximum turn rate occurs for a normal acceleration of about $n = 9$ g (pilot limit) and a velocity of about $V = 1000$ ft/s. Substitution into the turn rate equation gives the maximum turn rate of a manned aircraft of about $\dot{\gamma} = 32.2(9)/1000 = 0.290$ rad/s or 16.6 deg/s. Because the missile must have a speed advantage to intercept the aircraft, it must also have higher maneuverability to match the turn rate of the aircraft. For example, a missile with a velocity $V = 3000$ ft/s must have 27-g maneuverability to achieve a turn rate of $\dot{\gamma} = 16.6$ deg/s.

The rocket baseline missile and its data from Chapter 7 will be used to illustrate the drivers for turn rate performance. Assume that a climb maneuver is commanded for a typical launch condition of Mach 0.8 and 20,000-ft altitude. At this flight condition the velocity $V = 820$ ft/s, dynamic pressure $q = 436$ psf, launch weight $W_L = 500$ lb, and the launch center of gravity $x_{CG} = 84.6$ in. from the nose tip. The trim angle of attack and the control surface deflection based on the launch c.g. are derived from the wind tunnel data of Chapter 7. Based on the reference center of gravity for the wind tunnel data of $x_{CG} = 75.7$ in., the maximum trimmed angle of attack α and control surface deflection δ for the launch center of gravity are computed from

$$\begin{aligned}(C_{m_a})_{x_{CG}=84.6} &= (C_{m_a})_{x_{CG}=75.7} + C_{N_a}(84.6 - 75.7)/d \\ &= -0.40 + 0.68(8.9)/8 = 0.36 \text{ per deg}\end{aligned}$$

$$\begin{aligned}(C_{m_b})_{x_{CG}=84.6} &= (C_{m_b})_{x_{CG}=75.7} + C_{N_b}(84.6 - 75.7)/d \\ &= 0.60 + 0.27(8.9)/8 = 0.90 \text{ per deg}\end{aligned}$$

Note that the missile is statically unstable at launch ($C_{m_a} > 0$) and requires negative wing control deflection to trim. The control effectiveness is given by $\alpha/\delta = -C_{m_b}/C_{m_a} = -0.90/0.36 = -2.5$. The maximum wing local angle of attack $|\alpha'| = |\alpha + \delta| < 22$ deg. For a maximum angle of attack of the body of $\alpha = 30$ deg, the trim control deflection is $\delta = -12$ deg. Finally, compute

$$\dot{\gamma} = [436(0.349)(0.68)(30) + 436(0.349)(0.27)(-12) - 500(1)] / [(500/32.2)(820)]$$

$$= 0.164 \text{ rad/s or } 9.4 \text{ deg/s}$$

For a post-burnout flight condition of Mach 2 at 20,000-ft altitude, the missile has a higher turn rate. The missile is statically stable, with $\alpha/\delta = 0.75$. The turn rate

$$\dot{\gamma} = [2725(0.349)(0.60)(9.4) + 2725(0.349)(0.19)(12.6)] - 367(1)/(367/32.2)(2074) = 0.31 \text{ rad/s or } 18 \text{ deg/s}$$

The higher turn rate performance is due to higher dynamic pressure, statically stable missile, forward wing control, and lighter weight.

A metric for missile response time is the angle of attack sensitivity to turn rate, or $\alpha/\dot{\gamma}$. For the rocket baseline at Mach 0.8 launch and 20,000 ft in altitude, $\alpha/\dot{\gamma} = 30/9.4 = 3.2$ s. The response time metric for Mach 2 coast at 20,000 ft in altitude is smaller, $\alpha/\dot{\gamma} = 9.4/18 = 0.52$ s.

5.9 Coast Flight Performance

Coast velocity and the coast range are shown in Fig. 5.10 as a function of the coast time, weight, atmospheric density, reference area, zero-lift drag coefficient, and the initial velocity. The equation for coast velocity is

$$V_{EC} = V_{BC}/\{1 + t_{coast}/[2W_{BO}/(g_c S_{Ref} C_{D_0} V_{BC})]\}$$

Incremental flight range during coast is given by

$$R_{coast} = [2W_{BO}/(g_c S_{Ref} C_{D_0})] \ln\{1 + t_{coast}/[2W_{BO}/(g_c S_{Ref} C_{D_0} V_{BC})]\}$$

Examining the equation shows that the contributors to a long-range coast include low zero-lift drag coefficient and high altitude (low atmospheric density) flight. The

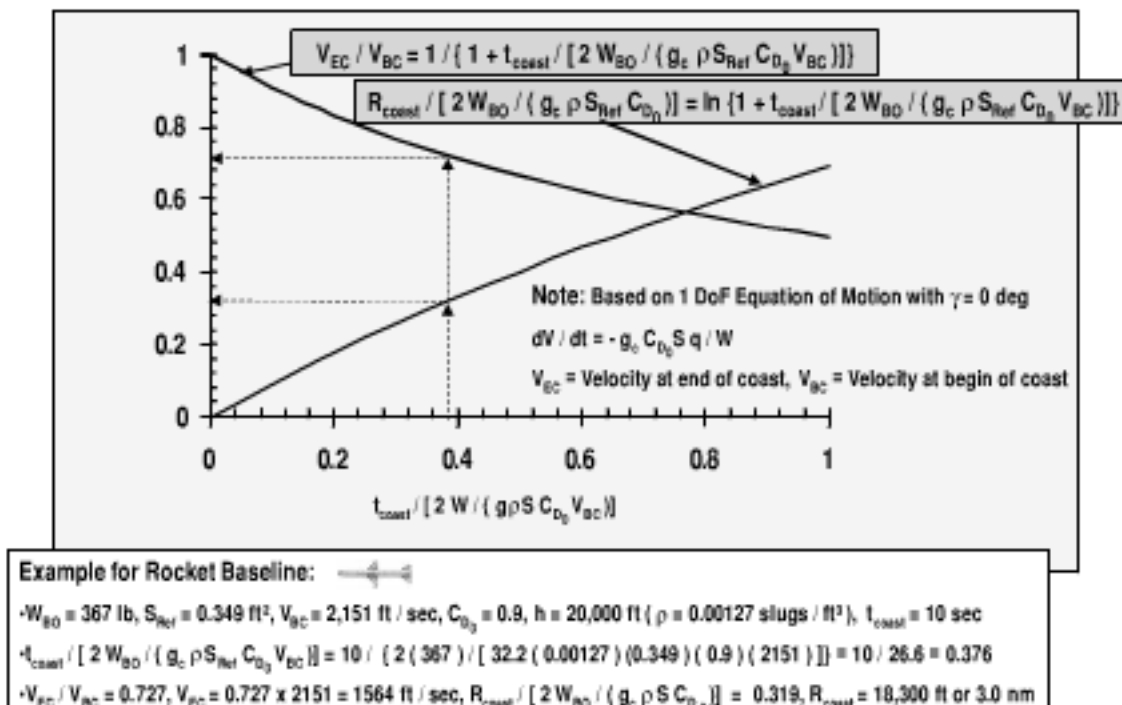


Fig. 5.10 For a long-range coast, maximize altitude and initial velocity.

assumptions for the coast equation are one-degree-of-freedom (1-DOF), constant altitude ($\gamma = 0$ deg) flight.

As an example for the rocket baseline missile, the coast weight is $W = 367$ lb and the reference area $S_{\text{Ref}} = 0.349 \text{ ft}^2$. For a burnout flight condition of Mach 2.1 at 20,000 ft in altitude ($\rho = 0.00127 \text{ slugs}/\text{ft}^3$), the zero-lift drag coefficient $C_{D_0} = 0.9$ and the beginning of coast velocity $V_{BC} = 2151 \text{ ft/s}$. The end of coast velocity after 10 s of coast is computed to be $V_{EC} = 1564 \text{ ft/s}$. The incremental range during coast $R_{\text{coast}} = 18,300 \text{ ft}$ or 3.0 n miles.

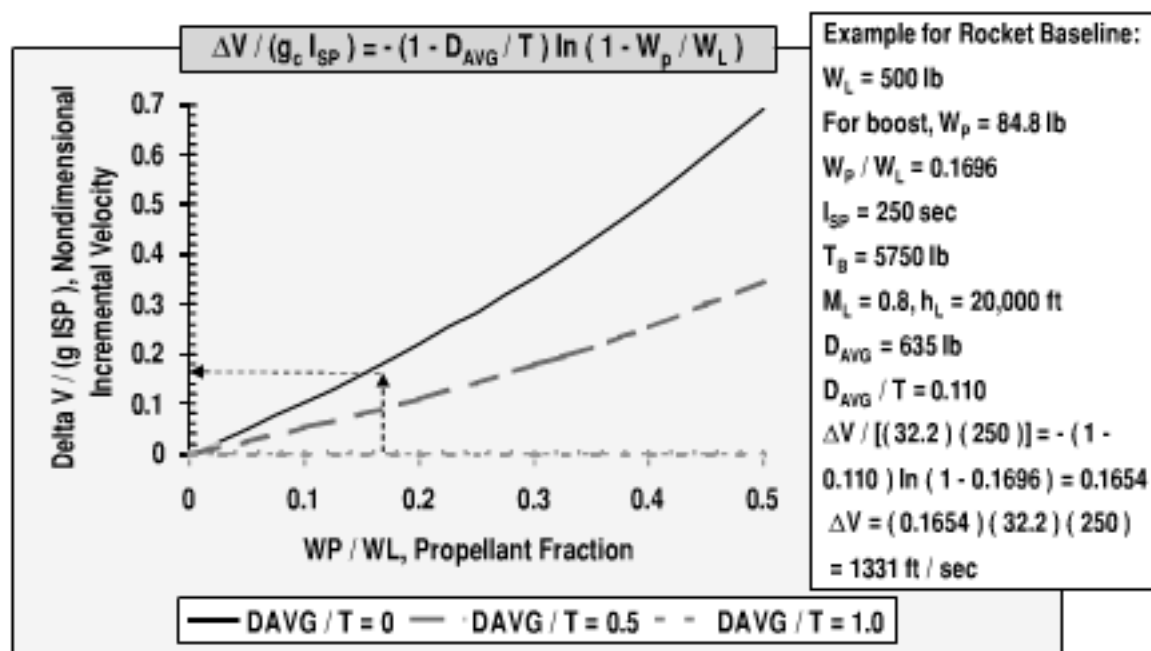
5.10 Boost Flight Performance

Incremental velocity due to the rocket motor burn is shown in Fig. 5.11 as a function of propellant weight fraction, specific impulse, average drag, and thrust. The equation is

$$\Delta V = -g_c I_{\text{SP}}(1 - D_{\text{AVG}}/T) \ln(1 - W_p/W_L)$$

High incremental velocity due to motor burn is provided by a high propellant weight fraction of the launch weight (W_p/W_L), low average drag D_{AVG} , high thrust T , and high specific impulse I_{SP} .

As an example, the incremental boost velocity is calculated for the rocket baseline missile, which has a launch weight $W_L = 500$ lb, boost propellant weight $W_p = 84.8$ lb, and boost specific impulse $I_{\text{SP}} = 250$ s. The assumed launch condition is Mach 0.8, 20,000 ft in altitude. After iterating, using an initial estimate of end-of-boost drag based on the theoretical end-of-boost velocity with no drag, the average drag between launch and the end of boost is found to be $D_{\text{AVG}} = 635$ lb. The incremental velocity due to boost for the rocket baseline is computed to be



Note: W_L = launch weight, W_p = propellant weight, I_{SP} = specific impulse, T_B = boost thrust, M_L = launch Mach number, h_L = launch altitude, D_{AVG} = average drag, ΔV = incremental velocity, g_0 = gravitation constant

Fig. 5.11 High propellant weight and high thrust provide high burnout velocity.

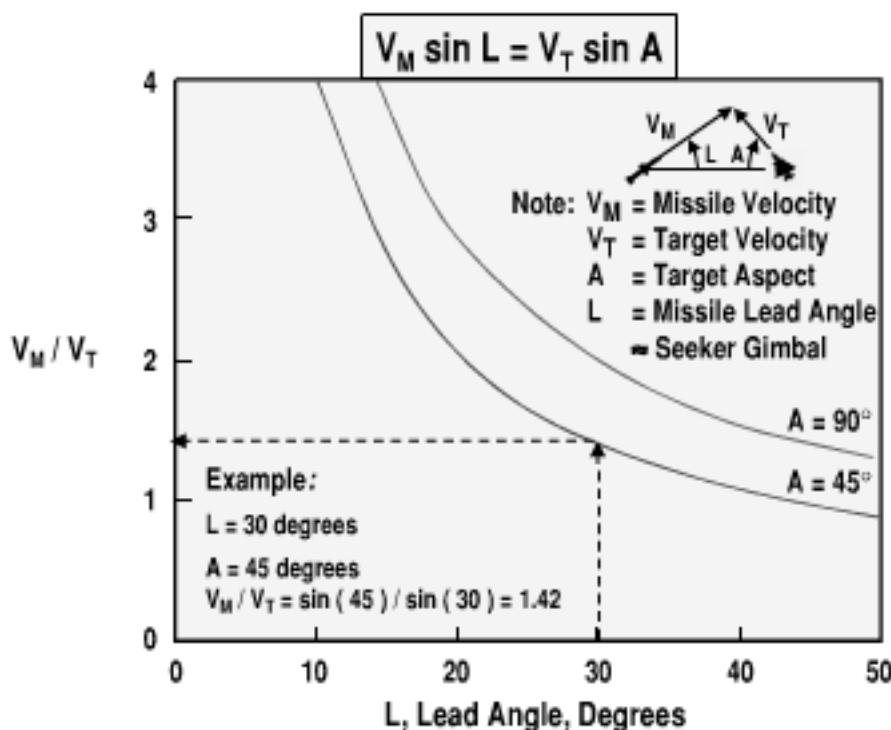


Fig. 5.12 High missile velocity and lead are required to intercept high-speed crossing targets.

$\Delta V = 1331$ ft/s. Including the effect of drag results in an end-of-boost velocity that is 93% of the theoretical velocity neglecting drag (2151 ft/s vs 2316 ft/s).

5.11 Intercept Lead Angle and Velocity

The average missile velocity and the lead angle required for intercept are shown in Fig. 5.12 as a function of target aspect and velocity. The equation $V_M \sin L = V_T \sin A$ is based on homing guidance. The figure is based on homing guidance. An assumption is that the seeker look angle is equal to the missile lead angle. The assumption is most applicable for constant altitude intercepts at a low angle of attack flight trajectory. Note from the figure that a high average missile velocity is required to intercept a target at an aspect angle of $A = 90$ deg (beam shot). Increasing the maximum lead angle and the seeker maximum gimbal angle reduces the required missile velocity for intercept.

As an example, assume a target that has an aspect angle $A = 45$ deg. Also assume that the maximum allowable lead angle is $L = 30$ deg, a typical gimbal limit for a seeker. For these assumptions, the missile must have an average velocity that is 42% greater than the velocity of the target to achieve an intercept.

5.12 Comparison with Performance Requirements

As shown in Fig. 5.13, after completing the missile flight performance computation, the next step in the missile configuration synthesis process is to compare the candidate missile design flight performance (e.g., range, time to target, off boresight) with the mission requirements for flight performance. If the candidate missile has insufficient flight performance, changes are made in the aerodynamic

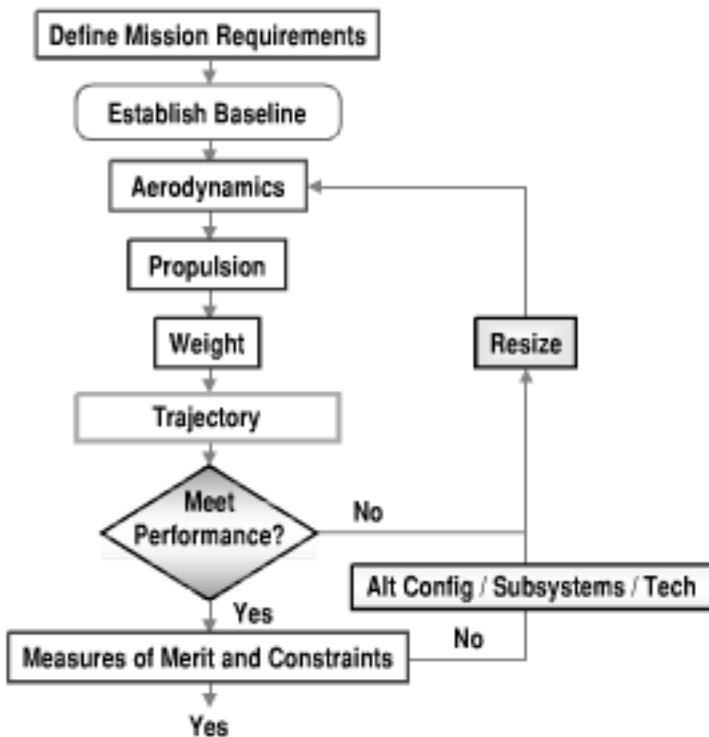


Fig. 5.13 Missile concept synthesis requires iteration.

configuration, propulsion, structure, and/or subsystems to improve the flight performance. The refined/resized missile is then sent through another cycle of evaluation. The iteration continues until there is a design convergence that meets the flight performance requirements.

5.13 Summary

Flight performance consideration in tactical missile design is oriented toward flight trajectory computation and comparison with the missile flight performance requirements. Flight performance requirements include range, time to target, and off boresight. This chapter presented equations of motion modeling, examples of flight performance drivers, typical flight performance for propulsion alternatives, and methods for predicting boost, coast, and turn performance. Much of the impact of changes in the missile aerodynamics, propulsion, and weight is in the area of flight performance. Converging to a design that harmonizes the aerodynamics, propulsion, and weight while also satisfying the flight performance requirements is a primary activity in missile configuration design.

Measures of Merit and Launch Platform Integration

Measures of merit and launch platform integration considerations in tactical missile design include robustness, warhead lethality, miss distance, carriage and launch observables, other survivability considerations, reliability, cost, and launch platform integration/firepower. Examples of the measures of merit/launch platform integration and conceptual design prediction methods are given in this chapter.

As shown in Fig. 6.1, the last step in missile configuration sizing is a comparison of the missile design with the measures of merit requirements and any constraints, such as launch platform compatibility. If the missile design satisfies the measures of merit and constraints, the design has converged, and we are finished. If not, the designer selects alternative configurations, subsystems, or technologies, and the design is reiterated until the measures of merit and constraints are satisfied.

Figure 6.2 illustrates the considerations of measures of merit and constraints for a balanced missile design. The aeromechanics performance of tactical missiles must be harmonized with other measures of merit such as robustness, warhead lethality, miss distance, carriage and launch observables, other survivability considerations, reliability, and cost, as well as constraints such as launch platform integration and firepower requirements.

6.1 Robustness

The first measure of merit to be discussed is robustness. Tactical missiles must have sufficient robustness to handle effects such as adverse weather, clutter, altitude variation, local climate, flight environment variations, uncertainty, and counter-countermeasures. This section of the text provides examples of requirements for robustness.

Adverse weather capability is a driving concern for tactical missiles. Cloud cover is a particular concern for sensors because clouds are pervasive worldwide. As shown in the National Oceanic and Atmospheric Administration (NOAA) typical satellite image of Fig. 6.3, clouds cover a large portion of the Earth. The figure shows that the average global annual cloud cover is about 61%. The average cloud cover over land is about 52%, and the average cloud cover over the oceans is about 65%. The figure is based on Ref. 12. Clouds tend to occur between 3000 and 20,000 ft elevation. Clouds may be thick, with thickness greater than 6000 ft. The average annual cloud cover shown in the figure is based on weather observers around the world. It is a composite of averages that vary widely with geographical location, season, and time of day.

An example of a geographical cloud system that changes regularly with the season and the time of day is the low-level, layered stratus clouds that cover much

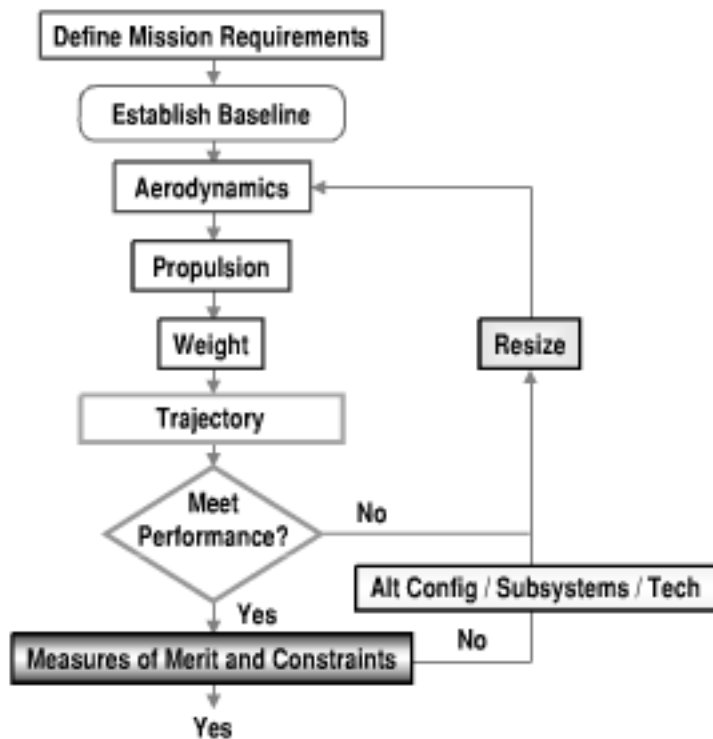


Fig. 6.1 Missile concept synthesis requires iteration.

of the world's oceans. Stratus clouds are more frequent during the summer months in the Eastern Pacific and the Eastern Atlantic and in the hours before sunrise.

Another example of a geographical cloud system that changes regularly with the season and the time of day is cumulonimbus. Cumulonimbus clouds are large columnar clouds that can extend to high altitude. These clouds are concentrated where surface temperatures are high and there is a general upward movement of the air. An example is a zone known as the Inter-Tropical Convergence Zone (ITCZ).

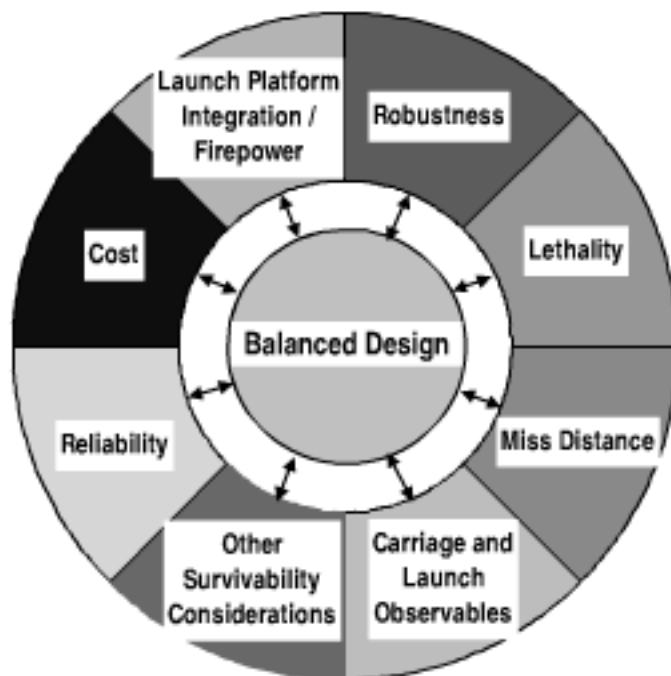


Fig. 6.2 Measures of merit and launch platform integration should be harmonized.

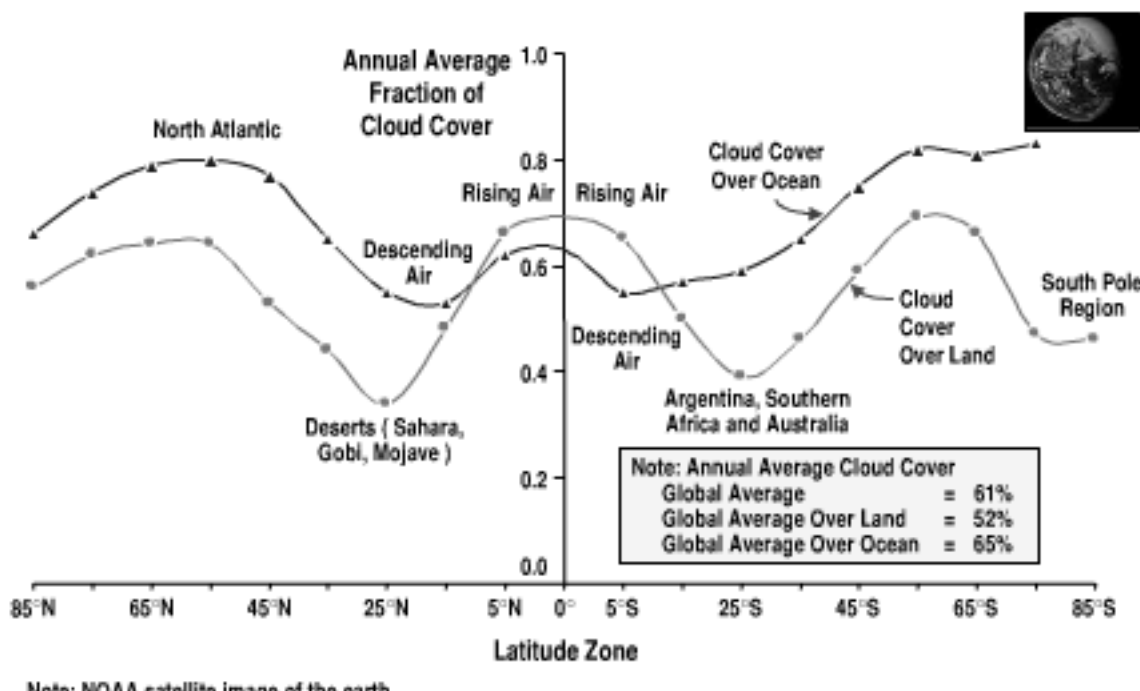


Fig. 6.3 Adverse weather and cloud cover are pervasive (from Ref. 12).

In the ITCZ the trade winds of the Northern Hemisphere converge with those of the Southern Hemisphere. Cumulonimbus clouds have high concentrations of droplets and ice crystals, which can grow to a large size. Cumulonimbus clouds are often responsible for the frequent summer afternoon rainfall of Southeast Asia, North America, and Europe, and rainfall in the Amazon basin during December, January, and February.

For the purpose of conceptual design, an assumed cloud base maximum height of 5 km, cloud maximum thickness of 2 km, and a maximum rain rate of 4 mm/h are considered to be cost-effective (e.g., 3σ) environmental requirements for tactical missile sensors. In a wet tropical climate, the probability of the rain rate exceeding 4 mm/h is less than 1%. In a desert environment the probability is less than 0.1%. It would be unnecessarily restrictive to require tactical sensors to operate in 100% weather conditions, such as severe thunderstorms. Note that a high-altitude missile with a downward looking seeker may have larger signal attenuation in rain than that of a low-altitude missile. This is due to a longer rain path.

Shown in Fig. 6.4, based on Ref. 13, is the attenuation vs wavelength for a representative atmospheric environment of cloud droplet density, rain rate, and humidity level. Note that, although passive electro-optical (EO) sensors have one-way transmission through rain of about 50% per kilometer, there is almost no transmission of an EO signal through clouds. Cloud droplets are small, about 5–20 μm in diameter, with dimensions comparable to the EO wavelength. The concentration is high, about 50–500 droplets per cm^3 . EO wavelengths are strongly diffracted around cloud droplets because of Mie electromagnetic scattering, which provides a concentration of the scatter in the forward direction. However, raindrops are about 2–6 mm in diameter (much larger than EO wavelengths) and cause less attenuation of an EO signal. Rain rate attenuation is due primarily to optical scattering. EO transmission through rain is a function of the size of the raindrops, rain rate, and the path length through the rain. EO passive sensors are limited from

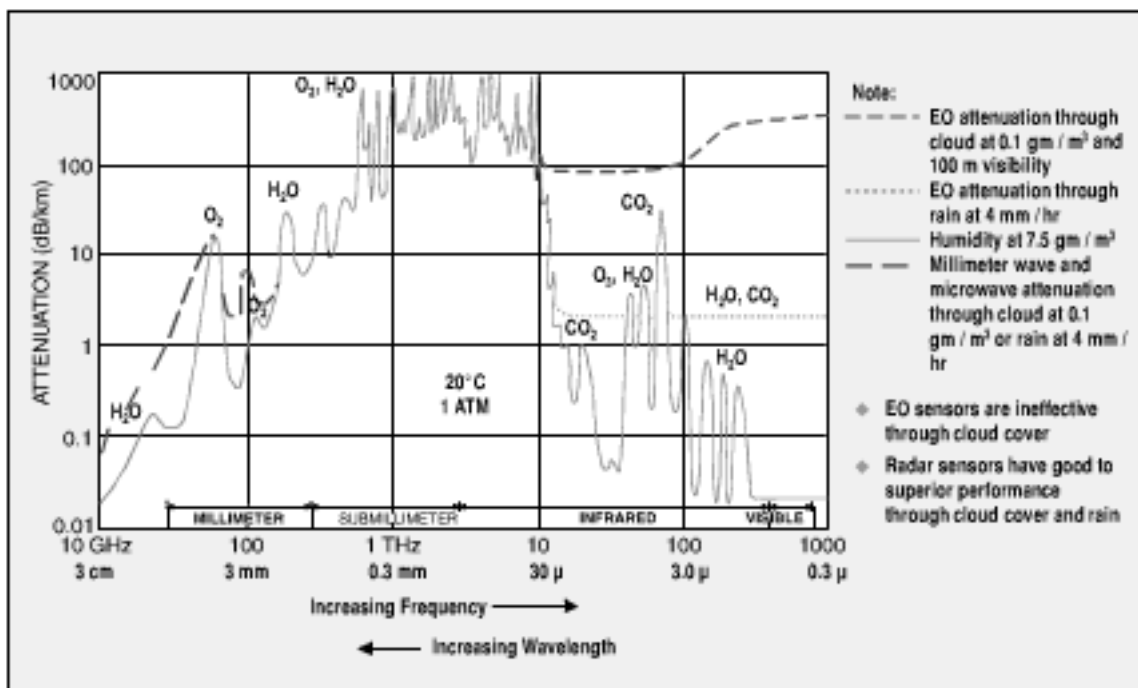


Fig. 6.4 Radar seekers are robust in adverse weather (from Ref. 13).

about 2 to 5 km of path length through the rain. EO focal plane array sensors for tactical missiles cover the wavelength range from ultraviolet (UV) through long-wave infrared (LWIR).

The best sensors for looking through cloud cover and rain are radar sensors. Radar sensors have negligible atmospheric attenuation at frequencies below 10 GHz. At higher frequencies, millimeter wave (mmW) sensors operating in cloud cover and rain are limited to about 2–5 km of path length through the clouds and rain, with the same implications as those discussed in the previous paragraph. Cloud droplets, which are much smaller than mmW wavelengths, absorb mmW radiation (much like a microwave oven). A different mechanism is responsible for the attenuation of a mmW signal through rain or snow. Raindrops and snowflakes are comparable in size to mmW wavelengths and cause Rayleigh and Mie electromagnetic scattering attenuation. Lower frequency radars, such as Ku-band radars, are less affected by cloud cover and rain rate.

As shown in Fig. 6.5, clouds tend to occur at elevation heights between 3000 and 20,000 ft, which covers most of the altitude of interest for tactical missiles. Also, as shown previously, cloud cover is a frequent occurrence. Because of the extent and frequency of cloud cover, EO sensors are often limited in their applications. The Low-Cost Autonomous Attack System (LOCAAS) and the Brilliant Anti-Tank (BAT) submunitions minimize the problem of cloud cover by operating at low altitude under most clouds. LOCAAS and BAT also fly at low velocity, to maximize the time available for target lock-on and homing under the constraint of a shallow look down angle. The “under the weather” operation is effective under most conditions except for the occurrence of fog, heavy rain, and obscurants. Search capability in operating at low altitude is improved by adding an additional wide field of view (FOV) sensor, such as passive imaging IR. For example, a wide FOV sensor could cue a narrow FOV sensor, such as a laser detection and ranging (LADAR) sensor, for target recognition, acquisition,

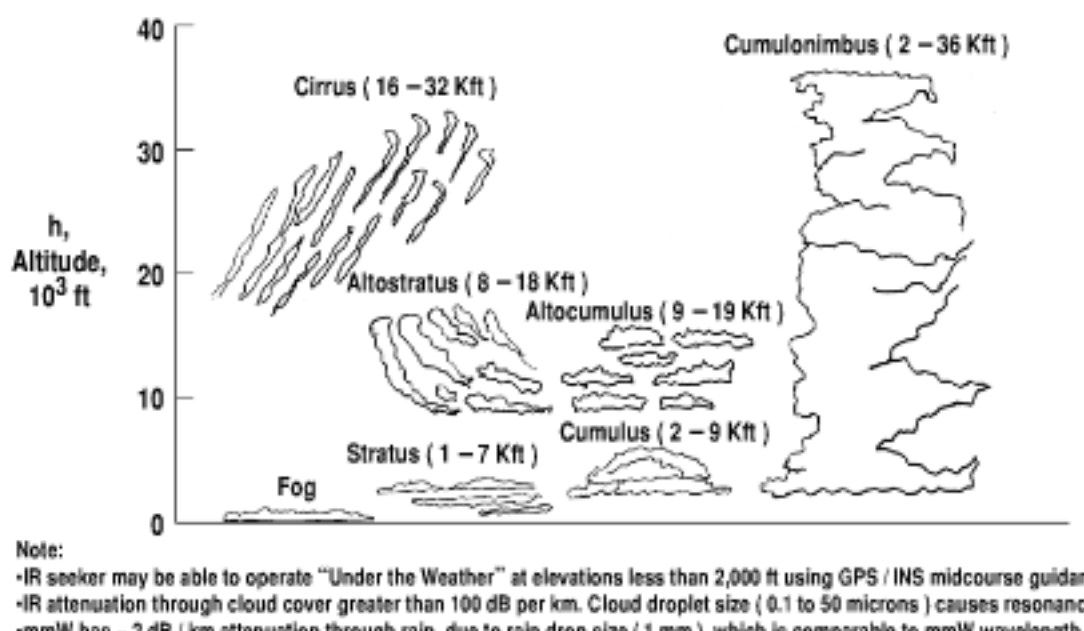


Fig. 6.5 Robust operation within the troposphere cloud cover requires radar seekers.

and fine tracking. However, as stated previously, for most missiles operating in adverse weather, especially supersonic missiles, the best sensors are radar sensors.

A comparison of sensor alternatives for precision strike missiles is shown in Fig. 6.6. The measures of merit are 1) performance in an adverse weather environment such as cloud cover, rain, snow, or dust; 2) automatic target recognition (ATR) performance in ground clutter; 3) sensor range; 4) performance against moving

Sensor	Adverse Weather Impact	ATR in Clutter	Range	Moving Target	FOV Cycle Time	Hypersonic Dome Compat.	Diameter Required	Weight and Cost
• SAR	●	○	●	○	●	●	○	·
• Active Imaging mmW	●	○	●	●	○	●	○	·
• Passive Imaging mmW	●	●	○	○	○	●	·	○
• Active Imaging IR (LADAR)	·	●	○	●	·	○	●	○
• Active Non-image IR (LADAR)	·	○	○	○	●	○	●	●
• Active Non-image mmW	●	·	●	○	●	●	●	○
• Passive Imaging IR	·	●	●	○	●	·	●	○
• Acoustic	●	○	·	○	●	·	·	●
• GPS / INS	●	●	●	·	●	●	●	●

Note: ● Superior ○ Good ○ Average · Poor

Fig. 6.6 Precision strike missile target sensors are complemented by GPS/INS sensors.

targets; 5) cycle time to cover the required field of view; 6) compatibility with a dome for a hypersonic application; 7) diameter required; and 8) weight/cost.

Synthetic aperture radar (SAR) is a preferred sensor for a precision strike missile. SAR has the flexibility required to cover an area search for single-cell target detection, then to switch to high resolution for target identification and targeting. SAR sensors can also provide high-accuracy profiling of the known terrain features around the target to provide a reference for global positioning system (GPS) coordinates of the target. Polarization provides a SAR sensor with the capability to extract information on the physical shape characteristics of the target. Other discriminates that improve the ATR performance of SAR include motion detection and three-dimensional imagery. The historical weight and cost of SAR sensors have been too high for an application of SAR as a tactical missile seeker. However, recent advances in electronics and inertial sensors have greatly reduced the weight and cost of a SAR seeker.

A passive imaging mmW sensor is the second choice for a future precision strike missile. Passive imaging mmW has an advantage over EO in its capability to see through cloud cover and the high contrast of metal objects in the millimeter wave spectrum. Advantages over active radar sensors include lower observables (passive), lower noise, and the avoidance of radar glint. The cold sky is about 35 K and is reflected by metal objects at millimeter wave frequencies. The temperature of terrestrial object clutter is about 300 K and is not reflected.

Other sensors for precision strike, listed in order of their projected application in the year 2010, include active imaging IR based on LADAR, passive imaging IR, active nonimaging radar, active nonimaging LADAR, passive nonimaging IR, visible, and acoustic/seismic. Sensors are available that cover the range of acoustic-to-visible. Because sensors have limitations in one or more areas, multimode sensors using sensor data fusion will be developed for future missiles. Multidimensional orthogonal discriminants that are likely to be used in sensor data fusion include angular resolution, range resolution, contrast, polarization, temporal (e.g., vibration, movement), multispectral, and gas composition signatures of the target. Because of the importance of adverse weather, radar and millimeter wave sensors are projected to be the primary sensors for many future precision strike missiles.

GPS/INS guidance is an enabling technology for precision navigation and the fusion of target sensor data in a clutter environment. Target clutter varies widely. For example, a SAM site situated in a populated area would probably be located in very high clutter, whereas a forested area could be moderate to high clutter, and a desert area could be low clutter. GPS accuracy in the wide area GPS enhancement (WAGE), differential, or relative modes has a navigation error less than 3 m. GPS combined with SAR precision mapping can provide near-real-time precision targeting of targets in clutter.

Shown in Fig. 6.7 are examples of the resolution for tactical missile imaging sensors. A LADAR sensor has the best resolution for target discrimination. It also provides three-dimensional imagery, enhancing ATR. The next best resolution is a passive imaging infrared sensor. IR sensors are in development with resolution up to 1000×1000 pixels. SAR has a resolution of about 0.3 m, independent of range. At very long range a SAR sensor has higher resolution than the other sensor alternatives. Finally, passive imaging mmW has relatively low resolution. Passive imaging mmW array sizes up to 40×26 elements have been produced, with apertures

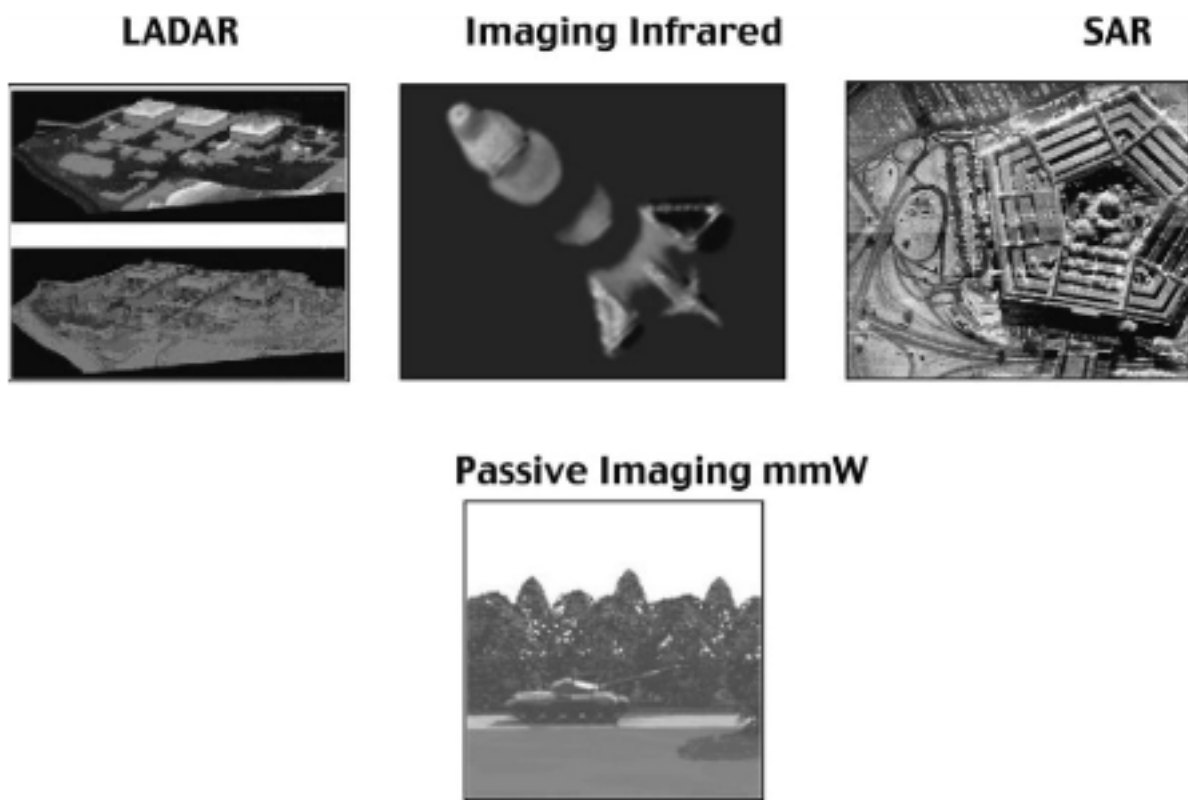
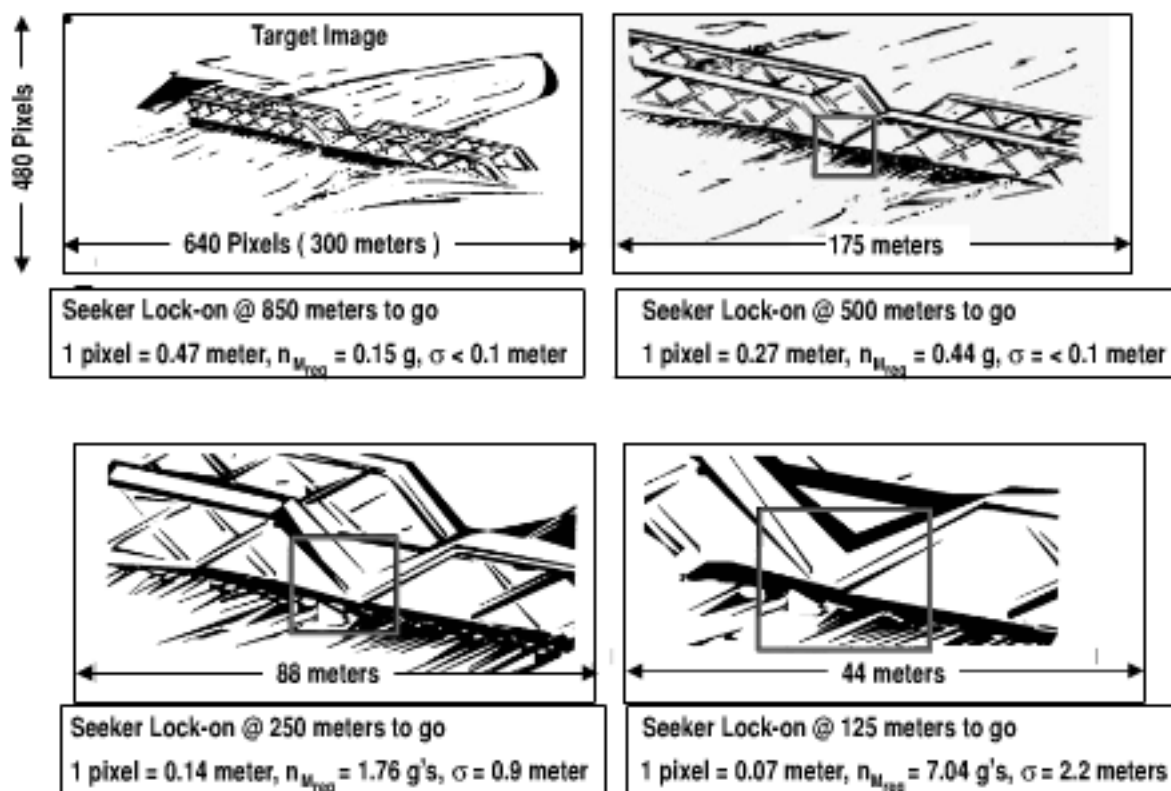


Fig. 6.7 Imaging seekers enhance target discrimination.

ranging from 0.4 to 1.2 m in diameter. The frequency and frame rate demonstrated to date are 89 GHz and 17 Hz, respectively. Passive imaging mmW is a relatively immature technology, and the resolution is expected to improve in the future.

Figure 6.8 illustrates the benefit of precision GPS/INS guidance. The example is a bridge target in adverse weather and in a high clutter environment consisting of a river and rolling terrain. In this example, a high-resolution (640×480 pixels) strapdown IIR seeker is used in terminal homing for precision strike. The aim point is the center pier of the bridge. Note that, even for a relatively large target such as the bridge in the figure, there is a large amount of clutter at the initial range of 850 m. The 20-deg FOV seeker provides a 300×230 m scene. Fortunately, the GPS/INS has precision accuracy (3 m), allowing delay of seeker lock-on and terminal guidance until the missile is closer to the target. As the missile closes on the target at the ranges of 500 and 250 m, note that there is less and less clutter. Finally, at a range-to-go of 125 m, note that there is almost no clutter within the seeker FOV. The GPS/INS accuracy of 3 m is comparable to the tracking accuracy of the seeker, allowing a smooth transition from midcourse navigation GPS/INS guidance to terminal seeker guidance. For a typical closing velocity of 300 m/s and a guidance update rate of 60 Hz, there are up to 25 guidance updates available to conduct ATR when the weapon is at a range-to-go of 125 m. The terminal accuracy is driven more by the airframe response than seeker tracking error. As a result of the GPS/INS precision guidance, the missile has higher probability of hitting the center pier aim point and dropping the center span of the bridge. The GPS/INS guided missile can be treated almost like an artillery projectile, with a high probability of impacting in the target area and a low probability of collateral damage.



Note: \square = Target Aim Point, GPS / INS Accuracy = 3 Meters, Seeker 640 x 480 Image, Seeker FOV = 20 Degrees, Proportional Guidance Navigation Ratio = 4, Velocity = 300 Meters / Sec, G&C Time Constant = 0.2 Second.

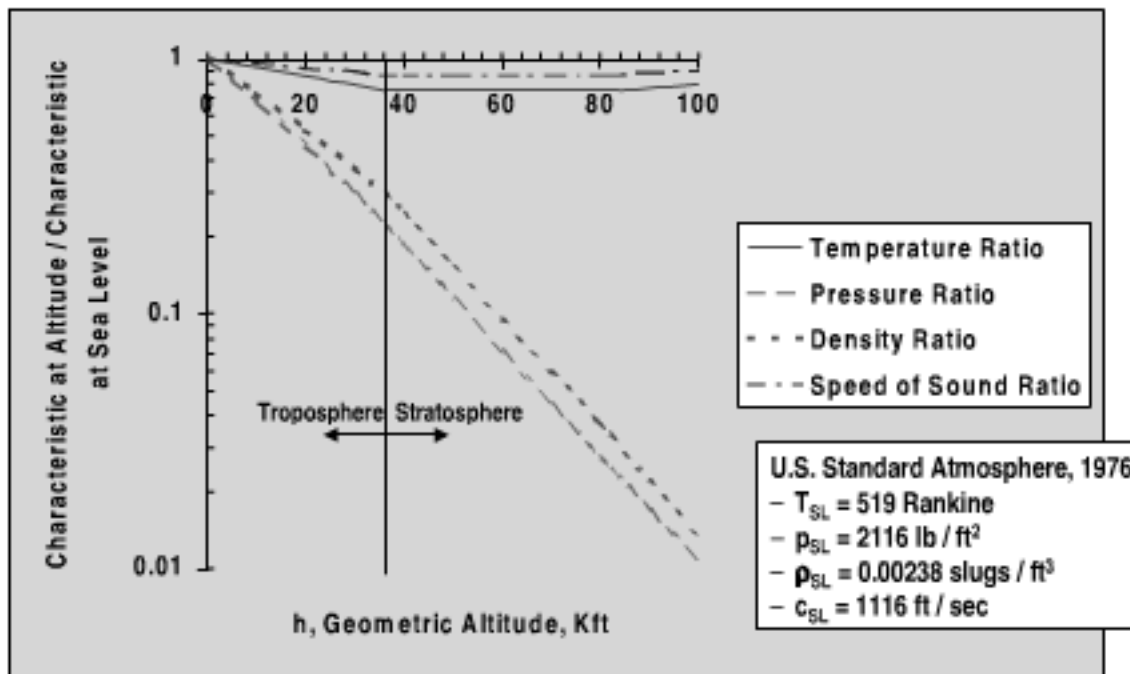
Fig. 6.8 GPS/INS provides robust seeker lock-on in adverse weather and clutter.

Benefits of tightly coupled integration of the INS with the GPS for navigation include high-precision position and velocity measurement and reduced jamming susceptibility. The availability of GPS to continuously update the inertial system allows the design trades to consider a lower precision and less expensive INS, while maintaining good navigation accuracy and antijam (A/J) performance.

Advanced GPS/INS receivers are based on a centralized Kalman filter that processes the raw data from all of the sensors (e.g., SAR, GPS receiver, INS). Tightly coupled GPS/INS is more robust against jamming because it is able to make pseudorange measurements from three, two, or even one satellite if one or more of the satellites are lost.

Also shown in the figure is the missile maneuverability requirement to correct the heading error at seeker lock-on. Because of the accuracy of GPS/INS, the maneuverability required is very low at long range and becomes significant (e.g., greater than 2 g) only if the seeker lock-on is less than 200 m to go.

Another consideration for design robustness is the variation in the flight environment design parameters with flight altitude. Figure 6.9 shows the variation of atmospheric temperature, pressure, density, and speed of sound as a function of altitude. Within the troposphere, temperature and speed of sound decrease with increasing altitude up to about 36,000 ft. The Mach number for a given velocity increases slightly with increasing altitude within the troposphere because of the decrease in the speed of sound with altitude. Most weather and clouds are within the troposphere. For flight within the stratosphere, above about 36,000 ft, temperature and speed of sound are nearly constant. The atmospheric pressure and density decrease rapidly with altitude in the troposphere as well as the stratosphere. The



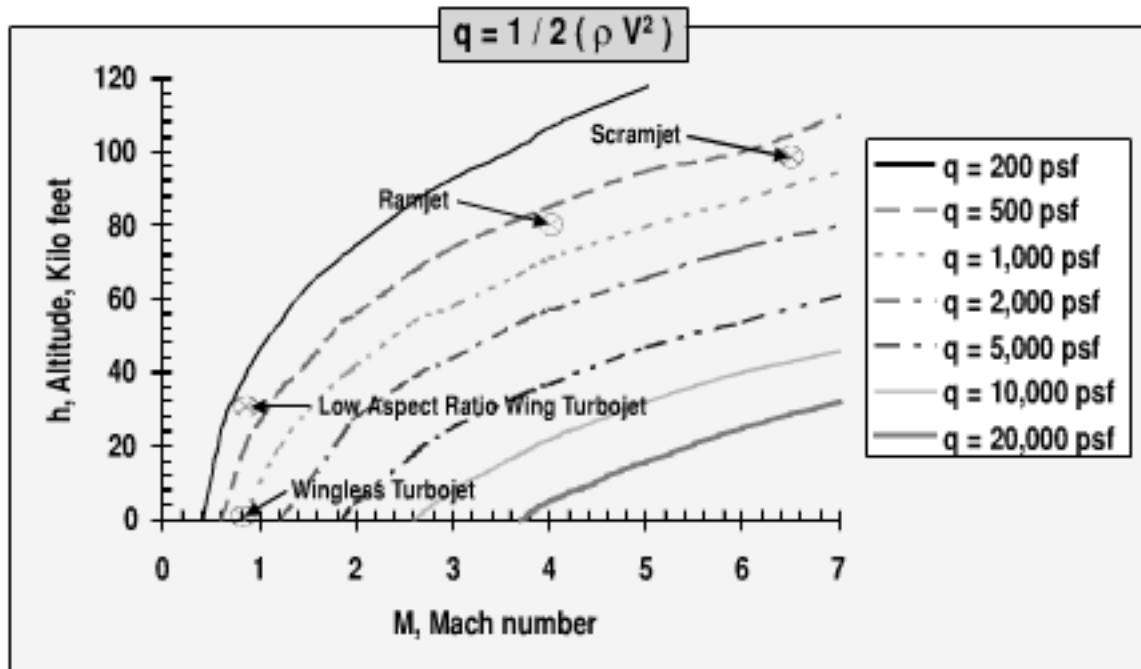
Note: T_{SL} = Temperature at sea level, p_{SL} = pressure at sea level, ρ_{SL} = density at sea level, c_{SL} = speed of sound at sea level

Fig. 6.9 Design robustness requires consideration of changes in parameters with altitude.

dynamic pressure, aerodynamic heating, and airbreathing propulsion thrust are a function of atmospheric density, and for a given velocity they also decrease rapidly with altitude. Rocket motor thrust for a typical (underexpanded) nozzle increases with altitude because of the decreasing atmospheric pressure. Data used to develop the figure are from the U.S. 1976 Standard Atmosphere.

Figure 6.10 shows the variation in dynamic pressure as a function of Mach number and altitude. Note that for a given Mach number the dynamic pressure decreases rapidly with altitude, similar to the decrease in atmospheric density with altitude. Most wingless missiles have their best aerodynamic efficiency (L/D)_{Max} at a dynamic pressure of about 700 psf. The figure shows the flight envelope of the optimum dynamic pressure as a function of Mach number and altitude. For a wingless turbojet flying at about Mach 0.8 (e.g., subsonic wingless cruise missile), the optimum flight altitude is sea level. Adding wings to the cruise missile results in a higher cruise altitude and a lower dynamic pressure for optimum aerodynamic efficiency. As shown in the figure, for a wingless ramjet missile flying at Mach 4, the optimum cruise altitude is about 80,000 ft. Finally, for a wingless scramjet missile flying at Mach 6.5, the optimum cruise altitude is about 100,000 ft.

The values of the atmospheric properties vary with different atmospheric models. The standard atmospheric model used for many design activities is the U.S. 1976 Standard Atmosphere. However, the worldwide weather and climate can provide significant differences in parameters such as temperature, density, and speed of sound. Shown in Fig. 6.11 are comparisons of cold, hot, polar, and tropic atmospheric models with the standard atmospheric model. Note that the values of the parameters can vary up to $+/- 26\%$ from the standard atmospheric model. The design of subsystems such as the rocket motor requires consideration of

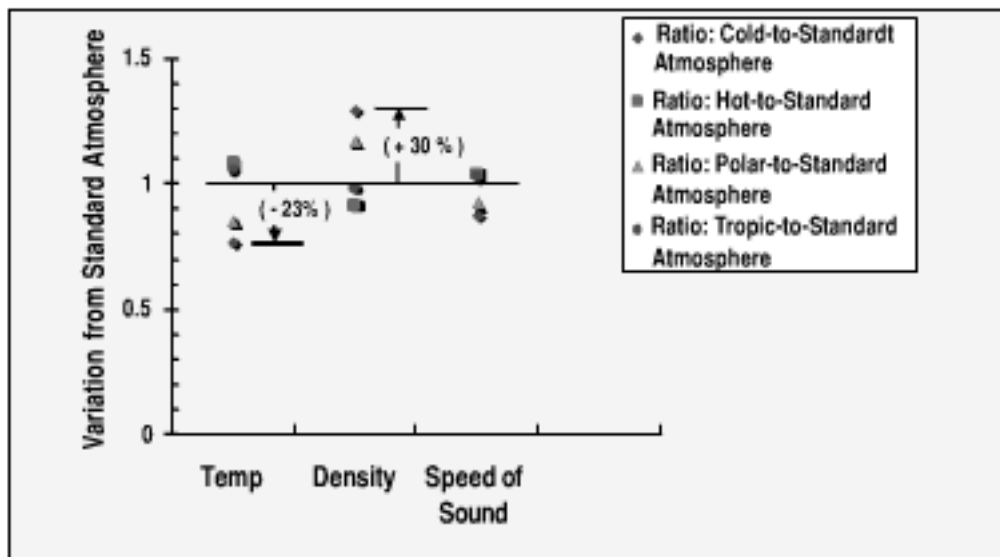
**Note:**

- U.S. 1976 Standard Atmosphere
- For Efficient Cruise, $(L/D)_{\max}$ for Cruising Lifting Body Typically Occurs for $500 \text{ lb/ft}^2 < q < 1,000 \text{ lb/ft}^2$
- $(L/D)_{\max}$ for Cruise Missile with Low Aspect Ratio Wing Typically Occurs for $200 \text{ lb/ft}^2 < q < 500 \text{ lb/ft}^2$

Fig. 6.10 Dynamic pressure varies with altitude and Mach number.

off-nominal design conditions, such as extreme hot and extreme cold atmospheric temperatures.

Shown in Fig. 6.12 is an example of the broad range of flight conditions that are encountered by a complex high-performance missile such as a ramjet. The example ramjet is launched at a subsonic Mach number, pitches up at high angle of attack, and is boosted to a supersonic Mach number while climbing. Following booster shutdown during the climb, the ramjet is ignited, and the missile

**Note:**

- Based on properties at sea level
- U.S. 1976 Standard Atmosphere: Temperature = 519 Deg. Rankine, Density = 0.002377 slugs / ft³, Speed of sound = 1116 ft / sec

Fig. 6.11 Design robustness requires consideration of type of atmosphere.

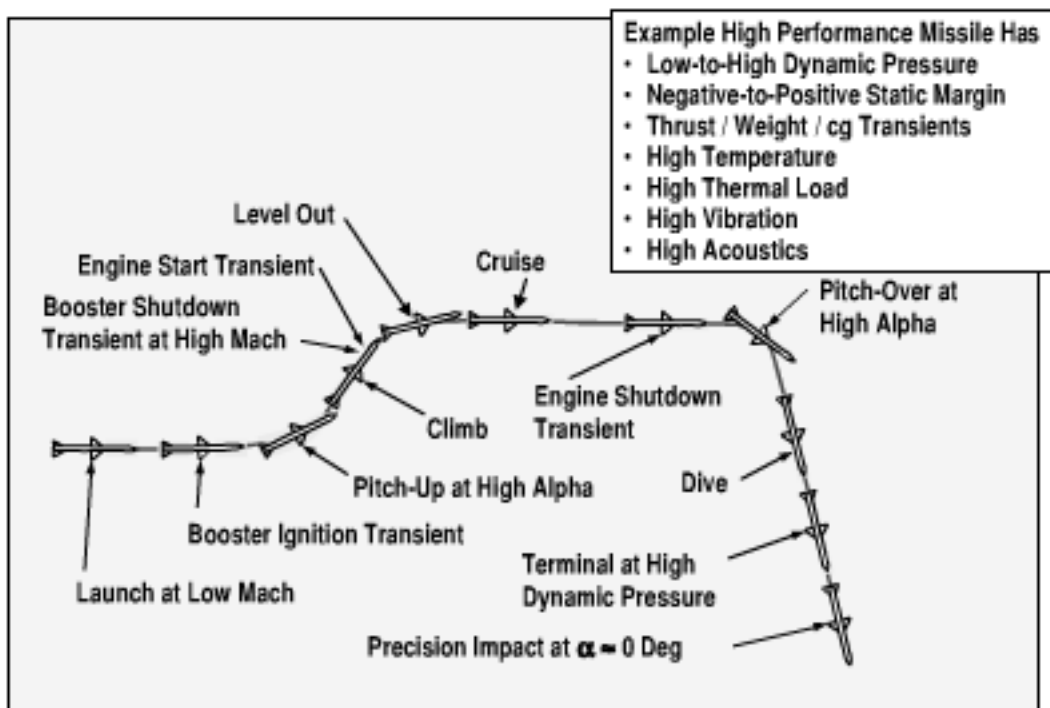


Fig. 6.12 Missile guidance and control must be robust for events and flight environment.

continues to climb under ramjet propulsion. As the missile approaches the optimum cruise altitude for ramjet cruise, a pitch-over maneuver is conducted to level off for constant altitude flight. The missile cruises at an optimum altitude until it approaches the target area. The engine may be shut down at the end of cruise, or if there is sufficient fuel, the engine may continue to operate to maximize the speed. A pitch-over maneuver at high angle of attack is initiated, and the missile dives toward the target. During the dive through the lower atmosphere, the dynamic pressure reaches a maximum. For a deeply buried target, the impact angle of attack is tightly controlled, to less than 1 deg, to avoid breaking up the warhead.

A modern control autopilot is required to handle the broad range of events, flight phases, and the flight environment of a high-performance missile. The autopilot is the brain of the missile. It provides flight control commands based on input data from the seeker, navigation, and stabilization sensors. Gains are multidimensional functions of complex parameters and are selected to maintain stable gain and phase margins. Special attention is given to the different flight phases. The autopilot design allows for sequencing between flight phases and fading in the different control gains for each phase. The flight phases may have low-to-high dynamic pressure, negative-to-positive static margin, and thrust/weight/center-of-gravity transients. Another consideration is designing robust subsystem hardware to handle a severe thermal, vibration, and acoustic environment.

Examples of design uncertainties of tactical missiles are illustrated in Fig. 6.13. The design uncertainty in engineering and manufacturing development (EMD) should ideally be small, for low risk in meeting mission requirements. Design uncertainty in EMD is usually a symmetrical, normal distribution of uncertainty with a relatively small deviation (e.g., $+/-5\%$, 1σ). Usually there is a single set of technologies for EMD based on a prior downselect of the technology alternatives. Note that the typical design uncertainty in conceptual design flight performance

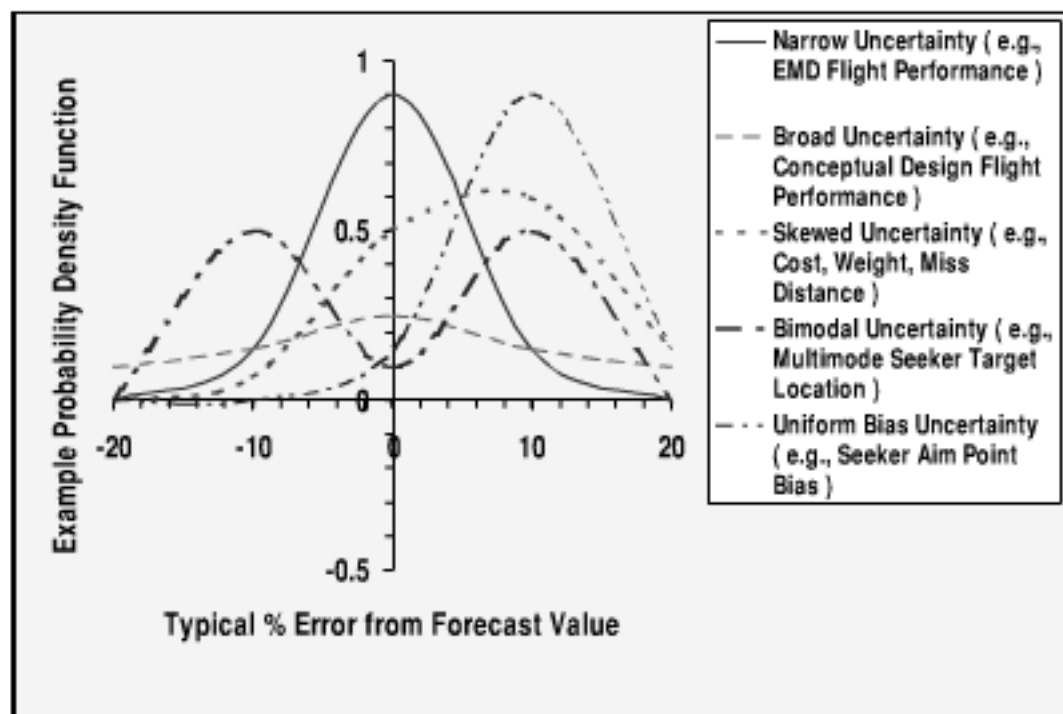


Fig. 6.13 Design robustness is required to handle uncertainty.

is much larger (e.g., $+/-15\%$, 1σ). The elements that contribute to conceptual design flight performance can have even larger uncertainty. For example, the uncertainty in the static margin of a nearly neutrally stable missile may be more than 100%. As a result of the larger uncertainty in conceptual design, alternative candidate technology solutions must usually be explored and developed. Different technologies have the potential to satisfy the mission requirements, but some have higher probability of success than others. The investment in the technology alternatives to quantify their performance and reduce their uncertainty will reduce the missile system design uncertainty and mature the design. Prior to EMD there is usually sufficient confidence to select the preferred technology from the set of alternatives.

Because of the large design uncertainty in conceptual design, it is important to evaluate the robustness of the conceptual design and the associated technology alternatives. Design robustness may be a factor in not selecting a technology that, although it may have higher potential performance or lower potential cost, is highly sensitive to uncertainty when there is insufficient funding or time to reduce the uncertainty.

Some uncertainty distributions are not a normal distribution. The third curve in the figure is a skewed uncertainty distribution. Examples of skewed distributions are cost, weight, and miss distance uncertainty. Usually the actual cost, weight, and miss distance measured during EMD tend to be higher than the original predictions. Conceptual design predictions are usually found later during the design maturation to be optimistic predictions. An approach used during conceptual design to compensate for the optimistic conceptual design prediction is to provide design margin for robustness. For example, during conceptual design the warhead lethal radius may be sized for a large (e.g., 3σ) miss distance. The fourth curve in the figure is a bimodal distribution. As an example of a bimodal distribution, a dual-mode seeker (e.g., millimeter wave/infrared) could measure two different

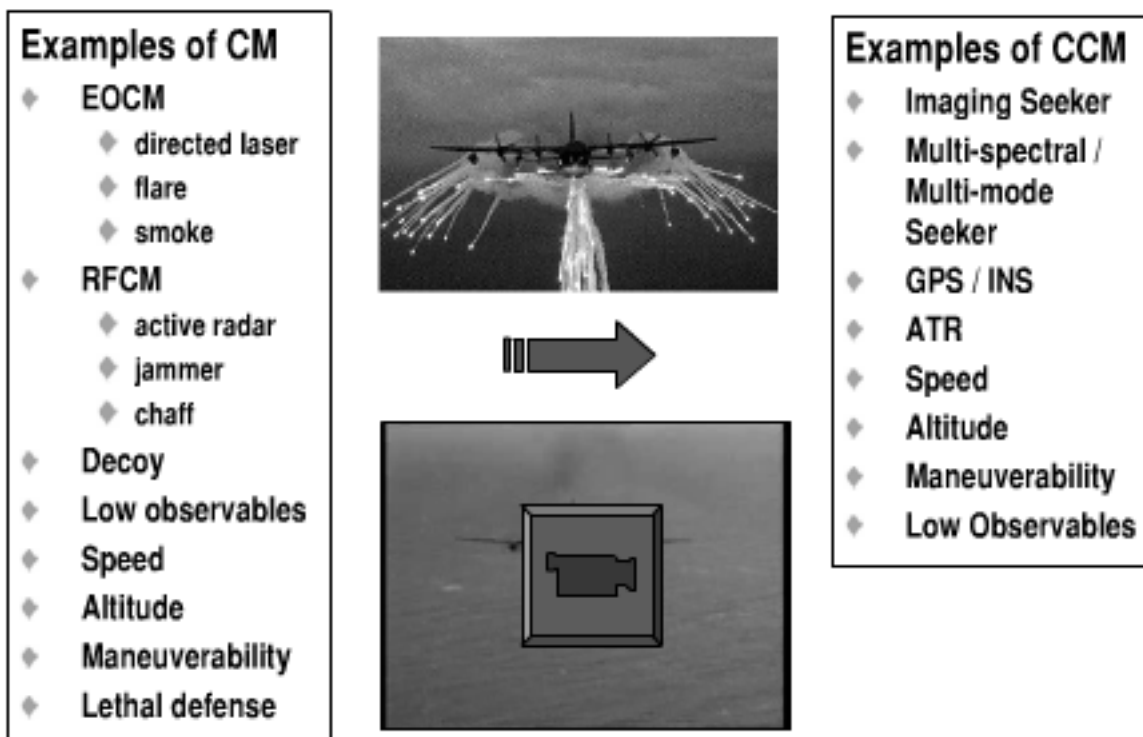


Fig. 6.14 Counter-countermeasures enhance the robustness.

locations of the target, with uncertainty in the target location from each sensor. The final curve in the figure is a distribution that is similar to a normal distribution, except for a bias. An example is a seeker that has an aim point bias, such as the IR seeker of an air intercept missile that homes on the hot plume aft of the target aircraft instead of the airframe centroid of the aircraft.

Examples of countermeasures to missiles are shown in Fig. 6.14. These are 1) electro-optical countermeasures (EOCM) against an IR missile seeker, such as directed energy lasers, flares, and smoke; 2) radar frequency countermeasures (RFCM) against a radar missile seeker, such as active radar ECM, jammers, and chaff; 3) decoys, such as towed decoys to induce homing on the decoy false target; 4) low observables, including contrail, RCS, and IR signature reduction; 5) high-speed flight, to defeat the missile seeker tracking and the warhead fusing; 6) high-altitude flight, to prevent seeker lock-on and exceed the missile flight envelope; 7) high maneuverability, to induce missile miss distance; and 8) lethal defense, to destroy the missile in flight.

Robust counter-countermeasures are often an asymmetric response based on technological surprise. An asymmetric counter-countermeasure may use new technology that was not envisioned when the countermeasure was originally developed by the threat. Examples of robust counter-countermeasures are shown in the figure. These are 1) imaging seeker, to provide the resolution required to separate the target from ejected or towed countermeasures; 2) multispectral/multimode seeker, to provide broadband discrimination of the target signature; 3) GPS/INS, to maintain a target intercept course if the seeker is jammed; 4) ATR, to pull the target out of the countermeasures; 5) high speed, to minimize the exposure time to countermeasures; 6) high-altitude flight, to avoid detection and exceed the threat flight envelope; 7) high maneuverability, to minimize miss distance from countermeasures; and 8) low observables from the missile plume visual, RCS, and IR signatures, to avoid detection.

Also shown in the figure are a photograph and a video of a dispensed flare countermeasure to missiles. Examples of counter-countermeasure that are used by missiles against flares include 1) high-resolution imaging seeker with sufficient pixels to maintain tracking of the larger target compared to the smaller flare(s) and 2) multispectral/multimode seeker to distinguish the energy distribution of the hot flare compared to that of the relatively cool target.

6.2 Warhead Lethality

The second measure of merit to be discussed is warhead lethality. Warhead lethality addressed in this text emphasizes blast fragmentation and kinetic energy warheads because of their impact on missile configuration design. Shaped charge warheads for anti-armor missions, although important for weapon system effectiveness, usually have a lesser effect on missile configuration design, and are not addressed in this text. Directed energy warheads, such as electromagnetic pulse (EMP) and high-power microwave (HPM) warheads, have not yet been shown to be of practical size for tactical missile application.

A design consideration for blast fragmentation warheads is their robustness against a variety of targets, such as the typical surface targets shown in Fig. 6.15. Targets may be large (e.g., buildings) or small (e.g., tanks), hard (e.g., bunkers) or soft (e.g., radar sites), mobile (e.g., TBMs) or fixed (e.g., bridges). New precision strike missiles should ideally have a capability against more than one type of target. An example is a combined capability to engage and defeat hardened buried targets in addition to defeating fixed and mobile surface targets. Benefits of producing a multipurpose missile that is effective against a broad range of targets include reduced unit production cost due to a larger production run and reduced logistic cost due to a simplified logistics organization.

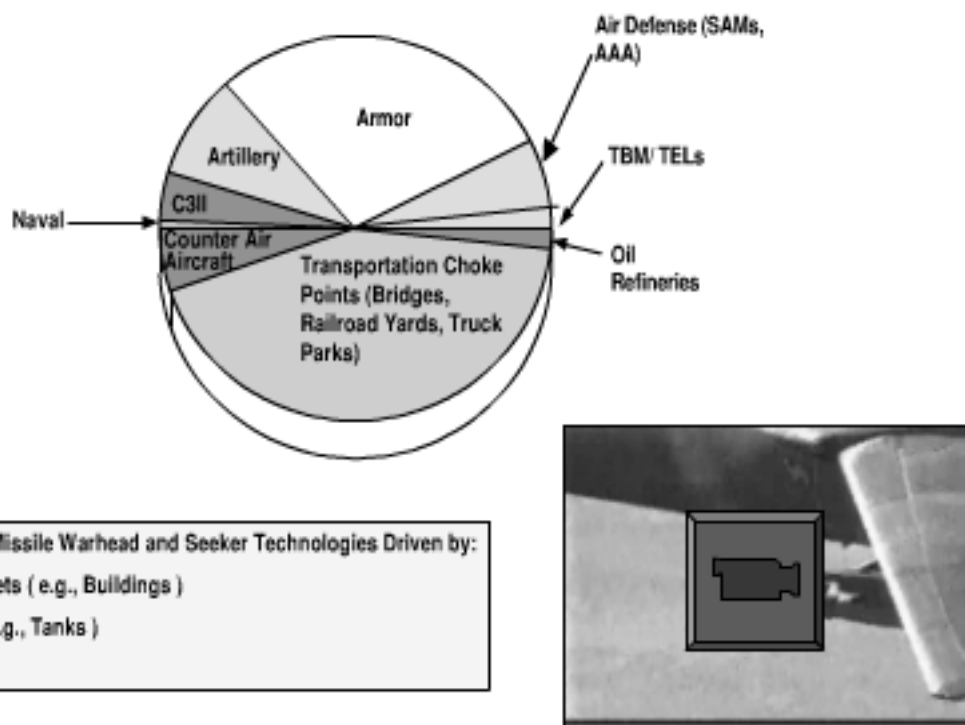


Fig. 6.15 Warheads for precision strike missiles must handle a broad range of targets.

◆ Anti-Fixed Surface Target Missiles (large size, wings, subsonic, blast frag warhead)



◆ Anti-Radar Site Missiles (ARH seeker, high speed, blast frag warhead)



◆ Anti-Ship Missiles (large size, blast frag warhead, and high speed or low altitude)



◆ Anti-Armor Missiles (small size, hit-to-kill, low cost, shape charge / EFP / KE warhead)



◆ Anti-Buried Target Missiles (large size, high fineness / penetrating warhead)



Permission of Missile Index. Copyright 1997©Missile.Index All Rights Reserved

Fig. 6.16 Examples of precision strike missiles (used with permission of Missile Index, 1997, online at <http://www.index.ne.jp/missile-e/>).

Shown in the computer video of the accompanying CD are examples of precision strike missiles that are used in missions against a building target, a single tank target, and a column of tanks target. The first example is a large laser guided bomb attacking a large building target of concrete/steel construction. The second example is a Maverick missile attacking a within-visual-range tank target. The third example is a Brimstone missile conducting a beyond-visual-range salvo attack against a column of tanks, using an autonomous millimeter wave seeker with automatic target recognition (ATR).

Figure 6.16 is an example of surface target types and the characteristics of current precision strike missiles. The missions for precision strike missiles cover a broad range of alternatives. Precision strike missile targets include fixed targets, radar sites, ships, armor, and buried targets. Most of the missile configuration drawings shown in the figure are from Missile.index (online at <http://www.index.ne.jp/missile-e/>).

In the case of *fixed targets* (which usually are of large size with hardness ranging from soft to hard), a blast fragmentation warhead or dispensed cluster submunitions are usually used. The current missiles for use against fixed targets are relatively large with wings for efficient subsonic flight. Current missiles in this category include AGM-154 JSOW, Apache, KEPD-350, BGM-109 Tomahawk, and AGM-142 Have Nap.

The second target category is *radar sites*. Radar sites are relatively soft, and a blast fragmentation warhead is usually used. Antiradar missiles have an antiradiation homing (ARH) seeker and generally fly at high supersonic Mach number, for launch aircraft survivability in a SAM engagement and to minimize threat radar shutdown before missile impact. Current missiles in this category include

AGM-88 HARM, AS-11 Kilter/Kh-58, ARMAT, AS-12 Kegler/Kh-27, and ALARM.

A third target category is *ship targets*. Ships are relatively hard targets and usually require a kinetic energy penetrating warhead, followed by blast fragmentation after penetration of the hull. Antiship missiles are generally large in size and have a large warhead. Antiship missiles are designed to survive ship defenses, relying on either speed or flying at low altitude in clutter to survive. Current antiship missiles include MM40 Exocet, AS-34 Kormoran, AS-17 Krypton/Kh-34, Sea Eagle, and SS-N-22 Sunburn/3M80.

A fourth category is *armor targets*. This includes tanks, armored personnel carriers, and other armored combat vehicles. Armor targets are small in size, mobile, and very hard. Typical anti-armor warheads include shaped charge, EFP, and kinetic energy penetrator. Most anti-armor missiles are small in size, have hit-to-kill accuracy, and are low cost. Examples are Hellfire/Brimstone, LOCAAS, MGM-140 ATACMS with submunitions, AGM-65 Maverick, and TRIGAT.

A final category is *buried targets*. Buried targets require a high fineness kinetic energy penetration warhead followed by blast fragmentation. Buried targets include underground command posts and bunkers. The current missiles in this category (CALCM, GBU-28, GBU-31 JDAM) are large and heavy. A technical concern is flight control at impact to avoid breaking up the warhead. Warhead design considerations include the shape of the nose, weight, case material, and diameter. Explosives and fuses must survive at high deceleration.

Examples of lightweight, air-launched multipurpose precision strike weapons and their system considerations are shown in Fig. 6.17. The selected examples are relatively lightweight air-launched missiles because of the importance of firepower. Firepower is especially important for lightweight fighter aircraft, helicopters, and UCAVs, which may have a firepower limitation because of a store weight limit. Current operational air-launched precision strike missiles that are relatively lightweight include AGM-65 Maverick, Small Smart Bomb, AGM-88 HARM, Brimstone/Longbow Hellfire, and LOCAAS. Measures of merit shown are the effectiveness against fixed-surface targets, effectiveness against moving targets, effectiveness against time-critical targets, effectiveness against buried targets, effectiveness in adverse weather, and the firepower loadout on the launch aircraft. Note that no one operational missile is superior in all areas. The Small Smart Bomb has good effectiveness against fixed-surface targets, has good effectiveness against buried targets, is capable of operation in adverse weather, and is relatively lightweight (100, 250, and 500 lb), providing high firepower. However, the Small Smart Bomb is relatively ineffective against moving targets and time-critical targets. A new lightweight precision strike missile that combines the attributes of a small smart bomb with the capability to handle moving targets and time-critical targets would be more robust. Examples of technologies that provide robustness to handle a broad range of targets include GPS/INS precision guidance, SAR or millimeter wave seeker for adverse weather homing, ducted rocket propulsion for higher speed and longer range, low drag airframe for higher average speed and longer range, multimode kinetic energy/blast fragmentation warhead, and lightweight subsystems for a lighter weight missile.

Figure 6.18, based on Ref. 14, shows the overpressure scaling for an explosive charge as a function of the charge weight and the distance from the charge to the

Weapon	Fixed Surface Targets ⁽¹⁾	Moving Targets ⁽²⁾	Time Critical Targets ⁽³⁾	Buried Targets ⁽⁴⁾	Adverse Weather ⁽⁵⁾	Firepower ⁽⁶⁾
Example New Missile	●	●	●	●	●	●
AGM-65	●	○	○	○	-	○
Small Smart Bomb	●	-	-	●	●	●
AGM-88	●	-	●	-	●	-
Hellfire / Brimstone / Longbow	○	●	○	-	●	●
LOCAAS	○	●	-	-	○	●

(1) - Large warhead desired. GPS / INS provides precision (3 meter) accuracy.

(2) - Seeker required for terminal homing.

(3) - High speed required → High payoff of rocket or ducted rocket propulsion and low drag.

(4) - Kinetic energy penetration required → High impact speed → High payoff of low drag and long length.

(5) - GPS / INS, SAR seeker, and imaging mmW seeker have high payoff.

(6) - Light weight required. Light weight also provides low cost.

Note:

- Superior
- Good
- Average
- Poor

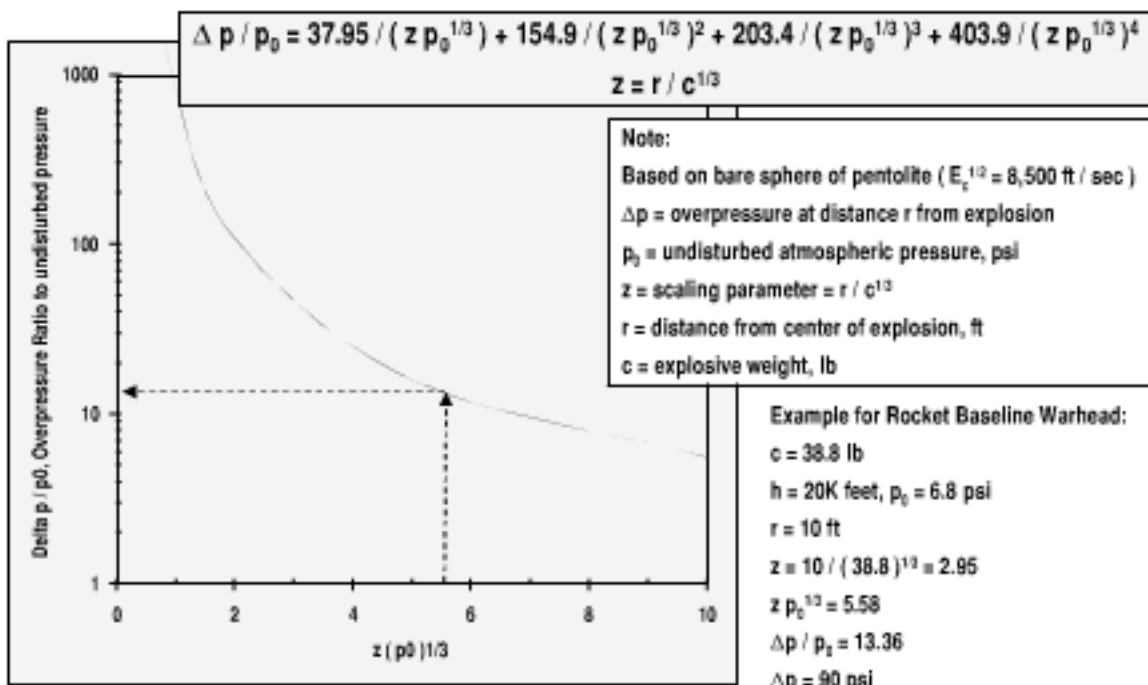
Fig. 6.17 Examples of lightweight air-launched multipurpose precision strike weapons.

target. Blast overpressure is given by the equation

$$\Delta p/p_0 = 37.95/(zp_0^{1/3}) + 154.9/(zp_0^{1/3})^2 + 203.4/(zp_0^{1/3})^3 + 403.9/(zp_0^{1/3})^4$$

The example is for a bare sphere of pentolite charge. Note that the overpressure is driven more by distance from the charge than by charge weight. The scaling parameter $z = r/c^{1/3}$ is used to relate overpressure to distance and charge weight. As an example, the rocket baseline warhead charge weight of 38.8 lb at a distance of 10 ft provides a maximum overpressure of 90 psi (6 atm). The scaling parameter z is computed to be 2.95. Comparing a smaller (10-lb) charge for the same value of z , the distance is 6.4 ft to achieve the same overpressure of 90 psi. A 36% reduction in miss distance has the same effect as a 290% increase in warhead weight. Because decreasing miss distance is more important to enhance lethality than increasing warhead weight, highly accurate missiles can have high lethality that is also combined with lighter weight, higher firepower, less collateral damage, and lower cost.

The kill and damage envelope for a typical aircraft target is shown in Fig. 6.19. The kill envelope is based on predicting the effects of the rocket baseline 77.7-lb warhead with spherical blast and a charge-to-metal ratio of 1. The altitude is assumed to be 20,000 ft. Other assumptions are that the minimum blast overpressure and the fragments impact kinetic energy to kill the target are 330 psi (22 atm) and 130,000 ft · lb/ft², respectively. For the 77.7-lb warhead, the kill overpressure and kill fragment impacts occur at a miss distance of about 5 ft. The envelope of significant damage is a miss distance of about 25 ft. At 25 ft the overpressure and kinetic energy impact are reduced to 24 psi and 5000 ft · lb/ft² respectively. For



Reference: US Army Ordnance Pamphlet ORDP-2 290-Warheads , 1980

Fig. 6.18 Blast is effective at small miss distance (from Ref. 14).

miss distance greater than 25 ft, there is a low probability of kill or even damage to the aircraft. Note from the figure that a highly accurate missile has a high kill probability, whereas a slightly less accurate missile has low kill probability.

Shown at the bottom of the figure is a video of a drone aircraft that is destroyed by the Sidewinder missile. The flight trajectory results in a small miss distance, with the missile impacting the target. The Sidewinder blast fragmentation warhead has preformed fragments of nearly uniform weight and size.

Photographs are shown in Fig. 6.20 of the fireball and fragments from small warhead detonations. The left section of the figure is the Hellfire missile warhead,

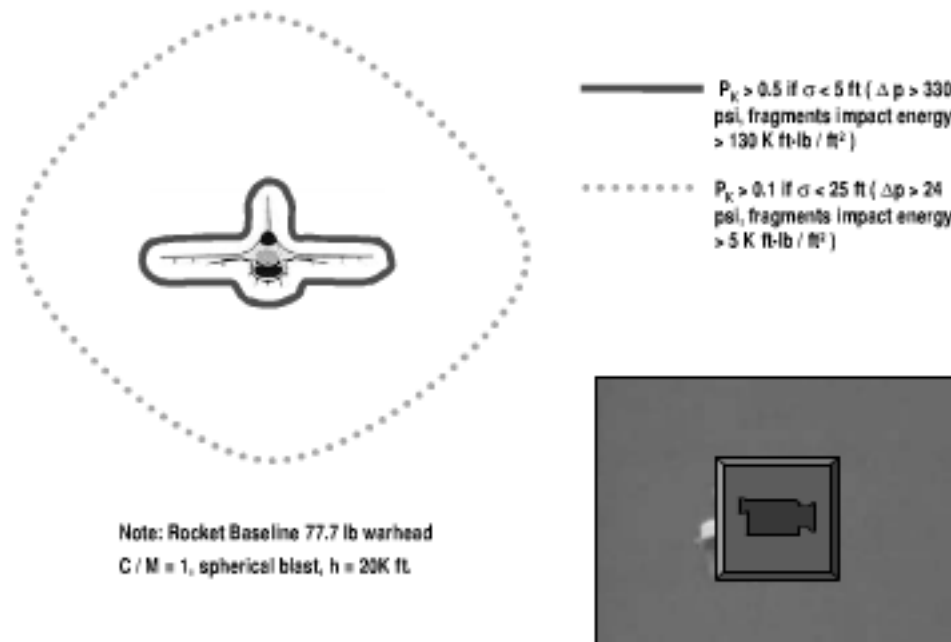


Fig. 6.19 Accuracy enhances the warhead lethality.

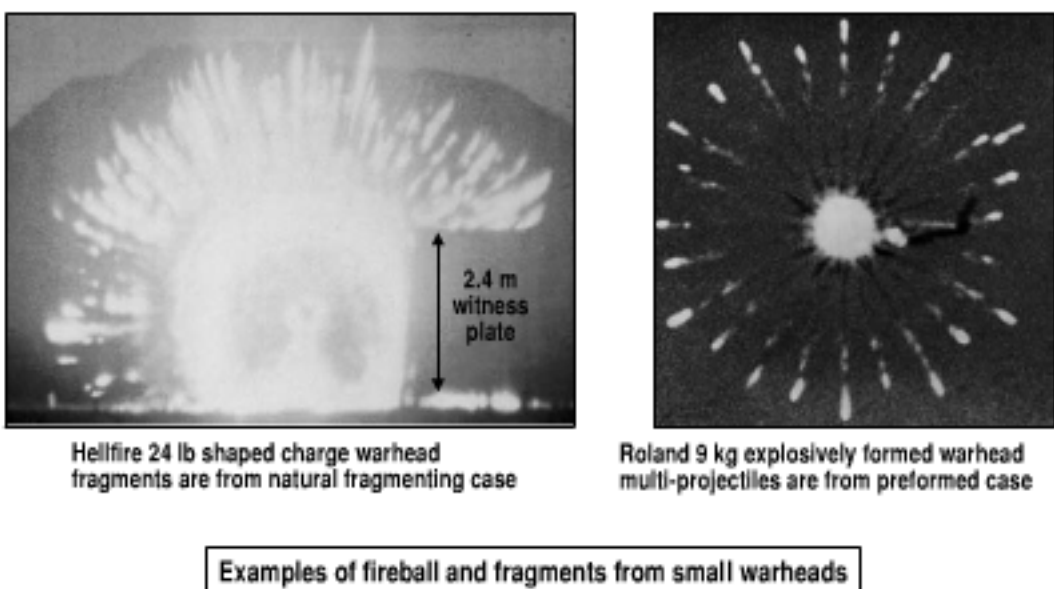


Fig. 6.20 Warhead blast and fragments are effective at small miss distance.

which weighs about 24 lb. Hellfire has a shaped charge warhead with a naturally fragmenting case. Note that the fireball and fragment coverage is larger than the 8-ft (2.4 m) witness plate. In the right section of the figure is a detonation of the Roland warhead (9 kg) against a helicopter drone target. Roland has a multiprojectile warhead. Dimples in the side of the warhead case provide explosively formed projectiles. Note that the tight fragment distribution extends beyond the target. These photographs illustrate that small warheads can be lethal if high accuracy is provided.

Figure 6.21 shows the kinetic energy of a blast fragmentation warhead as a function of charge-to-metal ratio. Kinetic energy is given by

$$KE = (1/2)M_m V_f^2 = E_c M_c / (1 + 0.5M_c/M_m)$$

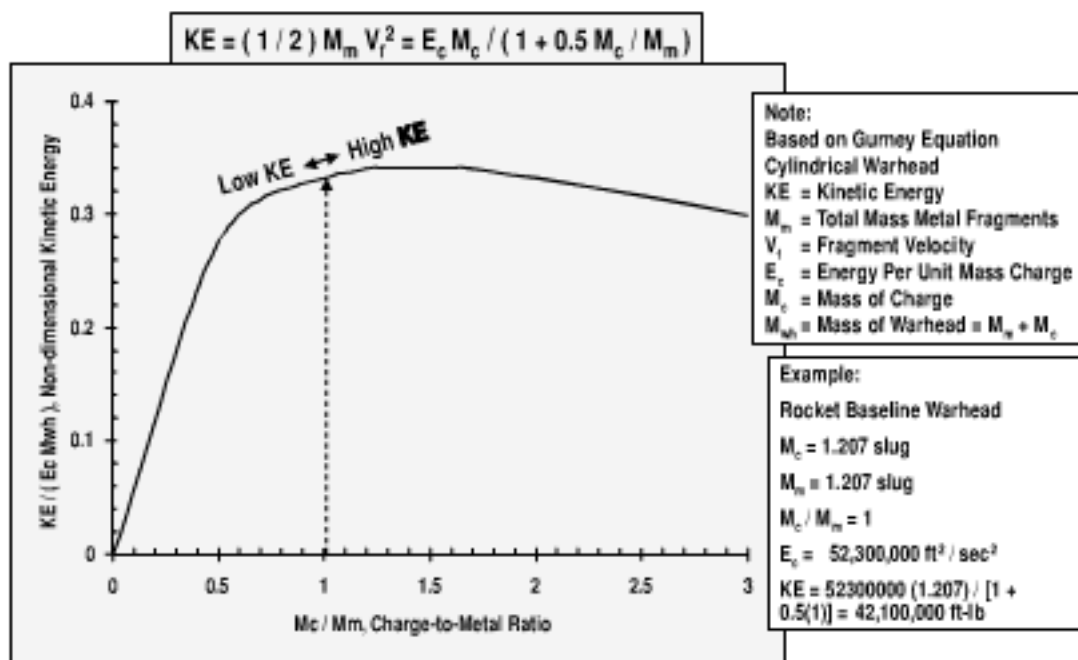


Fig. 6.21 High fragment kinetic energy requires high charge-to-metal ratio (from Ref. 15).

Results are based on the Gurney equation for a cylindrical warhead, from Ref. 15. Maximizing the total kinetic energy of the fragments is an optimization of the warhead charge-to-metal case mass ratio (M_c/M_m). A small value of charge-to-metal ratio has low kinetic energy because the small charge cannot accelerate the metal fragments to a high velocity. The charge-to-metal ratio should be greater than 1 for high kinetic energy. However, a very large value of the charge-to-metal ratio is not optimum. Although metal fragments are accelerated to high velocity, there are fewer fragments available to impact the target. The optimum value is $M_c/M_m \approx 1$.

As an example the rocket baseline warhead has a total weight of 77.7 lb and a charge-to-metal ratio of 1. The HMX explosive charge with the mass of 1.207 slugs provides a total energy $E_c = 52,300,000 \text{ ft} \cdot \text{lb}$. The total kinetic energy of the fragments is computed to be $\text{KE} = 42,100,000 \text{ ft} \cdot \text{lb}$. Again, note from the figure that the rocket baseline warhead charge-to-metal ratio of about 1 maximizes the total kinetic energy.

For a target kill by warhead fragments, probability of kill P_K is a function of the number of hits on the target and the fractional area of the target that is vulnerable. The equation is $P_K = 1 - (1 - A_V/A_P)^{n_{\text{hits}}}$. Figure 6.22 shows the probability of kill from fragments impacting a target with low vulnerable area ($A_V/A_P = 0.1$), a target with a moderate vulnerable area ($A_V/A_P = 0.5$), and a target with a large vulnerable area ($A_V/A_P = 0.9$). Although only a few warhead fragments are required to kill a soft target with a large vulnerable area, many fragment impacts are required on a hard target with a relatively small vulnerable area. As an example for a kill probability of 0.9, 22 hits are required on a hard target with a vulnerable area that is 10% of the presented area. However, only 1 hit is required against a soft target with a vulnerable area that is 90% of the presented area.

The number of fragment hits on the target is shown in Fig. 6.23 as a function of miss distance and warhead weight for a typical air-to-air missile warhead. It is based on the equation $n_{\text{hits}} = n_{\text{fragments}}[A_P/(4\pi\sigma^2)]$. The assumptions are a spherical blast with uniformly distributed fragments, charge-to-metal ratio equal to 1, an average fragment weight equal to 50 grains (3.2 g), and a target presented area equal to 20 ft^2 . The warhead and target characteristics are representative of an

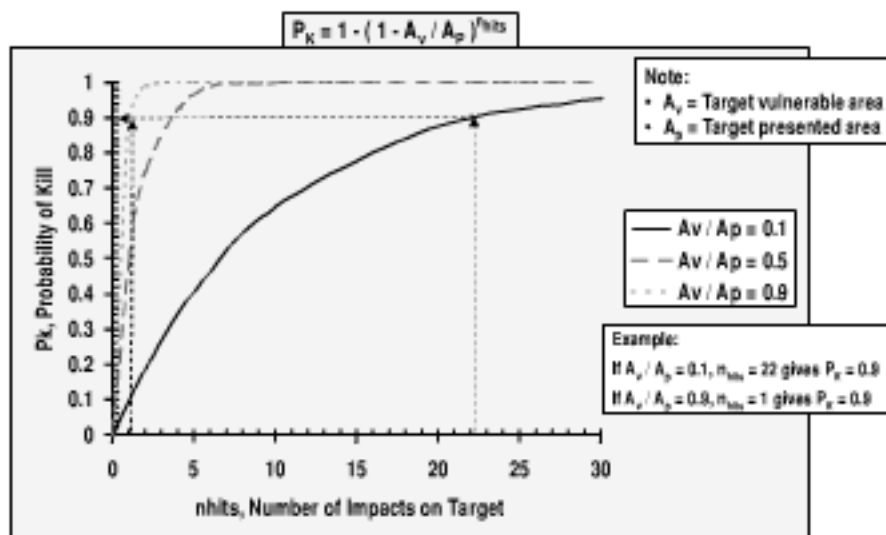


Fig. 6.22 Multiple impacts are effective against threat vulnerable area subsystems.

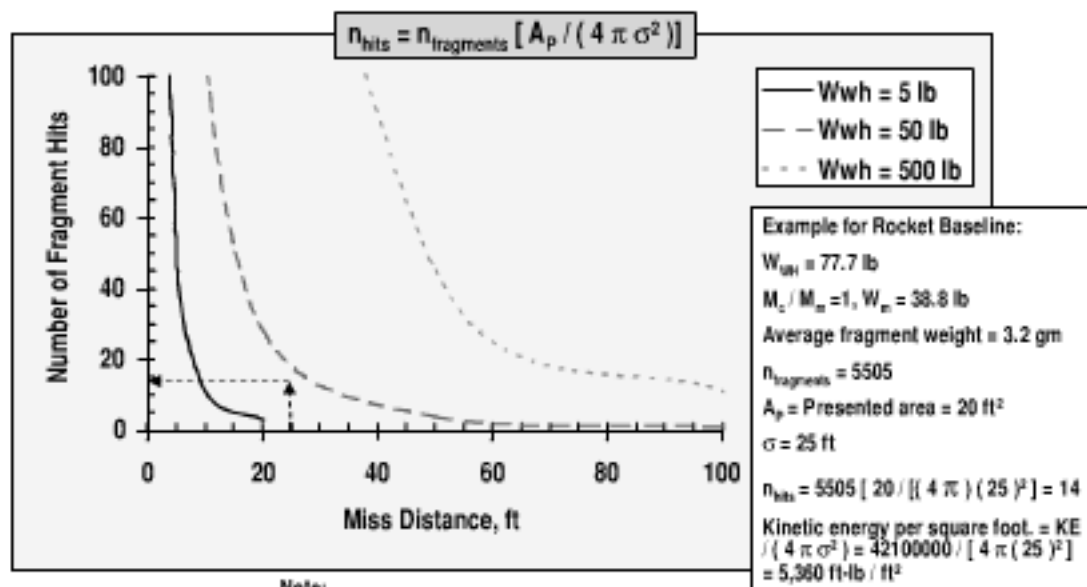


Fig. 6.23 Small miss distance improves the number of warhead fragment hits.

air target engagement. Again, note the value of guidance accuracy. At a small miss distance less than 10 ft, even a small 5-lb warhead will have multiple fragment hits on the target.

As an example, the rocket baseline 77.7-lb warhead has a charge-to-metal ratio of 1, providing a total fragment weight of 38.8 lb. For an average fragment weight of 3.2 g, there are 5505 fragments. For an assumed spherical blast with a miss distance of 25 ft, 14 fragments will impact a target with a presented area of 20 ft². The kinetic energy density of the fragments impacting on the target is 5360 ft · lb/ft².

Fragment initial velocity is a function of charge energy and the charge-to-metal ratio M_c/M_m . Figure 6.24, based on the Gurney equation, shows fragment initial velocity for a relatively modern explosive (HMX) compared to that of trinitrotoluene (TNT). The Gurney equation for fragment velocity is

$$V_f = (2E_c)^{\frac{1}{2}} [M_c/M_m] / (1 + 0.5M_c/M_m)^{\frac{1}{2}}$$

HMX has 35% more explosive energy than TNT (10,230 vs 7600 ft/s). Note from the figure that high fragment velocity V_f requires that $M_c/M_m > 1$. As an example, for an HMX explosive with $M_c/M_m = 1$, $V_f = 8353$ ft/s.

Penetration of the fragments from a blast fragmentation warhead is shown in Fig. 6.25 as a function of the miss distance and the fragment weight. Again, the value of small miss distance is apparent: fragments have much greater penetration at small miss distance. Warhead fragments are chunky, with high drag, and the fragment velocity decays rapidly with distance. In the example, a fragment that travels 10 ft has about four times the penetration of the target compared to a fragment that travels 100 ft. The data for the figure are based on a fragment initial velocity of 5000 ft/s, sea-level test, average fragment weight of 50 grains (3.2 g), and maximum fragment weight of 150 grains (9.7 g). Note that the average fragment weight for a typical air-to-air blast fragmentation warhead that

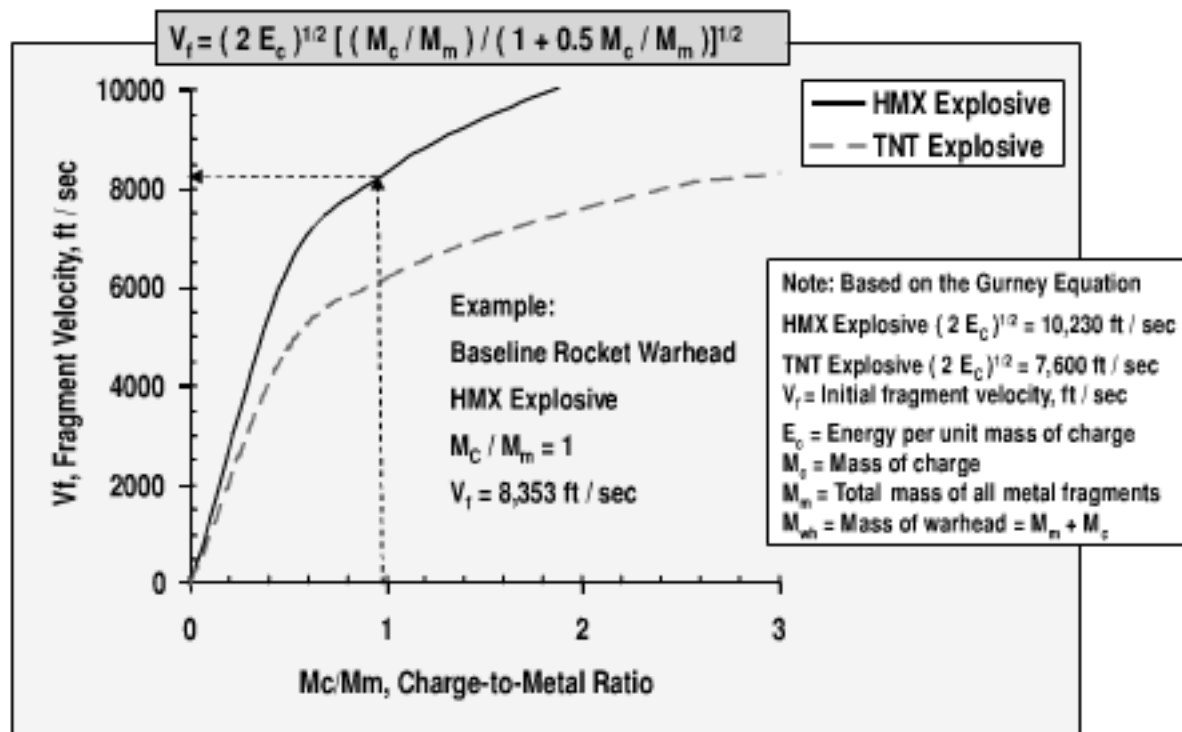
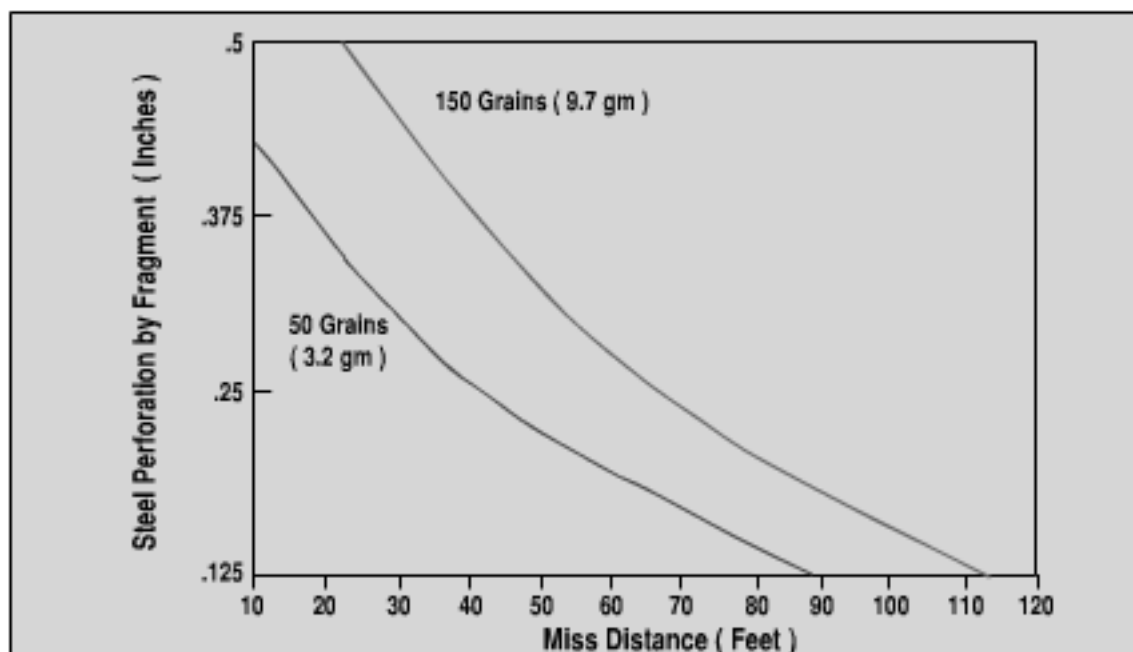


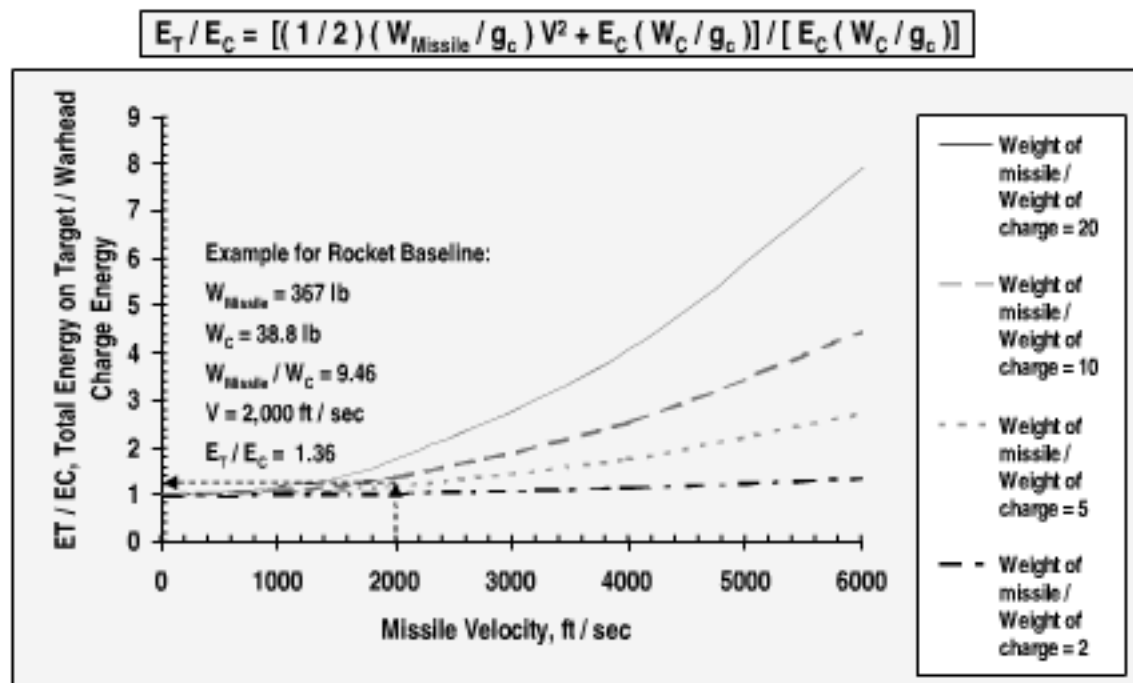
Fig. 6.24 High fragment velocity requires high charge-to-metal ratio.



Note: Typical air-to-air missile warhead

- Fragments initial velocity 5,000 ft/sec
- Sea level
- Average fragment weight 3.2 gm
- Fewer than 0.3% of the fragments weigh more than 9.7 gm

Fig. 6.25 Small miss distance improves the fragment penetration.



Note: Warhead explosive charge energy based on HMX, $(2 E_C)^{1/2} = 10,230 \text{ ft/sec}$

Fig. 6.26 Hypersonic hit-to-kill enhances the energy on target for missiles with small warheads.

uses preformed fragment is about 50 grains. Less than 0.3% of the fragments of a nominal 50-grain air-to-air blast fragmentation warhead weigh more than 150 grains. Preformed and multiprojectile blast fragmentation warheads for air targets have been developed with a broad range of fragment weight, ranging from 4 to 200 grains. The optimum fragment weight is a function of missile accuracy, target size, target hardness, and type of kill requirements.

The total energy on target from a missile impact is shown in Fig. 6.26. The total energy E_T on the target is assumed to be the sum of the warhead charge energy E_C plus the missile kinetic energy $[(1/2)(W_{\text{Missile}}/g_c)V^2]$. The warhead charge energy in the figure is based on an HMX explosive. Note that for a supersonic missile with a missile weight much larger than the warhead charge weight (e.g., $W_{\text{Missile}}/W_c > 20$), more of the total energy is due to the missile kinetic energy than the warhead charge energy. At a hypersonic closing velocity, the missile kinetic energy is sufficiently large so that for missiles that impact the target, a warhead charge may not be required.

As an example, for most direct hit intercepts, the rocket baseline missile often puts more energy on target from the missile kinetic energy than from the warhead charge. The rocket baseline has a burnout weight of 367 lb and a warhead charge weight of 38.8 lb. The missile weight is 9.46 times the warhead charge weight. At a relatively slow closing velocity of 2000 ft/s (e.g., 1200 ft/s missile velocity plus 800 ft/s head-on target velocity), the figure shows that the kinetic energy of the rocket baseline missile adds an additional 36% to the energy of the warhead charge.

Figure 6.27, based on Ref. 16, gives an example of kinetic energy warhead penetration distance through a target. It is based on the equation

$$P/d = [(l/d) - 1](\rho_P/\rho_T)^{\frac{1}{2}} + 3.67(\rho_P/\rho_T)^{\frac{1}{2}} [(\rho_T V^2)/\sigma_T]^{\frac{1}{3}}$$

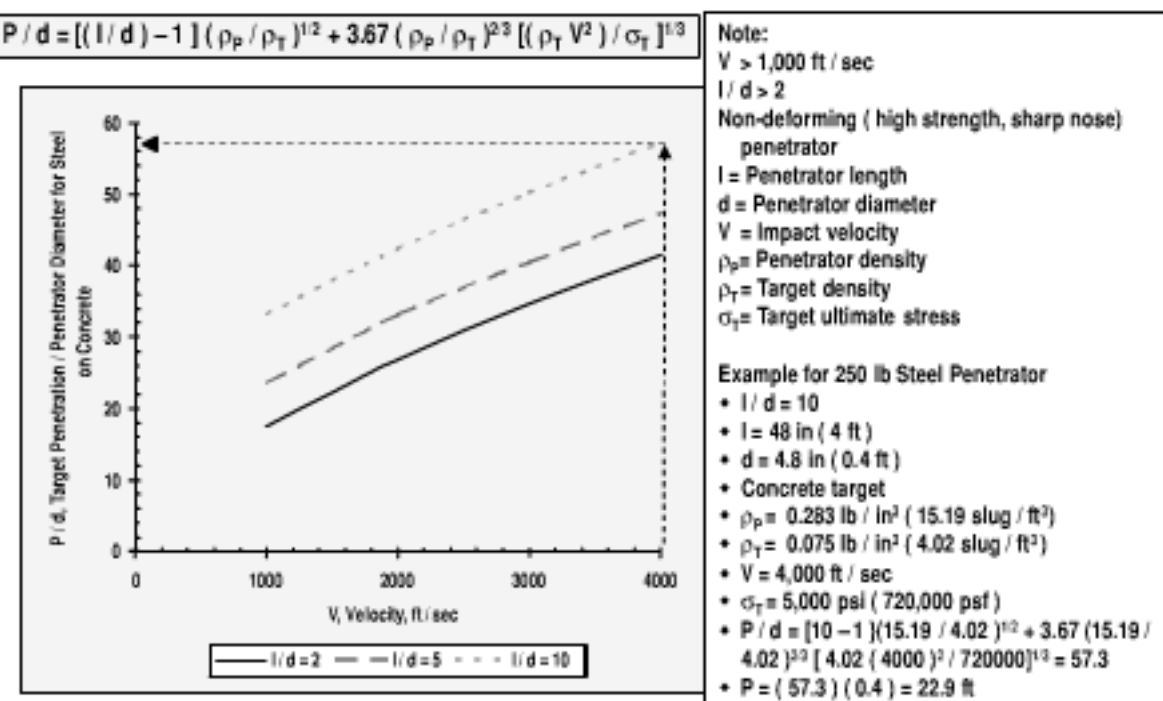


Fig. 6.27 Long-length kinetic energy warheads have enhanced penetration (from Ref. 16).

Assumptions for the equation are impact velocity $V > 1000 \text{ ft/s}$, penetrator length-to-diameter ratio $l/d > 2$, and a nondeforming penetrator. Requirements for a nondeforming penetrator include high hardness, high strength, and a sharp nose. Note that kinetic energy penetration is a function of the penetrator length, diameter, density, and velocity, as well as the target density and ultimate stress. Target penetration increases with penetrator length, diameter, density, and velocity. It also increases with lower target density and lower target ultimate stress.

An example is shown in the figure for a 250-lb steel penetrator that is 48 in. long and 4.8 in. in diameter. For a vertical impact at a velocity of 4000 ft/s, the penetration through a concrete target of 5000 psi strength is $P = 22.9 \text{ ft}$.

A higher density penetrator such as a tungsten carbide ($\rho = 0.540 \text{ lb/in}^3$) rod has advantages of greater penetration and smaller packaging volume. A 250-lb tungsten carbide penetrator with the same fineness ratio ($l/d = 10$) as the previous example has a diameter $d = 3.89 \text{ in.}$ and length $l = 38.9 \text{ in.}$. The penetration through concrete for an impact velocity $V = 4000 \text{ ft/s}$ is 27.7 ft. The tungsten carbide rod has 21% greater penetration than the steel rod (27.7 ft vs 22.9 ft). Another advantage of the tungsten carbide rod is greater hardness, resulting in less surface damage and deformation of the rod during penetration. The tungsten carbide rod also has better packaging, with 19% smaller diameter (3.9 in. vs 4.8 in.) and 24% shorter length (38.9 in. vs 48 in.).

Examples of kinetic kill missiles are shown in Fig. 6.28. These missiles have no warhead charge. The kinetic energy of the hypersonic missile provides the kill mechanism.

In the upper left corner of the figure is a drawing of the U.S. Navy Standard Missile 3 kinetic kill warhead. The SM 3 kinetic kill warhead replaces the current warhead and seeker of the Standard Missile 2. It is part of the Navy Theater Wide (NTW) upper-tier, sea-based capability for missile defense. The SM 3 kinetic kill



Fig. 6.28 Examples of kinetic kill missiles.

warhead includes a third-stage kick motor, strapdown imaging infrared seeker, guidance, autopilot, and reaction jet control.

The upper center photograph is the U.S. Army Patriot Advanced Capability (PAC-3) missile. The PAC-3 is a lower-tier missile defense system. Hit-to-kill accuracy is provided by a high resolution millimeter wave seeker and reaction jet control.

In the upper right section of the figure is a photograph of the U.S. Army Theater High Altitude Area Defense (THAAD) missile. The THAAD is an upper-tier, land-based missile defense system. Hit-to-kill accuracy is provided by a high resolution imaging infrared seeker and reaction jet control.

The bottom left photograph is the U.S. Army hypersonic Line-of-Sight Anti-Tank (LOSAT) missile. The LOSAT provides kinetic energy on target that exceeds that of a tank round, without requiring the heavy weight of a tank gun. It is particularly suitable for rapidly deployed, light forces. The LOSAT can be deployed using a C-130 aircraft, whereas an M-1 tank cannot be carried on a C-130 aircraft. Hit-to-kill accuracy is provided by the launch platform projecting a narrow beam laser spot on the target, laser beam rider guidance, and reaction jet control.

In the bottom right section of the figure is a video of LOSAT. Shown in the video are the lightweight transportation vehicle and firings against tank targets.

The United States is arguably the world leader in kinetic kill missile technology.

6.3 Miss Distance

The third measure of merit to be discussed is miss distance. Missile miss distance is important in missile configuration development because it impacts the required flight performance and the volume/weight required for an appropriately matched warhead.

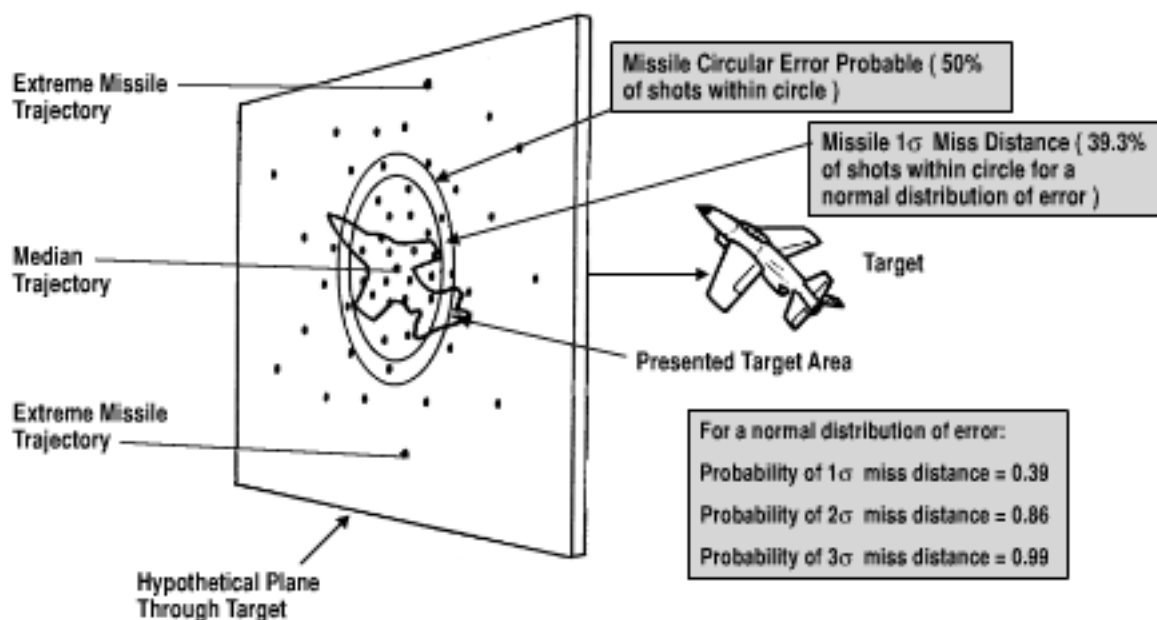
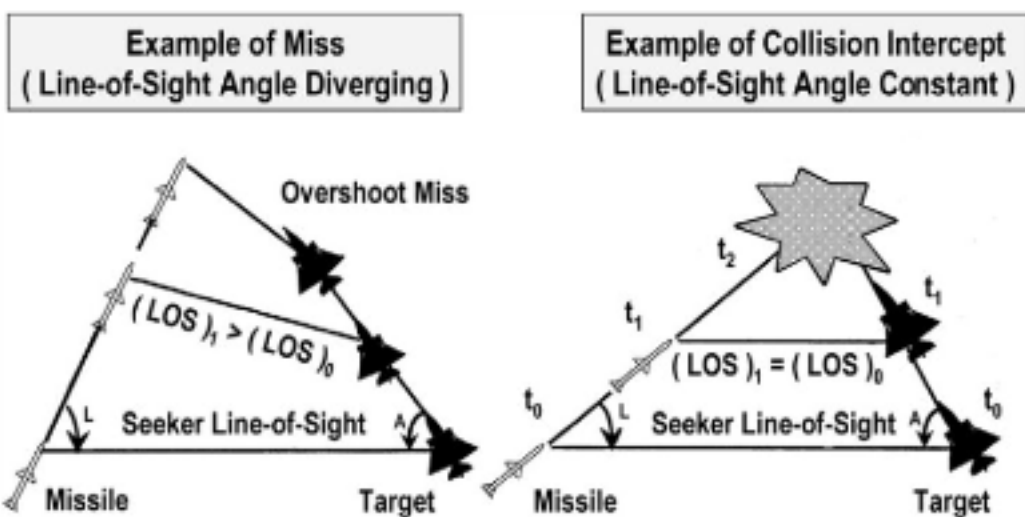


Fig. 6.29 CEP approximately equal to 1σ miss distance (from Ref. 17).

The definition of how miss distance relates to circular error probable (CEP) is shown in Fig. 6.29 from Ref. 17. The CEP is the radius of a circle within which 50% of the flight trajectories with the closest distance of the missile to the target (e.g., miss distance) are expected to occur. If the miss distance is a normal distribution (a common assumption for conceptual design), then the probability that the miss distance is less than the 1σ value of the normal distribution is 39%. A common assumption for conceptual design, consistent with design accuracy, is to use the terminology of CEP and 1σ miss distance interchangeably. The probabilities that the miss distance is less than 2 and 3σ are 86 and 99%, respectively. A conservative approach to blast fragmentation warhead design is to set the warhead lethal radius equal to the guidance estimate of the 3σ miss distance to provide a design margin for miss distance uncertainty.

Figure 6.30 compares an overshooting miss trajectory with a collision intercept trajectory. An efficient flight trajectory can be followed in terminal guidance by directing the missile with sufficient lead to a predicted intercept. A constant line-of-sight trajectory, or constant-looking course, is known as proportional guidance. In the left section of the figure, the line of sight between the missile and the target is increasing, resulting in an overshoot miss. In the right section of the figure, the line of sight between the missile and the target is constant, resulting in a collision intercept. Proportional guidance terminal homing is based on adjusting the rate of change in the missile heading proportional to the rate of change in the seeker line of sight to the target. The missile turning rate correction is usually designed to be three to five times the line-of-sight rotation rate.

The equations for the miss due to a maneuvering target and the miss due to an initial heading error are shown in Fig. 6.31 from Ref. 11. Note that the equation of motion of the missile flight trajectory against the maneuvering target and the equation of motion for an initial heading error have a discontinuity of the term $(t_0 - t)$ in their denominators. For a flight trajectory attempting to follow proportional guidance, as the time t approaches the total time of flight t_0 , the missile deviates from proportional guidance, resulting in a miss distance.

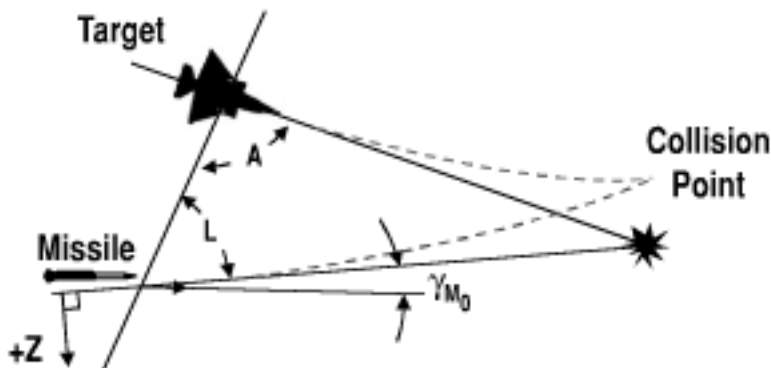


Note: L = Missile Lead
A = Target Aspect

Fig. 6.30 A collision intercept has constant bearing.

Note that the effective navigation ratio N' is a function of navigation ratio N , missile velocity V_M , target velocity V_T , and target aspect A . The navigation ratio N relates the change of flight path angle ($d\gamma/dt$) to the line-of-sight rate (dL/dt). The equation for the navigation ratio is $N = (d\gamma/dt)/(dL/dt)$, and the equation for the effective navigation ratio is $N' = N[V_M/(V_M - V_T \cos A)]$.

For conceptual design, the miss distance is usually evaluated for the cases of a constant maneuvering target and for an initial heading error at seeker lock-on.



$$\text{Maneuvering Target : } \tau \frac{d^2Z}{dt^2} + \frac{dZ}{dt} + N' \frac{Z}{t_0 - t} = \frac{-N'}{t_0 - t} \frac{\cos A}{\cos L} \frac{1}{2} a_T t^2$$

$$\text{Heading Error : } \tau \frac{d^2Z}{dt^2} + \frac{dZ}{dt} + N' \frac{Z}{t_0 - t} = -V_M \gamma_{M0}$$

Note: $t_0 - t = 0$ at intercept, causing discontinuity in above equations.
 $N' = \text{Effective navigation ratio} = N [V_M / (V_M - V_T \cos A)]$
 $N = \text{Navigation ratio} = (d\gamma/dt) / (dL/dt)$
 $\tau = \text{Missile time constant}$, $V_M = \text{Velocity of missile}$, $\gamma_{M0} = \text{Initial flight path angle error of missile}$, $t_0 = \text{Total time of flight}$, $a_T = \text{Acceleration of target}$, $V_T = \text{Velocity of target}$

Fig. 6.31 A maneuvering target and heading error cause missile miss for proportional guidance (from Ref. 11).

- ◆ Measure of missile ability to respond to target condition changes
- ◆ Equals elapsed time from input of target return until missile has completed 63% or $(1 - e^{-1})$ of corrective maneuver ($t = \tau$)
- ◆ Also called "rise time"
- ◆ Contributions to total guidance and control time constant
 - Control effectiveness
 - Control rate (actuator) dynamics
 - Dome error slope
 - Guidance and control filters (τ_{Filter})
 - Other dynamics (gyro dynamics, accelerometer, processor latency, etc.)
- ◆ Approach to estimate τ
 - $\tau = \tau_\delta + \tau_{\delta'} + \tau_{\text{Dome}}$

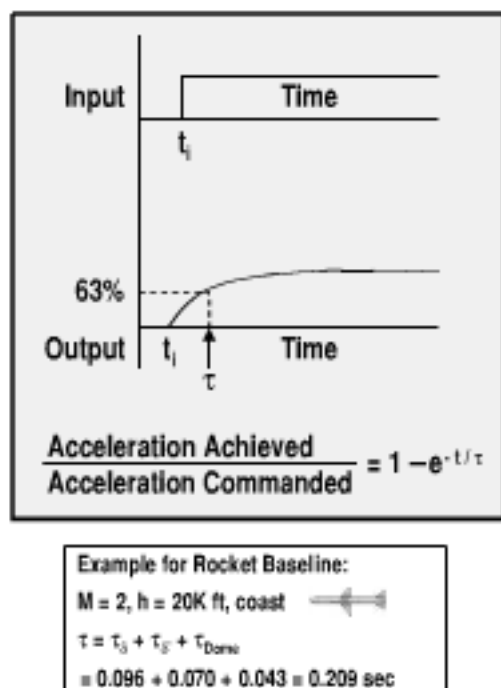


Fig. 6.32 Missile time constant causes miss distance.

Note that the miss distance due to smart target dynamic maneuvers such as sinusoidal maneuvers and corkscrew maneuvers is often larger. Also, for conceptual design, it is usually acceptable to evaluate the miss distance using proportional guidance. Note that augmented proportional guidance and modern guidance laws often provide smaller miss, particularly if the missile has an active, low-noise seeker that provides additional target information such as range, range rate, and target maneuvers acceleration.

Figure 6.32 shows the definition of time constant (τ_{Total}) that is used in this text. The contributors to the total time constant are assumed to be limited control effectiveness (τ_δ), control rate (actuator) dynamics ($\tau_{\delta'}$), and the dome error slope (τ_{Dome}). The time constant due to guidance and control filters (τ_{Filter}) and other contributors (gyro dynamics, accelerometer dynamics, digital processor latency, etc.) are not addressed because they usually have a lower impact on missile configuration design.

Missile time constant is an aggregate measure of the ability of the missile to respond to target condition changes. It is equal to the time elapsed from receiving an input for a required target correction until the missile has completed 63% or $(1 - e^{-1})$ of the required corrective maneuver. Missile time constant is also called "rise time." For this text it is assumed that the missile total time constant is the sum of the contributors:

$$\tau_{\text{Total}} = \tau_\delta + \tau_{\delta'} + \tau_{\text{Dome}}$$

As an example for the rocket baseline missile coasting at Mach 2 and 20,000-ft altitude, the missile time constant is

$$\tau = \tau_\delta + \tau_{\delta'} + \tau_{\text{Dome}} = 0.096 + 0.070 + 0.043 = 0.209 \text{ s}$$

For a 10-g command, the missile requires a time $t = \tau = 0.209 \text{ s}$ to achieve 63%

◆ Assume

- Control surface deflection limited
- Near neutral stability

◆ Equation of motion is

$$\alpha'' = [\rho V^2 S d C_{m_\delta} / (2 I_y)] \delta_{\text{Max}}$$

◆ Integrate to solve for α_{Max}

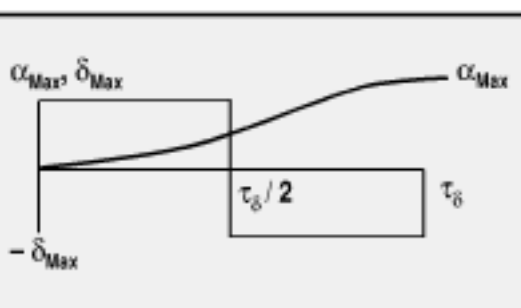
$$\alpha_{\text{Max}} = [\rho V^2 S d C_{m_\delta} / (8 I_y)] \delta_{\text{Max}} \tau_\delta^2$$

◆ τ_δ is given by

$$\tau_\delta = [8 I_y (\alpha_{\text{Max}} / \delta_{\text{Max}}) / (\rho V^2 S_{\text{Ref}} d C_{m_\delta})]^{1/2}$$

◆ Contributors to small τ_δ

- Low fineness (small $I_y / (S_{\text{Ref}} d)$)
- High dynamic pressure (low altitude / high speed)
- Large C_{m_δ}



Example for Rocket Baseline:
 $W = 367 \text{ lb}$, $d = 0.667 \text{ ft}$, $S_{\text{Ref}} = 0.349 \text{ ft}^2$, $I_y = 94.0 \text{ slugs ft}^2$,
 $V = 2,000 \text{ ft/sec}$, $h = 20 \text{ kft}$ ($\rho = 0.001267 \text{ slugs}/\text{ft}^3$),
 $\alpha_{\text{Max}} = 9.4 \text{ deg}$, $\delta_{\text{Max}} = 12.6 \text{ deg}$, $C_{m_\delta} = 51.6 \text{ per radian}$,
 $\tau_\delta = 0.096 \text{ sec}$

Fig. 6.33 Time constant τ_δ from limited pitching moment control effectiveness.

(or 6.3 g) of the command $[10(1 - e^{-1}) = 6.3]$. At a later time $t = 4\tau = 0.836 \text{ s}$, the missile achieves 98% (or 9.8 g) of the command $[10(1 - e^{-4}) = 9.8]$.

The time constant due to limited pitching moment control effectiveness is illustrated in Fig. 6.33. Assume that the flight control surface is deflection limited, operating in a race-break deflection profile (see figure). The assumption is valid if the flight control actuator is very fast ($\delta^* = \infty$) and the missile has near-neutral stability. The equation of motion for one degree of freedom is

$$\alpha'' = [\rho V^2 S d C_{m_\delta} / (2 I_y)] \delta_{\text{Max}}$$

Integrating the above equation to solve for α_{Max} gives

$$\alpha_{\text{Max}} = [\rho V^2 S d C_{m_\delta} / (8 I_y)] \delta_{\text{Max}} \tau_\delta^2$$

τ_δ is given by

$$\tau_\delta = [8 I_y (\alpha_{\text{Max}} / \delta_{\text{Max}}) / (\rho V^2 S_{\text{Ref}} d C_{m_\delta})]^{1/2}$$

The contributors to a small value of τ_δ are 1) low fineness [small $I_y / (S_{\text{Ref}} d)$]; 2) high dynamic pressure (low altitude/high speed); and 3) large pitching moment control effectiveness C_{m_δ} .

As an example of the time constant due to limited pitching moment control effectiveness, the rocket baseline missile has a burnout weight $W = 367 \text{ lb}$, diameter $d = 8 \text{ in.}$ (0.667 ft), reference area $S_{\text{Ref}} = 0.349 \text{ ft}^2$, and burnout pitch moment of inertia $I_y = 94.0 \text{ slugs-ft}^2$. At an intercept velocity and altitude of $V = 2000 \text{ ft/s}$ and $h = 20,000 \text{ ft}$, respectively, the maximum allowable angle of attack $\alpha_{\text{Max}} = 9.4 \text{ deg}$, the maximum control deflection $\delta_{\text{Max}} = 12.4 \text{ deg}$, and the pitching moment control effectiveness derivative $C_{m_\delta} = 51.6 \text{ per rad}$. The time constant due to limited pitching moment control effectiveness is computed to be

$$\tau_\delta = 0.096 \text{ s}$$

- ◆ Assume
 - Control surface rate limited ($\dot{\delta} = \dot{\delta}_{\text{Max}}$)
 - Near neutral stability
- ◆ Equation of motion for $\dot{\delta} = +/- \dot{\delta}_{\text{Max}}$
 $\ddot{\alpha} = [\rho V^2 S d C_{m\delta} / (2 I_y)] \dot{\delta}_{\text{Max}}$
- ◆ Equation of motion for “perfect” response $\dot{\delta} = \infty, \delta = \delta_{\text{Max}}$
 $\ddot{\alpha} = [\rho V^2 S d C_{m\delta} / (2 I_y)] \delta_{\text{Max}}$
- ◆ τ_{δ} is difference between actual response to α_{Max} and “perfect” (τ_{δ}) response
- ◆ Then

$$\tau_{\delta} = 2 \delta_{\text{Max}} / \dot{\delta}_{\text{Max}}$$

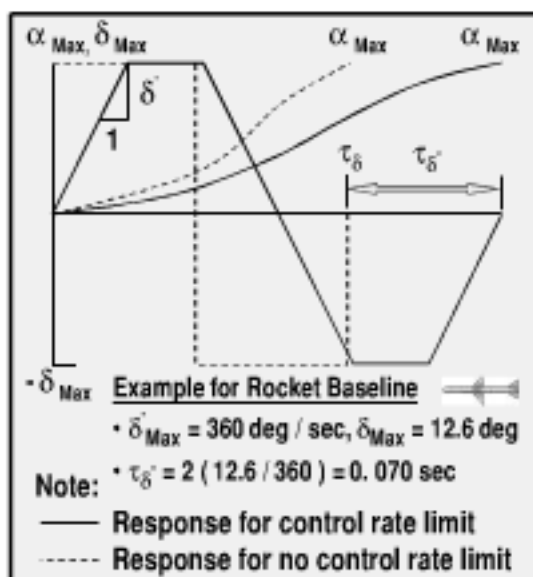


Fig. 6.34 Time constant τ_{δ} from the deflection rate limit of the flight control system.

The time constant due to flight control rate dynamics (e.g., actuator rate limit) is illustrated in Fig. 6.34. Assume that the flight control surface is rate limited ($\dot{\delta}^* = \dot{\delta}^*_{\text{Max}}$) and the missile has near-neutral stability. The one-degree-of-freedom equation of motion for $\dot{\delta}^* = \dot{\delta}^*_{\text{Max}}$ is

$$\ddot{\alpha}^* = [\rho V^2 S d C_{m\delta} / (2 I_y)] \dot{\delta}^*_{\text{Max}}$$

As a comparison, the equation of motion for a “perfect” response of $\dot{\delta}^* = \infty, \delta = \delta_{\text{Max}}$ is

$$\ddot{\alpha}^* = [\rho V^2 S d C_{m\delta} / (2 I_y)] \delta_{\text{Max}}$$

τ_{δ^*} is the difference between the actual response to α_{Max} and the “perfect” (τ_{δ}) response to α_{Max} . Then

$$\tau_{\delta^*} = 2 \delta_{\text{Max}} / \dot{\delta}^*_{\text{Max}}$$

As an example for the rocket baseline missile, the maximum wing control surface deflection rate $\dot{\delta}^*_{\text{Max}} = 360 \text{ deg/s}$ and the maximum wing control surface deflection $\delta_{\text{Max}} = 12.4 \text{ deg}$. The time constant due to pitching moment control rate dynamics is computed to be

$$\tau_{\delta^*} = 2(12.4 / 360) = 0.070 \text{ s}$$

The time constant due to radome error slope is illustrated in Fig. 6.35. The seeker radome error slope for a typical single high-fineness curved dome (e.g., single tangent ogive dome) is

$$|R| = 0.05(l_N/d - 0.5)[1 + 15(\Delta f/f)]/(d/\lambda)$$

The radome time constant (τ_{Dome}) is given by

$$\tau_{\text{Dome}} = N'(V_C / V_M)|R|(\alpha/\dot{\gamma})$$

- ◆ $|R| = 0.05 (l_N/d - 0.5) [1 + 15 (\Delta f/f)] / (d/\lambda)$
- ◆ $\tau_{\text{Dome}} = N' (V_C/V_M) |R| (\alpha/\gamma)$
- ◆ $\alpha/\gamma = \alpha (W/g_c) V_M / \{q S_{\text{Ref}} [C_{N_a} + C_{N_b} / (\alpha/\delta)]\}$
- ◆ Substituting gives $\tau_{\text{Dome}} = N' W V_C |R| / \{g_c q S_{\text{Ref}} [C_{N_a} + C_{N_b} / (\alpha/\delta)]\}$
- ◆ Contributors to small τ_{Dome}
 - Low body fineness (small W/S_{Ref})
 - Low dome error slope ($|R|$)
 - Low nose fineness (l_N/d)
 - Low angle of attack for control deflection (α/δ)
 - Low effective navigation ratio (N')
 - Low closing velocity (V_C)
 - Low bandwidth for frequency (Δf)
 - High seeker transmitter frequency (small λ)
 - High normal force due to angle of attack (C_{N_a})
 - High normal force due to control deflection (C_{N_b})
 - High dynamic pressure (q)

Example for Rocket Baseline at $V_M = 2000$ fps, $h = 20$ Kft, $q = 2745$ psf



Assume $V_T = 1,000$ fps, giving $V_C = 3,000$ fps

Assume $N' = 4$, $f = 10$ GHz, $\Delta f/f = 0.02$

Configuration data are $l_N/d = 2.4$, $d = 8$ in, $S_{\text{Ref}} = 0.349 \text{ ft}^2$, $W = 367$ lb, $C_{N_a} = 40$ per rad, $C_{N_b} = 15.5$ per rad, $\alpha/\delta = 0.75$

Compute $|R| = 0.0182 \text{ deg/deg}$, $\tau_{\text{Dome}} = 0.043 \text{ sec}$

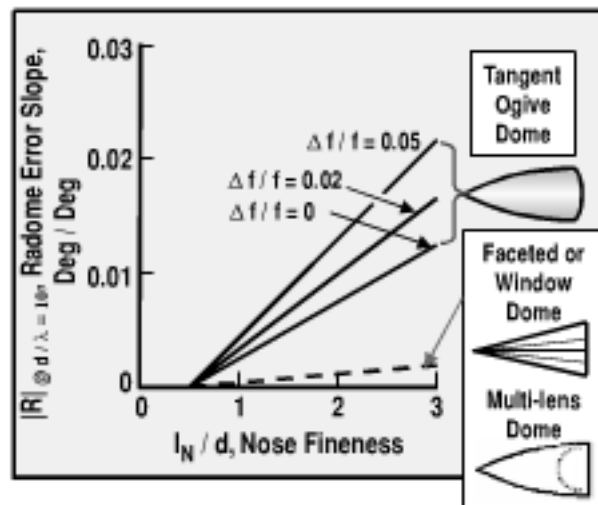


Fig. 6.35 Time constant τ_{Dome} from seeker radome error slope.

The angle of attack sensitivity to turn rate is given by

$$\alpha/\dot{\gamma} = \alpha/(W/g_c) V_M / \{q S_{\text{Ref}} [C_{N_a} + C_{N_b}/(\alpha/\delta)]\}$$

Substituting for $\alpha/\dot{\gamma}$ gives

$$\tau_{\text{Dome}} = N' W V_C |R| / \{g_c q S_{\text{Ref}} [C_{N_a} + C_{N_b}/(\alpha/\delta)]\}$$

The contributors to a small value of τ_{Dome} are 1) low weight per cross sectional area W/S_{Ref} , which implies a low value of body fineness ratio l/d ; 2) low dome error slope, $|R|$; hemispherical, faceted, window, or multilens domes have very small dome error slope; 3) low nose fineness l_N/d ; 4) low change in angle of attack with control deflection α/δ , such as a statically stable missile using wing control; 5) low effective navigation ratio N' ; 6) low closing velocity V_C , such as a tail chase intercept; 7) low bandwidth Δf for the seeker transmitter frequency; 8) high seeker transmitter frequency f , such as a millimeter wave radar; 9) high normal force derivative due to angle of attack C_{N_a} , such as a missile with a high aspect ratio large wing; 10) high normal force derivative due to control deflection C_{N_b} , such as wing control; and 11) high dynamic pressure, such as low altitude/high speed flight.

As an example for the rocket baseline missile, consider a head-on intercept of a target flying at an altitude of 20,000 ft and a velocity of $V_T = 1000$ ft/s. The assumed missile velocity is $V_M = 2000$ ft/s, providing a dynamic pressure $q = 2725$ psf, and a closing velocity $V_C = 3000$ ft/s. The seeker and guidance parameters are a frequency $f = 10$ GHz, frequency bandwidth $\Delta f = 0.02$, and effective navigation ratio $N' = 4$. Configuration data are a tangent ogive nose fineness ratio $l_N/d = 2.4$, seeker diameter $d = 8$ in., reference area $S_{\text{Ref}} = 0.349 \text{ ft}^2$,

burnout weight $W = 367$ lb, normal force angle of attack derivative $C_{N\alpha} = 40$ per rad, normal force control deflection derivative $C_{N\delta} = 15.5$ per rad, and angle of attack sensitivity $\alpha/\delta = 0.75$.

Computing the dome error slope and the dome time constant

$$|R| = 0.05(2.4 - 0.5)[1 + 15(0.02)]/(8/1.18) = 0.0182 \text{ deg/deg}$$

$$\tau_{\text{Dome}} = 0.043 \text{ s}$$

Note from the figure that hemispherical, faceted, window, and multilens domes have negligible dome error slope. The low error slope enhances the missile seeker tracking accuracy, reduces missile time constant, and reduces miss distance.

The rocket baseline has a proportional guidance effective navigation ratio $N' = 4$, burnout weight $W = 367$ lb, and reference area $S_{\text{Ref}} = 0.349 \text{ ft}^2$. For a Mach 2 head-on intercept against a 1000 ft/s target at an altitude $h = 20,000$ ft, the closing velocity is $V_C = 3000$ ft/s, dynamic pressure $q = 2720$ psf, and normal force derivative $C_{N\alpha} = 38$ per rad. Computing the time constant due to seeker dome error slope

$$\tau_{\text{Dome}} = 0.069 \text{ s}$$

Figure 6.36 shows the missile maneuver acceleration that is required to eliminate an initial heading error. The equation is

$$a_M = (V_M \gamma_{M_0} N' / t_0) (1 - t/t_0)^{N'-2}$$

It is based on proportional homing guidance for a missile with negligibly small time constant ($\tau = 0$). The required maneuverability to correct a heading error is

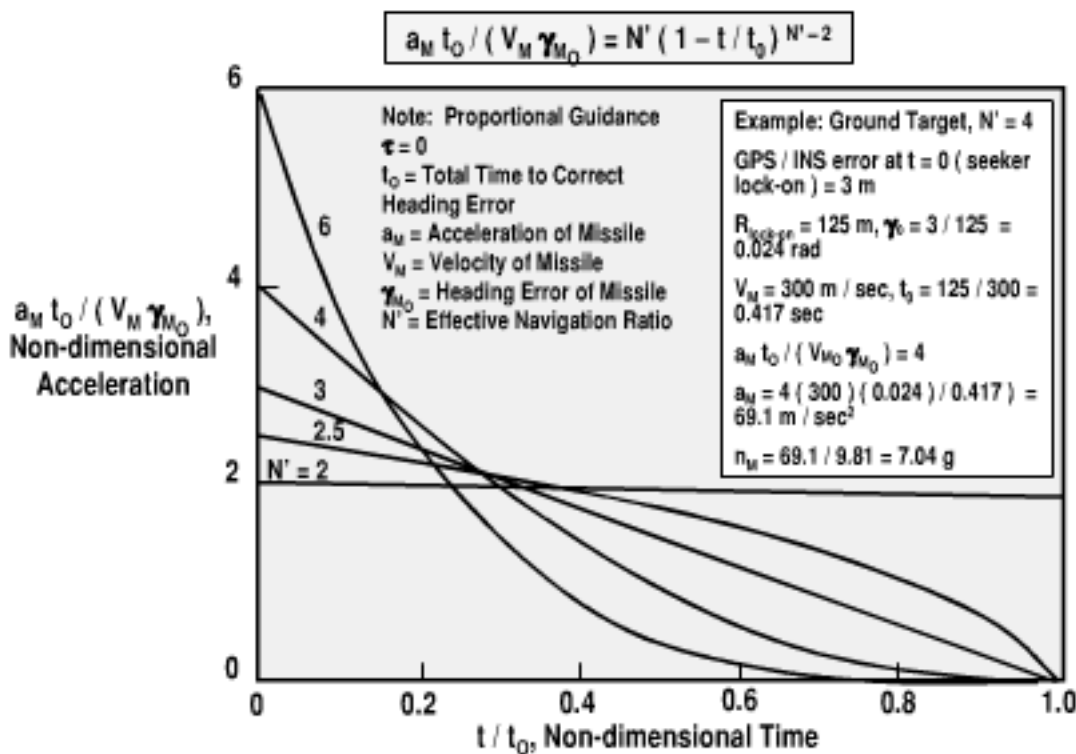


Fig. 6.36 Missile acceleration required for eliminating an initial heading error.

a function of the effective navigation ratio N' , the time elapsed since the initiation of guidance correction (t), the total time available to correct the heading error (t_0), the missile velocity V_M , and the initial heading error γ_{M_0} . Note that the missile maneuver acceleration to eliminate a heading error is largest at the initiation of the correction and decreases with time. Also note that for a large value of the effective navigation ratio N' , the initial missile acceleration is higher and the acceleration decreases more rapidly with time.

As an example of correcting an initial homing error against a ground target, assume that the GPS/INS midcourse guidance has an error of 3 m at $t = 0$ s (seeker lock-on). For a seeker lock-on range $R_{\text{lock-on}} = 125$ m, the initial heading error $\gamma_{M_0} = 0.024$ rad. Assume a missile velocity $V_M = 300$ m/s. Then the total time available to correct the heading error is $t_0 = 0.417$ s. For a missile effective navigation ratio $N' = 4$, the required maneuver acceleration $a_M = 69.1$ m/s², or $n_M = 7.04$ g'.

Miss distance due to heading error is a function of the time available to correct the error (t_0), missile time constant τ , heading error γ_{M_0} , missile velocity V_M , and the effective navigation ratio N' . Note from Fig. 6.37, based on an envelope of the adjoint method of Refs. 18 and 19, that miss distance due to heading error is lower for large values of navigation ratio. The figure also shows that the peak miss distance occurs if the guidance to correct the heading error is initiated at about one time constant before intercept. If guidance is initiated at about four to eight time constants prior to intercept, the miss distance is negligible.

As an example, assume the same conditions as those from the previous figure. These are 1) initial heading error against a ground target; 2) GPS/INS midcourse guidance with an error of 3 m at $t = 0$ s (seeker lock-on); 3) seeker lock-on range $R_{\text{lock-on}} = 125$ m; 4) missile velocity $V_M = 300$ m/s; 5) effective navigation ratio $N' = 4$; and 6) missile time constant $\tau = 0.2$ s. Then the initial heading error is $\gamma_0 = 0.024$ rad and total time available to correct the heading error

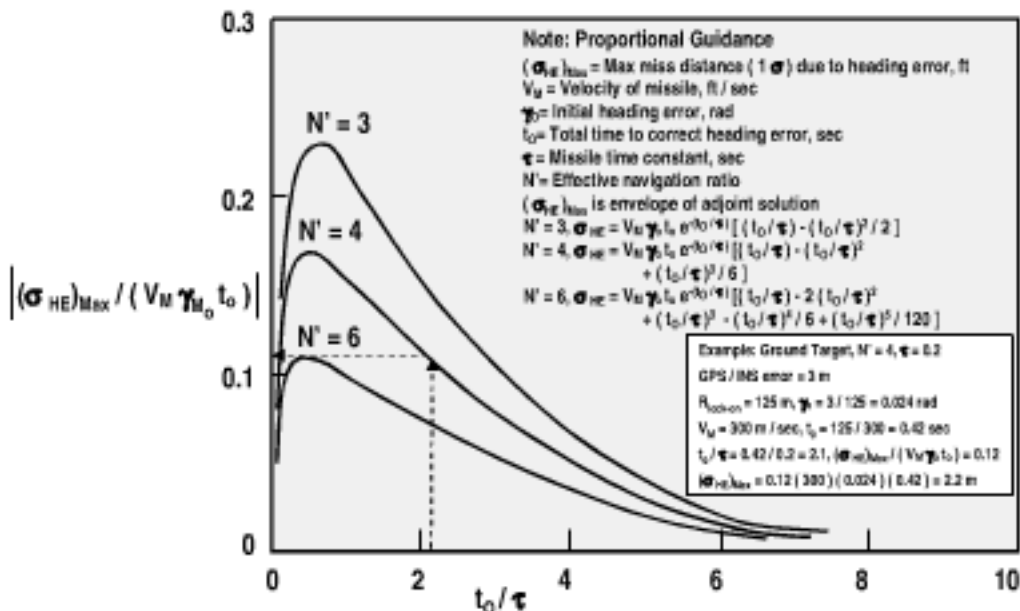


Fig. 6.37 Missle minimum range may be driven by four to eight time constants to correct an initial heading error (from Refs. 18, 19).

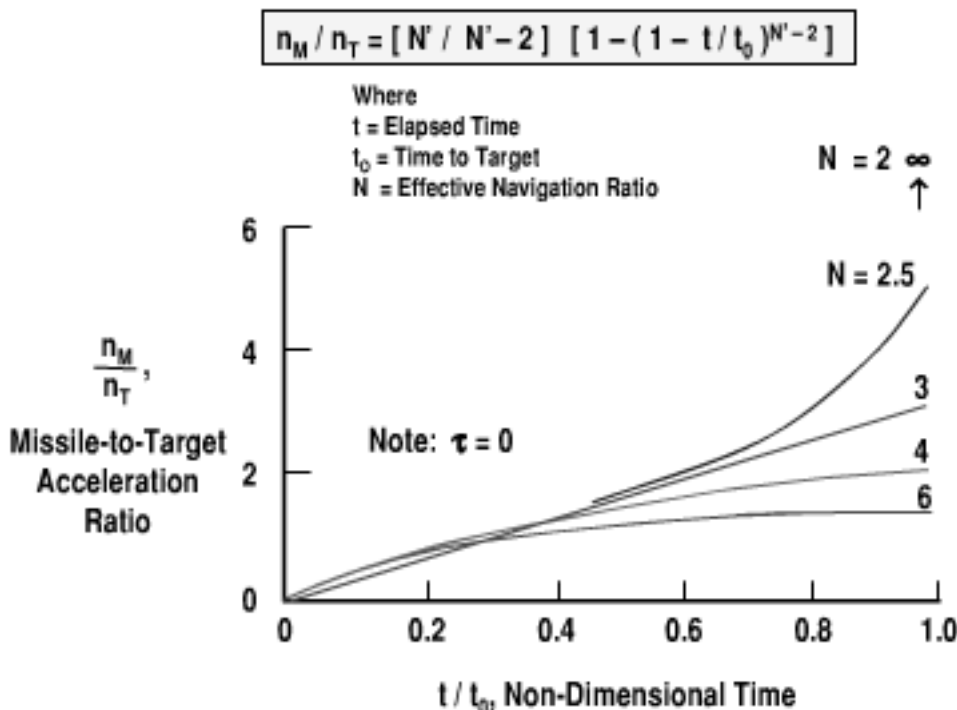


Fig. 6.38 Missile required maneuverability is about three times the target maneuverability.

is $t_0 = 0.417$ s. Compute the number of available time constants to correct the heading error as

$$t_0/\tau = 2.1$$

Finally, compute the envelope (maximum value) of the missile miss distance due to heading error

$$(\sigma_{HE})_{\text{Max}} = 2.2 \text{ m}$$

Figure 6.38 shows the missile maneuver acceleration required against a constant maneuvering target. It is based on proportional homing guidance for a missile with negligibly small time constant ($\tau = 0$). The equation is

$$n_M = n_T [N'/(N'-2)] \left[1 - \left(1 - \frac{t}{t_0}\right)^{N'-2} \right]$$

The required maneuverability against a maneuvering target is a function of the effective navigation ratio N' , time after the target initiates maneuvering t , and the total time to the target intercept t_0 . Note that the missile maneuver acceleration against a maneuvering target increases with time and has the largest value at intercept. A large value of the effective navigation ratio N' results in less required maneuverability at intercept. As a rule of thumb, the missile maneuverability must be about three times the maneuverability of the target.

Miss distance against a maneuvering target is a function of the time to go, missile time constant, target maneuverability, and the effective navigation ratio. Figure 6.39, based on the miss distance envelope of the adjoint method of Refs. 18

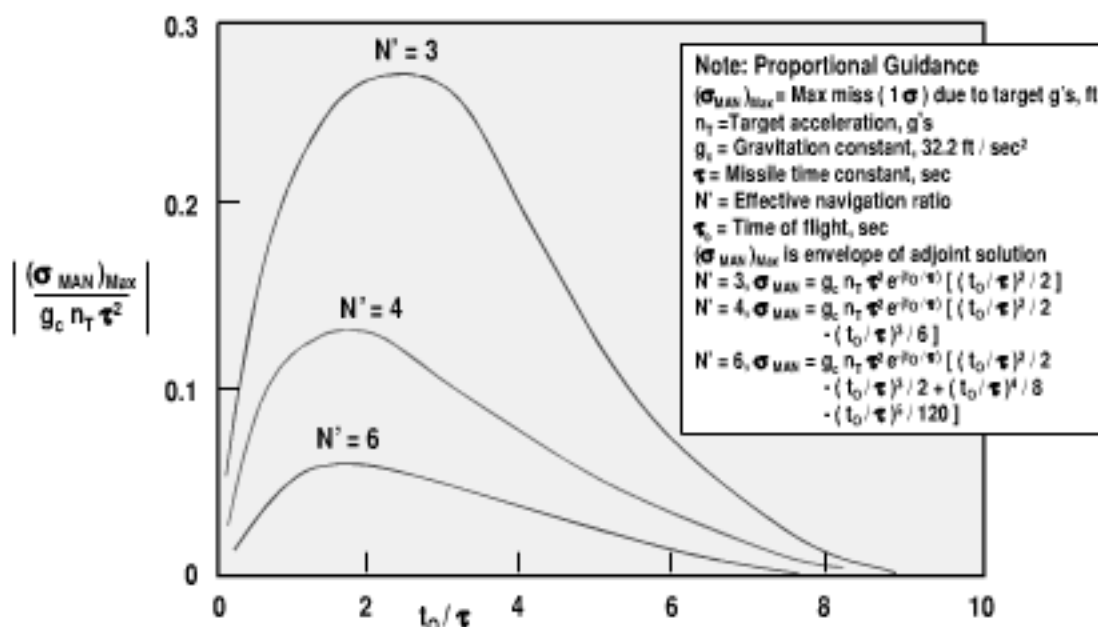


Fig. 6.39 Target maneuvers require about 6 to 10 time constants to settle out the miss distance (from Refs. 18, 19).

and 19, shows that peak miss distance occurs if the target initiates a constant acceleration maneuver at about two time constants prior to intercept. Note that a high value of navigation ratio gives smaller miss distance. The missile has negligible miss distance if the target initiates a maneuver at 6 to 10 time constants prior to intercept.

The adjoint results for both the initial heading error target and the maneuvering target showed that a high value of effective navigation ratio gives the smallest miss distance. However, a high value of effective navigation ratio increases the time constant due to dome error slope, contributing to miss distance. Also, a high value of effective navigation ratio makes the missile more sensitive to seeker noise, which has been neglected in this assessment. A missile that has a seeker with very low noise and high resolution, such as a LADAR or an imaging IR seeker, may be able to operate effectively at a high value of effective navigation ratio (e.g., $N' = 6$). However, most current tactical missile seekers have relatively high noise and relatively low resolution. Most of the current tactical missiles, especially radar missiles, operate most effectively at $3 < N' < 5$.

Figure 6.40 shows that the miss distance against a constant maneuvering target increases with increased missile time constant and target maneuverability. The figure is based on the adjoint envelope of proportional guidance with an effective navigation ratio $N' = 4$. Note that the miss distance is highly sensitive to time constant.

As an example, consider the rocket baseline missile coasting at Mach 2 and 20,000 ft in altitude. The time constant is $\tau = 0.209$ s. For a 5-g maneuvering target, the rocket baseline maximum miss distance is computed to be 0.9 ft. This computed result is probably optimistic because the adjoint method used in this text does not include other effects such as seeker noise that also contribute to miss distance.

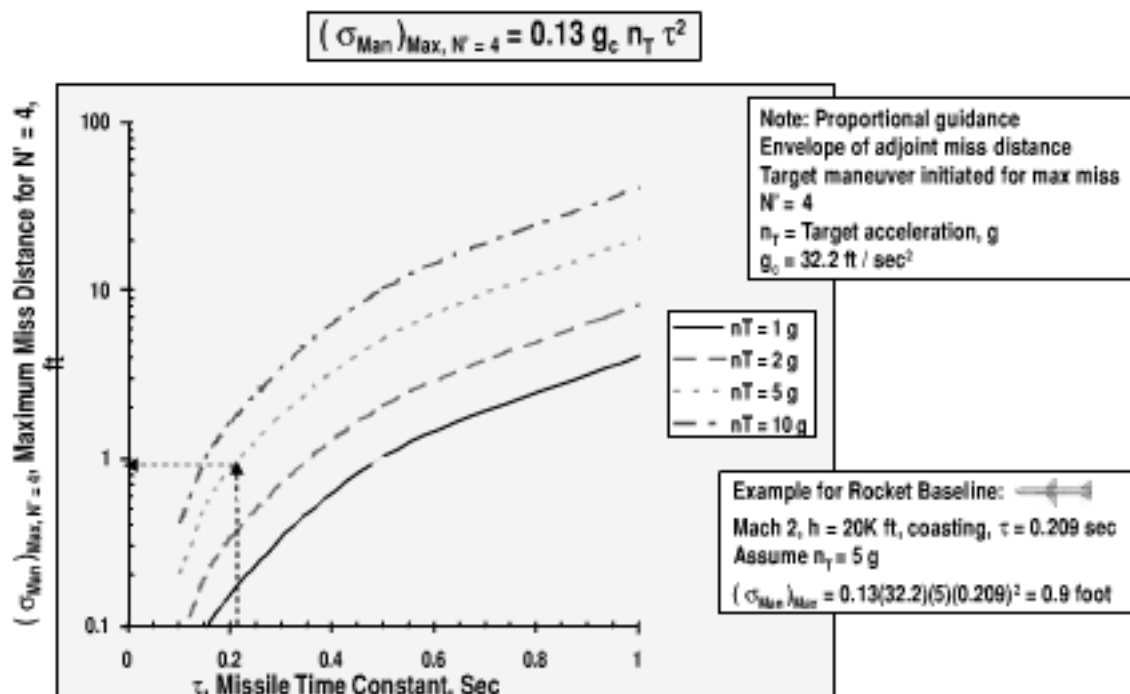


Fig. 6.40 Small time constant is required for a small miss against a maneuvering target.

6.4 Carriage and Launch Observables

The fourth measure of merit to be discussed is carriage and launch observables. Missile carriage and launch observables impact the survivability of the launch platform. Two areas of concern are the radar cross section for carriage on the launch platform and the missile plume visual signature. Missile carriage alternatives based on the consideration of observables are 1) internal carriage, which has the lowest radar cross section (RCS) in carriage; 2) conformal carriage, which provides reduced RCS in carriage; and 3) conventional external pylon or rail carriage, which has high RCS in carriage. The missile plume alternatives based on the consideration of visual observables are 1) minimum smoke motor, which has the lowest visual observables during launch (H_2O contrail); 2) reduced smoke motor, which has reduced observables during launch (HCl contrail); and 3) high smoke motor, which has high observables during launch (e.g., Al_2O_3 smoke).

As stated, the alternative approaches for missile carriage on aircraft include conventional external carriage, conformal carriage, and internal carriage. Conventional external carriage has the disadvantages of high RCS, high carriage drag, and potentially adverse aeroelastic stability, and control interactions with the aircraft platform. An advantage of external carriage is high firepower load-out, because of the large number of store attachment locations on the aircraft body and wings. Conformal carriage has an advantage of reduced RCS and lower drag compared to conventional carriage. A disadvantage is a need for specialized store and aircraft attachments for each type of aircraft. Internal carriage has the lowest carriage RCS and the lowest drag. A disadvantage of internal carriage is a reduction in firepower, by factors of up to two or four.

Figure 6.41 shows examples of internal carriage and load-outs for low observable fighters, bombers, and helicopters. In the upper left is shown the F-22

Center Weapon Bay Best for Ejection Launchers

F-22 Bay Loadout: 2 AIM-120C, 1 GBU-32



F-117 Bay Loadout: 1 GBU-27, 1 GBU-10



B-1 Bay Loadout: 8 AGM-69

VideoSide Weapon Bay Best for Rail Launchers

AMRAAM Loading in F-22 Bay



F-22 Side Bay Loadout: 1 AIM-9



RAH-66 Side Bay Loadout: 1 AGM-114, 2 FIM-92, 4 Hydra 70

Fig. 6.41 Weapon bay internal carriage and load-out examples.

internal center bay. The F-22 center bay typically has an outboard partition for air-to-air weapons (e.g., AMRAAMs) and an inboard partition for air-to-surface weapons (e.g., JDAM). LAU-142/A pneudraulic (pneumatic plus hydraulic) ejection launchers are provided for the AMRAAMs. The LAU-142 has a 9-in. stroke that ejects an AMRAAM from the bay at a velocity of 25 ft/s. The peak ejection acceleration is 40 g. Advantages of pneudraulic ejection compared to conventional pyrotechnic cartridge ejection include less logistics, faster turnaround for weapon loading, and a more nearly constant ejection force that allows a shorter ejection stroke. A conventional BRU-46/A bomb rack is provided for the GBU-32 JDAM (1000-lb class weapon). Examples of typical mixed weapon load-outs in the F-22 center bay are 1) two AMRAAMs (without compressed carriage) plus one 1000-lb JDAM, or 2) three compressed carriage AMRAAMs plus one 1000-lb JDAM. The F-22 center bay can also be set up for air-to-air weapons only, such as four conventional AMRAAMs (without compressed carriage) or six compressed carriage AMRAAMs. The F-117 internal weapons bay is shown in the top center of the figure. The F-117 weapons bay is similar to that of the F-22, except that it has about twice the payload weight capability. A typical load-out for the F-117 is two Paveway guided bombs (2000-lb class). Shown in the figure foreground is the GBU-27 laser guided bomb. Its warhead is based on the BLU-109 hardened structures penetrator bomb. In the background is the GBU-10 laser guided bomb. Its warhead is either the general-purpose Mk-84 bomb or the BLU-109 penetrator bomb. The B-1 bomber weapons bay is shown in the upper right of the figure. The B-1 has three bays. Each bay has a rotary launcher for ejection of missiles and bombs. An ejector rack assembly is provided for each weapon that is attached to the rotary launcher. The ejector rack assembly has a 30-in. spacing of the ejectors. Shown in the figure is a standard load-out of eight AGM-69 s per bay. The lower left section is a video of loading an AMRAAM missile into the center bay of the F-22 aircraft. In the

lower center of the figure is a photograph of an F-22 side bay. The F-22 has two side carriage bays. Each bay is capable of carrying a single Sidewinder missile on a LAU-141/A trapeze rail launcher. A trapeze launcher is required for lock-on before launch missiles. During the launch sequence the trapeze launcher extends the missile away from the aircraft, the missile seeker acquires the target, and the missile is launched. Following missile launch, the trapeze launcher retracts into the weapon bay and the bay doors are closed. It is noted that the LAU-141/A launcher has a deflector surface to keep the motor plume from entering the weapon bay. Finally, the lower right section of the figure is a photograph of the RAH-66 Comanche helicopter. The Comanche has two side bays with rail launchers. Each bay has a typical mixed mission (combined air-to-surface/air-to-air) load-out of one Hellfire missile plus two Stinger missiles plus four Hydra 70 rockets. For an air-to-surface-only mission, each bay can carry three Hellfire missiles, giving the Comanche a total load-out of six Hellfire missiles. As shown in the figure, the Comanche can also carry eight Hellfire missiles externally, at the expense of increased RCS.

Illustrated in Fig. 6.42 are the plume observables of high-smoke, reduced-smoke, and minimum-smoke propellants. The relatively old Sparrow missile rocket motor is a representative high-smoke motor. The high-smoke plume is shown in the upper left corner of the figure. The Sparrow has high-smoke Al_2O_3 particles from aluminum fuel. Shown in the upper center of the figure is an example of a reduced-smoke rocket motor. The AMRAAM is a more recent missile with a reduced-smoke motor. It still has a contrail of HCl from the ammonium perchlorate oxidizer. The HCl contrail occurs if the atmospheric temperature is less than -10°F , corresponding to altitudes greater than about 20,000 ft. Finally, the far upper right photograph is an example of a minimum-smoke rocket motor. The Javelin is a recent missile with a minimum-smoke motor. It has almost no smoke



High Smoke Example: AIM-7

Particles (e.g., metal fuel) at all atmospheric temperature.



Reduced Smoke Example: AIM-120

Contrail (HCl from AP oxidizer) at $< -10^{\circ}\text{F}$ Fahrenheit atmospheric temperature.



Minimum Smoke Example: Javelin

Contrail (H_2O) at $< -35^{\circ}\text{F}$ Fahrenheit atmospheric temperature.

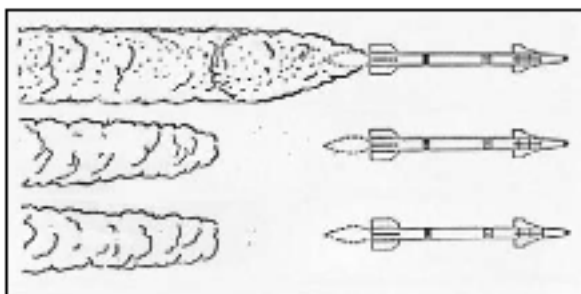


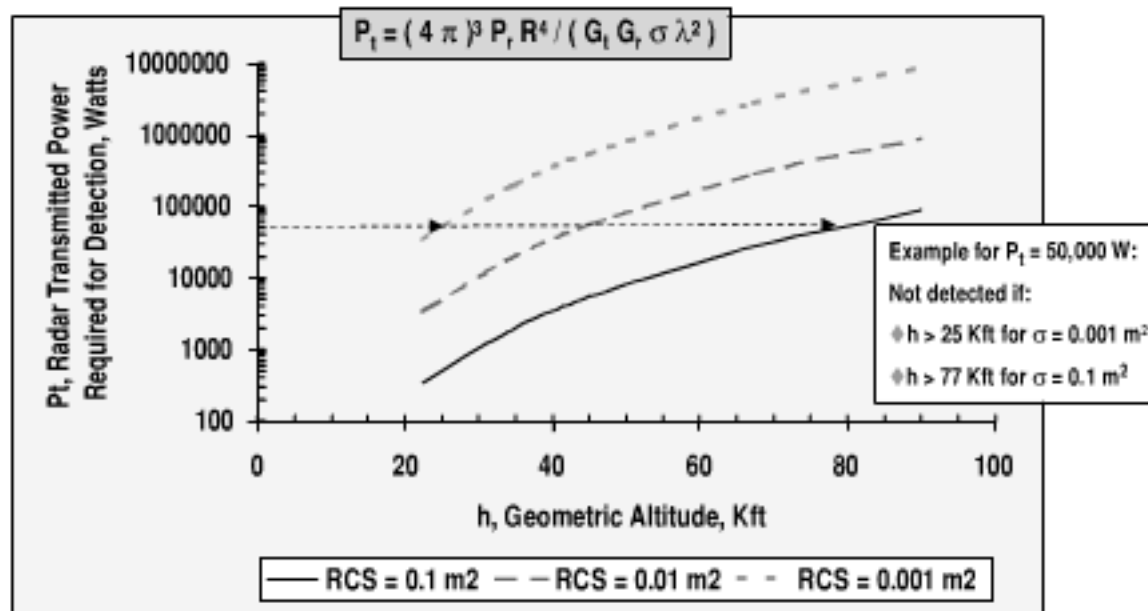
Fig. 6.42 Minimum-smoke propellant has low observables.

from either the launch motor or the flight motor, enhancing the survivability of the gunner. Minimum-smoke propellants can have an H₂O (ice) contrail if the atmospheric temperature is less than -35°F, corresponding to altitudes greater than about 27,000 ft.

The bottom left section of the figure shows typical contrails for high-smoke, reduced-smoke, and minimum-smoke motors. The bottom right section of the figure contains a video of missile systems with high-smoke (Sparrow), reduced-smoke (AMRAAM, Hellfire I), and minimum-smoke (Javelin, Hellfire II) propellants.

6.5 Other Survivability Considerations

The fifth measure of merit to be discussed is other survivability considerations. Missile RCS and the standoff distance from threat defenses are design considerations in the survivability of the missile. Shown in Fig. 6.43 is an example of a ground radar detection range against a missile with three assumed values of RCS and flying at altitudes from 22,000 ft to 90,000 ft. Results are based on the radar range equation discussed previously. The equation is $P_t = (4\pi)^3 P_r R^4 / (G_t G_r \sigma \lambda^2)$. The assumed values of the ground radar parameters for transmitted power P_t , received power P_r , transmitter gain G_t , receiver gain G_r , and wavelength λ are given in the figure. Note the dramatic increase in the required power of the ground radar to detect the missile if the missile flies at high altitude, which results in a large value of slant range R . Reducing the RCS also results in a large increase in the power required for the ground radar. An interesting tradeoff is the missile-required flight altitude vs RCS to avoid detection. As an example, assume that a typical threat



Note:
 ♦ Range Slant Angle = 20°, G_t = Transmitter Gain = 40 dB, G_r = Receiver Gain = 40 dB, λ = Wavelength = 0.03 m,
 P_r = Receiver Sensitivity = 10^{-14} Watts, σ = radar cross section (RCS)
 ♦ Based on Radar Range Equation

Fig. 6.43 High-altitude flight does not require low RCS for survivability.

fire control radar has a transmitted power of 50,000 W and is looking up at 20-deg elevation angle. A missile with a low value of RCS ($\sigma = 0.001 \text{ m}^2$) is not detected if it flies above 25,000 ft in altitude. Similarly a missile with a much larger RCS ($\sigma = 0.1 \text{ m}^2$) is not detected if it flies above 77,000 ft in altitude. Other approaches for survivability include mission planning to avoid the known threats and flight at very low altitude to provide terrain masking.

Insensitive munitions have high payoff in improving launch platform survivability. The critical subsystems are the rocket motor propellant/engine fuel and the warhead. In the United States the design considerations for insensitive munitions are based on MIL-STD-2105B. MIL-STD-2105B includes considerations of hardening against threat weapons, fast and slow cookoff fires, dropping the weapon, extremes in environmental temperature, missile vibration, and operation off an aircraft carrier. Hardening against threat weapons includes considerations of fragment impact and blast. Cookoff from a fire requires consideration of the type of fire (slow cookoff, fast cookoff) and the warhead or rocket motor reaction to the fire (e.g., burning, detonation). Drop shock sensitivity consideration is a particular concern for ground maintenance personnel dropping the missile during handling. The environmental temperature extremes range from very low temperatures that could damage the rocket motor to very high temperatures that could cause detonation of the warhead. Missile vibration consideration includes the dynamic acceleration imparted during store carriage on the launch platform. Finally, aircraft carrier operation includes the shock of aircraft landing sink rates as high as 18 ft/s.

6.6 Reliability

The sixth measure of merit to be discussed is reliability. Because missiles usually do not have redundancy and each subsystem must function reliably for success, missile system reliability is a product of the individual subsystem reliabilities. Figure 6.44 shows representative system and subsystem reliabilities for a tactical missile. For an operational missile the system reliability is usually between 90 and 99%, depending on the parts count and the type of subsystems/parts. Moving parts tend to be less reliable than nonmoving parts. For a typical missile an individual subsystem failure rate should be about one-tenth the system design failure rate to provide a balance of emphasis in the individual subsystem reliabilities. Design considerations for high reliability are to minimize the number of subsystems, minimize parts count, minimize moving parts, and minimize the complexity of the subsystems. It is noted that in recent years software reliability has replaced mechanical reliability as a major contributor to failure.

6.7 Cost

The seventh measure of merit to be discussed is cost. The relative importance of subsystems to missile cost is shown in Fig. 6.45. The seeker is usually the highest cost subsystem for a tactical missile, usually exceeding 25% of the missile production cost. Other subsystems that are high cost, usually exceeding 10% of the missile production cost, are the guidance and control subsystem and the propulsion subsystem. System assembly and system test are about 10% of the missile production cost for a moderately complex missile. For a complex missile, system assembly and system test may be more than 15% of the missile production cost.

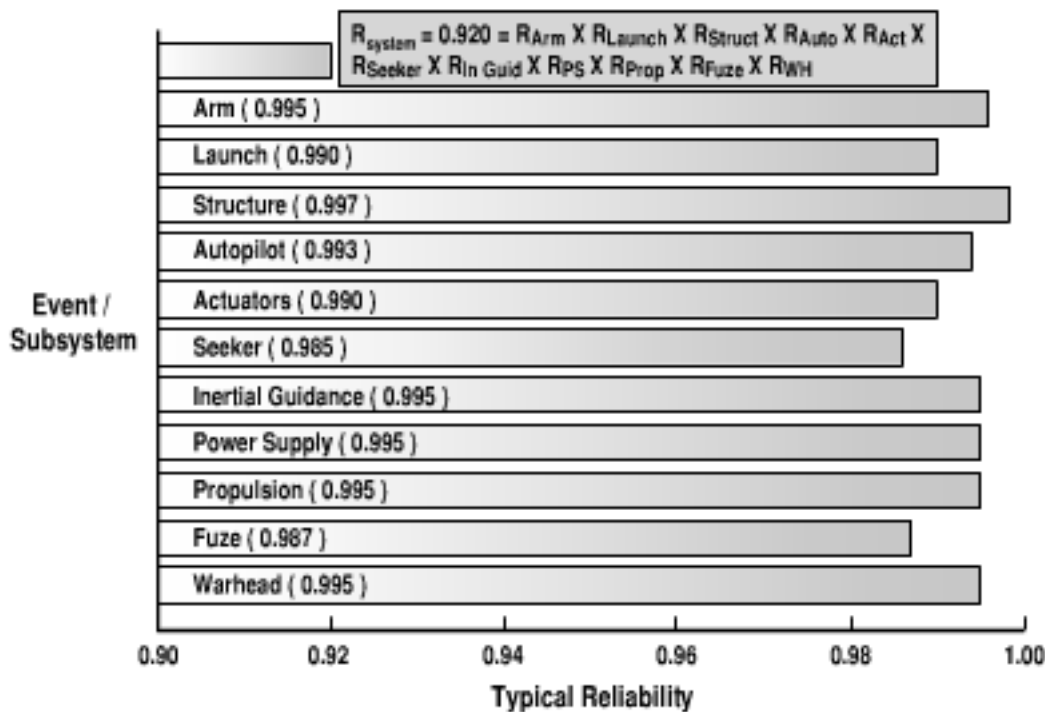


Fig. 6.44 High system reliability is provided by high subsystem reliability and low parts count.

For a simple missile, system assembly and test may be as low as 5% of the missile production cost.

Note that the relative subsystem costs shown in the figure are averages of rockets and airbreathing missiles. A difference in the cost of airbreathing missiles compared to rockets is the cost of the propulsion system and structure. The propulsion system and structure parts count/cost of airbreathing missiles are usually higher than that of rockets.

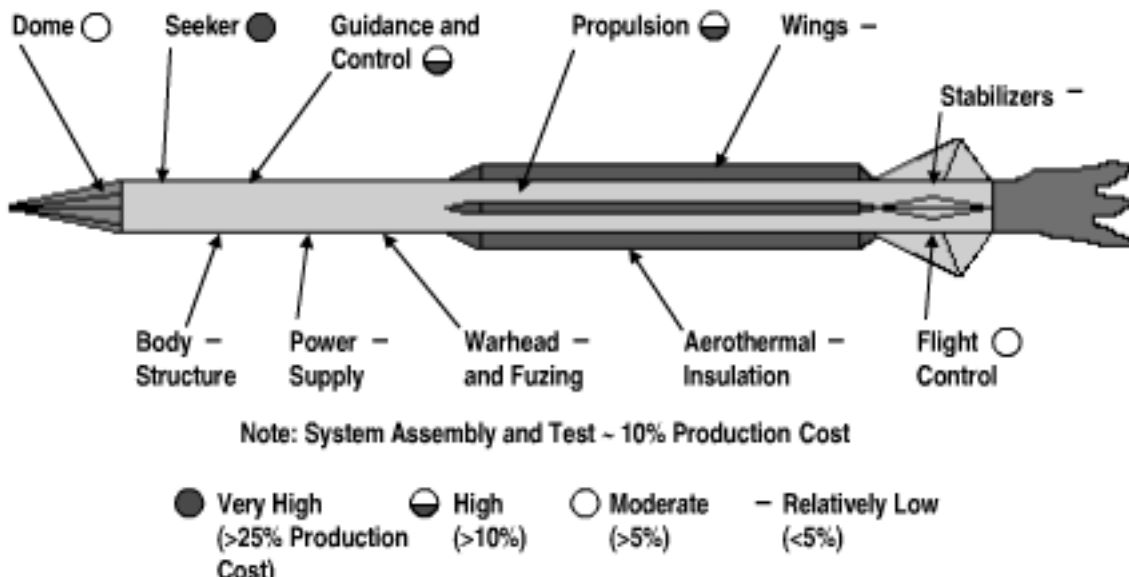


Fig. 6.45 Sensors, electronics, and propulsion drive missile production cost.

Seven primary drivers for missile cost are weight, production quantity (learning curve), parts count, logistics, production rate, culture/processes, and competition. The discussion will begin with a qualitative assessment of the last two drivers, followed by a more specific assessment of the first five drivers. Note that the culture of the strategic missile community, the unmanned air vehicle (UAV) community, and the aircraft community are different from that of the tactical missile community. For example, the tactical missile community usually puts the highest emphasis on reducing cost with less emphasis on performance, reliability, and the organization structure. In the other aerospace vehicle communities, the emphasis on performance, reliability, and a large organization structure is usually greater than the emphasis on reducing cost. A tactical missile may have 90% of the performance and reliability of a comparable size strategic missile at one-half the cost and two-thirds of the development time. Finally, it is not possible to provide specific examples in this text of how competition reduces cost; however, it is well known that competition drives down cost. Production buys with two competing contractors improve efficiency and may reduce the unit production cost by 50% compared to that of a sole-source contractor. Unfortunately, the downsizing of the number of contractors in the tactical missile community has reduced competition, and many tactical missile programs are being absorbed into the strategic missile, UAV, and aircraft communities. As a result, the cost of tactical missiles is likely to increase in the future.

As a first-order design consideration, production cost is a function of weight. The equation $C \approx \$6,900 W_L^{0.64}$ in Fig. 6.46 is based on correlating the data from Ref. 20. Cost C is in U.S. dollars and missile launch weight W_L is in pounds. The data are from tactical missile procurements by the U.S. Department of Defense in the year 1996. As an assessment of the scatter in the curve, note that the Hellfire and TOW missiles have large total production, mature learning curves (mature systems) and simple seekers. It is reasonable that their production costs should be lower than predicted. Note also that the Javelin is a relatively new missile just

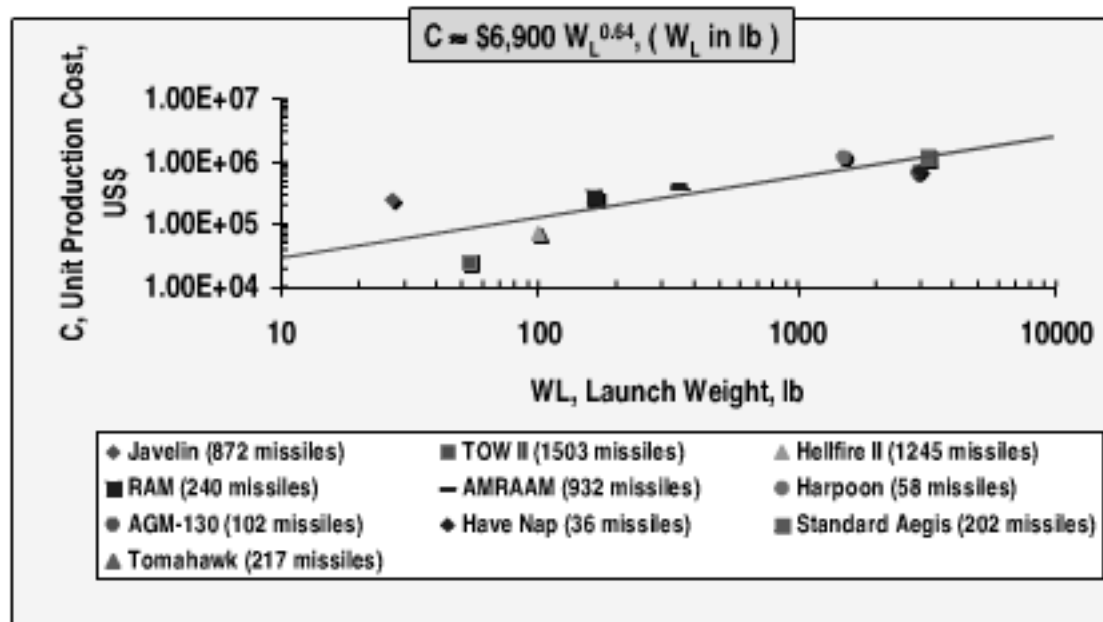


Fig. 6.46 Lightweight missiles are low cost (from Ref. 20).

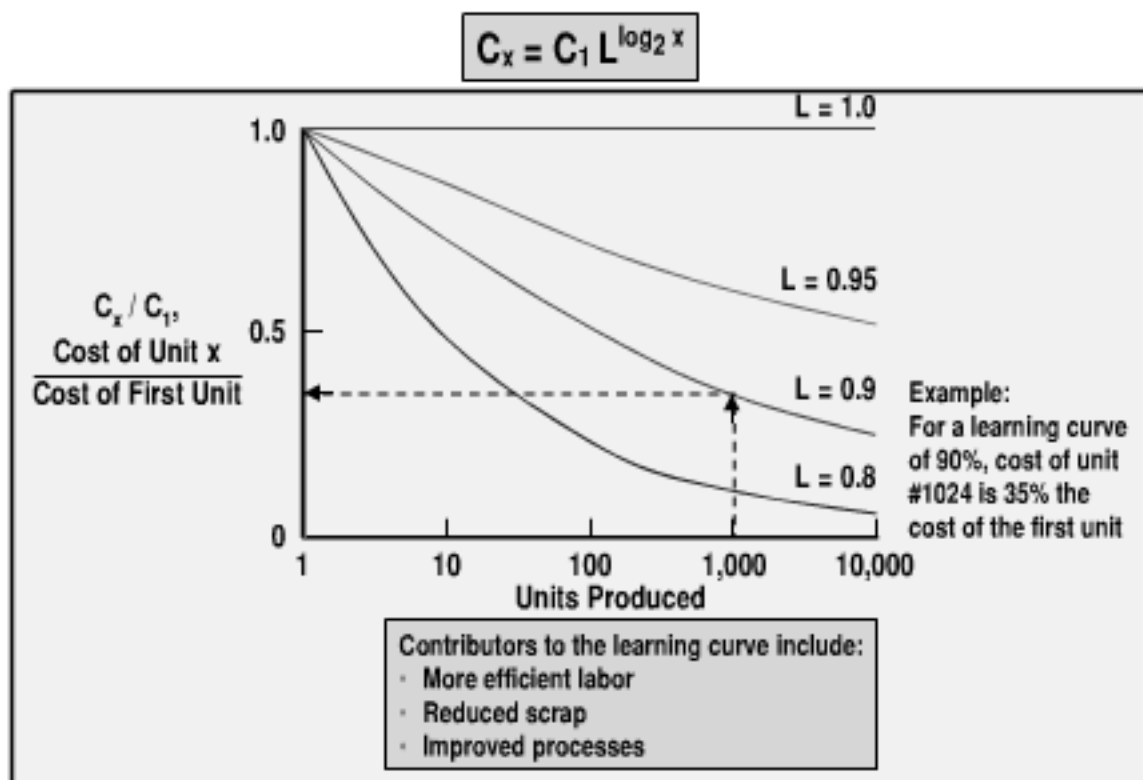


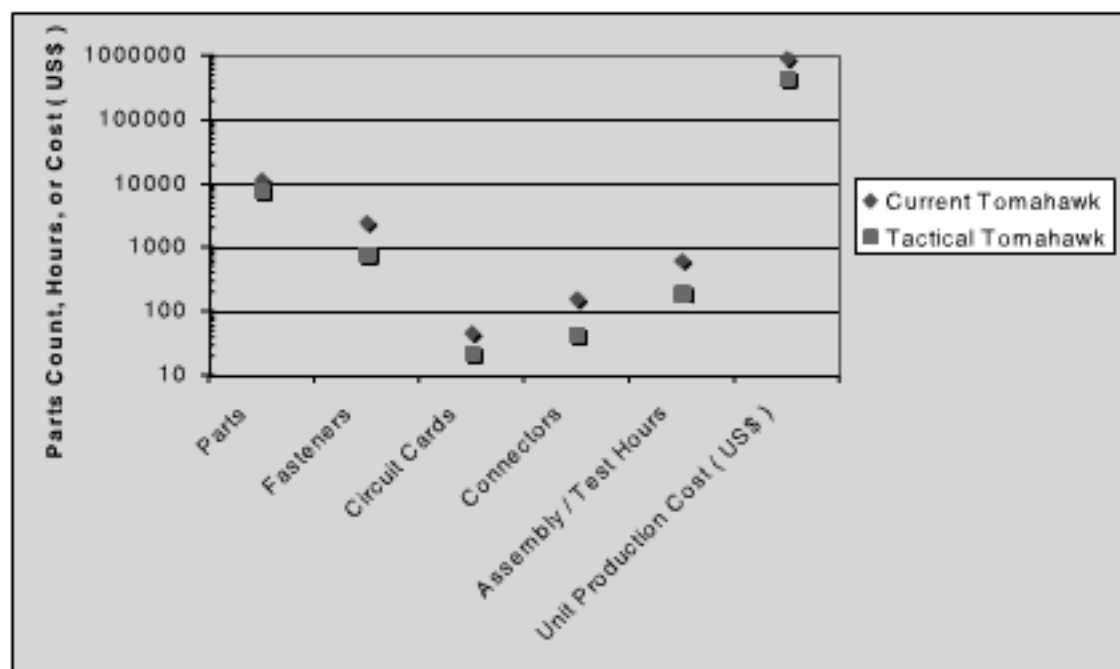
Fig. 6.47 Learning curve and large production reduce unit production cost.

entering production with a relatively immature learning curve. The Javelin also has a relatively complex imaging infrared seeker that uses relatively immature focal plane array technology. It is not surprising that production cost of the Javelin for the year 1996 is higher than predicted. The Javelin unit production cost should decrease in the future as more missiles are produced.

The unit production cost of a missile is dependent on the learning curve from the past production of the missile, given by the equation $C_x = C_1 L^{\log_2 x}$. C_x is the unit cost of the current missile, C_1 is the unit cost of the first production missile, and x is the number of missiles produced to date. The learning curve is extensively used to predict production cost, not only in the aerospace industry but also in other industries such as the automotive industry. The contributors to the learning curve include labor efficiency, scrap, and production process.

Figure 6.47 illustrates the impact of the learning curve and the number of units produced on missile production cost. As an example, for a typical value of the learning curve of $L = 90\%$, the cost of the 1024th missile is 35% of the cost of the first missile. However, note that changing a production process will change the learning curve. The production process that is used for the first missile is different from the production process that is used for the 1024th missile. The first missile is probably a developmental missile produced in the laboratory using soft tooling. The 1024th missile is probably a rate production missile produced in the factory using hard tooling.

New technology is in development that will enhance the production and reduce the cost of weapons. Examples of recent precision strike weapons that include low cost technologies include JDAM and JASSM. Technologies to reduce cost are also being introduced into existing weapons, with large savings. An example of cost reduction is the Tactical Tomahawk, shown in Fig. 6.48. It has a simple



Note: Tactical Tomahawk has superior flexibility (e.g., shorter mission planning, in-flight retargeting, BDI / BDA, modular payload) at lower parts count / cost and higher reliability. Enabling technologies for low parts count include: casting, pultrusion / extrusion, centralized electronics, and COTS.

Fig. 6.48 Low parts count reduces missile cost.

low-cost airframe with extruded wings. Low-cost commercial parts are used for guidance and control and for propulsion. The current Tomahawk has 11,500 parts, 2500 fasteners, 45 circuit cards, 160 connectors, and requires 610 assembly/test hours. The Tactical Tomahawk is projected to have 35% fewer parts, 68% fewer fasteners, 51% fewer circuit cards, 72% fewer connectors, and 68% fewer assembly/test hours, resulting in a projected 50% reduction in cost. The Tactical Tomahawk also has superior flexibility (e.g., shorter mission planning time, capability for in-flight targeting, capability for battle damage indication/battle damage assessment, modular payload) and higher reliability at the same launch weight as the current Tomahawk.

Logistics considerations in tactical missile cost are addressed in Fig. 6.49. The figure compares a simple surface-to-air missile system (Stinger) that has low cost, wooden round logistics to more complex missiles (PAC-3, THAAD) that have higher cost logistics from an entourage of vehicles and support personnel for transportation, maintenance, launch, fire control, and command and control. Shown in the bottom right section of the figure is a video that compares the operational logistics of the relatively simple Stinger to that of the relatively complex PAC-3 and THAAD.

Shown in Fig. 6.50 are examples of the impact of missile weight on the support manpower requirements for tactical missiles. A typical maximum lift requirement per person is between 50 and 100 lb. For man-portable missiles such as Stinger, a single gunner can prepare and launch the missile. As an example of a moderately heavy missile, the 190-lb Sidewinder requires two to four personnel to install the missile on the launch aircraft. A heavier missile, such as a 500-lb Sparrow, requires additional support personnel plus ground support equipment. Finally, a very heavy

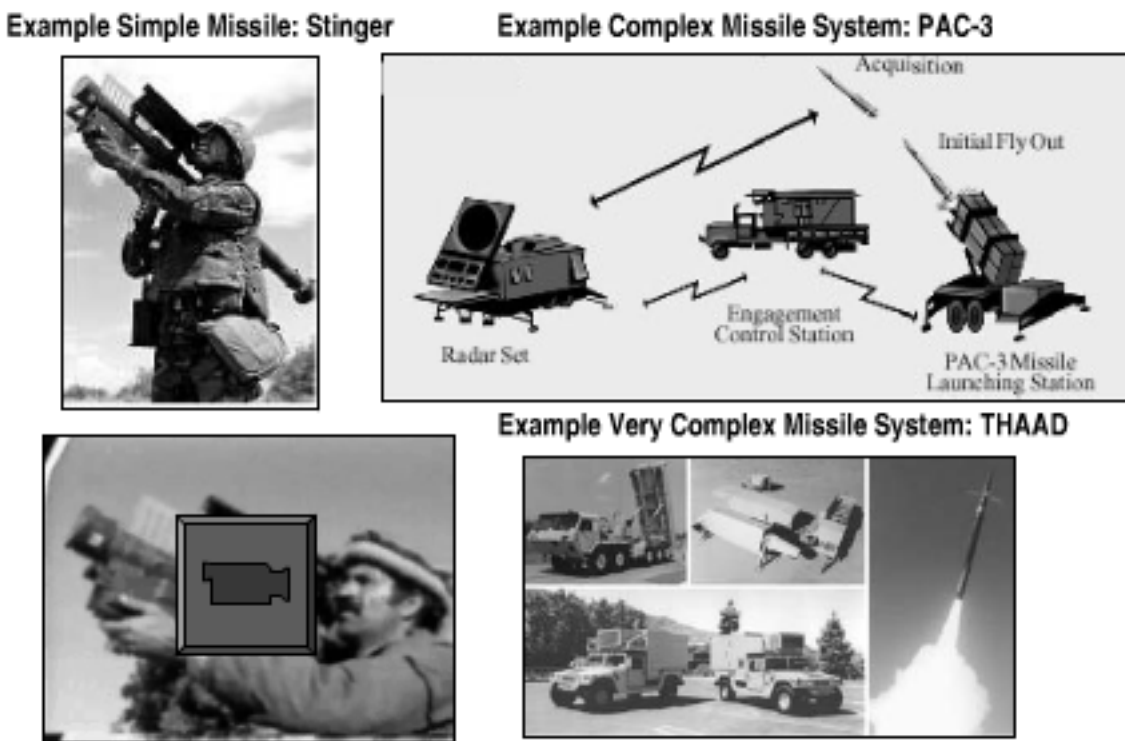


Fig. 6.49 Logistics cost is lower for simple missile systems.

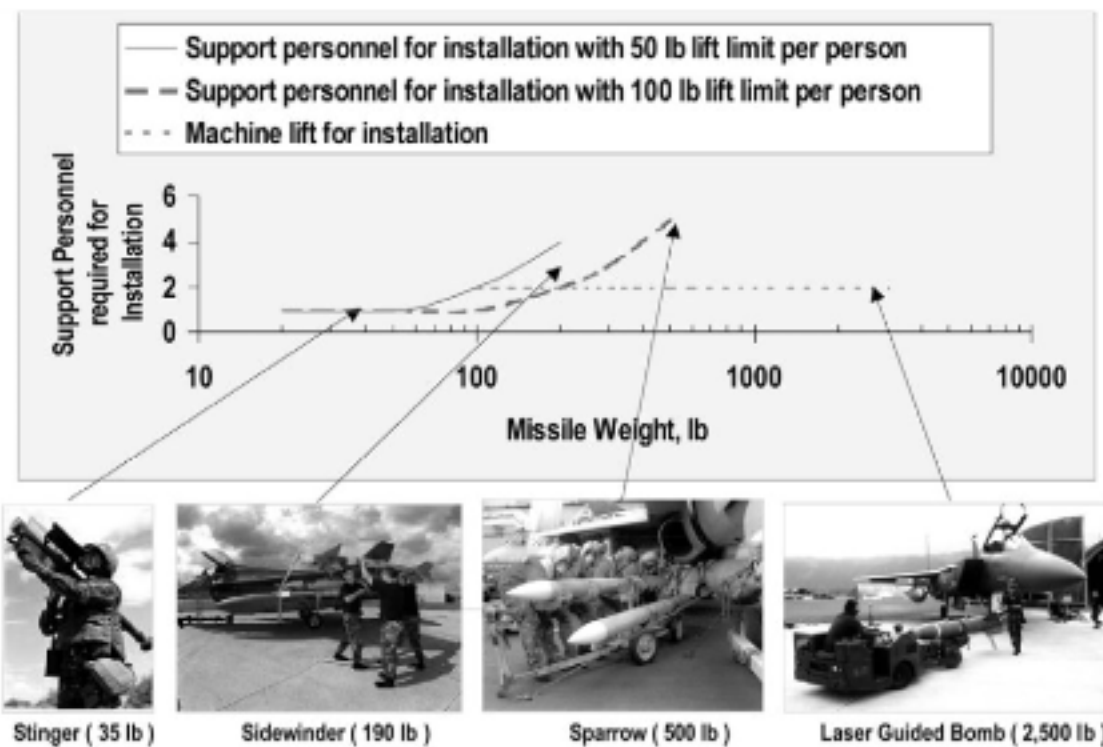


Fig. 6.50 Logistics is simpler for lightweight missiles.

Copperhead Seeker and Electronics Production



Patriot Control Section Production



Video of Hellfire Seeker and Electronics Production

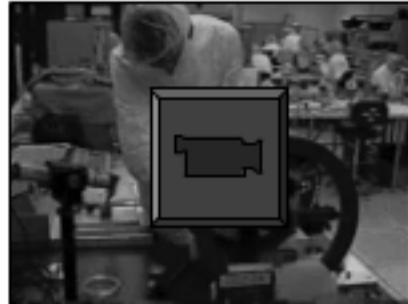


Fig. 6.51 Tactical missile culture is driven by the rate production of sensors and electronics.

weapon, such as a laser guided bomb, requires specialized, heavy ground support equipment.

Missile production cost is sensitive to production rate. There is normally an economy of high-rate production. High-rate production allows hard tooling, which is usually more efficient. The work force is also usually more efficient in rate production. A difference of the tactical missile culture compared to the related cultures of the strategic missile, UAV, and combat aircraft communities is the emphasis on low-cost manufacturing and high rate production. Tactical missile production rate may be more than 5000 missiles per year. This may be 10 times the production rate of a strategic missile and 100 times the production rate of a UAV or combat aircraft.

Examples of relatively high-rate production processes are shown Fig. 6.51. Shown in the left side of the figure is an example of the Copperhead seeker and electronics production. The top right section of the figure is an example of the Patriot flight control production. In the bottom right section of the figure is a video of the Hellfire seeker and electronics production processes. The production processes of the Copperhead, Patriot, and Hellfire weapons are labor intensive with some automation of electronics, such as circuit boards. System assembly and system test are a significant portion of the production cost. A simpler missile that is produced at a very high rate, such as TOW, is less labor intensive. The production process for TOW is highly automated. There is relatively little assembly and testing. Missile system assembly and system tests are a relatively small portion of the TOW production cost. At the other extreme is the Phoenix missile. The Phoenix is a very complex missile that is produced at a low rate and is very labor intensive. The production process for the Phoenix has little automation. Missile subsystem, subsystem assembly, and system tests are a large portion of the Phoenix production cost.

Note that a skilled labor force is desirable for tactical missile production. Skilled production workers provide enhanced reliability and reduce the scrap/cost.

6.8 Launch Platform Integration

Launch platform integration sets constraints on the missile that must be considered early in the development process. Moreover, the design process requires iteration to harmonize the outputs from the diverse areas of mission/scenario definitions, missile requirements, aircraft integration, missile concepts, and technologies. In a few cases it may be possible to modify a launch platform to accommodate a new missile, but in most cases this is not an option. Generally the launch platform is a constraint that drives the missile design. For example, AMRAAM was originally developed as a lightweight radar missile for carriage on the wing tips of the F-16, which has a 300-lb weight limit. Later, AMRAAM was modified to a compressed carriage configuration (clipped wings and tails) to better accommodate internal carriage in the F-22 center weapons bay. Missiles are driven as much by launch platform compatibility as other measures of merit. Weapon compatibility with all launch platforms has high payoff in the neckdown benefit cost savings of fewer missile logistics systems.

In an ideal world new combat aircraft development would be conducted in concert with new missile development for a more cost-effective weapon system. Examples of system-level trades include aircraft maneuverability vs missile maneuverability and aircraft observables vs missile standoff range. The reality is that new aircraft are developed based on the current weapons with little consideration of the new weapons or the new missile technology that is in development. The lack of consideration of new weapons may be due to a concern of the aircraft developer that the consideration of new weapons may endanger the aircraft program funding.

Carriage constraints for missiles on surface ships, submarines, and aircraft are shown in Fig. 6.52. Cross-platform compatibility is desirable for a missile system. A larger total buy of missiles for cross-platform application has the benefits of lower unit production cost and lower logistics cost. In the United States, the vertical launch system (VLS) is a standard carriage and launch system for missiles on surface ships. The VLS geometry constraints are $22 \times 22 \times 256$ in. The maximum weight constraint is 3400 lb. U.S. submarines have a similar standard launcher that is circular in cross section. The submarine canister launch system (CLS) has a diameter constraint of 22 in. and a length constraint of 256 in. Maximum missile weight for the CLS is the same as that of the VLS, 3400 lb. The VLS and CLS also have a maximum limit on the total impulse delivered in the event of hangfire, to avoid burning through the launch platform structure. Finally, aircraft launch platforms for missiles include tactical fighters, bombers, helicopters, and UCAVs. Shown in the figure is an example of a fighter aircraft, the F-18C. The F-18C carries weapons externally on pylons and rails. Other aircraft, such as the F-22, RAH-66, and B-1, have an additional capability of internal carriage. Internal launchers include vertical ejection, rail trapeze, and rotary ejection. Missile span constraint for aircraft carriage is about 24×24 in. Length constraint is about 168 in. and the maximum allowable missile weight varies from about 500 to 3000 lb, depending on the aircraft. There is a strong desire for lightweight missiles

Launch Platform	Launcher	Maximum Body Shape	Maximum Length	Maximum Weight
Surface Ships	Surface VLS	Square Missile	256"	3400 lb
Submarines	Sub-CLS	Round Missile	256"	3400 lb
Aircraft	External Rail / Eject Internal Vert Eject Internal Trap Rail Internal Rotary	-24" x 24" ~168"	~500 lb to 3000 lb	

Fig. 6.52 Missile shape, size, and weight are driven by launch platform compatibility.

to maximize the firepower of small aircraft such as the F-18C, Comanche, and Predator. Maintaining high firepower for small aircraft is important. For example, around the year 2010 50% of the U.S. Navy fleet combat aircraft are expected to be F-18Cs.

New technology development for weapon compatibility and high firepower includes low volume propulsion, ordnance, and airframe; store carriage and store separation wind-tunnel tests; computational fluid dynamics (CFD) predictions; and finite element modeling (FEM) predictions.

Figure 6.53 illustrates how day/night operation, firepower objectives, and weapons load-out impact the maximum allowable weight of a precision strike missile. Shown are examples for the F-18C and F-18E aircraft. Note that the F-18C aircraft has less capability than the F-18E in all load-out configurations. The figure shows a large difference in the maximum allowable missile weight for day vs night operation. The difference is due to the additional fuel that must be reserved for night operation off an aircraft carrier. The maximum weapon weight shown in the curves must also be reduced to account for limits in asymmetric carriage (2500 lb maximum weight for inboard asymmetric carriage and 1500 lb maximum weight for outboard asymmetric carriage). Finally, note the reduction in maximum allowable missile weight as the load-out configuration is changed from that of a clean aircraft carrying only precision strike missile(s) to other configuration load-outs. Five other load-out configurations are the precision strike missile(s) plus either 1) a centerline fuel tank, 2) two inboard fuel tanks, 3) a centerline fuel tank plus two Sidewinder air-to-air missiles, 4) a centerline fuel tank plus two antiradiation missiles (ARM), or 5) two inboard fuel tanks plus two Sidewinders. Note that the maximum allowable weight of a single precision strike missile on the F-18E is about 4800 lb under ideal conditions. At the other extreme is an F-18C operating under limited conditions. For an F-18C operating at night with two inboard fuel tanks and two Sidewinders, the maximum allowable weight of a single precision strike missile is much lower, about 1800 lb. In the case of carriage

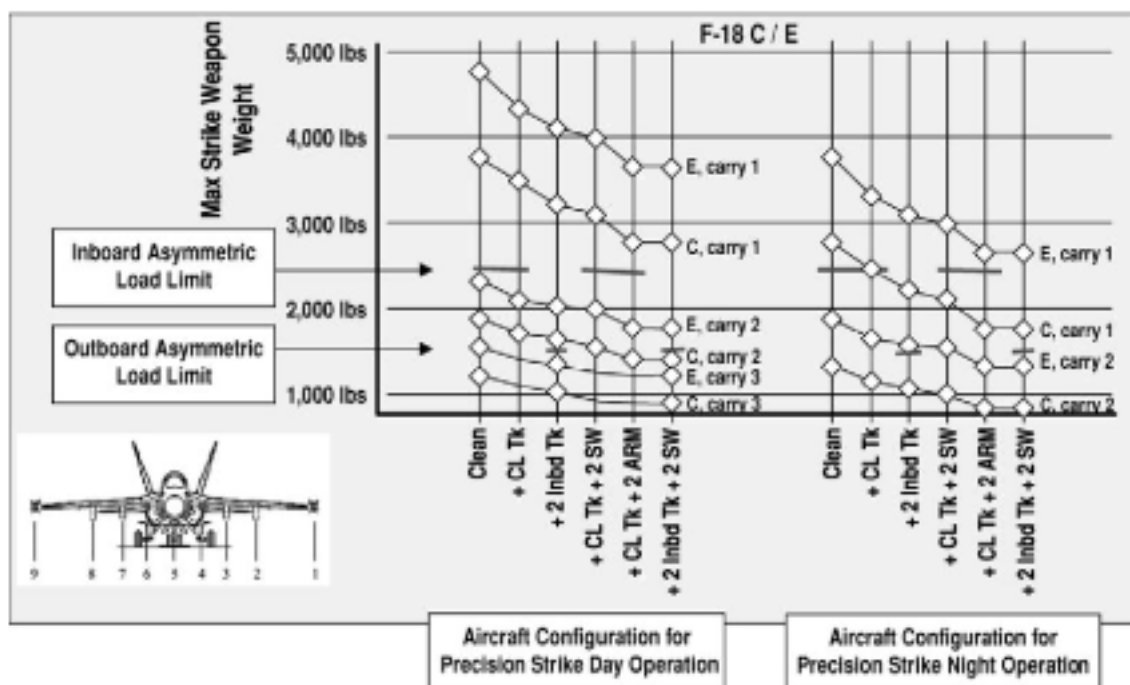


Fig. 6.53 Lightweight missiles enhance firepower.

of two precision strike missiles, the F-18E under ideal conditions can carry a missile weighing up to 2400 lb. At the other extreme for an F-18C load-out of two precision strike missiles, operating at night with the addition of two inboard fuel tanks and two Sidewinders requires that the precision strike missile weigh less than 900 lb. A precision strike missile weight of about 1400 lb is probably a good compromise for the example of F-18C/E aircraft integration. It allows two weapons on the F-18C for unrestricted day operation, two weapons on the F-18E for near unrestricted night flight operation, and three weapons on the F-18E for day operation with two inboard fuel tanks.

In addition to firepower, weight, and fit, other considerations in missile/aircraft integration include the following:

- 1) Missile seeker field of regard (FOR) design consideration that the aircraft does not obscure the seeker FOR.
- 2) Launch rail clearance design consideration of the miss distance at the minimum launch range. The missile has tip-off angular rates in pitch, yaw, and roll because of the clearance between the missile hangers/shoes and the launcher rail.
- 3) Launcher rail retention design consideration to avoid an inadvertent release of the missile prior to launch. It must also release reliably during the motor firing to avoid a hang-fire.
- 4) Launcher aeroelasticity design consideration of the miss distance at minimum range. Tip-off rates are imparted by the flexible launcher.
- 5) Aircraft local flowfield α , β design consideration of safe separation.
- 6) Aircraft maneuvering design consideration of safe separation.
- 7) Aircraft stability and control design consideration with attached stores. The changes in the aircraft flowfield and center of gravity from a stores load-out impact the aircraft flying qualities.
- 8) Helicopter rotor downwash design consideration of missile miss distance at minimum range.
- 9) Aircraft bay acoustics design consideration of missile factor of safety.



F-18 Store Compatibility Test in AEDC 16T



AV-8 Store Compatibility Test in AEDC 4T

Types of Wind Tunnel Testing for Store Compatibility

- Flow field mapping with probe
- Flow field mapping with store
- Captive trajectory simulation
- Drop testing



Example Stores with Flow Field Interaction: Kh-41 / AA-10

Fig. 6.54 Store separation wind-tunnel tests are required for missile/aircraft compatibility.

10) Aircraft bay vibration design consideration of missile factor of safety.

Aircraft store compatibility wind-tunnel tests are conducted to determine store carriage loads and store separation forces, moments, and trajectories. Figure 6.54 shows wind-tunnel installations of aircraft and store models. Note that a typical aircraft store load-out has closely spaced stores. The local airflow around a store is difficult to predict. There is a complex flowfield interaction of a store with the aircraft and also with the adjacent stores.

The types of wind-tunnel testing for store compatibility include the following:

- 1) Flowfield mapping with a pitot static pressure probe to measure the local static pressure, total pressure, and local angle of attack.
- 2) Flowfield mapping with an instrumented store model on a sting to measure the forces and moments on the store immersed in the aircraft flowfield.
- 3) Captive trajectory simulation of an instrumented store model on a sting.
- 4) Drop testing of store models. The store models are constructed of lead, tungsten, or even gold to provide weight scaling to simulate full-scale buoyancy in the wind-tunnel test.

Figure 6.55 shows examples of missile carriage on U.S. standard rail and ejection launchers. The launcher provides the mechanical and electrical interface between the missile and the launch aircraft. The mechanical interface includes the attachment, structural support, and the launch mechanism. The electrical interface supports the cockpit controls and displays, enabling the pilot to launch the missile. In the upper left of the figure is an AGM-114 Hellfire II missile on a helicopter rail launcher. Rail launchers are particularly suited to lightweight, high-thrust missiles such as the Hellfire. The Hellfire weighs 100 lb, with a launch thrust-to-weight ratio of about 30:1. The Hellfire has a semilaser seeker with a field of regard of ± 30 deg.



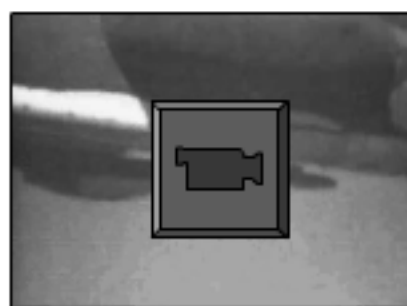
Example Rail Launcher: Hellfire / Brimstone



Example Ejection Launcher: AGM-86 ALCM



Video of Hellfire / Brimstone Carriage / Launch



Video of AGM-86 Carriage / Launch

Fig. 6.55 Rail-launched missile and ejection-launched missile examples.

Most precision strike missiles use ejection launch. In the upper right corner of the figure is an AGM-86 ALCM precision strike missile that is installed on a rotary launcher of a bomb bay. The ALCM is ejected from the bay at an ejection velocity of about 20 ft/s. The ejection stroke is about 12 in., providing an average acceleration of about 6 g. The ejection launcher contains cartridges that provide the downward velocity and a downward pitch rate to the missile at launch, aiding safe and accurate separation. Suspension of the missile is such that the missile center of gravity is midway between the ejectors. A concern during launch is the local angle of attack and the local angle of sideslip because of the proximity of the store to the aircraft and the effect on the missile flight trajectory, especially at high dynamic pressure. Up to eight ALCM missiles can be carried on a rotary launcher in each bay of the B-1, B-2, and B-52 bombers. The ALCM has compressed carriage (switch blade wing, folded tails), providing a high load-out in the bomb bay. The wings and tails are unfolded immediately after separation from the bay. Concerns for internal bay carriage include bay acoustics, bay vibration, flowfield angularities near the aircraft, and safe separation at high dynamic pressure.

The left bottom section of the figure is a video of the rail launcher loading of the Brimstone missile. The missile slides onto the rail and into a "shotgun" connector that interfaces with the aircraft avionics. The right bottom section is a video of the loading, carriage, ejection launch, separation, and flight of the ALCM missile. Note the deployment of the compressed carriage switchblade wing and the folded tails.

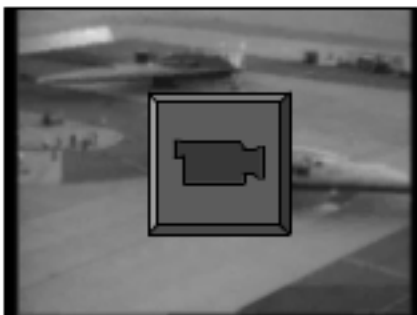
Examples are shown in Fig. 6.56 of safe separation of a rail launched AMRAAM from an F-16 and the clean separation of two laser guided bombs dropped from an F-117. In the bottom right corner is a computer video from the Northrop Grumman Corporation, showing the clean separation of a rapid bomb drop (about one per



AMRAAM Rail Launch from F-16



Laser Guided Bombs Drop from F-117



Video of Rapid Drop (16 Bombs) from B-2

Fig. 6.56 Examples of safe store separation.

second) from the B-2 bomber. A rapid bomb drop is desirable to minimize the exposure time with the high observables from the open weapon bay. Exposure time less than 10 s is desirable to prevent threat radars from establishing a track file.

The videos in Fig. 6.57 show aircraft store compatibility problems. The upper left video shows examples of unsafe store separation of tanks, bombs, and missiles. The upper right video is a hang-fire of a rocket motor. Shown in the bottom video is an example of aircraft aeroelastic instability due to a large/heavy store.

Store suspension requirements for ejection launchers, based on U.S. military standard MIL-A-8591, are summarized in Fig. 6.58. Shown are the store weight and the store dimension parameters for light-weight stores (up to 100 lb), medium-weight stores (101 to 1450 lb), and heavy-weight stores (over 1451 lb). Suspension alternatives are 30-in. and 14-in. suspension systems. For an ejected store weight up to 100 lb, only the 14-in. suspension can be used. A lightweight (up to 100 lb) missile requires a lug height and an ejector pad area of 0.75 in. and 4.0×26.0 in., respectively. For a medium-weight missile, with a weight between 101 and 1450 lb, either the 14-in. suspension or a 30-in. suspension may be used. Medium-weight ejected stores have larger required lug height and ejector pad area. They also require lug wells. The required lug wells could have a strong impact on the missile internal structure design. For example, in some cases the rocket motor overlaps the missile center of gravity. Accommodating the lug wells in the rocket motor case is difficult and expensive. A strong back may be required, similar to that of the AGM-69 SRAM missile. For a heavy missile with a weight that is over 1451 lb, only the 30-in. suspension can be used. MIL-STD-8591 requires that the lugs have a deeper well if the missile weighs more than 1451 lb.

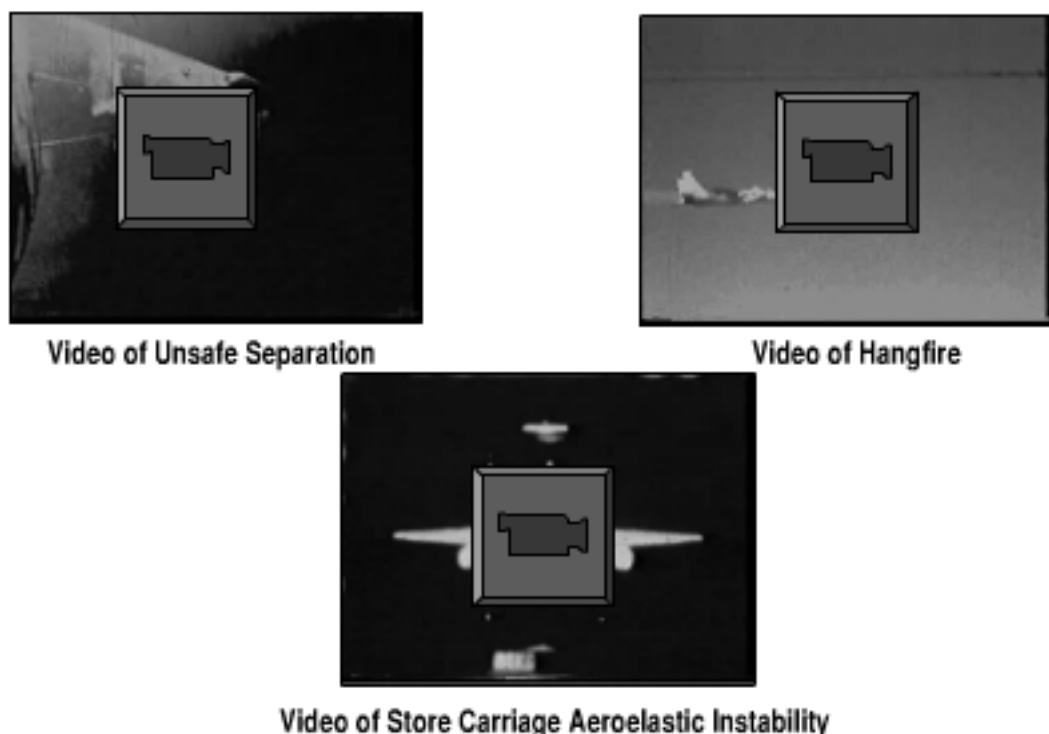


Fig. 6.57 Examples of store compatibility problems.

Examples of missile rail launchers that are compatible with MIL-STD-8591 are shown in Fig. 6.59. Rail launchers usually suspend the missile at two locations, a forward hanger and an aft hanger. Some rail launchers suspend the missile at three locations for added stiffness. The launcher shown in the top of the figure is the LAU-7. The LAU-7 rail launcher has a store weight limit of 300 lb and a store diameter limit of 7 in. The LAU-7 is a standard launcher for the Sidewinder missile. It has forward and aft hangers with a shoe width of 2.26 in.

Store Weight / Parameter	30 Inch Suspension	14 Inch Suspension
+ Weight Up to 100 lb • Lug height (in) • Min ejector area (in x in)	Not Applicable ↓	Yes 0.75 4.0 x 26.0
+ Weight 101 to 1,450 lb • Lug height (in) • Min lug well (in) • Min ejector area (in x in)	Yes 1.35 0.515 4.0 x 36.0	Yes 1.00 0.515 .0 x 26.0
+ Weight Over 1,451 lb • Lug height (in) • Min lug well (in) • Min ejector area (in x in)	Yes 1.35 1.080 4.0 x 36.0	Not Applicable ↓

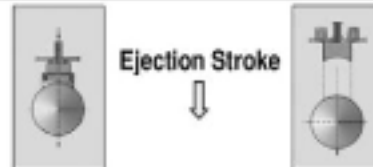


Fig. 6.58 MIL-STD-8591 ejection launcher requirements.

Rail Launcher	Forward Hanger	Aft Hanger
LAU-7 Sidewinder Launcher 	→ 2.260 ← 	→ 2.260 ← 
LAU 117 Maverick Launcher 	→ 1.14 ← 	→ 7.23 ← 

Note: Dimensions in inches.

- LAU 7 rail launched store weight and diameter limits are ≤ 300 lb, ≤ 7 in
- LAU 117 rail launched store weight and diameter limits are ≤ 600 lb, ≤ 10 in

Fig. 6.59 MIL-STD-8591 rail launcher examples.

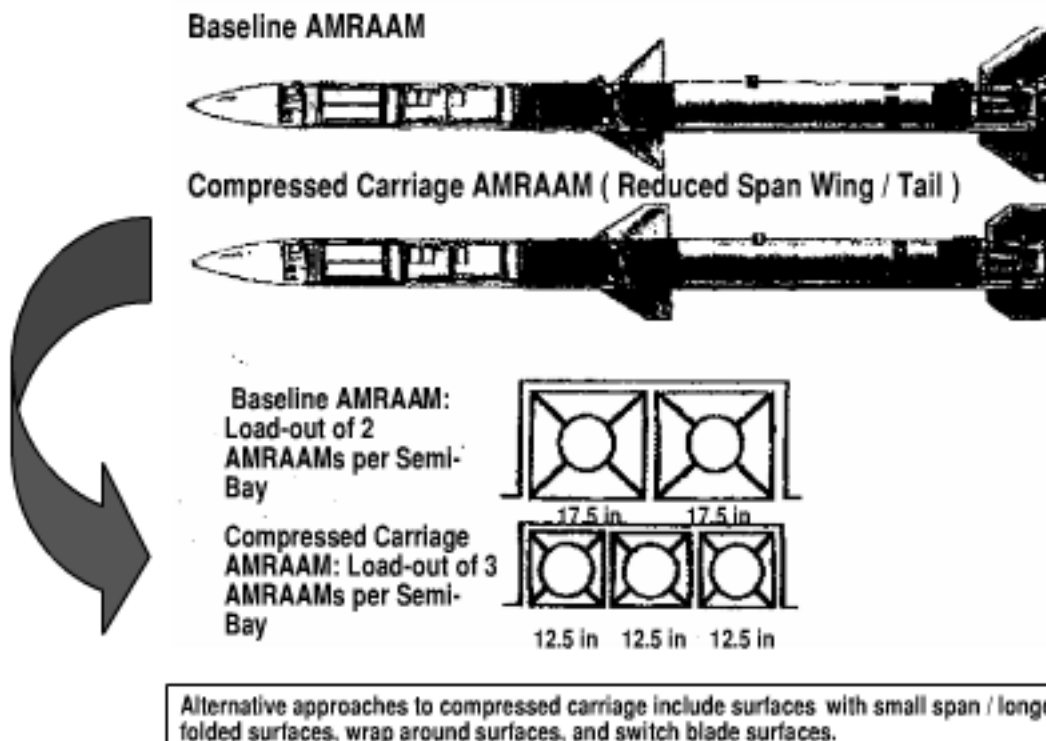


Fig. 6.60 Compressed carriage missiles provide higher firepower for aircraft with internal weapon bays.

The LAU-117 rail launcher, shown in the bottom of the figure, has a store weight limit of 600 lb and a store diameter limit of 10 in. The LAU-117 is a standard launcher for the Maverick missile. It has a forward hanger with a shoe width of 1.14 in. and an aft hanger with a shoe width of 7.23 in.

A missile that has reduced span surfaces during carriage allows closer spacing of the adjacent missiles on the launch platform. Approaches for compressed carriage include reduced span/longer chord surfaces, folded surfaces, wraparound surfaces, and switch blade surfaces. Figure 6.60 illustrates the benefits of compressed carriage. The F-22 internal center weapons bay typically has two partitions, with one partition for air-to-air (e.g., AMRAAM) missiles. A baseline AMRAAM load-out in an F-22 center bay partition allows two missiles per partition. However, compressed carriage AMRAAM can be packaged three missiles per partition, a 50% increase in the firepower load-out. For an air-to-air mission only, both partitions of the F-22 center bay are allocated to air-to-air missiles, allowing a bay load-out of six compressed carriage AMRAAMs.

Air-launched missiles must have sufficient robustness in their design to accommodate a broad environment during storage and during launch platform carriage. Table 6.1 has examples of environmental requirements for temperature, humidity, rain, wind, salt fog, vibration, shock, and acoustics. An example of concern at the temperature extremes is propulsion and warhead safety, reliability, and performance. Another concern is the effect of high rain rate, such as seeker dome erosion at high carriage velocity. A third example of an environmental concern is corrosion from salt fog, particularly for naval operation. An advantage of internal bay carriage over external carriage is that many of the carriage environment concerns are alleviated. However, some carriage environment concerns could be greater for internal carriage than that of external carriage. Examples include high vibration and acoustic loads when the internal carriage bay doors are open at a flight condition with high dynamic pressure.

Table 6.1 Robustness is required to satisfy carriage and storage environmental requirements

Environmental parameter	Example of environmental requirement
Temperature	-60 to 160°F
Humidity	5 to 100%
Rain	120 mm/h
Wind	100 km/h steady 150 km/h gusts
Salt fog	3 g/mm ² per year
Vibration	10 g rms
Shock	MIL STD 810, 648, 1670A Drop height 0.5 m 100 g 10 ms, half sine wave
Acoustic	160 dB

6.9 Summary

This chapter addressed the broad considerations of measures of merit and launch platform integration. Examples of measures of merit for tactical missiles were presented. Considerations for robustness included the effectiveness of alternative sensors operating in adverse weather and clutter, the capability in off-design flight conditions, changes in performance with uncertainty, and the performance in countermeasures. Considerations for warhead lethality included warhead effectiveness against a broad range of targets, synergy with guidance accuracy, and the type of warhead (e.g., blast fragmentation, kinetic energy). Considerations for miss distance included the miss distance due to an initial heading error at seeker lock-on, miss distance due to a maneuvering target, and the contributions to the missile time constant by limited control effectiveness, flight control dynamics, and seeker dome error slope. Included in the considerations for carriage and launch observables were launch platform carriage RCS and missile plume visual signature for reduced observables. Other survivability considerations included missile radar cross section, missile flight altitude, and insensitive munitions. Considerations for reliability included the number of subsystems, parts count, types of parts, and subsystem complexity. Cost considerations included weight, production quantity/learning curve, parts count, logistics, production rate, culture/processes, and competition. Considerations for launch platform integration included fire-power, weight, fit, store separation, aircraft stability and control, aircraft aeroelasticity, hangfire, vibration, compatibility with standard launchers, and the flight environment.

Sizing Examples

This chapter presents examples of sizing tactical missile configurations and examples of computer-aided sizing tools for conceptual design. The topics presented are rocket baseline missile air-to-air range requirement, rocket baseline missile wing sizing for maneuverability, rocket baseline missile weight and miss distance harmonization, ramjet baseline missile range robustness, ramjet propulsion and fuel alternatives, ramjet missile surface target impact velocity, and computer-aided sizing tools for conceptual design.

7.1 Air-to-Air Range Requirement

The rocket baseline missile will be used to illustrate the establishment and substantiation of an air-to-air missile flight range requirement, wing sizing for maneuverability, and the harmonization of missile weight/miss distance. The first example is sizing the rocket baseline missile to meet an air-to-air flight range requirement.

The air-to-air missile flight range in this example is derived from the speed and range required for standoff survivability of the launch aircraft. The assumed requirement is to provide an F-pole range that allows a kill of a head-on threat outside the threat weapon launch range. For air-to-air combat, the visual detection range by the threat is $R_D \approx 3.3$ n miles. This sets the required F-pole range of 3.3 n miles. The assumed altitude and speed of the launch aircraft, target aircraft, and missile for this analysis are $h = 20,000$ ft in altitude; $V_L = 820$ ft/s (Mach 0.8); $V_T = 820$ ft/s; and $V_M = 2 V_T = 1640$ ft/s.

The assumed air-to-air scenario is shown in Fig. 7.1. The required launch range R_L and F-pole range are functions of the missile average velocity V_M , missile time of flight t_f , and the target average velocity V_T . To provide an $R_{F\text{-pole}} = 3.3$ n miles, the rocket baseline missile must be launched at 10.0 n miles from the target and have a flight range of 6.7 n miles within 24.4 s. Because the launch range is greater than the visual detection range, a noncooperative target identification (NCTID) capability is required for the launch aircraft fire control system to avoid fratricide to friendly or neutral aircraft.

The typical ranges at which a pilot can detect and recognize an aircraft target are shown in Fig. 7.2. The detection range and the recognition range are functions of the aircraft contrast, aircraft presented area, and the threshold contrast. Note that detection range is reduced as the contrast is reduced. A design consideration for aircraft integration of tactical missiles is to use a paint scheme for the missile (e.g., gray) that matches the paint scheme of the launch aircraft. Note that for an assumed launch aircraft contrast $C = 0.2$, launch aircraft presented area $S = 50$ ft², and threshold contrast $C_T = 0.02$, the visual detection range by the threat is $R_D = 3.3$ n miles. The visual recognition range is 29% of the detection range,

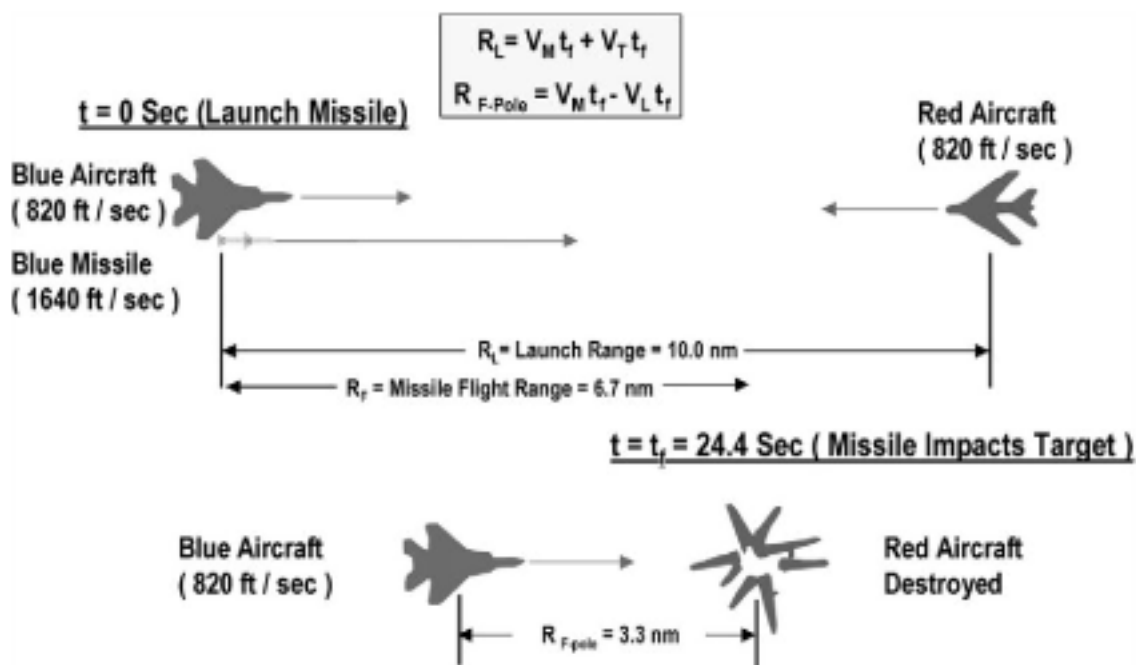


Fig. 7.1 Air-to-air engagement scenario.

giving $R_R = 0.29 R_D = 1.0$ n miles. Assumptions for this analysis are:

- 1) The threat does not have NCTID or a beyond-visual-range missile.
- 2) The threat will launch a within-visual-range missile (e.g., Sidewinder type) when it is within visual detection range.
- 3) Probability of detection by the threat is $P_D = 0.5$.
- 4) Threat pilot visual acuity angle θ is the foveal angle of the eye = $\theta_F = 0.8$ deg.
- 5) The weather is clear.

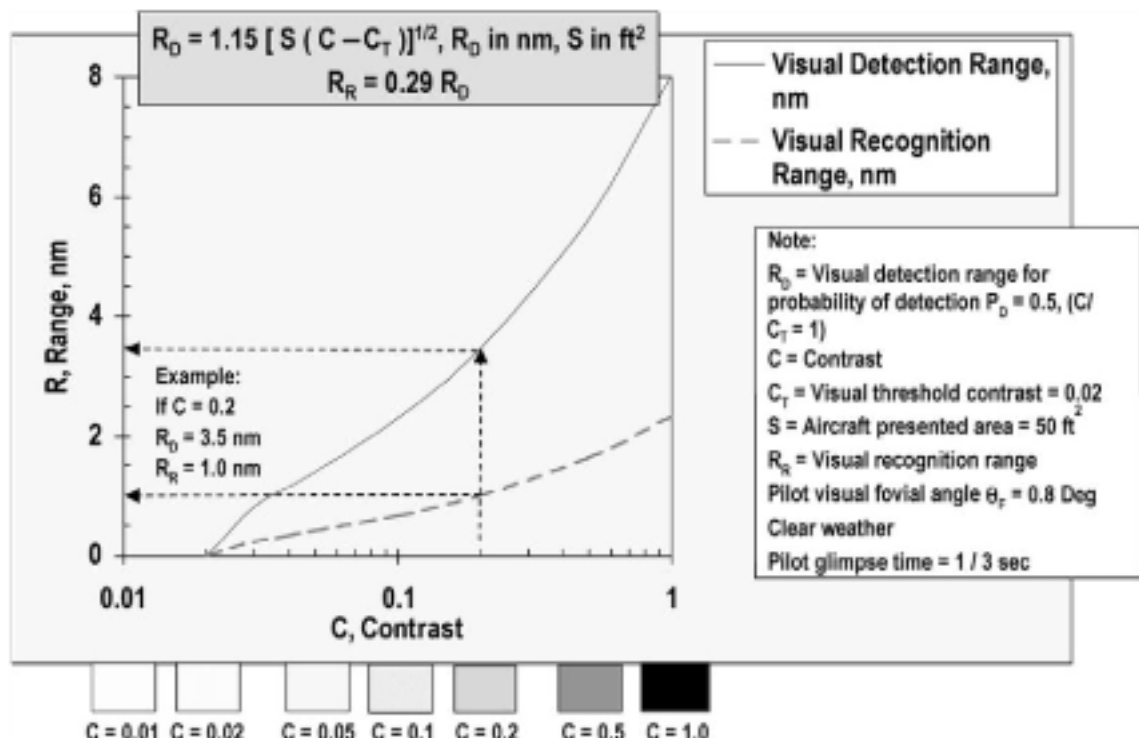


Fig. 7.2 Target contrast and size drive visual detection and recognition range.

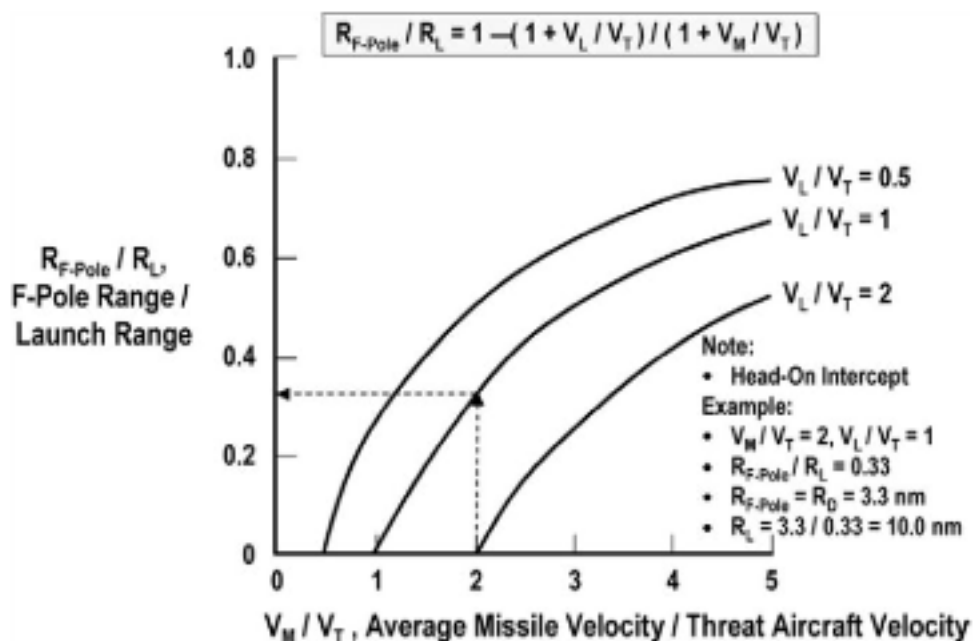


Fig. 7.3 Benefit of high missile velocity for air-to-air standoff range.

6) Threat pilot glimpse time for an air-to-air search = 1/3 s.

At the bottom of the figure is a grayscale of contrast ranging from $C = 0.01$ to 1.0 . Note that it is difficult to distinguish the difference between the contrast and the white background for $C = 0.02$.

Figure 7.3 shows the relative standoff range for air-to-air combat. It is a function of missile velocity, threat aircraft velocity, and the launch aircraft velocity. An assumption is a head-on intercept engagement. Note that the longest F-pole range is for a missile velocity that is much greater than the threat aircraft target velocity.

As an example, assume that the average missile velocity is twice that of the target ($V_M / V_T = 2$), and the velocity of the launch aircraft is equal to that of the target ($V_L / V_T = 1$). If the F-pole range is required to be the same as the detection range, then $R_{F\text{-Pole}} = R_D = 3.3 \text{ n miles}$. Finally, the missile launch range is calculated to be $R_L = 10.0 \text{ n miles}$.

As shown in Fig. 7.4, the missile flight range that is required to intercept a target is a function of the launch range, missile velocity, target velocity, and the target aspect. Note that a higher speed missile reduces the required flight range for a tail chase intercept and increases the required flight range for a head-on intercept.

As an example, using the rocket baseline missile flight range, assume the head-on intercept engagement discussed previously. For an average missile velocity $V_M = 1640 \text{ ft/s}$ and an average target velocity of $V_T = 820 \text{ ft/s}$, the flight range is 67% of the launch range. For a launch range $R_L = 10.0 \text{ n miles}$, the required missile flight range $R_F = 6.67 \text{ n miles}$.

Note from the figure that the missile flight range requirement is greatest for a tail chase intercept. If the target in the engagement discussed previously were retreating from the launch aircraft, the required flight range for the same assumptions of launch range ($R_L = 10.0 \text{ n miles}$), missile average velocity ($V_M = 1640 \text{ ft/s}$), and target average velocity ($V_T = 820 \text{ ft/s}$), the required flight range of the missile is increased by 200% (20.0 n miles vs 6.67 n miles).

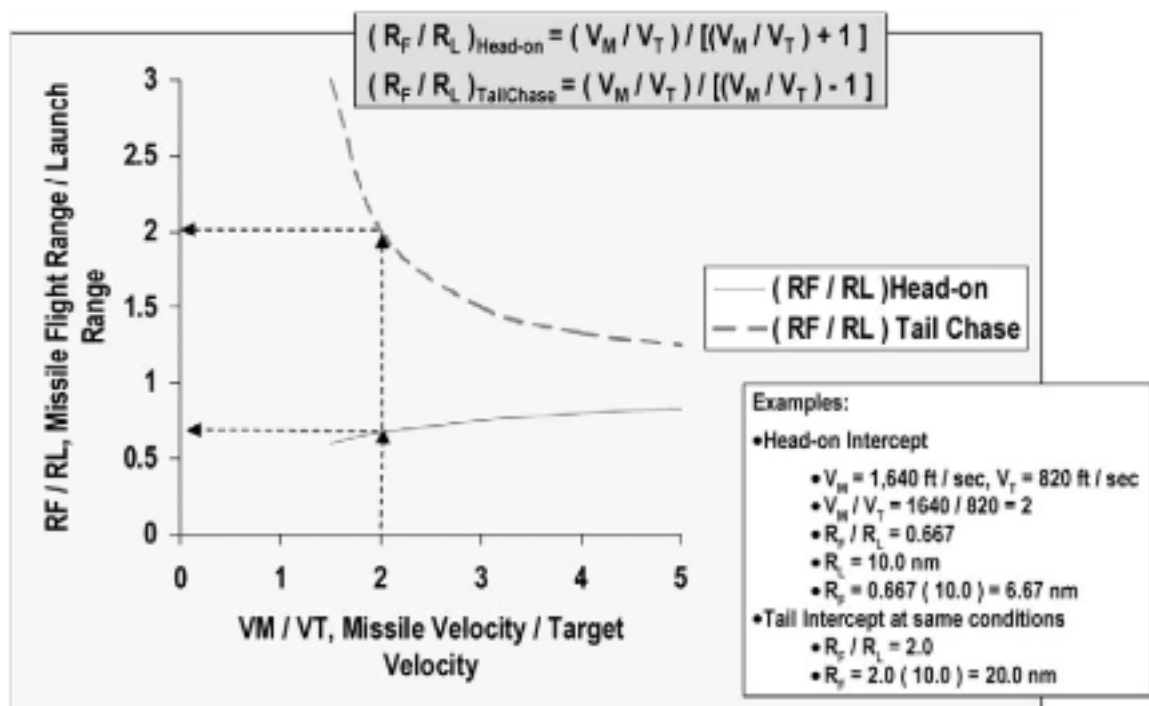
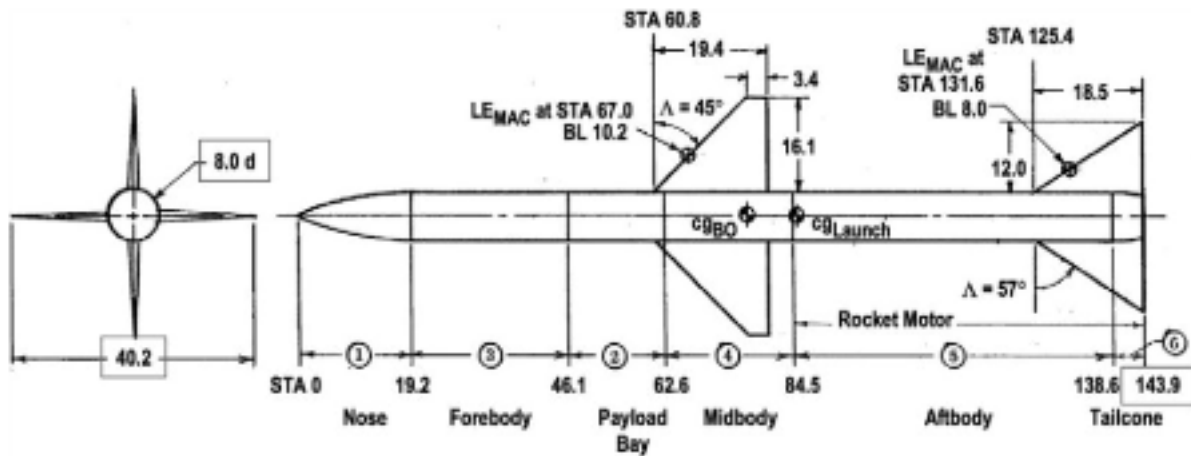


Fig. 7.4 Missile flight range requirement is greatest for a tail chase intercept.

Figure 7.5 from Ref. 21 is a configuration drawing of the rocket baseline missile, which is similar to the Sparrow missile. Note that the diameter $d = 8 \text{ in.}$, total wing span $b_w = 40.2 \text{ in.}$, and length $l = 143.9 \text{ in.}$ Shown is the length of the rocket motor and the section lengths/bulkhead locations. The missile is divided into the nose, forebody, payload bay, midbody, aftbody, and the tailcone sections of the missile. The wing geometry in the figure includes the wing span, sweep angle, location of the mean aerodynamic chord, length of the root chord and its location, and the length of the tip chord. The tail geometry shown in the figure includes the tail span sweep angle, location of the mean aerodynamic chord, length of the root chord, and the location of the root chord.

The rocket baseline missile weight and balance statement is given in Table 7.1, derived from Ref. 21. Note that the burnout weight $W_{BO} = 367 \text{ lb}$, the launch



Note: Dimensions in inches

Fig. 7.5 Drawing of the rocket baseline missile configuration (from Ref. 21).

Table 7.1 Mass properties of the rocket baseline missile

Component	Weight, lb	Center of gravity station, in.
1) Nose (radome)	4.1	12.0
3) Forebody	12.4	30.5
Guidance	46.6	32.6
2) Payload bay	7.6	54.3
Warhead	77.7	54.3
4) Midbody	10.2	73.5
Controls	61.0	75.5
5) Aftbody	0.0	—
Rocket motor case	47.3	107.5
Insulation	23.0	117.2
6) Tailcone	6.5	141.2
Nozzle	5.8	141.2
Fixed surfaces	26.2	137.8
Movable surfaces	38.6	75.5
Burnout total	367.0	76.2
Propellant	133.0	107.8
Launch total	500.0	84.6

weight $W_L = 500$ lb, and the propellant weight $W_P = 133$ lb. The center-of-gravity location is 84.6 in. from the nose tip at launch and 76.2 in. from the nose tip at burnout. There is a large forward movement (1.05 diameters) in the center of gravity during motor burn, resulting in excess static margin. The total weight of the aluminum airframe structure, wing and tail surfaces, and the steel motor case is 30% of the missile launch weight.

Reference 21 also provides the rocket baseline missile geometric data, material data, configuration reference data, and propulsion data. Table 7.2, based on Ref. 21, shows data on the body and movable wing surfaces. The material for the body airframe, wing, and tail structure is aluminum 2219-T81. The radome is pyroceram.

In Table 7.2 additional information is provided on the movable wings, fixed aft stabilizers, and the configuration reference values. The configuration reference area for the rocket baseline missile is $S_{Ref} = 0.349 \text{ ft}^2$. It is the body cross-sectional area. The configuration reference length of the rocket baseline missile is $l_{Ref} = d = 8 \text{ in.}$ (0.667 ft). It is the body diameter.

Also shown in Table 7.2 are additional configuration reference values, rocket motor performance data, and propellant characteristics. The pitch/yaw moment of inertia is 117.0 slugs- ft^2 at launch and 94.0 slugs- ft^2 at burnout. The rocket motor boost thrust and boost burn time are 5750 lb and 3.26 s, respectively. The sustain thrust and sustain burn time are 1018 lb and 10.86 s, respectively. Boost and sustain propellant weight are 84.8 and 48.2 lb, respectively.

Finally, the conclusion of the table, based on Ref. 21, provides data on the rocket motor case and nozzle. The structural material for the motor case and the nozzle housing is 4130 steel, with a yield strength of 170,000 psi. The rocket motor case length and thickness are 59.4 and 0.074 in., respectively. The nozzle expansion ratio and length are 6.2 and 4.9 in., respectively.

Table 7.2 Rocket baseline missile definition

Body	
Dome material	Pyroceam
Airframe material	Aluminum 2219-T81
Length, in.	143.9
Diameter, in.	8.0
Thickness, in.	0.16
Fineness ratio	17.99
Volume, ft ³	3.82
Wetted area, ft ²	24.06
Nozzle area, ft ²	0.078
Boattail fineness ratio	0.38
Nose fineness ratio	2.40
Nose bluntness	0.0
Boattail angle, deg	7.5
Movable surfaces (forward)	
Material	Aluminum 2219-T81
Area, ft ² (2 panels exposed)	2.55
Wetted area, ft ² (4 panels)	10.20
Aspect ratio (exposed)	2.82
Taper ratio	0.175
Root chord, in.	19.4
Tip chord, in.	3.4
Span, in. (exposed)	32.2
LE sweep, deg	45.0
MAC, in.	13.3
Thickness ratio	0.044
Section type	Modified double wedge
Section leading edge angle, deg	10.01
X MAC, in.	67.0
Y MAC, in. (from root chord)	6.2
Actuator rate limit, deg/s	360.0
Fixed surfaces (aft)	
Material	Aluminum 2219-T81
Modulus of elasticity, 10 ⁶ psi	10.5
Area, ft ² (2 panels exposed)	1.54
Wetted area, ft ² (4 panels)	6.17
Aspect ratio (exposed)	2.59
Taper ratio	0.0
Root chord, in.	18.5
Tip chord, in.	0.0
Span, in. (exposed)	24.0
LE sweep, deg	57.0
MAC, in.	12.3
Thickness ratio	0.027

(continued)

Table 7.2 Rocket baseline missile definition (continued)

Section type	Modified double wedge
Section leading edge angle, deg	6.17
X MAC, in.	131.6
Y MAC, in. (from root chord)	4.0
Reference values	
Reference area, ft ²	0.349
Exit diameter, in.	3.78
Reference length, ft	0.667
Moment of inertia at launch, slugs·ft ²	117.0
Moment of inertia at burnout, slugs·ft ²	94.0
Rocket motor performance (standard temperature and pressure)	
Burning time, s (boost/sustain)	3.26/10.86
Maximum pressure, psi	2042
Average pressure, psi (boost/sustain)	1769/301
Average thrust, lbf (boost/sustain)	5750/1018
Total impulse, lbf-s (boost/total)	18720/29800
Specific impulse, lbf-s/lbm (boost/sustain)	250/230.4
Propellant	
Weight, lbm (boost/sustain)	84.8/48.2
Flame temperature at 1000 psi, °F	5282/5228
Propellant density, lbm/in. ³	0.065
Characteristic velocity, ft/s	5200
Burn rate at 1000 psi, in./s	0.5
Burn rate pressure exponent	0.3
Burn rate sensitivity with temperature, % / °F	0.10
Pressure sensitivity with temperature, % / °F	0.14
Rocket motor case	
Yield strength, psi	170,000
Material	4130 Steel
Modulus of elasticity, psi	29.5×10^6 psi
Length, in.	59.4
Outside diameter, in.	8.00
Thickness, in. (minimum)	0.074
Burst pressure, psi	3140
Volumetric efficiency	0.76
Dome ellipse ratio	2.0
Nozzle	
Housing material	4130 Steel
Exit geometry	Contoured (equiv. 15°)
Throat area, in. ²	181
Expansion ratio	6.2
Length, in.	4.9

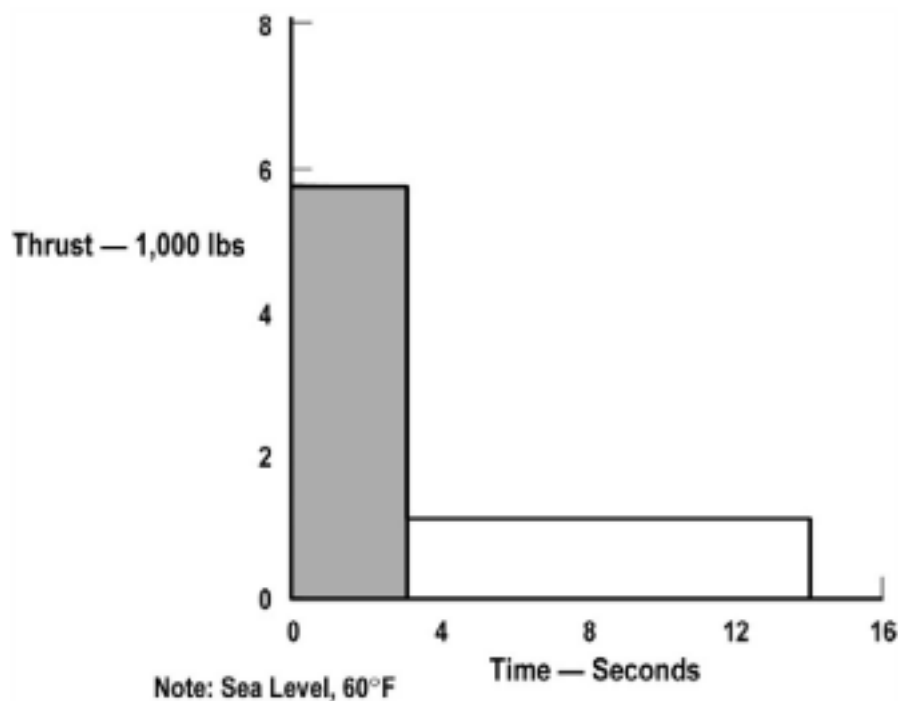


Fig. 7.6 Rocket baseline missile has a boost-sustain thrust-time history.

A graph of the rocket baseline thrust-time history is shown in Fig. 7.6. The boost thrust is 5.6 times the sustain thrust (5750 vs 1018 lb). The sustain burn time is 3.3 times the boost burn time (10.86 vs 3.26 s).

Figure 7.7a from Ref. 21 shows the rocket baseline missile pitching moment and normal force coefficients as a function of angle of attack and Mach number. The figure is based on undeflected control surfaces. Note that the pitching moment coefficient and normal force coefficient decrease with increasing supersonic Mach number. The reference center-of-gravity location for the aerodynamic data is 75.7 in. from the nose tip, slightly forward of the burnout center of gravity.

Figure 7.7b shows other aerodynamic data consisting of the rocket baseline missile normal force derivative due to control surface deflection, zero-lift drag coefficient, corrections to the axial force coefficient due to control surface deflection and angle of attack, and pitching moment derivative due to control surface deflection. The power-off (coast) drag is higher because of the additional drag from the base pressure. Note the decrease in the aerodynamic coefficients and derivatives with increasing supersonic Mach number.

The maximum forward flight-range performance for an assumed Mach 0.7 launch and Mach 1.5 termination is shown in Fig. 7.8, based on Ref. 21. The flight range increases with high altitude launch because of the lower drag and higher L/D at high altitude. For sea-level flight the sustain thrust Mach number is Mach 1.5, the same as the end-of-boost Mach number.

Off-boresight maneuverability performance of the rocket baseline missile is shown in Fig. 7.9 from Ref. 21. The best turn performance is at low altitude with high angle of attack. Note that the missile envelope shown in the figure is not constrained by seeker gimbal angle or a requirement for lock-on before launch. A typical seeker gimbal angle limit (e.g., ± 30 deg) and a requirement for lock-on before launch would limit the missile off-boresight envelope to about ± 30 deg. A seeker with high gimbal angle (e.g., ± 90 deg) and a lock-on after launch capability facilitate a large off-boresight envelope.

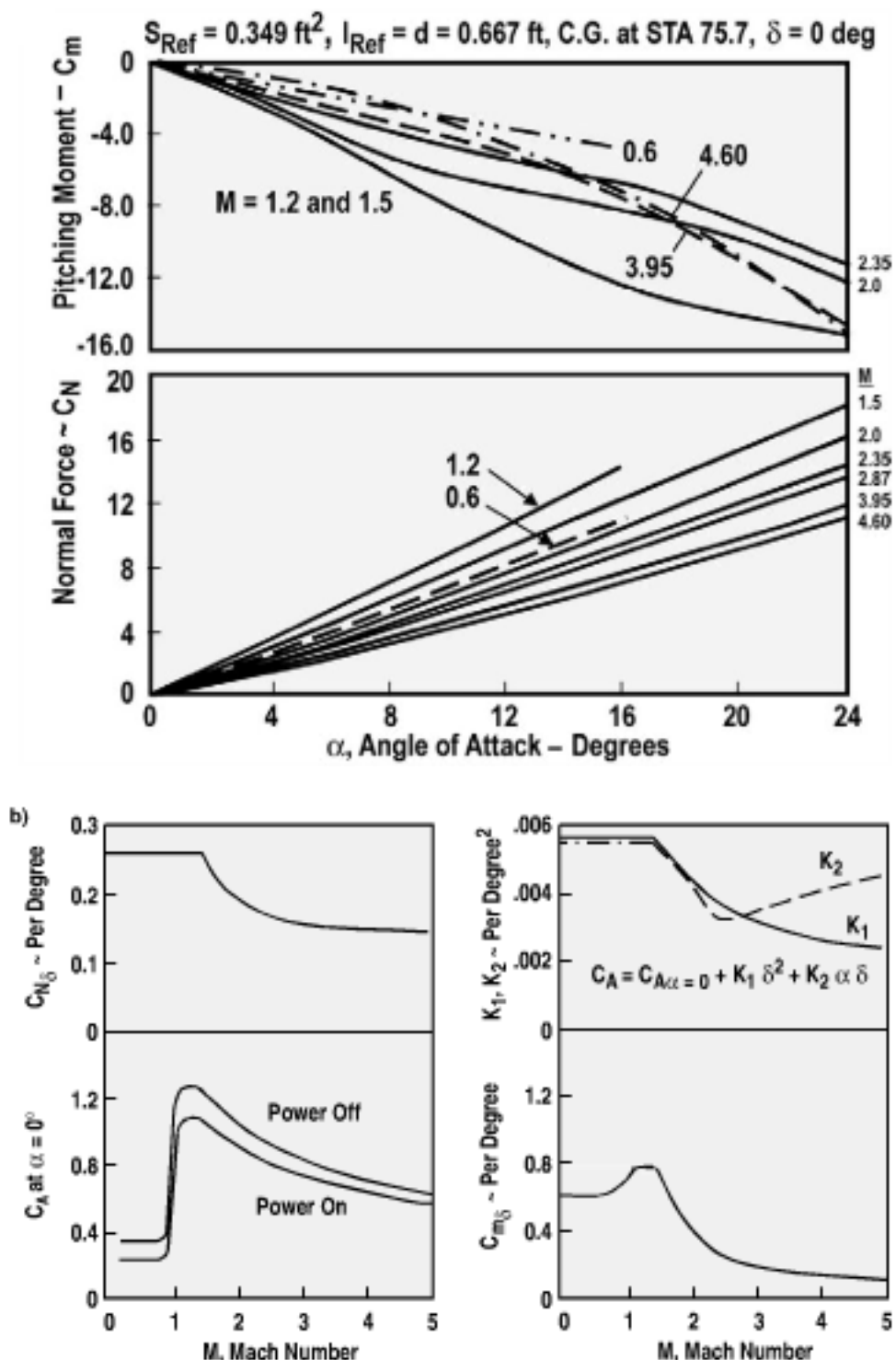


Fig. 7.7 Rocket baseline missile aerodynamic characteristics (from Ref. 21): a) pitching moment and normal force coefficients as a function of angle attack and Mach number; b) other aerodynamic data as a function of Mach number.

A flight performance sensitivity study was conducted of the rocket baseline missile to determine the most significant parameters and the required accuracy for prediction methods. Note from Fig. 7.10 that the flight range is most sensitive to specific impulse, propellant weight, zero-lift drag coefficient, drag due to lift, and static margin.

The prediction methods for specific impulse, zero-lift drag coefficient, and drag due to lift usually have sufficient accuracy (e.g., $\pm 5\%$, 1σ) for conceptual

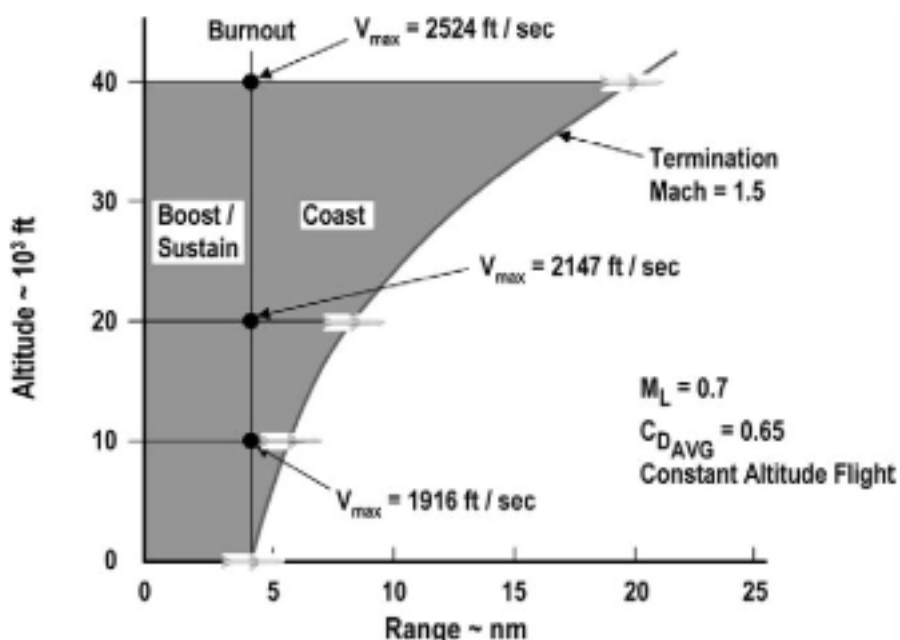


Fig. 7.8 High altitude launch enhances the rocket baseline flight range (from Ref. 21).

design. However, there is often large uncertainty in predicting the subsystem packaging volume available for the propellant weight and predicting the static margin. Inboard profile drawings and wind-tunnel tests are required to reduce the design uncertainty.

The assumptions for the conceptual design analysis of the boost-sustain flight trajectory are one degree of freedom, constant altitude, and thrust greater than weight. The simplified equation for axial acceleration based on thrust, drag, and weight is

$$n_X = (T - D)/W$$

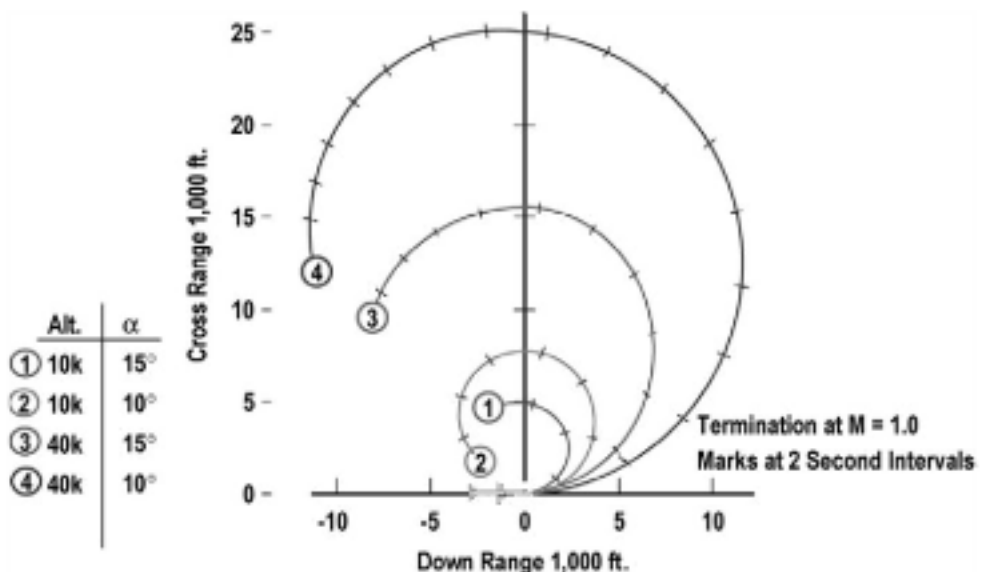


Fig. 7.9 Low-altitude launch and maneuvers at high angles of attack enhance rocket baseline turn performance (from Ref. 21).

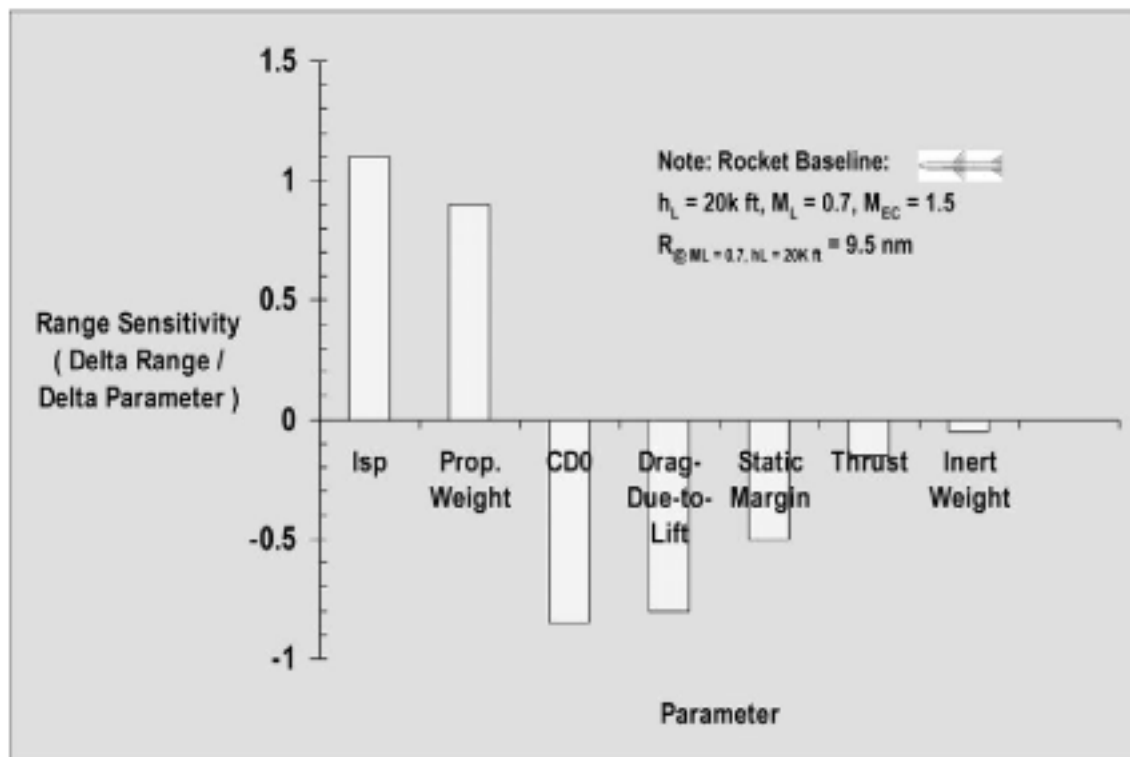


Fig. 7.10 Rocket baseline missile flight range is driven by the parameters of specific impulse, propellant weight, drag, and static Margin.

Missile weight varies with burn rate and time

$$W = W_L - W_P t / t_B$$

Missile drag is approximated by

$$D = C_D q S$$

Figure 7.11 shows the rocket baseline missile axial acceleration during the boost, sustain, and coast phases of flight. During boost the acceleration is positive (increasing flight velocity), during sustain the acceleration is nearly zero (nearly constant flight velocity), and during coast the acceleration is negative (decreasing flight velocity). The assumed flight conditions are:

- 1) Total time of flight $t_f = 24.4 \text{ s}$ (required to provide F-pole range).
- 2) Launch Mach number $M_L = 0.8$.
- 3) Launch altitude $h_L = 20,000 \text{ ft}$.
- 4) Boost thrust $T_B = 5750 \text{ lb}$.
- 5) Boost time $t_B = 3.26 \text{ s}$.
- 6) Sustain thrust $T_S = 1018 \text{ lb}$.
- 7) Sustain time $t_S = 10.86 \text{ s}$.
- 8) Drag $D = 99 \text{ lb}$ at launch (Mach 0.8).
- 9) Drag $D = 1020 \text{ lb}$ during sustain (Mach 2.1).
- 10) Launch weight $W_L = 500 \text{ lb}$.
- 11) Propellant weight $W_P = 133 \text{ lb}$.

Note that the aerodynamic efficiency of the rocket baseline missile is relatively low for most of the flight conditions shown in the figure. For the 1-g constant

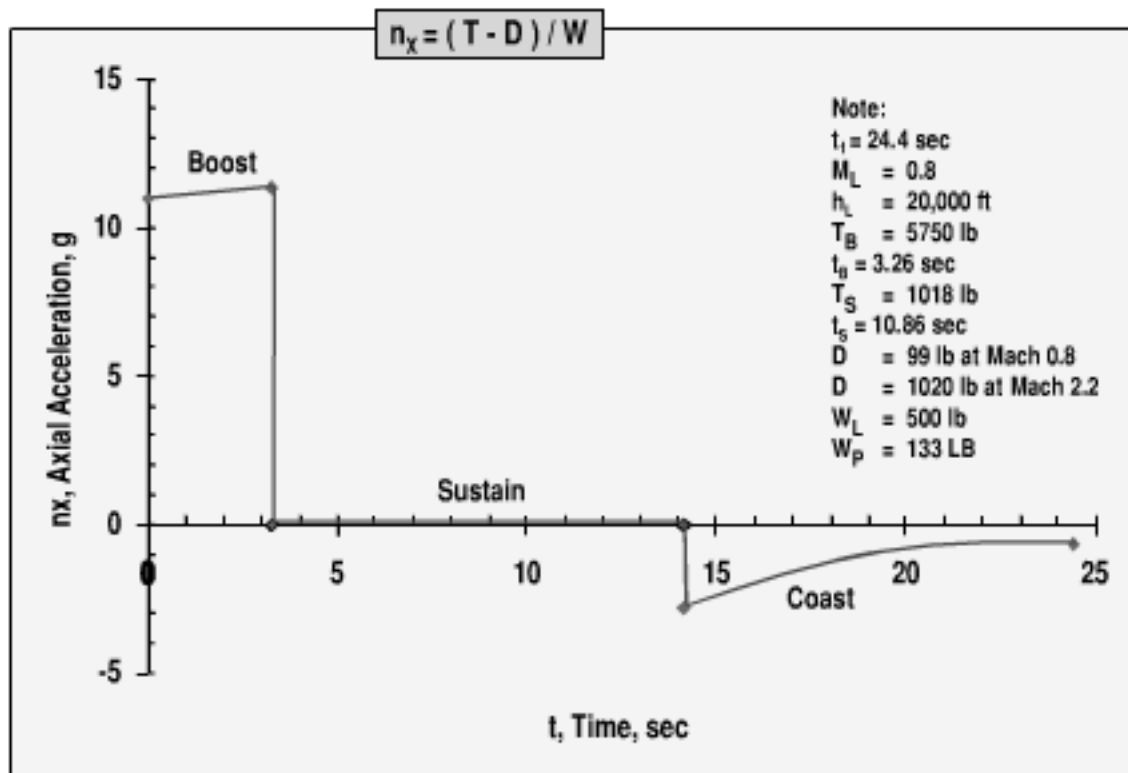


Fig. 7.11 Example of rocket baseline axial acceleration.

altitude flyout, the lift is equal to the missile weight. At the Mach 0.8, 20,000-ft altitude launch condition, the L/D is relatively high ($L/D = 500/99 = 5.1$). At the end of the Mach 2.1 sustain, the L/D is very low ($L/D = 367/1020 = 0.36$). For most of the flight the L/D is much lower than $(L/D)_{\text{Max}}$. The rocket baseline missile would have to fly at much higher altitude and nearly constant (cruise) velocity to fly at $(L/D)_{\text{Max}}$.

The incremental velocity during boost (ΔV) is a function of launch weight W_L , propellant weight W_P , thrust T , average drag D_{AVG} , and specific impulse I_{SP} . The velocity at the end of coast V_{EC} is a function of the begin-of-coast velocity V_{BC} , burnout weight W_{BO} , atmospheric density ρ , reference area S_{Ref} , zero-lift drag coefficient C_{D_0} , and coast time t_C . Figure 7.12 shows the rocket baseline missile velocity vs time history for the flight phases of boost, sustain, and coast. The launch conditions are Mach 0.8, 20,000 ft in altitude. The peak (sustain) velocity is 2151 ft/s. The velocity at the end of 24.4 s time of flight is 1588 ft/s. Note that the missile has a rapid velocity increase during boost, nearly constant velocity during sustain, and a velocity decay during coast.

The rocket baseline missile flight range is shown in Fig. 7.13 as a function of time. The launch conditions are Mach 0.8, 20,000 ft in altitude. Note that the flight range at a time of flight $t_f = 24.4$ s exceeds the requirement by 15% (7.7 vs 6.7 n miles). The rocket baseline achieves the required flight range of 6.7 n miles at a time that is 14% shorter than the required time of flight (21 vs 24.4 s).

The total flight range R is the sum of the incremental flight range during boost (ΔR_{boost}), the incremental range during sustain ($\Delta R_{\text{sustain}}$), and the incremental range during coast (ΔR_{coast}). The incremental range during boost is a function of the propellant weight W_P , launch weight W_L , specific impulse I_{SP} , thrust T ,

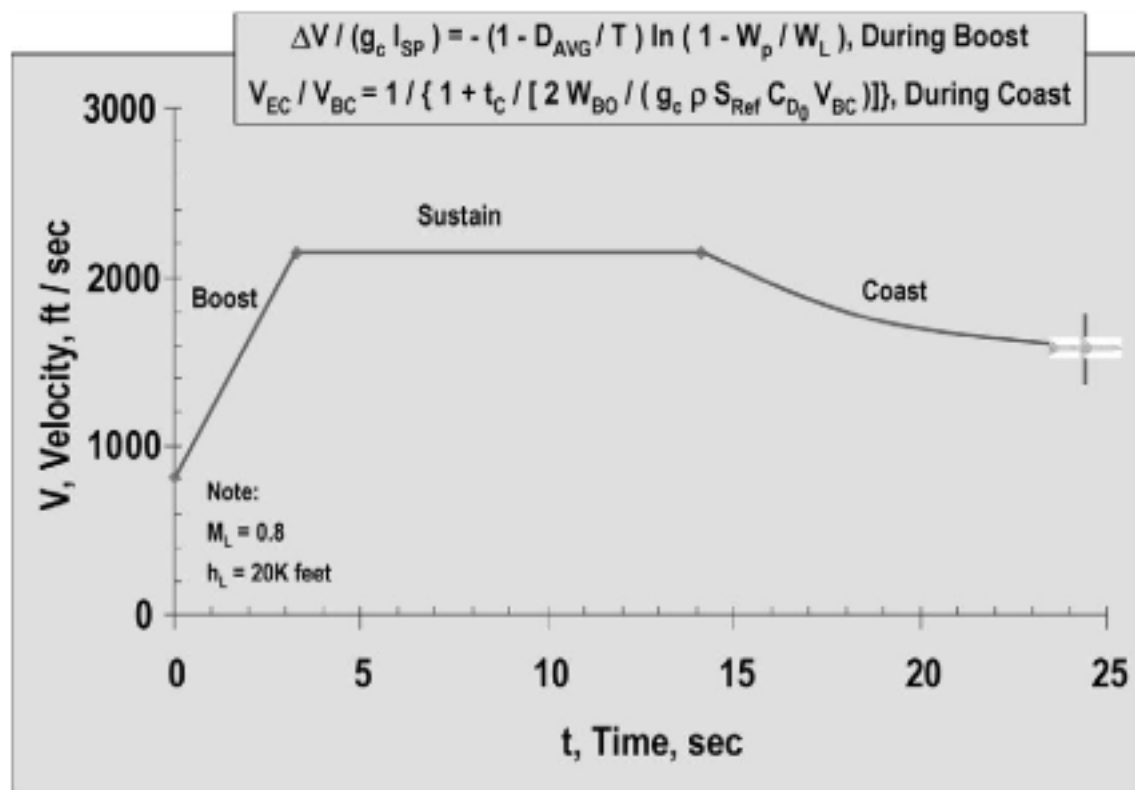


Fig. 7.12 Example of rocket baseline missile velocity vs time.

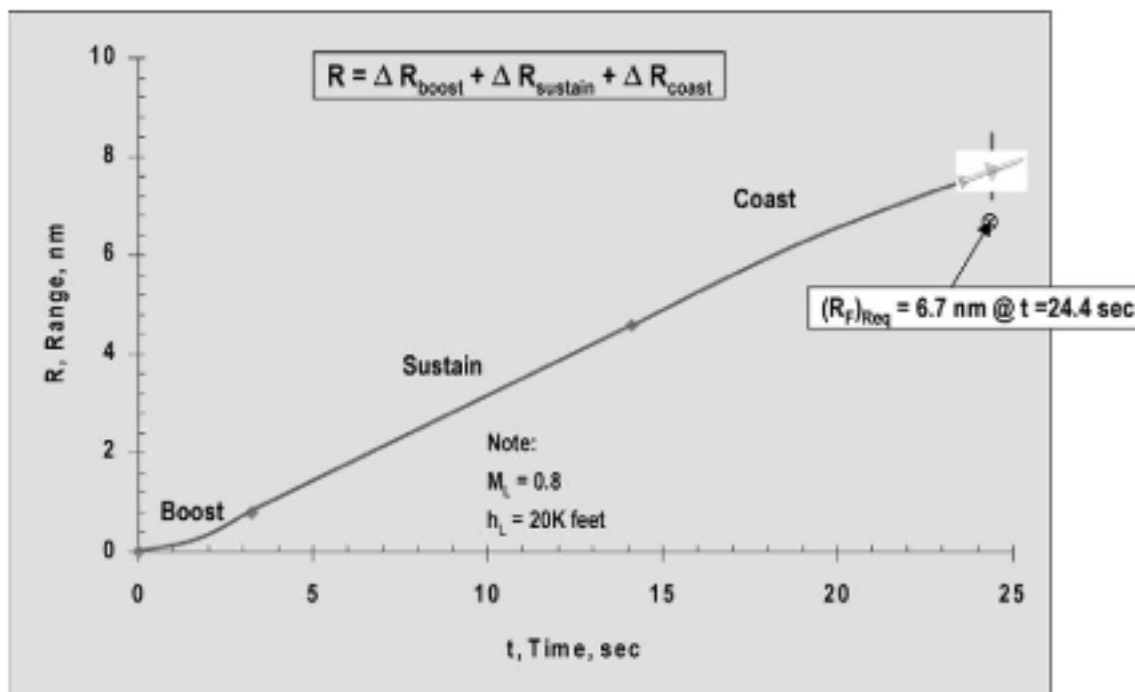


Fig. 7.13 Range and time to target of rocket baseline missile exceed the requirements.

average drag D_{AVG} , launch velocity V_L , and the boost time t_B . The equation for the incremental range during boost is

$$\begin{aligned}\Delta R_{\text{boost}} &= (V_L + \Delta V/2)t_B \\ &= \{V_L + [-g_c I_{\text{SP}}(1 - D_{\text{AVG}}/T) \ln(1 - W_p/W_L)]/2\}(t_B) \\ &= [820 - 32.2(250)(1 - 635/5750) \ln(1 - 84.8/500)/2](3.26) \\ &= 4842 \text{ ft} = 0.79 \text{ n mile}\end{aligned}\quad (3.26)$$

The incremental range during sustain ($\Delta R_{\text{sustain}}$) is a function of the propellant weight W_P , missile weight at the begin of sustain W_{BS} , specific impulse I_{SP} , thrust T , average drag D_{AVG} , velocity at the begin of sustain V_{BS} , and the sustain burn time t_S . The equation for the incremental velocity during sustain is

$$\begin{aligned}\Delta R_{\text{sustain}} &= (V_{BS} + \Delta V/2)t_S \\ &= \{V_{BS} + [-g_c I_{\text{SP}}(1 - D_{\text{AVG}}/T) \ln(1 - W_p/W_{BS})]/2\}(t_S) \\ &= [2151 - 32.2(230.4)(1 - 1020/1018) \ln(1 - 48.2/415.2)/2](10.86) \\ &= 23,350 \text{ ft} \\ &= 3.84 \text{ n miles}\end{aligned}$$

The incremental range during coast (ΔR_{coast}) is a function of the begin-of-coast velocity V_{BC} , burnout weight W_{BO} , atmospheric density ρ , reference area S_{Ref} , zero-lift drag coefficient C_{D_0} , and the coast time t_C . The equation for the incremental range during coast is

$$\begin{aligned}\Delta R_{\text{coast}} &= \left[2W/\left(g_c \rho S_{\text{Ref}} C_{D_0}\right)\right] \ln\{1 + t_C/[2W/(g_c \rho S_{\text{Ref}} C_{D_0} V_{BC})]\} \\ &= \{2(367)/[(32.2)(0.00127)(0.349)(0.9)]\} \\ &\quad \ln\{1 + 10.28/[(2)(367)/[(32.2)(0.00127)(0.349)(0.9)(2150)]]\} \\ &= 18,685 \text{ ft} \\ &= 3.07 \text{ n miles}\end{aligned}$$

Finally, the total flight range for 24.4 s of flight is

$$R = \Delta R_{\text{boost}} + \Delta R_{\text{sustain}} + \Delta R_{\text{coast}} = 0.79 + 3.84 + 3.07 = 7.7 \text{ n miles}$$

7.2 Wing Sizing for Maneuverability

The next sizing example for the rocket baseline missile is wing sizing to meet a maneuverability requirement. In this example, the wing size is evaluated against an assumed maneuverability requirement of 30 g, required for small miss distance. Also assume flight conditions of Mach 2, 20,000 ft in altitude, and 367 lb in weight (burnout).

The maximum local angle of attack of the rocket baseline missile wing is 22 deg, established by wing stall. The relationship of the local wing angle of attack to the

body angle of attack is

$$\alpha_{\text{Wing}} = \alpha'_{\text{Max}} = (\alpha + \delta)_{\text{Max}} = 22 \text{ deg.}$$

The rocket baseline missile static margin is $\alpha = 0.75\delta$, giving $\alpha_{\text{Body}} = \alpha_{\text{Tail}} = 9.4 \text{ deg}$. The maneuverability contribution from the isolated body is

$$(n_Z)_{\text{Body}} = q S_{\text{Ref}} (C_N)_{\text{Body}} / W = 2725(0.349)(1.28)/367 = 3.3g \text{ (from body)}$$

The aerodynamic contribution from the tail at Mach 2, with an angle of attack $\alpha_{\text{Tail}} = 9.4 \text{ deg}$, is $(C_N)_{\text{Tail}} (S_{\text{Ref}}/S_{\text{Tail}}) = 0.425$. The maneuverability contribution from the isolated tail is

$$\begin{aligned} (n_Z)_{\text{Tail}} &= q S_{\text{Tail}} [(C_N)_{\text{Tail}} (S_{\text{Ref}}/S_{\text{Tail}})] / W \\ &= 2725(1.54)(0.425)/367 = 4.8g \text{ (from tail)} \end{aligned}$$

The wing must be designed to meet the shortfall in maneuverability. Compute

$$(n_Z)_{\text{Wing}} = (n_Z)_{\text{Required}} - (n_Z)_{\text{Body}} - (n_Z)_{\text{Tail}} = 30 - 3.3 - 4.8 = 21.9g$$

The aerodynamic contribution from the wing at Mach 2, with an effective angle of attack of $\alpha_{\text{Wing}} = 22 \text{ deg}$, is $(C_N)_{\text{Wing}} (S_{\text{Ref}}/S_{\text{Wing}}) = 1.08$. The required wing area is therefore

$$\begin{aligned} S_W &= (n_Z)_{\text{Wing}} W / \{q[(C_N)_{\text{Wing}} (S_{\text{Ref}}/S_{\text{Wing}})]\} \\ &= 21.9(367) / [(2725)(1.08)] = 2.76 \text{ ft}^2 \end{aligned}$$

Note that the wing area of the rocket baseline missile $(S_W)_{\text{RocketBaseline}} = 2.55 \text{ ft}^2$. The rocket baseline requires about 8% additional wing area to satisfy the maneuverability requirement of 30 g at Mach 2, 20,000 ft in altitude. Although an 8% larger wing also increases the missile weight by about 1% (367 to 370.1 lb), the increased weight of 3.1 lb has a negligible effect on missile maneuverability, speed, and flight range.

7.3 Weight and Miss Distance Harmonization

The last example of sizing for the rocket baseline missile is weight/miss distance harmonization. A sensitivity study was conducted to determine which parameters have the greatest impact on weight and miss distance for the rocket baseline missile. Table 7.3 from Ref. 22 shows that there is strong synergistic benefit in reducing both weight and miss distance by increasing the nozzle expansion ratio, increasing the motor volumetric efficiency, and increasing the motor characteristic velocity. For example, a 10% increase in motor volumetric efficiency (0.76 to 0.84) reduces the missile weight by 14% (500 to 432 lb) and also reduces the miss distance by 45% (62 to 34 ft). In addition to the strong synergistic impact of nozzle expansion ratio, motor volumetric efficiency, and characteristic velocity, other sensitivities that have a strong impact on either weight or miss distance, but not a strong impact on both, are reducing the number of tails, reducing the number of wings, reducing the static margin, increasing the wing sweep, increasing the nose fineness ratio, decreasing the boattail fineness ratio, increasing the sustain thrust, and moving the wing forward.

Table 7.3 Rocket baseline missile parametric weight and miss distance sensitivity (from Ref. 22)

Parameter	Baseline	Sensitivity	W*	σ^*
		variation		
Fixed surface number of panels	4	3	+0.054	+0.100 ^a
Movable surface number of panels	4	2	+0.071	+0.106 ^a
Design static margin	0.40	0.30	+0.095	+0.167 ^a
Wing movable surface sweep, deg	45.0	49.5	-0.205 ^a	+0.015
Tail fixed surface thickness ratio	57.0	60.0	+0.027	+0.039
Wing movable surface thickness ratio	0.044	0.034	+0.041	+0.005
Nose fineness ratio	2.4	2.6	-0.016	-0.745 ^a
Rocket chamber sustain pressure, lb/in. ²	301	330	-0.076	-0.045
Boattail fineness ratio	0.38	0.342	+0.096	+0.140 ^a
Nozzle expansion ratio	6.2	6.82	-0.114 ^b	-0.181 ^a
Motor volumetric efficiency	0.76	0.84	-0.136 ^b	-0.453 ^b
Propellant density, lb/in. ³	0.065	0.084	-0.062	+0.012
Boost thrust, lb	5,750	6,325	+0.014	-0.018
Sustain thrust, lb	1,018	1,119	+0.088	+0.246 ^a
Characteristic velocity, ft/s	5,200	5,720	-0.634 ^b	-0.767 ^b
Wing location, percent total length	47.5	42.75	+0.181 ^a	-0.036

Baseline: weight = 500 lb, miss distance = 62.3 ft
 W^* = weight sensitivity for parameter variation = $\Delta W/W$
 σ^* = miss distance sensitivity for parameter variation = $\Delta\sigma/\sigma$

^aStrong impact. ^bSynergy, with strong impact.

Missile parameters were selected that resulted in the lightest weight and smallest miss distance missiles without exceeding the state of the art. These parameters and their values for the four missiles (baseline, lightest weight, smallest miss distance, and harmonized missile) are shown in Table 7.4 from Ref. 22. The harmonized missile compared to the baseline missile has the following characteristics:

- 1) Higher fineness nose (2.6 vs 2.4).
- 2) Higher expansion nozzle (15 vs 6.2).
- 3) Higher sustain pressure (1000 vs 301 psi).
- 4) Smaller boattail fineness (0.21 vs 0.38).
- 5) Fewer wing panels (two vs four).
- 6) Fewer tail panels (three vs four).
- 7) Higher wing leading edge sweep (55 vs 45 deg).
- 8) Smaller static margin at launch (0 vs 0.4 diameter).
- 9) Higher propellant density (0.084 vs 0.065 lb/in.³).
- 10) Higher propellant loading for higher motor volumetric efficiency (84 vs 76%).

The measures of merit comparison of the harmonized missile with the baseline missile shows that the harmonized missile has lighter weight (390 vs 500 lb), smaller miss distance (17 vs 62 ft), and shorter length (115 vs 144 in.). A

Table 7.4 Minimum weight, minimum miss, and harmonized missile properties (from Ref. 22)

Parameter	Baseline value	Missile configured for minimum		
		Weight	Miss distance	Harmonized
Judicious changes				
Boost thrust, lb	5,750	3,382	3,382	3,382
Wing location, percent of total length to 1/4 MAC	47.5	47	44	46
Wing taper ratio	0.18	0.2	0.2	0.2
Nose fineness ratio	2.4	3.2	2.55 ^a	2.6
Nose blunting ratio	0.0	0.05	0.05	0.05
Expansion ratio	6.2	15 ^a	15	15
Sustain chamber pressure, psi	301	1,000 ^a	1,000	1,000
Boattail fineness ratio	0.38	0.21	0.21 ^a	0.21
Tail leading edge sweep, deg	57	50	50	50
Technology limited changes				
No. wing panels	4	2	2 ^a	2
No. tail panels	4	3	3 ^a	3
Wing thickness ratio	0.044	0.030	0.030	0.030
Wing leading edge sweep, deg	45	55 ^a	55	55
Static margin at launch, diameter	0.4	0.0	0.0 ^a	0.0
Propellant density, lb/in. ³	0.065	0.084 ^a	0.084	0.084
Motor volumetric efficiency	0.76	0.84 ^a	0.84	0.84
Measures of Merit				
Total weight, lb	500	385.9 ^a	395.0	390.1
Miss distance, ft	62.3	63.1	16.2 ^a	16.6
Time to target, s	21.6	23.8	23.6	23.8
Length, in.	144	112.7 ^a	114.7	114.9
Mach no. at burnout	2.20	2.08	2.09	2.07
Weight of propellant, lb	133	78.3 ^a	85.4	85.9
Wing area, in. ²	368.6	175.5 ^a	150.7	123.8
Tail area, in. ²	221.8	109.1 ^a	134.5	112.0

^aValue of driving parameter.

comparison of the harmonized missile with the minimum weight missile shows that the harmonized missile is only slightly heavier (390 vs 386 lb). It is also slightly longer (115 vs 113 in.). Comparing the harmonized missile with the minimum miss distance missile shows that the harmonized missile has only slightly larger miss distance (17 vs 16 ft). The harmonized missile was selected based on synergistic parameters for weight and miss distance that are within the state of the art.

The configuration of the harmonized missile, which has lighter weight and smaller miss distance, is compared with the baseline missile in Fig. 7.14 from Ref. 22. Note the 22% smaller size of the harmonized missile compared to the baseline. The harmonized missile is also 22% lighter in launch weight and has a

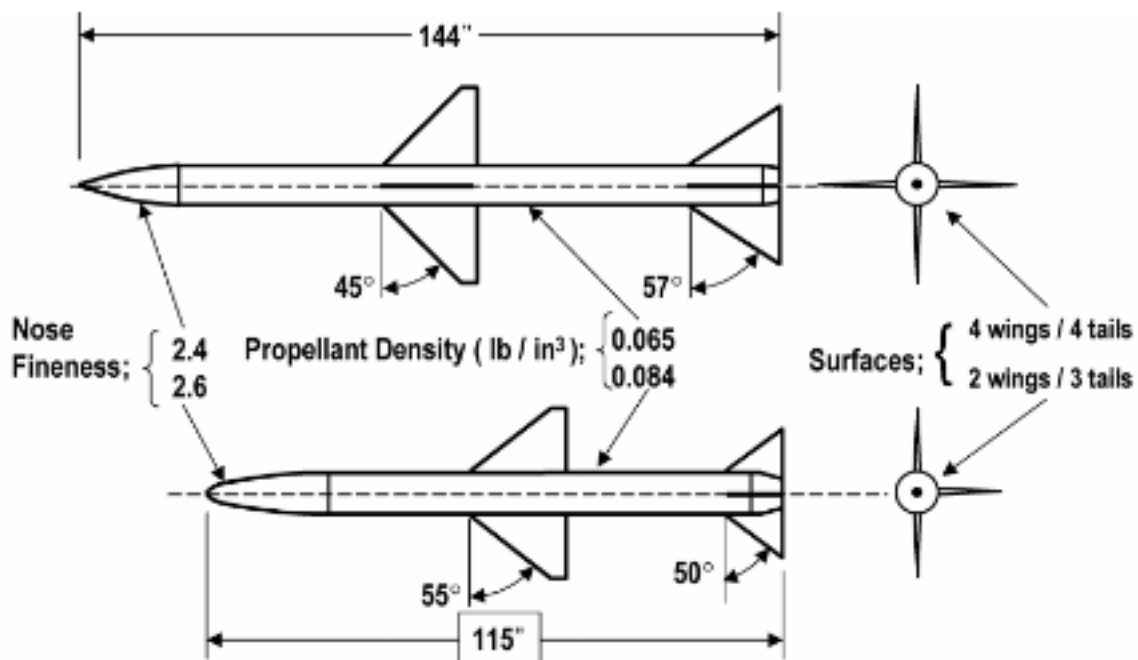


Fig. 7.14 Baseline missile vs harmonized missile (from Ref. 22).

73% reduction in miss distance. A slight disadvantage for the harmonized missile is 10% longer time of flight for a flight range of 6.7 n miles. However, the time of flight of the harmonized missile still meets the F-Pole requirement of 24.4 s to 6.7 n miles.

7.4 Ramjet Missile Range Robustness

A generic baseline of a ramjet missile, derived from the Advanced Strategic Air Launched Missile (ASALM), is used to illustrate the typical characteristics of ramjet powered missiles. Sizing examples are presented for flight range robustness, alternative propulsion systems, alternative fuels, and surface impact velocity.

The baseline ramjet engine is sized for cruise at Mach numbers up to Mach 4.0 at 80,000 ft in altitude and up to Mach 3.0 at sea level. An integral solid rocket motor boosts the missile to a ramjet thrust takeover Mach number of about 2.5. The rocket motor case becomes the ramjet combustor after rocket motor burnout. Unlike the rocket missile baseline, the ramjet missile baseline is able to cruise at constant velocity and high altitude, providing an aerodynamic efficiency near $(L/D)_{\text{Max}}$.

The baseline ramjet configuration is shown in Fig. 7.15. It is a chin inlet integral rocket ramjet based on Ref. 21. The aerodynamic configuration has a conical nose with a half-angle of 17.7 deg, followed by a nearly circular cross-sectional body. The average diameter $d = 20.375$ in. The ASALM diameter and length were set by the diameter and length constraints to efficiently package eight ASALM missiles with the B-1 rotary launcher/weapons bay. Flight control is provided by four tail surfaces. The tails are folded for compressed carriage in the weapons bay. Tail span after deployment is 41.4 in. The missile uses bank-to-turn maneuvering to minimize the sideslip air flowing into the inlet. The fuel is liquid hydrocarbon RJ-5 ramjet fuel, packaged in a fuel tank around the inlet duct. Shown in the figure are the section bulkhead locations and lengths for the nose, forebody, payload bay,

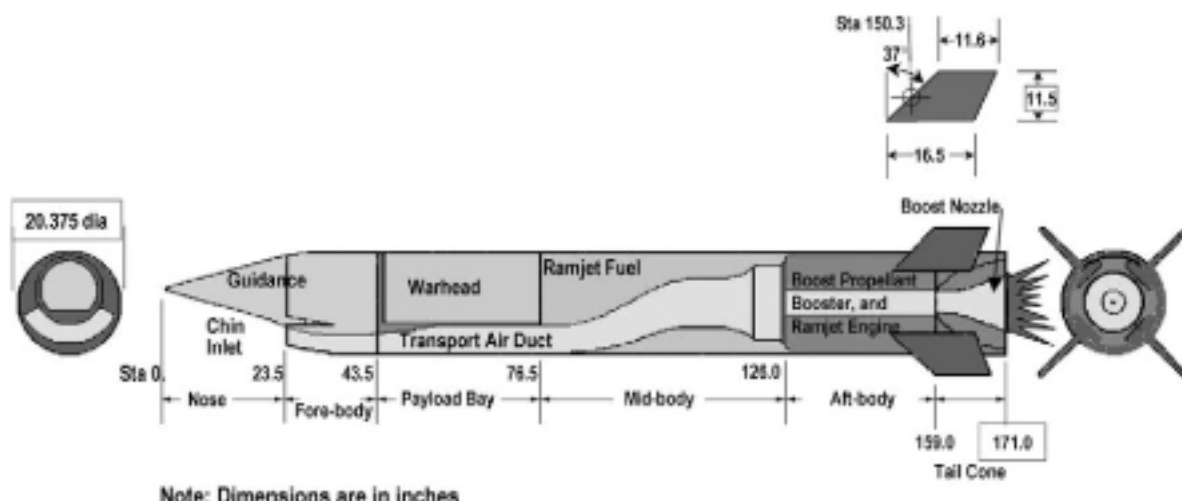


Fig. 7.15 Ramjet baseline is a chin inlet integral rocket ramjet (IRR) (from Ref. 21).

midbody, aftbody, and tail cone sections. Also shown are frontal and aft views of the nose and tail sections. Finally, a planform view is provided of the tail geometry, showing the tail leading edge sweep, root chord location and length, tip chord length, and the tail span.

Shown in Table 7.5 from Ref. 21 is a weight and balance statement of the ramjet baseline. The launch weight $W_L = 2230$ lb and the end of cruise weight $W_{EC} = 1263$ lb. The fuel weight $W_f = 476$ lb and the booster propellant weight $W_P = 449$ lb. There is a small forward movement (0.07 diameter) in its center of gravity during the ramjet cruise portion of flight. The center of gravity at the start of cruise is 83.2 in. from the nose tip. The center of gravity at the end of cruise is 81.8 in. from the nose tip. The total weight of the titanium airframe structure, inlet, and fins is 17% of the launch weight.

The ramjet baseline geometric and material definition of the inlet, body, and tails are from Ref. 21. Shown in Table 7.6 are data on the inlet, body, and tails. The missile has a hot structure. The body structure and inlet are uninsulated titanium with internal insulation to protect the subsystems. The tails are made of a titanium built-up structure. A ballistic actuator located inside each tail unfolds the tail after the missile separates from the launch aircraft. The combustor is constructed from Inconel super alloy with internal insulation. The dome material is silicon nitride.

Also shown in Table 7.6 are data on the missile reference geometry parameters. The ramjet baseline missile reference area $S_{Ref} = 2.264 \text{ ft}^2$ is based on the cross-sectional area. The reference length $l_{Ref} = d_{Ref} = 1.698 \text{ ft}$ is based on an equivalent circular diameter of the cross-sectional area.

The definitions of the propulsion parameters and the flowpath are shown in Fig. 7.16 based on Ref. 21. The ramjet baseline inlet captures the air that flows over one-third of the nose (120 deg). Note the thrust-drag accounting system, where the nose corrected drag accounts for the air captured by the inlet. The flowpath is described by stations 1 (freestream conditions) through 6 (nozzle exit). The largest flowpath areas are located at the subsonic combustion stations 3 (flame holder plane) and 4 (combustor exit), each having an area of 287 in.². The other areas of the flowpath are the inlet throat (41.9 in.²), diffuser exit (77.3 in.²), nozzle throat (103.1 in.²), and the nozzle exit (233.6 in.²). The smallest area in the flowpath is the inlet throat, which is 15% of the combustor area.

Table 7.5 Mass properties of the ramjet baseline missile

Component	Weight, lb	CG Sta, in
Nose	15.9	15.7
Forebody	42.4	33.5
Guidance	129.0	33.5
Payload bay	64.5	60.0
Warhead	510.0	60.0
Midbody	95.2	101.2
Inlet	103.0	80.0
Electrical	30.0	112.0
Hydraulic	20.0	121.0
Fuel Distribution	5.0	121.0
Aftbody	44.5	142.5
Engine	33.5	142.5
Tailcone	31.6	165.0
Exit duct	31.0	165.0
Controls	37.0	164.0
Fins, 4	70.0	157.0
End of cruise	1262.6	81.8
Ramjet fuel, 11900 in. ³	476.0	87.0
Start of cruise	1738.6	83.2
Boost Nozzle, ejected	31.0	164.0
Frangible port	11.5	126.0
End of boost	1781.1	84.9
Boost propellant	449.0	142.5
Booster ignition	2230.1	96.5

Axial force and normal force coefficients of the ramjet baseline are presented as a function of Mach number and angle of attack in Fig. 7.17a from Ref. 21. Note the decrease in the aerodynamic coefficients with increasing supersonic Mach number. Also note that the axial force is nearly equal to the zero-lift drag coefficient. The reference center of gravity for the aerodynamic data is 82.5 in. from the nose tip, representative of the cruise center of gravity.

Pitching moment coefficient of the ramjet baseline is presented in Fig. 7.17b from Ref. 21. Pitching moment is a function of Mach number and angle of attack. Again, the reference center of gravity location for the aerodynamic data is 82.5 in. from the nose tip. Note the small value of pitching moment and the relatively small variation with angle of attack and Mach number. This enhances the control effectiveness and reduces the trim drag of the missile.

Zero-lift drag coefficient and the stability and control derivatives of the ramjet baseline are presented as a function of Mach number (Fig. 7.17c). The zero-lift drag coefficient is based on power-on flight. Note the decrease of the zero-lift drag coefficient and the stability and control derivatives with increasing supersonic Mach number. The figure is from Ref. 21.

Net thrust of the ramjet baseline is shown in Fig. 7.18 as a function of Mach number and altitude for an equivalence ratio of 1 (i.e., stoichiometric combustion)

Table 7.6 Ramjet baseline missile definition

Inlet	
Type	Mixed compression
Material	Titanium
Conical forebody half-angle, deg	17.7
Ramp wedge angle, deg	8.36
Capture area, ft ²	0.79
Throat area, ft ²	0.29
Body	
Dome material	Silicon nitride
Airframe material	Titanium
Combustor material	Insulated inconel
Length, in.	171.0
Diameter, in.	20.375
Fineness ratio	8.39
Volume, ft ³	28.33
Wetted area, ft ²	68.81
Base area, ft ² (cruise)	0.58
Boattail fineness ratio	—
Nose half-angle, deg	17.7
Nose length, in.	23.5
Tail (Exposed)	
Material	Titanium
Area (2 panels), ft ²	2.24
Wetted area (4 panels), ft ²	8.96
Aspect ratio (exposed)	1.64
Taper ratio	
Root chord, in.	16.5
Span, in. (exposed)	23.0
LE sweep, deg	37.0
MAC, in.	
Thickness ratio	0.04
Section type	Modified double wedge
Section leading edge angle, deg	9.1
X MAC, in.	150.5
Y MAC, in. (from root chord)	5.4
Reference values	
Reference area, ft ²	2.264
Reference length, ft	1.698

and an assumed combustion temperature of 4000°R. The Mach number range is from 2 to 4 and the altitude range is from sea level to 80,000 ft. Note that the peak thrust is produced at about Mach 3.5. For conceptual design purposes, it is assumed that thrust is proportional to the equivalence ratio for values of $\varphi < 1$.

Specific impulse of the ramjet baseline is shown in Fig. 7.19 as a function of Mach number. The data are based on an assumed combustion temperature of

$(C_{D_0})_{\text{Nose Corrected}} = (C_{D_0})_{\text{Nose Uncorrected}} \times (1 - A_c/S_{\text{REF}})$	
A_c	Inlet capture area
A_{IT}	Inlet throat area
S_{REF}	Reference area
A_s	Nozzle throat area
I_{SP}	Specific impulse
ϕ	Equivalence ratio — operating fuel / air ratio divided by fuel / air ratio for stoichiometric combustion

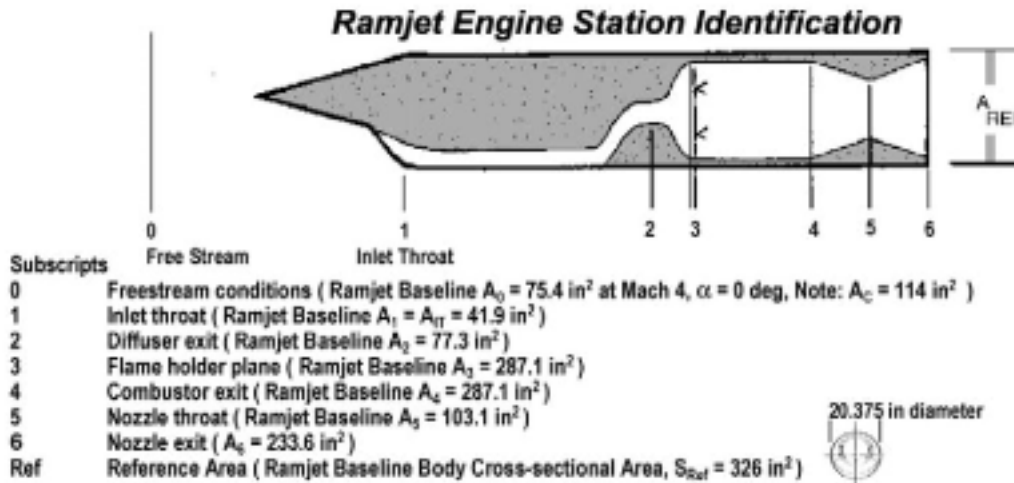


Fig. 7.16 Engine nomenclature and flowpath geometry for ramjet baseline (from Ref. 21).

4000°R and fuel-to-air ratio less than or equal to stoichiometric. The peak value of specific impulse occurs at a Mach number of about Mach 3.5. The specific impulse of the ramjet baseline is nearly independent of altitude if the equivalence ratio is less than or equal to stoichiometric.

The performance of the rocket boost motor is shown in Fig. 7.20 from Ref. 21. The booster thrust and burn time are 22,000 lb and 5.05 s, respectively. The booster thrust-to-launch-weight ratio is 9.9:1. A high thrust-to-weight ratio is required to provide safe separation from the launch aircraft and to minimize the propellant that is required for boost to the ramjet thrust takeover Mach number (about Mach 2.5). The incremental flight range during boost is about 1.3 n miles for a launch Mach number of 0.8. The end-of-boost burnout Mach number varies from Mach 2.3 to Mach 2.7, depending on the launch altitude.

Flight-range performance for constant altitude flight is shown in Fig. 7.21 from Ref. 21. Note that the ramjet is much more efficient in high-altitude flight than in low-altitude flight. Also note that the Breguet range equation prediction of flight range has about 10% error in predicting the flight range of the ramjet baseline (e.g., 500 n miles prediction vs 450 n miles actual for Mach 3,60,000-ft-altitude cruise).

A flight performance sensitivity study was conducted to define the most significant parameters of the ramjet baseline and the required accuracy for prediction methods. Note from Fig. 7.22 that flight range is most sensitive to the ramjet specific impulse, fuel weight, zero-lift drag coefficient, and the ramjet thrust. The flight range is relatively insensitive to inert weight and lift curve slope, especially for low-altitude flight (high dynamic pressure).

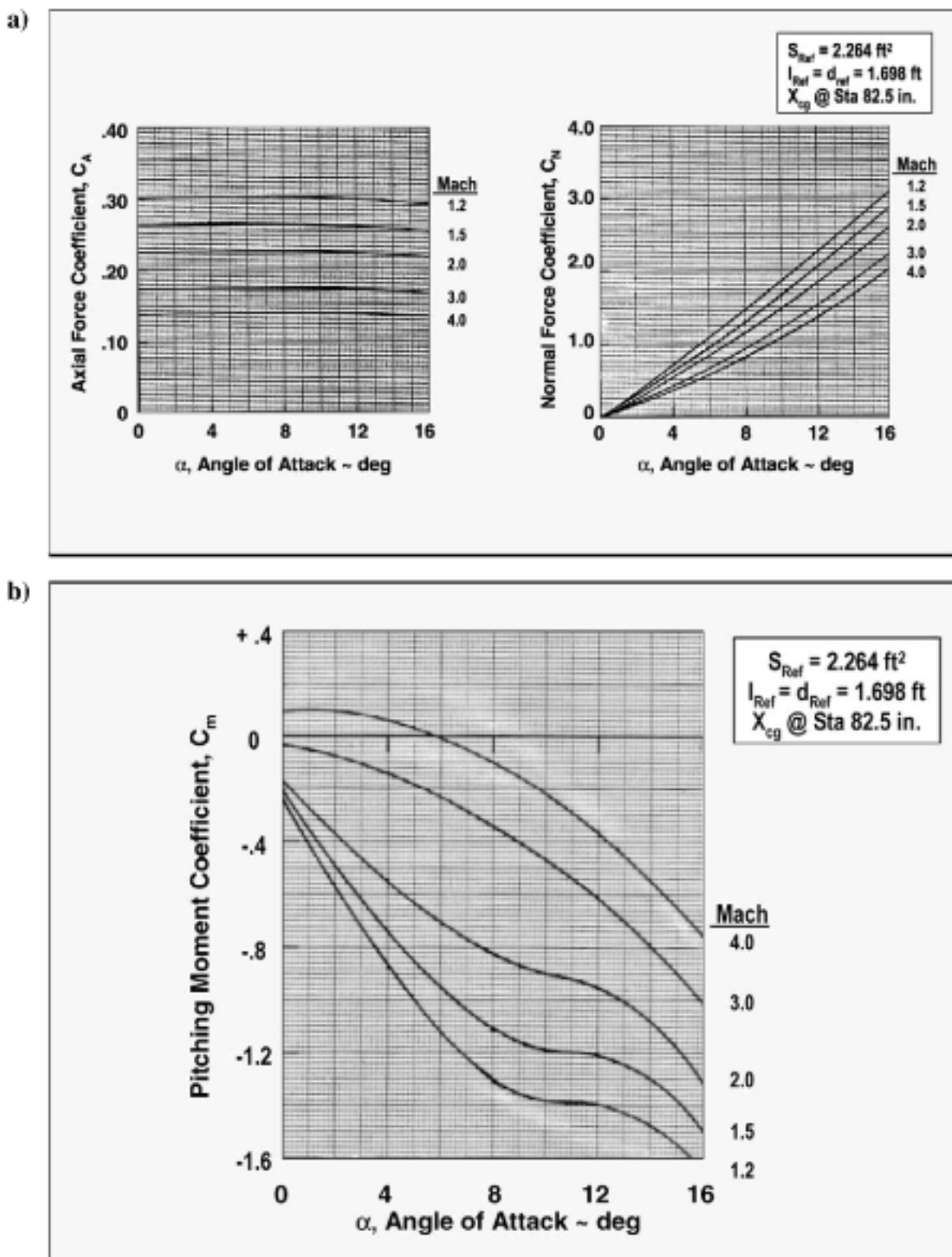


Fig. 7.17 Aerodynamic characteristics of the ramjet baseline missile (from Ref. 21):
 a) axial force and normal force coefficients as a function of Mach number and angle of attack and b) pitching moment coefficient as a function of Mach number and angle of attack.

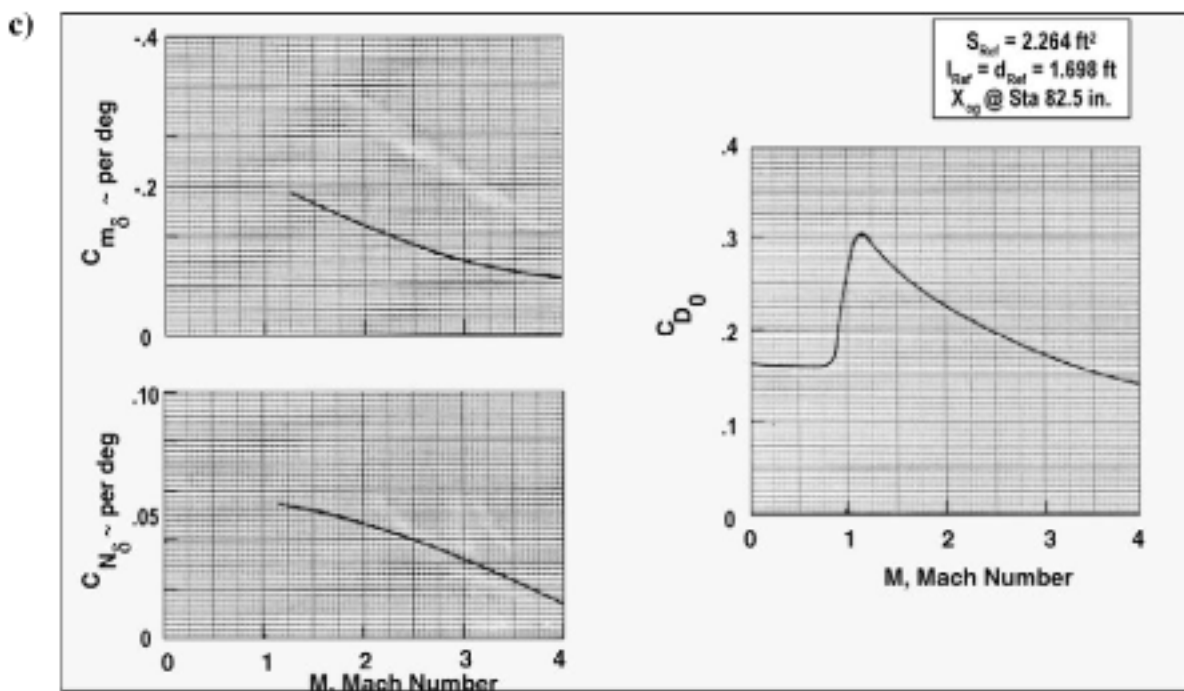


Fig. 7.17 (Cont.) Aerodynamic characteristics of the ramjet baseline missile (from Ref. 21): c) zero-lift drag coefficient and stability and control derivatives as a function of Mach number.

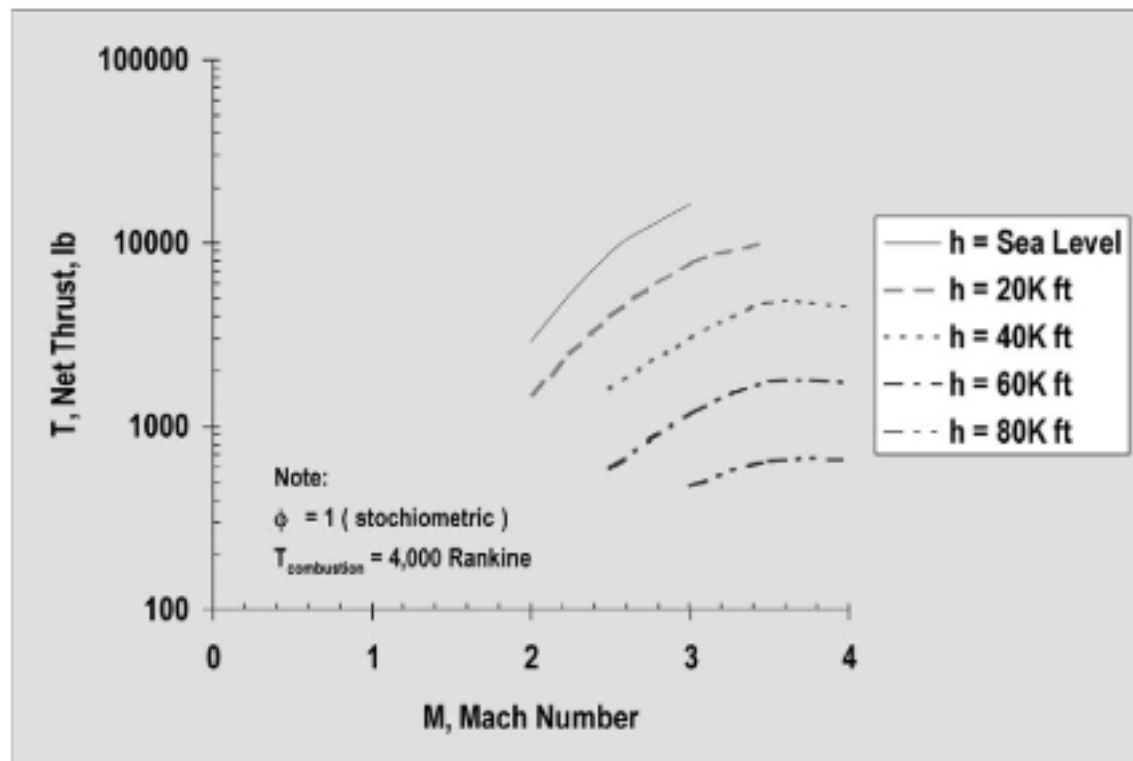


Fig. 7.18 Thrust modeling of ramjet baseline.

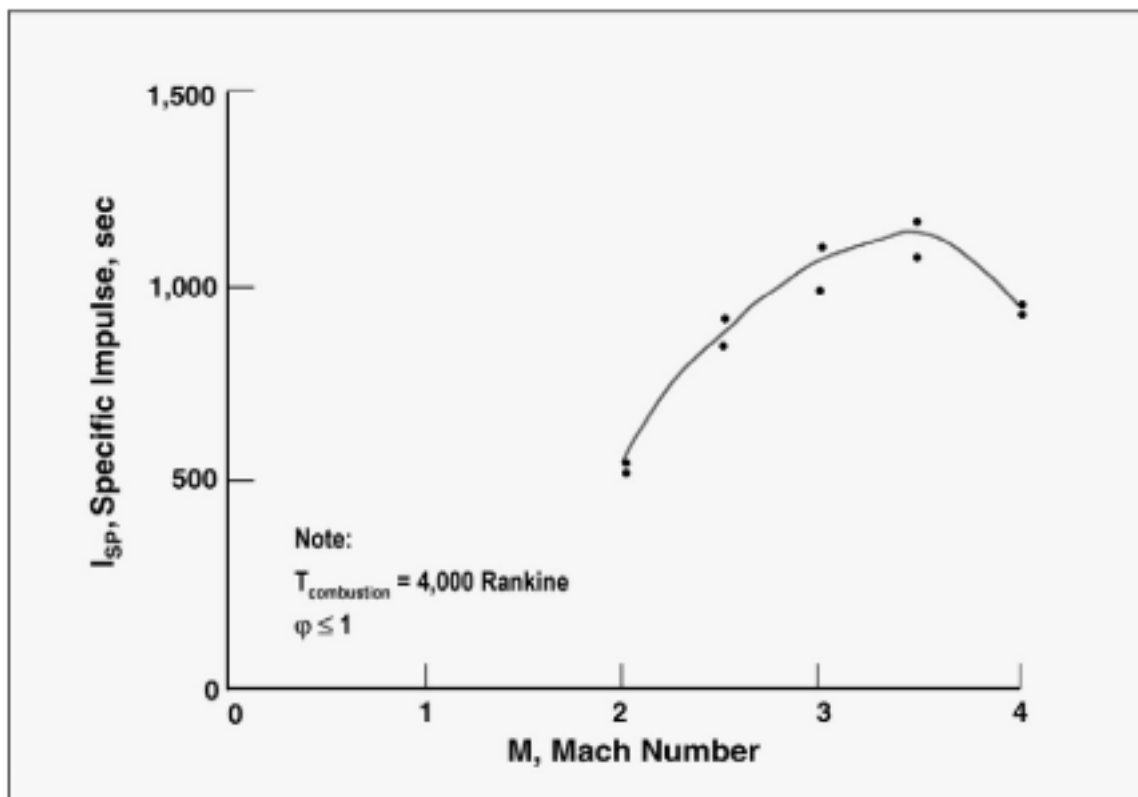


Fig. 7.19 Specific impulse modeling of ramjet baseline.

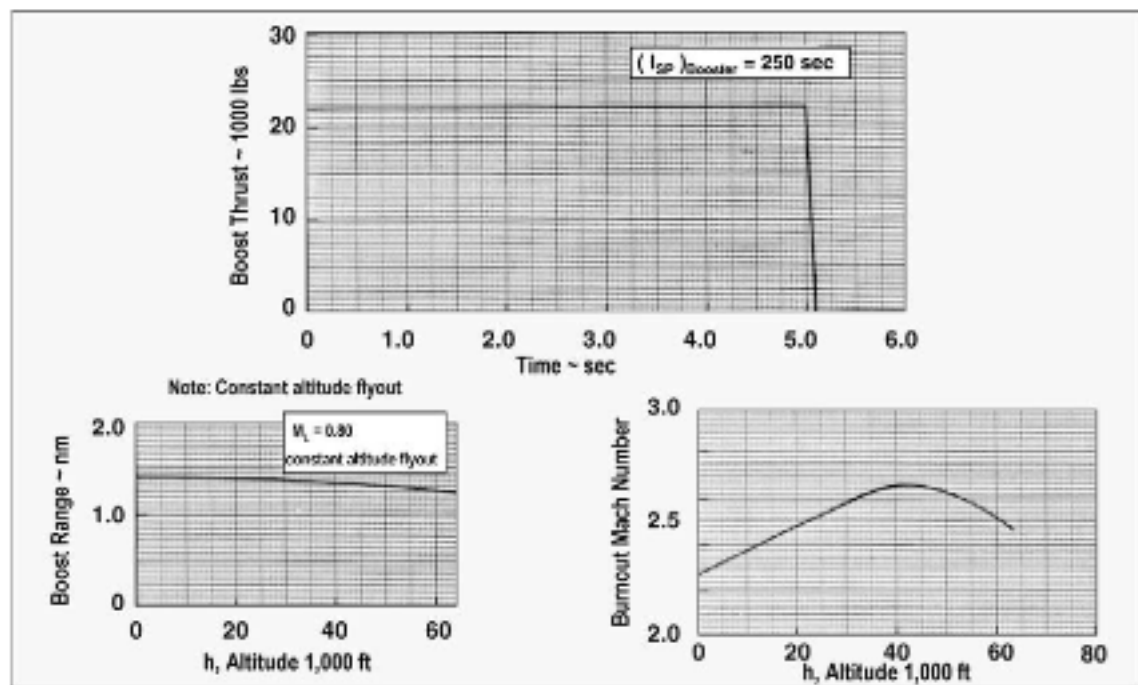


Fig. 7.20 Rocket booster acceleration/performance of ramjet baseline (from Ref. 21).

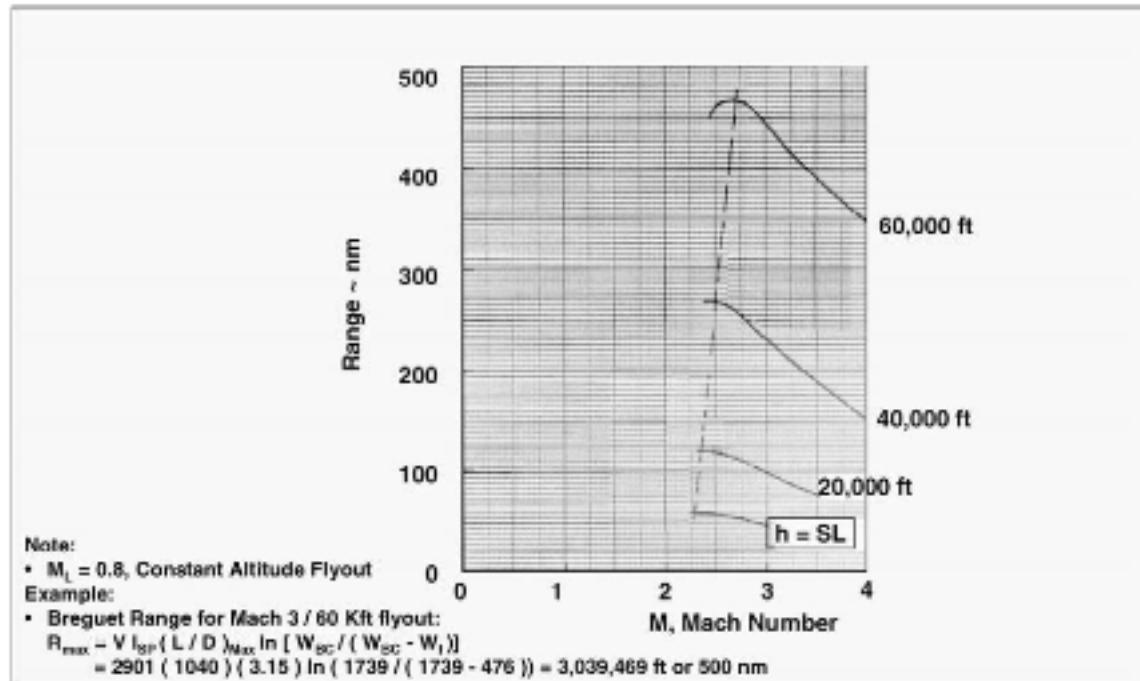


Fig. 7.21 Flight performance modeling of ramjet baseline.

The prediction methods for ramjet specific impulse, zero-lift drag coefficient, and ramjet thrust usually have sufficient accuracy (e.g., $\pm 5\%$, 1σ) for conceptual design. However, there is often large uncertainty in predicting the subsystem packaging volume available to package the fuel, providing uncertainty in the fuel weight. Inboard profile drawings are required to reduce the uncertainty.

The uncertainties in the values of the ramjet baseline parameters that define the cruise flight range are used to determine the uncertainty in flight range, as

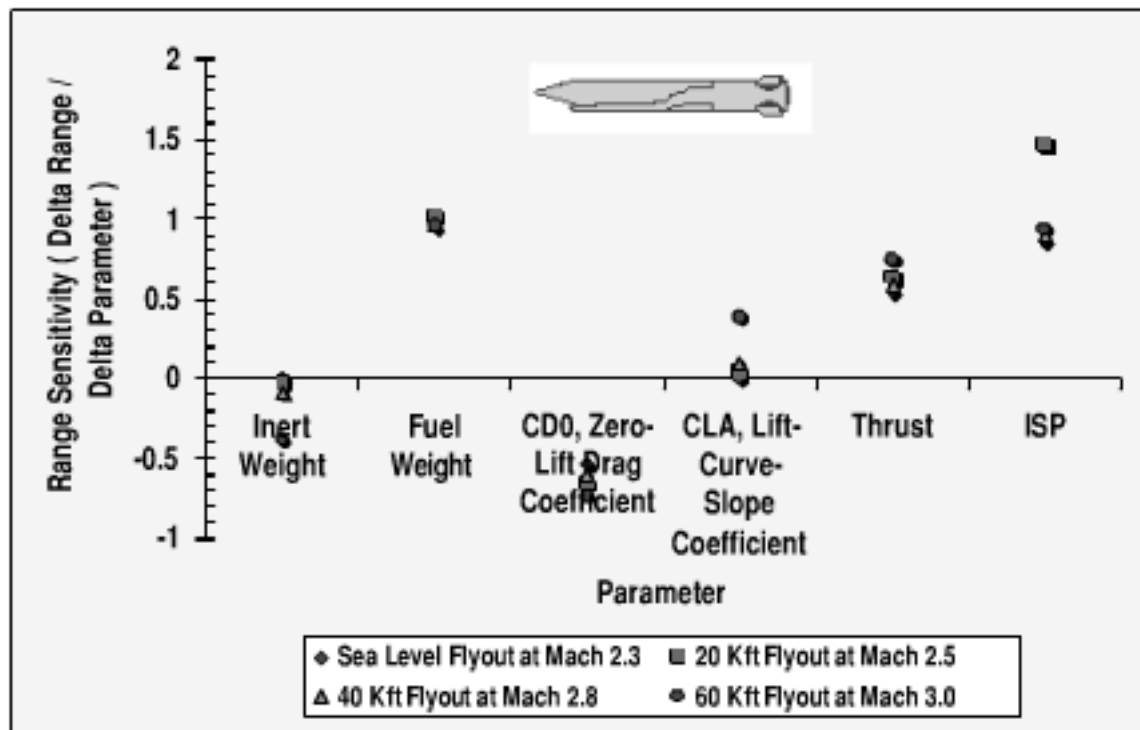


Fig. 7.22 Ramjet baseline range is driven by the I_{SP} , fuel weight, thrust, and the zero-lift drag coefficient.

Table 7.7 Ramjet baseline flight range uncertainty is $\pm 7\%$, 1σ

Parameter	Baseline value at Mach 3.0 / 60,000 ft	Uncertainty in parameter	$\Delta R/R$ due to uncertainty
1. Inert weight	1205 lb	$\pm 2\%, 1\sigma$	$\pm 0.8\%, 1\sigma$
2. Ramjet fuel weight	476 lb	$\pm 1\%, 1\sigma$	$\pm 0.9\%, 1\sigma$
3. Zero-lift drag coefficient	0.17	$\pm 5\%, 1\sigma$	$\pm 4\%, 1\sigma$
4. Lift curve slope coefficient	0.13/deg	$\pm 3\%, 1\sigma$	$\pm 1\%, 1\sigma$
5. Cruise thrust, $\phi = 0.39$	458 lb	$\pm 5\%, 1\sigma$	$\pm 2\%, 1\sigma$
6. Specific impulse	1040 s	$\pm 5\%, 1\sigma$	$\pm 5\%, 1\sigma$
Level of maturity of ramjet baseline based on flight demo of prototype and subsystem tests			
Wind-tunnel tests			
Direct connect, freejet, and booster firing propulsion tests			
Structure test			
Hardware-in-loop simulation			
Total flight range uncertainty at Mach 3.0/60,000 ft flyout			
$\Delta R/R = [(\Delta R/R)_1^2 + (\Delta R/R)_2^2 + (\Delta R/R)_3^2 + (\Delta R/R)_4^2 + (\Delta R/R)_5^2 + (\Delta R/R)_6^2]^{1/2}$			
$= \pm 6.9\%, 1\sigma$			
$R = 445 \text{ nm} \pm 31 \text{ nm}, 1\sigma$			

shown in Table 7.7. The assumed cruise flight conditions are Mach 3.0 at 60,000 ft in altitude. The parameters are inert weight, ramjet fuel weight, zero-lift drag coefficient, lift curve slope coefficient, cruise thrust ($\phi = 0.39$), and specific impulse. The level of maturity of the ramjet baseline used in this text is based on an advanced technology demonstration (ATD) of a flight prototype of the ASALM missile. Subsystem technology tests included wind-tunnel tests; direct connect, inlet, and freejet propulsion tests; booster firings; structure test; and hardware-in-loop simulation.

The total flight range uncertainty for Mach 3.0, 60,000-ft cruise flight is assumed to be the root-sum-of-the-squares (RSS) of the contributors:

$$\begin{aligned}\Delta R/R = & \pm \sqrt{[(\Delta R/R)_1^2 + (\Delta R/R)_2^2 + (\Delta R/R)_3^2 + (\Delta R/R)_4^2 \\ & + (\Delta R/R)_5^2 + (\Delta R/R)_6^2]} = \pm 6.9\%, 1\sigma\end{aligned}$$

The ramjet baseline missile cruise flight range with uncertainty is therefore $R = 445 \text{ n miles} \pm 31 \text{ n miles}, 1\sigma$. There is a 99% confidence (3σ) in achieving a cruise range exceeding 352 n miles.

Note that, because the engine burnout is at 60,000 ft in altitude, the missile has additional range available in gliding from the high altitude.

7.5 Ramjet Propulsion/Fuel Alternatives

The second example of ramjet missile sizing is the effect of propulsion system alternatives and fuel alternatives on the missile flight range. Shown in Fig. 7.23 is a comparison of the baseline liquid-fuel ramjet with the propulsion/fuel alternatives

Propulsion / Configuration	Fuel Type / Volumetric Performance (BTU / in ³) / Density (lb / in ³)	Fuel Volume (in ³) / Fuel Weight (lb)	ISP (sec) / Cruise Range at Mach 3.5, 60K ft (nm)
Liquid-Fuel Ramjet	RJ-5 / 581 / 0.040	11900 / 476	1120 / 390
			
Ducted Rocket (Low Smoke)	Solid Hydrocarbon / 1132 / 0.075	7922 / 594	677 / 294
			
Ducted Rocket (High Performance)	Boron / 2040 / 0.082	7922 / 649	769 / 366
			
Solid- Fuel Ramjet	Boron / 2040 / 0.082	7056 / 579	1170 / 496
			
Slurry-Fuel Ramjet	40% JP-10, 60% boron carbide / 1191 / 0.050	11900 / 595	1835 / 770
			

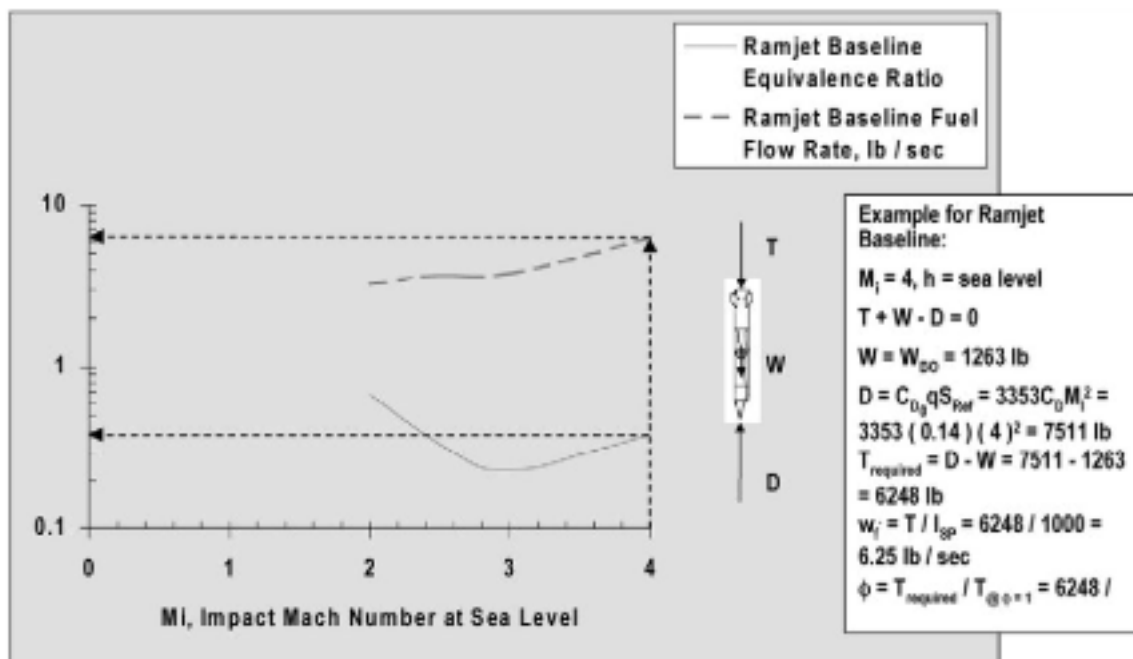
Note: ■ Flow Path ■ Available Fuel $R_{\text{cruise}} = VL_p(L/D) \ln [W_{\text{oc}} / (W_{\text{oc}} - W_t)]$

Fig. 7.23 Slurry-fuel ramjet provides extended range.

of low-smoke ducted rocket, high-performance ducted rocket, solid-fuel ramjet, and slurry-fuel ramjet propulsion. The comparison is conducted for a volume-limited missile. Note that the solid hydrocarbon ducted rocket has 75% of the range of the baseline liquid-fuel ramjet. Although a solid hydrocarbon ducted rocket has less range than a liquid-fuel ramjet, other attributes such as simpler logistics and higher acceleration capability may make it attractive for some missions. The high-performance boron ducted rocket has 94% of the range of the liquid-fuel ramjet. A tradeoff could be made of the simpler logistics and higher acceleration of the ducted rocket vs the lower observables of the liquid-fuel ramjet plume. The solid boron fuel ramjet has 27% longer range than the liquid-fuel ramjet (496 vs 390 n miles). Although boron fuel has much higher volumetric performance and density than liquid hydrocarbon fuel, some of the potential performance benefit is lost in design integration. As shown in the figure, a grain cavity must be provided for the burn area, reducing the volumetric efficiency of the solid-fuel ramjet. Disadvantages of the solid-fuel ramjet are increased plume observables and the lack of a throttle capability compared to the liquid hydrocarbon fuel ramjet. Finally, the slurry-fuel ramjet (40% JP-10, 60% boron carbide) has almost twice the range of the liquid-fuel ramjet. The adverse characteristic of the high observables of the plume of the slurry fuel ramjet must be traded off with the outstanding range performance. Another design consideration is the need for a higher performance fuel pump because of the highly viscous slurry fuel.

7.6 Ramjet Missile Surface Impact Velocity

The last example of ramjet missile sizing is the thrust and fuel flow rate requirement to achieve a high velocity impact on a surface target. It illustrates the process



Note: Ramjet baseline, vertical impact at sea level, steady state velocity at impact, T = thrust, W = weight, D = drag, W_{bo} = burnout weight, C_{D_0} = zero-lift drag coefficient, M_I = impact Mach number, T_{required} = required thrust for steady state flight, w_f = fuel flow rate, I_{sp} = specific impulse, ϕ = equivalence ratio ($\phi = 1$ stoichiometric)

Fig. 7.24 Liquid-fuel ramjet can provide a high velocity impact.

of matching thrust and fuel flow rate to the required values for flight performance. Figure 7.24 and the previous cruise performance data for the ramjet baseline show that the liquid-fuel ramjet has a low thrust and a low fuel flow rate requirement in the efficient cruise at high altitude. The thrust for efficient cruise at Mach 3, 60,000 ft in altitude is $T = 458$ lb. At Mach 3, 60,000 ft in altitude, the dynamic pressure, fuel flow rate, and equivalence ratio are 945 psf, 0.46 lb/s, and 0.39, respectively. The liquid-fuel ramjet can also provide the higher thrust that is required for a high-impact speed on a surface target. The thrust required for a Mach 4 vertical impact on a sea-level target is much larger, $T = 6248$ lb. At Mach 4, sea-level impact, the dynamic pressure is 23,700 psf, fuel flow rate is 6.25 lb/s, and $\phi = 0.38$. Operating over the broad range of throttle ratio (13.6 to 1) is pushing the state of the art in combustion stability technology and fuel pump technology. Note that the baseline ramjet missile was also designed for cruise at Mach 3.0, sea-level flight, and has been flight tested at Mach 2.5, sea-level flight. A heavier structure would be required for Mach 4.0, sea-level flight.

7.7 Computer-Aided Sizing for Conceptual Design

The final sizing examples are computer-aided sizing for conceptual missile design. Two fundamental requirements for computer programs used in conceptual design are fast turnaround time and ease of use. Fast turnaround is necessary to search a broad solution space with a sufficient number of iterations for design convergence. A good design code connects the missile physical parameters directly to a trajectory code that calculates flight performance. The conceptual design methods should be simple physics-based methods, incorporating only the most important driving parameters. Baseline missile data should be imbedded in the code to facilitate startup.

More detailed computational methods are used later in preliminary design when the number of alternative geometric, subsystem, and flight parameters has been reduced to a smaller set of alternatives. As an example, it is inappropriate to use computational fluid dynamics (CFD) in conceptual design. The mathematical considerations of CFD (e.g., mesh size, time interval, numerical stability, turbulence modeling, smoothing) are impediments to the fast turnaround time that is required for conceptual design. Similarly, a 6-DOF trajectory simulation is inappropriate during conceptual design for the convenient evaluation of guided flight. The development of the required autopilot for 6-DOF guided flight is time consuming, diverting emphasis from other more appropriate considerations. Similarly, missile optimization codes are generally inappropriate for conceptual design. Optimization in conceptual design is best left to the creativity and the intuition of the designer. Optimization codes work best when there is a continuous smooth variation in parameters, which is usually not the case in conceptual design. For example, optimization codes do not work well in comparing ramjet propulsion vs rocket propulsion. The CFD, 6-DOF guided flight trajectory simulations and optimization codes have seductive "precision." However, more often than not their accuracy in conceptual design is worse than simpler methods. Simpler aerodynamic and simulation methods, combined with a well-defined baseline missile and the designer's creativity and intuition, are a preferable approach for alternatives selection, sizing, and optimization. They are invariably more accurate and robust. Reference 23 and the tactical missile design (TMD) Spreadsheet discussed in this text are examples of conceptual design computer-aided sizing methods that are fast and that usually have sufficient accuracy for the relative screening of missile concept alternatives.

The following discussion of the ADAM missile simulation program²³ is provided as an example of a computer program that generally meets the conceptual design criteria of fast turnaround, ease of use, and applicability to a broad range of configurations and flight conditions. ADAM is a DOS code that runs on a personal computer. ADAM may have compatibility problems with higher speed computers. It may require a compatible timing hardware emulation setting, to reduce the rate at which the computer's timer sends timing. The aerodynamics predictions are based on Refs. 4 and 5. The aerodynamic methods cover subsonic to hypersonic Mach numbers and angles of attack up to 180 deg. The ADAM aerodynamics module calculates force and moment coefficients, static and dynamic stability derivatives, trim conditions, control effectiveness, and center-of-pressure location. Modeling of the equations of motion can be in three, four, five, or even six degrees of freedom (unguided flight). The three-degrees-of-freedom flight trajectory model runs faster than real time. A 30-s time of flight requires about 8 s of run time. The 6-DOF flight trajectory simulation is used to analyze the nutation/precession modes of missiles during their unguided portion of flight, as well as unguided bombs and projectiles. It requires longer run time. For homing missiles, proportional guidance is used as well as other guidance laws. The input to the flight trajectory module is provided automatically by the aerodynamics module, simplifying the user input. The benchmark missiles used in the aerodynamics module have corrected coefficients and derivatives based on wind-tunnel data. Greater than 50 input parameters are available. The input default is the baseline missile parameters, simplifying the input data preparation.

The baseline missiles in ADAM include air-to-air (e.g., Archer), surface-to-air (e.g., Patriot), air-to-surface (e.g., Hellfire), and surface-to-surface (e.g., ATACMS). The aerodynamic modeling of the body includes the diameter, nose configuration (geometry, fineness, bluntness), body bulge, boattail, and length. The body cross section may be circular or elliptical. Up to three surfaces (stabilizers, wings, and controls) can be specified. The geometric modeling of each surface includes the location, leading edge root and tip station, span, trailing edge root and tip station, thickness, control surface deflection limit, and the number of surfaces. The program models the missile center-of-gravity variation from launch to burnout. For propulsion, the thrust is modeled as a two-value thrust profile of a given time duration. The propellant weight of each thrust-time phase can also be specified. The target can be fixed or moving. Down range and cross range of the target are specified, as well as the target altitude and velocity. Launch conditions for the missile are specified, including altitude, velocity, launch angle, and the guidance law. The output of the three-degrees-of-freedom pitch simulation modeling includes a drawing of the missile geometry with dimensions, aerodynamic coefficients and derivatives, center-of-pressure location, flight performance parameters (velocity, trim angle of attack, acceleration, range, trim control surface deflection) vs time, and missile miss distance.

A second computer technique suitable for conceptual design is spreadsheet analysis. Figure 7.25 shows the design parameters of the TMD Spreadsheet. It is based on the methods and data presented in this text. The TMD Spreadsheet runs in Windows on a personal computer.

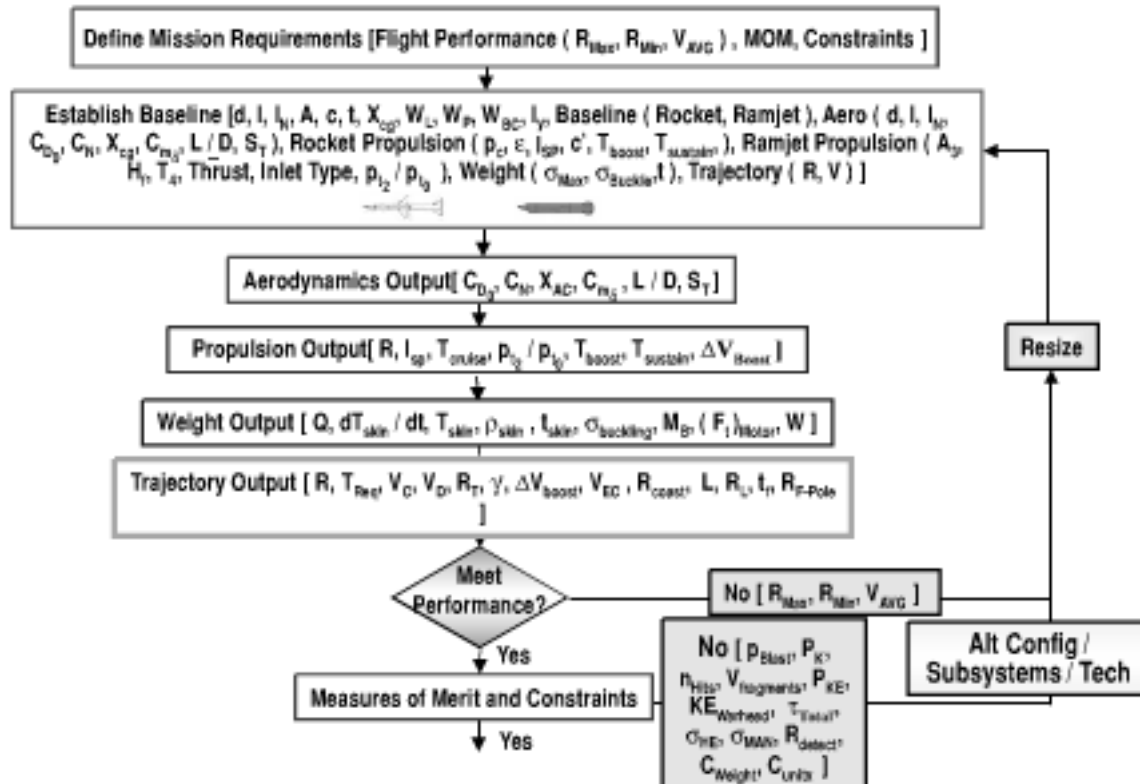


Fig. 7.25 Example of spreadsheet-based conceptual sizing computer code, TMD spreadsheet.

Aerodynamics of the missile body is from slender body theory⁴ and crossflow theory.⁵ Fixed and movable surface aerodynamics are based on linear wing theory and Newtonian impact theory.^{4,5} The methods are applicable to low aspect ratio wing and wingless configuration at angles of attack up to 90 deg.

For a ramjet the propulsion module output includes the inlet total pressure recovery, specific impulse, and thrust.^{7,9,10} The ramjet thrust and specific impulse predictions include the oblique and normal shock losses in total pressure. The rocket motor thrust and specific impulse are based on the isentropic flow equations adjusted for the change in specific heat ratio with temperature.

The system and subsystem weight scaling (i.e., density scaling) and material data (e.g., stress-strain vs temperature) in the TMD Spreadsheet weight module are from this text. Predictions of aerodynamic heating and surface temperature rate are from Ref. 11. Finally, the body localized buckling stress due to bending moment and axial loads, motor case stress, and the required motor case and airframe thickness are based on the methods used in this text.

Flight trajectory methods are based on closed-form analytical methods. Cruise range prediction is the Breguet range equation. The thrust required for steady cruise, steady climb, and steady dive is based on Ref. 3. Turn radius, turn rate, boost velocity, coast velocity, coast range, missile homing lead angle, launch range, and the F-pole range are based on the methods used in this text.

Warhead blast pressure is based on Ref. 14. Fragment velocity, kill probability, number of warhead fragments impacting the target, kinetic energy warhead penetration, and penetrator kinetic energy are based on Ref. 15 and the methods used in this text. Kinetic energy penetration depth is based on Ref. 16. Miss distance prediction and parameters (e.g., missile time constant, heading error, maneuvering target acceleration) are based on this text, Ref. 18, and Ref. 19. Survivability detection range is based on this text. Finally, production cost due to weight and the learning curve are based on this text, using data from Ref. 20.

Following definition of mission requirements and selection of a baseline configuration (either rocket or ramjet), the aerodynamics spreadsheet module is exercised. It calculates zero-lift drag coefficient, normal force coefficient, aerodynamic center location, pitching moment control effectiveness, lift-to-drag ratio, and the required tail stabilizer surface area. The aerodynamics spreadsheet module output, along with the default data of the baseline missile, is an input into a propulsion spreadsheet. The propulsion spreadsheet provides an estimate of range, velocity, thrust, and specific impulse.

A weight spreadsheet is used next to revise the missile weight. It includes an estimate of aerodynamic heating, surface temperature, required airframe and motor case thickness, localized buckling stress, bending moment, motor case stress, total weight, moment of inertia, and the density/weight of subsystems.

The flight trajectory spreadsheet has analytical expressions for one- and two-degrees-of-freedom trajectories. The output of the flight trajectory spreadsheet includes flight range, thrust required for steady flight, steady climb velocity, steady dive velocity, turn radius, turn rate, velocity and range at the end of boost and coast, seeker lead angle for proportional homing guidance, required launch range, time of flight, and F-pole range.

Finally, the designer compares the output of the flight trajectory spreadsheet against the mission flight performance requirements. If the missile design does not

meet the performance requirements, the process is repeated until the requirements are satisfied. The modularity of the spreadsheet and the default baseline missile data reduce the time required for data input in the next iteration.

Once flight performance requirements are met, the measures of merit (warhead lethality, miss distance, survivability, cost) and launch platform constraints are evaluated. Warhead lethality parameters include the blast pressure, kill probability, number of fragments impacting the target, fragment velocity, kinetic energy penetration, and the kinetic energy impacting the target for hit-to-kill missiles. Miss distance parameters include the missile time constant, miss distance due to an initial heading error, and the miss distance due to a maneuvering target. The survivability assessment includes the detection range based on the missile radar cross section and altitude. A cost prediction is made based on the missile weight, learning curve, and the number of units produced. Again, the missile design is iterated until the measures of merit and constraints are satisfied.

7.8 Verification Process

The verification process of a computer sizing code includes comparing the source code with the original algorithms, comparing results with another computer code, and when possible comparing the results with test data.

Verification of the TMD Spreadsheet was based on comparing the source code with the equations from this text, comparing results with the ADAM code, and also comparing the results with the text examples. The rocket and ramjet baselines, which are based on test data, were used in the verification of the TMD Spreadsheet.

An example of the TMD Spreadsheet verification is the air-to-air range requirement discussed previously in this chapter. The example launch condition is Mach 0.8 launch at 20,000 ft altitude. In the example the rocket baseline missile flies straight ahead at constant altitude. Based on the F-pole requirement, the missile must fly 6.7 n miles in less than 24.4 s. In this example the ADAM computer program gives a time of flight of 18.4 s. The TMD Spreadsheet gives a time of flight that is 14% longer ($t_f = 21.0$ s). As discussed previously, the flight range of the rocket baseline is most sensitive to the parameters of specific impulse, propellant weight, zero-lift drag coefficient, drag-due-to-lift, and static margin. Results may also be sensitive to the equations of motion. The TMD Spreadsheet result was based on the analytical equations of motion for boost and glide that are described in this text. The ADAM result was based on the three degree-of-freedom equations of motion using proportional guidance. In this example, specific impulse, weight, and static margin were specified. An examination of the two solutions shows that the major contributor to the difference in time of flight is attributable to the difference in zero-lift drag coefficient. For example, at Mach 2, the ADAM prediction of zero-lift drag coefficient during coast is $(C_{D_0})_{\text{coast}} = 0.53$. The TMD Spreadsheet prediction is much higher [$(C_{D_0})_{\text{coast}} = 0.96$]. Wind tunnel data for the rocket baseline is an even larger value, $(C_{D_0})_{\text{coast}} = 1.05$. Because the uncertainty in zero-lift drag coefficient has an impact on flight range and time to target, it is desirable to correct the TMD Spreadsheet with wind tunnel data to reduce the uncertainty. The wind tunnel data on the rocket baseline missile can be used to reduce the uncertainty.

7.9 Summary

Chapter 7 provided examples of the sizing process for a rocket-powered missile, examples of the sizing process for a ramjet-powered missile, and examples of computer programs for conceptual design. The Sparrow missile was used as a baseline missile to illustrate 1) the flight performance sizing to meet an air-to-air standoff range requirement, 2) wing sizing for maneuverability, and 3) weight and miss distance harmonization. A ramjet missile based on the Advanced Strategic Air Launched Missile was used to illustrate 1) the robustness in the uncertainty of the cruise flight range, 2) propulsion and fuel alternatives, and 3) surface target impact velocity. Finally, examples were shown of computer-aided sizing codes for conceptual design. ADAM is a DOS-based aerodynamic sizing code that includes a time-marching numerical solution of the equations of motion. TMD Spreadsheet is a Windows-based sizing code consisting of a spreadsheet based on the analytical methods of this text.

Development Process

The relationship of tactical missile design to the development process is presented in this chapter. The development process addresses the areas of technology assessment/roadmap, phases of development and the relationship to design, technology readiness level (TRL), frequency of new missile system follow-on programs, integration of missile subsystems development with the missile system development, examples of development tests and facilities, an example of technology development, examples of missile state-of-the-art advancement, and new technologies for tactical missiles.

8.1 Technology Assessment/Roadmap

Technology assessment and roadmapping identify the technology drivers, key decision points, critical paths, and the resource needs for technology development. The purpose of a technology roadmap is to establish the time-phase relationships for the required missile technology development activity. This includes 1) development of plans for technology development and validation, 2) identification of the technology options, 3) setting time-phased technology goals, and 4) development of a plan for technology transition. The technology plan provides an approach in maturing the missile technology through the development phases. As a result of technology development, the level of maturity will move from that of exploratory development, to advanced technology development, to a prototype demonstration. For most new missiles a technology development, risk reduction, and maturity demonstration activity is required prior to entering engineering and manufacturing development (EMD).

An optimum allocation of funding for technology investment is a difficult task. Some technologies may have the potential to satisfy the requirements but may be highly immature. There may be insufficient time or insufficient funding available to mature the technology to the required level of performance/cost or confidence. As a result, the highly immature technologies would not be included in the technology roadmap. Other technologies may be mature with high confidence in their performance/cost. However, the technologies may fall short of meeting the requirements, and a funding investment may do little to improve the performance/cost. As a result, the mature technologies would not be included in the technology roadmap. Technologies that would be included in the technology roadmap are those that have high potential payoff and can mature within the available time and funding.

8.2 Phases of Development/Design Maturity

Summarized in Fig. 8.1 is the technology development and design validation process for tactical missile systems. Technology development is focused on the

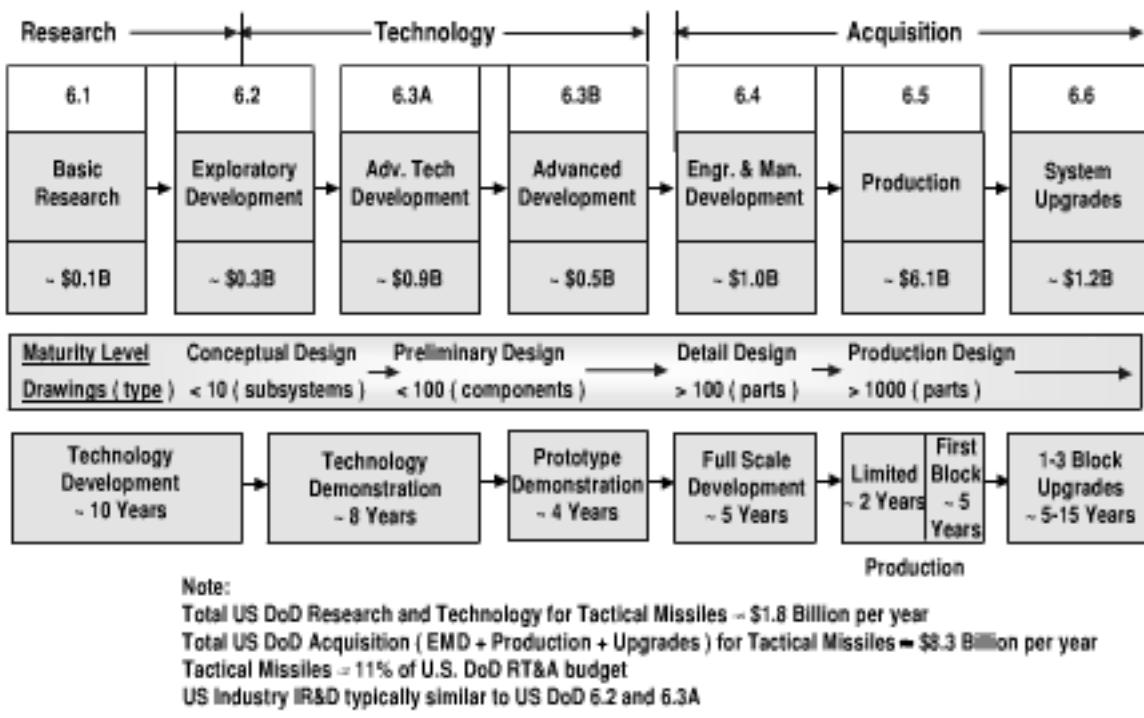


Fig. 8.1 Relationship of the design maturity level to the research, technology, and acquisition process.

key enabling technologies that are driven by the requirements but that are in need of additional development and demonstration for a required level of maturity. The technology development program addresses alternative approaches and risk mitigation. It has exit criteria for each phase and an exit plan in the event of failure. The technology development and demonstration activities lead to a level of readiness for entry into EMD.

Early technology work addresses laboratory tests and demonstrations of a critical component of a subsystem in a representative environment but not necessarily a full-scale environment. The next step of technology development is a laboratory or a flight demonstration of a subsystem in a representative, but not a full-scale, environment. This is followed by either a laboratory demonstration or a flight advanced technology demonstration (ATD) of a subsystem in a full-scale environment. Finally, there is a flight demonstration, based on either an advanced concept technology demonstration (ACTD) or a program definition and risk reduction (PDRR) of a full-scale prototype missile in a full-scale environment. This is required for a missile to enter into EMD.

The figure also shows the relationship of missile design to the development process of research, technology, and acquisition. Conceptual design is most often conducted during the exploratory development phase of missile development. A primary objective of exploratory development is to investigate and evaluate technology alternatives. The advanced technology development phase of missile development is intended to mature the enabling technologies of key subsystems. Although conceptual design may be conducted during advanced development, preliminary design methods are usually more appropriate. Preliminary design continues during advanced development demonstration of the prototype missile.

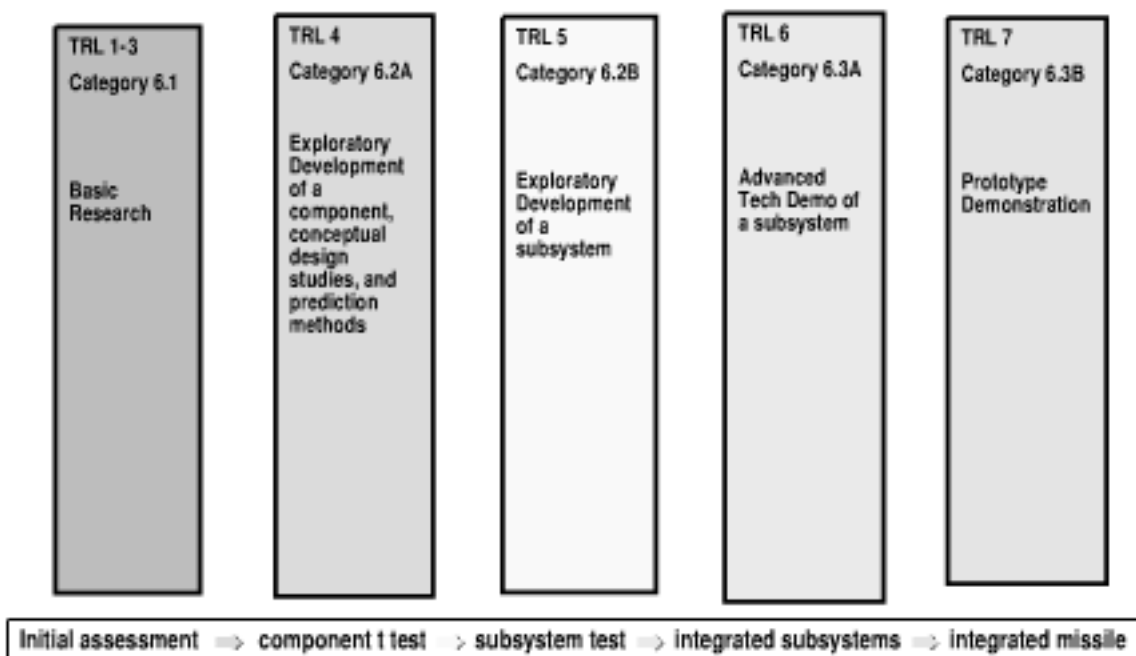


Fig. 8.2 Technology readiness level (TRL).

Following successful demonstration of a prototype, the program moves into EMD. At this point more detail design methods are appropriate for the operational missile. However, the assessment of possible future block upgrades may require the reintroduction of preliminary design and conceptual design activities.

Conceptual design and sensitivity studies should be conducted early in the exploratory development process and continued into advanced development. Many of the cost and performance drivers may be locked in during the conceptual design phase. It is therefore important to evaluate quickly a large number of alternatives that cover the feasible design solution space.

Figure 8.2 relates the maturity of a subsystem or technology for application to a missile system. The technology levels that characterize the type of funding are derived from the TRL model developed by NASA. TRLs for tactical missile technology may be characterized as follows.

1) TRL 1-3 is basic research. The category of funding is 6.1. The technology goals for this category generally have limited consideration of the constraints of other component interactions or a specific application for the technology. An example of a basic research program is determining the basic strength characteristics of a high temperature composite material, which may have numerous applications (e.g., missiles, aircraft, spacecraft). The differences of TRL 1-3 are the degree of consideration of the interaction with the other components of the subsystem and consideration of applications.

2) TRL 4 is laboratory development and laboratory test demonstration of a component. The category of funding is 6.2A exploratory development. In this category a component is usually developed and tested in a representative environment but not a full-scale environment. The component usually has general application (e.g., follow-on to AMRAAM, follow-on to JASSM). Conceptual design and analysis studies are also conducted in this category. These set the technology in a military

context. Analytical prediction methods are usually developed under this category of funding. The accuracy of the analytical predictions is established by the laboratory experiments under this category.

3) TRL 5 is laboratory development or demonstration of a subsystem. The subsystem usually has full-scale components and is tested in a representative but not full-scale environment. The category of funding is 6.2B exploratory development category.

4) TRL 6 is laboratory or flight ATD of a full-scale subsystem in a full-scale environment with integration of some of the other subsystems and some of the other new technologies of a follow-on missile system. This is the concept definition phase of program development. The category of funding is 6.3A advanced technology development.

5) TRL 7 flight demonstration is based on either an ACTD or a PDRR full-scale prototype in a full-scale environment. The category of funding is 6.3B advanced development. All of the new critical technologies and subsystems are demonstrated. A driving consideration is to assure the system engineering and the development of management confidence in the technologies. TRL 7 is normally performed where the technology and/or subsystem application is critical and high risk. The technology availability date (TAD) for entry into EMD is based on successfully completing TRL 7.

Indicators of design maturity include the number of drawings to describe the design and the number of alternative concepts that are currently under consideration. These are shown in Fig. 8.3. Conceptual design may be characterized by approximately five drawings for each concept, describing perhaps five subsystems. A large number of alternative missile system concepts, perhaps 10, are in evaluation

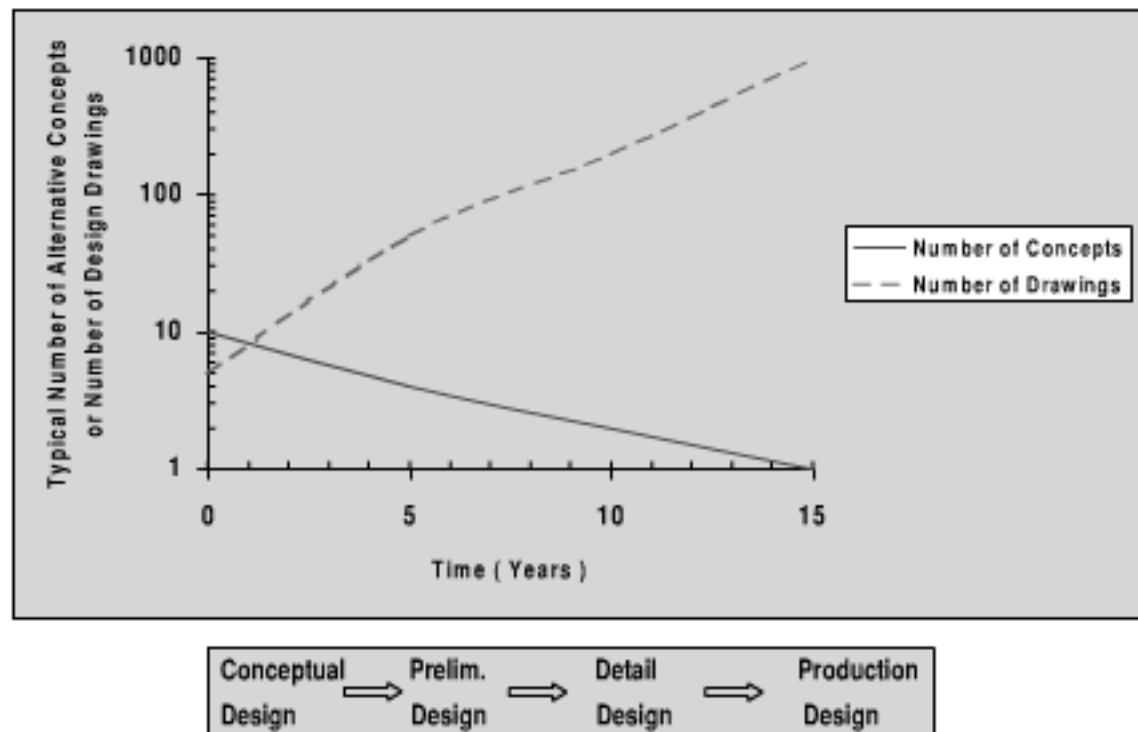


Fig. 8.3 Conceptual design has broad alternatives while detail design has high definition.

during conceptual design. Conceptual design drawings include the overall dimensions of the missile, major subsystems layout, and the major subsystems mass properties. The next step is preliminary design. Preliminary design drawings of a prototype missile are usually characterized by up to 100 drawings with greater detail and showing up to 100 components. Preliminary design drawings have fully dimensioned subsystems, inboard layouts showing the subsystems, individual subsystem and component drawings, and dimension tolerances. A fewer number of alternative missile system concepts, perhaps four, are under evaluation during preliminary design. Following preliminary design, the next step is detail design. Detail design for EMD usually requires more than 100 drawings and often has more than 1000 drawings. EMD drawings have even more detail, including drawings of each part, detailed work assembly instructions, and descriptions of the manufacturing processes. During EMD there is usually only one design concept (e.g., sole-source contractor) or perhaps at most two design concepts (two competitive contractors).

8.3 Tactical Missile Follow-On Programs

Figure 8.4 shows that the frequency of a follow-on program to a tactical missile is about every 24 years for U.S. missiles. Once a missile is in production, it usually has a long lifetime, including block upgrades. However, eventually a capability is needed that is not easily achievable through a block upgrade, requiring a follow-on missile development. Examples are shown in the figure of the driving requirements in the follow-on missile programs. These are the improved maneuverability of AIM-9X, improved speed and range of AIM-120 and AGM-88, improved accuracy of PAC-3, lighter weight and improved gunner survivability (lower observables,

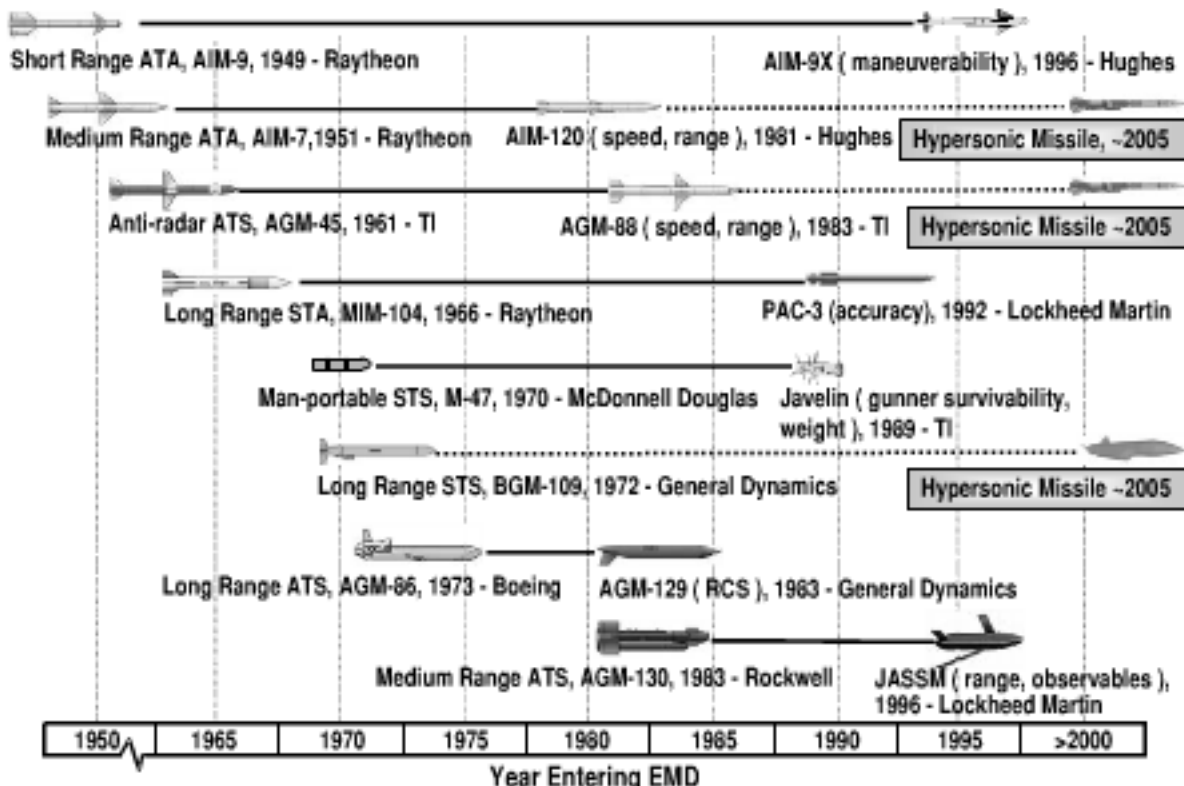


Fig. 8.4 U.S. tactical missile follow-on programs occur about every 24 years.

launch-and-leave) of Javelin, reduced radar cross section of AGM-129, and the longer range and lower observables of JASSM. It is interesting to note that in almost no case does a missile follow-on program go to the incumbent contractor of the current missile.

There may be opportunities for a new start for a U.S. hypersonic airbreathing missile around the year 2005. A hypersonic airbreathing missile provides longer range and faster time-to-target. Opportunities include follow-on programs for the AIM-120 AMRAAM, AGM-88 HARM, and the BGM-109 Tomahawk missiles.

8.4 Subsystem Integration

Figure 8.5 shows the design validation and technology development process for tactical missiles. A primary integration tool for the design validation/development process is missile system simulation. The initial simulations used in conceptual and preliminary design are digital simulations. As missile guidance and control hardware becomes available, a hardware-in-loop (HWL) simulation is also developed. HWL simulation incorporates the missile guidance and control hardware (e.g., seeker, gyros, accelerometers, actuators, autopilot). It also includes a simulated target signal for the seeker to track. Hybrid computers are used in HWL simulation. Fast analog computers simulate the rapidly changing parameters, such as the flight trajectory equations of motion. Digital computers simulate the more slowly changing parameters, such as the forces and moments from aerodynamics and propulsion. HWL and digital simulations are the primary system analysis tools used during missile flight tests. For example, simulation results based on wind-tunnel data are validated with flight test results. HWL and digital simulations are also used to determine the cause of flight test anomalies.

Launch platform integration is considered from the start of the subsystems development activities, continuing as they evolve into a missile system. In the propulsion area, static firings and insensitive munition tests are conducted before

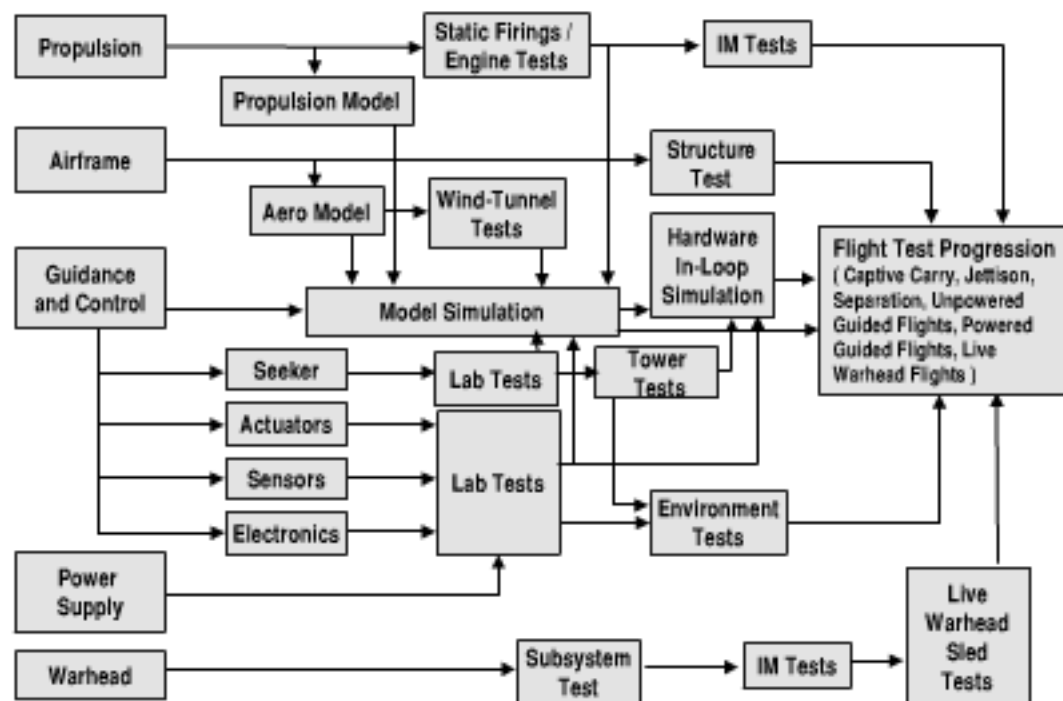


Fig. 8.5 Design validation/technology development is an integrated process.

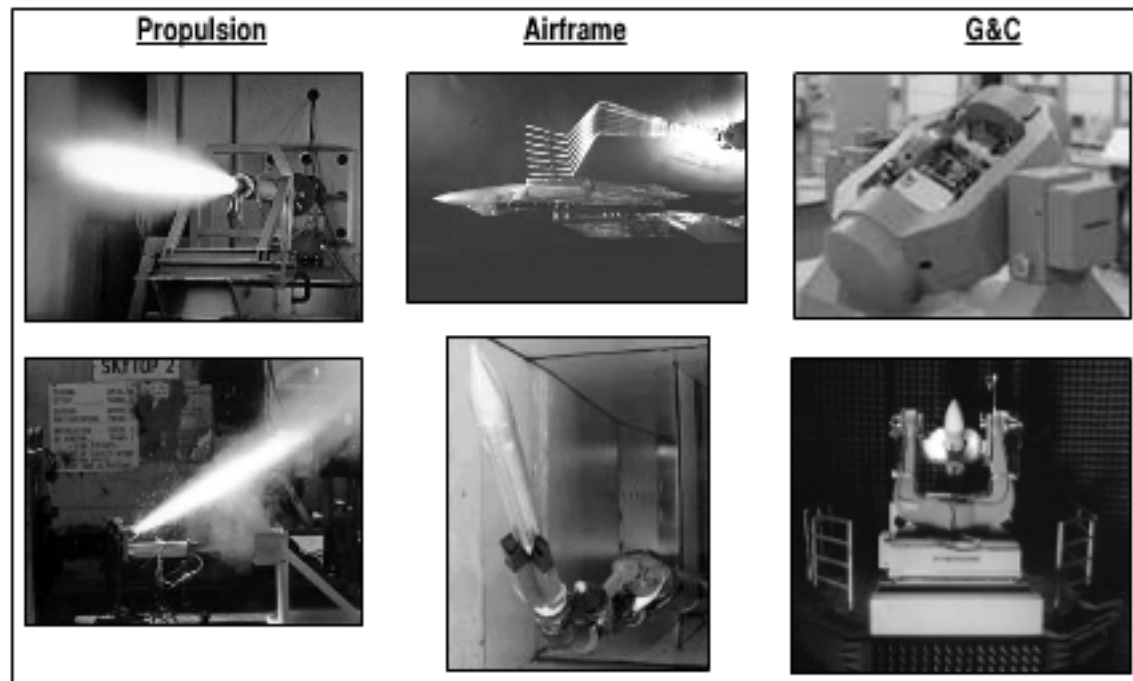
a missile with a live rocket motor is fired from a launch platform. In the airframe area, wind-tunnel testing of air-launched missiles includes not only the basic aerodynamic configuration development but also store separation wind-tunnel tests. In the guidance and control area, laboratory tests are conducted in a simulated ground and flight environment for the missile seeker, flight control gyros and accelerometers, flight control actuators, and electronics. The laboratory tests include environmental tests that simulate the operational temperature and vibration. The missile modeling and simulation activities include safe separation analysis. Similar to the propulsion area, the warhead has insensitive munition tests prior to firing a missile with a live warhead from the launch platform. Flight test validation is a progressive activity of increasing complexity. The objective of progressively complex testing is to minimize risk and enhance safety in the flight test activity. For example, a typical progression of flight demonstration for an air-launched missile begins with captive carriage of the missile and ends with launches of the missile with a live warhead. Intermediate flight tests are store jettison tests, safe separation tests, unpowered guided flights with an inert warhead, and powered guided flights with an inert warhead.

Examples of missile development tests and test facilities are shown in Figs. 8.6a–b. Figure 8.6a gives examples of propulsion, airframe, and guidance and control tests. The top left propulsion test is a static rocket motor firing. Measurements are made of thrust vs time. Additional measurements may also be made of the side forces and moments to evaluate thrust misalignment. The bottom left photograph is an example of a thrust vector control test. Measurements are made of the six forces and moments provided by the TVC. The top middle photograph is an example of a store separation test in a transonic wind tunnel. The time-lapse photograph shows a simulated flight trajectory of a store ejected from the F-22 aircraft. Shown in the bottom middle photograph is a ramjet missile model in the ONERA wind-tunnel facility. The wind tunnel test acquires six component aerodynamic force and moment data, surface pressure data, and flowfield data across the Mach number, angle of attack, angle of roll, and control surface deflection envelope. The top right photograph is a rate table for HWL simulation. The rate table provides simulated flight trajectory pitch, yaw, and roll rates for rate-sensitive guidance and control hardware such as gyros and seekers. In the bottom right of the figure is a photograph of a HWL simulation of the AMRAAM missile. The AMRAAM seeker is mounted on a rate table surrounded by an anechoic chamber that contains the simulated target.

The left portion of Fig. 8.6b shows examples of development testing of warheads. Shown in the center and upper right portions of the figure are examples of missile system level tests. The bottom right portion of the figure is a video of development tests.

In the top left photograph, a Hellfire missile warhead is detonated next to an 8 × 8 ft witness plate. The warhead fragments that penetrate the witness plate provide information on the size and distribution of the fragments. The bottom left of the figure is a more sophisticated warhead arena test conducted at the U.S. Naval Air Warfare Center, China Lake, California. The top center photograph is a missile systems environmental test to demonstrate the reliability and performance of guidance and control hardware at low temperature. The bottom center photograph is an example of a flight test of a surface-to-air missile. The Aster FSAF 15 missile is demonstrating stability and control and maneuverability at high angles of attack.

a)



b)

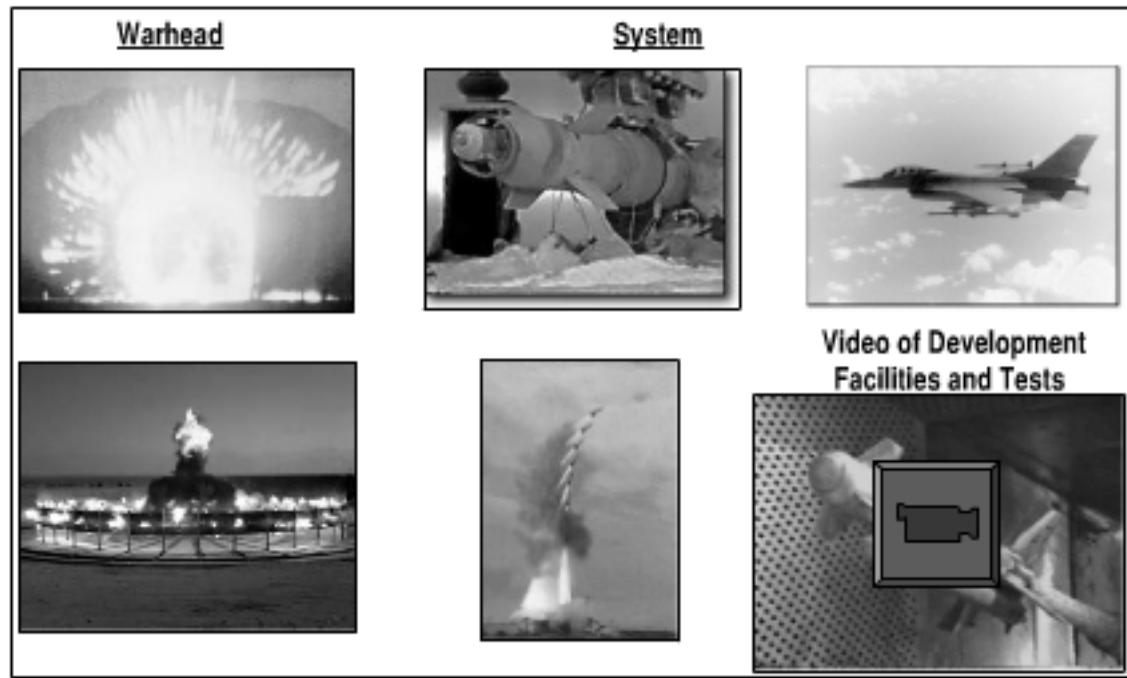


Fig. 8.6 Examples of missile development tests and facilities for a) propulsion, airframe, and guidance and control tests and b) development testing of warheads and missile system level tests.

The top right photograph shows an aircraft with a weapon load-out that is launching an AMRAAM missile. In addition to store separation and weapon effectiveness tests, the flight tests also provide information on the aircraft stability and control, aeroelasticity, and flying qualities with various store arrangements over the Mach number and altitude flight envelope. Finally, the bottom right section of the figure is a video of development facilities and testing for tactical missiles. Included are examples of a wind-tunnel test, hardware-in-loop simulation, warhead sled test,

TVC flight demonstration, insensitive munitions test, propellant development, and an environmental test.

8.5 Example of Technology Development

An example of a technology development activity is shown Fig. 8.7. It illustrates the maturity development and risk reduction activities of missile aerodynamics. Conceptual design is usually based on predicted aerodynamics without test data for the configuration. Preliminary design may also be initially based on prediction. The accuracy of the aerodynamics is improved when wind-tunnel data become available. Relatively low fidelity simulation (e.g., 3-DOF digital) is conducted during conceptual design to provide an initial estimate of flight performance and stability and control. The 6-DOF digital simulation and the hardware-in-loop simulation are usually initiated during preliminary design, continuing with refinement through flight test. The 6-DOF simulation provides an integration of aerodynamics with flight control and other subsystems.

Examples of the state of the art in preliminary design codes are Missile DATCOM, M3HAX, SUPL, and NSWC AP98. The Missile DATCOM (Data Compendium) computer code²⁴ was developed under the sponsorship of the U.S. Air Force Research Laboratory, Wright-Patterson Air Force Base, Ohio. The generalized methods are applicable to wing-body-tail configurations with circular and elliptical body cross section. Surfaces may be at arbitrary roll orientation and deflection. Missile DATCOM is more applicable to preliminary design because of the large number of input parameters and the time required to prepare the input data and to analyze the output from the computer program. Missile DATCOM has 405 subroutines.

- ◆ Conceptual Design (5 to 50 input parameters) Prediction
- ◆ Preliminary Design (50 to 200 input parameters) Prediction
 - ◆ Missile DATCOM: Attribute—low cost
 - ◆ NEAR M3HAX: Attribute—modeling vortex shedding
 - ◆ NEAR SUPL: Attribute—paneling complex geometry
 - ◆ NSWC AP98: Attribute—frequently updated
- ◆ Wind Tunnel Test Verification
 - ◆ Body buildup force and moment
 - ◆ Pressure distribution
 - ◆ Control effectiveness
 - ◆ Flow field
 - ◆ Store carriage and separation
 - ◆ Plume, heat transfer, and dynamic stability (may be required)
 - ◆ Inlet (if applicable)
- ◆ 3 to 6 DOF Digital Simulation
- ◆ Hybrid Hardware-in-loop Simulation
- ◆ Detail Design (over 200 input parameters)
- ◆ Flight Test Validation

Fig. 8.7 Example of aerodynamic technology development.

The Nielsen Engineering and Research (NEAR) M3HAX computer code [see Nielsen Engineering & Research (NEAR) Aerodynamic Software Products online at <http://www.nearinc.com/near/software.htm>] is based on the equivalent angle-of-attack method. It includes the effects of vortex shedding, configuration geometry, and Mach number. M3HAX is applicable to wing-body-tail configurations at high angles of attack, arbitrary roll angle, and arbitrary control surface deflection. The output includes static and dynamic forces and moments. The NEAR M3HAX code is more applicable to preliminary design because it does not automatically transfer output data to a conceptual design sizing code.

The NEAR SUPL computer code [see Nielsen Engineering & Research (NEAR) Aerodynamic Software Products online at <http://www.nearinc.com/near/software.htm>] is a supersonic panel method that models up to two different surfaces at different locations, including the effect of fin-body interference. The body and fin separation vortices are tracked aft of the separation point. Either two-dimensional shock expansion theory or Newtonian impact theory can be selected to provide lifting surface pressure calculations. SUPL is limited to relatively low angles of attack and control surface deflection. The code handles arbitrary surface geometry and roll angle. It is more applicable to preliminary design because of the time required to model the surface panels.

The U.S. Naval Surface Warfare Center, Dahlgren, Virginia, Aeroprediction Code AP98²⁵ includes bodies of elliptical cross section, high angles of attack, arbitrary control surface deflection, and arbitrary roll angle. The output includes forces, moments, pressure distribution, load distribution, and the airframe temperature response. Although it is user friendly for preliminary design, a deficiency for conceptual design application is that the output does not automatically feed a conceptual design code.

Figure 8.7 also shows the relationship of aerodynamics to the development of missile flight trajectory simulation, detail design, and flight test validation. Wind-tunnel testing develops the aerodynamic configuration and verifies the conceptual and preliminary design prediction. The wind-tunnel testing is a progressive series of increasing complexity. The initial tests are simple body buildup evaluations of aerodynamic configuration alternatives. Data are six component forces and moments with undeflected control surfaces. Following body buildup tests, a missile baseline is selected and a follow-on test is conducted to determine the pressure distribution over the missile. The data are used for the air loads prediction. The next test is a control effectiveness test. In the control effectiveness test the control surfaces are systematically deflected in "pure" pitch, yaw, or roll and asymmetric combined pitch, yaw, and roll configurations over their limits. The combined control deflections measure cross coupling forces and moments. Another wind tunnel test is a flowfield test. The flowfield test investigates the quality of the flow over the missile. Areas of concern include flow separation and shock-wave/boundary-layer interaction. Flowfield measurements may be made using a laser velocimeter, wind-tunnel model paint, oil flow over model, smoke, water bubbles, or schlierens. Aircraft store carriage and separation wind-tunnel tests were discussed previously. Other wind-tunnel tests such as thrust plume, reaction jet plume, heat transfer, and dynamic stability testing may not be required, depending upon the missile characteristics. Similarly, inlet tests would be required for airbreathing missiles.

The aerodynamic data from the wind-tunnel tests are used to provide increasing confidence in the digital and hardware-in-loop simulations. During conceptual

design only a few (typically fewer than 50) aerodynamic parameters are required. However, for detail design, over 200 aerodynamic parameters may be required in the simulation.

The flight test missile may have about 50 channels available for telemetry. Aerodynamic data of interest include missile acceleration, angle of attack, Mach number, control surface deflection, and hinge moment.

8.6 Examples of State-of-the-Art Advancement

Examples are shown of the missile state-of-the-art advancement in the areas of air-to-air missile maneuverability and supersonic airbreathing missile cruise Mach number. An assessment of the state-of-the-art advancement in air-to-air missile maneuverability is shown in Fig. 8.8. The figure is based on the maximum angle of attack of the missiles at the date of their initial operational capability (IOC). Note that there is a trend of increased angle of attack capability, especially for short-range air-to-air missiles. Aerodynamic control missiles are limited by technology to about a 35-deg angle of attack. For very high angles of attack, unconventional flight control (i.e., thrust vector control, reaction jet/jet interaction control) is required. Examples of modern highly maneuverable missiles with unconventional flight control are the Archer AA-11, Mica, and AIM-9X.

Ramjet propulsion has been investigated as early as the 1940s and has been used on several production missile systems in the United States, United Kingdom, France, and Russia. Figure 8.9 shows a history of the state-of-the-art advancement for supersonic/hypersonic airbreathing missiles over the last 50 years. A number of liquid-fuel ramjet demonstrations have been conducted. As shown in the figure, the cruise Mach number demonstrations have provided higher confidence in the capability for efficient hypersonic cruise. Ramjets have demonstrated supersonic

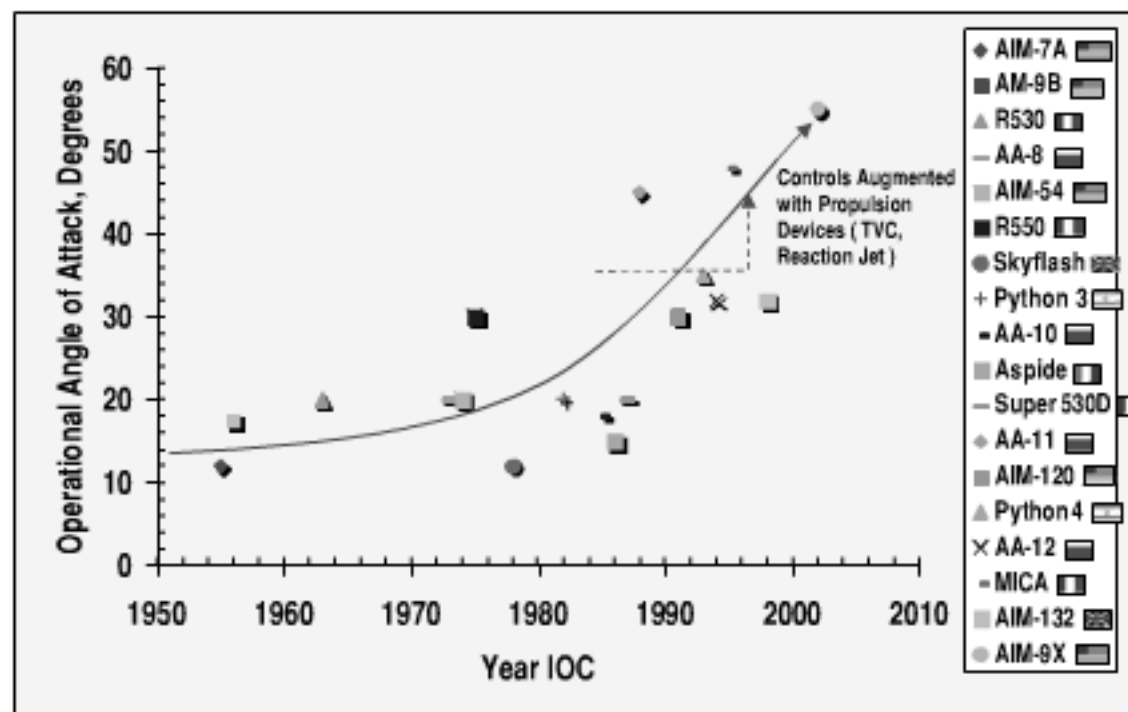


Fig. 8.8 Example of missile technology state-of-the-art advancement: air-to-air missile maneuverability.

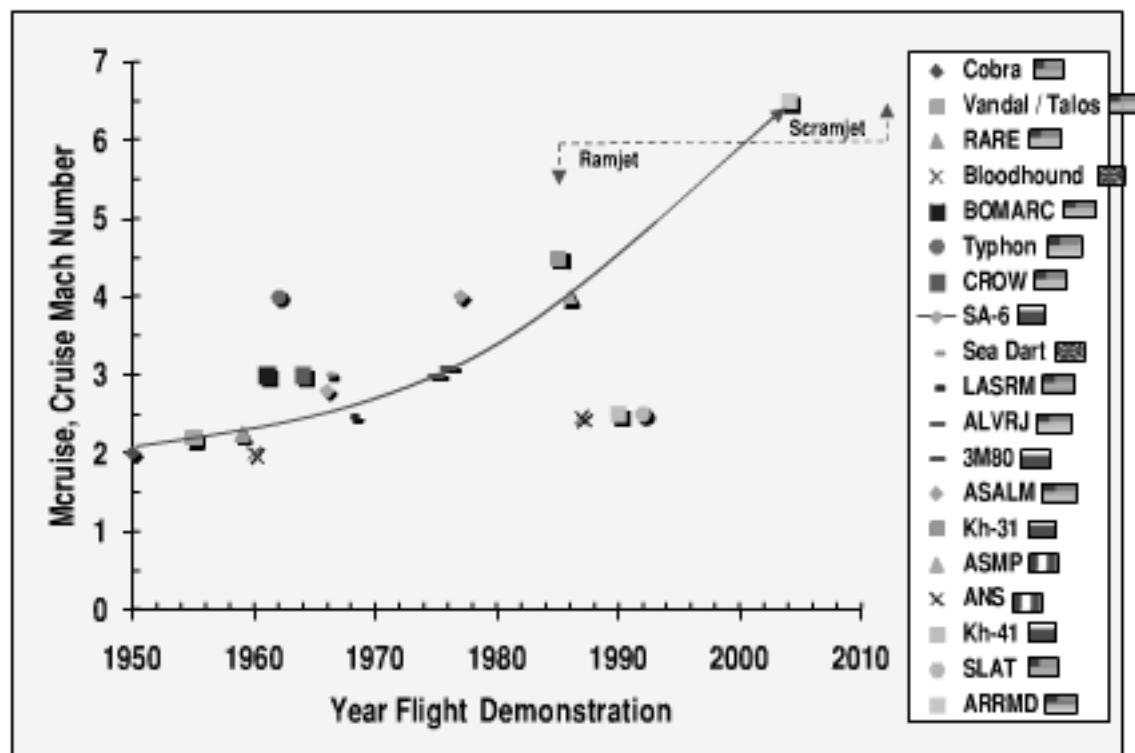


Fig. 8.9 Example of missile technology state-of-the-art advancement: supersonic air-breathing missiles.

and hypersonic cruise up to Mach 4.5. A future flight demonstration of a scramjet engine may demonstrate Mach 6.5 cruise around the year 2004. Because France and Russia have maintained a steady commitment to ramjet propulsion technology and have ramjet missile systems that are currently deployed, France and Russia are arguably the world leaders in ramjet missiles.

8.7 New Technologies for Tactical Missiles

An assessment of new technologies for tactical missiles is shown in Fig. 8.10. High payoff technologies are as follows.

1) *Dome*. Faceted/window and multilens domes have reduced dome error slope, resulting in improved guidance accuracy, low observables, and low drag at supersonic speed. Multispectral domes are an enabling technology for multispectral/multimode seekers.

2) *Seeker*. Multispectral/multimode imaging seekers provide enhanced performance for automatic target recognition in countermeasures and clutter. SAR seekers have good effectiveness in adverse weather and ground clutter. Strap-down seekers and uncooled IR seekers reduce parts count and seeker cost. High gimbal angle seekers enhance the off-boresight capability.

3) *Guidance and control*. GPS/INS will permit a low-cost seekerless missile to be used against fixed targets. Using in-flight digital trajectory flight prediction and derived flight conditions from the GPS/INS, missiles will continuously optimize the flight trajectory to maximize performance parameters. Advancements in ATR technology will provide new capabilities of near-real-time ATR and lower false alarm rate.

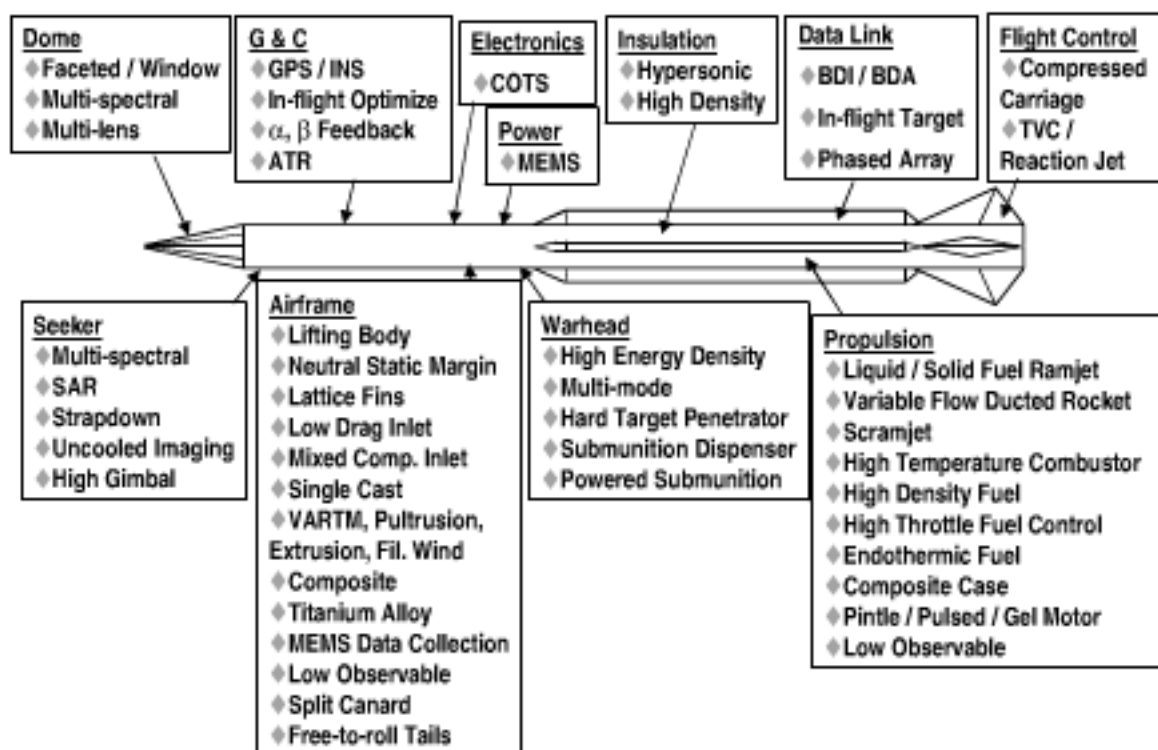


Fig. 8.10 New technologies for tactical missiles.

4) *Electronics.* Processing capability is ceasing to be a limitation for the application of commercial off-the-shelf (COTS) processors to sensor data fusion and near-real-time trajectory optimization to missiles.

5) *Airframe.* Lifting body airframes provide enhanced maneuverability and efficiency. Enhancements are also provided by neutral static margin. Split canard control and free-to-roll tails also provide enhanced maneuverability. Lattice fins have advantages of smaller hinge movement and higher control effectiveness. Low drag, mixed compression, and improved pressure recovery inlets are in development for hypersonic missiles. Increased usage will be made of castings, vacuum assisted resin transfer molding, pultrusion, extrusion, and filament winding to reduce parts count and cost. Composite and titanium materials will find use in hypersonic missiles. Low-cost/small-size MEMS sensors will be used for data collection and for health monitoring. Airframe shaping and materials technology will provide continued reduction in observables.

6) *Power.* Microturbine generator technology will offer a greater than 15–20 times weight advantage compared to a conventional battery.

7) *Warhead.* Higher explosive warheads such as the U.S. Navy China Lake CL-20 will be developed. Modular warheads will be developed. Kinetic energy warheads will be developed for hard and penetrating deeply buried targets. Submunition dispensers and autonomous submunitions will be developed to counter mobile, time-critical targets.

8) *Insulation.* Higher density insulation will be developed for hypersonic missiles.

9) *Propulsion.* Ramjet, variable flow ducted rocket, and scramjet airbreathing propulsion will be developed for hypersonic missiles. High temperature combustors will be developed. Higher density slurry and solid fuels will provide high

volumetric performance. Endothermic fuels will provide higher specific impulse, shorter combustor length, and cooling for scramjets. Composites will reduce weight. Thrust management technologies will be developed for pintle, pulse, and gel motors. Reduced observable propellants will continue development.

10) *Data link.* BDI/BDA will be provided by a data link of target imagery from an imaging IR seeker. Phased array antennas will be developed that provide high data rate and mission flexibility. In-flight retargeting will be developed to counter mobile targets.

11) *Flight control.* Compressed carriage aerodynamic surfaces will be developed for internal carriage. Unconventional flight control will continue development.

8.8 Summary

Chapter 8 addressed the development process for tactical missiles. The areas of discussion included the development activities and time frame for the phases of basic research, exploratory development, advanced technology development, advanced development, and engineering and manufacturing development; the levels of design and drawing maturity as related to the stage of missile system development; and missile follow-on program frequency and examples of follow-on programs. Also discussed was the process for integration of missile subsystems (propulsion, airframe, guidance and control, power supply, warhead) development to the missile system development/integration activities (e.g., hardware-in-loop simulation, environmental tests, launch platform compatibility). The process leading to a flight demonstration of the missile system was discussed, along with missile development tests and facilities, and the state-of-the-art advancement and the new technologies for tactical missiles.

Summary and Lessons Learned

This final chapter is a summary of the material presented in this text, a reiteration of conceptual design criteria, and a discussion of lessons learned from the author's experience in the development of tactical missiles and their technologies. The following is a discussion of fourteen guidelines in the development of conceptual designs for tactical missiles.

9.1 Iterate the System-of-Systems Analysis

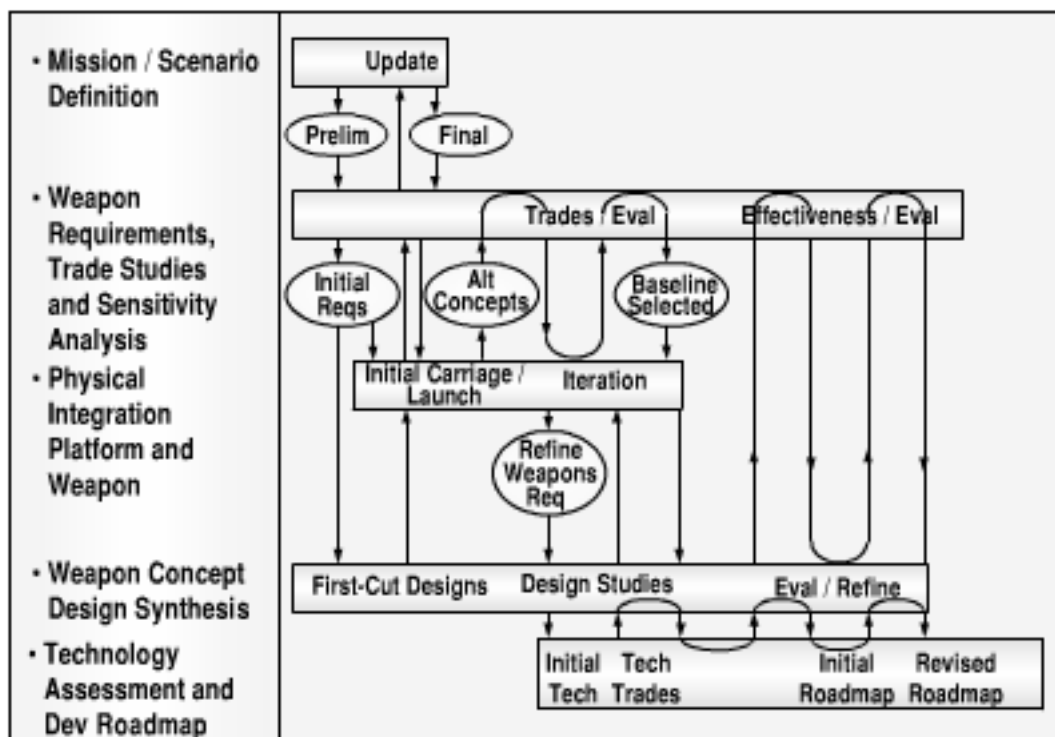
Again, Fig. 9.1 illustrates that the missile design process requires a broad assessment of alternatives and iteration at all levels. A common mistake is to select a design too quickly without sufficient consideration of the system-of-systems alternatives.

9.2 Exploit Diverse Skills

Figure 9.2 illustrates that the missile design activity is an opportunity to harmonize diverse inputs early in the development process. The military customer has the lead in providing the "requirements pull" initial input for the mission/scenario definition task and in providing the relative weighting for the system measures of merit. The mission/scenario definition and the relative weighting of the measures of merit may be modified later as a result of the "technology push" of the available capability in the time frame of interest. The system-of-systems weapon requirements, trade studies, and sensitivity analysis are usually conducted by operations analysis personnel. System integration engineers usually lead the task to integrate the missile with the launch platform. Missile design engineers lead the task to synthesize the alternative missile concepts. Finally, technical specialists provide the lead input for the technology push of potentially available technical capability and the technology development roadmap.

9.3 Apply Creative Skills

Missile design is a creative process that requires unique skills. Missile design requires 1) consideration of a broad range of alternatives; 2) projecting into the future (e.g., 5–15 years) the state of the art, threat, scenarios and military doctrine, and alternative concepts; 3) recognizing and distilling the most important, key drivers from a large number of possibilities; and 4) developing a synergistic/balanced combination of high leverage configurations, subsystems, and technologies.



Note: Typical design cycle for conceptual design is usually 3 to 9 months

Fig. 9.1 Iterate, iterate, iterate.

9.4 Identify High-Payoff Measures of Merit

One objective of missile design is to identify and quantify the high-payoff measures of merit. Because missiles are cost constrained, it is not possible to use the latest state of the art for all areas. Measures of merit such as range, time to target, robustness, lethality, miss distance, survivability, observables, reliability, and weight affect the missile cost. As illustrated in Fig. 9.3, judicious selection must be made for a balanced, cost-effective design.



Fig. 9.2 Exploit diverse skills.

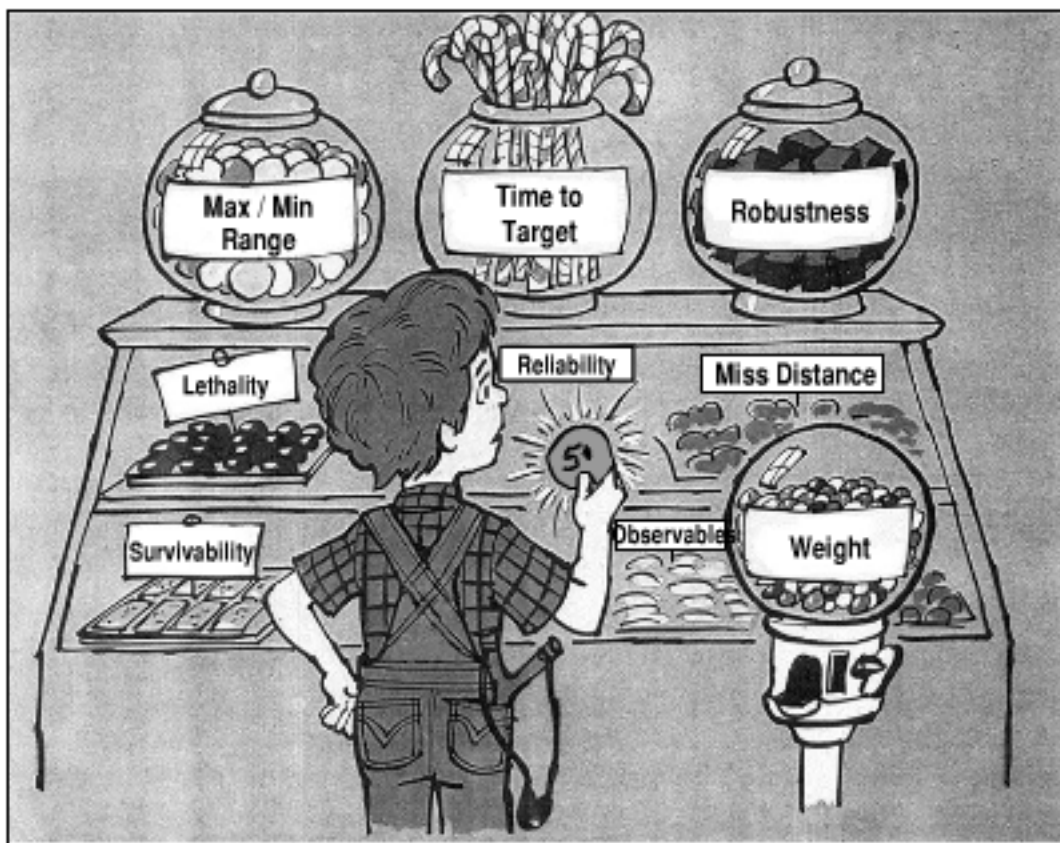


Fig. 9.3 Identify and quantify the high-payoff measures of merit.

Note that participation by the military customer is required to obtain a consensus on the relative weighting of the system measures of merit. As an example, for a typical volume- and weight-limited missile, one contractor may overly emphasize the warhead lethality and, as a result, develop a larger warhead at the expense of range. Another contractor may overly emphasize the launch platform survivability and, as a result, develop a longer range missile at the expense of warhead lethality and the required weight. The customer preference of lethality vs launch platform survivability should be a driver in the relative weighting of the measures of merit.

9.5 Start with a Good Baseline Design

Starting with a good baseline enhances the accuracy and speed of the design process. As illustrated in Fig. 9.4, the selection of a baseline missile should not be biased by previous experience.

9.6 Conduct Balanced Tradeoffs

As shown in Fig. 9.5, what is important is in the eye of the beholder. The missile designer must harmonize the subsystems to create a cost-effective design.

9.7 Evaluate a Broad Range of Alternatives

There are many configuration candidates for a missile design. A balanced, optimum conceptual design requires the consideration of a broad range of alternatives. For example, Fig. 9.6 shows air-to-air missile alternatives that are very different in their aerodynamic configurations. As expected, aircraft launch platform constraints

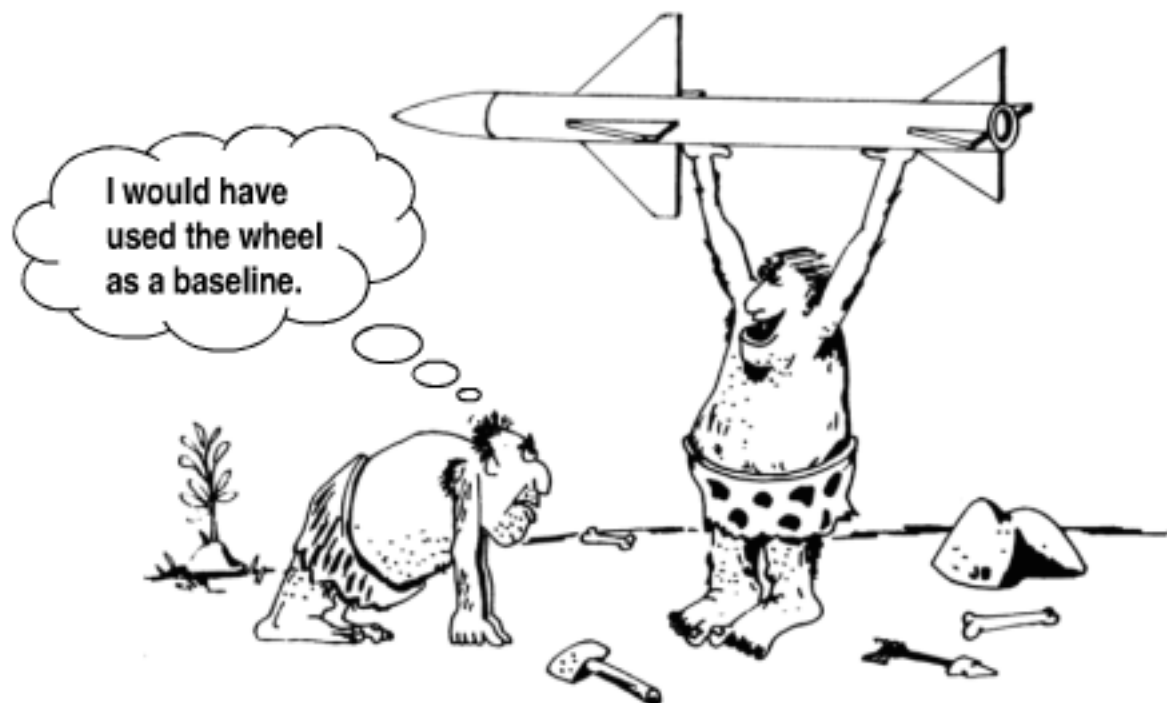


Fig. 9.4 Start with good baseline.

and supersonic flight result in air-to-air missiles with high fineness ratio. Also, the relatively soft/small air target results in a relatively small warhead. Although all of the missiles have high maneuverability (e.g., $30+ g$), the approach to surface area and geometry varies widely. Some missiles have wings, whereas others are wingless. Flight control alternatives include thrust vector control, tail control, canard control, and wing control. Finally, propulsion alternatives include rocket, ducted rocket, and ramjet.

9.8 Refine the Design

Figure 9.7 illustrates a natural bias on the part of the developer of a missile that changes to the current missile are not necessary. The pride of authorship reflects the time and money that went into developing the missile. However, time does not

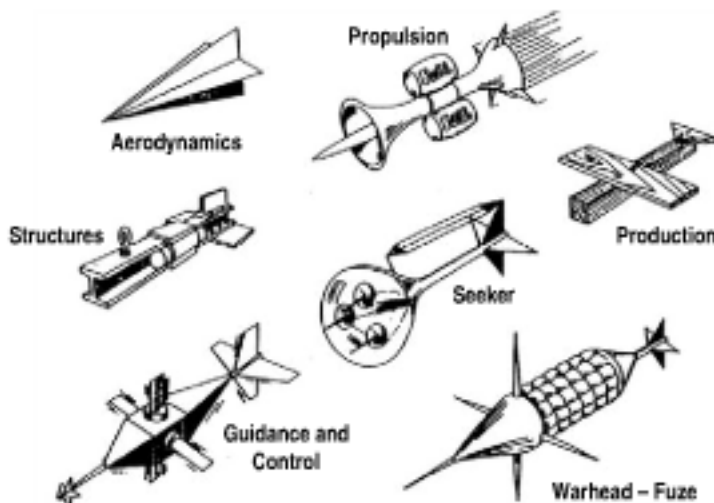


Fig. 9.5 Conduct unbiased tradeoffs.



Note: Although all of the above are supersonic air-to-air missiles, they have different configuration geometry

Fig. 9.6 Evaluate many alternatives.

stand still. The developer of a missile should not ignore new technology because of a “not invented here” attitude. A good design should eventually be replaced by a better design.

9.9 Evaluate Technology Risk

Immature technologies often have unknown and adverse interactions with other subsystems. Unfortunately, the technical specialist will often present only the favorable features of a technology. A technology should not be inserted into a future EMD or production program unless the technology is mature and the risk, performance, schedule, and cost have been fully characterized. Figure 9.8 illustrates that there may be hidden, perhaps even disguised, problems of using a new, highly immature technology.



Fig. 9.7 Evaluate and refine as often as possible.



Fig. 9.8 Beware of highly immature technologies (they may have hidden system problems).

9.10 Maintain Real-Time Documentation

As illustrated in Fig. 9.9, a good practice is to maintain real-time documentation of the assumptions and results during the design study, rather than waiting until the end. A common mistake is to delay the documentation until the end of the study. However, key assumptions and results may be lost during the study unless there is timely and accurate documentation. Also, there may be insufficient time to complete the documentation before moving on to other activities.

9.11 Develop Good Documentation

Figure 9.10 lists documentation requirements for tactical missile conceptual design. Good documentation should provide a traceable flow-down of information from the system-level requirements to subsystem requirements to component performance to the technology rationale. The output of the missile design process includes the following.

- 1) Literature review bibliography.
- 2) Sketches of alternative concepts.
- 3) Justification of the recommended concept(s), including reasons for the



Fig. 9.9 Keep track of assumptions and results.

concept(s) being selected, measures of merit, design tradeoffs, criteria for selection, and advantages compared with alternative concepts. Measures of merit include maximum range, minimum range, maximum speed, and accuracy.

4) Aerodynamics and propulsion characteristics, including aerodynamic stability, aerodynamic control effectiveness, normal force, axial force, specific impulse, thrust, weight of propellant/fuel, and the methods used for prediction.

5) Mission flight profiles of the preferred concept(s).



Technology Roadmap

Unit production cost

Weight and balance

Three-view drawing of preferred concept (s)

Traceability of system driving MIRs

Sensitivity of system / subsystem parameters

Mission flight profiles of preferred concept (s)

Aero and propulsion characteristics

Justification of recommended concept(s)

Sketches of alternative concepts

Literature review bibliography

Fig. 9.10 Maintain good documentation.

- 6) Sensitivity of the system/subsystem parameters to measures of merit.
- 7) Traceability of the system driving most important requirements (MIR).
- 8) Three-view drawing of preferred concept(s), including an outboard profile showing external features and dimensions, and inboard profiles showing subsystems and their dimensions.
- 9) Weight and balance statement, including subsystems weight, subsystems location, launch and burnout center of gravity, launch and burnout moments of inertia, and the methods used for weight and balance.
- 10) Unit production cost, including the number of units that are produced, the learning curve, and the basis for the learning curve.
- 11) Technology roadmap of technologies that require development to demonstrate maturity and readiness for an operational application. The technology roadmap includes the required schedule and milestones for timely insertion of technology into an operational system.

9.12 Utilize Group Skills

Tactical missile conceptual design is conducted by a small group of engineers in an advanced programs department. The advanced programs/conceptual design team is usually part of a larger organization. A system design engineer leads the conceptual design activity, with support from about 10 engineers, representing the key technical areas. It is important that the design team function as a synergistic group rather than a set of individuals with primary interests in promoting their individual technical areas.

Figure 9.11, based on Ref. 26, shows that the size of the conceptual design team is about 2% of the engineering organization. The size of the typical advanced programs/conceptual design organization is about 10–30 engineers, with about two engineers in each broad technical area (e.g., system design, aerodynamics, propulsion, structures, performance, flight control, guidance and navigation, sen-

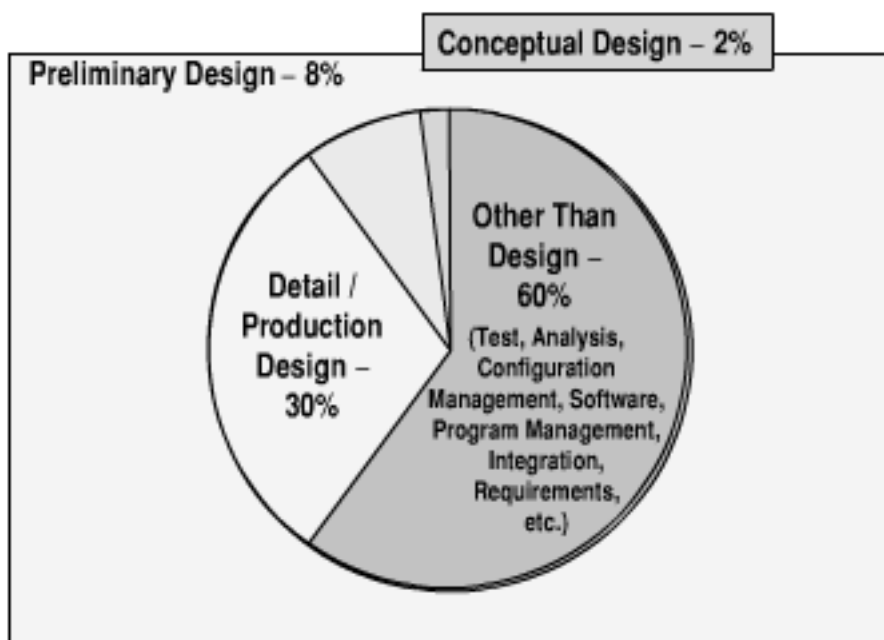


Fig. 9.11 Develop skills for a small work group (from Ref. 26).

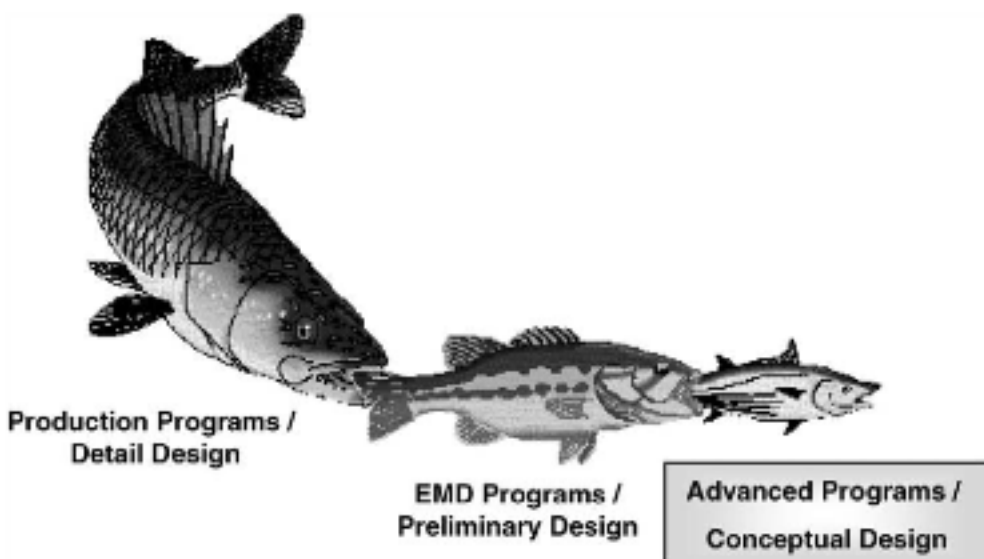


Fig. 9.12 Be agile to survive in the food chain.

sors, warhead, system effectiveness, cost). Usually there is a senior engineer as a mentor for each junior engineer. Most of the junior engineers move out of the conceptual design organization after a few years. The junior system engineers often become program managers, while the junior technical specialists may move on to either providing technical support to specific programs or to conducting more detailed work in their technical specialty.

9.13 Balance the Tradeoff of Importance Versus Priority

The advanced programs/conceptual design team works on future business opportunities that are important but that have relatively low priority in comparison to the more near-term concerns of the larger organization. As illustrated in Fig. 9.12, it is important to be agile to survive in the dynamic environment of the shifting priority for the EMD and production programs. When the large programs get into trouble, there is a tendency to “mortgage the future” or “eat the seed corn” by taking away the funding and personnel in advanced programs. In many organizations the senior engineering managers and program managers began their careers in advanced programs/conceptual design. There may be unspoken management support for conceptual design and advanced programs in spite of the relatively low priority and the lack of a short-term return on investment.

9.14 Iterate the Configuration Design

Figure 9.13 shows one last time that the conceptual design sizing process requires iteration, iteration, and iteration. A conceptual design is only as good as the number of iterations and the number of alternatives considered.

9.15 Configuration Sizing Conceptual Design Criteria

Table 9.1 shows conceptual design configuration sizing criteria for tactical missiles that were presented in this text. An examination of the configuration characteristics of the current tactical missiles, missile sizing method parameters,

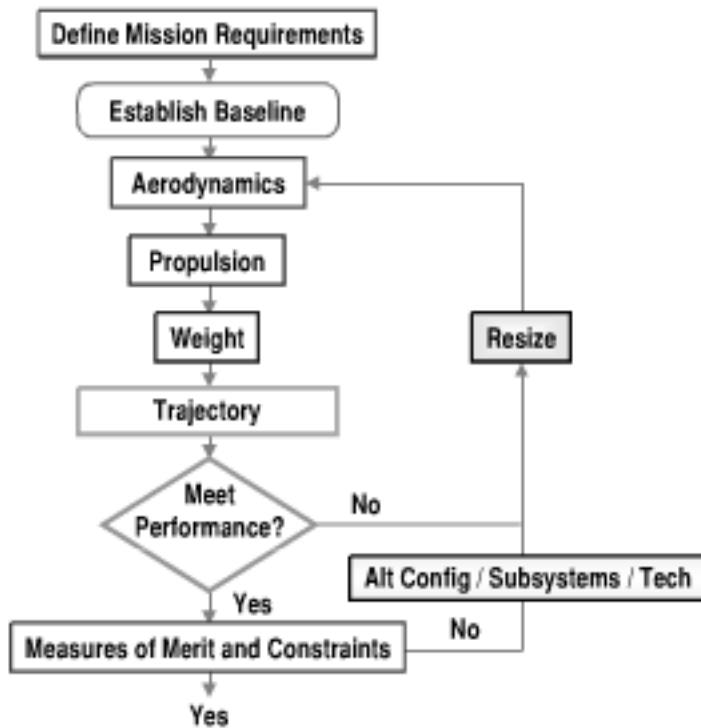


Fig. 9.13 Iterate, iterate, iterate.

Table 9.1 Configuration sizing conceptual design criteria

Configuration sizing parameter	Design criteria
Flight performance related	
Body fineness ratio	$5 < l/d < 25$
Nose fineness ratio	$l_N/d \approx 2$ if $M > 1$
Boattail diameter ratio	$0.6 < d_B/d_{Ref} < 1.0$
Cruise dynamic pressure	$q < 1000$ psf
Missile homing velocity	$V_M/V_T > 1.5$
Ramjet combustion temperature	>4000°F
Oblique shocks prior to inlet normal shock	>1 oblique shock if $M > 3.0$, >2 if $M > 3.5$
Inlet spillage	Shock on cowl lip at M_{max} cruise
Guidance and control related	
Body bending frequency	$\omega_{BB} > 2\omega_{ACT}$
Trim control power	$\alpha/\delta > 1$
Stability and control cross coupling	<30%
Airframe time constant	$\tau < 0.2$ s
Missile maneuverability	$n_M/n_T > 3$
Proportional guidance ratio	$3 < N' < 5$

and missile design activities suggests configuration design criteria. The table has 14 configuration design criteria related to the areas of flight performance and guidance and control. Configuration design criteria related to flight performance include missile body fineness ratio, nose fineness ratio, boattail ratio, cruise dynamic pressure, missile homing velocity, ramjet combustion temperature, oblique shocks prior to the inlet normal shock, and inlet spillage. A design criterion for the missile body fineness ratio (length-to-diameter ratio) is that it should be between 5 and 25 to harmonize tradeoffs of drag, subsystem packaging available volume, launch platform integration, seeker and warhead effectiveness, and body bending. The nose fineness (nose length-to-diameter ratio) for supersonic missiles should be approximately 2 to avoid high drag at high speed without degrading seeker performance. Boattail diameter ratio (boattail-diameter-to-maximum-missile-diameter ratio) should be greater than 0.6 for supersonic missiles to avoid increased drag at high speed. A design criterion for efficient cruise flight is that the dynamic pressure be less than 1000 psf. Missile velocity should be at least 50% greater than the target velocity to capture the target. Ramjet combustion temperature should be greater than 4000°F for high specific impulse and thrust at Mach numbers greater than 3.5. Efficient inlet integration for supersonic missiles requires at least one oblique shock prior to the inlet normal shock for good inlet total pressure recovery at Mach numbers greater than 3.0. For Mach numbers greater than 3.5, at least two oblique shocks prior to the inlet normal shock are desirable for inlet total pressure recovery. Finally, the forebody shock wave should impact the inlet cowl lip at the highest Mach number cruise condition to minimize the spillage drag at lower Mach number.

Configuration design criteria related to guidance and control include the flight control actuator frequency, trim control power, stability and control derivatives cross coupling, airframe time constant, missile maneuverability, and proportional guidance ratio. Body bending frequency in the first mode should be greater than twice the flight control actuator frequency if possible, to avoid the complication and risk of notch filters. Trim control power (trim-angle-of-attack-to-control-surface-deflection ratio) should be greater than 1 for maneuverability. Stability and control derivatives cross coupling should be less than 30% for efficient dynamics. The missile airframe time constant should be less than 0.2 s for precision accuracy (3 m). Contributors to a low value of the airframe time constant include high maneuverability capability, neutral static margin, high rate control surface actuators, low dome error slope, and a low noise seeker. Missile maneuverability should be at least three times the target maneuverability for small miss distance. Finally, the proportional guidance ratio should be between 3 and 5 to minimize miss distance. Values less than 3 result in excessive time to correct heading error, whereas values greater than 5 make the missile overly sensitive to noise input from the seeker and the dome error slope.

9.16 Wrap-Up

Missile design is a creative and iterative process that includes system-of-systems considerations, missile sizing, and flight trajectory evaluation. Because many of the cost and performance drivers may be “locked in” early during the design process, the emphasis of this text has been on conceptual design.

Missile design is an opportunity to harmonize diverse inputs early in the missile development process. The military customer, operations analysts, system integration engineers, conceptual design engineers, technical specialists, and others work together in harmonizing the mission/scenario definition, system-of-system requirements, launch platform integration, missile concept synthesis, and technology assessment/roadmaps.

Missile conceptual design is a highly integrated process requiring synergistic compromise and tradeoffs of many parameters. The synthesis of an effective compromise requires balanced emphasis in subsystems, unbiased tradeoffs, and the evaluation of many alternatives. It is important to keep track of assumptions to maintain traceable results. Starting with a well-defined baseline that has similar propulsion and performance expedites design convergence and provides a more accurate design.

Conceptual design is an open-ended problem and has no single right answer. The available starting point information is never sufficient to provide only one solution. The design engineer makes assumptions in coming up with candidate concepts, subsystems, and technologies to satisfy mission requirements and cover the solution space. Weighting of the most important measures of merit is required in coming up with a cost-effective solution. The military customer buy-in is important in achieving a consensus weighting of the most important measures of merit. Trade studies are conducted to investigate the impact of design parameters. Sensitivity analyses are also conducted to evaluate the effects of uncertainty in the design and the benefit of new technology. The missile is designed for robustness to handle risk and uncertainty of both a deterministic and a stochastic nature.

Finally, a good conceptual design code is a physics-based code that connects the missile geometric, physical, and subsystem performance parameters directly into a flight trajectory evaluation. Good conceptual design codes do not automatically change the design or resize automatically. It is best that the missile designer make the creative decisions.

Appendix A Nomenclature

The figures and tables in this text are designed as a stand-alone set of information. In most cases it is possible to use a figure or table without referring to the text or referring to other figures and tables. When practical the symbols are defined in the figures and tables. As a complement, a list of symbols is provided in this section.

a	= speed of sound
A	= target aspect angle or aspect ratio
A_0	= freestream air inlet capture area
A_3	= combustor flame holder entrance area
A_B	= propellant burn area
A_C	= inlet capture area
a_M	= acceleration of missile
A_P	= target presented area
A_{Ref}	= reference area
A_T	= throat area
A_V	= target vulnerable area
b	= span
b_w	= wing span
B	= bandwidth or billion
C	= contrast, explosive charge weight, coefficient, chord length, or cost
C_I	= cost of 1st unit
c	= heat capacity or type of loading
c^*	= characteristic velocity
C_A	= axial force coefficient
C/C_T	= actual-contrast-to-threshold-contrast ratio
c_d	= discharge coefficient
C_D	= drag coefficient
C_{D_0}	= zero-lift drag coefficient
$(C_{D_0})_{\text{Base}}$	= base drag coefficient at zero angle of attack
$(C_{D_0})_{\text{Body,PowerOff}}$	= body zero lift drag coefficient with power off
$(C_{D_0})_{\text{Body,PowerOn}}$	= body zero lift drag coefficient with power on
cg_{BO}	= center of gravity at burnout
cg_{Launch}	= center of gravity at launch
C_{I_s}	= rolling moment derivative due to sideslip
$C_{I_{ba}}$	= rolling moment derivative due to roll control deflection
$C_{I_{by}}$	= rolling moment derivative due to yaw control deflection

C_{I_ϕ}	= rolling moment derivative due to roll angle
C_{L_a}	= lift curve slope due to angle of attack
C_m	= pitching moment coefficient
C_{MAC}	= mean aerodynamic chord
C_{m_a}	= pitching moment derivative due to angle of attack
C_{m_z}	= pitching moment derivative due to pitch control deflection
C_N	= normal force coefficient
$C_{N\alpha}$	= normal force derivative due to angle of attack
C_{N_z}	= normal force derivative due to pitch control deflection
$(C_N)_{wing}$	= wing normal force coefficient
C_{n_δ}	= yawing moment derivative due to angle of sideslip
$C_{n_{\delta_a}}$	= yawing moment derivative due to roll control deflection
$C_{n_{\delta_r}}$	= yawing moment derivative due to yaw control deflection
c_R	= root chord
c_{skin}	= heat capacity of airframe skin
C_{skin}	= specific heat ratio of wall material
C_T	= threshold contrast
C_x	= cost of unit x
d	= diameter
D	= drag force
D_0	= zero-lift drag
D_{AVG}	= average drag
d_{bemi}	= diameter of hemisphere
d_{Ref}	= reference diameter
dt	= incremental time
E	= Young's modulus of elasticity
E_c	= energy per unit mass of charge
E_T	= total energy
f	= frequency
f/a	= fuel-to-air ratio
F	= force or noise factor
F_t	= tensile stress
$(F_t)_{HoopStress}$	= hoop tensile stress
$(F_t)_{LongitudinalStress}$	= longitudinal tensile stress
F_{TU}	= ultimate tensile stress
g_c	= gravitational constant (32.2 ft/s^2)
G_r	= gain of receiver antenna
G_t	= gain of transmitter antenna
h	= altitude or inlet height
H_f	= heating value of fuel
h_L	= launch altitude
I	= moment of inertia
I_{SP}	= specific impulse
I_t	= total impulse (average thrust \times time)
I_y	= yaw moment of inertia
K	= Boltzman's constant or thickness constant
k	= conductivity
l	= length

l_B	= length of body
L	= lift force, lead angle, learning curve, or loss factor
l/d	= length/diameter
L/D	= lift/drag
l_N	= length of nose
l_N/d	= nose fineness ratio
l_{Ref}	= reference length
M	= Mach number or moment
$M_{\Delta \text{LE}}$	= Mach number perpendicular to leading edge
M_0	= freestream Mach number
M_∞	= freestream Mach number
M_B	= bending moment
M_C	= mass of charge of warhead
M_i	= impact Mach number
M_L	= launch Mach number
M_m	= mass of metal case of warhead
M_{wh}	= mass of warhead
N	= normal force, noise, or navigation ratio
N'	= effective navigation ratio
n	= number of pulses
n_{hits}	= number of hits
n_M	= missile maneuver acceleration g
n_T	= target maneuver acceleration g
n_X	= acceleration g in longitudinal direction
n_Z	= acceleration g in vertical direction
p	= pressure
P	= penetration, load, or power
p_0	= freestream pressure
$P_{B,C}$	= baseline parameter, corrected (actual data)
$P_{B,U}$	= baseline parameter, uncorrected
p_{blast}	= blast pressure
p_c	= chamber pressure
$P_{CD,C}$	= conceptual design parameter, corrected
$P_{CD,U}$	= conceptual design parameter, uncorrected
p_e	= exit pressure
P_K	= probability of kill
P_{KE}	= penetration of kinetic energy warhead
P_r	= power received
p_t	= total pressure
P_t	= power transmitted
p_{t_0}	= total pressure of freestream
p_{t_2}	= total pressure after normal shock
q	= dynamic pressure, $\frac{1}{2}\rho V^2$
Q	= heat flux
r	= radius, recovery factor, or propellant burn rate
R	= range, radius, dome error slope, or reliability
R_{boost}	= boost range
R_{coast}	= coast range

R_D	= detection range
R_F	= flight range
$R_{F\text{-Pole}}$	= standoff range at missile intercept
R_L	= launch range
$R_{\text{Lock-on}}$	= seeker lock-on range
R_R	= recognition range
R_{sustain}	= sustain range
R_T	= turn radius
S	= area or signal
S_{hemi}	= cross-sectional area of hemisphere
S/N	= signal-to-noise ratio
S_{Ref}	= reference area
S_T	= tail area
S_W	= wing area
t	= time or thickness
T	= thrust, temperature, or tail
T_0	= freestream temperature
t_0/τ	= number of time constants for intercept
T_4	= combustor temperature
t/t_0	= fraction of time-to-go
t_B	= rocket motor burn time
T_B	= boost thrust
t_C	= coast time
t_f	= time of flight
t_{MAC}	= maximum thickness of mean aerodynamic chord
T_{\max}	= maximum temperature
t_S	= rocket motor sustain time
T_{skin}	= skin temperature
$(T_{\text{skin}})_i$	= skin initial temperature
t_{skin}	= thickness of wall material
V	= velocity
V_{BC}	= velocity at begin of coast
V_{BS}	= velocity at begin of sustain
V_C	= climb velocity
V_D	= dive velocity
V_e	= nozzle exit velocity
V_{EC}	= velocity at end of coast
V_f	= fragment velocity
V_L	= launch velocity
V_M	= missile velocity
V_T	= target velocity
V_∞	= freestream velocity
W	= weight or wing
W_{BC}	= weight at the beginning of coast
W_{BO}	= weight at burnout
W_c	= weight of warhead charge
W_f	= weight of fuel
W_f'	= fuel flow rate

W_L	= launch weight
W_m	= weight of warhead metal case (fragments)
W_{Missile}	= missile weight
W_P	= propellant weight
w_p	= propellant burn rate
x	= distance or number of missiles produced
x_{AC}	= aerodynamic center location
$(x_{AC})_{\text{wing}}$	= wing aerodynamic center location
x_{CP}	= center-of-pressure location
x_{CG}	= center-of-gravity location
y_{cp}	= lateral location of center of pressure
z	= warhead scaling parameter
z_{skin}	= airframe skin thickness
α	= angle of attack or thermal diffusivity
α'	= local effective angle of attack
α_{Trim}	= trim angle of attack
$\alpha/\dot{\gamma}$	= angle of attack sensitivity to turn rate
α/δ	= change in angle of attack with control deflection
β	= angle of sideslip
δ	= control deflection or body angle
δ_{LE}	= section leading edge angle
δ_{\max}	= maximum control deflection
δ_{trim}	= control deflection for trim
ε	= nozzle expansion ratio (exit area/throat area) or strain
ϕ	= equivalence ratio (actual fuel-to-air compared to stoichiometric) or missile roll angle
γ	= specific heat ratio (≈ 1.4 for air, ≈ 1.2 for rocket motor) or flight path angle
$\dot{\gamma}$	= turn rate
γ_C	= climb angle
γ_D	= dive angle
γ_{M_0}	= missile initial heading error
η	= efficiency ($n = 1$ is 100% efficient)
λ	= taper ratio (tip chord/root chord) or wavelength
θ	= missile pitch attitude, beam width, or shock angle
θ_F	= vision foveal angle
ρ	= density
ρ_M	= missile average density
ρ_p	= density of penetrator warhead
ρ_{skin}	= density of wall material
ρ_T	= density of target
ρ_∞	= freestream density
σ	= radar cross section, stress, standard deviation, or miss distance
σ_{buckling}	= buckling stress
σ_{HE}	= miss distance due to heading error
σ_{MAN}	= miss distance due to target maneuver acceleration
σ_{Max}	= maximum stress
σ_{ult}	= ultimate stress

σ_{yield}	= yield stress
τ	= time constant
τ_{Dome}	= time constant due to dome error slope
τ_{Filter}	= time constant due to guidance filers
τ_{Total}	= total time constant
τ_δ	= time constant due control deflection
$\tau_{\dot{\delta}}$	= time constant due control deflection rate
ω_{BB}	= first mode body bending frequency
ζ	= damping coefficient
Δ	= incremental
Λ	= leading edge sweep
AVG	= average
C.G.	= center of gravity
CP	= center of pressure
F-Pole	= standoff range at missile intercept
$2a$	= major axis of ellipse
$2b$	= minor axis of ellipse

Appendix B

Acronyms

AAA	= anti-aircraft artillery
AAM	= air-to-air missile
ACTD	= advanced concept technology demonstration
ADAM	= advanced design of aerodynamic missiles
AEDC	= Arnold Engineering and Development Center
AGM	= air-to-ground missile
AIM	= air intercept missile
A/J	= antijam
AOA	= angle of attack or assessment of alternatives
ARM	= antiradiation missile
ARRMD	= Affordable Rapid Response Missile Demonstrator
ASALM	= Advanced Strategic Air Launched Missile
ATA	= air to air
ATD	= advanced technology demonstration
ATR	= automatic target recognition
ATS	= air to surface
BAT	= Brilliant Anti-Tank
BDA	= battle damage assessment
BDI	= battle damage indication
BL	= baseline or body line
BTT	= bank to turn
C3I	= command, control, communication, intelligence
C4ISR	= command, control, communication, computers, intelligence, surveillance, reconnaissance
CCM	= counter-countermeasures
CEP	= circular error probable
CFD	= computational fluid dynamics
CL	= centerline
CLS	= canister launch system
CL Tk	= centerline tank carriage
CM	= cruise missile
COTS	= commercial off-the-shelf
DCR	= dual combustor ramjet-scramjet
DOD	= Department of Defense
DOF	= degree of freedom
DOS	= disk operating system
ECM	= electronic countermeasures

EFP	= explosively formed projectile
EMD	= engineering and manufacturing development
EMP	= electromagnetic pulse
EO	= electro-optical
EOCM	= electro-optical countermeasures
FEM	= finite element modeling
FMRAAM	= Future Medium Range Air-to-Air Missile
FOR	= field of regard
FOS	= factor of safety
FOV	= field of view
GPS	= Global Positioning System
HE	= high explosive or heading error
HM	= hypersonic missile
HMX	= Her Majesty's Explosive
HPM	= high-power microwave
HWL	= hardware in the loop
IIR	= imaging infrared
INS	= inertial navigation system
IOC	= initial operational capability
IR	= infrared
IRR	= integral rocket ramjet
ITCV	= Inter-Tropical Convergence Zone
JI	= jet interaction
KE	= kinetic energy
LADAR	= laser detection and ranging
LE	= leading edge
LOCAAS	= Low Cost Autonomous Attack System
LOS	= line of sight angle
LWIR	= long-wave infrared
MAC	= mean aerodynamic chord
MEOP	= maximum effective operating pressure
MD	= miss distance
MEMS	= micro-machined electro-mechanical systems
MIL STD	= military standard
MIR	= most important requirements
mmW	= millimeter wave
MRAAM	= medium range air-to-air missile
MWIR	= midwave infrared
NCTID	= noncooperative target identification
OP	= operating pressure
PBX	= plastic bonded explosive
PH	= precipitation hardened
PDRR	= program definition and risk reduction
PGM	= precision guided munitions
RAM	= radar absorbing material
RCS	= radar cross section
RDX	= Royal Demolition Explosive
RF	= radar frequency

RFCM	= radar frequency countermeasure
RJ	= ramjet or reaction jet
RSS	= root-sum-of-the-squares
RT	= room temperature
RT&A	= research, technology, and acquisition
SAM	= surface-to-air missile
SAR	= synthetic aperture radar
SL	= sea level
SOTA	= state of the art
STA	= station or surface to air
STD	= standard
STS	= surface to surface
STT	= skid to turn
SW	= Sidewinder
TAD	= technology availability date
TBM	= theater ballistic missiles
TCT	= time-critical target
TE	= trailing edge
TEL	= transporter, erector, launcher
TK	= tank
TLE	= target location error
TM	= telemetry
TMD	= tactical missile design
TNT	= trinitrotoluene
TRL	= technology readiness level
TURB	= turbulent
TVC	= thrust vector control
UAV	= unmanned air vehicle
UCAV	= unmanned combat air vehicle
VLS	= vertical launch system
WAGE	= Wide Area GPS Enhancement
WBS	= work breakdown structure
W/H	= warhead
XLDB	= cross-linked double-base

Appendix C

Conversion Factors

Table C.1 Conversion of English to metric units

Parameter	English unit	Metric unit	Multiply by
Acceleration	ft/s ²	m/s ²	0.3048
Area	ft ²	m ²	0.09294
Area	in. ²	m ²	6.452E-04
Density	lbm/in. ³	kg/m ³	2.767E+04
Density	lbm/ft ³	kg/m ³	16.02
Density	lb·s ² /in. ⁴	kg/m ³	1.069E+07
Density	slug/ft ³	kg/m ³	515.4
Energy	Btu	J	1055
Energy	ft-lbf	J	1.3557
Force	lbf	N	4.4484
Heat capacity	Btu/lbm/°F	J/kg/°C	4188
Heat transfer rate	Btu/ft ² /s	W/m ²	1.135E+04
Heat transfer coefficient	Btu/h/ft ² /°F	W/m ² /°C	5.6786
Length	ft	m	0.3048
Length	in.	m	0.0254
Length	mile	m	1609
Length	n mile	m	1853
Mass	lbm	kg	0.4535
Mass	lbf·s ² /in.	kg	1200
Mass	slug	kg	14.59
Mass flow rate	lbm/h	kg/s	1.260E-04
Mass flow rate	lbm/s	kg/s	0.4535
Moment of inertia	ft-lbf·s ²	kg·m ²	1.3557
Moment of inertia	in.-lbf·s ²	kg·m ²	0.113
Power	Btu/h	W	0.2931
Power	hp	W	745.71
Pressure	lbf/ft ²	Pa	47.89
Pressure	lbf/in. ²	Pa	6897
Pressure	atm	Pa	1.013E+05
Specific heat	Btu/lbm/°F	J/kg/°C	4186
Temperature	°F	°C	(°F - 32) 0.5556

(continued)

Table C.1 Conversion of English to metric units (continued)

Parameter	English unit	Metric unit	Multiply by
Temperature	°F	K	(°F + 460) 0.5556
Temperature	°R	K	0.5556
Thermal conductivity	Btu/h/ft/°F	W/m/°C	1.7307
Torque	ft-lbf	N-m	1.3557
Torque	in.-lbf	N-m	0.113
Velocity	ft/s	m/s	0.3048
Viscosity, absolute	lbf-s/ft ²	N-s/m ²	47.87
Viscosity, absolute	lbm-s/ft	N-s/m ²	1.4881
Viscosity, kinematic	ft ² /s	m ² /s	0.09294
Volume	ft ³	m ³	0.02831
Volume	in. ³	m ³	1.639E-05
Volume	U.S. gal	m ³	0.003785

References

- ¹AIAA *Aerospace Design Engineers Guide*, AIAA, Washington, DC, 1993.
- ²Chin, S. S., *Missile Configuration Design*, McGraw-Hill, New York, 1961.
- ³Mason, L. A., Devan, L., and Moore, F. G., "Aerodynamic Design Manual for Tactical Weapons," NSWCTR 81-156, 1981.
- ⁴Pitts, W. C., Nielsen, J. N., and Kaattari, G. E., "Lift and Center of Pressure of Wing-Body-Tail Combinations at Subsonic, Transonic, and Supersonic Speeds," NACA Rept. 1307, 1959.
- ⁵Jorgensen, L. H., "Prediction of Static Aerodynamic Characteristics for Space-Shuttle-Like, and Other Bodies at Angles of Attack from 0° to 180°," NASA TND 6996, Jan. 1973.
- ⁶Hoak, D. E., et al., "USAF Stability and Control Datcom," AFWAL TR-83-3048, Global Engineering Documents, Irvine, CA, 1978.
- ⁷Cox, H. H., "Internal Aerodynamics," North American Aircraft Lecture Course, April 1968.
- ⁸Kinroth, G. D., and Anderson, W. R., "Ramjet Design Handbook," AFWAL TR 80-2003, June 1980.
- ⁹"Technical Aerodynamics Manual," North American Rockwell Corp., DTIC AD 723823, June 1970.
- ¹⁰Oswatitsch, K., "Pressure Recovery for Missiles with Reaction Propulsion at High Supersonic Speeds," NACA TM-1140, 1948.
- ¹¹Jerger, J. J., *Systems Preliminary Design Principles of Guided Missile Design*, Van Nostrand, Princeton, NJ, 1960.
- ¹²Schneider, S. H., *Encyclopedia of Climate and Weather*, Oxford Univ. Press, Oxford, England, UK, 1996.
- ¹³Priessner, "Attenuation by Atmospheric Gases, Clouds, and Rain," 1979.
- ¹⁴U.S. Army Ordnance Pamphlet ORDP-20-290-Warheads, 1980.
- ¹⁵Carleone, J. (ed.), *Tactical Missile Warheads*, Vol. 155, Progress in Astronautics and Aeronautics, AIAA, Washington, DC, 1993.
- ¹⁶Christman, D. R., and Gehring, J. W., "Analysis of High-Velocity Projectile Penetration Mechanics," *Journal of Applied Physics*, Vol. 37, 1966.
- ¹⁷Heaston, R. J., and Smoots, C. W., "Precision Guided Munitions," GACIAC Rept. HB-83-01, May 1983.
- ¹⁸Donatelli, G. A., and Fleeman, E. L., "Methodology for Predicting Miss Distance for Air Launched Missiles," AIAA Paper 82-0364, Jan. 1982.
- ¹⁹Bennett, R. R., and Mathews, W. E., "Analytical Determination of Miss Distances for Linear Homing Navigation Systems," Hughes Tech. Memo 260, Hughes Aircraft, 31 March 1952.
- ²⁰Nicholas, T., and Rossi, R., *US Missile Data Book*, 1996, Data Search Associates, Orange County, CA, 1996.

- ²¹Bithell, R. A., and Stoner, R. C., "Rapid Approach for Missile Synthesis," AFWAL TR 81-3022, Vol. 1, March 1982.
- ²²Fleeman, E. L., and Donatelli, G. A., "Conceptual Design Procedure Applied to a Typical Air-Launched Missile," AIAA Paper 81-1688, Aug. 1981.
- ²³Hindes, J. W., "Advanced Design of Aerodynamic Missiles (ADAM)," Oct. 1993.
- ²⁴Bruns, K. D., Moore, M. E., Stoy, S. L., Vukelich, S. R., and Blake, W. B., "Missile Datcom," AFWAL-TR-91-3039, April 1991.
- ²⁵Moore, F. G., McInvile, R. M., and Hymer, T. C., "Application of the 1998 Version of the Aeroprediction Code," *Journal of Spacecraft and Rockets*, Vol. 36, No. 5, Sept.-Oct. 1999.
- ²⁶Nicolai, L. M., "Designing a Better Engineer," *Aerospace America*, April 1992.

Bibliography

System Design

- Ashley, H., *Engineering Analysis of Flight Vehicles*, Dover, New York, 1974.
- Ball, R. E., *The Fundamentals of Aircraft Combat Survivability Analysis and Design*, AIAA, New York, 1985.
- Defense Technical Information Center, <http://www.dtic.mil/>
- "DoD Index of Specifications and Standards," <http://www.dtic.mil/stinet/str/dodiss4-fields.html>
- Eichblatt, E. J., *Test and Evaluation of the Tactical Missile*, AIAA, Washington, DC, 1989.
- Fleeman, E. L., "Aeromechanics Technologies for Tactical and Strategic Guided Missiles," AGARD Paper, FMP Meeting, London, May 1979.
- Fleeman, E. L., "Tactical Missile Design," AIAA Short Course, AIAA, Reston, VA, Aug. 2000.
- Giragosian, P. A., "Rapid Synthesis for Evaluating Missile Maneuverability Parameters," *10th AIAA Applied Aerodynamics Conference*, AIAA, Washington, DC, June 1992.
- Hogan, J. C., et al., "Missile Automated Design (MAD) Computer Program," AFRPL TR 80-21, March 1980.
- Lee, R. G. (Ed.), *Guided Weapons*, Third Edition, Brassey's, London, 1998.
- Lindsey, G. H., and Redman, D. R., "Tactical Missile Design," Naval Postgraduate School, Monterey, CA, 1986.
- "Missile System Flight Mechanics," AGARD CP270, May 1979.
- Nicolai, L. M., *Fundamentals of Aircraft Design*, METS, Inc., San Jose, CA, 1984.
- "Periscope," <http://www.periscope.usni.com>
- Rapp, G. H., "Performance Improvements with Sidewinder Missile Airframe," AIAA Paper 79-0091, Jan. 1979.
- Raymer, D. P., *Aircraft Design, A Conceptual Approach*, AIAA, Washington, DC, 1989.
- "Aircraft Stores Interface Manual (ASIM)," <http://www.asim.net>
- "Advanced Sidewinder Missile AIM-9X Cost Analysis Requirements Description (CARD)," <http://web2.deskbook.osd.mil/valhtml/2/2B/2B4/2B4T01.htm>

Aerodynamics

- Briggs, M. M., *Systematic Tactical Missile Design, Tactical Missile Aerodynamics: General Topics*, Vol. 141, Progress in Astronautics and Aeronautics, AIAA, Washington, DC, 1992.
- Briggs, M. M. (Ed.), "Aeromechanics Survey and Evaluation, Vol. 1-3," Naval Surface Warfare Center, NSWC/DL TR-3772, Dahlgren, VA, Oct. 1977.
- Burns, K. A., Deters, K. J., Haley, C. P., and Kihlken, T. K., "Viscous Effects on Complex Configurations," WL-TR-95-3060, 1995.

- Dillenius, M. F. E., et al., "Engineering-, Intermediate-, and High-Level Aerodynamic Prediction Methods and Applications," *Journal of Spacecraft and Rockets*, Vol. 36, No. 5, Sept.-Oct., 1999.
- Mendenhall, M. R., et al., *Proceedings of NEAR Conference on Missile Aerodynamics*, NEAR, Mountain View, CA, 1989.
- "Missile Aerodynamics," NATO AGARD LS-98, Feb. 1979.
- "Missile Aerodynamics," NATO AGARD CP-336, Feb. 1983.
- "Missile Aerodynamics," NATO AGARD CP-493, April 1990.
- "Missile Aerodynamics," NATO RTO-MP-5, Nov. 1998.
- Nielsen, J. N., *Missile Aerodynamics*, McGraw-Hill, New York, 1960.
- Nielsen, J. N., "Missile Aerodynamics - Past, Present, Future," AIAA Paper 79-1818, 1979.
- Nielsen, J. N., and Pitts, W. C., "Wing-Body Interference at Supersonic Speeds with an Application to Combinations with Rectangular Wings," NACA TN 2677, April 1952.

Propulsion

- Bonney, E. A., et al., "Propulsion, Structures and Design Practice," *Principles of Guided Missile Design*, Van Nostrand, Princeton, NJ, 1956.
- Chemical Propulsion Information Agency, <http://www.jhu.edu/~cpia/index.html>
- Mahoney, J. J., *Inlets for Supersonic Missiles*, AIAA, Washington, DC, 1990.
- Sutton, G. P., *Rocket Propulsion Elements*, J Wiley, New York, 1986.
- "Tri-Service Rocket Motor Trade-off Study, Missile Designer's Rocket Motor Handbook," Chemical Propulsion Information Agency, CPIA 322, Columbia, MD, May 1980.

Materials

- Budinski, K. G., and Budinski, M. K., *Engineering Materials Properties and Selection*, Prentice-Hall, Upper Saddle River NJ, 1999.
- "Matweb's Material Properties Index Page," <http://www.matweb.com>
- "NASA Ames Research Center Thermal Protection Systems Expert (TPSX) and Material Properties Database," <http://asm.arc.nasa.gov/tpsx/tpsxhome.shtml>

Guidance and Control

- Proceedings of AGARD G&C Panel Conference on Guidance & Control of Tactical Missiles*, AGARD LS-52, May 1972.
- Zarchan, P., *Tactical and Strategic Missile Guidance*, Vol. 124, Progress in Astronautics and Aeronautics, AIAA, Washington, DC, 1990.

Index

- Acceleration
 - initial heading error, 160, 161
 - longitudinal, 1, 2, 194, 195
 - maneuver, 1, 2, 160–163,
 - maneuvering target, 162, 163
- Aerodynamic heating, 83, 101, 112, 113
- Aerodynamic center, 29, 32, 33, 35, 36, 38, 40, 53, 214, 215
- Aeroelasticity, 20, 29, 177, 226
- Aircraft integration, 164–168, 175–183, 185, 202
- Air loads, 47, 107–110, 228
- Air-to-air missile, 6, 7, 12, 13, 17, 22, 46, 49, 71, 106, 148, 151, 165, 166
- Air-to-surface missile, 6, 7, 71, 165, 166, 183, 185, 187, 215, 217, 229, 235
- Altitude, 3, 6–9, 14, 23, 27, 29, 61, 62, 64, 66, 80, 101, 103, 115, 117, 119, 121, 122, 124, 125, 129–132, 136, 137, 139, 141, 144, 157, 159, 166–168, 192, 196, 202, 204–206, 211, 213, 226
- Aluminum, 21, 77, 84, 86, 87, 96–99, 101, 103, 104, 106, 166, 189
- Angular resolution, 17, 19, 20, 134, 135, 141, 142, 153, 163
- Annular, inlet 69, 70–73
- Antenna, 10, 19, 231, 232
- Aspect ratio, 30–33, 35, 49, 216
- Atmosphere, 137, 138
- Axial force, 117–119, 192, 193, 204, 239
- Bank-to-turn, 36, 37, 48–50, 71, 202
- Base area, 23, 25
- Base drag (base pressure drag), 22–25
- Baseline missile, 5, 13–17, 185–213
- Beam range, 115, 116, 126
- Beam width, 20
- Bending moment, 35, 106–111
- Binder, 84, 85
- Blast, 17, 145, 146, 168, 216, 217
- Blast, tube 38, 87, 88
- Blunt, nose 24, 33, 215
- Boattail drag, 25, 26
- Body
 - Bending, 3, 17, 20, 21, 117, 216, 243
 - center of pressure, 29
 - drag coefficient, 23, 24, 35
- Boost-glide trajectory, 61, 194–198
- Booster, 14, 61–64, 67–69, 76, 189, 191, 204, 206
- Breguet range equation, 62, 119, 120, 206, 216
- Buckling, 106, 107, 110, 112, 216
- Burn area, 78, 79, 81, 82, 212
- Burn rate, 78, 79, 82, 83, 195
- Canard, 12, 30, 33, 35–40, 42–44, 46, 52, 53, 55, 71, 112, 159, 231, 236
- Canister Launch System (CLS), 175, 176
- Captive flight, 94, 225
- Capture efficiency, inlet, 73, 74
- Carriage, 36–38, 61, 67, 69, 70, 89, 93, 94, 107, 110, 129, 164–166, 168, 175, 176, 178, 182, 183, 202, 228, 232
- Casting, 94–97, 101, 231
- Center of gravity, 14, 33, 42, 45, 52, 53, 55, 92, 139, 177, 179, 189, 203, 215, 240
- Center of pressure, 29, 32, 33, 36, 38, 40, 53, 214, 215
- Ceramic, 96, 97, 99, 100, 105
- Chamber pressure, 78–81, 83, 87, 191
- Characteristic velocity, 78, 79, 81, 199, 200
- Charge, warhead, 145–151
- Circular error probable (CEP), 8, 47–49, 140, 141, 145, 146, 148–150, 153–163, 177, 185, 198–199, 202, 215–217, 234, 243
- Climb, 120, 121, 123, 139, 216
- Cloud, 129–134
- Clutter, 19, 129, 133–135, 144, 230
- Coast, 23, 24, 35, 82, 83, 117, 124, 125, 195–198, 216, 217, 225
- Collision course, 154, 155
- Combustion chamber, 61, 67, 83, 202–206
- Communication, 10–12, 231, 232
- Composite material, 35, 86, 90, 96–101, 103–105, 110, 111, 221, 231, 232
- Composite propellant, 84, 85
- Compressed carriage, 36–38, 165, 175, 179, 180, 182, 183, 202, 232
- Computer aided sizing, 213–217, 227, 228
- Conceptual design, 3–6, 13–16, 52, 55–57, 72, 116, 117, 139, 140, 154–156, 193, 194, 205, 210, 213–217, 220–223, 227–229, 235,

- Conical nose, 73–75, 92, 93, 202
 Contrast, 134, 185–187
 Control effectiveness, 3, 4, 8, 14, 29, 35, 36, 38–44, 46–49, 51, 52, 55, 56, 118, 119, 123, 124, 156, 157, 159, 192, 193, 204, 214, 216, 228, 231, 239, 242, 243
 Control, types of
 all movable, 38, 40, 41
 canard, 30, 36, 39, 42, 43, 52, 71, 231
 flap, 38, 40, 41
 tail, 36–41, 52, 71, 202, 204, 205, 207, 208
 unconventional, 12, 30, 37, 46–48, 153, 225, 229
 wing, 36, 44, 45, 71, 123, 124, 189, 190, 192, 193
 Cost, 1, 4, 5, 6, 8, 9, 11, 12, 36, 46, 49, 64, 68, 71, 83, 85–89, 94–98, 100, 101, 104, 106, 111, 112, 129–131, 133, 134, 140, 143, 144, 145, 168–175, 216, 217, 219, 221, 230, 231, 234, 237, 240, 243, 244
 Counter measures, 141, 230
 Cross coupling, stability and control, 49, 55, 56, 228, 242, 243
 Cross flow, 26–29, 122, 216
 Cruciform design, 34, 36, 48, 49, 69–71, 188
 Cruise missile, 1, 2, 7–10, 22, 35–38, 59, 61, 62, 137, 138
 Cruise trajectory, 14, 15, 61–64, 119–121, 137–139, 202, 206, 210, 211, 213, 216, 230, 242, 243
 Damping characteristics, 51
 Degrees of freedom, 116–118, 125, 214–217, 227, 228
 Delta wing, 35, 36
 Density, 16, 77, 78, 84, 85, 90, 91, 99, 103–105, 119, 136–138, 152, 199, 200, 212, 216, 231
 Design,
 conceptual, 3–6, 13, 14, 52, 56, 72, 116, 117, 139, 140, 154, 155, 193, 194, 205, 210, 213–215, 222–224, 227, 228, 236, 238–244
 criteria, 52, 55, 56, 94, 214, 241–243
 detailed, 220–223, 228, 229,
 loads, 28, 93, 94, 106–110, 178, 183, 216, 228
 preliminary, 57, 116, 117, 223, 224, 227, 228
 Detection range, 19, 20, 134, 141, 167, 185, 186, 216, 217
 Development process, 94, 170, 175, 219–233
 Diameter considerations, 17–21
 Discharge coefficient, 80
 Dome
 bandpass, 111, 112
 error slope, 22, 29, 44, 48, 49, 156, 158–160, 163, 230, 243
 material alternatives, 111, 112
 stress, 111–113
 Double base propellant, 85
 cross flow, 27
 definition of, 17, 18
 skin friction, 23, 24
 wave, 23, 24, 33, 34
 Ducted rocket, 50, 60, 62–64, 144, 145, 212, 231
 Dynamic pressure, 1, 18, 28–30, 37, 66, 119, 121, 122, 124, 137–139, 159, 179, 206, 213, 243
 Dynamic stability, 214, 228
 Effective navigation ratio, 155, 159–162
 Ejection launch, 108–110, 175, 176, 178–181
 Electro-optical, 111–113, 131–136, 141
 End burning grain, 79, 81–83
 Engine nomenclature, 14, 15, 203, 204, 206
 Environment, 86, 91, 101, 131, 133–137, 139, 183, 220–222, 225, 226
 Exit
 pressure, 65–67
 velocity, 62, 63
 Expansion ratio, 79–81, 189, 191, 199, 200
 Faceted dome, 22, 48, 159, 160, 230
 Factor of safety, 93, 94, 177, 178
 Fineness ratio, 3, 8, 17, 20–25, 27, 73, 92, 93, 95, 144, 152, 157–160, 199, 200, 214, 236, 242, 243
 Firepower, 3, 9, 89, 129, 144, 145, 164–166, 176, 177, 183
 Flight loads, 28, 93, 94, 106–110, 178, 183, 216, 228
 Flight path angle, 118, 120, 121, 123, 124
 Flight performance, 5–7, 12, 13, 61, 62, 89, 90, 92, 115–127, 139, 153, 170, 192, 194, 196–198, 209, 210, 212–214, 216, 217, 227, 240, 242–244
 Flow path geometry, 14, 15, 87, 88, 203, 206
 Flow separation, 25, 47, 68, 69, 228
 Flow types
 laminar, 100, 101
 turbulent, 100–103
 Forebody types
 conical, 73, 75, 76, 92, 93, 202, 203
 hemispherical, 22, 24, 159, 160
 tangent ogive, 22, 158–160, 189
 Four degrees of freedom, 117, 214
 Fragment, 145–151, 168, 216
 Free-to-roll tails, 36, 39, 40, 42, 43, 231
 Freestream Mach number, 41, 62, 63, 66, 67, 73, 74, 203, 206
 Frequency, 19–21, 40, 49, 132, 135, 159, 242, 243
 Fuel
 alternatives, 3–5, 8, 28, 50, 61–64, 77, 83–85,

- Gain, 139, 167
Gas generator, 64
Global positioning system (GPS), 133–136, 141, 144, 145, 161, 230, 231
Grain configuration, 64, 77, 79, 81–83
Graphite, 87, 88, 97–101, 103–105
Ground handling loads, 86, 93, 94, 110, 168
- Hardware in the loop, 211, 224–229
Heading error, 115, 136, 154, 155, 160–163, 216, 217, 242, 243
Heat capacity, 103, 104
Heat flux, 101, 102
Heat sink, 61, 104, 112, 113
Heat transfer, 100–102, 112–114, 228
Heating, aerodynamic, 24, 59, 83, 100, 101, 103, 112–114, 136, 216, 228
Heating value of fuel, 16, 66, 77, 212
Hemispherical nose, 24, 110, 111, 159, 160
Hinge moment, 38, 40, 41, 44, 45, 229–231
Hoop stress, 110, 111
Horizontal flight, 117, 122–125, 195–198
Hypersonic Mach number, 26, 32, 53, 54, 59–63, 75, 78, 100, 112, 122, 151, 214, 229–231
Hypersonic missile, 1, 2, 9–11, 72, 101, 102, 105, 112, 152, 153, 223, 224, 229–231
- Imaging seeker, 12, 133–135, 141, 142, 153, 163, 171, 230–232
Impulse
 specific, 14–16, 59–62–66, 77–81, 83, 84, 119, 120, 125, 193, 195–198, 205, 206, 209–211, 216, 231, 232, 242, 243
 total, 118, 119, 175,
Induced roll, 29, 38–40, 42, 44, 45, 48–51, 55, 56, 227, 228
Inertia, moment of, 92, 93, 118, 137, 189, 191, 216, 239, 240
Inertial navigation system (INS), 134–136, 141, 144, 161, 230, 231
Infrared (IR) seeker, 12, 22, 111, 112, 132–135, 140, 141, 153, 230–232
Inlet
 alternatives, 14, 15, 49, 50, 59, 69, 70–72, 202, 203
 capture efficiency, 14, 15, 49, 70, 72–75, 202, 203, 216
 integration, 28, 68, 69, 75, 202, 203, 211, 242, 243
In-line surfaces, 37, 38
Insensitive munition, 85, 168, 224–227
Insulation, 86–89, 101, 103–106, 203, 231
Interdigitated surfaces, 36–38
Internal carriage, 164–166, 175, 179, 182, 183, 231, 232
IR dome, 22, 111, 112
Isentropic flow 65–67 216
Kill probability, 2, 135, 145, 146, 148, 185, 186, 216, 217
Laminar flow, 100, 101
Lattice fins, 40–42, 231
Launcher, 37, 165, 166, 175, 177, 178, 180, 181
Launch platform integration, 3, 4, 7–10, 17, 27–29, 36, 37, 50, 64, 67–70, 74, 86, 89, 93, 94, 107, 108, 110, 129, 130, 143, 144, 153, 164–167, 172, 173, 175–183, 202, 206, 217, 224, 225, 233–236, 242–244
Launch range, 9, 115, 116, 185–188, 216
Lead angle, 126, 154, 216
Learning curve, 170, 171, 216, 217, 239, 240
Length considerations, 3, 4, 6, 8, 21, 29, 61, 66–69, 78, 81, 91, 107, 108, 152, 175, 200–202, 215, 231, 232
Lessons learned, 233–244
Lethality, 4, 8, 129, 130, 142–153, 217, 234, 235
Lift, 38, 39, 42, 44, 119, 120, 196
Lifting body, 26–29, 48, 49, 95, 96, 231
Lift-to-drag ratio, 26–30, 40, 44, 50, 62, 117, 119–122, 137, 138, 196, 202
Limit stress, 97–99, 106, 107, 109–113, 152, 216
Linear wing theory, 30, 31, 54, 216
Line-of-sight, 48, 49, 153–155
Load distribution, 47, 107–110, 228
Loads, 28, 93, 94, 99, 106, 109, 111, 144, 183, 216, 228
Local angle of attack, 30–32, 38, 39, 42, 44, 101, 123, 177–179, 198, 199
Logistics, 8, 50, 89, 93, 143, 165, 170, 172, 175, 212
- Mach angle, 73
Maneuverability, 1, 4–7, 12, 29, 30, 40, 42, 44, 47–52, 57, 70, 71, 89, 90, 107, 108, 115, 116, 118, 119, 123, 136, 141, 160, 160, 162, 163, 175, 185, 192, 194, 198, 199, 223, 225, 226, 229, 231, 236, 242, 243
Manufacturing process, 42, 95–97, 111, 223
Mass ratio, 147–151
Material density, 91, 99, 101–105, 152, 178, 216, 231
Material strength, 97–99, 111, 112, 152, 189, 216, 221
Maximum angle of attack, 3, 6, 31, 52, 53, 123, 157, 229
Maximum effective operating pressure, 93, 94, 111
Maximum lift coefficient, 26, 52, 53
Maximum range, 14, 61, 62, 115, 116, 119, 192, 194, 238, 239
Maximum speed, 59, 60–63, 77, 78, 238, 239
Mean aerodynamic chord (MAC), 32–36, 54, 188
Measures of merit, 4–8, 12, 111, 129–175, 200,

- Minimum smoke, 80, 85, 164
 Miss distance, 8, 47–49, 140, 141, 145, 146, 148–150, 153–163, 177, 185, 198–202, 215–217, 234, 243
 Missiles, types of, 6, 7, 143, 144
 Mission definition, 3–5, 185–188, 216, 233, 244
 Mission requirements, 3–13, 17, 89, 126, 139, 140, 196, 197, 216, 219, 223, 238, 239, 244
 Moment of inertia, 92, 93, 118, 157, 189, 191, 216, 239, 240
 Monocoque construction, 96
 Motor case, 21, 44, 81, 86, 87, 93, 94, 96, 104–106, 110, 111, 180, 189, 191, 202, 216
- Natural frequency, 17, 20, 21, 49, 242, 243
 Navigation ratio, 155, 159–163
 Nitrocellulose, 85
 Noise, 17, 19, 134, 156, 163, 243
 Nomogram, 107–109
 Normal distribution, 139–141, 154
 Normal force
 due to angle of attack, 26, 27, 30–32, 51–54, 56, 118, 119, 123, 124, 159, 192, 193, 198, 199, 204, 207
 due to control deflection, 14, 31, 39, 42–44, 50–52, 118, 119, 123, 124, 159, 192, 193, 198, 199, 204, 208
 Normal force coefficient
 body, 26, 32, 56, 57, 199
 wing, 30–32, 56, 57, 199
 tail, 31, 32, 52, 53, 56, 57, 199
 total, 14, 32, 42, 44, 50, 52, 56, 57, 117, 118, 122, 192, 193, 204, 207, 216, 239
 Nose geometry, 1, 17, 21, 22, 24, 92, 93, 144, 158, 159, 160, 188, 202, 203, 205, 215
 Nose fineness, 3, 8, 21–25, 91, 144, 152, 158–160, 190, 199–201, 215, 242, 243
 Nose inlet, 69–74
 Nozzle
 discharge coefficient, 80, 81
 exit area, 14, 15, 79, 80, 87, 88, 191, 203, 206
 exit pressure, 65–67, 88
 expansion ratio, 65–67, 79–81, 189, 191, 200, 201
 exit velocity, 62, 63
 Oblique shock, 41, 42, 69, 70, 72–75, 216, 242, 243
 Off boresight, 12, 13, 22, 47–49, 115, 116, 126, 192, 194, 230
 One degree of freedom, 117, 118, 124, 125, 157, 158, 194
 Optimum
 climb, 120, 121, 138, 139
 cruise, 14, 15, 28, 61, 64, 119–122, 137–139, 196, 202, 206, 210, 211, 213, 229, 230, Parts count, 95–97, 168–170, 172, 230, 231
 Penetration, 11, 12, 144, 149–152, 216, 217
 Pintle motor, 62, 83, 84, 231, 232
 Pitching moment, 14, 15, 51–53, 55–57, 118, 157, 158, 192, 193, 204, 207
 Planform, 30–32, 34–38, 91, 188, 202, 203
 Point load, 108, 109
 Precision strike
 accuracy, 6, 7, 134–136, 144, 243
 missiles, 2, 6–12, 133, 134, 142–145, 171, 176, 177, 179
 Preliminary design, 57, 116, 117, 214, 220, 223, 224, 227, 228
 Pressure
 base, 23, 25, 192, 193
 chamber, 78–81, 83, 87, 88
 recovery, 70, 72, 74–76, 216, 231, 243
 Probability of kill, 2, 146, 148, 216, 217
 Production process, 83, 95–97, 143, 168, 169, 171, 174
 Progressive thrust, 81, 82
 Propellant
 flow rate, 78–84, 119, 195, 212, 213
 properties, 84–87, 189, 191
 selection, 3, 4, 84, 85
 Proportional guidance, 126, 135, 136, 154, 155, 160–163, 215–217, 243
 Pulse motor, 82, 83, 231, 232
 Pultrusion, 95–97, 232
- Radar
 beam width, 19, 20
 cross section, 1, 19, 21, 22, 28, 29, 35, 38, 40, 41, 141, 142, 164, 166, 167, 168, 217, 223, 224
 range, 18, 19, 167, 168
 Radial burn, 79–83
 Radome, 21, 111, 112, 158, 159, 189, 190
 Rail launch, 165, 166, 175, 177, 179–183
 Rain, 111, 112, 131–133, 183
 Ramjet, 14–16, 49, 50, 59–71, 73–77, 104, 119, 120, 137–139, 202–214, 216, 217, 225, 229, 231, 234, 236, 242, 243
 Range sensitivity, 89, 90, 193, 195, 206, 210
 Rate of climb, 120, 121, 123, 124, 216
 Rate of dive, 120, 121, 216
 Reaction jet, 29, 37, 48, 49, 117, 153, 229
 Recognition range, 185–187
 Recovery factor, 100, 101
 Recovery temperature, 100, 101
 Rectangular planform, 35, 36
 Reduced smoke, 164, 166, 167, 231, 232
 Regressive thrust, 81, 82
 Reliability, 168, 170, 172, 175, 225, 226, 234
 Robustness, 7, 8, 115, 129–142, 202, 234, 244
 Rocket motor, 6, 21, 60–63, 77–88, 93, 94, 96,

- Roll
 attitude, 48, 49, 227, 228
 orientation, 37, 38, 49, 227, 228
 stabilization, 48, 50, 56
Rolling airframe, 36, 37, 49, 50
- Safety, 84, 85, 93–95, 109–111, 177, 178, 183, 225
Scramjet, 59–62, 137, 231
Seeker, 3, 4, 12, 17, 19–22, 29, 44, 48, 89, 111, 112, 115, 126, 131–135, 139–142, 144, 152–156, 159–161, 163, 166, 168, 171, 174, 177, 178, 192, 216, 224, 225, 226, 230, 231, 243
Seeker dome, 21, 22, 29, 44, 49, 89, 111–113, 133, 134, 156, 158–160, 163, 183, 189, 190, 203, 205, 230, 231, 243
Sensitivity, 4, 14, 15, 89, 193, 195, 199–202, 206, 210, 221, 233, 239, 244
Ship integration, 9, 175, 176
Shock angle, 41, 42, 69, 70, 72–76
Shock wave, 23, 24, 33, 34, 41, 42, 46, 47, 66, 67, 69, 70, 72–76, 112, 113, 216, 228, 242, 243
Sideslip, angle of, 48, 49, 179, 202
Six degrees of freedom, 117, 214, 227
Skid-to-turn, 37, 44, 48, 49, 70, 71
Skin friction drag, 22, 23, 33
Slender body theory, 26–29, 54, 122, 215, 216
Slender wing theory, 31, 215, 216
Smoke, 80, 84–86, 141, 164, 166, 167
Solid propellant rocket, 61–63, 78–88, 109–111, 125, 126, 166–169, 188–203
Sound, speed of, 66, 88, 137
Specific heat, 65–67, 73, 80, 81
Specific impulse
 ducted rocket, 60, 64, 212
 ramjet, 14–16, 60–62, 64–66, 75, 205, 206, 209–211, 216, 217, 231, 239, 243
 rocket, 46, 60–62, 77–81, 83, 84, 119, 125, 126, 193, 195, 196, 216, 217, 239
 scramjet, 60, 61, 62
 turbojet, 60, 61, 62
Split canard, 12, 39, 42–44, 231
Spreadsheet, 215–217
Stability and control, 4, 26, 29, 32, 33, 36, 37, 42, 44, 49, 51–56, 115, 118, 119, 157, 158, 164, 204, 207, 214, 225–228, 239, 242, 243
State-of-the-art, 1–3, 6, 7, 14, 200, 201, 212, 214, 227, 229, 230, 233, 234
Static margin, 3, 6, 12, 51–57, 137, 140, 189, 199–201, 217, 231, 243
Steady flight, 120, 121, 123, 216
Steel, 21, 86, 87, 96–101, 106, 107, 110, 111, 152, 189, 191
Stagnation temperature, 101, 103, 112, 113
separation, 37, 51, 93, 121, 176–180, 206, 224–226, 228
Strength, 86, 87, 94, 97–101, 111, 112, 152
Stress, 24, 81, 83, 95, 97, 98, 100, 106, 109–113, 152, 216
Structure design, 1, 2, 5, 6, 20, 21, 28, 36, 42, 87, 93, 94, 96, 101, 103, 104, 106–111, 180, 203
Structural weight, 62, 71, 89, 91, 99, 101, 106, 107, 189, 203, 204, 213
Submarine integration, 9, 175
Subsystems, 4–6, 13, 14, 25, 28, 38, 42, 49, 52, 62, 72, 79, 88–90, 104, 129, 130, 137, 144, 145, 148, 168, 169, 216, 220–222, 224–227, 233, 235, 239, 240, 244
Surface planform, 30, 31, 34–36, 43, 45, 91, 188, 203, 235, 236
Surface-to-air missile, 6, 7, 47, 70, 71, 172, 173, 215, 225, 226
Surface-to-surface missile, 6, 7, 143, 144, 145, 146, 147–168, 185, 216, 217, 223, 234, 235
Sustain flight, 79–83, 189, 191, 192, 194–201
Synthetic aperture radar (SAR), 134, 136, 230, 231
System analysis, 4, 5, 8–13, 221, 225, 227, 233, 234, 239, 240, 243, 244
- Tactical Missile Design Spreadsheet, 214–217
Tail
 arrangement, 36–38, 71, 188, 200–203
 control, 33, 36–42, 52, 71, 72, 159, 235, 236
 force, 14, 32, 38, 41, 53, 56, 57, 199, 204, 208
 sizing, 1–4, 8, 26, 32, 51–55, 200–202, 216
Tangent ogive nose, 21, 158, 159
Target
 acquisition, 2, 3, 132–136, 141, 166
 aspect, 22, 126, 155, 159, 187
 damage, 11, 135, 145, 146, 172
 detection, 4, 14, 19, 20, 123, 132, 134, 185, 186
 kill, 2, 12, 135, 144, 185–187, 216, 217
 recognition, 133–135, 143, 145–153, 185, 186, 230, 231
 types, 12, 135, 136, 142–144, 147–152, 155, 156, 161–164, 212, 213, 215
Technology
 assessment, 1–5, 59, 60, 135, 171, 211, 213, 219, 220, 229–234, 237, 244
 availability date, 139, 141, 219, 220, 222, 229, 230
 development, 9, 62, 95, 100, 104, 111, 134, 171, 172, 175, 176, 219–234
 readiness level, 12, 13, 139–141, 211, 213, 219–222, 229, 230, 240
 roadmap, 4, 5, 219, 233, 234, 239, 240, 244

- Tensile stress, 97, 98, 111
 Terminal guidance, 48, 49, 135, 154, 155, 159–164
 Test, 5, 13, 96, 168, 169, 172, 174, 178, 211, 217, 224, 225–229
 Thermal diffusivity, 103, 104
 Thermal stress, 97, 109, 110, 112, 113
 Thickness of
 airframe, 20, 102–105, 107, 109, 110, 112, 216
 motor case, 20, 86, 87, 106, 107, 110, 111, 216
 surface, 34, 42, 112, 215
 Thin wall cylinder, 20, 105, 107, 109
 Threat radar, 144, 167, 168, 186
 Three degrees of freedom, 117, 214, 215, 217
 Throat, nozzle, 14, 78–81, 83, 87, 203, 206
 Thrust
 considerations, 3, 6, 8, 46, 47, 49, 59, 61–64, 75, 76, 78–84, 110, 117–123, 125, 137, 139, 176, 194, 202, 203, 206, 212, 213, 215, 216, 231, 239
 ramjet, 14, 15, 59, 62–67, 75, 76, 137, 202, 204, 206, 208, 210–213, 216, 227, 228, 243
 rocket, 14, 15, 59, 61–63, 78–83, 110, 125, 137, 191, 192, 194, 196–201, 206, 209, 216, 225, 226
 Thrust vector control, 12, 29, 30, 37, 46–48, 225, 226, 238
 Time to climb, 120, 121, 123, 124, 216
 Time constant, 29, 56, 156–163, 216, 217, 242, 243
 Time-critical target, 8–12, 60–62, 144, 145, 231
 Titanium, 86, 96, 97, 100, 101, 203, 231
 TNT, 149, 150
 Total impulse, 118, 119, 175
 Trajectory
 boost-coast, 82, 83
 boost-sustain-coast, 82, 83, 192, 194–198
 boost-glide, 61, 62, 139
 climb, 120, 121, 123, 124, 139, 216
 cruise, 14, 61, 62, 119, 120, 137, 138, 139, 206, 210–212, 216
 dive, 120, 121, 139, 216
 turn, 47–50, 192, 194
 Trapezoidal planform, 35, 36
 Triangular planform, 35, 36
 Tri-tail, 36–38
 Trim angle of attack, 38–40, 42, 51–53, 123, 124, 215, 243
 Trim normal force coefficient, 39, 42, 52, 53, 123, 124
 Turbine, 59, 231
 Turbojet engine, 59–63, 137, 138
 Turbulent flow, 23, 101–103
 Turn radius, 115, 116, 122, 216
 Turn rate, 115, 116, 118, 119, 123, 124, 154, 159, 216
 Two degrees of freedom, 117, 216
 Uncertainty, 47, 94, 111, 139–141, 154, 194, 210, 211, 217, 244
 Undamped natural frequency, 17, 20, 21, 49, 243
 Underexpanded nozzle, 80, 81, 137
 Uniform load, 108–110
 Unguided flight trajectory, 51, 214
 Unit cost, 143, 170–172, 175, 239, 240
 Unmanned
 air vehicle, 9, 10, 94, 170
 combat air vehicle, 9, 10
 Unpowered flight, 23, 24, 35, 82, 83, 117, 124, 125, 195–198, 216, 217, 225

 Velocity
 burnout, 14, 77, 78, 106, 194, 196–198, 206, 209
 coast, 124, 125, 194–198, 216
 cruise, 14, 16, 61, 62, 74, 75, 120, 122, 137, 138, 202, 206, 210–212, 229, 230
 sustain, 125, 126, 194, 196–198
 Vertical Launch System, (VLS) 86, 175, 176
 Volumetric
 Efficiency, 64, 81–83, 86, 199–201, 212
 Performance, 64, 77, 84, 85, 212, 231, 232
 Vortices, 37, 39, 44, 45, 228
 Vulnerable area, 148

 Wall temperature, 101–103
 Warhead
 blast fragmentation, 17, 142–151, 154, 216, 217
 kinetic energy, 142, 144–149, 151–153, 216, 217, 231
 Weather, 129–137, 144, 145, 230, 231
 Weight reduction, 7, 9, 10, 29, 64, 67–69, 71, 86, 88, 89, 94–101, 103–107, 110, 111, 134, 144, 145, 153, 175–177, 199–202, 223, 224, 231
 Weight statement, 14, 15, 188, 189, 203, 204, 239, 240
 Wetted area, 23, 190, 205
 Wind tunnel, test 5, 28, 107, 176, 178, 194, 211, 214, 217, 224–228
 Window dome, 21, 22, 159, 160, 230, 231
 Wing
 aerodynamic center, 17, 32, 33, 35, 38, 53, 54
 area, 3, 6, 8, 17, 31, 34, 45, 185, 188, 190, 198, 199
 arrangement, 8, 37, 38, 179, 188, 200, 201, 202
 center of pressure, 17, 32, 33, 35, 38, 53, 54
 characteristics, 28–30, 35, 36, 53, 122, 179, 189, 190, 198–202
 control, 31, 33, 36, 37, 44, 45, 56, 70, 71, 123,

- location, 33, 44, 45, 53–55, 69–71, 188, 200–202, 215
mean aerodynamic chord (mac), 32–36, 54, 188, 190
normal force, 17, 29–32, 44, 56, 57, 118, 122, 159, 160, 185, 192, 193, 198, 199
planform, 3, 4, 8, 17, 33–36, 188, 200–202, 216
rectangular wing, 35, 36
section, 34, 35, 113, 190
size considerations, 3, 4, 8, 17, 29, 30, 198–202
sizing, 3, 4, 6, 8, 17, 44, 55, 57, 185, 199–202
sweep, 33–36, 188, 190, 199, 200
trapezoidal wing, 35, 36, 188
Wing-body-tail, 32, 37, 38, 44, 45, 53, 56, 57, 227, 228
Wing theory, aerodynamic linear, 30–33, 54, 216
slender, 31, 32, 216
X tail, 50, 51
Yawing moment, 55, 56, 117
Yield strength, 93, 94, 97–99, 106, 107, 109, 111, 112, 152
Zero lift drag of body, 23, 24, 27, 35, 122
wing drag, 33–35
tail, 34, 35
total, 14, 15, 18, 19, 23, 24, 35, 76, 77, 115, 117, 119, 124, 192, 193, 195, 196, 198, 204, 206, 207, 210, 211, 216, 217